

INFLUENCE OF RUBBING ON ROTOR DYNAMICS

NASA Contract No. NAS8-36719

FINAL REPORT

Part 2 of 2

Prepared for George C. Marshall Space Flight Center  
Marshall Space Flight Center,  
Alabama 35812

by

Agnes Muszynska  
Donald E. Bently  
Wesley D. Franklin  
Robert D. Hayashida  
Lori M. Kingsley  
Arthur E. Curry

Bently Rotor Dynamics Research Corporation

BENTLY NEVADA CORPORATION  
P.O. Box 157  
MINDEN, NEVADA 89423

March 1989

# TABLE OF CONTENTS

## PART 1

1. INTRODUCTION . . . . .	9
1.1 Original Scope of the Research on "Influence of Rubbing on Rotor Dynamics" Solicited by NASA . . . . .	9
1.2 Scope of This Report . . . . .	9
2. ROTOR-TO-STATIONARY ELEMENT RUB-RELATED VIBRATION PHENOMENA IN ROTATING MACHINERY. LITERATURE SURVEY . . . . .	11
2.1 Introduction . . . . .	11
2.2 Rub Malfunction in Rotating Machinery . . . . .	11
2.3 Thermal Effect of Rub . . . . .	12
2.4 Dry Whip . . . . .	12
2.5 Physical Phenomena Occurring During Rubbing . . . . .	13
2.5.1 Friction . . . . .	13
2.5.2 Impacting . . . . .	13
2.5.3 Torsional Load . . . . .	14
2.5.4 Coupling Effect . . . . .	14
2.5.5 Stiffening Effect . . . . .	14
2.5.6 Other Effects . . . . .	14
2.6 Analysis of Rubbing Rotors . . . . .	14
2.7 Vibration Response of Rubbing Rotors . . . . .	16
2.8 Deadband Malfunction - Twin Brother of Rub . . . . .	17
2.9 Summary . . . . .	17
2.10 References . . . . .	18
3. CHARACTERIZATION OF RUB PHENOMENA IN ROTATING MACHINERY . . . . .	25
3.1 Definitions . . . . .	25
3.2 Rub-Related Changes in the Rotating Machine Force Balance and Dynamic Stiffness . . . . .	25
3.2.1 Coupling Effect . . . . .	25
3.2.2 Stiffening Effect . . . . .	25
3.2.3 Friction Effect . . . . .	26
3.2.4 Impacting Effect . . . . .	26
3.2.5 Fluid Dynamic Forces and Thermal Unbalance . . . . .	27
3.3 Rub Location . . . . .	27
3.4 Conditions Leading to Rub . . . . .	27
3.5 Transient Character of Rub-Related Effects . . . . .	28
3.6 Rub-Related Modifications of the Rotating Machine Vibrational Response . . . . .	28
3.6.1 Frequency . . . . .	28
3.6.2 Amplitude . . . . .	28
3.6.3 Mode of Shaft Centerline . . . . .	28
3.7 Summary . . . . .	29
4. HPFTP SIMULATING RUBBING ROTOR RIG INITIAL DESIGN DATA . . . . .	33
4.1 Modelling Data for HPFTP . . . . .	33
4.2 Scaled Rotor Rig Model Data . . . . .	33

4.3	Computer Calculation of Natural Frequencies and Mode Shapes . . . . .	34
4.4	Summary . . . . .	35
5.	HPFTP SEAL-SIMULATING OIL-LUBRICATED BEARING SELECTION AND TESTS . . . . .	39
5.1	Introduction . . . . .	39
5.2	Seal-Simulating Oil Bearing Tests . . . . .	39
	5.2.1 Introduction . . . . .	39
	5.2.2 Test Procedure . . . . .	39
	5.2.3 Static Test . . . . .	39
	5.2.4 Dynamic Test . . . . .	39
	5.2.5 Results of Static Perturbation Testing of the 2.5 Mil Radial Clearance Bearing . . . . .	40
	5.2.6 Results of Dynamic Perturbation Testing of the 2.5 Mil Radial Clearance Bearing . . . . .	40
	5.2.7 Results of Static Perturbation Testing of the 5.5 Mil Radial Clearance Bearing . . . . .	40
5.3	Mathematical Model Used for Oil-Lubricated Bearing Test Data Interpretation . . . . .	41
	5.3.1 Static Test . . . . .	42
	5.3.2 Dynamic Test . . . . .	42
5.4	Summary . . . . .	43
6.	RUBBING ROTOR RIG SIMULATING HPFTP . . . . .	53
6.1	Rotor Rig . . . . .	53
6.2	Instrumentation of the Rubbing Rotor Rig Simulating HPFTP . . . . .	53
	6.2.1 Vibration Transducers . . . . .	53
	6.2.2 Data Acquisition and Processing Instrumentation . . . . .	53
	6.2.3 Description of Data Presentation Format . . . . .	54
	6.2.4 Auxiliary Instrumentation . . . . .	54
6.3	Summary . . . . .	55
7.	HPFTP SIMULATING RUBBING ROTOR RIG PRELIMINARY EXPERIMENTAL RESULTS . . . . .	59
7.1	Test Objective and Experiment Conditions . . . . .	59
7.2	Test Results . . . . .	59
7.3	Internal Friction Instability . . . . .	60
7.4	Summary . . . . .	61
8.	EFFECTS OF RUB ON ROTOR AND STATOR RUBBING SURFACES . . . . .	121
8.1	Objective of the Study . . . . .	121
8.2	Description of Rub Blocks for Surface Rub-Related Damage Study . . . . .	121
8.3	Friction Measurement Fixture and Coefficient of Friction Algorithm . . . . .	121
8.4	Results of Surface Friction Coefficient Measurements . . . . .	123
8.5	Effects of Rotor-to-Stator Rub on Rubbing Surfaces . . . . .	123
	8.5.1 Test Procedure . . . . .	123
	8.5.2 Metallographic Analysis of Rub Surface Photographs . . . . .	123
	8.5.3 Conclusions From Material Property Experiments . . . . .	124
8.6	Summary . . . . .	125

9.	TWO-BENDING-MODE RUBBING ROTOR RIG AND IDENTIFICATION OF ITS DYNAMIC CHARACTERISTICS . . . . .	143
9.1	Objective . . . . .	143
9.2	Two-Bending-Mode Rubbing Rotor Experimental Rig . . . . .	143
	9.2.1 High Frequency Accelerometer . . . . .	144
	9.2.2 Rub-Related Electrical Contact Device . . . . .	144
9.3	Results of Stator Compliance Tests . . . . .	144
9.4	Identification of Rotor Rig Modal Parameters via Synchronous Dynamic Stiffness Testing . . . . .	145
	9.4.1 Mathematical Model of the Rotor at the First Lateral Mode . . . . .	145
	9.4.2 Synchronous Response . . . . .	146
	9.4.3 The First Mode Identification of Rotor Parameters Using Synchronous Perturbation Testing . . . . .	148
	9.4.4 Mathematical Model of the Rotor With Two Lateral Modes . . . . .	150
	9.4.5 Forced Solution . . . . .	151
	9.4.6 Two-Mode Identification of Rotor Parameters Using Synchronous Perturbation Testing . . . . .	153
9.5	Summary . . . . .	155
10.	EXPERIMENTAL RESULTS OF PARTIAL ROTOR-TO-STATOR RUB FROM TWO-MODE ROTOR RIG	
10.1	Introduction . . . . .	173
10.2	Test Procedure . . . . .	173
10.3	No-Rub Test . . . . .	173
10.4	Results From Rub Tests . . . . .	173
10.5	Results Obtained From Displacement Probes Versus Results Obtained From Accelerometers . . . . .	175
10.6	Investigation of Multiple Partial Rub With Full 360 Degree Rub Fixture . . . . .	176
10.7	Summary . . . . .	177
11.	MATHEMATICAL MODEL OF THE RUBBING ROTOR MECHANICAL SYSTEM . . . . .	255
11.1	Initial Assumptions . . . . .	255
11.2	Mathematical Model . . . . .	255
11.3	Calculation of Rotor-to-Stator Rub Contact Normal Force . . . . .	258
11.4	Rub-Related Impact Model . . . . .	260
11.5	Summary . . . . .	261
12.	RESULTS OF THE ROTOR-TO-STATOR RUBBING EXPERIMENTAL TESTING OF THE HPFTP SIMULATING ROTOR RIG . . . . .	265
12.1	Introduction . . . . .	265
12.2	Experiment With Mass Unbalance in Turbine Disk . . . . .	265
12.3	Experiment With Mass Unbalance in Third Pump Impeller Disk . . . . .	266
12.4	Summary . . . . .	266

PART 2

13.	RESULTS OF THE ROTOR-TO-STATOR RUB CONTACT STUDY . . . . .	527
13.1	Introduction . . . . .	527
13.2	Rotor-to-Stator Rub Contact Experiments . . . . .	527
	13.2.1 Rub Contact Time Versus Rotative Speed Test Conditions . . . . .	527
	13.2.2 Test Procedure and Transient Test Data . . . . .	527
	13.2.3 Steady-State Test Results . . . . .	528
	13.2.4 Discussion on Results From Rub Tests . . . . .	528

13.3	Rub Contact Analytical Study . . . . .	529
13.4	Experimental Results on the Second Harmonic Generation Versus Rubbing Rotor/Stator Contact . . . . .	531
13.5	Summary . . . . .	532
14.	<b>ROTOR-TO-STATOR RUB COMPUTER SIMULATION PROGRAM DEVELOPMENT AND OPERATION . . . . .</b>	<b>639</b>
14.1	Introduction . . . . .	639
14.2	General Description of the Program . . . . .	639
14.3	Program Initialization . . . . .	639
14.4	Linear Synchronous Response Calculations . . . . .	640
	14.4.1 Linear Equations and Their Solution . . . . .	640
	14.4.2 Linear Synchronous Response Plots: Exit Data . . . . .	643
14.5	Nonlinear Timebase Calculation . . . . .	643
	14.5.1 Nonlinear Equations . . . . .	643
	14.5.2 Numerical Method . . . . .	644
	14.5.3 Accuracy Sensitivity . . . . .	645
	14.5.4 Nonlinear Timebase Plots: Exit Data . . . . .	645
	14.5.5 Extension of the Nonlinear Timebase Calculations . . . . .	645
	14.5.6 Program Termination . . . . .	645
14.6	Summary . . . . .	646
15.	<b>RESULTS FROM COMPUTER SIMULATION PROGRAM . . . . .</b>	<b>663</b>
15.1	Introduction . . . . .	663
15.2	Determination of the System Dynamic Parameters Using the Linear Synchronous Response Part of the Computer Program . . . . .	663
15.3	Results From the Nonlinear Timebase Portion of the Computer Program . . . . .	663
	15.3.1 Results From the Calculations With the Unbalance and the Radial Preload at the Third Disk . . . . .	664
	15.3.2 Results From the Calculations With the Unbalance in the Second Disk and the Radial Preload at the Third Disk . . . . .	664
15.4	Summary . . . . .	665
16.	<b>CONCLUSIONS . . . . .</b>	<b>739</b>
	<b>APPENDIX 1. DATA REDUCTION OF THE HPFTP HOT FIRE TAPES . . . . .</b>	<b>747</b>
	A.1.1 Introduction . . . . .	747
	A.1.2 Data Reduction . . . . .	747
	A.1.3 Conclusions and Recommendations . . . . .	748
	<b>APPENDIX 2. "INFLUENCE OF RUBBING ON ROTOR DYNAMICS," by A. Muszynska, W. D. Franklin, and R. D. Hayashida. Paper Presented at the Third Conference on Advanced Earth-to-Orbit Propulsion Technology, Huntsville, Alabama, 10-12 May 1988. . . . .</b>	<b>779</b>
	<b>APPENDIX 3. INSTRUMENTATION DATA . . . . .</b>	<b>797</b>
	• 3000 and 7000 Series Proximity Transducer Systems	
	• Acceleration Transducer System	
	• ADRE <sup>o</sup>	
	• 24000 Digital Vector Filter 2	
	• Digital Vector Filter 3	
	• ADRE <sup>o</sup> 3	

## 13. RESULTS OF THE ROTOR-TO-STATOR RUB CONTACT STUDY.

### 13.1 Introduction

Rotor dynamic behavior depends considerably on how much the specific physical phenomena accompanying rotor rubbing against the stator are involved. One of the factors which might represent a measure of severity of rub is the time of the rotor and stator physical contact, as a fraction of the rotor precessional period. In this chapter this problem is outlined.

### 13.2 Rotor-to-Stator Rub Contact Experiments

A series of tests of rubbing rotor was performed on the two-mode rotor rig. The rotor/stator contact was carefully measured and correlated with the rotor vibrational response.

#### 13.2.1 Rub Contact Time Versus Rotative Speed Test Conditions

The two-mode rubbing rotor rig is used for this series of tests. The system consists of a horizontal two-disk rotor supported at each end by a relatively rigid bronze sleeve-type bearing (Oilite) (Fig. 9.2). A one-half horsepower AC motor drives the rotor through a flexible coupling. When observed from the motor end of the shaft, rotation is in the clockwise direction.

The compliant rub fixture, also used in the previous experiments, is mounted between the two rotor disks (Fig. 9.3). The X-Y displacement probes providing the shaft radial displacement data are mounted next to the outboard disk. The rub fixture plunger can move in the horizontal direction perpendicular to the rotor axis. The plunger motion is observed by another displacement probe. Plunger motion data is then correlated with the rub contact timing signal in a timebase format. A Keyphasor probe mounted vertically at the motor end of the system provides the once-per-turn reference signal from which all phase angles are measured in the direction against rotation. The shaft observing vertical and horizontal displacement probes are installed at 0 and 270 degrees respectively. For this entire series of experiments the plunger mechanism preload is constant, and equals 3.34 lb. The rub block material is aluminum.

#### 13.2.2 Test Procedure and Transient Test Data

A controlled unbalance force inserted at the rotor inboard disk is used to generate the required level of synchronous vibration needed to investigate the relationship between rotor-to-stator rub contact time (dwelling time) and rotor rotative speed. Rotor speeds range from 1200 rpm to 4350 rpm passing through the rotor first and second balance resonances at approximately 1570 rpm and 4020 rpm respectively. It should be noted that these speeds represent the rotors first and second balance resonances under normal operating conditions without rub.

The unbalance mass employed for this series of experiments is 2.0 grams at 180 degrees (relative to the Keyphasor notch) and located at the inboard disk at a radius of 1.2 inches. This relatively high mass unbalance is needed to generate the desired rub condition over the operational speed range. For reference, transient data in Bodé plot format is presented for both balanced and unbalanced (controlled unbalance) states (Figures 13.1 to 13.4). Transient data indicates maximum vibration amplitudes through both the first and second balance resonances of approximately 4.0 and 28.0 mils for balanced and unbalanced states respectively. Slow roll amplitudes have been maintained at less than .5 mils at all times.

A set of Bodé plots (Figures 13.5 and 13.6) as well as spectrum cascade plots (Figures 13.7 and 13.8) of the rotor response during rotor-to-stator rub are also given. As compared with the "no rub" case (Figures 13.1 to 13.4) the occurrence of rub modified the rotor responses. Figure 13.9 presents the numerical values for the rotor-to-stator rub contact time and corresponding elapsed shaft rotation for each chosen operating speed. Figure 13.10 presents the data from Figure 13.9 graphically.

### 13.2.3 Steady-State Test Results

Steady state data (at constant rotative speed) of the rotor vibrational response is captured for each chosen rotative speed and presented in both 1x filtered (synchronous) and unfiltered orbit/timebase formats (Figures 13.11 to 13.84).

The vertical and horizontal timebase data used to generate each orbit is presented in a format to simplify graphical reconstruction of the orbit. Vertical timebase data is seen to the right of each orbit while horizontal timebase data is seen below. The scaling of each data type (orbit or timebase) plot is arbitrarily selected, again for purposes of presentation. Absolute amplitude scaling for each pair of timebase data used to generate the associated orbit will be the same whereas the amplitude scaling for each orbit must be read specifically from each graph.

In addition, the rub plunger motion (compliant stator-simulating boundary mechanism) and the associated rub-generated electrical contact signal are presented below the vertical timebase data. It is important to understand that the electrical contact signal may be generated by rub at any point over the rub clock's 180-degree half-circle surface. Therefore, this signal does not have an angular reference fixed to a specific probe location, as is the case with the vertical and horizontal displacement probes. To determine where rub occurs from an orbit alone may be difficult. It is necessary to establish when a rub occurred in the time domain to determine the corresponding rub location on each given orbit. Together with the vertical and horizontal vibration data, rub phase information may be obtained. Of interest are the phase angles at which a rub condition initiates and terminates, related to the phase angles of the rotor's heavy and high spots.

### 13.2.4 Discussion on Results From Rub Test

Precessional motion of the rotor given in terms of the 1x filtered orbits represents rotor vibrations due to the controlled unbalance. The steady-state unfiltered orbits clearly indicate modification of the "normal" vibration response of the rotor due to rub. When the occurrence of rub is essentially a "clean" once-per-turn event and the rotor-to-stator contact is light, the resulting unfiltered orbit is still close to circular. In fact, some of the unfiltered orbits are so perfectly circular that a rub condition, although cleanly indicated by the electrical contact signal, is not obvious. The "circular" shape of the orbit is an indication of the rotor system's highly symmetrical characteristics, specifically, orthogonal stiffnesses in the vertical and horizontal directions. The "system's" stiffnesses include the rotor as well as the associated bearings and support stiffnesses.

Given the time scale on each electrical contact signal timebase plot, the shaft dwelling time during rub is graphically obtained for each rotative speed. The amount of shaft rotation during the period of contact for each chosen rotative speed is then calculated. A tabular listing of this information is given in Figure 13.9. Further inspection of this data indicates local maxima of rub contact time corresponding to the rotor modified first, twice first, and second resonant frequencies.

The rotor/stator contact values are presented in the form of the angle  $\beta$  which is defined as "the amount of shaft revolutions encountered while the shaft is in contact with the rub

block for each specific operating speed." The angle  $\beta$  is plotted versus shaft rotative speed (rpm) (Figure 13.10a). The data from Figure 13.9 generates a curve similar in shape to that of a rotor vibrational response amplitude due to unbalance during run-up. The 1x response amplitude is overlaid on the graph. Over the range of operating speeds for this experiment, the rotor would normally (operation without rub) experience only two distinct resonances (Figures 13.3 and 13.4); however, Figure 13.10 indicates three peaks of the angle  $\beta$ . The peaks at 1820 and 4105 rpm correspond to the rotor's (modified by rub) first and second balance resonance frequencies respectively. The peak at 3610 rpm occurs due to the rub-induced excitation. Note that the speed at which this occurs (3610 rpm) is approximately twice that of the system's modified first balance resonance (1820 rpm). The data between 3400 and 3800 rpm is somewhat inconsistent due to the excitation of the first balance resonance.

The rotor-to-stator contact arc related to the generalized 360 degree period of fundamental 1x response versus rotative speed is presented in Figure 13.10b. The bottoms of the contact arc lines correspond to rub inception, the tops correspond to rub cessation. The 1x vertical phase is overlaid on the graph. As the resonant range of rotative speeds rub occurs twice per period. The rub inception somewhat follows the 1x response phase.

It is apparent that the phenomena of rub during machine operation modify the system's natural frequencies as well as the dynamic motion of the rotor. Strong subsynchronous rub-related vibration components are generated. They have frequencies of predominantly 1/2 running speed ( $1/2\times$ ) when rotative speed is at and above twice the first balance resonance. Super-synchronous components, including two and three times running speed ( $2\times$ ,  $3\times$ ), are also present though much less pronounced (Figures 13.7 and 13.8).

During rub, the obstacle encountered acts like an additional bearing or support, thus momentarily increasing the observed dynamic stiffness of the system. A comparison of the pure unbalanced rotor response Bodé plots (Figures 13.3 and 13.4) with those during rub (Figures 13.5 and 13.6) clearly indicates that resonance occurs at higher frequencies as a result of the rub-induced system stiffening effect.

The motion of the rotor is modified by rub as indicated by the unfiltered orbits. The orbit's deviation from a pure circular or elliptical shape caused by the rubbing shows a rich variety, and is rotative speed dependent. The rotor rebounding motion proved to be dependent not only on the position of the rotor unbalance, but also the compliance of the stator against which rub occurs, thus the time that the rotor spends in contact with the stator depends on several conditions. The rub contact time data generated indicates that changes in the dwelling time closely follow the nature of the rotor vibration response amplitudes and phases.

### 13.3 Rub Contact Analytical Study

It is believed that the "dwelling time," i.e., the time of the rotor-to-stationary part contact and the following changes in the rotor vibration responses may be used as the diagnostic information for determination of the severity of rub (Ref. [4], Section 2.10). In this section a simplified model of the phenomenon is discussed.

Assuming that during the rotor normal operation its lateral vibrational response is harmonic, the occurrence of the rotor-to-stationary part contact causes a truncation of the harmonic wave, as measured by one lateral probe (Fig. 13.85). The truncated wave  $f(t)$  with the period  $\frac{2\pi}{\omega}$  where  $\omega$  [ $\frac{\text{rad}}{\text{s}}$ ] is rotor precessional frequency has the following functional form in between one period time:

$$f(t) = \begin{cases} A = B \cos \omega t_0 & \text{for } 0 < t < t_0 \\ B \cos \omega t & \text{for } t_0 < t < \frac{2\pi}{\omega} - t_0 \\ A = B \cos \omega t_0 & \text{for } \frac{2\pi}{\omega} - t_0 < t < \frac{2\pi}{\omega} \end{cases} \quad (13.1)$$

where  $2t_0$  is rotor total dwelling time (maintaining contact with the stationary part) per one period of vibration. Applying the Fourier transformation, this function can be presented as follows:

$$f(t) = \frac{a_0}{2} + \sum_{\nu=1}^{\infty} a_{\nu} \cos \nu \omega t \quad (13.2)$$

where

$$a_{\nu} = \frac{\omega}{\pi} \int_0^{\frac{2\pi}{\omega}} f(t) \cos \nu \omega t \, dt, \quad \nu = 0, 1, 2, \dots \quad (13.3)$$

Introducing (13.1) into (13.3), the amplitudes of the static displacement and harmonics are obtained:

$$\begin{aligned} a_0 &= \frac{2B}{\pi} (\omega t_0 \cos \omega t_0 - \sin \omega t_0) \\ a_1 &= \frac{B}{2\pi} (\sin 2\omega t_0 + 2\pi - 2\omega t_0) \\ a_2 &= \frac{B}{6\pi} (\sin 3\omega t_0 - 3 \sin \omega t_0) \\ &----- \\ a_{\nu} &= \frac{B}{\nu\pi} \left[ \frac{1}{\nu+1} \sin (\nu+1)\omega t_0 - \frac{1}{\nu-1} \sin (\nu-1)\omega t_0 \right] \end{aligned} \quad (13.4)$$

All amplitudes depend on the "dwelling time"  $t_0$ , thus, it is indirectly responsible for modifications of the rotor vibrational responses.

The time  $t_0$  can be expressed in terms of the arc  $\varphi$  of the rotor precessional motion, as follows:

$$\begin{aligned} t_0 [\text{sec}] &= \frac{\pi \varphi [\text{deg}]}{360 \omega [\text{rad/s}]} = \frac{\varphi [\text{deg}]}{12\omega [\text{Hz}]} \\ t_0 [\text{min}] &= \frac{\varphi [\text{deg}]}{720 \omega [\text{rpm}]} \end{aligned} \quad (13.5)$$

where in brackets the corresponding units are given. Introducing Eq. (13.5) into (13.4) the amplitudes become expressed in terms of the arc  $\varphi$ :

$$\begin{aligned}
 a_0 &= \frac{2B}{\pi} \left[ \frac{\pi \varphi}{360} \cos \frac{\varphi}{2} - \sin \frac{\varphi}{2} \right] \\
 a_1 &= \frac{B}{2\pi} \left[ \sin \varphi + 2\pi - \frac{\pi \varphi}{180} \right]
 \end{aligned}
 \tag{13.6}$$

-----

$$a_\nu = \frac{B}{\nu\pi} \left\{ \frac{1}{\nu+1} \sin \left[ (\nu+1) \frac{\varphi}{2} \right] - \frac{1}{\nu-1} \left[ \sin (\nu-1) \frac{\varphi}{2} \right] \right\}
 \tag{13.7}$$

The arc  $\varphi = 360^\circ$  theoretically corresponds to the full annular rub. Practically the model is valid only for  $\varphi < 180^\circ$ . In this range the static displacement, as well as harmonic amplitudes  $a_2$ ,  $a_3$  are negative, while the first harmonic amplitude  $a_1$  is positive. This means that the second and third harmonics are  $180^\circ$  out of phase of the first one.

The amplitudes of the first four components of (13.2) and the amplitude ratios versus angle  $\varphi$  are illustrated in Fig. 13.86.

The model of rub-related straight truncation of the rotor lateral response wave form is very simplified, and only roughly qualitatively can describe the rub phenomena. The results of a series of experiments described in the next section contest the use of this model.

#### 13.4 Experimental Results On The Second Harmonic Generation Versus Rubbing Rotor/Stator Contact

The same two-mode rotor rig, as described in Section 13.2 was used for this series of experiments. The rubbing rotor vibrational data from the rotative speed range 1260 to 2920 rpm was reduced, and in particular, the second harmonics (2x) of the vibrational responses were extracted (Figs 13.87 to 13.103). Presented along with the fundamental term (1x) and the rotor/stator contact time gives an idea on how much the rub affects the second harmonics. The summary of results is given in Table 13.1 and in Fig. 13.104. The experimental results in Fig 13.104 are presented together with the theoretical curve of 2x to 1x response component amplitude ratio, discussed in the previous section. Highly scattered experimental points hardly follow the theoretical curve. The results look rather chaotic. Plotted versus rotative speed the 2x to 1x response component amplitude ratio (Fig. 13.105) exhibits clear increase of 2x component at first balance resonance speed and at about 2300 rpm. The latter speed is a half of the second resonance. At this speed the resonance of 2x component occurs independently of rub mechanism. This resonance occurs due to the rotor lateral asymmetry together with the radial preload (due to gravity in the considered case). The dramatic phase change of the 2x component causing 2x orbit to flip over from reverse to forward direction confirms that the 2x horizontal then vertical resonances occur in a short span of the rotative speed (Figs. 13.100 to 13.103).

The increase of 2x to 1x vibration amplitude component ratio at the first balance resonance is obvious. However, in this case there also exist two sources contributing to that increase. At high 1x amplitudes the system stiffness nonlinearity becomes significant, and causes the 2x component to occur. More severe rub around the 1x resonant speed, as a result of higher rotor/stator normal force (see Section 11.3) also contributes to the 2x component growth. It was difficult, however, to separate all these effects in the vibrational response.

The 2x to 1x amplitude ratio looks uncorrelated from the rotor/stator contact arc. Especially puzzling are results in the range of rotative speeds between 1800 and 2000 rpm (Fig. 13.105). In spite of relatively long time rubbing contact, the amplitude ratio remains very low.

TABLE 13.1 Synchronous and Second Harmonic Vibration Response Versus Rotor/Stator Contact Arc

Rotative Speed $\omega$ [rpm]	Synchronous (1x) Horizontal Amplitude [mils]	Synchronous (1x) Vertical Amplitude [mils]	2x Horizontal Amplitude [mils]	2x Vertical Amplitude [mils]	Horizontal 1x to 2x Amplitude Ratio	Vertical 1x to 2x Amplitude Ratio	Rub time to 1x Vibration Period Ratio, $\Delta t \omega$	Contact arc $\varphi = \Delta t \omega 360$ [Degrees]
1262	2.3	2.8	0.2	0.2	0.09	0.07	0.13	48.5°
1302	2.5	3.1	0.3	0.2	0.12	0.06	0.16	50°
1345	3.1	4.1	0.2	0.1	0.06	0.02	0.14	50°
1404	4.2	5.8	0.07	0.1	0.02	0.02	0.31	112°
1456	5.5	8.3	0.37	0.1	0.07	0.01	0.54	194.5°
1500	6.6	10.4	0.9	0.4	0.14	0.04	0.5	180°
1593	5.2	11.9	3.2	1.5	0.62	0.13	0.48	173°
1646	5.7	12.3	4.1	1.9	0.72	0.15	0.48	173°
1736	9.1	17.1	4.7	2.4	0.52	0.14	0.5	180°
1834	3.9	8.8	0.5	0.3	0.13	0.03	0.64	230°
1933	2.5	5.7	0.4	0.4	0.16	0.07	0.68	245°
1975	2.2	5	0.7	0.3	0.32	0.06	0.68	245°
2059	6.4	4.2	3.7	1.9	0.58	0.45	0.46	166°
2292	6.5	1.1	1.9	1.9	0.29	1.73	0.53	191°
2442	6.9	2.6	1.3	1.1	0.19	0.42	0.38	137°
2737	3.1	2.4	0.2	0.1	0.06	0.04	0.6	216°
2917	2.9	2.6	0.19	0.13	0.07	0.05	0.72	259°

The range of the rotative speeds for which this test was performed was limited to the value of twice first balance resonance speed. For higher speeds the rotor-to-stator rub generates 1/2x vibration component, thus the second harmonic of the fundamental 1/2x frequency becomes 1x, and is difficult to separate from the unbalance-related response.

### 13.5 Summary

The study on the rotor-to-stator rub contact as a factor correlated to the severity of rub is outlined in this chapter. When there is no additional radial preload on the shaft the contact time follows the values of the vibration amplitudes of the fundamental component. Thus, at resonant speeds, the rotor-to-stator contact is longer than in non-resonant ranges of rotative speeds. The second harmonic component exhibits also an increase in the 1x resonant range. The judgment on severity of rub based on the 2x to 1x amplitude ratio seems however inappropriate. The experimental results show widely scattered and rather chaotic data.

ORIGINAL PAGE IS  
OF POOR QUALITY

BENTLY  
NEVADA  
CORP.

RUNUP

PLANT ID: BRDRC  
TRAIN ID: TEST  
MACHINE ID: ROTOR KIT  
SOLID DATA: Uncomp INB VERT

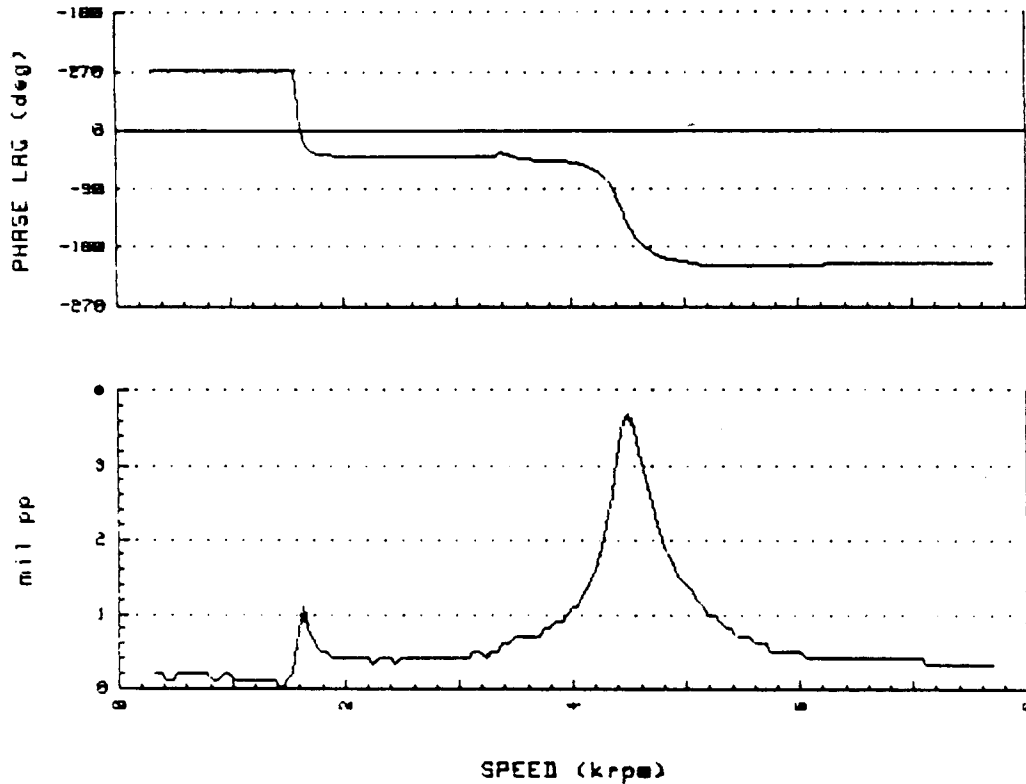


FIGURE 13.1 BODÉ PLOT OF THE ROTOR FILTERED SYNCHRONOUS VIBRATION RESPONSE DURING RUN-UP, AS SEEN BY THE INBOARD VERTICAL DISPLACEMENT PROBE. BALANCED ROTOR, NO RUB.

BENTLY  
NEVADA  
CORP.

RUNUP

PLANT ID: BRDRC  
TRAIN ID: TEST  
MACHINE ID: ROTOR KIT  
SOLID DATA: Uncomp OUTB VERT

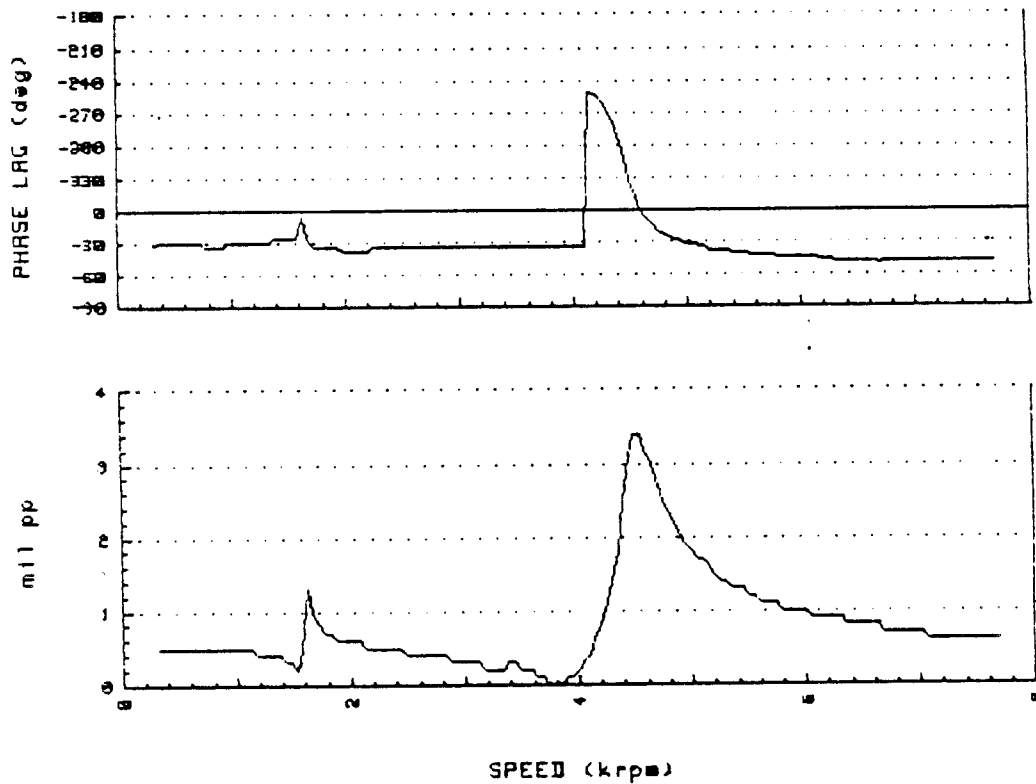


FIGURE 13.2 BODÉ PLOT OF THE ROTOR FILTERED SYNCHRONOUS VIBRATION RESPONSE DURING RUN-UP, AS SEEN BY THE OUTBOARD VERTICAL DISPLACEMENT PROBE. BALANCED ROTOR, NO RUB.

BENTLY  
NEVADA  
CORP.

RUNUP

PLANT ID: BRDRC  
TRAIN ID: TEST  
MACHINE ID: ROTOR KIT  
SOLID DATA: Uncomp INB VERT

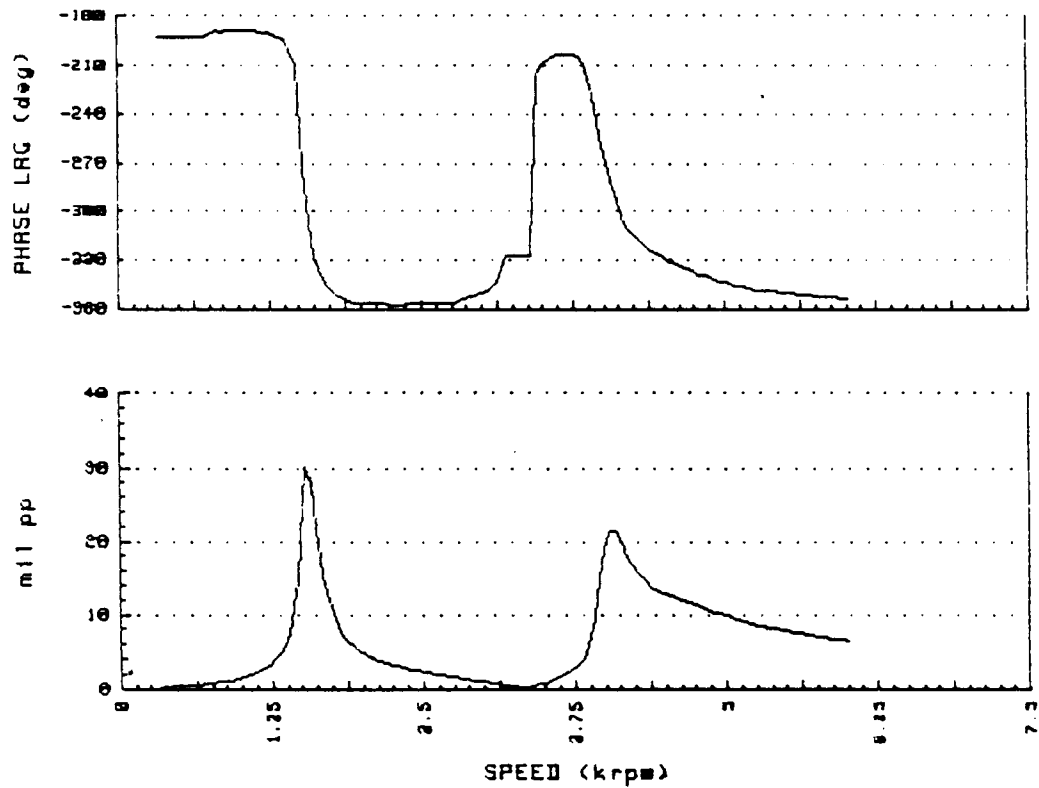


FIGURE 13.3 BODÉ PLOT OF THE ROTOR FILTERED SYNCHRONOUS VIBRATION RESPONSE DURING RUN-UP, AS SEEN BY THE INBOARD VERTICAL DISPLACEMENT PROBE. UNBALANCE: 2.0 GRAMS, 180 DEGREES, RADIUS 1.2 INCHES AT THE INBOARD DISK. NO RUB.

BENTLY  
NEVADA  
CORP.

RUNUP

PLANT ID: BRDRC  
TRAIN ID: TEST  
MACHINE ID: ROTOR KIT  
SOLID DATA: Uncomp OUTB VERT

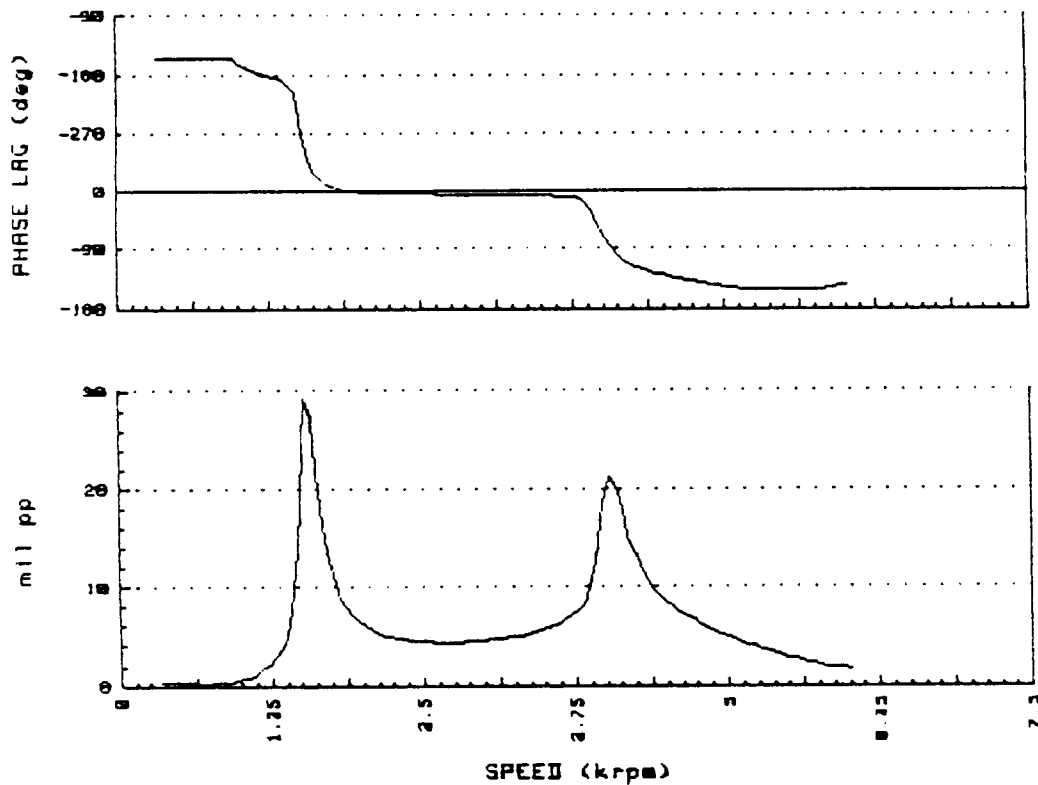


FIGURE 13.4 BODÉ PLOT OF THE ROTOR FILTERED SYNCHRONOUS VIBRATION RESPONSE DURING RUN-UP, AS SEEN BY THE OUTBOARD VERTICAL DISPLACEMENT PROBE. UNBALANCE: 2.0 GRAMS, 180 DEGREES, RADIUS 1.2 INCHES AT THE INBOARD DISK. NO RUB.

BENTLY  
NEVADA  
CORP.

RUNUP

PLANT ID: BRDRC  
TRAIN ID: TEST  
MACHINE ID: ROTOR KIT  
SOLID DATA: Uncomp INB VERT

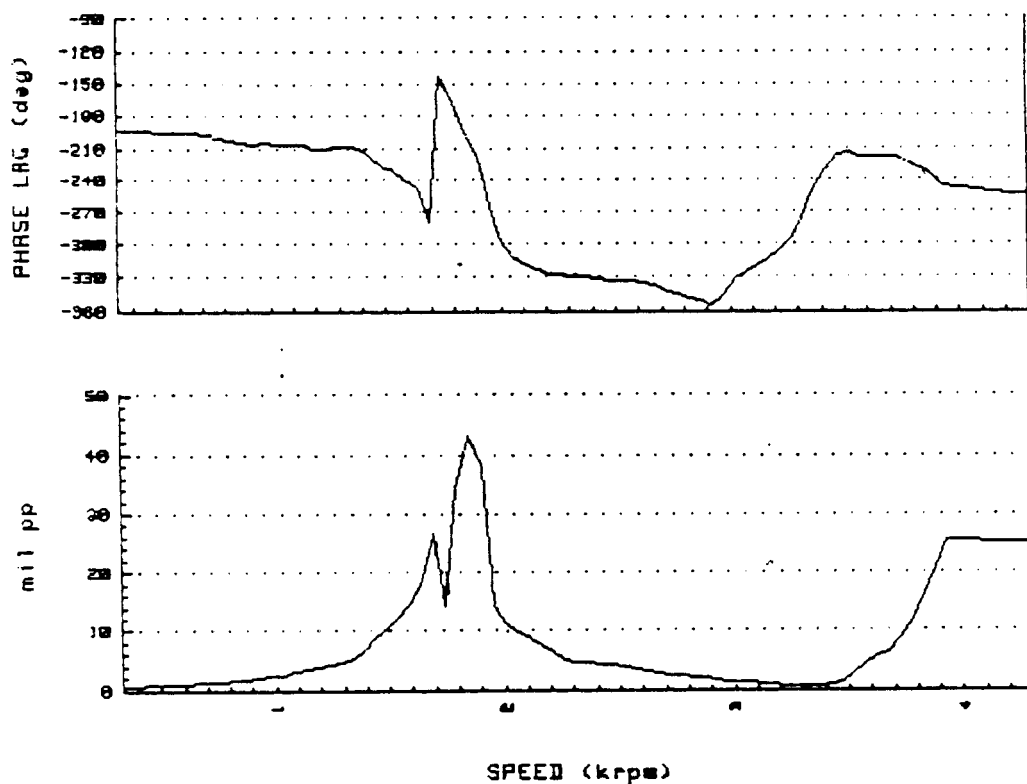


FIGURE 13.5 BODÉ PLOT OF THE ROTOR FILTERED SYNCHRONOUS VIBRATION RESPONSE WITH RUB DURING RUN-UP, AS SEEN BY THE INBOARD VERTICAL DISPLACEMENT PROBE. 3.34 LB. PRELOAD AT THE PLUNGER. UNBALANCE: 2.0 GRAMS, 180 DEGREES, RADIUS 1.2 INCHES AT THE INBOARD DISK.

BENTLY  
NEVADA  
CORP.

RUNUP

PLANT ID: BRDRC  
TRAIN ID: TEST  
MACHINE ID: ROTOR KIT  
SOLID DATA: Uncomp OUTB VERT

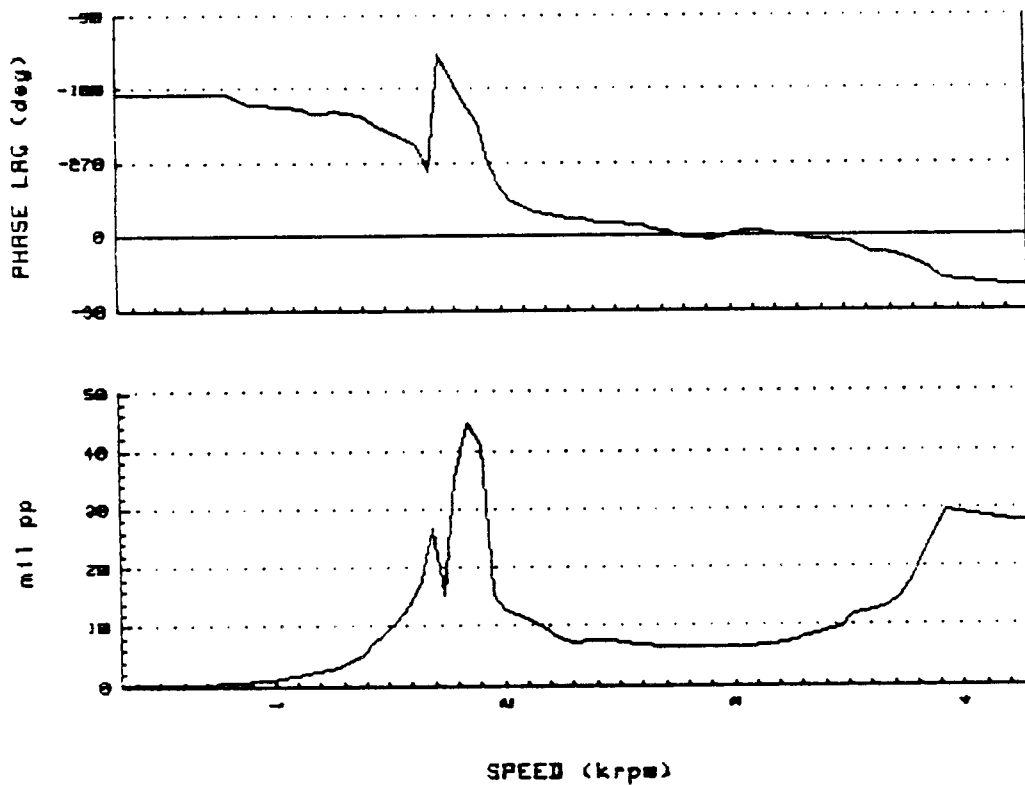


FIGURE 13.6 BODÉ PLOT OF THE ROTOR FILTERED SYNCHRONOUS VIBRATION RESPONSE WITH RUB DURING RUN-UP, AS SEEN BY THE OUTBOARD VERTICAL DISPLACEMENT PROBE. 3.34 LB. PLUNGER PRELOAD. UNBALANCE: 2.0 GRAMS, 180 DEGREES, RADIUS 1.2 INCHES AT THE INBOARD DISK.

BENTLY  
NEVADA  
CORP.

RUNUP

PLANT ID:  
TRAIN ID:  
MACHINE ID:  
PROBE ID:

BRDRC  
TEST  
ROTOR KIT  
INB VERT

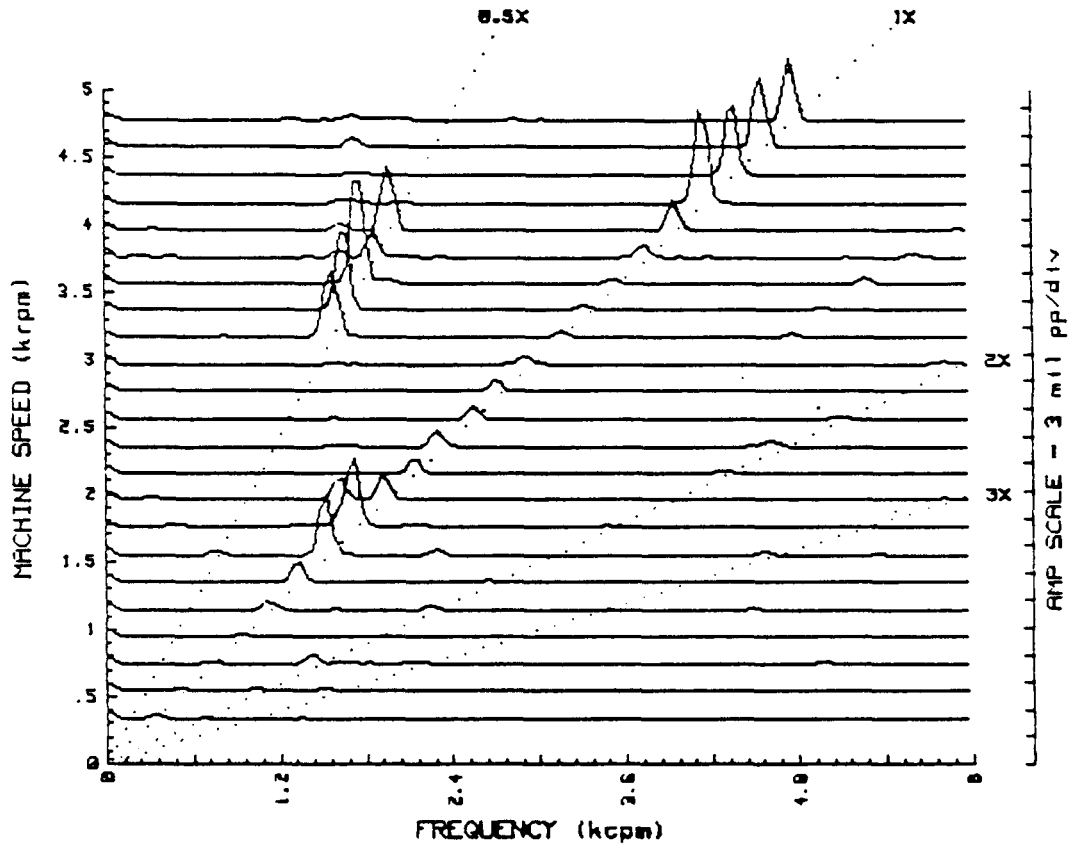


FIGURE 13.7 SPECTRUM CASCADE PLOT OF THE ROTOR VIBRATION RESPONSE WITH RUB DURING RUN-UP, AS SEEN BY THE INBOARD VERTICAL DISPLACEMENT PROBE. 3.34 LB. PLUNGER PRELOAD. UNBALANCE: 2.0 GRAMS, 180 DEGREES, RADIUS 1.2 INCHES AT THE INBOARD DISK.

BENTLY  
NEVADA  
CORP.

RUNUP

PLANT ID:  
TRAIN ID:  
MACHINE ID:  
PROBE ID:

BRDRC  
TEST  
ROTOR KIT  
OUTB VERT

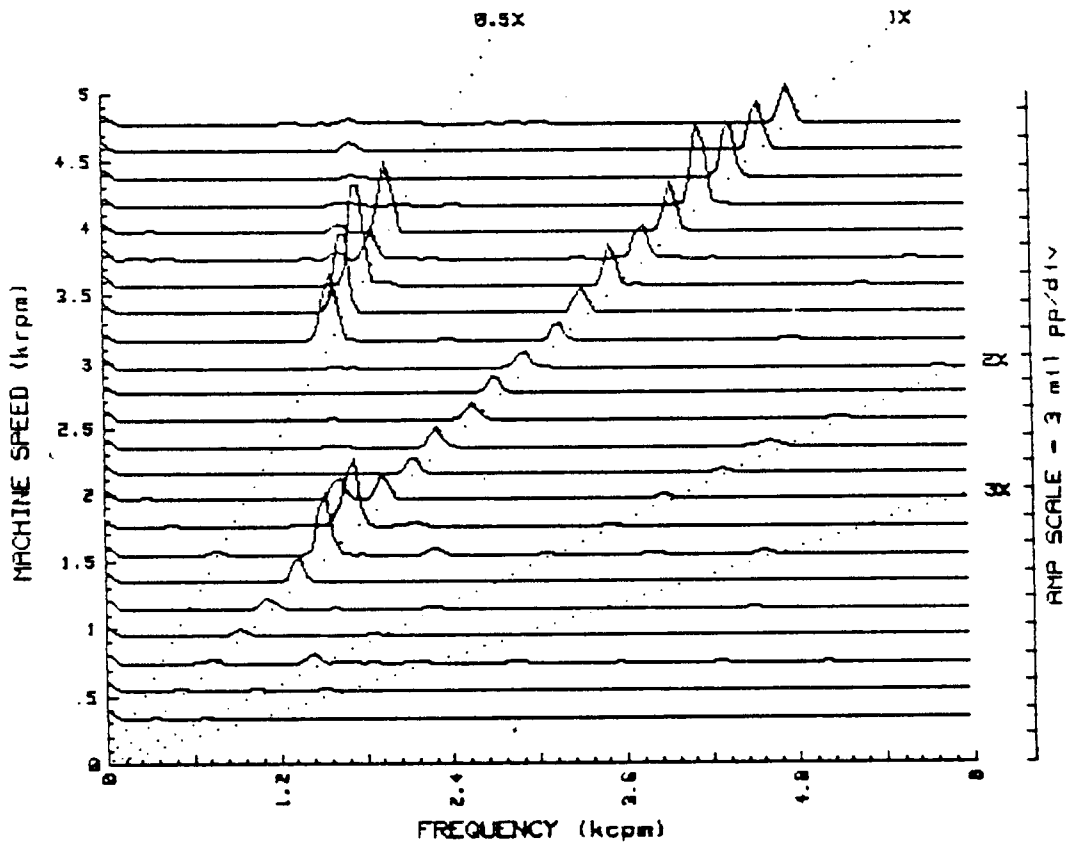


FIGURE 13.8

SPECTRUM CASCADE PLOT OF THE ROTOR VIBRATION RESPONSE WITH RUB DURING RUN-UP, AS SEEN BY THE OUTBOARD VERTICAL DISPLACEMENT PROBE. 3.34 LB. PLUNGER PRELOAD. UNBALANCE: 2.0 GRAMS, 180 DEGREES, RADIUS 1.2 INCHES AT THE INBOARD DISK.

SHAFT RPM $\omega$	RUB CONTACT TIME (mS) $t_r$	SHAFT REVOLUTIONS DURING RUB ( $\beta$ )
4307	4.54	.3263
4227	5.00	.3522
4116	5.71	.3920
4056	5.55	.3718
3950	4.54	.2990
3865	4.76	.3067
3780	6.89	.4340
3670	8.69	.5310
3621	4.76	.2800
3246	3.84	.2080
3150	3.07	.1600
3062	2.40	.1240
3016	2.40	.1220
2910	1.78	.0860
2845	2.63	.1247
2713	1.92	.0869
2645	2.50	.1100
2517	1.61	.0670
2464	3.90	.1600
2335	3.96	.1550
2269	3.96	.1500
2204	4.46	.1640
2155	4.46	.1640
2094	5.55	.1930
2021	5.55	.1870
1971	7.35	.2415
1931	8.33	.2680
1828	11.10	.3380
1778	4.80	.1420
1711	5.90	.1690
1645	5.95	.1630
1586	4.70	.1200
1508	5.20	.1300
1455	4.46	.1082
1405	4.46	.1040
1340	9.25	.2060
1301	4.46	.0968
1262	4.80	.1010

$$\beta = (\omega t_r / 60) 10^{-3}$$

FIGURE 13.9 TABULAR LISTINGS OF DATA USED TO GENERATE FIGURE 13.10. TABLE LISTS CONTACT TIME DURING RUB AND THE CORRESPONDING SHAFT ORBITING ARC DURING CONTACT FOR EACH GIVEN SHAFT SPEED.

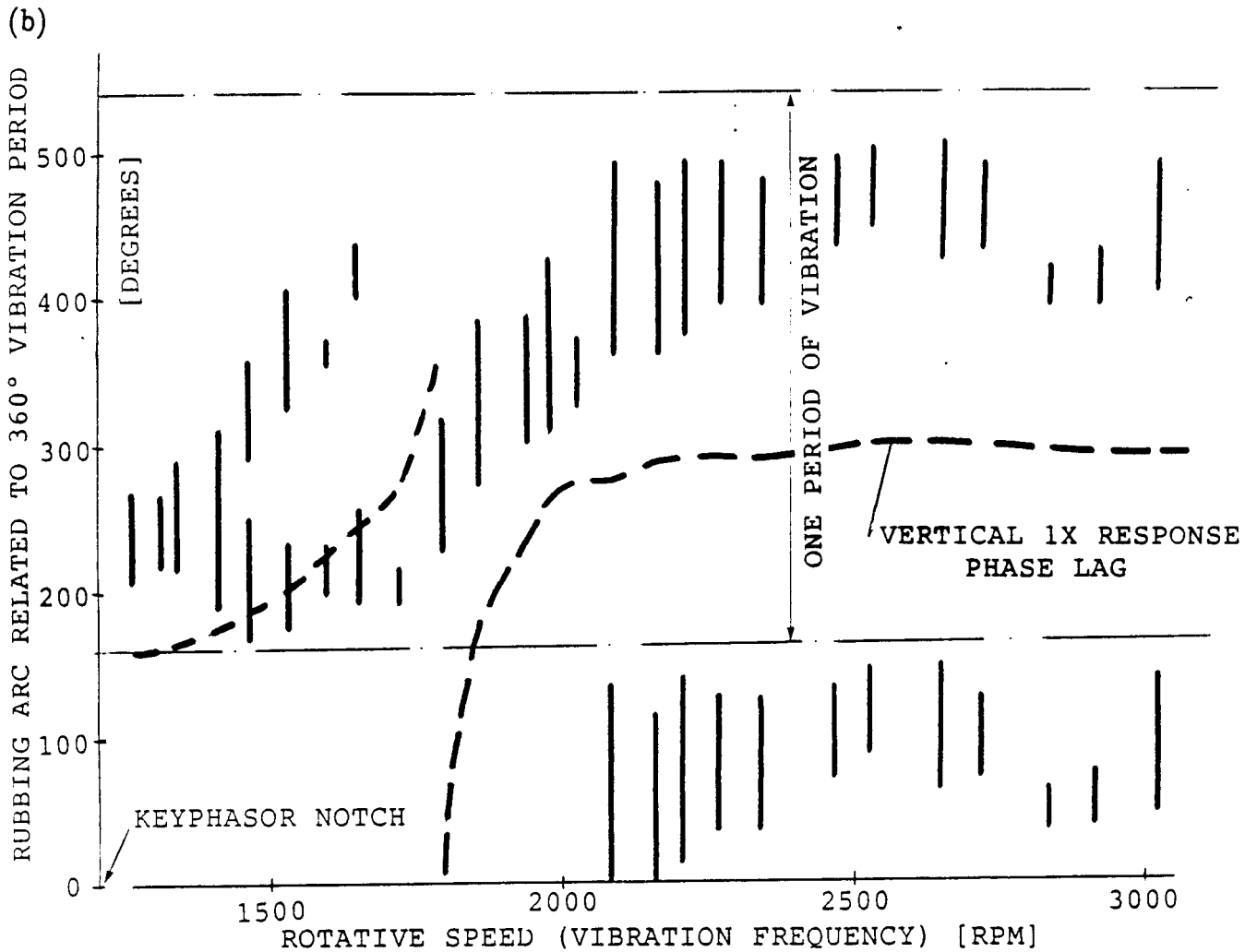
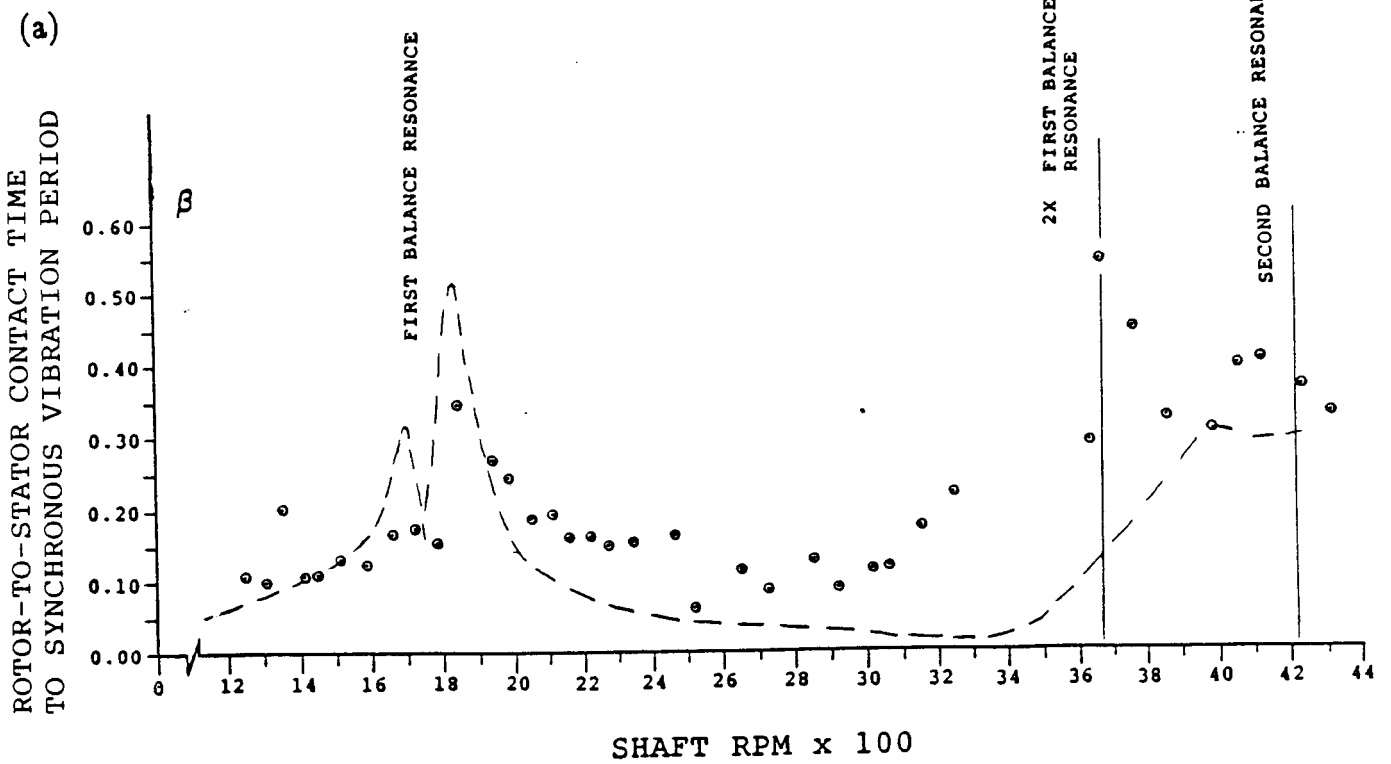


FIGURE 13.10 (a) ROTOR-TO-STATOR CONTACT IN TERMS OF THE AMOUNT OF ROTOR REVOLUTIONS VERSUS ROTATIVE SPEED; (b) ROTOR-TO-STATOR CONTACT ARC RELATED TO THE GENERALIZED 360 DEGREE PERIOD VERSUS ROTATIVE SPEED.



ORIGINAL PAGE IS  
OF POOR QUALITY

PROBE #1 ID: OUTBRD VERT DIS      ORIENTATION= 90 DEG  
1X FILTERED                            1X VECTOR= 7.10 MILS PK-PK @-142

PROBE #2 ID: OUTBRD HOR DISP      ORIENTATION= 0 DEG  
1X FILTERED                            1X VECTOR= 6.00 MILS PK-PK @-219

ROTATION: CW  
RPM(START)= 1259 RPM(END)= 1258

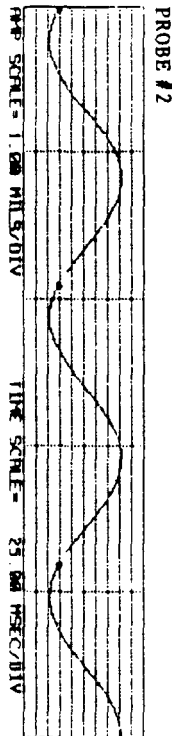
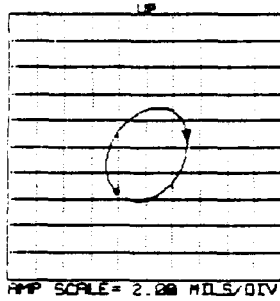


FIGURE 13.12 STEADY-STATE ORBIT AND TIMEBASE WAVE OF ROTOR VIBRATIONAL RESPONSE. 3.34 LB. PLUNGER PRELOAD. UNBALANCE: 2.0 GRAMS., 180 DEGREES, RADIUS 1.2 INCHES. FILTERED 1X RUB. ROTATIVE SPEED: 1258 RPM.



**ORIGINAL PAGE IS  
OF POOR QUALITY**

PROBE #1 ID: OUTBRD VERT DIS  
1X FILTERED

ORIENTATION- 90 DEG  
1X VECTOR- 7.80 MILS PK-PK @-144

PROBE #2 ID: OUTBRD HOR DISP  
1X FILTERED

ORIENTATION- 0 DEG  
1X VECTOR- 6.00 MILS PK-PK @-208

ROTATION: CW  
RPM(START)- 1299 RPM(END)- 1299

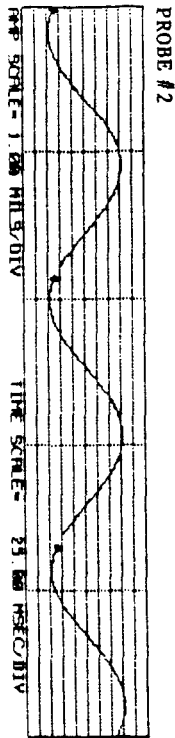
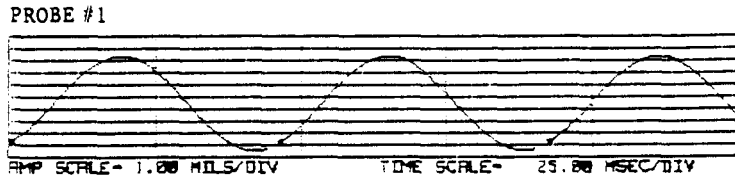
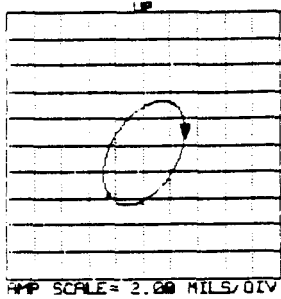


FIGURE 13.14 STEADY-STATE ORBIT AND TIMEBASE WAVE OF ROTOR VIBRATIONAL RESPONSE. 3.34 LB. PLUNGER PRELOAD. UNBALANCE: 2.0 GRAMS., 180 DEGREES, RADIUS 1.2 INCHES. FILTERED 1X RUB. ROTATIVE SPEED: 1299 RPM.



ORIGINAL PAGE IS  
OF POOR QUALITY

PROBE #1 ID: OUTBRD VERT DIS  
1X FILTERED

ORIENTATION= 90 DEG  
1X VECTOR= 10.80 MILS PK-PK @-148

PROBE #2 ID: OUTBRD HOR DISP  
1X FILTERED

ORIENTATION= 0 DEG  
1X VECTOR= 7.80 MILS PK-PK @-220

ROTATION: CW  
RPM(START)= 1340 RPM(END)= 1340

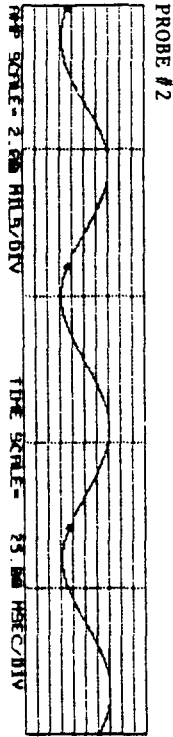
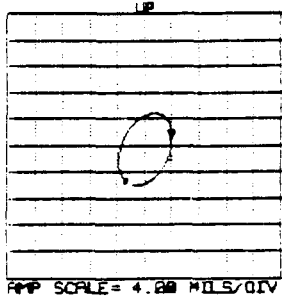


FIGURE 13.16 STEADY-STATE ORBIT AND TIMEBASE WAVE OF ROTOR VIBRATIONAL RESPONSE. 3.34 LB. PLUNGER PRELOAD. UNBALANCE: 2.0 GRAMS., 180 DEGREES, RADIUS 1.2 INCHES. FILTERED 1X RUB. ROTATIVE SPEED: 1340 RPM.

BENTLY  
NEVADA  
CORP.

PLANT ID: S.R.D.R.C  
TRAIN ID: NASA RUB RIG  
MACHINE ID: RUB ORBITS

ORIGINAL PAGE IS  
OF POOR QUALITY

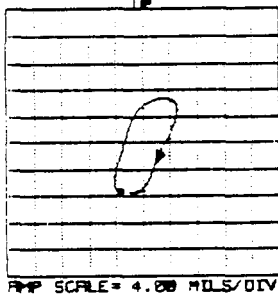
PROBE #1 ID: OUTBRD VERT DIS  
UNFILTERED

ORIENTATION= 90 DEG  
MAX AMP= 14.70 MILS PK-PK

PROBE #2 ID: OUTBRD HOR DISP  
UNFILTERED

ORIENTATION= 0 DEG  
MAX AMP= 9.40 MILS PK-PK

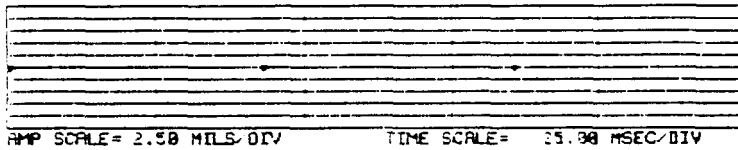
ROTATION: CW  
RPM(START)= 1406 RPM(END)= 1405



PROBE #1



PROBE #3



NO CONTACT



CONTACT

PROBE #4

PROBE #3 ID: RUB PLUNGER INBRD  
UNFILTERED

ORIENTATION= 0 DEG  
MAX AMP= 0.00 MILS PK-PK

PROBE #4 ID: ELEC CONTACT INBRD  
UNFILTERED

ORIENTATION= 0 DEG  
MAX AMP= 11.80 MILS PK-PK

ROTATION: CW  
RPM(START)= 1406 RPM(END)= 1405

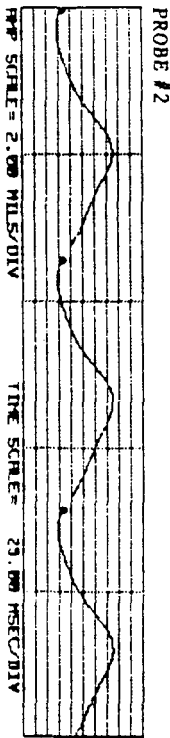


FIGURE 13.17 STEADY-STATE ORBIT AND TIMEBASE WAVE OF ROTOR VIBRATIONAL RESPONSE AND ASSOCIATED RUB PLUNGER MOTION. RUB CONTACT TIME: 4.46 ms. SHAFT REVOLUTIONS DURING RUB CONTACT = .1040 ROTATIONS. 3.34 LB. PLUNGER PRELOAD. UNBALANCE: 2.0 GRAMS., 180 DEGREES, RADIUS 1.2 INCHES. UNFILTERED 1x RUB. ROTATIVE SPEED: 1406 RPM.

ORIGINAL PAGE IS  
OF POOR QUALITY

PROBE #1 ID: OUTBRD VERT DIS  
1X FILTERED

ORIENTATION= 90 DEG  
1X VECTOR= 15.40 MILS PK-PK @-161

PROBE #2 ID: OUTBRD HOR DISP  
1X FILTERED

ORIENTATION= 0 DEG  
1X VECTOR= 9.90 MILS PK-PK @-212

ROTATION: CW  
RPM(START)= 1407 RPM(END)= 1406

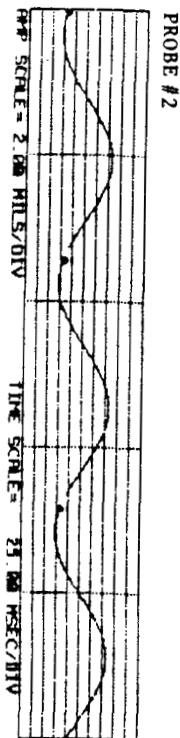
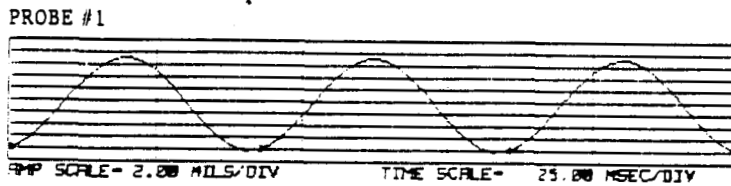
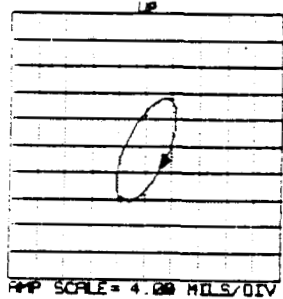


FIGURE 13.18 STEADY-STATE ORBIT AND TIMEBASE WAVE OF ROTOR VIBRATIONAL RESPONSE. 3.34 LB. PLUNGER PRELOAD. UNBALANCE: 2.0 GRAMS., 180 DEGREES, RADIUS 1.2 INCHES. FILTERED 1X RUB. ROTATIVE SPEED: 1406 RPM.



PROBE #1 ID: OUTBRD VERT DIS      ORIENTATION= 90 DEG  
 1X FILTERED                            1X VECTOR= 20.50 MILS PK-PK @-169  
  
 PROBE #2 ID: OUTBRD HOR DISP      ORIENTATION= 0 DEG  
 1X FILTERED                            1X VECTOR= 10.30 MILS PK-PK @-218  
  
 ROTATION: CW  
 RPM(START)= 1457 RPM(END)= 1457

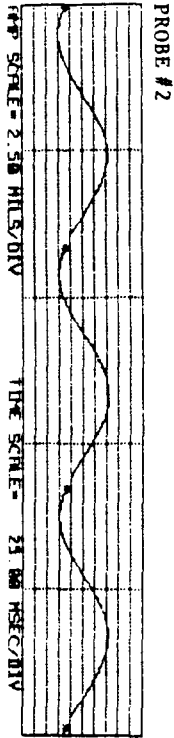
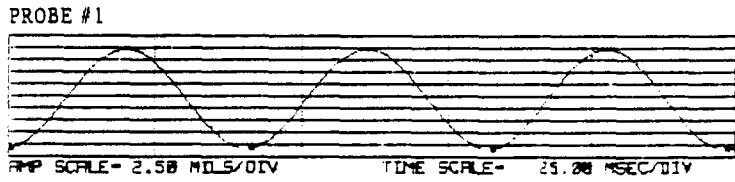
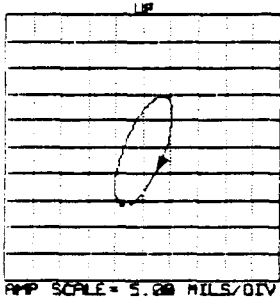
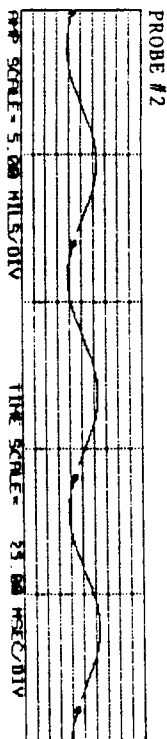
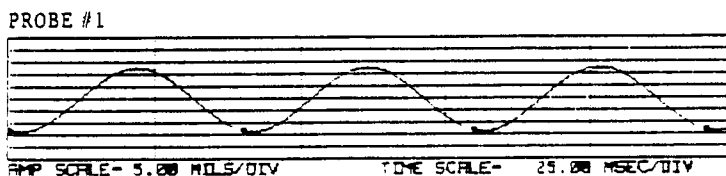
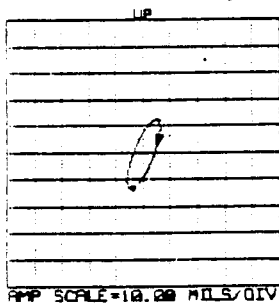


FIGURE 13.20    STEADY-STATE ORBIT AND TIMEBASE WAVE OF ROTOR  
 VIBRATIONAL RESPONSE. 3.34 LB. PLUNGER PRELOAD. UN-  
 BALANCE: 2.0 GRAMS., 180 DEGREES, RADIUS 1.2 INCHES.  
 FILTERED 1X RUB. ROTATIVE SPEED: 1457 RPM.



PROBE #1 ID: OUTBRD VERT DIS      ORIENTATION= 90 DEG  
 1X FILTERED                              1X VECTOR= 25.10 MILS PK-PK @-190  
  
 PROBE #2 ID: OUTBRD HOR DISP      ORIENTATION= 0 DEG  
 1X FILTERED                              1X VECTOR= 12.30 MILS PK-PK @-230  
  
 ROTATION: CW  
 RPM(START)= 1504 RPM(END)= 1505



ORIGINAL PAGE IS  
 OF POOR QUALITY

FIGURE 13.22 STEADY-STATE ORBIT AND TIMEBASE WAVE OF ROTOR VIBRATIONAL RESPONSE. 3.34 LB. PLUNGER PRELOAD. UNBALANCE: 2.0 GRAMS., 180 DEGREES, RADIUS 1.2 INCHES. FILTERED 1X RUB. ROTATIVE SPEED: 1505 RPM.

ORIGINAL PAGE IS  
OF POOR QUALITY

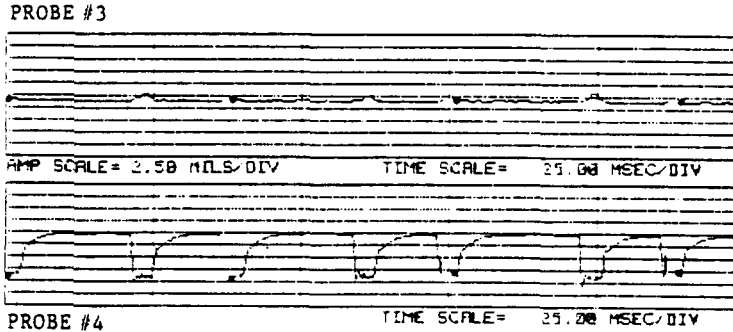
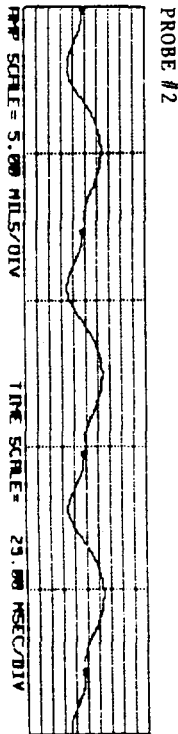
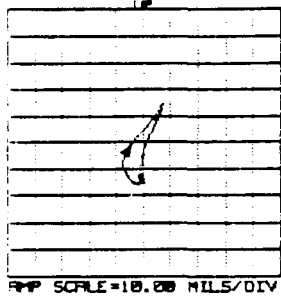
BENTLY  
NEVADA  
CORP.

PLANT ID: B.R.D.R.C  
TRAIN ID: NASA RUB RIG  
MACHINE ID: RUB ORBITS

PROBE #1 ID: OUTBRD VERT DIS UNFILTERED      ORIENTATION= 90 DEG  
MAX AMP= 30.40 MILS PK-PK

PROBE #2 ID: OUTBRD HOR DISP UNFILTERED      ORIENTATION= 0 DEG  
MAX AMP= 14.60 MILS PK-PK

ROTATION: CW  
RPM(START)= 1580 RPM(END)= 1579



PROBE #3 ID: RUB PLUNGER INBRD UNFILTERED      ORIENTATION= 0 DEG  
MAX AMP= 1.90 MILS PK-PK

PROBE #4 ID: ELEC CONTACT INBRD UNFILTERED      ORIENTATION= 0 DEG  
MAX AMP= 10.40 MILS PK-PK

ROTATION: CW  
RPM(START)= 1586 RPM(END)= 1585

FIGURE 13.23 STEADY-STATE ORBIT AND TIMEBASE WAVE OF ROTOR VIBRATIONAL RESPONSE AND ASSOCIATED RUB PLUNGER MOTION. RUB CONTACT TIME: 4.70 ms. SHAFT REVOLUTIONS DURING RUB CONTACT = .1200 ROTATIONS. 3.34 LB. PLUNGER PRELOAD. UNBALANCE: 2.0 GRAMS., 180 DEGREES, RADIUS 1.2 INCHES. UNFILTERED 1x RUB. ROTATIVE SPEED: 1579 RPM.

ORIGINAL PAGE IS  
OF POOR QUALITY

PROBE #1 ID: OUTBRD VERT DIS      ORIENTATION= 90 DEG  
1X FILTERED                              1X VECTOR= 29.20 MILS PK-PK @-212

PROBE #2 ID: OUTBRD HOR DISP      ORIENTATION= 0 DEG  
1X FILTERED                              1X VECTOR= 12.60 MILS PK-PK @-243

ROTATION: CW  
RPM(START)= 1580 RPM(END)= 1580

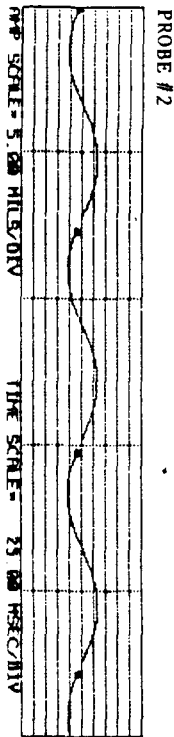
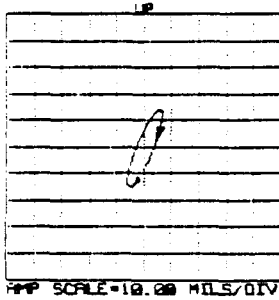


FIGURE 13.24 STEADY-STATE ORBIT AND TIMEBASE WAVE OF ROTOR VIBRATIONAL RESPONSE. 3.34 LB. PLUNGER PRELOAD. UNBALANCE: 2.0 GRAMS., 180 DEGREES, RADIUS 1.2 INCHES. FILTERED 1X RUB. ROTATIVE SPEED: 1580 RPM.

ORIGINAL PAGE IS  
OF POOR QUALITY

BENTLY  
NEVADA  
CORP.

PLANT ID: B.R.D.R.C  
TRAIN ID: NASA RUB RIG  
MACHINE ID: RUB ORBITS

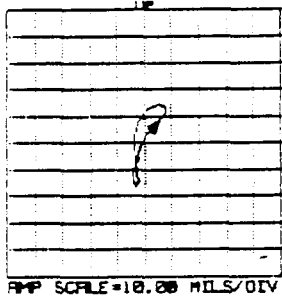
PROBE #1 ID: OUTBRD VERT DIS  
UNFILTERED

ORIENTATION= 90 DEG  
MAX AMP= 32.50 MILS PK-PK

PROBE #2 ID: OUTBRD HOR DISP  
UNFILTERED

ORIENTATION= 0 DEG  
MAX AMP= 15.80 MILS PK-PK

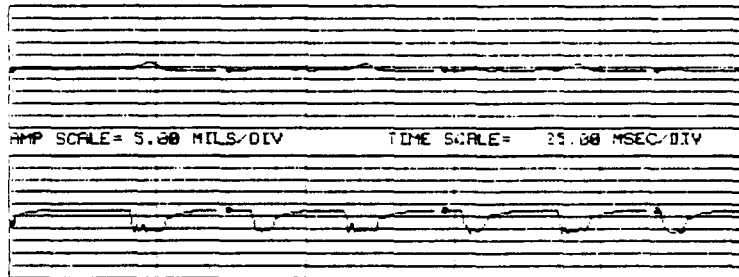
ROTATION: CW  
RPM(START)= 1644 RPM(END)= 1646



PROBE #1

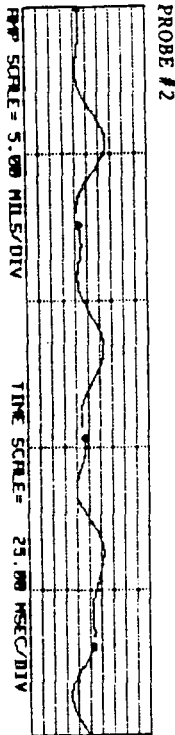


PROBE #3



PROBE #4

TIME SCALE = 25.00 MSEC/DIV



PROBE #3 ID: RUB PLUNGER INBRD  
UNFILTERED

ORIENTATION= 0 DEG  
MAX AMP= 3.30 MILS PK-PK

PROBE #4 ID: ELEC CONTACT INBRD  
UNFILTERED

ORIENTATION= 0 DEG  
MAX AMP= 9.30 MILS PK-PK

ROTATION: CW  
RPM(START)= 1645 RPM(END)= 1645

FIGURE 13.25

STEADY-STATE ORBIT AND TIMEBASE WAVE OF ROTOR VIBRATIONAL RESPONSE AND ASSOCIATED RUB PLUNGER MOTION. RUB CONTACT TIME: 5.95 ms. SHAFT REVOLUTIONS DURING RUB CONTACT = .1630 ROTATIONS. 3.34 LB. PLUNGER PRELOAD. UNBALANCE: 2.0 GRAMS., 180 DEGREES, RADIUS 1.2 INCHES. UNFILTERED 1x RUB. ROTATIVE SPEED: 1646 RPM.

ORIGINAL PAGE IS  
OF POOR QUALITY

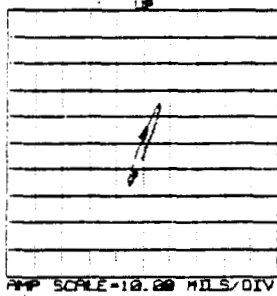
PROBE #1 ID: OUTBRD VERT DIS  
1X FILTERED

ORIENTATION- 90 DEG  
1X VECTOR- 31.40 MILS PK-PK 9-224

PROBE #2 ID: OUTBRD HOR DISP  
1X FILTERED

ORIENTATION- 0 DEG  
1X VECTOR- 11.90 MILS PK-PK 9-238

ROTATION: CW  
RPM(START)- 1645 RPM(END)- 1646



PROBE #1

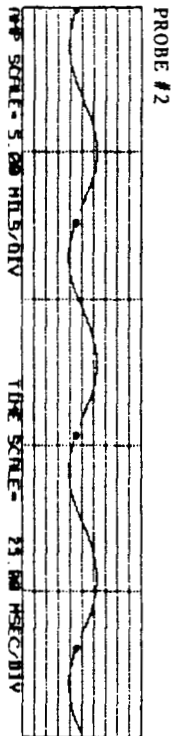


FIGURE 13.26 STEADY-STATE ORBIT AND TIMEBASE WAVE OF ROTOR VIBRATIONAL RESPONSE. 3.34 LB. PLUNGER PRELOAD. UNBALANCE: 2.0 GRAMS., 180 DEGREES, RADIUS 1.2 INCHES. FILTERED 1X RUB. ROTATIVE SPEED: 1646 RPM.

BENTLY  
NEVADA  
CORP.

PLANT ID: B.R.D.R.C  
TRAIN ID: NASA RUB RIG  
MACHINE ID: RUB ORBITS

ORIGINAL PAGE IS  
OF POOR QUALITY

PROBE #1 ID: OUTBRD VERT. DIS  
UNFILTERED

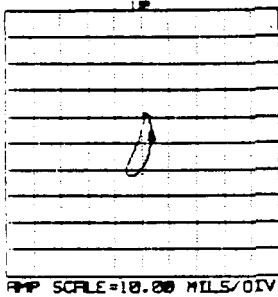
ORIENTATION= 90 DEG  
MAX AMP= 24.30 MILS PK-PK

PROBE #2 ID: OUTBRD HOR DISP  
UNFILTERED

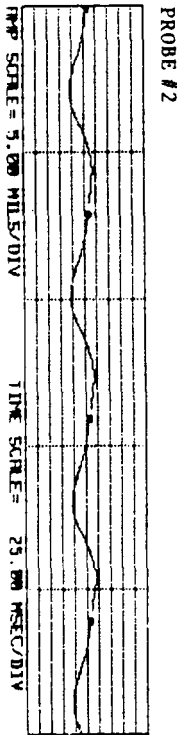
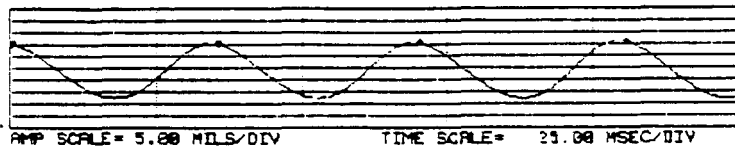
ORIENTATION= 0 DEG  
MAX AMP= 9.30 MILS PK-PK

ROTATION: CW

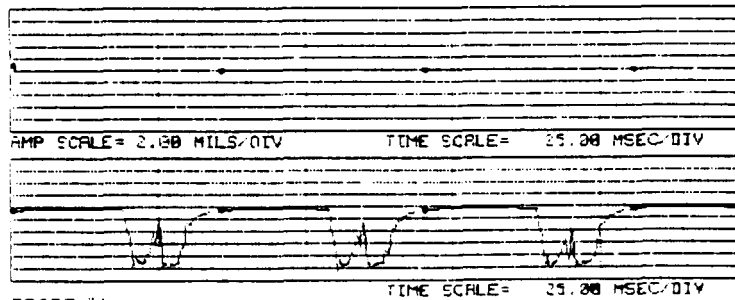
RPM(START)= 1713 RPM(END)= 1711



PROBE #1



PROBE #3



PROBE #4

PROBE #3 ID: RUB PLUNGER INBRD  
UNFILTERED

ORIENTATION= 0 DEG  
MAX AMP= 0.00 MILS PK-PK

PROBE #4 ID: ELEC CONTACT INBRD  
UNFILTERED

ORIENTATION= 0 DEG  
MAX AMP= 10.10 MILS PK-PK

ROTATION: CW

RPM(START)= 1712 RPM(END)= 1711

FIGURE 13.27 STEADY-STATE ORBIT AND TIMEBASE WAVE OF ROTOR VIBRATIONAL RESPONSE AND ASSOCIATED RUB PLUNGER MOTION. RUB CONTACT TIME: 5.90 ms. SHAFT REVOLUTIONS DURING RUB CONTACT = .1690 ROTATIONS. 3.34 LB. PLUNGER PRELOAD. UNBALANCE: 2.0 GRAMS., 180 DEGREES, RADIUS 1.2 INCHES. UNFILTERED 1x RUB. ROTATIVE SPEED: 1711 RPM.

ORIGINAL PAGE IS  
OF POOR QUALITY

PROBE #1 ID: OUTBRD VERT DIS  
1X FILTERED

ORIENTATION= 90 DEG  
1X VECTOR= 22.30 MILS PK-PK @-351

PROBE #2 ID: OUTBRD HOR DISP  
1X FILTERED

ORIENTATION= 0 DEG  
1X VECTOR= 8.60 MILS PK-PK @-308

ROTATION: CW  
RPM(START)= 1714 RPM(END)= 1715

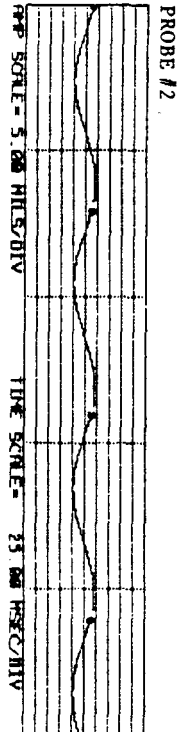
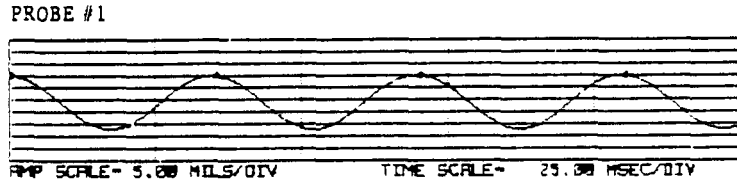
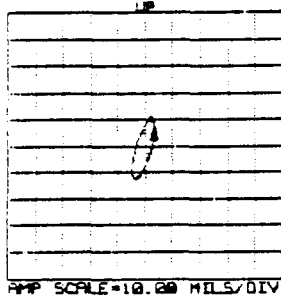


FIGURE 13.28 STEADY-STATE ORBIT AND TIMEBASE WAVE OF ROTOR VIBRATIONAL RESPONSE. 3.34 LB. PLUNGER PRELOAD. UNBALANCE: 2.0 GRAMS., 180 DEGREES, RADIUS 1.2 INCHES. FILTERED 1X RUB. ROTATIVE SPEED: 1715 RPM.



ORIGINAL PAGE IS  
OF POOR QUALITY

PROBE #1 ID: OUTBRD VERT DIS  
1X FILTERED

ORIENTATION= 90 DEG  
1X VECTOR= 15.10 MILS PK-PK @-4

PROBE #2 ID: OUTBRD HOR DISP  
1X FILTERED

ORIENTATION= 0 DEG  
1X VECTOR= 9.60 MILS PK-PK @-303

ROTATION: CW  
RPM(START)= 1778 RPM(END)= 1784

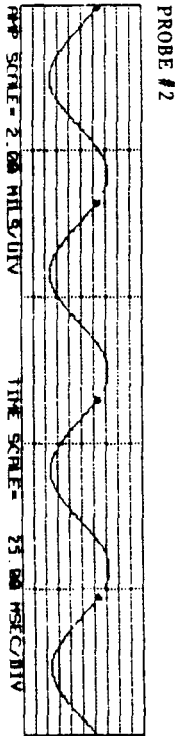
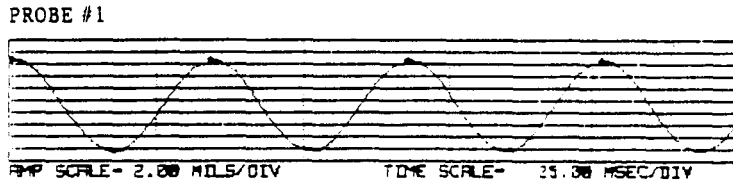
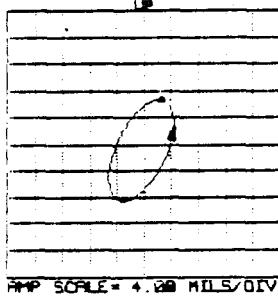


FIGURE 13.30 STEADY-STATE ORBIT AND TIMEBASE WAVE OF ROTOR VIBRATIONAL RESPONSE. 3.34 LB. PLUNGER PRELOAD. UNBALANCE: 2.0 GRAMS., 180 DEGREES, RADIUS 1.2 INCHES. FILTERED 1X RUB. ROTATIVE SPEED: 1784 RPM.

ORIGINAL PAGE IS  
OF POOR QUALITY

BENTLY  
NEVADA  
CORP.

PLANT ID: 3.R.D.R.C  
TRAIN ID: NASA RUB RIG  
MACHINE ID: RUB ORBITS

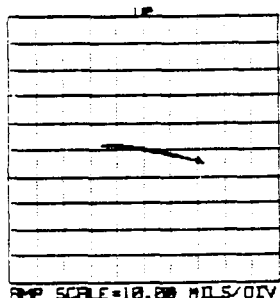
PROBE #1 ID: OUTBRD VERT 91S  
UNFILTERED

ORIENTATION= 90 DEG  
MAX AMP= 8.90 MILS PK-PK

PROBE #2 ID: OUTBRD HOR DISP  
UNFILTERED

ORIENTATION= 0 DEG  
MAX AMP= 37.90 MILS PK-PK

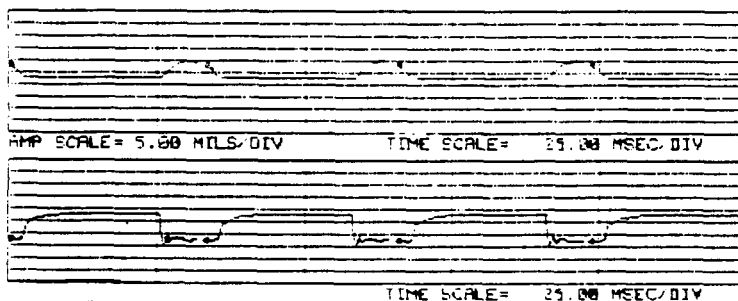
ROTATION: CW  
RPM(START)= 1833 RPM(END)= 1835



PROBE #1



PROBE #3



PROBE #4

PROBE #3 ID: RUB PLUNGER INBRD  
UNFILTERED

ORIENTATION= 0 DEG  
MAX AMP= 7.70 MILS PK-PK

PROBE #4 ID: ELEC CONTACT INBRD  
UNFILTERED

ORIENTATION= 0 DEG  
MAX AMP= 12.80 MILS PK-PK

ROTATION: CW  
RPM(START)= 1829 RPM(END)= 1829

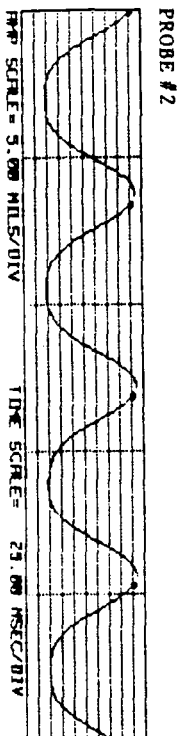


FIGURE 13.31 STEADY-STATE ORBIT AND TIMEBASE WAVE OF ROTOR VIBRATIONAL RESPONSE AND ASSOCIATED RUB PLUNGER MOTION. RUB CONTACT TIME: 11.10 ms. SHAFT REVOLUTIONS DURING RUB CONTACT = .3380 ROTATIONS. 3.34 LB. PLUNGER PRELOAD. UNBALANCE: 2.0 GRAMS., 180 DEGREES, RADIUS 1.2 INCHES. UNFILTERED 1x RUB. ROTATIVE SPEED: 1835 RPM.

ORIGINAL PAGE IS  
OF POOR QUALITY

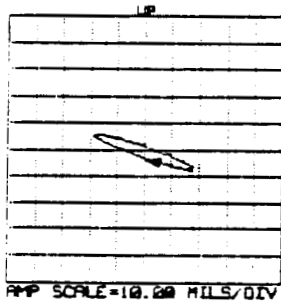
PROBE #1 ID: OUTBRD VERT DIS  
1X FILTERED

ORIENTATION= 90 DEG  
1X VECTOR= 13.00 MILS PK-PK @-175

PROBE #2 ID: OUTBRD HOR DISP  
1X FILTERED

ORIENTATION= 0 DEG  
1X VECTOR= 36.40 MILS PK-PK @-337

ROTATION: CW  
RPM(START)= 1834 RPM(END)= 1834



PROBE #1

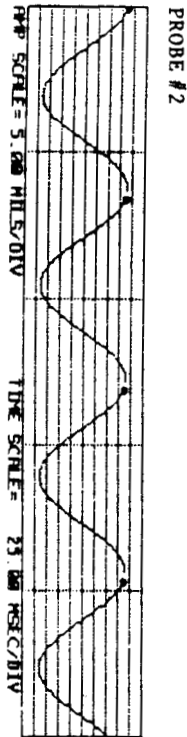
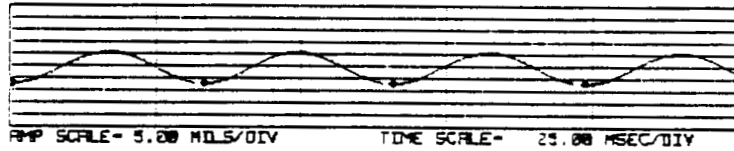


FIGURE 13.32 STEADY-STATE ORBIT AND TIMEBASE WAVE OF ROTOR VIBRATIONAL RESPONSE. 3.34 LB. PLUNGER PRELOAD. UNBALANCE: 2.0 GRAMS., 180 DEGREES, RADIUS 1.2 INCHES. FILTERED 1X RUB. ROTATIVE SPEED: 1834 RPM.

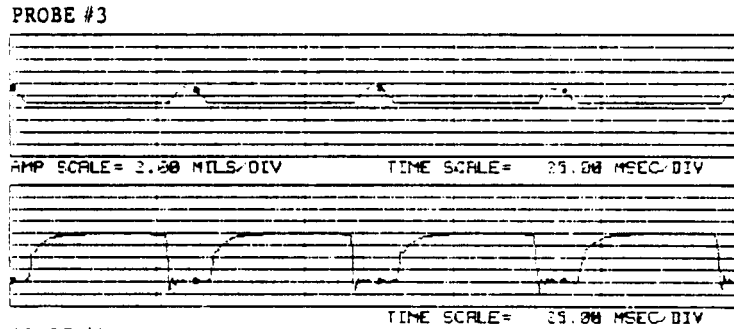
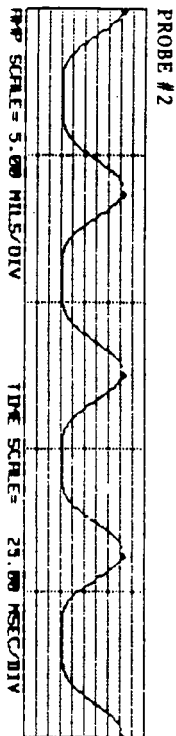
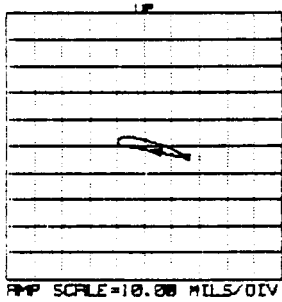
BENTLY  
NEVADA  
CORP.

PLANT ID: B.R.D.R.C  
TRAIN ID: NASA RUB RIG  
MACHINE ID: RUB ORBITS

PROBE #1 ID: OUTBRD VERT DIS UNFILTERED      ORIENTATION= 90 DEG  
MAX AMP= 10.10 MILS PK-PK

PROBE #2 ID: OUTBRD HOR DISP UNFILTERED      ORIENTATION= 0 DEG  
MAX AMP= 25.50 MILS PK-PK

ROTATION: CW  
RPM(START)= 1929 RPM(END)= 1929



NO CONTACT  
CONTACT

PROBE #3 ID: RUB PLUNGER INBRD UNFILTERED      ORIENTATION= 0 DEG  
MAX AMP= 2.80 MILS PK-PK

PROBE #4 ID: ELEC CONTACT INBRD UNFILTERED      ORIENTATION= 0 DEG  
MAX AMP= 9.70 MILS PK-PK

ROTATION: CW  
RPM(START)= 1930 RPM(END)= 1931

FIGURE 13.33 STEADY-STATE ORBIT AND TIMEBASE WAVE OF ROTOR VIBRATIONAL RESPONSE AND ASSOCIATED RUB PLUNGER MOTION. RUB CONTACT TIME: 8.33 ms. SHAFT REVOLUTIONS DURING RUB CONTACT = .2680 ROTATIONS. 3.34 LB. PLUNGER PRELOAD. UNBALANCE: 2.0 GRAMS., 180 DEGREES, RADIUS 1.2 INCHES. UNFILTERED 1x RUB. ROTATIVE SPEED: 1929 RPM.

ORIGINAL PAGE IS  
OF POOR QUALITY

PROBE #1 ID: OUTBRD VERT DIS      ORIENTATION= 90 DEG  
1X FILTERED                              1X VECTOR= 6.50 MILS PK-PK @-236

PROBE #2 ID: OUTBRD HOR DISP      ORIENTATION= 0 DEG  
1X FILTERED                              1X VECTOR= 24.90 MILS PK-PK @-348

ROTATION: CW  
RPM(START)= 1928 RPM(END)= 1930

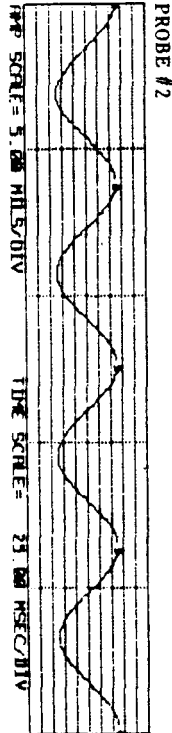
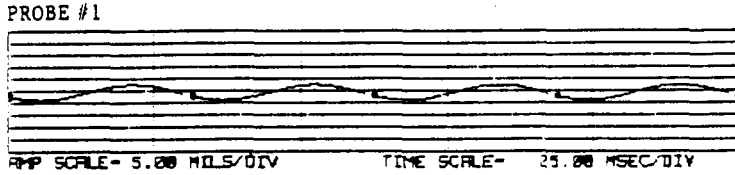
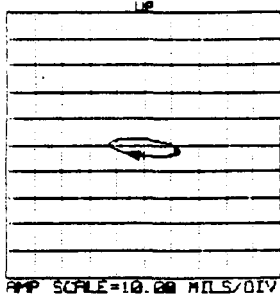


FIGURE 13.34 STEADY-STATE ORBIT AND TIMEBASE WAVE OF ROTOR VIBRATIONAL RESPONSE. 3.34 LB. PLUNGER PRELOAD. UNBALANCE: 2.0 GRAMS., 180 DEGREES, RADIUS 1.2 INCHES. FILTERED 1X RUB. ROTATIVE SPEED: 1930 RPM.



ORIGINAL PAGE IS  
OF POOR QUALITY

PROBE #1 ID: OUTBRD VERT DIS  
1X FILTERED

ORIENTATION= 90 DEG  
1X VECTOR= 7.40 MILS PK-PK @-266

PROBE #2 ID: OUTBRD HOR DISP  
1X FILTERED

ORIENTATION= 0 DEG  
1X VECTOR= 19.50 MILS PK-PK @-356

ROTATION: CW  
RPM(START)= 1970 RPM(END)= 1971

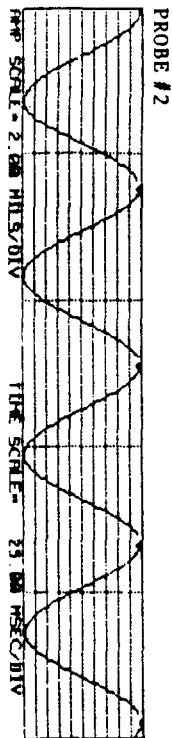
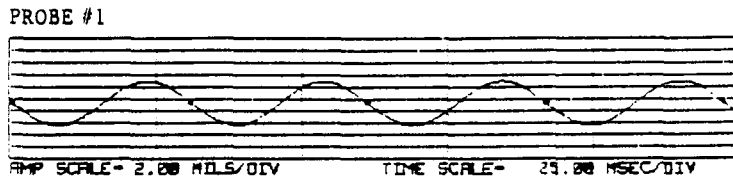
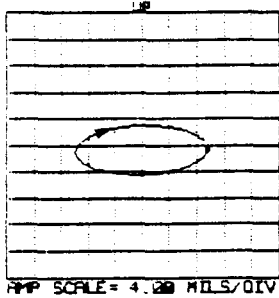


FIGURE 13.36 STEADY-STATE ORBIT AND TIMEBASE WAVE OF ROTOR VIBRATIONAL RESPONSE. 3.34 LB. PLUNGER PRELOAD. UNBALANCE: 2.0 GRAMS., 180 DEGREES, RADIUS 1.2 INCHES. FILTERED 1X RUB. ROTATIVE SPEED: 1971 RPM.

ORIGINAL PAGE IS  
OF POOR QUALITY

BENTLY  
NEVADA  
CORP.

PLANT ID: B.R.D.R.C  
TRAIN ID: NASA RUB RIG  
MACHINE ID: RUB ORBITS

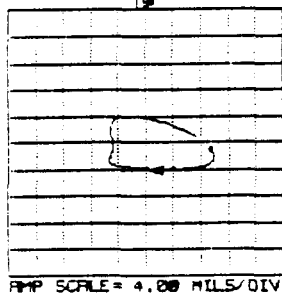
PROBE #1 ID: OUTBRD VERT DIS  
UNFILTERED

ORIENTATION= 90 DEG  
MAX AMP= 8.20 MILS PK-PK

PROBE #2 ID: OUTBRD HOR DISP  
UNFILTERED

ORIENTATION= 0 DEG  
MAX AMP= 15.90 MILS PK-PK

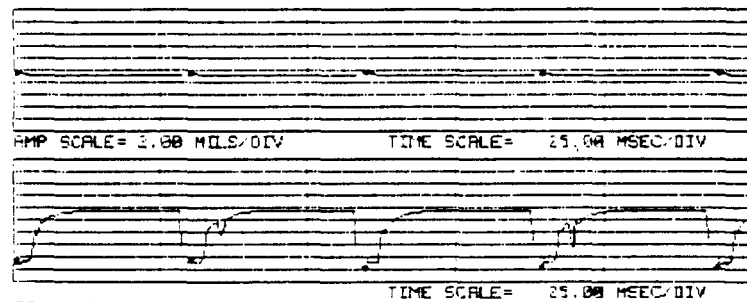
ROTATION: CW  
RPM(START)= 2017 RPM(END)= 2019



PROBE #1



PROBE #3



PROBE #4

PROBE #3 ID: RUB PLUNGER INBRD  
UNFILTERED

ORIENTATION= 0 DEG  
MAX AMP= .50 MILS PK-PK

PROBE #4 ID: ELEC CONTACT INBRD  
UNFILTERED

ORIENTATION= 0 DEG  
MAX AMP= 9.90 MILS PK-PK

ROTATION: CW  
RPM(START)= 2022 RPM(END)= 2024

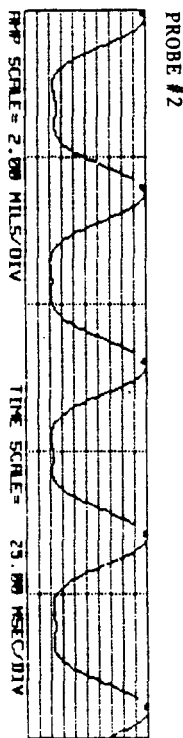


FIGURE 13.37 STEADY-STATE ORBIT AND TIMEBASE WAVE OF ROTOR VIBRATIONAL RESPONSE AND ASSOCIATED RUB PLUNGER MOTION. RUB CONTACT TIME: 5.55 ms. SHAFT REVOLUTIONS DURING RUB CONTACT = .1870 ROTATIONS. 3.34 LB. PLUNGER PRELOAD. UNBALANCE: 2.0 GRAMS., 180 DEGREES, RADIUS 1.2 INCHES. UNFILTERED 1x RUB. ROTATIVE SPEED: 2019 RPM.

PROBE #1 ID: OUTBRD VERT DIS      ORIENTATION= 90 DEG  
                   1X FILTERED                    1X VECTOR= 9.10 MILS PK-PK 3-274  
  
 PROBE #2 ID: OUTBRD HOR DISP      ORIENTATION= 0 DEG  
                   1X FILTERED                    1X VECTOR= 15.60 MILS PK-PK 3-8  
  
 ROTATION: CW  
 RPM(START)= 2019 RPM(END)= 2020

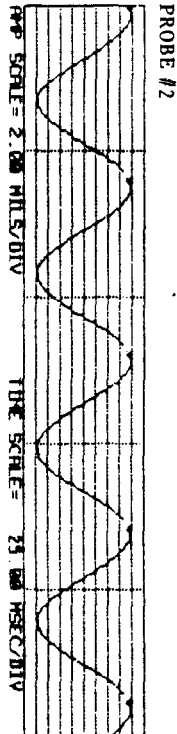
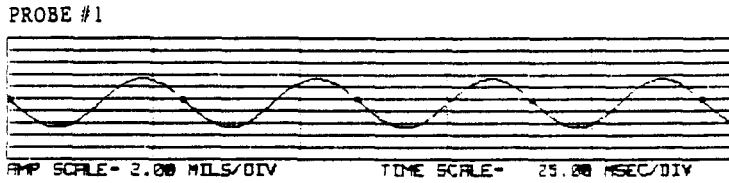
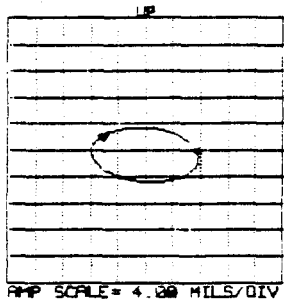


FIGURE 13.38 STEADY-STATE ORBIT AND TIMEBASE WAVE OF ROTOR VIBRATIONAL RESPONSE. 3.34 LB. PLUNGER PRELOAD. UNBALANCE: 2.0 GRAMS., 180 DEGREES, RADIUS 1.2 INCHES. FILTERED 1X RUB. ROTATIVE SPEED: 2020 RPM.



ORIGINAL PAGE IS  
OF POOR QUALITY

PROBE #1 ID: OUTBRD VERT DIS  
1X FILTERED

ORIENTATION= 90 DEG  
1X VECTOR= 9.20 MILS PK-PK @-271

PROBE #2 ID: OUTBRD HOR DISP  
1X FILTERED

ORIENTATION= 0 DEG  
1X VECTOR= 11.70 MILS PK-PK @-21

ROTATION: CW  
RPM(START)= 2084 RPM(END)= 2085

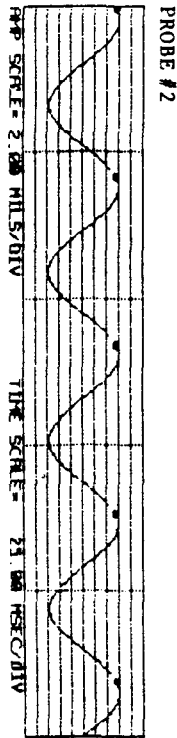
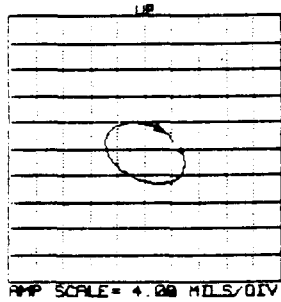


FIGURE 13.40 STEADY-STATE ORBIT AND TIMEBASE WAVE OF ROTOR VIBRATIONAL RESPONSE. 3.34 LB. PLUNGER PRELOAD. UNBALANCE: 2.0 GRAMS., 180 DEGREES, RADIUS 1.2 INCHES. FILTERED 1X RUB. ROTATIVE SPEED: 2085 RPM.



ORIGINAL PAGE IS  
OF POOR QUALITY

PROBE #1 ID: OUTBRD VERT DIS      ORIENTATION= 90 DEG  
1X FILTERED                              X VECTOR= 8.40 MILS PK-PK @-293

PROBE #2 ID: OUTBRD HOR DISP      ORIENTATION= 0 DEG  
1X FILTERED                              X VECTOR= 8.50 MILS PK-PK @-25

ROTATION: CW  
RPM(START)= 2158 RPM(END)= 2159

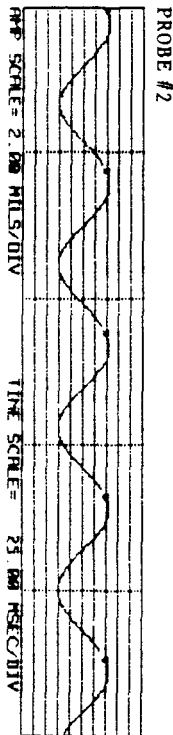
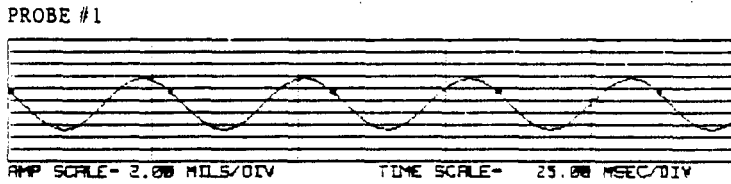
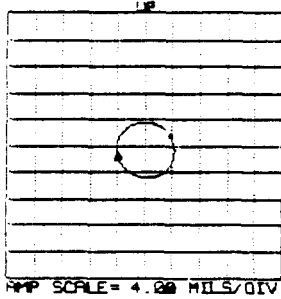


FIGURE 13.42 STEADY-STATE ORBIT AND TIMEBASE WAVE OF ROTOR VIBRATIONAL RESPONSE. 3.34 LB. PLUNGER PRELOAD. UNBALANCE: 2.0 GRAMS., 180 DEGREES, RADIUS 1.2 INCHES. FILTERED 1X RUB. ROTATIVE SPEED: 2159 RPM.

ORIGINAL PAGE IS  
OF POOR QUALITY.

BENTLY  
NEVADA  
CORP.

PLANT ID: 3.R.D.R.C  
TRAIN ID: NASA RUB RIG  
MACHINE ID: RUB ORBITS

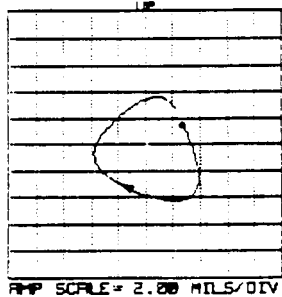
PROBE #1 ID: OUTBRD VERT DIS  
UNFILTERED

ORIENTATION= 90 DEG  
MAX AMP= 8.70 MILS PK-PK

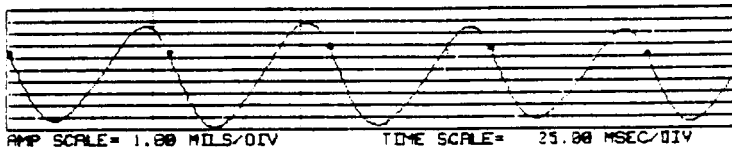
PROBE #2 ID: OUTBRD HOR DISP  
UNFILTERED

ORIENTATION= 0 DEG  
MAX AMP= 8.80 MILS PK-PK

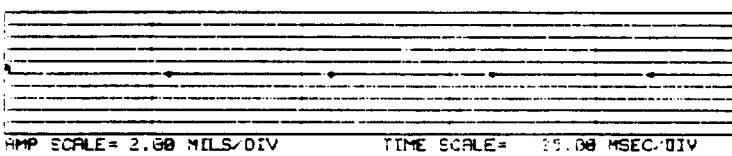
ROTATION: CW  
RPM(START)= 2198 RPM(END)= 2197



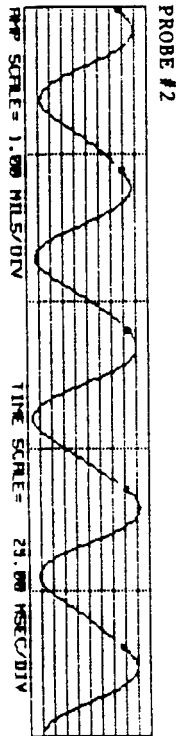
PROBE #1



PROBE #3



PROBE #4



PROBE #3 ID: RUB PLUNGER INBRD  
UNFILTERED

ORIENTATION= 0 DEG  
MAX AMP= 0.00 MILS PK-PK

PROBE #4 ID: ELEC CONTACT INBRD  
UNFILTERED

ORIENTATION= 0 DEG  
MAX AMP= 9.50 MILS PK-PK

ROTATION: CW  
RPM(START)= 2204 RPM(END)= 2206

FIGURE 13.43 STEADY-STATE ORBIT AND TIMEBASE WAVE OF ROTOR VIBRATIONAL RESPONSE AND ASSOCIATED RUB PLUNGER MOTION. RUB CONTACT TIME: 4.46 ms. SHAFT REVOLUTIONS DURING RUB CONTACT = .1640 ROTATIONS. 3.34 LB. PLUNGER PRELOAD. UNBALANCE: 2.0 GRAMS., 180 DEGREES, RADIUS 1.2 INCHES. UNFILTERED 1x RUB. ROTATIVE SPEED: 2197 RPM.

ORIGINAL PAGE IS  
OF POOR QUALITY

PROBE #1 ID: OUTBRD VERT DIS      ORIENTATION= 90 DEG  
1X FILTERED                              1X VECTOR= 8.10 MILS PK-PK @-294

PROBE #2 ID: OUTBRD HOR DISP      ORIENTATION= 0 DEG  
1X FILTERED                              1X VECTOR= 8.00 MILS PK-PK @-25

ROTATION: CW  
RPM(START)= 2201 RPM(END)= 2201

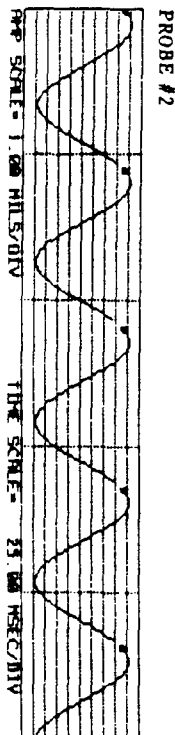
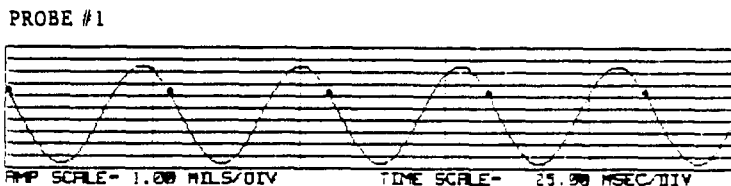
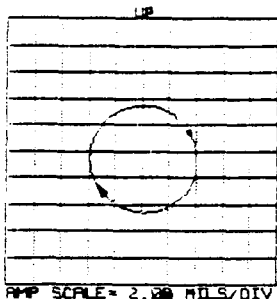


FIGURE 13.44 STEADY-STATE ORBIT AND TIMEBASE WAVE OF ROTOR VIBRATIONAL RESPONSE. 3.34 LB. PLUNGER PRELOAD. UNBALANCE: 2.0 GRAMS., 180 DEGREES, RADIUS 1.2 INCHES. FILTERED 1X RUB. ROTATIVE SPEED: 2201 RPM.

ORIGINAL PAGE IS  
OF POOR QUALITY

BENTLY  
NEVADA  
CORP.

PLANT ID: B.R.D.R.C  
TRAIN ID: NASA RUB RIG  
MACHINE ID: RUB ORBITS

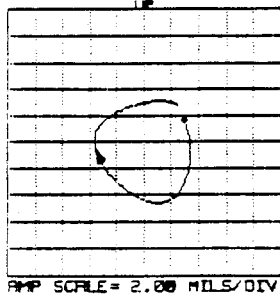
PROBE #1 ID: OUTBRD VERT DIS  
UNFILTERED

ORIENTATION= 90 DEG  
MAX AMP= 8.00 MILS PK-PK

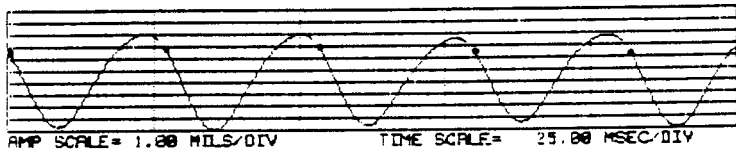
PROBE #2 ID: OUTBRD HOR DISP  
UNFILTERED

ORIENTATION= 0 DEG  
MAX AMP= 7.60 MILS PK-PK

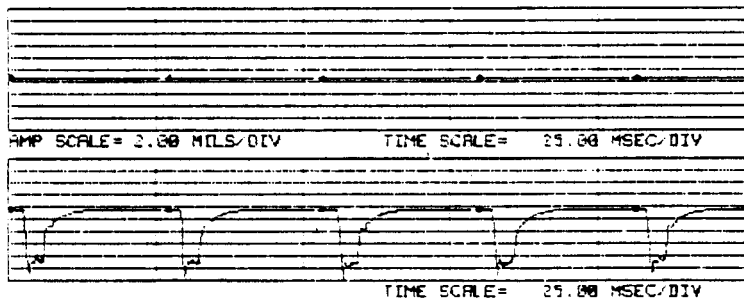
ROTATION: CW  
RPM(START)= 2262 RPM(END)= 2261



PROBE #1



PROBE #3



PROBE #4

PROBE #3 ID: RUB PLUNGER INBRD  
UNFILTERED

ORIENTATION= 0 DEG  
MAX AMP= .10 MILS PK-PK

PROBE #4 ID: ELEC CONTACT INBRD  
UNFILTERED

ORIENTATION= 0 DEG  
MAX AMP= 11.10 MILS PK-PK

ROTATION: CW  
RPM(START)= 2270 RPM(END)= 2269

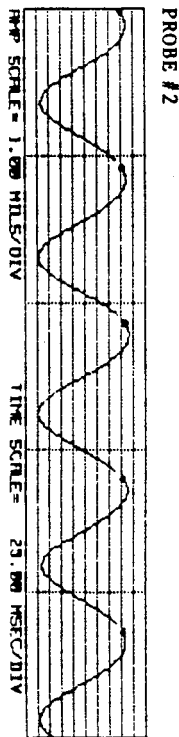


FIGURE 13.45 STEADY-STATE ORBIT AND TIMEBASE WAVE OF ROTOR VIBRATIONAL RESPONSE AND ASSOCIATED RUB PLUNGER MOTION. RUB CONTACT TIME: 3.96 ms. SHAFT REVOLUTIONS DURING RUB CONTACT = .1500 ROTATIONS. 3.34 LB. PLUNGER PRELOAD. UNBALANCE: 2.0 GRAMS., 180 DEGREES, RADIUS 1.2 INCHES. UNFILTERED 1x RUB. ROTATIVE SPEED: 2261 RPM.



BENTLY  
NEVADA  
CORP.

PLANT ID: B.R.D.R.C  
TRAIN ID: NASA RUB RIG  
MACHINE ID: RUB ORBITS

ORIGINAL PAGE IS  
OF POOR QUALITY

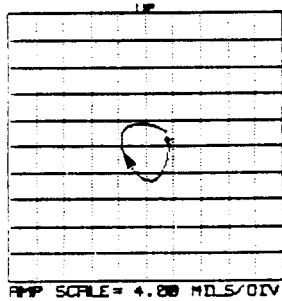
PROBE #1 ID: OUTBRD VERT DIS  
UNFILTERED

ORIENTATION= 90 DEG  
MAX AMP= 8.70 MILS PK-PK

PROBE #2 ID: OUTBRD HOR DISP  
UNFILTERED

ORIENTATION= 0 DEG  
MAX AMP= 8.10 MILS PK-PK

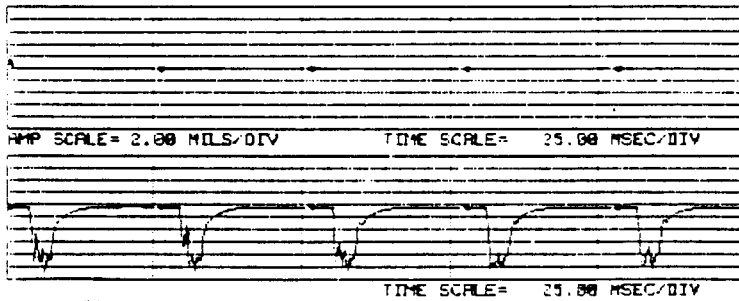
ROTATION: CW  
RPM(START)= 2331 RPM(END)= 2331



PROBE #1



PROBE #3



PROBE #4

PROBE #3 ID: RUB PLUNGER INBRD UNFILTERED  
ORIENTATION= 0 DEG  
MAX AMP= 0.00 MILS PK-PK

PROBE #4 ID: ELEC CONTACT INBRD UNFILTERED  
ORIENTATION= 0 DEG  
MAX AMP= 10.40 MILS PK-PK

ROTATION: CW  
RPM(START)= 2335 RPM(END)= 2335

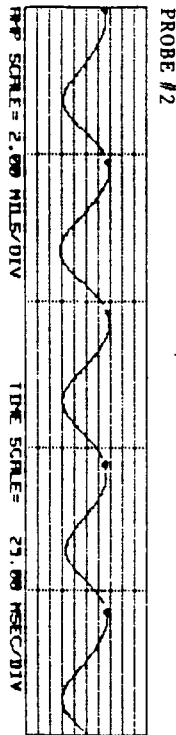


FIGURE 13.47 STEADY-STATE ORBIT AND TIMEBASE WAVE OF ROTOR VIBRATIONAL RESPONSE AND ASSOCIATED RUB PLUNGER MOTION. RUB CONTACT TIME: 3.96 ms. SHAFT REVOLUTIONS DURING RUB CONTACT = .1550 ROTATIONS. 3.34 LB. PLUNGER PRELOAD. UNBALANCE: 2.0 GRAMS., 180 DEGREES, RADIUS 1.2 INCHES. UNFILTERED 1x RUB. ROTATIVE SPEED: 2331 RPM.

ORIGINAL PAGE IS  
OF POOR QUALITY

PROBE #1 ID: OUTBRD VERT DIS      ORIENTATION= 90 DEG  
1X FILTERED                              1X VECTOR= 7.90 MILS PK-PK @-291

PROBE #2 ID: OUTBRD HOR DISP      ORIENTATION= 0 DEG  
1X FILTERED                              1X VECTOR= 7.30 MILS PK-PK @-26

ROTATION: CW  
RPM(START)= 2330 RPM(END)= 2331

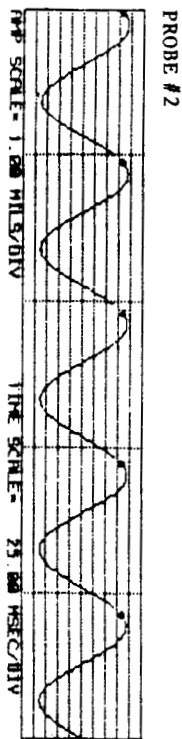
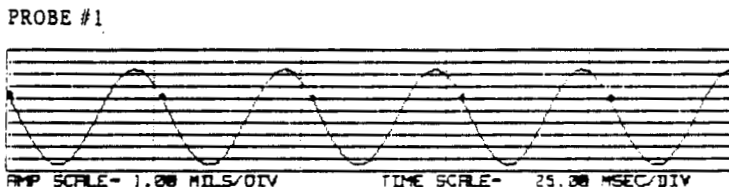
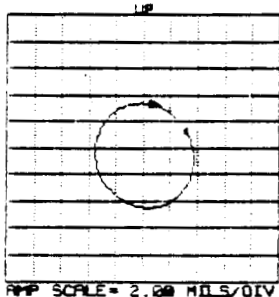


FIGURE 13.48 STEADY-STATE ORBIT AND TIMEBASE WAVE OF ROTOR VIBRATIONAL RESPONSE. 3.34 LB. PLUNGER PRELOAD. UNBALANCE: 2.0 GRAMS., 180 DEGREES, RADIUS 1.2 INCHES. FILTERED 1X RUB. ROTATIVE SPEED: 2331 RPM.

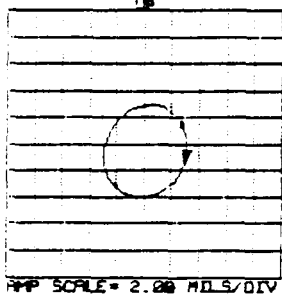


ORIGINAL PAGE IS  
OF POOR QUALITY

PROBE #1 ID: OUTBRD VERT DIS      ORIENTATION= 90 DEG  
1X FILTERED                              1X VECTOR= 7.00 MILS PK-PK @-299

PROBE #2 ID: OUTBRD HOR DISP      ORIENTATION= 0 DEG  
1X FILTERED                              1X VECTOR= 6.10 MILS PK-PK @-23

ROTATION: CW  
RPM(START)= 2462 RPM(END)= 2462



PROBE #1

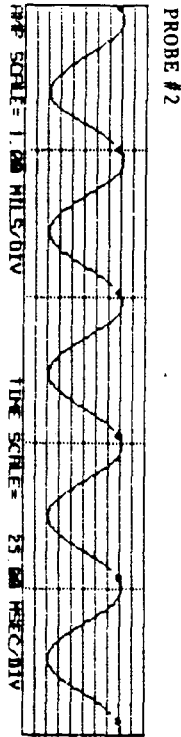
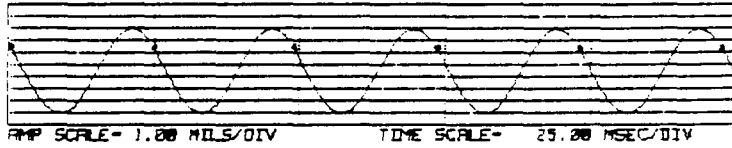


FIGURE 13.50      STEADY-STATE ORBIT AND TIMEBASE WAVE OF ROTOR VIBRATIONAL RESPONSE. 3.34 LB. PLUNGER PRELOAD. UNBALANCE: 2.0 GRAMS., 180 DEGREES, RADIUS 1.2 INCHES. FILTERED 1X RUB. ROTATIVE SPEED: 2462 RPM.



PROBE #1 ID: OUTBRD VERT DIS  
1X FILTERED

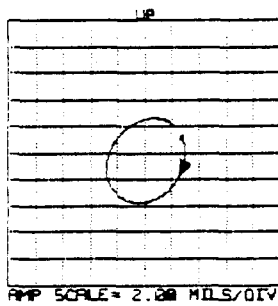
ORIENTATION= 90 DEG  
1X VECTOR= 6.40 MILS PK-PK @-301

PROBE #2 ID: OUTBRD HOR DISP  
1X FILTERED

ORIENTATION= 0 DEG  
1X VECTOR= 5.80 MILS PK-PK @-20

ROTATION: CW

RPM(START)= 2520 RPM(END)= 2519



PROBE #1

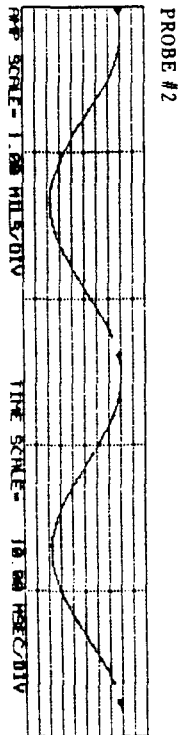


FIGURE 13.52 STEADY-STATE ORBIT AND TIMEBASE WAVE OF ROTOR VIBRATIONAL RESPONSE. 3.34 LB. PLUNGER PRELOAD. UNBALANCE: 2.0 GRAMS., 180 DEGREES, RADIUS 1.2 INCHES. FILTERED 1X RUB. ROTATIVE SPEED: 2519 RPM.



PROBE #1 ID: OUTDRD VERT DIS      ORIENTATION= 90 DEG  
 1X FILTERED                            1X VECTOR= 6.10 MILS PK-PK @-300  
  
 PROBE #2 ID: OUTBRD HOR DISP      ORIENTATION= 0 DEG  
 1X FILTERED                            1X VECTOR= 5.40 MILS PK-PK @-14  
  
 ROTATION: CW  
 RPM(START)= 2650 RPM(END)= 2647

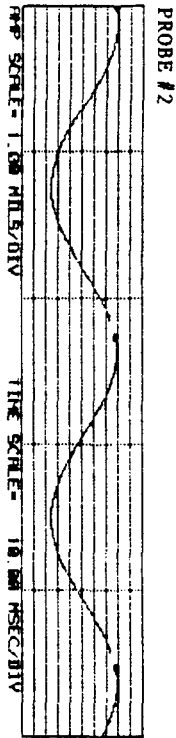
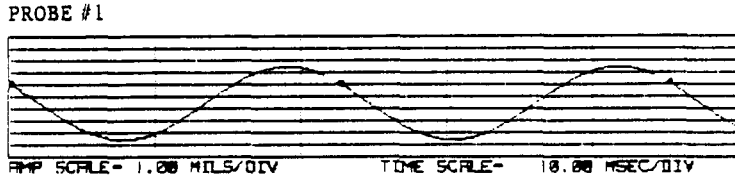
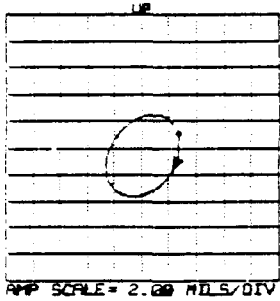


FIGURE 13.54 STEADY-STATE ORBIT AND TIMEBASE WAVE OF ROTOR VIBRATIONAL RESPONSE. 3.34 LB. PLUNGER PRELOAD. UNBALANCE: 2.0 GRAMS., 180 DEGREES, RADIUS 1.2 INCHES. FILTERED 1X RUB. ROTATIVE SPEED: 2647 RPM.

ORIGINAL PAGE IS  
OF POOR QUALITY

BENTLY  
NEVADA  
CORP.

PLANT ID: B.R.D.R.C  
TRAIN ID: NASA RUB RIG  
MACHINE ID: RUB ORBITS

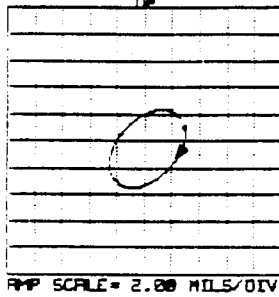
PROBE #1 ID: OUTBRD VERT DIS  
UNFILTERED

ORIENTATION= 90 DEG  
MAX AMP= 5.80 MILS PK-PK

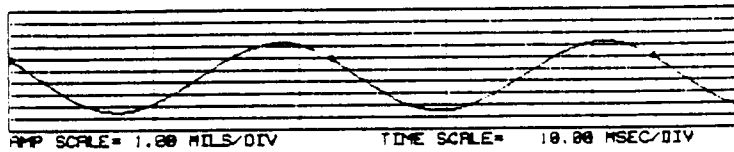
PROBE #2 ID: OUTBRD HOR DISP  
UNFILTERED

ORIENTATION= 0 DEG  
MAX AMP= 5.50 MILS PK-PK

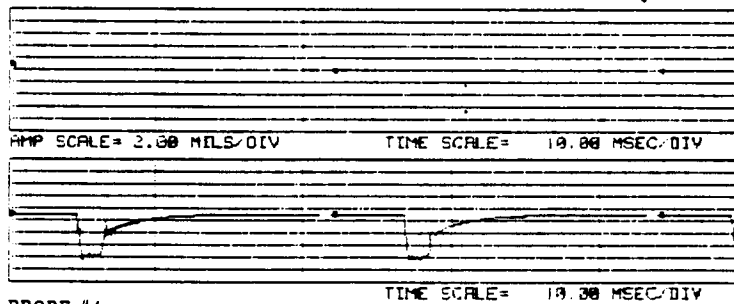
ROTATION: CW  
RPM(START)= 2714 RPM(END)= 2713



PROBE #1



PROBE #3



PROBE #4

PROBE #3 ID: RUB PLUNGER INBRD  
UNFILTERED

ORIENTATION= 0 DEG  
MAX AMP= 0.00 MILS PK-PK

PROBE #4 ID: ELEC CONTACT INBRD  
UNFILTERED

ORIENTATION= 0 DEG  
MAX AMP= 7.60 MILS PK-PK

ROTATION: CW  
RPM(START)= 2713 RPM(END)= 2712

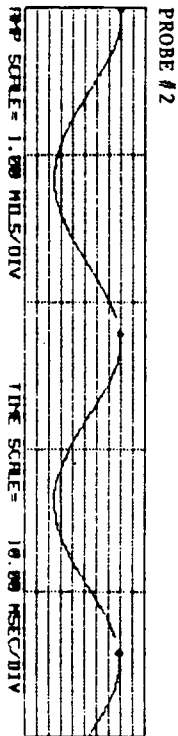


FIGURE 13.55 STEADY-STATE ORBIT AND TIMEBASE WAVE OF ROTOR VIBRATIONAL RESPONSE AND ASSOCIATED RUB PLUNGER MOTION. RUB CONTACT TIME: 1.92 ms. SHAFT REVOLUTIONS DURING RUB CONTACT = .0869 ROTATIONS. 3.34 LB. PLUNGER PRELOAD. UNBALANCE: 2.0 GRAMS., 180 DEGREES, RADIUS 1.2 INCHES. UNFILTERED 1x RUB. ROTATIVE SPEED: 2713 RPM.

PROBE #1 ID: OUTBRD VERT DIS      ORIENTATION= 90 DEG  
 1X FILTERED                            1X VECTOR= 5.80 MILS PK-PK @-300  
  
 PROBE #2 ID: OUTBRD HOR DISP      ORIENTATION= 0 DEG  
 1X FILTERED                            1X VECTOR= 5.50 MILS PK-PK @-7  
  
 ROTATION: CW  
 RPM(START)= 2712 RPM(END)= 2713

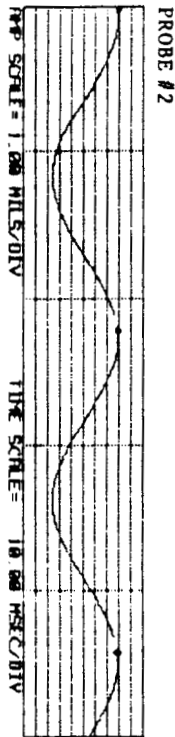
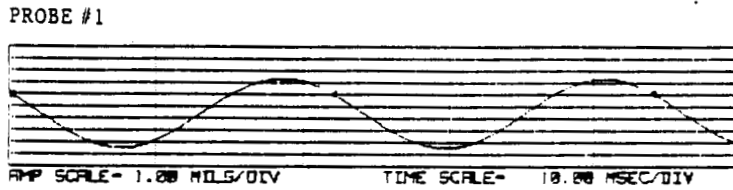
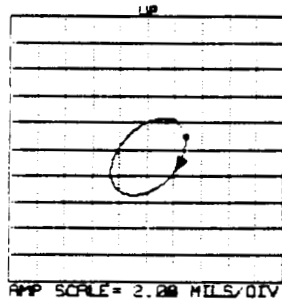


FIGURE 13.56 STEADY-STATE ORBIT AND TIMEBASE WAVE OF ROTOR VIBRATIONAL RESPONSE. 3.34 LB. PLUNGER PRELOAD. UNBALANCE: 2.0 GRAMS., 180 DEGREES, RADIUS 1.2 INCHES. FILTERED 1x RUB. ROTATIVE SPEED: 2713 RPM.



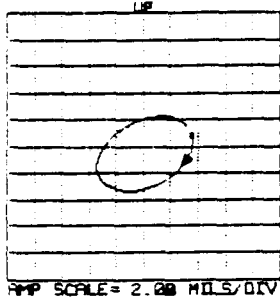
PROBE #1 ID: OUTBRD VERT DIS  
1X FILTERED

ORIENTATION= 90 DEG  
1X VECTOR= 5.50 MILS PK-PK @-296

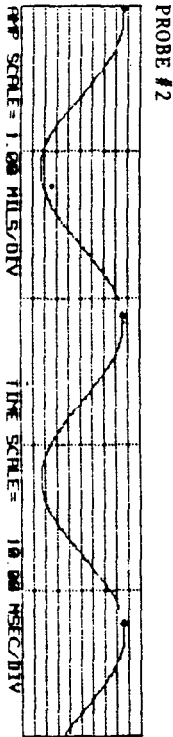
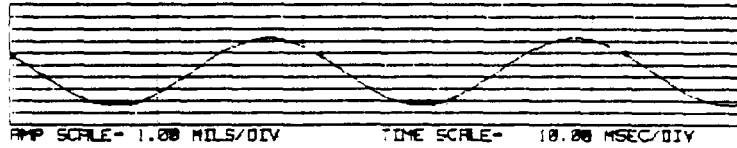
PROBE #2 ID: OUTBRD HOR DISP  
1X FILTERED

ORIENTATION= 0 DEG  
1X VECTOR= 7.00 MILS PK-PK @-7

ROTATION: CW  
RPM(START)= 2839 RPM(END)= 2839



PROBE #1



ORIGINAL PAGE IS  
OF POOR QUALITY

FIGURE 13.58 STEADY-STATE ORBIT AND TIMEBASE WAVE OF ROTOR VIBRATIONAL RESPONSE. 3.34 LB. PLUNGER PRELOAD. UNBALANCE: 2.0 GRAMS., 180 DEGREES, RADIUS 1.2 INCHES. FILTERED 1X RUB. ROTATIVE SPEED: 2839 RPM.

GENTLY  
NEVADA  
CORP.

PLANT ID: B.R.D.R.C  
TRAIN ID: NASA RUB RIG  
MACHINE ID: RUB ORBITS

ORIGINAL PAGE IS  
OF POOR QUALITY

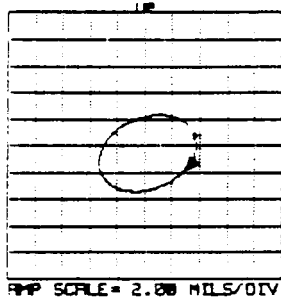
PROBE #1 ID: OUTBRD VERT DIS  
UNFILTERED

ORIENTATION= 90 DEG  
MAX AMP= 5.70 MILS PK-PK

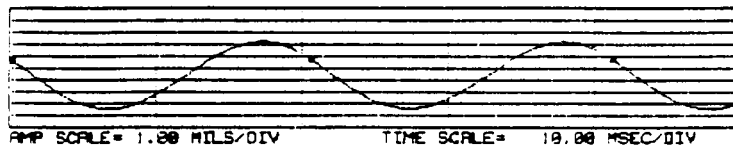
PROBE #2 ID: OUTBRD HOR DISP  
UNFILTERED

ORIENTATION= 0 DEG  
MAX AMP= 7.10 MILS PK-PK

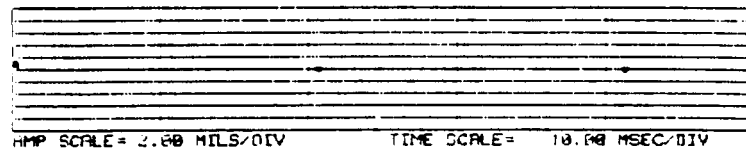
ROTATION: CW  
RPM(START)= 2910 RPM(END)= 2910



PROBE #1



PROBE #3



PROBE #4

PROBE #3 ID: RUB PLUNGER INBRD  
UNFILTERED

ORIENTATION= 0 DEG  
MAX AMP= 0.00 MILS PK-PK

PROBE #4 ID: ELEC CONTACT INBRD  
UNFILTERED

ORIENTATION= 0 DEG  
MAX AMP= 9.30 MILS PK-PK

ROTATION: CW  
RPM(START)= 2908 RPM(END)= 2911

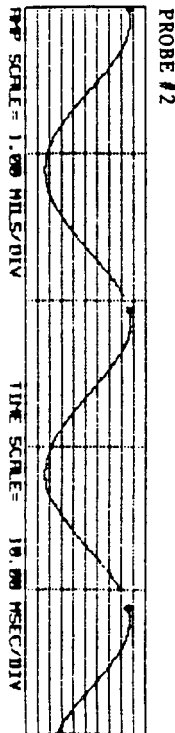


FIGURE 13.59

STEADY-STATE ORBIT AND TIMEBASE WAVE OF ROTOR VIBRATIONAL RESPONSE AND ASSOCIATED RUB PLUNGER MOTION. RUB CONTACT TIME: 1.78 ms. SHAFT REVOLUTIONS DURING RUB CONTACT = .0860 ROTATIONS. 3.34 LB. PLUNGER PRELOAD. UNBALANCE: 2.0 GRAMS., 180 DEGREES, RADIUS 1.2 INCHES. UNFILTERED 1x RUB. ROTATIVE SPEED: 2910 RPM.

ORIGINAL PAGE IS  
OF POOR QUALITY

PROBE #1 ID: OUTBRD VERT DIS      ORIENTATION= 90 DEG  
1X FILTERED                              1X VECTOR= 5.70 MILS PK-PK @-294

PROBE #2 ID: OUTBRD HOR DISP      ORIENTATION= 0 DEG  
1X FILTERED                              1X VECTOR= 7.20 MILS PK-PK @-11

ROTATION: CW  
RPM(START)= 2910 RPM(END)= 2910

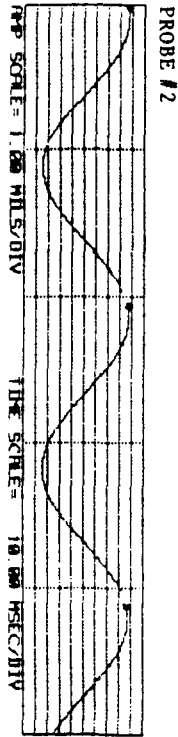
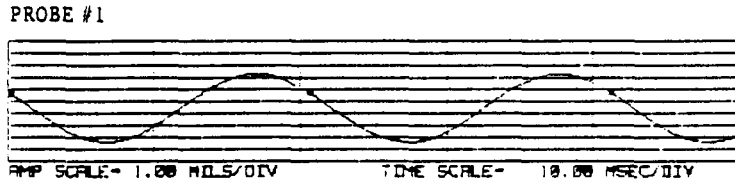
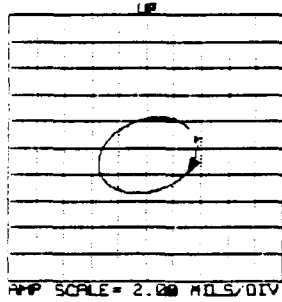


FIGURE 13.60 STEADY-STATE ORBIT AND TIMEBASE WAVE OF ROTOR VIBRATIONAL RESPONSE. 3.34 LB. PLUNGER PRELOAD. UNBALANCE: 2.0 GRAMS., 180 DEGREES, RADIUS 1.2 INCHES. FILTERED 1x RUB. ROTATIVE SPEED: 2910 RPM.



ORIGINAL PAGE IS  
OF POOR QUALITY

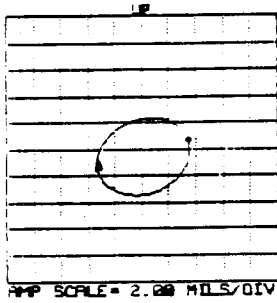
PROBE #1 ID: OUTBRD VERT DIS  
1X FILTERED

ORIENTATION- 90 DEG  
1X VECTOR- 5.80 MILS PK-PK @-293

PROBE #2 ID: OUTBRD HOR DISP  
1X FILTERED

ORIENTATION- 0 DEG  
1X VECTOR- 6.90 MILS PK-PK @-14

ROTATION: CW  
RPM(START)- 3018 RPM(END)- 3016



PROBE #1

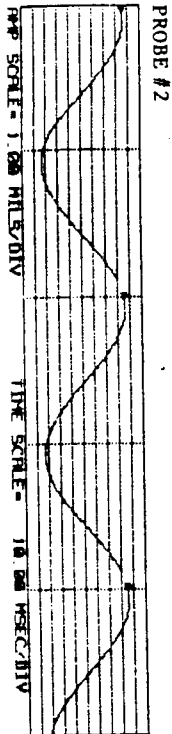
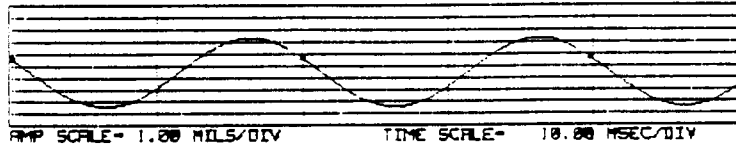


FIGURE 13.62 STEADY-STATE ORBIT AND TIMEBASE WAVE OF ROTOR VIBRATIONAL RESPONSE. 3.34 LB. PLUNGER PRELOAD. UNBALANCE: 2.0 GRAMS., 180 DEGREES, RADIUS 1.2 INCHES. FILTERED 1X RUB. ROTATIVE SPEED: 3016 RPM.

ORIGINAL PAGE IS  
OF POOR QUALITY

BENTLY  
NEVADA  
CORP.

PLANT ID: B.R.D.R.C  
TRAIN ID: NASA RUB RIG  
MACHINE ID: RUB ORBITS

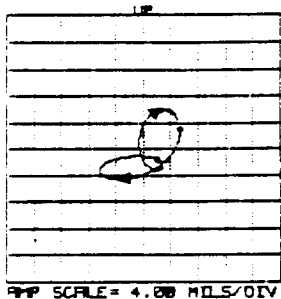
PROBE #1 ID: OUTBRD VERT DIS  
UNFILTERED

ORIENTATION= 90 DEG  
MAX AMP= 10.60 MILS PK-PK

PROBE #2 ID: OUTBRD HOR DISP  
UNFILTERED

ORIENTATION= 0 DEG  
MAX AMP= 11.80 MILS PK-PK

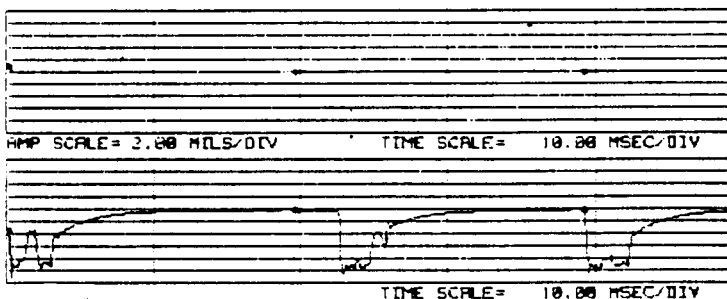
ROTATION: CW  
RPM(START)= 3066 RPM(END)= 3067



PROBE #1



PROBE #3



PROBE #4

PROBE #3 ID: RUB PLUNGER INBRD UNFILTERED  
ORIENTATION= 0 DEG  
MAX AMP= 0.00 MILS PK-PK

PROBE #4 ID: ELEC CONTACT INBRD UNFILTERED  
ORIENTATION= 0 DEG  
MAX AMP= 10.90 MILS PK-PK

ROTATION: CW  
RPM(START)= 3062 RPM(END)= 3062

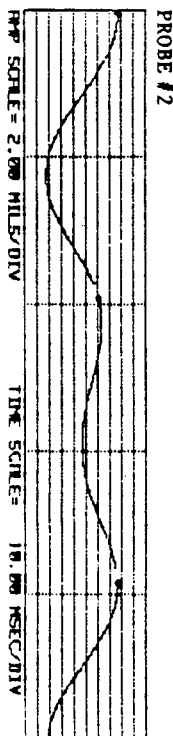


FIGURE 13.63 STEADY-STATE ORBIT AND TIMEBASE WAVE OF ROTOR VIBRATIONAL RESPONSE AND ASSOCIATED RUB PLUNGER MOTION. RUB CONTACT TIME: 2.40 ms. SHAFT REVOLUTIONS DURING RUB CONTACT = .1240 ROTATIONS. 3.34 LB. PLUNGER PRELOAD. UNBALANCE: 2.0 GRAMS, 180 DEGREES, RADIUS 1.2 INCHES. UNFILTERED 1x RUB. ROTATIVE SPEED: 3067 RPM.





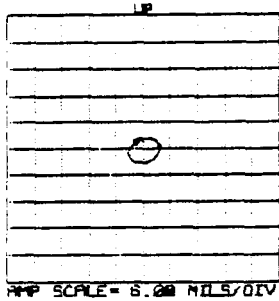
PROBE #1 ID: OUTBRD VERT DIS  
1X FILTERED

ORIENTATION= 90 DEG  
1X VECTOR= 5.60 MILS PK-PK @-285

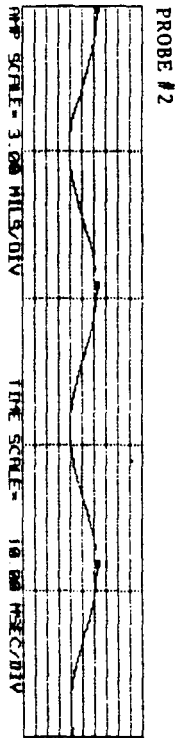
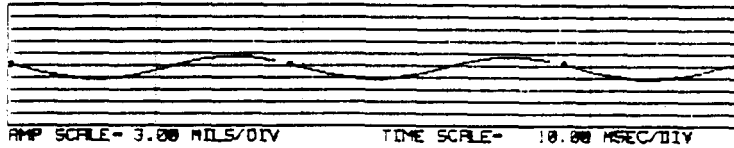
PROBE #2 ID: OUTBRD HOR DISP  
1X FILTERED

ORIENTATION= 0 DEG  
1X VECTOR= 6.80 MILS PK-PK @-3

ROTATION: CW  
RPM(START)= 3151 RPM(END)= 3150



PROBE #1



ORIGINAL PAGE IS  
OF POOR QUALITY

FIGURE 13.66 STEADY-STATE ORBIT AND TIMEBASE WAVE OF ROTOR VIBRATIONAL RESPONSE. 3.34 LB. PLUNGER PRELOAD. UNBALANCE: 2.0 GRAMS., 180 DEGREES, RADIUS 1.2 INCHES. FILTERED 1X RUB. ROTATIVE SPEED: 3150 RPM.

BENTLY  
NEVADA  
CORP.

PLANT ID: B.R.D.R.C  
TRAIN ID: NASA RUB RIG  
MACHINE ID: RUB ORBITS

ORIGINAL PAGE IS  
OF POOR QUALITY

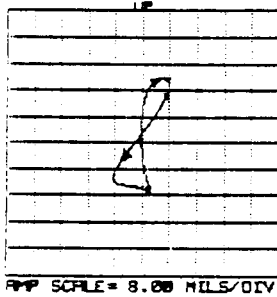
PROBE #1 ID: OUTBRD VERT DIS  
UNFILTERED

ORIENTATION= 90 DEG  
MAX AMP= 34.70 MILS PK-PK

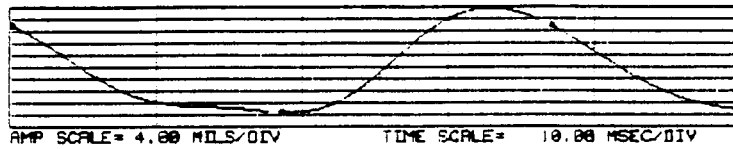
PROBE #2 ID: OUTBRD HOR DISP  
UNFILTERED

ORIENTATION= 0 DEG  
MAX AMP= 17.50 MILS PK-PK

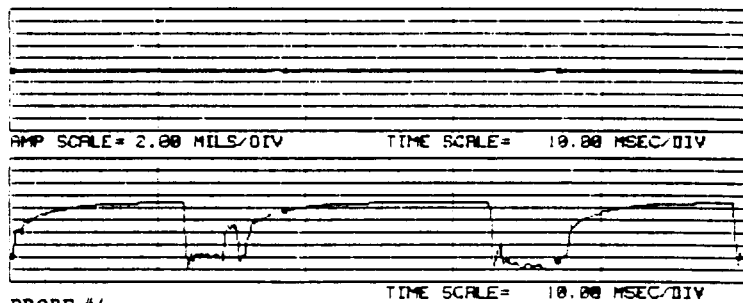
ROTATION: CW  
RPM(START)= 3245 RPM(END)= 3248



PROBE #1



PROBE #3



PROBE #4

PROBE #3 ID: RUB PLUNGER INBRD UNFILTERED  
ORIENTATION= 0 DEG  
MAX AMP= .10 MILS PK-PK

PROBE #4 ID: ELEC CONTACT INBRD UNFILTERED  
ORIENTATION= 0 DEG  
MAX AMP= 10.60 MILS PK-PK

ROTATION: CW  
RPM(START)= 3246 RPM(END)= 3246

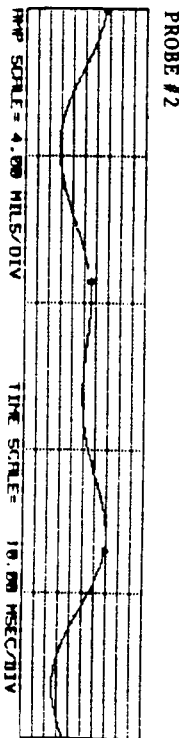


FIGURE 13.67 STEADY-STATE ORBIT AND TIMEBASE WAVE OF ROTOR VIBRATIONAL RESPONSE AND ASSOCIATED RUB PLUNGER MOTION. RUB CONTACT TIME: 3.84 ms. SHAFT REVOLUTIONS DURING RUB CONTACT = .2080 ROTATIONS. 3.34 LB. PLUNGER PRELOAD. UNBALANCE: 2.0 GRAMS., 180 DEGREES, RADIUS 1.2 INCHES. UNFILTERED 1x RUB. ROTATIVE SPEED: 3248 RPM.

ORIGINAL PAGE IS  
OF POOR QUALITY

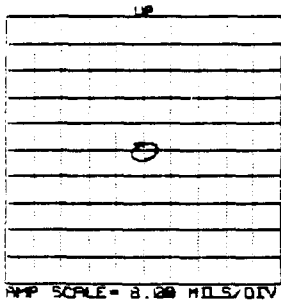
PROBE #1 ID: OUTBRD VERT DIS  
1X FILTERED

ORIENTATION= 90 DEG  
1X VECTOR= 5.10 MILS PK-PK @-279

PROBE #2 ID: OUTBRD HOR DISP  
1X FILTERED

ORIENTATION= 0 DEG  
1X VECTOR= 7.40 MILS PK-PK @-353

ROTATION: CW  
RPM(START)= 3246 RPM(END)= 3246



PROBE #1

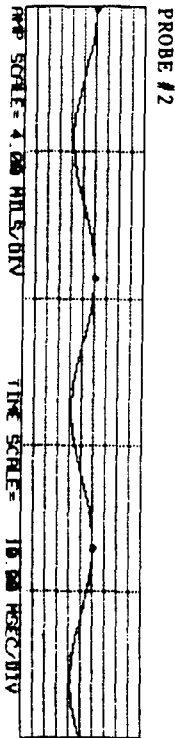


FIGURE 13.68 STEADY-STATE ORBIT AND TIMEBASE WAVE OF ROTOR VIBRATIONAL RESPONSE. 3.34 LB. PLUNGER PRELOAD. UNBALANCE: 2.0 GRAMS., 180 DEGREES, RADIUS 1.2 INCHES. FILTERED 1X RUB. ROTATIVE SPEED: 3246 RPM.

BENTLY  
NEVADA  
CORP.

PLANT ID: B.R.D.R.C  
TRAIN ID: NASA RUB RIG  
MACHINE ID: RUB ORBITS

ORIGINAL PAGE IS  
OF POOR QUALITY

PROBE #1 ID: OUTBRD VERT DIS  
UNFILTERED

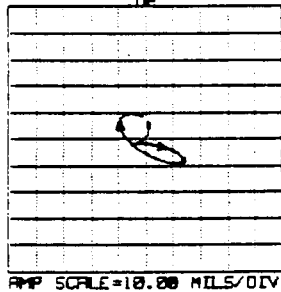
ORIENTATION= 90 DEG  
MAX AMP= 18.70 MILS PK-PK

PROBE #2 ID: OUTBRD HOR DISP  
UNFILTERED

ORIENTATION= 0 DEG  
MAX AMP= 23.70 MILS PK-PK

ROTATION: CW

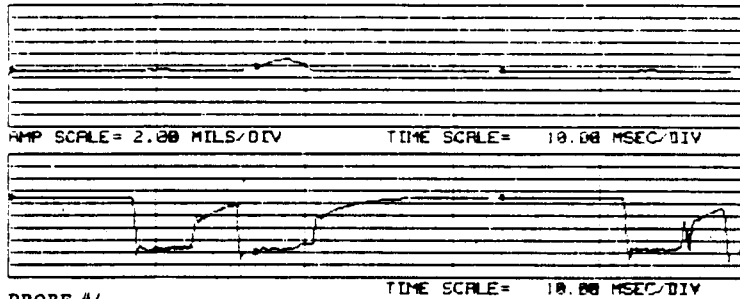
RPM(START)= 3622 RPM(END)= 3629



PROBE #1



PROBE #3



PROBE #4

PROBE #3 ID: RUB PLUNGER INBRD  
UNFILTERED

ORIENTATION= 0 DEG  
MAX AMP= 2.10 MILS PK-PK

PROBE #4 ID: ELEC CONTACT INBRD  
UNFILTERED

ORIENTATION= 0 DEG  
MAX AMP= 10.30 MILS PK-PK

ROTATION: CW

RPM(START)= 3621 RPM(END)= 3621

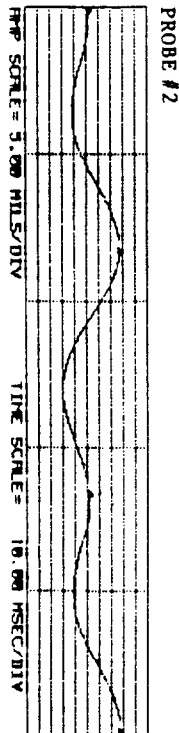
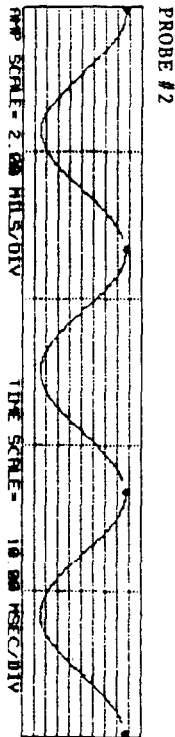
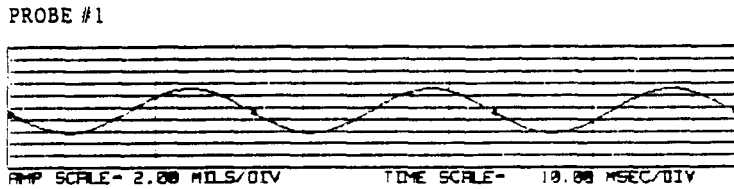
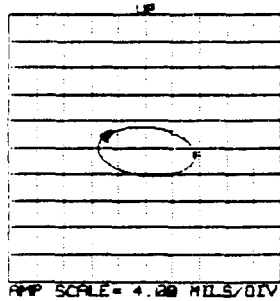


FIGURE 13.69

STEADY-STATE ORBIT AND TIMEBASE WAVE OF ROTOR VIBRATIONAL RESPONSE AND ASSOCIATED RUB PLUNGER MOTION. RUB CONTACT TIME: 4.76 ms. SHAFT REVOLUTIONS DURING RUB CONTACT = .2800 ROTATIONS. 3.34 LB. PLUNGER PRELOAD. UNBALANCE: 2.0 GRAMS., 180 DEGREES, RADIUS 1.2 INCHES. UNFILTERED 1x RUB. ROTATIVE SPEED: 3629 RPM.

PROBE #1 ID: OUTBRD VERT DIS      ORIENTATION= 90 DEG  
 1X FILTERED                            1X VECTOR= 7.30 MILS PK-PK @-261  
  
 PROBE #2 ID: OUTBRD HOR DISP      ORIENTATION= 0 DEG  
 1X FILTERED                            1X VECTOR= 14.30 MILS PK-PK @0  
  
 ROTATION: CW  
 RPM(START)= 3621 RPM(END)= 3629



ORIGINAL PAGE IS  
 OF POOR QUALITY

FIGURE 13.70 STEADY-STATE ORBIT AND TIMEBASE WAVE OF ROTOR VIBRATIONAL RESPONSE. 3.34 LB. PLUNGER PRELOAD. UNBALANCE: 2.0 GRAMS., 180 DEGREES, RADIUS 1.2 INCHES. FILTERED 1X RUB. ROTATIVE SPEED: 3629 RPM.



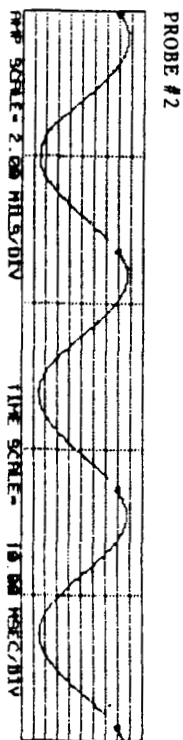
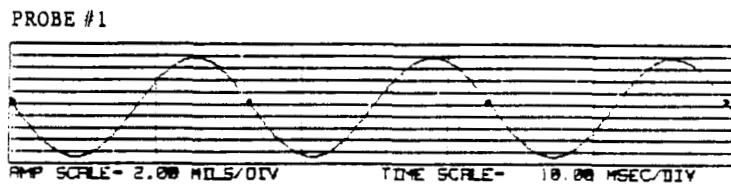
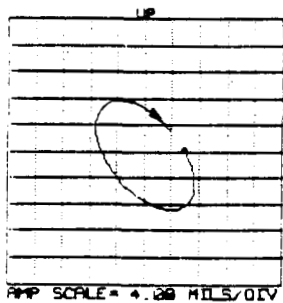
PROBE #1 ID: OUTBRD VERT DIS  
1X FILTERED

ORIENTATION= 90 DEG  
X VECTOR= 16.60 MILS PK-PK @-274

PROBE #2 ID: OUTBRD HOR DISP  
1X FILTERED

ORIENTATION= 0 DEG  
X VECTOR= 14.50 MILS PK-PK @-36

ROTATION: CW  
RPM(START)= 3671 RPM(END)= 3671



ORIGINAL PAGE IS  
OF POOR QUALITY

FIGURE 13.72 STEADY-STATE ORBIT AND TIMEBASE WAVE OF ROTOR VIBRATIONAL RESPONSE. 3.34 LB. PLUNGER PRELOAD. UNBALANCE: 2.0 GRAMS., 180 DEGREES, RADIUS 1.2 INCHES. FILTERED 1X RUB. ROTATIVE SPEED: 3671 RPM.



PROBE #1 ID: OUTBRD VERT DIS      ORIENTATION= 90 DEG  
 1X FILTERED                            1X VECTOR= 16.10 MILS PK-PK @-282  
  
 PROBE #2 ID: OUTBRD HOR DISP      ORIENTATION= 0 DEG  
 1X FILTERED                            1X VECTOR= 13.00 MILS PK-PK @-41  
  
 ROTATION: CW  
 RPM(START)= 3789 RPM(END)= 3792

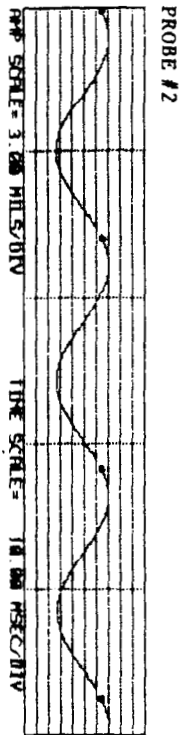
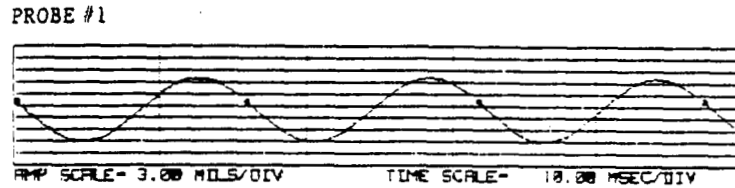
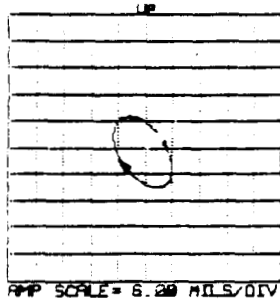


FIGURE 13.74 STEADY-STATE ORBIT AND TIMEBASE WAVE OF ROTOR VIBRATIONAL RESPONSE. 3.34 LB. PLUNGER PRELOAD. UNBALANCE: 2.0 GRAMS., 180 DEGREES, RADIUS 1.2 INCHES. FILTERED 1X RUB. ROTATIVE SPEED: 3792 RPM.



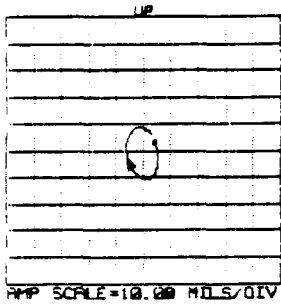
PROBE #1 ID: OUTBRD VERT DIS  
1X FILTERED

ORIENTATION= 90 DEG  
1X VECTOR= 19.70 MILS PK-PK @-291

PROBE #2 ID: OUTBRD HOR DISP  
1X FILTERED

ORIENTATION= 0 DEG  
1X VECTOR= 11.60 MILS PK-PK @-34

ROTATION: CW  
RPM(START)= 3868 RPM(END)= 3868



PROBE #1

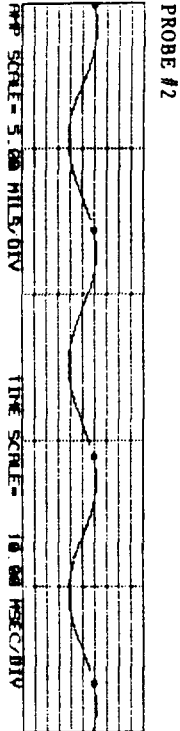
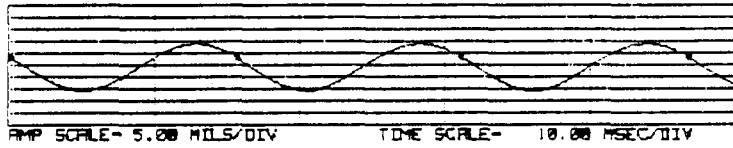


FIGURE 13.76 STEADY-STATE ORBIT AND TIMEBASE WAVE OF ROTOR VIBRATIONAL RESPONSE. 3.34 LB. PLUNGER PRELOAD. UNBALANCE: 2. GRAMS., 180 DEGREES, RADIUS 1.2 INCHES. FILTERED 1X RUB. ROTATIVE SPEED: 3868 RPM.



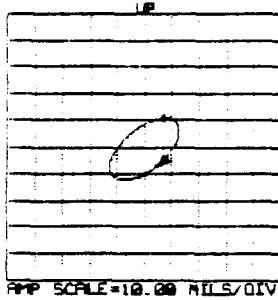
PROBE #1 ID: OUTBRD VERT DIS  
1X FILTERED

ORIENTATION= 90 DEG  
1X VECTOR= 22.70 MILS PK-PK @-359

PROBE #2 ID: OUTBRD HOR DISP  
1X FILTERED

ORIENTATION= 0 DEG  
1X VECTOR= 25.50 MILS PK-PK @-53

ROTATION: CW  
RPM(START)= 4055 RPM(END)= 4055



PROBE #1

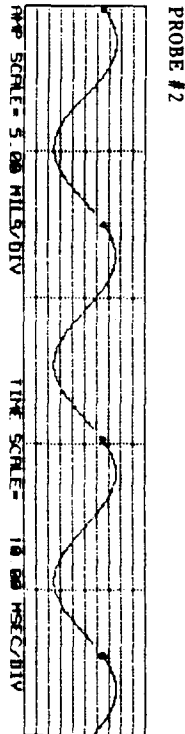


FIGURE 13.78 STEADY-STATE ORBIT AND TIMEBASE WAVE OF ROTOR VIBRATIONAL RESPONSE. 3.34 LB. PLUNGER PRELOAD. UNBALANCE: 2.0 GRAMS., 180 DEGREES, RADIUS 1.2 INCHES. FILTERED 1X RUB. ROTATIVE SPEED: 4055 RPM.

BENTLY  
NEVADA  
CORP.

PLANT ID: B.R.D.R.C  
TRAIN ID: NASA RUB RIG  
MACHINE ID: RUB ORBITS

ORIGINAL PAGE IS  
OF POOR QUALITY

PROBE #1 ID: OUTBRD VERT DIS  
UNFILTERED

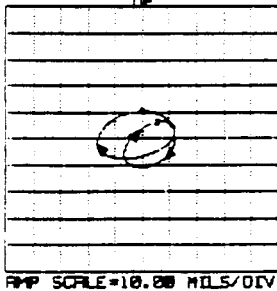
ORIENTATION= 90 DEG  
MAX AMP= 21.40 MILS PK-PK

PROBE #2 ID: OUTBRD HOR DISP  
UNFILTERED

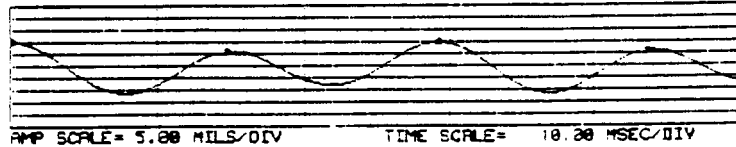
ORIENTATION= 0 DEG  
MAX AMP= 28.30 MILS PK-PK

ROTATION: CW

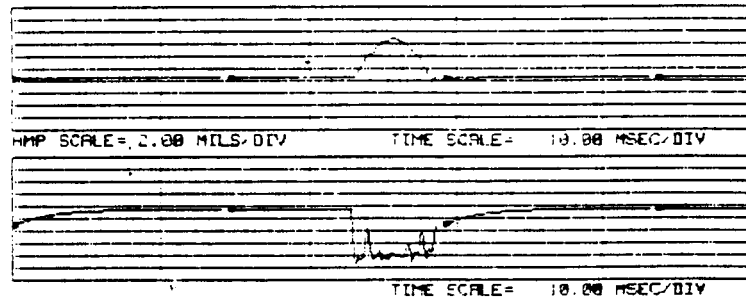
RPM(START)= 4117 RPM(END)= 4120



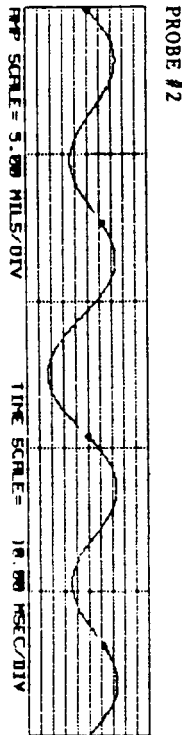
PROBE #1



PROBE #3



PROBE #4



PROBE #3 ID: RUB PLUNGER INBRD  
UNFILTERED

ORIENTATION= 0 DEG  
MAX AMP= 6.60 MILS PK-PK

PROBE #4 ID: ELEC CONTACT INBRD  
UNFILTERED

ORIENTATION= 0 DEG  
MAX AMP= 9.00 MILS PK-PK

ROTATION: CW

RPM(START)= 4118 RPM(END)= 4116

FIGURE 13.79

STEADY-STATE ORBIT AND TIMEBASE WAVE OF ROTOR VIBRATIONAL RESPONSE AND ASSOCIATED RUB PLUNGER MOTION. RUB CONTACT TIME: 5.71 ms. SHAFT REVOLUTIONS DURING RUB CONTACT = .3920 ROTATIONS. 3.34 LB. PLUNGER PRELOAD. UNBALANCE: 2.0 GRAMS., 180 DEGREES, RADIUS 1.2 INCHES. UNFILTERED 1x RUB. ROTATIVE SPEED: 4120 RPM.

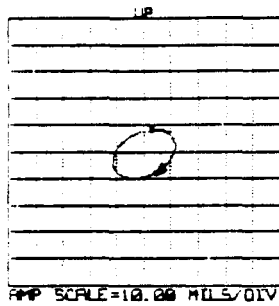
PROBE #1 ID: OUTBRD VERT DIS  
1X FILTERED

ORIENTATION= 90 DEG  
1X VECTOR= 18.20 MILS PK-PK @-1

PROBE #2 ID: OUTBRD HOR DISP  
1X FILTERED

ORIENTATION= 0 DEG  
1X VECTOR= 23.10 MILS PK-PK @-72

ROTATION: CW  
RPM(START)= 4117 RPM(END)= 4119



PROBE #1

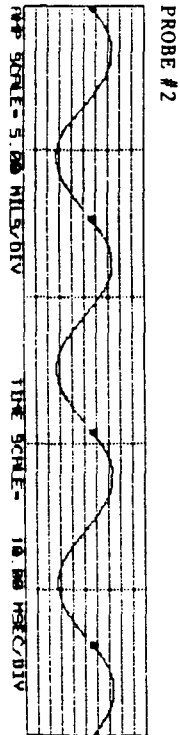


FIGURE 13.80 STEADY-STATE ORBIT AND TIMEBASE WAVE OF ROTOR VIBRATIONAL RESPONSE. 3.34 LB. PLUNGER PRELOAD. UNBALANCE: 2.0 GRAMS., 180 DEGREES, RADIUS 1.2 INCHES. FILTERED 1X RUB. ROTATIVE SPEED: 4119 RPM.

BENTLY  
NEVADA  
CORP.

PLANT ID: B.R.D.R.C  
TRAIN ID: NASA RUB RIG  
MACHINE ID: RUB ORBITS

ORIGINAL PAGE IS  
OF POOR QUALITY

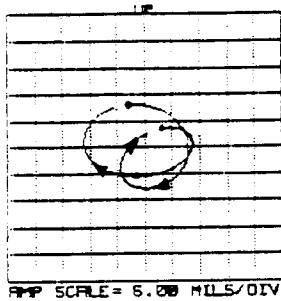
PROBE #1 ID: OUTBRD VERT DIS  
UNFILTERED

ORIENTATION= 90 DEG  
MAX AMP= 19.10 MILS PK-PK

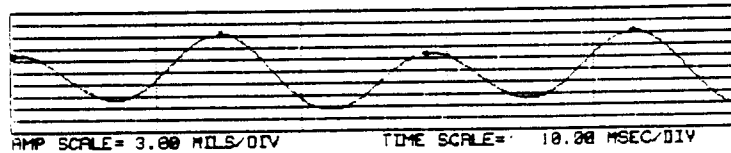
PROBE #2 ID: OUTBRD HOR DISP  
UNFILTERED

ORIENTATION= 0 DEG  
MAX AMP= 23.80 MILS PK-PK

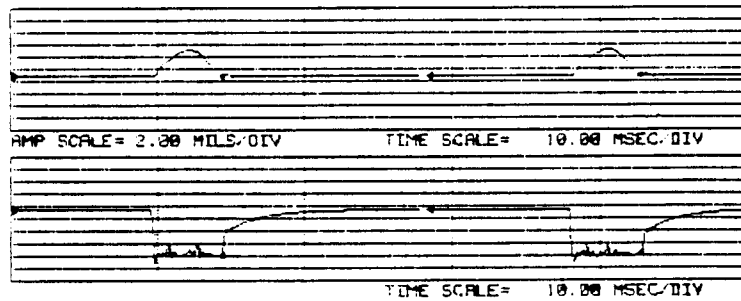
ROTATION: CW  
RPM(START)= 4225 RPM(END)= 4226



PROBE #1



PROBE #3



NO CONTACT  
CONTACT

PROBE #4

PROBE #4 ID: RUB PLUNGER INBRD  
UNFILTERED

ORIENTATION= 0 DEG  
MAX AMP= 4.60 MILS PK-PK

PROBE #3 ID: ELEC CONTACT INBRD  
UNFILTERED

ORIENTATION= 0 DEG  
MAX AMP= 8.60 MILS PK-PK

ROTATION: CW  
RPM(START)= 4227 RPM(END)= 4227

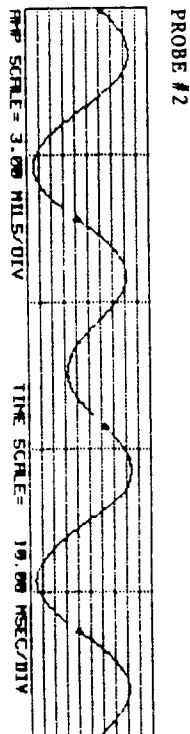


FIGURE 13.81 STEADY-STATE ORBIT AND TIMEBASE WAVE OF ROTOR VIBRATIONAL RESPONSE AND ASSOCIATED RUB PLUNGER MOTION. RUB CONTACT TIME: 5.00 ms. SHAFT REVOLUTIONS DURING RUB CONTACT = .3522 ROTATIONS. 3.34 LB. PLUNGER PRELOAD. UNBALANCE: 2.0 GRAMS., 180 DEGREES, RADIUS 1.2 INCHES. UNFILTERED 1x RUB. ROTATIVE SPEED: 4226 RPM.

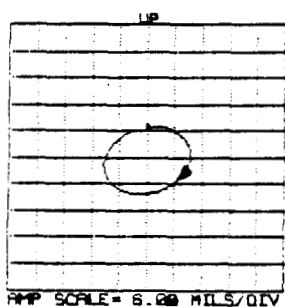
PROBE #1 ID: OUTBRD VERT DIS  
1X FILTERED

ORIENTATION= 90 DEG  
1X VECTOR= 15.20 MILS PK-PK @-4

PROBE #2 ID: OUTBRD HOR DISP  
1X FILTERED

ORIENTATION= 0 DEG  
1X VECTOR= 18.80 MILS PK-PK @-86

ROTATION: CW  
RPM(START)= 4228 RPM(END)= 4228



PROBE #1

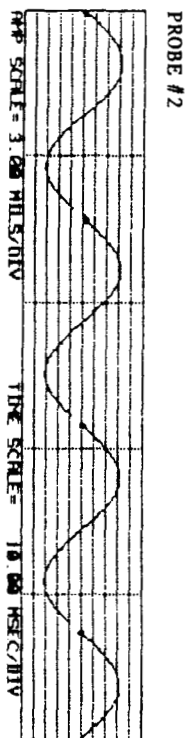
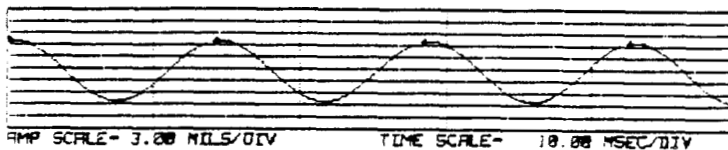


FIGURE 13.82 STEADY-STATE ORBIT AND TIMEBASE WAVE OF ROTOR VIBRATIONAL RESPONSE. 3.34 LB. PLUNGER PRELOAD. UNBALANCE: 2.0 GRAMS., 180 DEGREES, RADIUS 1.2 INCHES. FILTERED 1X RUB. ROTATIVE SPEED: 4228 RPM.

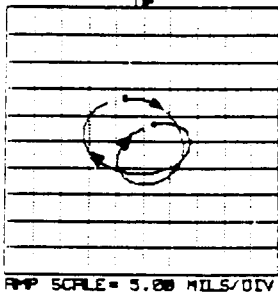
SENTLY  
NEVADA  
CORP.

PLANT ID: B.R.D.R.C  
TRAIN ID: NASA RUB RIG  
MACHINE ID: RUB ORBITS

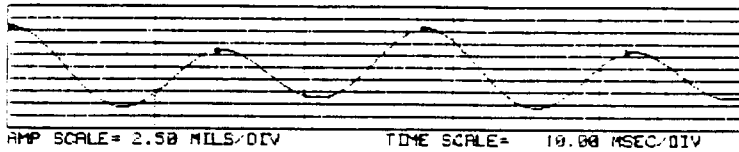
PROBE #1 ID: OUTBRD VERT DIS UNFILTERED      ORIENTATION= 90 DEG  
MAX AMP= 16.30 MILS PK-PK

PROBE #2 ID: OUTBRD HOR DISP UNFILTERED      ORIENTATION= 0 DEG  
MAX AMP= 19.60 MILS PK-PK

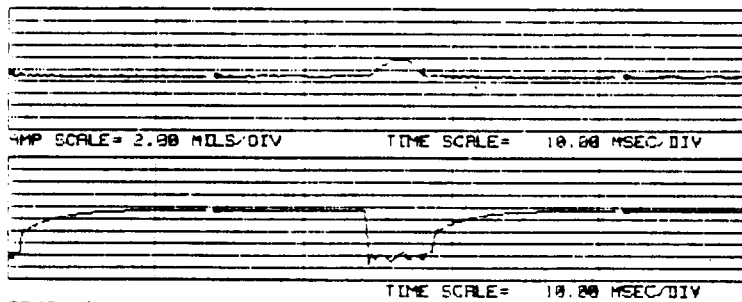
ROTATION: CW  
RPM(START)= 4311 RPM(END)= 4307



PROBE #1



PROBE #3



PROBE #4

PROBE #3 ID: RUB PLUNGER INBRD UNFILTERED      ORIENTATION= 0 DEG  
MAX AMP= 2.90 MILS PK-PK

PROBE #4 ID: ELEC CONTACT INBRD UNFILTERED      ORIENTATION= 0 DEG  
MAX AMP= 8.80 MILS PK-PK

ROTATION: CW  
RPM(START)= 4310 RPM(END)= 4308

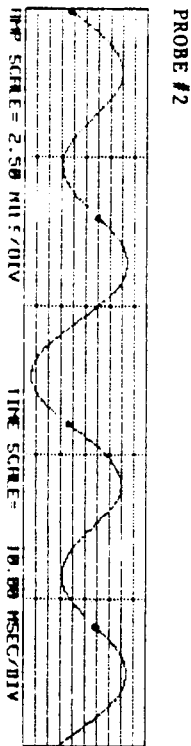


FIGURE 13.83 STEADY-STATE ORBIT AND TIMEBASE WAVE OF ROTOR VIBRATIONAL RESPONSE AND ASSOCIATED RUB PLUNGER MOTION. RUB CONTACT TIME: 4.54 ms. SHAFT REVOLUTIONS DURING RUB CONTACT = .3263 ROTATIONS. 3.34 LB. PLUNGER PRELOAD. UNBALANCE: 2.0 GRAMS., 180 DEGREES, RADIUS 1.2 INCHES. UNFILTERED 1x RUB. ROTATIVE SPEED: 4307 RPM.

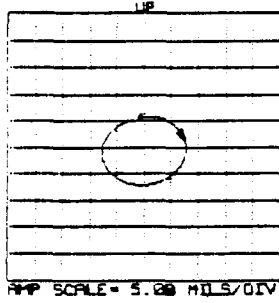
PROBE #1 ID: OUTBRD VERT DIS  
 1X FILTERED

PROBE #2 ID: OUTBRD HOR DISP  
 1X FILTERED

ORIENTATION= 90 DEG  
 1X VECTOR= 12.90 MILS PK-PK 3-5

ORIENTATION= 0 DEG  
 1X VECTOR= 15.50 MILS PK-PK 3-92

ROTATION: CW  
 RPM(START)= 4308 RPM(END)= 4307



PROBE #1

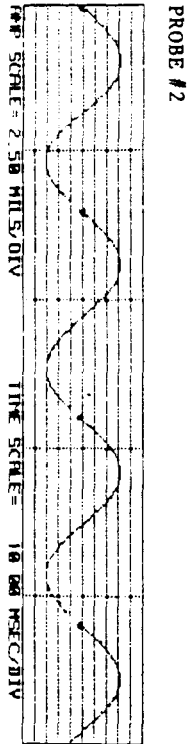
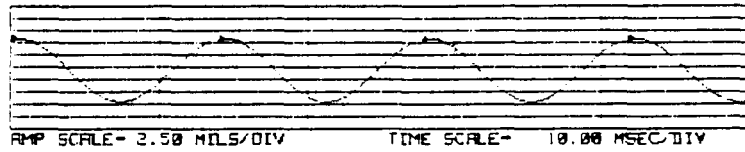


FIGURE 13.84 STEADY STATE ORBIT AND TIMEBASE WAVE OF ROTOR VIBRATIONAL RESPONSE. 3.34 LB. PLUNGER PRELOAD. UNBALANCE: 2.0 GRAMS., 180 DEGREES, RADIUS 1.2 INCHES AT THE INBOARD DISK, FILTERED 1x RUB ROTATIVE SPEED: 4307 RPM.

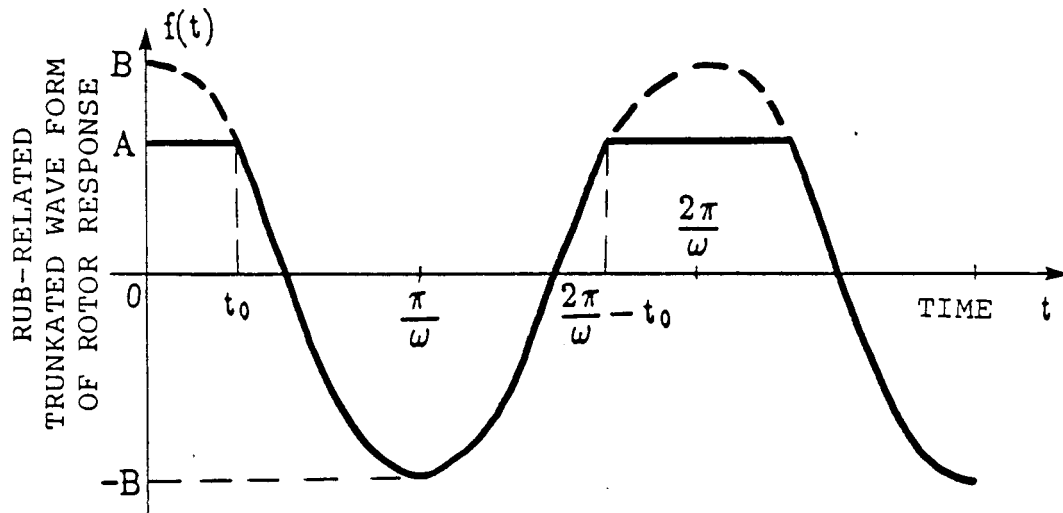


FIGURE 13.85 ROTOR RESPONSE HARMONIC WAVE TRUNCATED DUE TO ROTOR-TO-STATOR RUB.

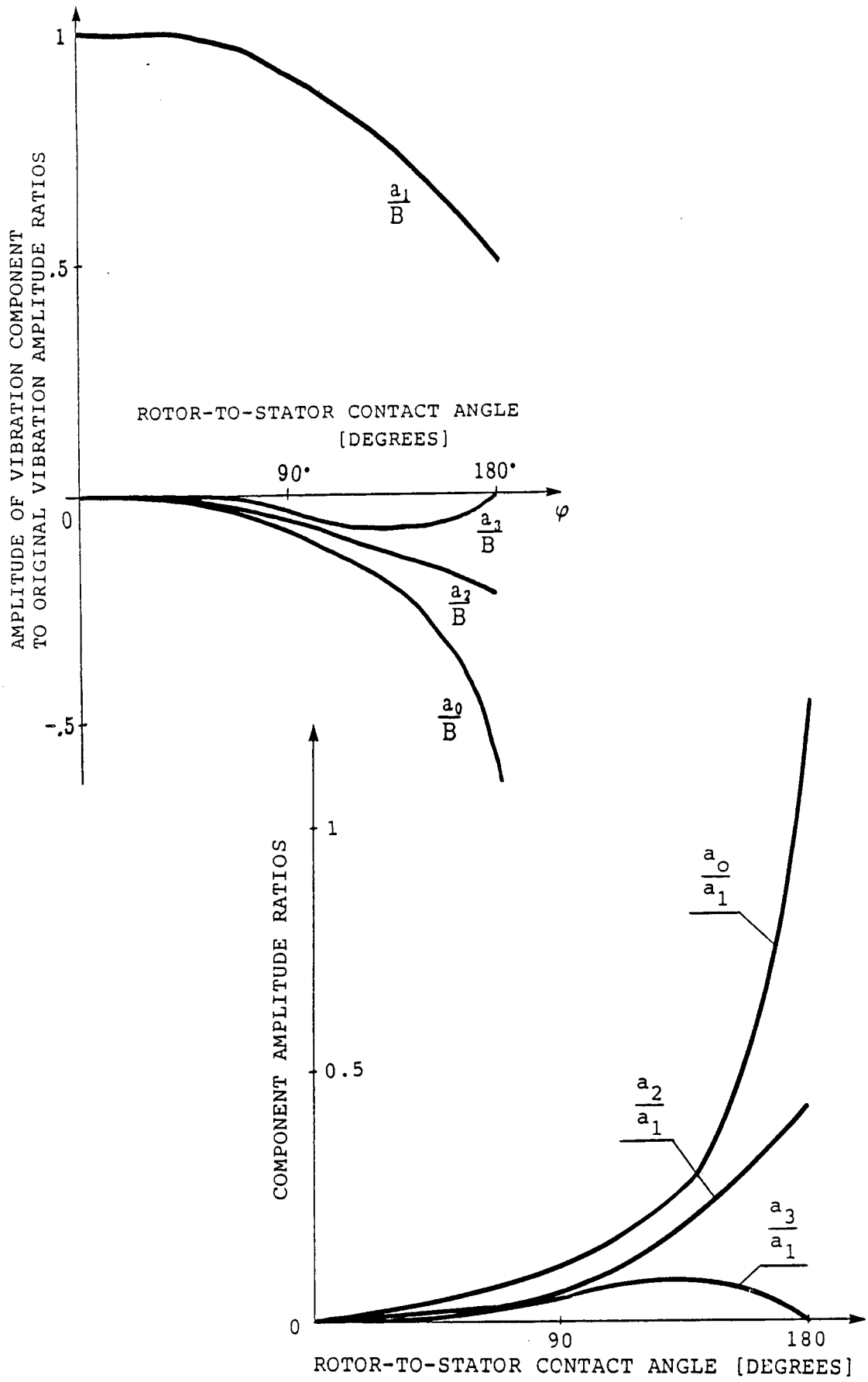


FIGURE 13.86 AMPLITUDES OF FOUR COMPONENTS OF VIBRATIONAL RESPONSE AND THE AMPLITUDE RATIOS VERSUS ROTOR/STATOR CONTACT ARC





ORIGINAL PAGE IS  
OF POOR QUALITY

ROTATION: CW  
RPM(START)= 1345 RPM(END)= 1341

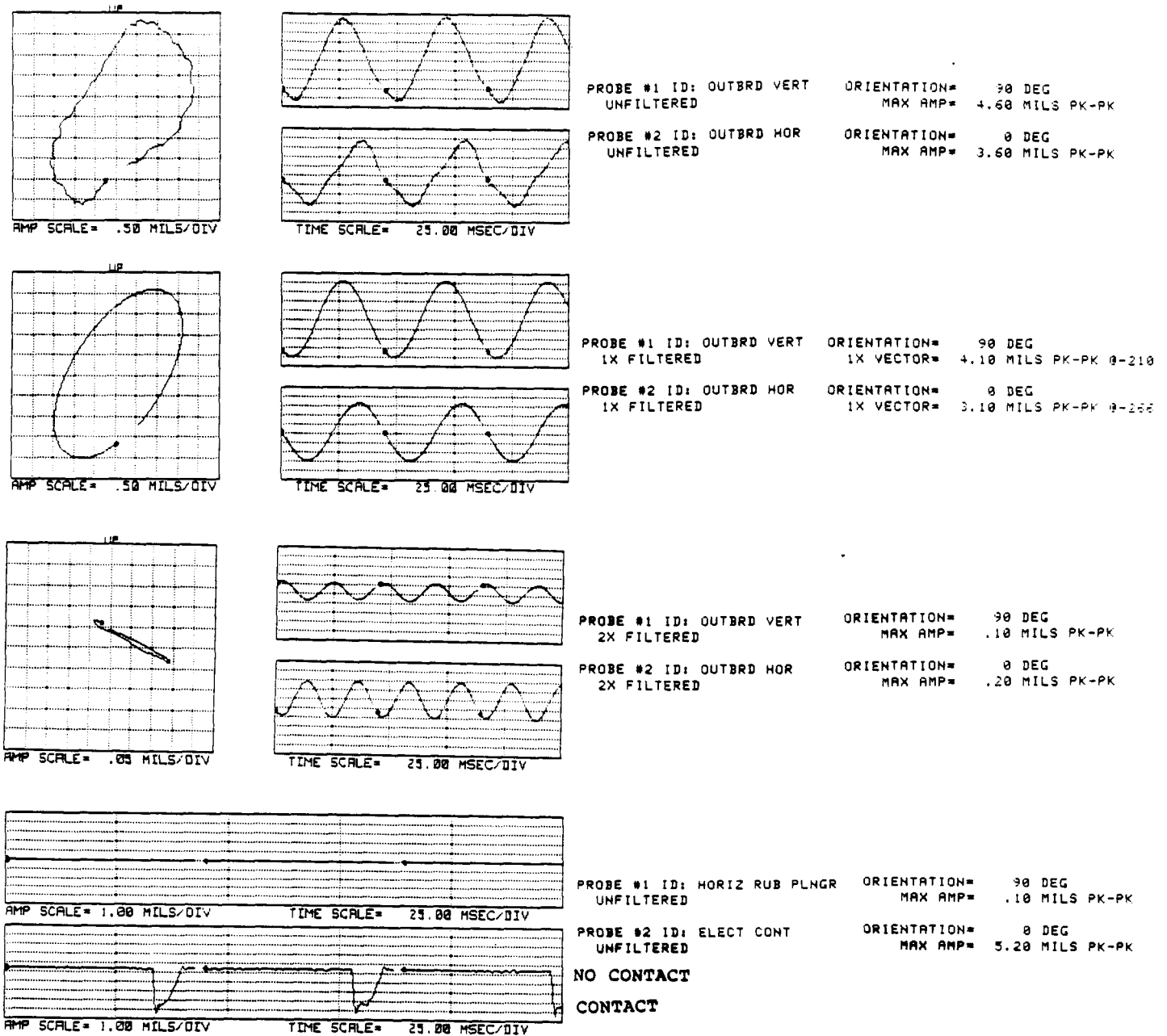
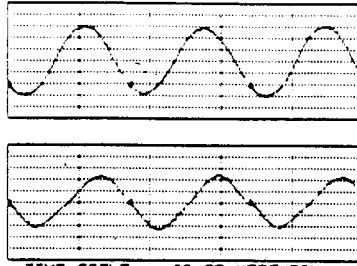
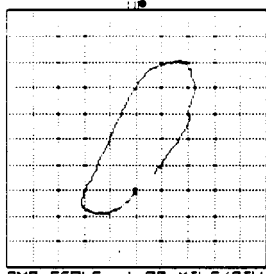


FIGURE 13.89

RUBBING ROTOR VIBRATIONAL RESPONSE AT 1345 RPM.  
UNFILTERED, 1X FILTERED AND 2X FILTERED SIGNALS.  
TIME BASE OF THE PLUNGER MOTION AND  
ROTOR-TO-STATOR CONTACT TIME (BOTTOM)

ROTATION: CW  
 RPM(START)= 1404 RPM(END)= 1407

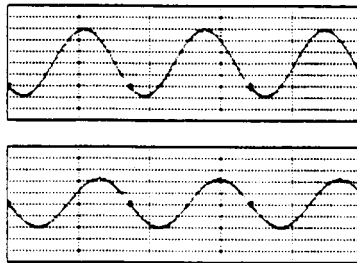
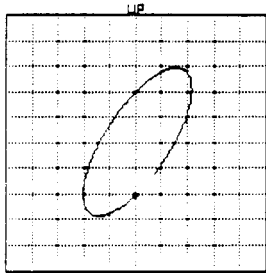


PROBE #1 ID: OUTBRD VERT  
 UNFILTERED

ORIENTATION= 90 DEG  
 MAX AMP= 6.00 MILS PK-PK

PROBE #2 ID: OUTBRD HOR  
 UNFILTERED

ORIENTATION= 0 DEG  
 MAX AMP= 4.80 MILS PK-PK

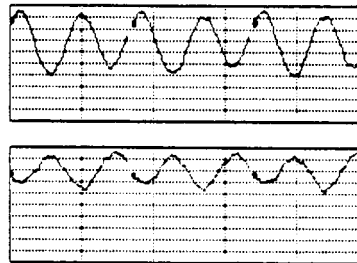
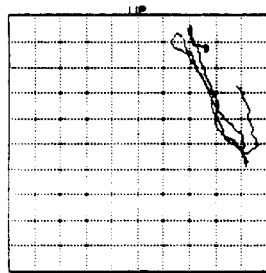


PROBE #1 ID: OUTBRD VERT  
 1X FILTERED

ORIENTATION= 90 DEG  
 1X VECTOR= 5.30 MILS PK-PK @-219

PROBE #2 ID: OUTBRD HOR  
 1X FILTERED

ORIENTATION= 0 DEG  
 1X VECTOR= 4.20 MILS PK-PK @-262

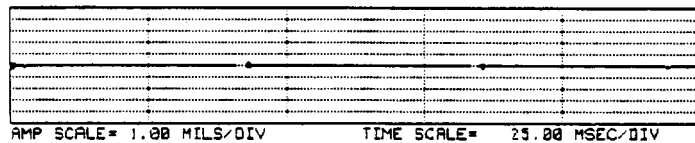


PROBE #1 ID: OUTBRD VERT  
 2X FILTERED

ORIENTATION= 90 DEG  
 MAX AMP= .11 MILS PK-PK

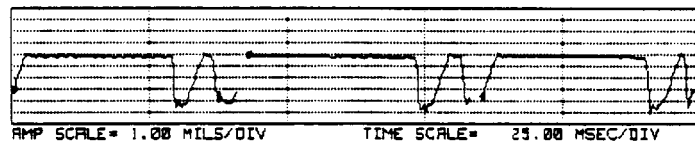
PROBE #2 ID: OUTBRD HOR  
 2X FILTERED

ORIENTATION= 0 DEG  
 MAX AMP= .07 MILS PK-PK



PROBE #1 ID: HORIZ RUB PLNGR  
 UNFILTERED

ORIENTATION= 90 DEG  
 MAX AMP= .10 MILS PK-PK



PROBE #2 ID: ELECT CONT  
 UNFILTERED

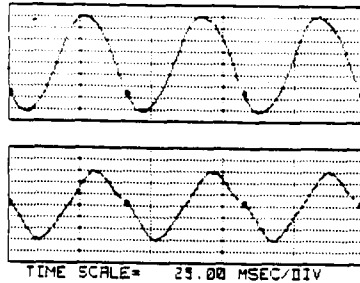
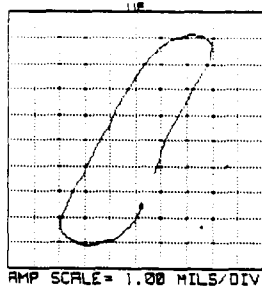
ORIENTATION= 0 DEG  
 MAX AMP= 5.30 MILS PK-PK

NO CONTACT  
 CONTACT

FIGURE 13.90

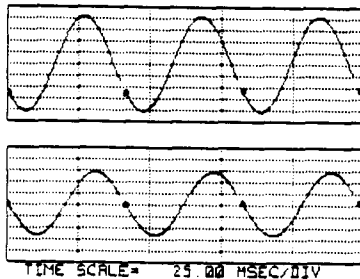
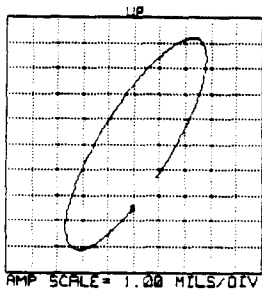
RUBBING ROTOR VIBRATIONAL RESPONSE AT 1404 RPM.  
 UNFILTERED, 1X FILTERED AND 2X FILTERED SIGNALS.  
 TIME BASE OF THE PLUNGER MOTION AND  
 ROTOR-TO-STATOR CONTACT TIME (BOTTOM)

ROTATION: CW  
 RPM(START)= 1456 RPM(END)= 1454



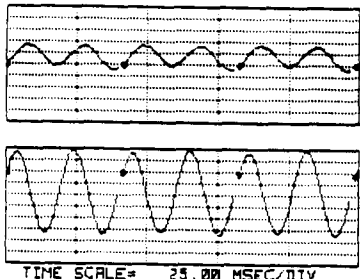
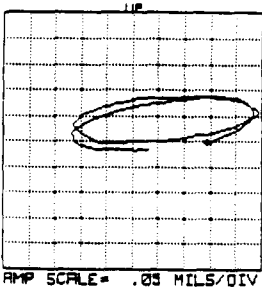
PROBE #1 ID: OUTBRD VERT  
 UNFILTERED  
 PROBE #2 ID: OUTBRD HOR  
 UNFILTERED

ORIENTATION= 90 DEG  
 MAX AMP= 8.30 MILS PK-PK  
 ORIENTATION= 0 DEG  
 MAX AMP= 6.10 MILS PK-PK



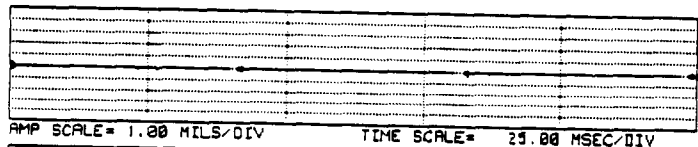
PROBE #1 ID: OUTBRD VERT  
 1X FILTERED  
 PROBE #2 ID: OUTBRD HOR  
 1X FILTERED

ORIENTATION= 90 DEG  
 1X VECTOR= 8.30 MILS PK-PK @-229  
 ORIENTATION= 0 DEG  
 1X VECTOR= 5.50 MILS PK-PK @-165



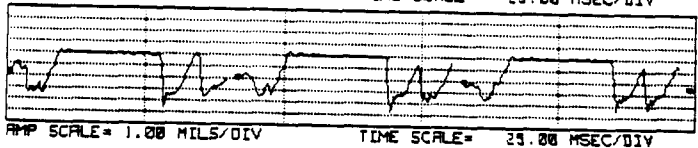
PROBE #1 ID: OUTBRD VERT  
 2X FILTERED  
 PROBE #2 ID: OUTBRD HOR  
 2X FILTERED

ORIENTATION= 90 DEG  
 MAX AMP= .11 MILS PK-PK  
 ORIENTATION= 0 DEG  
 MAX AMP= .37 MILS PK-PK



PROBE #1 ID: HORIZ RUB PLNGR  
 UNFILTERED  
 PROBE #2 ID: ELECT CONT  
 UNFILTERED

ORIENTATION= 90 DEG  
 MAX AMP= .10 MILS PK-PK  
 ORIENTATION= 0 DEG  
 MAX AMP= 5.10 MILS PK-PK

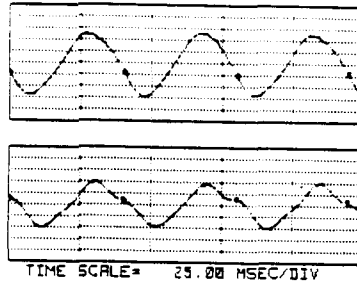
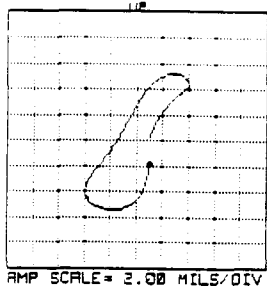


NO CONTACT  
 CONTACT

FIGURE 13.91

RUBBING ROTOR VIBRATIONAL RESPONSE AT 1456 RPM.  
 UNFILTERED, 1X FILTERED AND 2X FILTERED SIGNALS.  
 TIME BASE OF THE PLUNGER MOTION AND  
 ROTOR-TO-STATOR CONTACT TIME (BOTTOM). NOTE THE  
 THE 2X ORBIT IS REVERSE.

ROTATION: CW  
 RPM(START)= 1500 RPM(END)= 1498

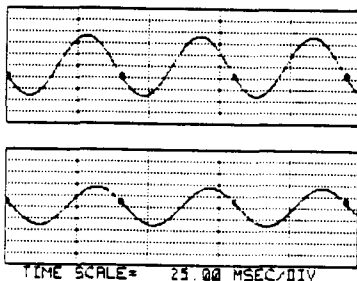
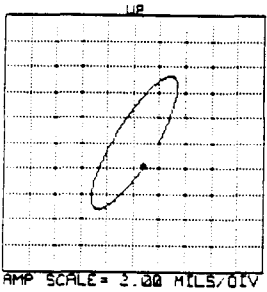


PROBE #1 ID: OUTBRD VERT  
 UNFILTERED

ORIENTATION= 90 DEG  
 MAX AMP= 11.00 MILS PK-PK

PROBE #2 ID: OUTBRD HOR  
 UNFILTERED

ORIENTATION= 0 DEG  
 MAX AMP= 3.10 MILS PK-PK

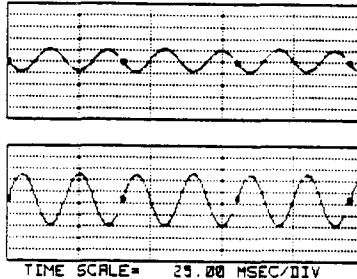
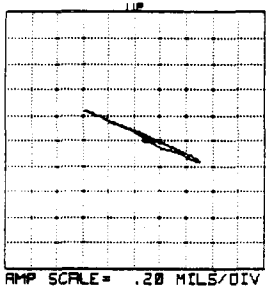


PROBE #1 ID: OUTBRD VERT  
 1X FILTERED

ORIENTATION= 90 DEG  
 1X VECTOR= 10.40 MILS PK-PK @-243

PROBE #2 ID: OUTBRD HOR  
 1X FILTERED

ORIENTATION= 0 DEG  
 1X VECTOR= 5.60 MILS PK-PK @-276

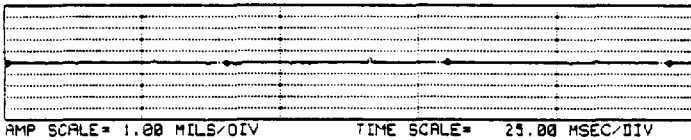


PROBE #1 ID: OUTBRD VERT  
 2X FILTERED

ORIENTATION= 90 DEG  
 MAX AMP= .40 MILS PK-PK

PROBE #2 ID: OUTBRD HOR  
 2X FILTERED

ORIENTATION= 0 DEG  
 MAX AMP= .90 MILS PK-PK

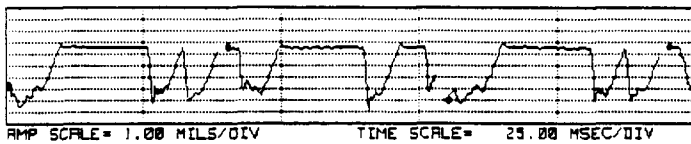


PROBE #1 ID: HORIZ RUB PLNGR  
 UNFILTERED

ORIENTATION= 90 DEG  
 MAX AMP= .50 MILS PK-PK

PROBE #2 ID: ELECT CONT  
 UNFILTERED

ORIENTATION= 0 DEG  
 MAX AMP= 5.90 MILS PK-PK



NO CONTACT

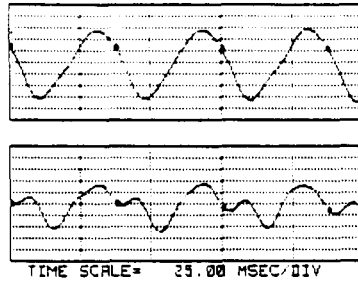
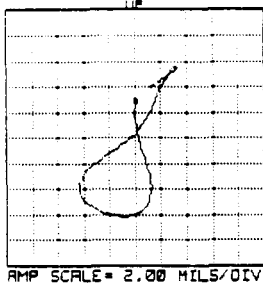
CONTACT

FIGURE 13.92

RUBBING ROTOR VIBRATIONAL RESPONSE AT 1500 RPM.  
 UNFILTERED, 1X FILTERED AND 2X FILTERED SIGNALS.  
 TIME BASE OF THE PLUNGER MOTION AND  
 ROTOR-TO-STATOR CONTACT TIME (BOTTOM).

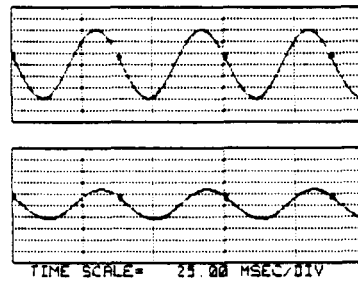
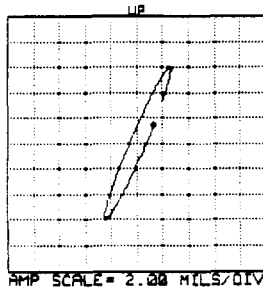
ORIGINAL PAGE IS  
OF POOR QUALITY

ROTATION: CW  
RPM(START)= 1593 RPM(END)= 1593



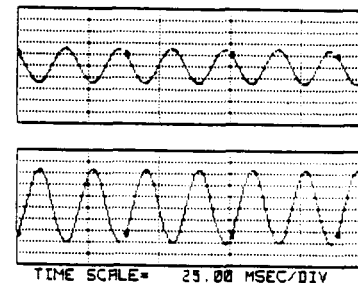
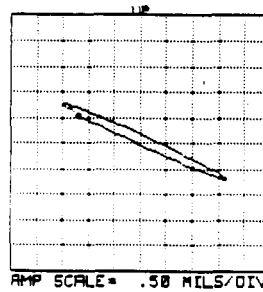
PROBE #1 ID: OUTBRD VERT  
UNFILTERED  
PROBE #2 ID: OUTBRD HOR  
UNFILTERED

ORIENTATION = 90 DEG  
MAX AMP = 12.70 MILS PK-PK  
ORIENTATION = 0 DEG  
MAX AMP = 3.40 MILS PK-PK



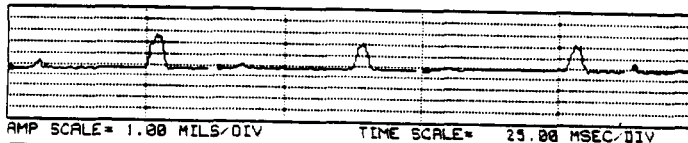
PROBE #1 ID: OUTBRD VERT  
1X FILTERED  
PROBE #2 ID: OUTBRD HOR  
1X FILTERED

ORIENTATION = 90 DEG  
1X VECTOR = 11.90 MILS PK-PK @-278  
ORIENTATION = 0 DEG  
1X VECTOR = 5.20 MILS PK-PK @-292



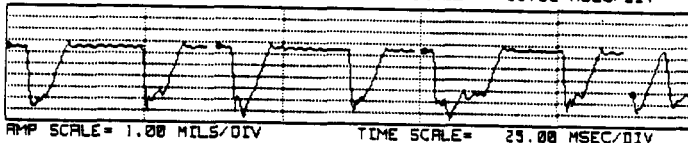
PROBE #1 ID: OUTBRD VERT  
2X FILTERED  
PROBE #2 ID: OUTBRD HOR  
2X FILTERED

ORIENTATION = 90 DEG  
MAX AMP = 1.50 MILS PK-PK  
ORIENTATION = 0 DEG  
MAX AMP = 2.20 MILS PK-PK



PROBE #1 ID: HORIZ RUB PLNGR  
UNFILTERED

ORIENTATION = 90 DEG  
MAX AMP = 3.20 MILS PK-PK



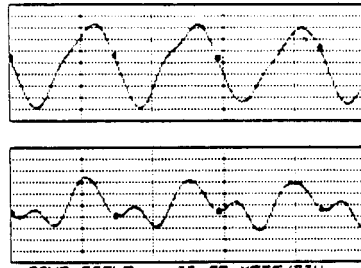
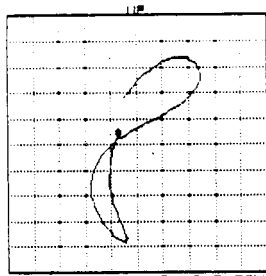
PROBE #2 ID: ELECT CONT  
UNFILTERED  
NO CONTACT  
CONTACT

ORIENTATION = 0 DEG  
MAX AMP = 6.40 MILS PK-PK

FIGURE 13.93

RUBBING ROTOR VIBRATIONAL RESPONSE AT 1593 RPM.  
UNFILTERED, 1X FILTERED AND 2X FILTERED SIGNALS.  
TIME BASE OF THE PLUNGER MOTION AND  
ROTOR-TO-STATOR CONTACT TIME (BOTTOM). NOTE  
THAT THE 2X ORBIT IS REVERSE.

ROTATION: CW  
 RPM(START)= 1646 RPM(END)= 1650

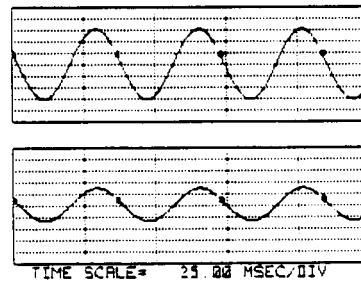
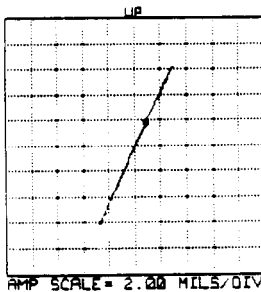


PROBE #1 ID: OUTBRD VERT  
 UNFILTERED

ORIENTATION= 90 DEG  
 MAX AMP= 14.40 MILS PK-PK

PROBE #2 ID: OUTBRD HOR  
 UNFILTERED

ORIENTATION= 0 DEG  
 MAX AMP= 9.30 MILS PK-PK

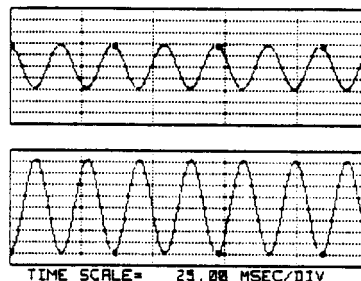
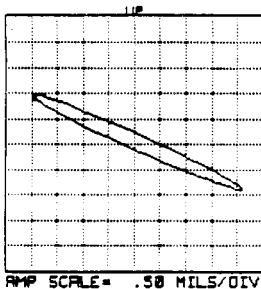


PROBE #1 ID: OUTBRD VERT  
 1X FILTERED

ORIENTATION= 90 DEG  
 1X VECTOR= 12.30 MILS PK-PK @-292

PROBE #2 ID: OUTBRD HOR  
 1X FILTERED

ORIENTATION= 0 DEG  
 1X VECTOR= 5.70 MILS PK-PK @-283

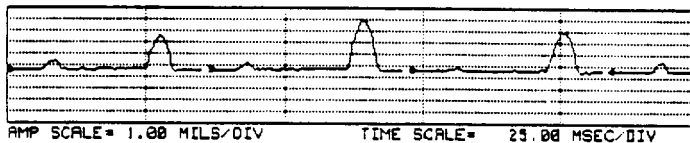


PROBE #1 ID: OUTBRD VERT  
 2X FILTERED

ORIENTATION= 90 DEG  
 MAX AMP= 1.90 MILS PK-PK

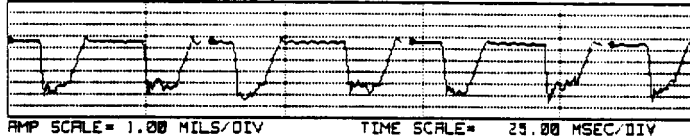
PROBE #2 ID: OUTBRD HOR  
 2X FILTERED

ORIENTATION= 0 DEG  
 MAX AMP= 4.10 MILS PK-PK



PROBE #1 ID: HORIZ RUB PLNGR  
 UNFILTERED

ORIENTATION= 90 DEG  
 MAX AMP= 4.50 MILS PK-PK



PROBE #2 ID: ELECT CONT  
 UNFILTERED

ORIENTATION= 0 DEG  
 MAX AMP= 5.50 MILS PK-PK

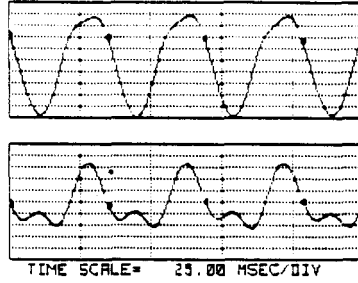
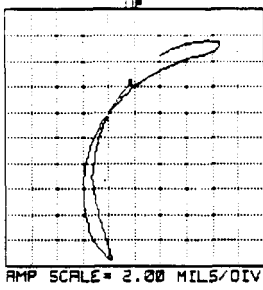
NO CONTACT  
 CONTACT

FIGURE 13.94

RUBBING ROTOR VIBRATIONAL RESPONSE AT 1646 RPM.  
 UNFILTERED, 1X FILTERED AND 2X FILTERED SIGNALS.  
 TIME BASE OF THE PLUNGER MOTION AND  
 ROTOR-TO-STATOR CONTACT TIME (BOTTOM)

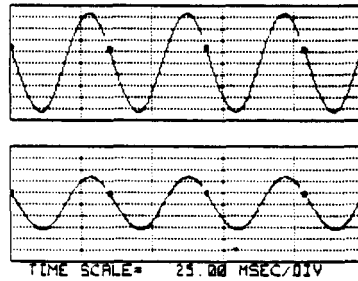
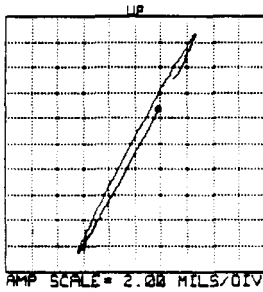
ROTATION: CW  
 RPM(START)= 1736 RPM(END)= 1736

ORIGINAL PAGE IS  
 OF POOR QUALITY



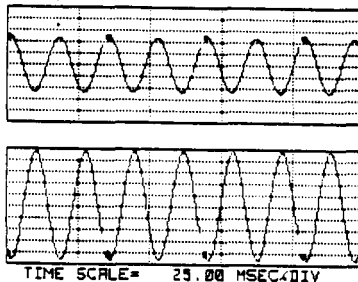
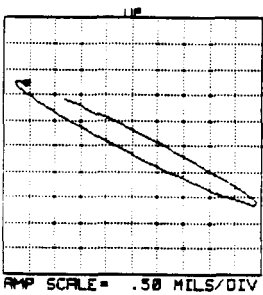
PROBE #1 ID: OUTBRD VERT  
 UNFILTERED  
 PROBE #2 ID: OUTBRD HOR  
 UNFILTERED

ORIENTATION= 90 DEG  
 MAX AMP= 17.70 MILS PK-PK  
 ORIENTATION= 0 DEG  
 MAX AMP= 11.30 MILS PK-PK



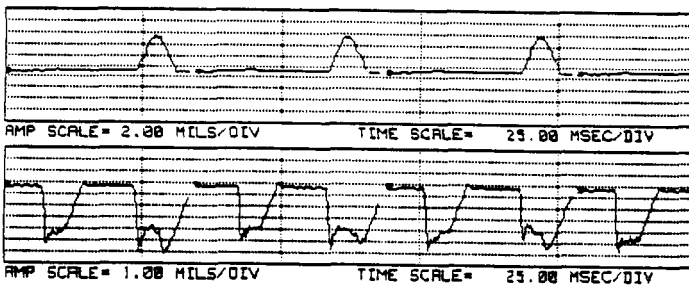
PROBE #1 ID: OUTBRD VERT  
 1X FILTERED  
 PROBE #2 ID: OUTBRD HOR  
 1X FILTERED

ORIENTATION= 90 DEG  
 1X VECTOR= 17.10 MILS PK-PK @-291  
 ORIENTATION= 0 DEG  
 1X VECTOR= 9.10 MILS PK-PK @-286



PROBE #1 ID: OUTBRD VERT  
 2X FILTERED  
 PROBE #2 ID: OUTBRD HOR  
 2X FILTERED

ORIENTATION= 90 DEG  
 MAX AMP= 2.40 MILS PK-PK  
 ORIENTATION= 0 DEG  
 MAX AMP= 4.70 MILS PK-PK



PROBE #1 ID: HORIZ RUB PLNGR  
 UNFILTERED  
 PROBE #2 ID: ELECT CONT  
 UNFILTERED  
 NO CONTACT  
 CONTACT

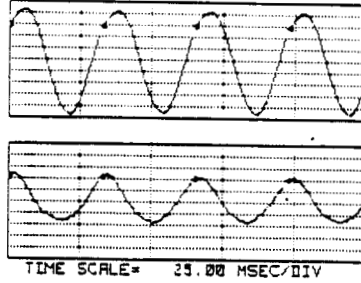
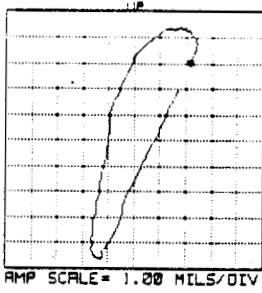
ORIENTATION= 90 DEG  
 MAX AMP= 7.00 MILS PK-PK  
 ORIENTATION= 0 DEG  
 MAX AMP= 6.20 MILS PK-PK

FIGURE 13.95

RUBBING ROTOR VIBRATIONAL RESPONSE AT 1736 RPM.  
 UNFILTERED, 1X FILTERED AND 2X FILTERED SIGNALS.  
 TIME BASE OF THE PLUNGER MOTION AND  
 ROTOR-TO-STATOR CONTACT TIME (BOTTOM)

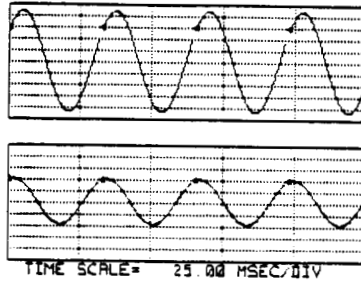
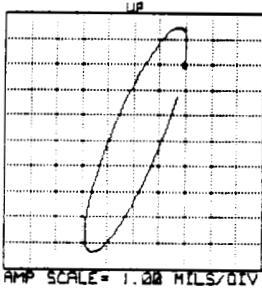
ORIGINAL PAGE IS  
OF POOR QUALITY

ROTATION: CW  
RPM(START)= 1834 RPM(END)= 1835



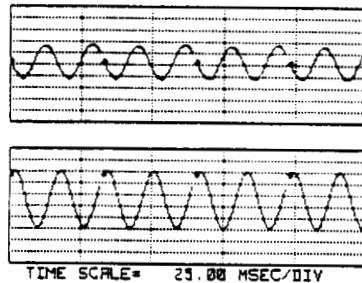
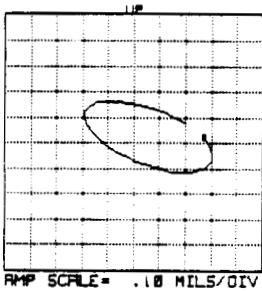
PROBE #1 ID: OUTBRD VERT  
UNFILTERED  
PROBE #2 ID: OUTBRD HOR  
UNFILTERED

ORIENTATION = 90 DEG  
MAX AMP = 3.00 MILS PK-PK  
ORIENTATION = 0 DEG  
MAX AMP = 4.20 MILS PK-PK



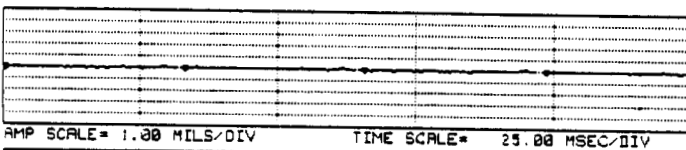
PROBE #1 ID: OUTBRD VERT  
1X FILTERED  
PROBE #2 ID: OUTBRD HOR  
1X FILTERED

ORIENTATION = 90 DEG  
1X VECTOR = 3.00 MILS PK-PK 0-43  
ORIENTATION = 0 DEG  
1X VECTOR = 3.90 MILS PK-PK 0-11



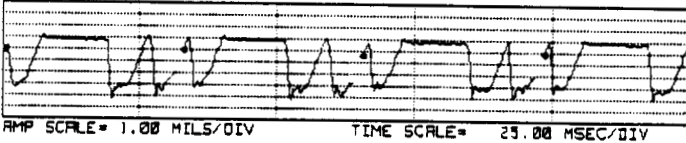
PROBE #1 ID: OUTBRD VERT  
2X FILTERED  
PROBE #2 ID: OUTBRD HOR  
2X FILTERED

ORIENTATION = 90 DEG  
MAX AMP = .30 MILS PK-PK  
ORIENTATION = 0 DEG  
MAX AMP = .50 MILS PK-PK



PROBE #1 ID: HORIZ RUB PLNGR  
UNFILTERED

ORIENTATION = 90 DEG  
MAX AMP = .30 MILS PK-PK



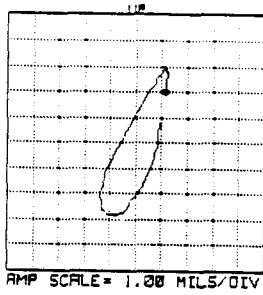
PROBE #2 ID: ELECT CONT  
UNFILTERED  
NO CONTACT  
CONTACT

ORIENTATION = 0 DEG  
MAX AMP = 5.50 MILS PK-PK

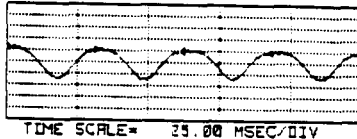
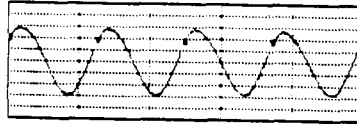
FIGURE 13.96

RUBBING ROTOR VIBRATIONAL RESPONSE AT 1834 RPM.  
UNFILTERED, 1X FILTERED AND 2X FILTERED SIGNALS.  
TIME BASE OF THE PLUNGER MOTION AND  
ROTOR-TO-STATOR CONTACT TIME (BOTTOM). NOTE  
THAT THE 2X ORBIT IS REVERSE.

ROTATION: CW  
 RPM(START)= 1933 RPM(END)= 1938



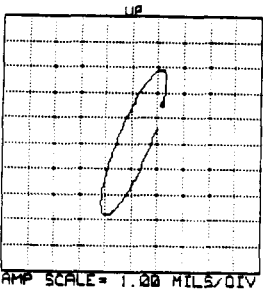
AMP SCALE= 1.00 MILS/DIV



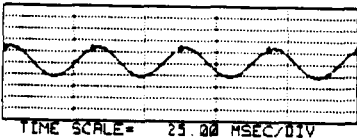
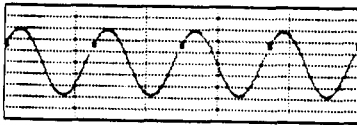
TIME SCALE= 25.00 MSEC/DIV

PROBE #1 ID: OUTBRD VERT  
 UNFILTERED  
 PROBE #2 ID: OUTBRD HOR  
 UNFILTERED

ORIENTATION= 90 DEG  
 MAX AMP= 5.80 MILS PK-PK  
 ORIENTATION= 0 DEG  
 MAX AMP= 2.70 MILS PK-PK



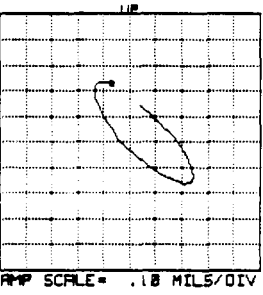
AMP SCALE= 1.00 MILS/DIV



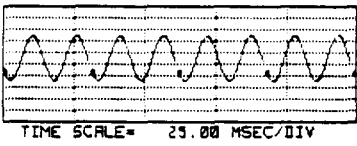
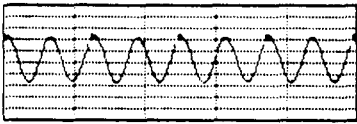
TIME SCALE= 25.00 MSEC/DIV

PROBE #1 ID: OUTBRD VERT  
 1X FILTERED  
 PROBE #2 ID: OUTBRD HOR  
 1X FILTERED

ORIENTATION= 90 DEG  
 1X VECTOR= 5.70 MILS PK-PK @-51  
 ORIENTATION= 0 DEG  
 1X VECTOR= 2.50 MILS PK-PK @-13



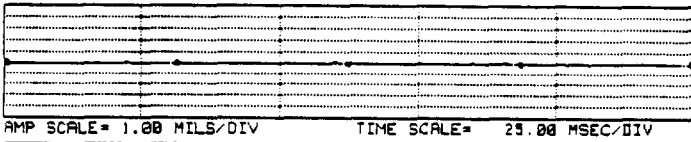
AMP SCALE= .10 MILS/DIV



TIME SCALE= 25.00 MSEC/DIV

PROBE #1 ID: OUTBRD VERT  
 2X FILTERED  
 PROBE #2 ID: OUTBRD HOR  
 2X FILTERED

ORIENTATION= 90 DEG  
 MAX AMP= .40 MILS PK-PK  
 ORIENTATION= 0 DEG  
 MAX AMP= .40 MILS PK-PK

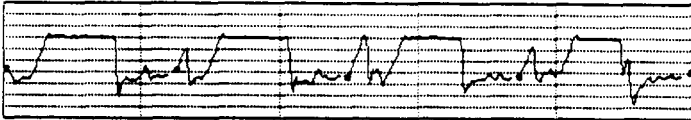


AMP SCALE= 1.00 MILS/DIV

TIME SCALE= 25.00 MSEC/DIV

PROBE #1 ID: HORIZ RUB PLNGR  
 UNFILTERED

ORIENTATION= 90 DEG  
 MAX AMP= .20 MILS PK-PK



AMP SCALE= 1.00 MILS/DIV

TIME SCALE= 25.00 MSEC/DIV

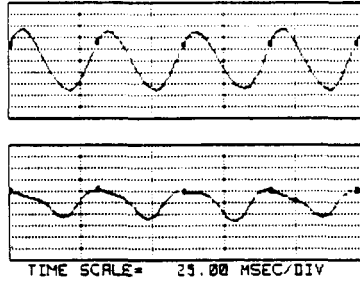
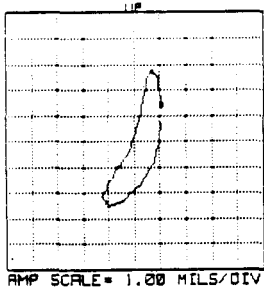
PROBE #2 ID: ELECT CONT  
 UNFILTERED  
 NO CONTACT  
 CONTACT

ORIENTATION= 0 DEG  
 MAX AMP= 6.00 MILS PK-PK

FIGURE 13.97

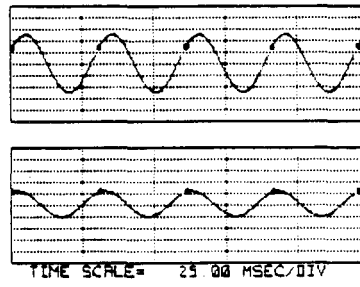
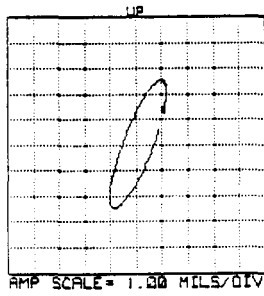
RUBBING ROTOR VIBRATIONAL RESPONSE AT 1933 RPM. UNFILTERED, 1X FILTERED AND 2X FILTERED SIGNALS. TIME BASE OF THE PLUNGER MOTION AND ROTOR-TO-STATOR CONTACT TIME (BOTTOM). NOTE THAT THE 2X ORBIT IS REVERSE.

ROTATION: CW  
 RPM(START)= 1975 RPM(END)= 1974



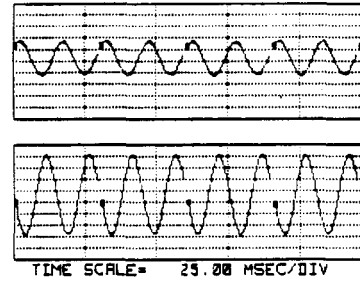
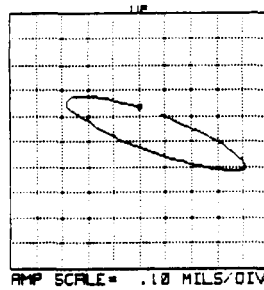
PROBE #1 ID: OUTBRD VERT  
 UNFILTERED  
 PROBE #2 ID: OUTBRD HOR  
 UNFILTERED

ORIENTATION= 90 DEG  
 MAX AMP= 5.30 MILS PK-PK  
 ORIENTATION= 0 DEG  
 MAX AMP= 2.80 MILS PK-PK



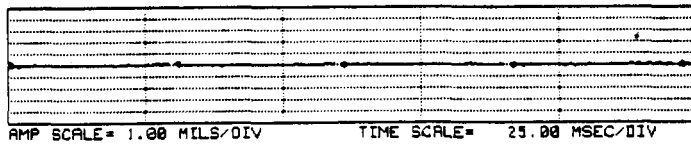
PROBE #1 ID: OUTBRD VERT  
 1X FILTERED  
 PROBE #2 ID: OUTBRD HOR  
 1X FILTERED

ORIENTATION= 90 DEG  
 1X VECTOR= 5.00 MILS PK-PK 3-50  
 ORIENTATION= 0 DEG  
 1X VECTOR= 2.20 MILS PK-PK 9-17



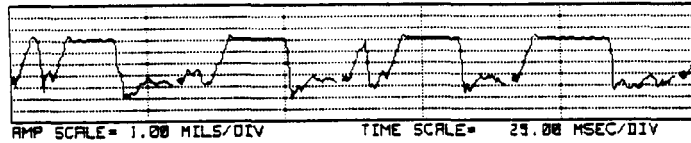
PROBE #1 ID: OUTBRD VERT  
 2X FILTERED  
 PROBE #2 ID: OUTBRD HOR  
 2X FILTERED

ORIENTATION= 90 DEG  
 MAX AMP= .30 MILS PK-PK  
 ORIENTATION= 0 DEG  
 MAX AMP= .70 MILS PK-PK



PROBE #1 ID: HORIZ RUB PLNGR  
 UNFILTERED

ORIENTATION= 90 DEG  
 MAX AMP= .30 MILS PK-PK



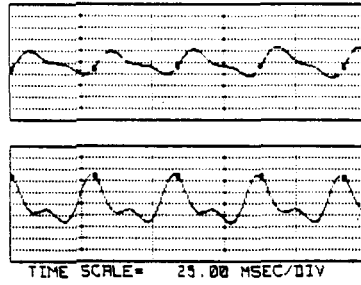
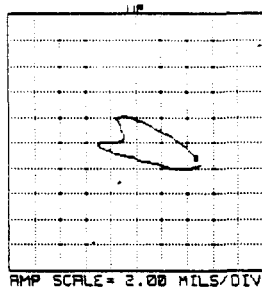
PROBE #2 ID: ELECT CONT  
 UNFILTERED  
 NO CONTACT  
 CONTACT

ORIENTATION= 0 DEG  
 MAX AMP= 5.50 MILS PK-PK

FIGURE 13.98

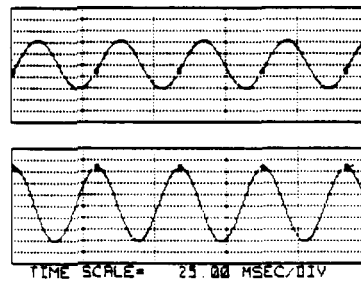
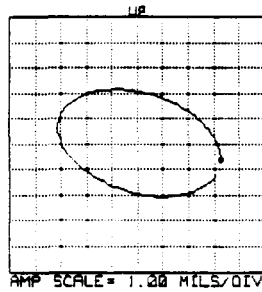
RUBBING ROTOR VIBRATIONAL RESPONSE AT 1975 RPM. UNFILTERED, 1X FILTERED AND 2X FILTERED SIGNALS. TIME BASE OF THE PLUNGER MOTION AND ROTOR-TO-STATOR CONTACT TIME (BOTTOM). NOTE THAT THE 2X ORBIT IS REVERSE.

ROTATION: CW  
 RPM(START)= 2059 RPM(END)= 2052



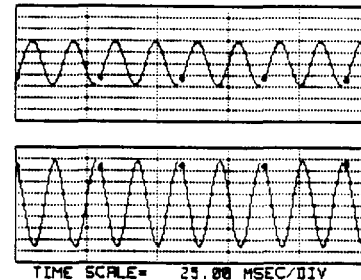
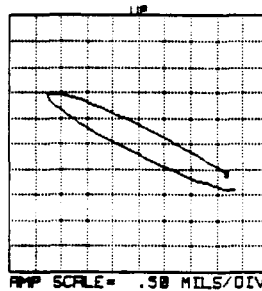
PROBE #1 ID: OUTBRD VERT  
 UNFILTERED  
 PROBE #2 ID: OUTBRD HOR  
 UNFILTERED

ORIENTATION= 90 DEG  
 MAX AMP= 5.40 MILS PK-PK  
 ORIENTATION= 0 DEG  
 MAX AMP= 3.40 MILS PK-PK



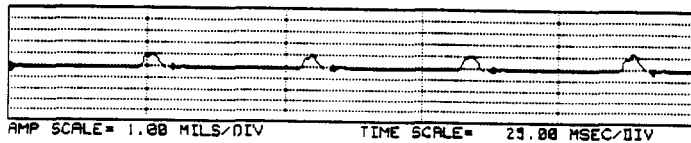
PROBE #1 ID: OUTBRD VERT  
 1X FILTERED  
 PROBE #2 ID: OUTBRD HOR  
 1X FILTERED

ORIENTATION= 90 DEG  
 1X VECTOR= 4.20 MILS PK-PK @-101  
 ORIENTATION= 0 DEG  
 1X VECTOR= 6.40 MILS PK-PK @-355



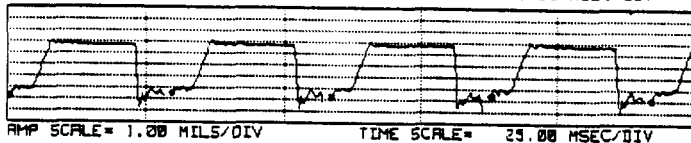
PROBE #1 ID: OUTBRD VERT  
 2X FILTERED  
 PROBE #2 ID: OUTBRD HOR  
 2X FILTERED

ORIENTATION= 90 DEG  
 MAX AMP= 1.90 MILS PK-PK  
 ORIENTATION= 0 DEG  
 MAX AMP= 3.70 MILS PK-PK



PROBE #1 ID: HORIZ RUB PLNGR  
 UNFILTERED

ORIENTATION= 90 DEG  
 MAX AMP= 1.50 MILS PK-PK



PROBE #2 ID: ELECT CONT  
 UNFILTERED

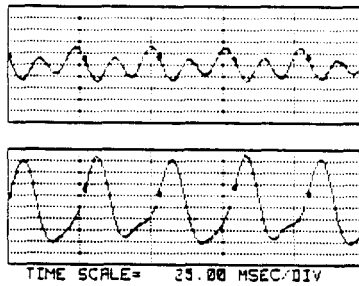
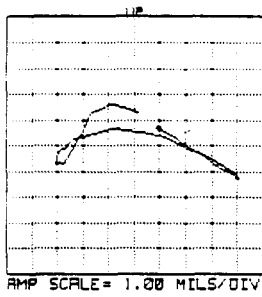
ORIENTATION= 0 DEG  
 MAX AMP= 6.10 MILS PK-PK

NO CONTACT  
 CONTACT

FIGURE 13.99

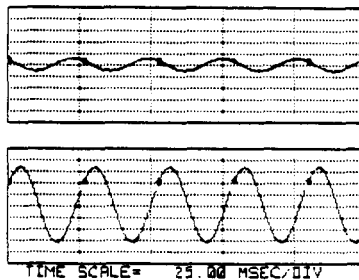
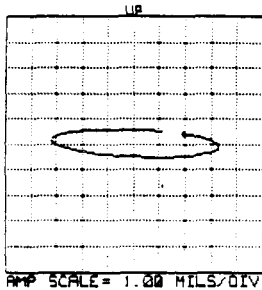
RUBBING ROTOR VIBRATIONAL RESPONSE AT 2059 RPM.  
 UNFILTERED, 1X FILTERED AND 2X FILTERED SIGNALS.  
 TIME BASE OF THE PLUNGER MOTION AND  
 ROTOR-TO-STATOR CONTACT TIME (BOTTOM). NOTE  
 THAT THE 2X ORBIT IS REVERSE.

ROTATION: CW  
 RPM(START)= 2292 RPM(END)= 2291



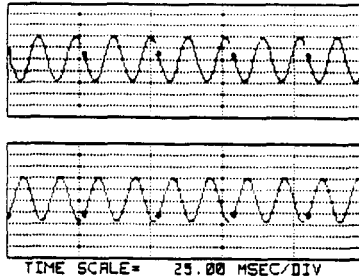
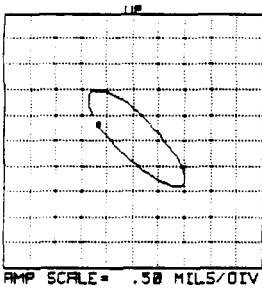
PROBE #1 ID: OUTBRD VERT  
 UNFILTERED  
 PROBE #2 ID: OUTBRD HOR  
 UNFILTERED

ORIENTATION= 90 DEG  
 MAX AMP= 3.00 MILS PK-PK  
 ORIENTATION= 0 DEG  
 MAX AMP= 7.70 MILS PK-PK



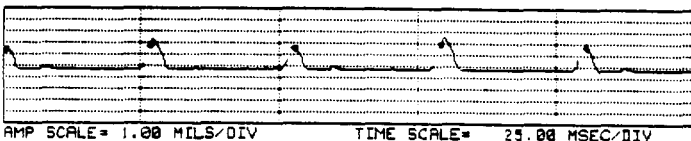
PROBE #1 ID: OUTBRD VERT  
 1X FILTERED  
 PROBE #2 ID: OUTBRD HOR  
 1X FILTERED

ORIENTATION= 90 DEG  
 1X VECTOR= 1.10 MILS PK-PK @-300  
 ORIENTATION= 0 DEG  
 1X VECTOR= 6.50 MILS PK-PK @-47



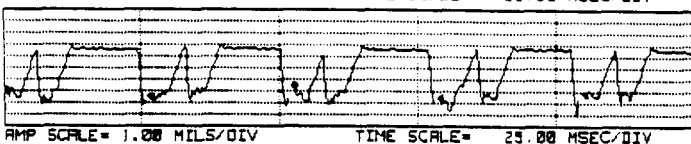
PROBE #1 ID: OUTBRD VERT  
 2X FILTERED  
 PROBE #2 ID: OUTBRD HOR  
 2X FILTERED

ORIENTATION= 90 DEG  
 MAX AMP= 1.90 MILS PK-PK  
 ORIENTATION= 0 DEG  
 MAX AMP= 1.90 MILS PK-PK



PROBE #1 ID: HORIZ RUB PLNGR  
 UNFILTERED

ORIENTATION= 90 DEG  
 MAX AMP= 2.90 MILS PK-PK



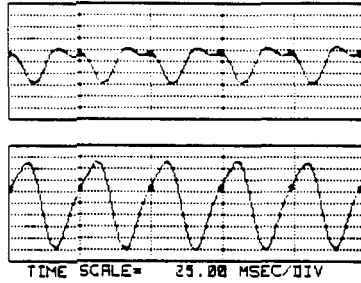
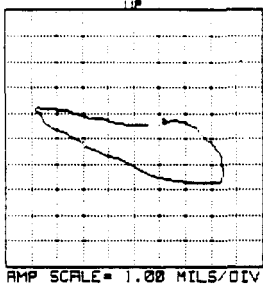
PROBE #2 ID: ELECT CONT  
 UNFILTERED  
 NO CONTACT

ORIENTATION= 0 DEG  
 MAX AMP= 6.00 MILS PK-PK

CONTACT

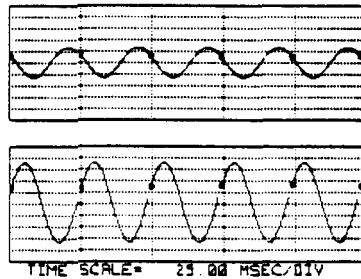
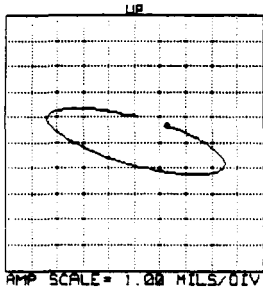
FIGURE 13.100 RUBBING ROTOR VIBRATIONAL RESPONSE AT 2292 RPM. UNFILTERED, 1X FILTERED AND 2X FILTERED SIGNALS. TIME BASE OF THE PLUNGER MOTION AND ROTOR-TO-STATOR CONTACT TIME (BOTTOM). NOTE THAT THE 2X ORBIT IS REVERSE.

ROTATION: CW  
 RPM(START)= 2442 RPM(END)= 2443



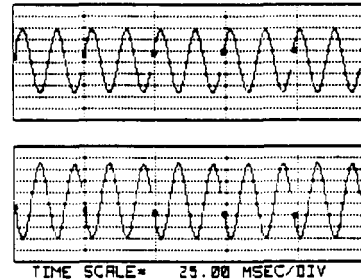
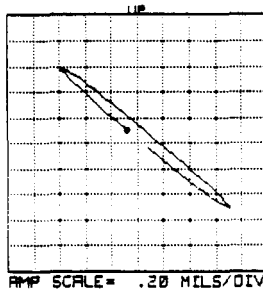
PROBE #1 ID: OUTBRD VERT  
 UNFILTERED  
 PROBE #2 ID: OUTBRD HOR  
 UNFILTERED

ORIENTATION= 90 DEG  
 MAX AMP= 3.20 MILS PK-PK  
 ORIENTATION= 0 DEG  
 MAX AMP= 7.60 MILS PK-PK



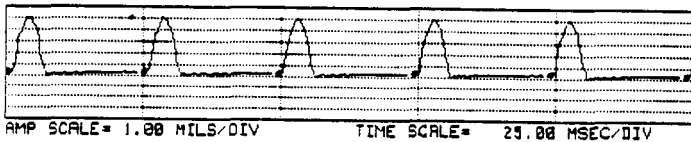
PROBE #1 ID: OUTBRD VERT  
 1X FILTERED  
 PROBE #2 ID: OUTBRD HOR  
 1X FILTERED

ORIENTATION= 90 DEG  
 1X VECTOR= 2.60 MILS PK-PK @-290  
 ORIENTATION= 0 DEG  
 1X VECTOR= 6.90 MILS PK-PK @-62



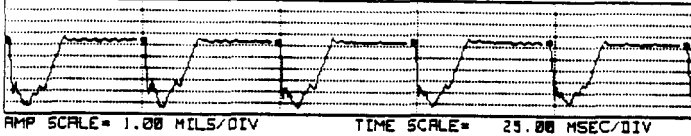
PROBE #1 ID: OUTBRD VERT  
 2X FILTERED  
 PROBE #2 ID: OUTBRD HOR  
 2X FILTERED

ORIENTATION= 90 DEG  
 MAX AMP= 1.10 MILS PK-PK  
 ORIENTATION= 0 DEG  
 MAX AMP= 1.30 MILS PK-PK



PROBE #1 ID: HORIZ RUB PLNGR  
 UNFILTERED

ORIENTATION= 90 DEG  
 MAX AMP= 5.10 MILS PK-PK



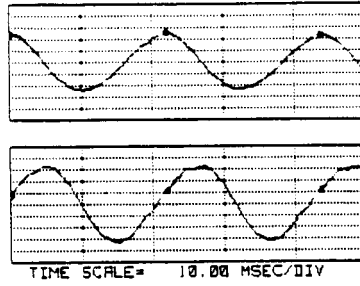
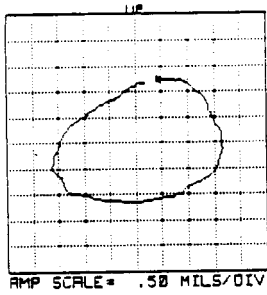
PROBE #2 ID: ELECT CONT  
 UNFILTERED

ORIENTATION= 0 DEG  
 MAX AMP= 6.20 MILS PK-PK

NO CONTACT  
 CONTACT

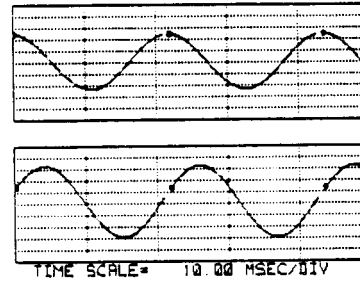
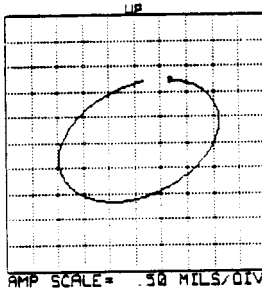
FIGURE 13.101 RUBBING ROTOR VIBRATIONAL RESPONSE AT 2442 RPM. UNFILTERED, 1X FILTERED AND 2X FILTERED SIGNALS. TIME BASE OF THE PLUNGER MOTION AND ROTOR-TO-STATOR CONTACT TIME (BOTTOM). NOTE THAT THE 2X ORBIT IS FORWARD.

ROTATION: CW  
 RPM(START)= 2737 RPM(END)= 2738



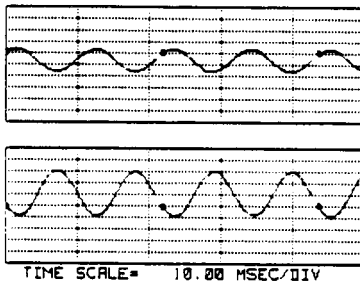
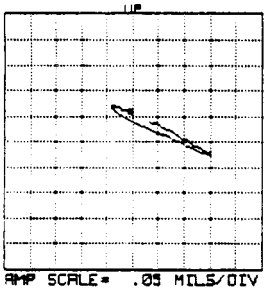
PROBE #1 ID: OUTBRD VERT  
 UNFILTERED  
 PROBE #2 ID: OUTBRD HOR  
 UNFILTERED

ORIENTATION= 90 DEG  
 MAX AMP= 2.50 MILS PK-PK  
 ORIENTATION= 0 DEG  
 MAX AMP= 3.30 MILS PK-PK



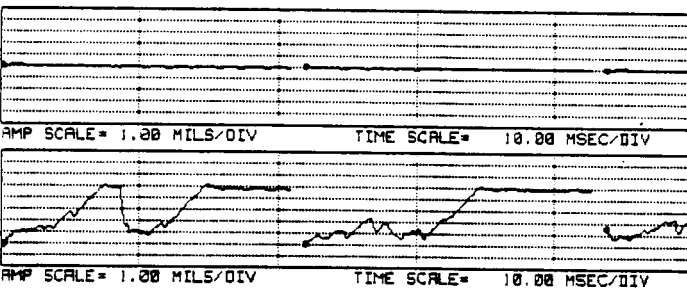
PROBE #1 ID: OUTBRD VERT  
 1X FILTERED  
 PROBE #2 ID: OUTBRD HOR  
 1X FILTERED

ORIENTATION= 90 DEG  
 1X VECTOR= 2.40 MILS PK-PK 0-351  
 ORIENTATION= 0 DEG  
 1X VECTOR= 3.10 MILS PK-PK 0-53



PROBE #1 ID: OUTBRD VERT  
 2X FILTERED  
 PROBE #2 ID: OUTBRD HOR  
 2X FILTERED

ORIENTATION= 90 DEG  
 MAX AMP= .10 MILS PK-PK  
 ORIENTATION= 0 DEG  
 MAX AMP= .20 MILS PK-PK

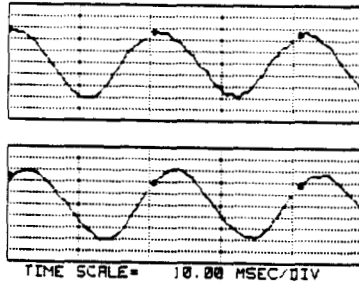
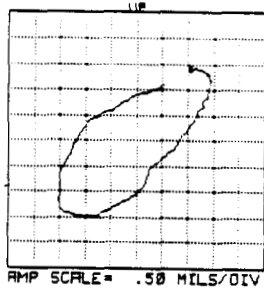


PROBE #1 ID: HORIZ RUB PLNGR  
 UNFILTERED  
 PROBE #2 ID: ELECT CONT  
 UNFILTERED  
 NO CONTACT  
 CONTACT

ORIENTATION= 90 DEG  
 MAX AMP= .30 MILS PK-PK  
 ORIENTATION= 0 DEG  
 MAX AMP= 5.30 MILS PK-PK

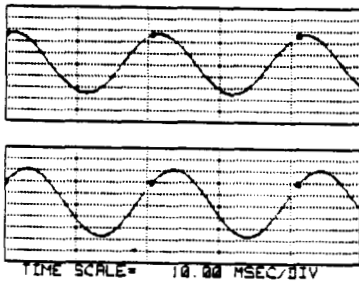
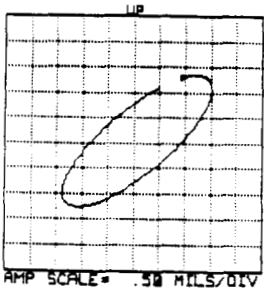
FIGURE 13.102 RUBBING ROTOR VIBRATIONAL RESPONSE AT 2737 RPM. UNFILTERED, 1X FILTERED AND 2X FILTERED SIGNALS. TIME BASE OF THE PLUNGER MOTION AND ROTOR-TO-STATOR CONTACT TIME (BOTTOM). NOTE THAT THE 2X ORBIT IS REVERSE.

ROTATION: CW  
 RPM(START)= 2919 RPM(END)= 2920



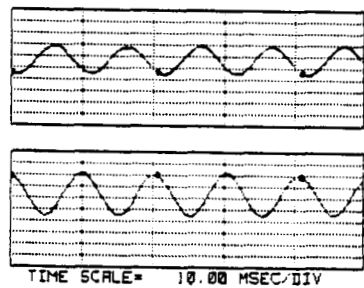
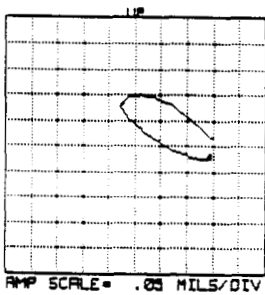
PROBE #1 ID: OUTBRD VERT  
 UNFILTERED  
 PROBE #2 ID: OUTBRD HOR  
 UNFILTERED

ORIENTATION= 90 DEG  
 MAX AMP= 2.90 MILS PK-PK  
 ORIENTATION= 0 DEG  
 MAX AMP= 3.10 MILS PK-PK



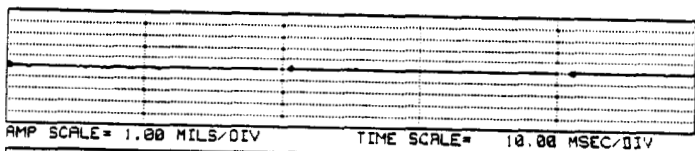
PROBE #1 ID: OUTBRD VERT  
 1X FILTERED  
 PROBE #2 ID: OUTBRD HOR  
 1X FILTERED

ORIENTATION= 90 DEG  
 1X VECTOR= 2.60 MILS PK-PK @-10  
 ORIENTATION= 0 DEG  
 1X VECTOR= 2.90 MILS PK-PK @-48



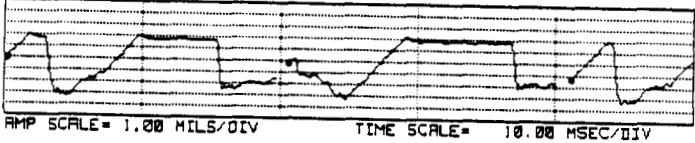
PROBE #1 ID: OUTBRD VERT  
 2X FILTERED  
 PROBE #2 ID: OUTBRD HOR  
 2X FILTERED

ORIENTATION= 90 DEG  
 MAX AMP= .13 MILS PK-PK  
 ORIENTATION= 0 DEG  
 MAX AMP= .19 MILS PK-PK



PROBE #1 ID: HORIZ RUB PLNGR  
 UNFILTERED

ORIENTATION= 90 DEG  
 MAX AMP= .20 MILS PK-PK



PROBE #2 ID: ELECT CONT  
 UNFILTERED  
 NO CONTACT  
 CONTACT

ORIENTATION= 0 DEG  
 MAX AMP= 5.50 MILS PK-PK

FIGURE 13.103 RUBBING ROTOR VIBRATIONAL RESPONSE AT 2919 RPM. UNFILTERED, 1X FILTERED AND 2X FILTERED SIGNALS. TIME BASE OF THE PLUNGER MOTION AND ROTOR-TO-STATOR CONTACT TIME (BOTTOM). NOTE THAT THE 2X ORBIT IS FORWARD.

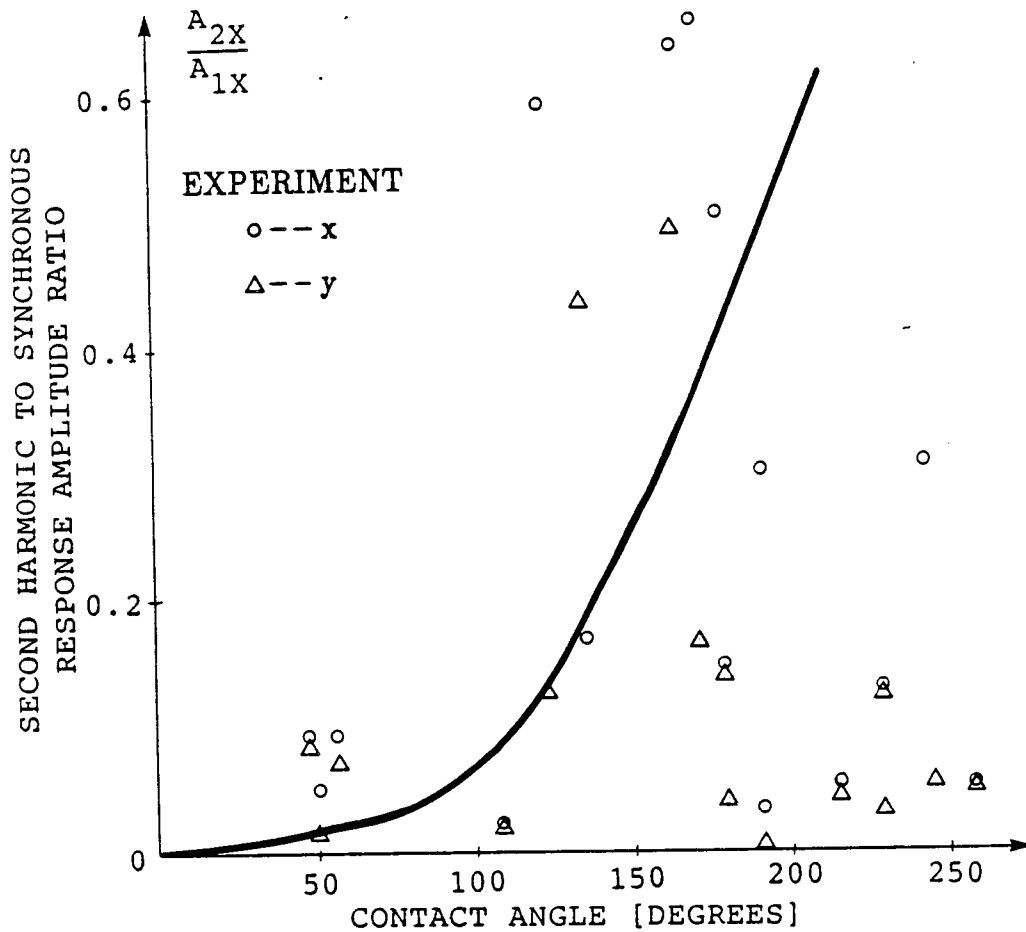


FIGURE 13.104 SECOND HARMONIC (2X) TO FUNDAMENTAL COMPONENT (1X) AMPLITUDE RATIO VERSUS ROTOR/STATOR CONTACT ARC. THEORETICAL CURVE AND EXPERIMENTAL DATA

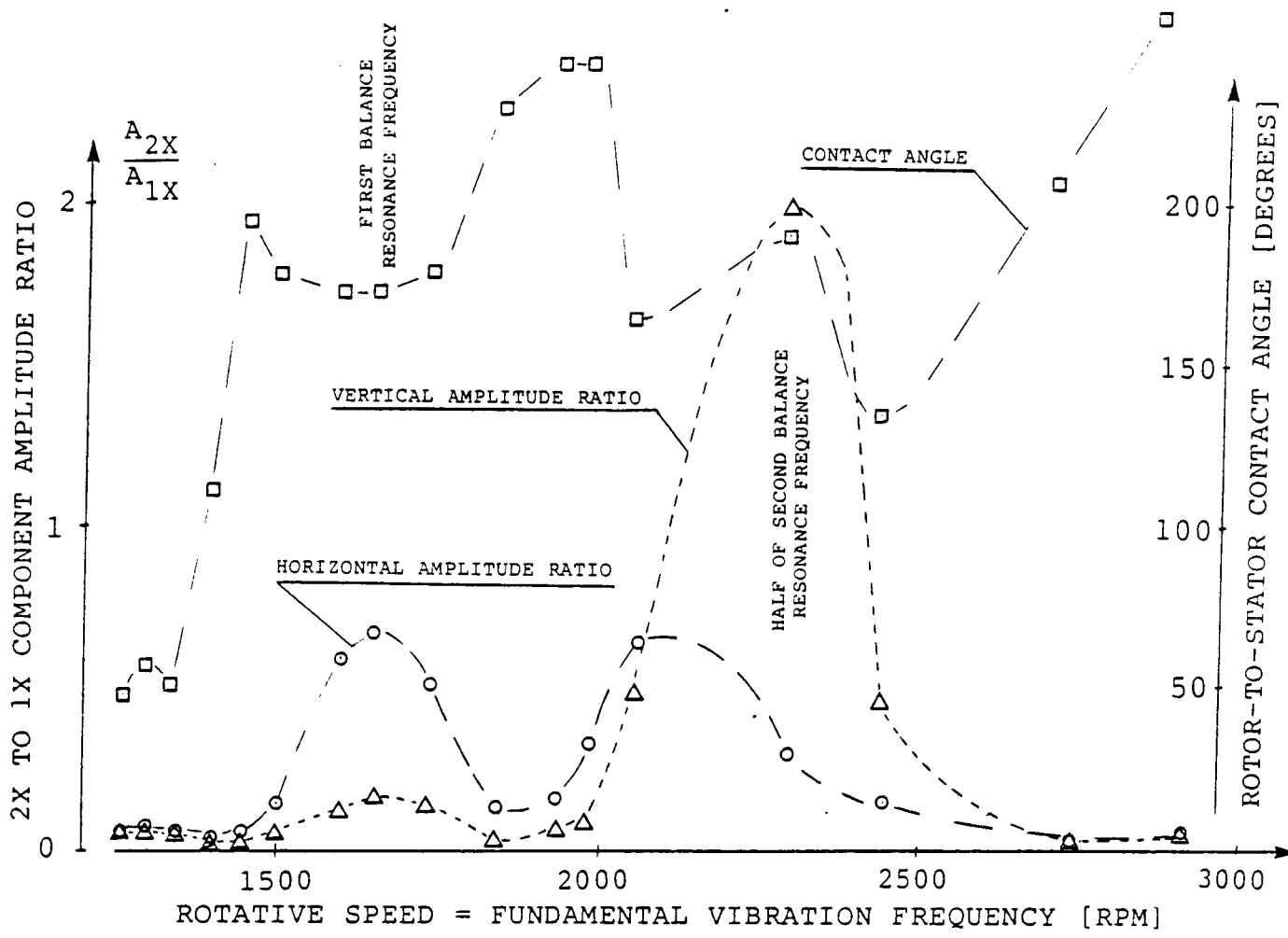


FIGURE 13.105 SECOND HARMONIC (2X) TO FUNDAMENTAL COMPONENT (1X) AMPLITUDE RATIO AND ROTOR/STATOR CONTACT ARC VERSUS ROTATIVE SPEED. EXPERIMENTAL RESULTS.

## 14. ROTOR-TO-STATOR RUB COMPUTER SIMULATION PROGRAM DEVELOPMENT AND OPERATION.

### 14.1 Introduction

This computer program was written to help explore the effects of rotor-to-stator contact on the vibrational response of rotating machines operating under rubbing conditions. This chapter of the report outlines the program development and operation. A few numerical test results used to guide its development are presented.

### 14.2 General Description of the Program

The computer program objective is to calculate the rotor response during rotor-to-stator rub conditions. The rotor/bearing/seal/stator basic system is presented in Fig. 14.1.

The program is designed for the IBM PC computer and is written in Pascal language. The computer program is composed of two major subprograms: (1) the linear rotor/bearing system synchronous response with no rub, and (2) the timebase response of the nonlinear system with rub at a selected rotative speed. The first of the subprograms allows the user to calculate the synchronous response of the system versus rotative speed, producing transient type data which may be displayed in Bodé plot format. This allows for easy identification of the system resonances and modal characteristics indicating at which rotative speeds the largest vibration amplitudes occur. This information is eventually used to determine rotative speeds at which rotor motion should be investigated more closely by taking into account the rub nonlinear effects in the timebase response, the second portion of the program. It is at these rotative speeds the rotor-to-stator contact occurs. This portion of the program allows a more detailed analysis of the shaft vibrational response caused by external and rub-related excitation forces at the desired rotative speed, by calculating (using numerical integration) the shaft centerline motion versus time. In addition to the linear parameters of the shaft and support structure, the nonlinear timebase response subprogram uses the nonlinear properties imposed on the rotating system by outside support structures with limited clearance. Since these structures are non-rotating, the tangential forces generated due to the rotor/stator relative surface velocities are considered as well as the nonlinear modification of the system support structure. The following sections provide a more detailed description of the computer program operation.

### 14.3 Program Initialization

The overall program sequence is shown on the first page of the flow chart section (Fig. 14.2). Each of the larger program blocks is expanded and presented in Figs. 14.3 to 14.10 to show the program operation in more detail. The rotor system being modeled along with the identification/location of the input parameters and calculated output motion is shown in Figure 14.1. Program operation begins with the computer setting aside the memory required to store the output motion data. This consists of data buffers for both the linear and nonlinear responses at each of the three mass stations,  $A_x$ , and each of the bearing/seal locations,  $B_x$ , plus buffers indicating positions and times of rotor-to-stator contact. Once the data storage area has been reserved, the linear parameters for the system need to be entered. The parameters necessary to allow computation of the synchronous response include the following parameters: the system modal mass at each mass station, the stiffness for each shaft section, the external damping at each mass location, the rotational unbalance force vector, the radial constant preload force and its associated angle, and the fluid radial damping, fluid average circumferential velocity ratio, fluid radial stiffness, and radial clearance at each of the bearing/seal locations. To enter a new value for a system

parameter, it is necessary to select the subgroup from the screen menu which contains the desired parameter. The program then lists the individual elements within the subgroup and their current values. The parameter to be changed can be selected from the list and the new value entered. The program will then update the parameter values for the subgroup allowing verification of the new value. This process can be repeated until all the input elements of the subgroup are as desired. At this point in the data entry process, to return to the list of available parameter subgroups the exit selection in the screen menu should be used. Once back to the list of parameter subgroups, a different subgroup may be selected, and the above process described repeated to change the individual values within the new subgroup. This whole data entry process is repeated until all individual parameter values are set to the desired values. After the system parameters have been entered and verified, the exit selection in the subgroup menu initiates the storage of the parameter values on the mass storage medium, allowing them to be recalled and used as the starting values for future calculations. At this stage the program begins the execution of the synchronous response calculations.

#### 14.4 Linear Synchronous Response Calculation

The first user input required with the synchronous response calculation determines whether the routine needs to be executed. If the synchronous vibration response is not required, the program skips the calculation and proceeds to the nonlinear parameter input routine described in Section 14.5. Otherwise, the program prompts for the rotative speed range over which the synchronous calculations are to be performed and the rotative speed increment between calculations. The data entry process for these variables is the same as for the input of the other linear system parameters previously described. Once this data has been entered, the program proceeds to calculate the linear synchronous response of the rotor at axial locations A1, A2, A3 (disk locations), B1, B2, B3, and B4 (bearing/seal locations).

##### 14.4.1 Linear Equations and Their Solution

The linear equations of motion for the model being used (Figure 14.1) are the same as described in Chapter 11 (Eqs. (11.1) to (11.8)). With slightly modified rotation, they are as follows:

$$D_1 \dot{\tilde{z}}_1 + \tilde{z}_1(K_{b_1} + K_1 - j\lambda_1 \Omega D_1) - K_1 z_1 = 0 \quad (14.1)$$

$$M_1 \ddot{\tilde{z}}_1 + D_{s_1} \dot{\tilde{z}}_1 + (K_1 + K_2)z_1 - K_1 \tilde{z}_1 - K_2 \tilde{z}_2 = F_{u_1} e^{j(\omega t + \epsilon_1)} + F_{p_1} e^{j\gamma_1} \quad (14.2)$$

$$D_2 \dot{\tilde{z}}_2 + \tilde{z}_2(K_{b_2} + K_2 + K_3 - j\lambda_2 \Omega D_2) - K_2 z_1 - K_3 z_2 = 0 \quad (14.3)$$

$$M_2 \ddot{\tilde{z}}_2 + D_{s_2} \dot{\tilde{z}}_2 + (K_3 + K_4)z_2 - K_3 \tilde{z}_2 - K_4 \tilde{z}_3 = F_{u_2} e^{j(\omega t + \epsilon_2)} + F_{p_2} e^{j\gamma_2} \quad (14.4)$$

$$D_3 \dot{\tilde{z}}_3 + \tilde{z}_3(K_{b_3} + K_4 + K_5 - j\lambda_3 \Omega D_3) - K_4 z_2 - K_5 z_3 = 0 \quad (14.5)$$

$$M_3 \ddot{z}_3 + D_{S_3} \dot{z}_3 + (K_5 + K_6)z_3 - K_5 \bar{z}_3 - K_6 \bar{z}_4 = F_{u_3} e^{j(\omega t + \epsilon_3)} + F_{p_3} e^{j\gamma_3} \quad (14.6)$$

$$D_4 \dot{\bar{z}}_4 + \bar{z}_4 (K_{b_4} + K_6 + K_7 - j\lambda_4 \Omega D_4) - K_6 z_3 = 0 \quad (14.7)$$

Since the equations represent a linear system, the response to each forcing function can be computed separately and the results summed to get the complete response. Starting with the unbalance responses, the following solutions are assumed:

$$\begin{aligned} z_1 &= A_1 e^{j(\omega t + \alpha_1)} & \bar{z}_1 &= B_1 e^{j(\omega t + \beta_1)} \\ z_2 &= A_2 e^{j(\omega t + \alpha_2)} & \bar{z}_2 &= B_2 e^{j(\omega t + \beta_2)} \\ z_3 &= A_3 e^{j(\omega t + \alpha_3)} & \bar{z}_3 &= B_3 e^{j(\omega t + \beta_3)} \\ & & \bar{z}_4 &= B_4 e^{j(\omega t + \beta_4)} \end{aligned} \quad (14.8)$$

The coordinates  $z_i$  describe rotor responses at the disk stations. The coordinates  $\bar{z}_i$  describe responses at each bearing/seal location. Also, since synchronous responses have been assumed, the rotor response frequency is rotative speed,  $\omega$ . Substituting the responses into Eqs. (14.1) through (14.7) with  $F_{p_1} = F_{p_2} = F_{p_3} = 0$  results in the following algebraic equations

$$\begin{aligned} B_1 e^{j(\omega t + \beta_1)} (K_{b_1} + K_1 + jD_1 \omega (1 - \lambda_1)) - K_1 A_1 e^{j(\omega t + \alpha_1)} &= 0 \\ A_1 e^{j(\omega t + \alpha_1)} (K_1 + K_2 - m_1 \omega^2 + jD_{S_1} \omega) - K_1 B_1 e^{j(\omega t + \beta_1)} - K_2 B_2 e^{j(\omega t + \beta_2)} &= F_{u_1} e^{j(\omega t + \epsilon_1)} \\ B_2 e^{j(\omega t + \beta_2)} (K_{b_2} + K_2 + K_3 + jD_2 \omega (1 - \lambda_2)) - K_2 A_1 e^{j(\omega t + \alpha_1)} - K_3 A_2 e^{j(\omega t + \alpha_2)} &= 0 \\ A_2 e^{j(\omega t + \alpha_2)} (K_3 + K_4 - m_2 \omega^2 + jD_{S_2} \omega) - K_3 B_2 e^{j(\omega t + \beta_2)} - K_4 B_3 e^{j(\omega t + \beta_3)} &= F_{u_2} e^{j(\omega t + \epsilon_2)} \\ B_3 e^{j(\omega t + \beta_3)} (K_{b_3} + K_4 + K_5 + jD_3 \omega (1 - \lambda_3)) - K_4 A_2 e^{j(\omega t + \alpha_2)} - K_5 A_3 e^{j(\omega t + \alpha_3)} &= 0 \\ A_3 e^{j(\omega t + \alpha_3)} (K_5 + K_6 - m_3 \omega^2 + jD_{S_3} \omega) - K_5 B_3 e^{j(\omega t + \beta_3)} - K_6 B_4 e^{j(\omega t + \beta_4)} &= F_{u_3} e^{j(\omega t + \epsilon_3)} \end{aligned} \quad (14.9)$$

$$B_4 e^{j(\omega t + \beta_4)} (K_{b_4} + K_6 + K_7 + jD_4 \omega (1 - \lambda_4)) - K_6 A_3 e^{j(\omega t + \alpha_3)} = 0$$

These equations can be solved to obtain the response amplitudes and phase angles  $A_1, \alpha_1, A_2, \alpha_2, A_3, \alpha_3, B_1, \beta_1, B_2, \beta_2, B_3, \beta_3, B_4,$  and  $\beta_4$ .

For the static preload response the following solutions are assumed:

$$\begin{aligned} z_1 &= A_{01} e^{j\alpha_{01}} & \bar{z}_1 &= B_{01} e^{j\beta_{01}} \\ z_2 &= A_{02} e^{j\alpha_{02}} & \bar{z}_2 &= B_{02} e^{j\beta_{02}} \\ z_3 &= A_{03} e^{j\alpha_{03}} & \bar{z}_3 &= B_{03} e^{j\beta_{03}} \\ & & \bar{z}_4 &= B_{04} e^{j\beta_{04}} \end{aligned} \quad (14.10)$$

When these solutions (14.10) are substituted into Eqs. (14.1) through (14.7) with  $F_{u_1} = F_{u_2} = F_{u_3} = 0$ , the following algebraic equations are obtained:

$$\begin{aligned} B_{01} e^{j\beta_{01}} (K_{b_1} + K_1) - K_1 A_{01} e^{j\alpha_{01}} &= 0 \\ A_{01} e^{j\alpha_{01}} (K_1 + K_2) - K_1 B_{01} e^{j\beta_{01}} - K_2 B_{02} e^{j\beta_{02}} &= F_{p_1} e^{j\gamma_1} \\ B_{02} e^{j\beta_{02}} (K_{b_2} + K_2 + K_3) - K_2 A_{01} e^{j\alpha_{01}} - K_3 A_{02} e^{j\alpha_{02}} &= 0 \\ A_{02} e^{j\alpha_{02}} (K_3 + K_4) - K_3 B_{02} e^{j\beta_{02}} - K_4 B_{03} e^{j\beta_{03}} &= F_{p_2} e^{j\gamma_2} \\ B_{03} e^{j\beta_{03}} (K_{b_3} + K_4 + K_5) - K_4 A_{02} e^{j\alpha_{02}} - K_5 A_{03} e^{j\alpha_{03}} &= 0 \\ A_{03} e^{j\alpha_{03}} (K_5 + K_6) - K_5 B_{03} e^{j\beta_{03}} - K_6 B_{04} e^{j\beta_{04}} &= F_{p_3} e^{j\gamma_3} \\ B_{04} e^{j\beta_{04}} (K_{b_4} + K_6 + K_7) - K_6 A_{03} e^{j\alpha_{03}} &= 0 \end{aligned} \quad (14.11)$$

These equations are solved to get the values of  $A_{01}, \alpha_{01}, A_{02}, \alpha_{02}, A_{03}, \alpha_{03}, B_{01}, \beta_{01}, B_{02}, \beta_{02}, B_{03}, \beta_{03}, B_{04},$  and  $\beta_{04}$ .

The maximum amplitude and its angle are then computed by combining the synchronous and static preload solutions (14.8) and (14.10). These results are then compared with the

specified radial clearances at the bearing/seal locations B1, B2, B3, and B4 to determine whether rubs would have occurred. This potential rub information is placed in the "RUB" and "ANGLE" data buffers which may be displayed the same way as the computed vibration responses.

#### 14.4.2 Linear Synchronous Response Plots : Exit Data

The linear system synchronous response data and the potential rotor-to-stator rub data may be plotted using a Bodé format or listed in a tabular format. Both formats may be displayed on the computer screen or hard copied using the graphics printer. To display the desired data, one must select the data location from the list on the available menu. Once the desired location is selected, the program prompts to determine if the data is to be plotted or tabularly listed, and if it is to be hard copied or only displayed on the computer screen. Once the prompts have been answered, the program executes the desired action. When all the desired information has been displayed, one must select the exit option within the plot location selection menu in order to continue to the nonlinear numerical integration portion of the program.

#### 14.5 Nonlinear Timebase Calculation

As with the linear solutions, the first task within the nonlinear portion of the program is to determine whether the nonlinear calculations need to be performed. If the nonlinear calculations are not required, they may be skipped and the program proceeds to the prompt to exit the program. If they are to be performed, the additional parameters necessary to complete the calculations must be entered.

These include the initial displacements and velocities at each location (initial conditions), the stator stiffness, the coefficient of friction between the rotor and stator surfaces, and the impact restitution coefficient at each of the potential rub locations, plus the program control variables, namely operating speed, number of revolutions to compute, and the number of computational steps per revolution.

If the linear calculations by the first portion of the program were performed, the initial displacements and velocities are calculated from the synchronous responses; therefore, any values entered during the data input process will not be used by the program. The initial conditions in the parameter table are also not used when the nonlinear calculations are being extended. The process of extending the nonlinear calculations is discussed in Section 14.5.5; for now it is sufficient to realize that the initial conditions for the current calculation are obtained from the previous calculation, and their input into the parameter table is not required.

The actual program operation to select and change any of these parameters is identical to the process used to enter the parameters for the synchronous vibration response calculations. When the parameters have been set to the desired values, selection of the exit option in the group menu allows the program to proceed with the actual numerical calculations of the shaft centerline motion.

#### 14.5.1 Nonlinear Equations

The nonlinear program uses the same physical model as the linear system; however, the equations of motion must be slightly modified to include the effects due to rub at the bearing/seal "B" locations. Eqs. (14.1), (14.3), (14.5), and (14.7) are modified to

$$D_1 \dot{\tilde{z}}_1 / \kappa_1 + \tilde{z}_1 (K_{b_1} + K_1 - j\lambda_1 \Omega D_1) - K_1 z_1 + f_1 (K_{r_1} (|\tilde{z}_1| - C_1) (1 + j\mu_1)) = 0 \quad (14.12)$$

$$D_2 \dot{\tilde{z}}_2 / \kappa_2 + \tilde{z}_2 (K_{b_2} + K_2 + K_3 - j\lambda_2 \Omega D_2) - K_2 z_1 - K_3 z_2 + f_2 (K_{r_2} (|\tilde{z}_2| - C_2) (1 + j\mu_2)) = 0 \quad (14.13)$$

$$D_3 \dot{\tilde{z}}_3 / \kappa_3 + \tilde{z}_3 (K_{b_3} + K_4 + K_5 - j\lambda_3 \Omega D_3) - K_4 z_2 - K_5 z_3 + f_3 (K_{r_3} (|\tilde{z}_3| - C_3) (1 + j\mu_3)) = 0 \quad (14.14)$$

$$D_4 \dot{\tilde{z}}_4 / \kappa_4 + \tilde{z}_4 (K_{b_4} + K_6 + K_7 - j\lambda_4 \Omega D_4) - K_6 z_3 + f_4 (K_{r_4} (|\tilde{z}_4| - C_4) (1 + j\mu_4)) = 0 \quad (14.15)$$

where  $f_i = 1$  and  $\kappa_i =$  current restitution coefficient input value if  $(|\tilde{z}_i| - C_i) \geq 0$  and  $f_i = 0$  and  $\kappa_i = 1$  if  $(|\tilde{z}_i| - C_i) < 0$  ( $i = 1, 2, 3, 4$ ), where  $C_i$  are allowable radial clearances at each bearing or seal.

For non-rub conditions,  $(\tilde{z}_i - C_i) < 0$ , the modified equations (14.12) to (14.15) reduce to the original linear equations. Since rub can only occur at the "B" locations, the equations of motion for the responses at the "A" locations remain the same as for the linear solutions.

Instead of assuming a solution form and substituting it into the original equations as was done to get the linear solution, the numerical integration algorithm used requires that each equation be solved for its highest order derivative. For example, Eqs. (14.12) and (14.2) become:

$$\dot{\tilde{z}}_1 = \kappa_1 [K_1 z_1 - \tilde{z}_1 (K_{b_1} + K_1 - j\lambda_1 \Omega D_1) - f_1 (K_{r_1} (|\tilde{z}_1| - C_1) (1 + j\mu_1))] / D_1$$

$$\ddot{\tilde{z}}_1 = [F_{u_1} e^{j(\omega t + \epsilon_1)} + F_p e^{j\gamma_1} - D_s \dot{\tilde{z}}_1 - (K_1 + K_2) z_1 + K_1 \tilde{z}_1 + K_2 \tilde{z}_2] / M_1$$

The remaining equations are similarly solved for their highest order derivatives.

#### 14.5.2 Numerical Method

The RUNGE-KUTTA algorithm then uses the values calculated for the highest order derivatives, along with the current state of the system, (shaft positions and velocities) to predict the state of the system at some point in the future. This process continues until the motion for the specified period has been calculated. The accuracy and numerical stability of the RUNGE-KUTTA algorithm is very sensitive to the step size between computed points. Large step sizes provide increased computational speed at the cost of reduced accuracy and stability, since both accuracy and stability depend on the product of the step size and the value of the highest order derivative. This program uses a variable step size, based on the percentage change (2 percent) between the value for the new point and the current point, to optimize both the computational speed and accuracy. This produces relatively large step changes when the function is producing slowly changing values, which increases computational speed, and then decreases the step size during

periods of rapid change in values to preserve the accuracy. When the change is too high, the step size is reduced by one-half, and the calculation restarted. This process is repeated until the maximum change in amplitude requirements is met, or the numerical precision of the computer is exceeded. At this point, the new value is transferred into the current value location. If the time coincides with the next data sample time, it is stored in the data buffer. Otherwise, the program returns to the previous time that did not produce acceptable results, and retries that time with the new current values. This process is repeated until the sample data buffer is complete. Figure 14.11 illustrates this process by showing the steps for a possible computation sequence between two data sample times. Since any change from the value of zero will produce percentage changes greater than allowed, the program also has an amplitude threshold (0.01 mils) which overrides the change requirements between points if the new value is less than the threshold. The threshold and percent change parameters should be picked carefully as they significantly affect both the computational speed and accuracy.

### 14.5.3 Accuracy Sensitivity

Since the transient response is much more susceptible to computational errors than the forced response, it makes a good subject to study the sensitivity of the computational accuracy with these parameters. Such tests were performed in a test environment which allowed computation at only one plane of motion. Figures 14.12 to 14.17 present computed output shaft waveforms for a 5 mil initial displacement in a system with no damping. Each figure lists the system parameters used in the computations above the waveform plot. The actual response should be a cosine wave with a 5 mil amplitude at the system's resonant frequency; any deviation from this ideal waveform is due to errors generated during the numerical solution. Note that the response in Figure 14.17 would be the numerical solution produced using 64 points per revolution period with no percentage change correction to the step size, as the threshold exceeds the maximum response amplitude.

### 14.5.4 Nonlinear Timebase Plots: Exit Data

Once the computations are performed and data buffers have been completed, the nonlinear motion display selection menu is displayed. The nonlinear display selection process operates similarly to that for the synchronous response, the only difference being the plot format is orbit/timebase instead of Bodé. After all the desired data has been presented, the exit selection in the menu is used to continue to the calculation extension program function.

### 14.5.5 Extension of the Nonlinear Timebase Calculations

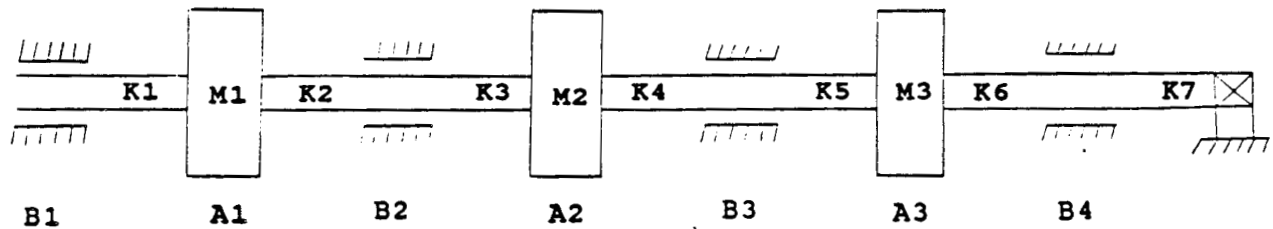
The program prompts to determine whether the nonlinear calculations need to be extended. The extension can be used to continue the computational period until a steady-state solution is obtained by using the values at the last computed point as the initial conditions for another computational period. This process can be continued until the steady-state solution has been obtained.

### 14.5.6 Program Termination

If the nonlinear calculations are not to be extended, the program prompts for program termination. If Exit program is selected, control is returned to the computer's operating system; if not, the program is restarted at the data entry for the synchronous response calculations.

## 14.6 Summary

This chapter presented the description of the computer simulation program and its operation. The rubbing rotor/bearing/seal system to be modeled was defined and the equations describing its motion were presented. The manipulation of these equations required by the program to produce transformed equations compatible with the linear synchronous response and nonlinear timebase calculations is also described. The numerical solution technique and tests used to determine the sensitivity of the numerical solutions to control parameters is presented, along with a description of the modifications made to the primary numerical solution technique to minimize the effects of the control parameters on the final solution.



**Bx** are bearing/seal stations with the fluid stiffness, fluid damping, fluid average circumferential velocity ratio, clearance, coefficient of friction, restitution coefficient, and stator stiffness as program input parameters. Motion at each point is calculated for output.

**Ax** are mass stations with the modal mass, and external damping as program input parameters. Motion at each point is calculated for output.

**Kx** are the rotor system modal stiffnesses between the stations Ax and Bx as shown above; they are also program input parameters.

FIGURE 14.1 ROTOR/SUPPORT SYSTEM MODELLED BY COMPUTER PROGRAM.

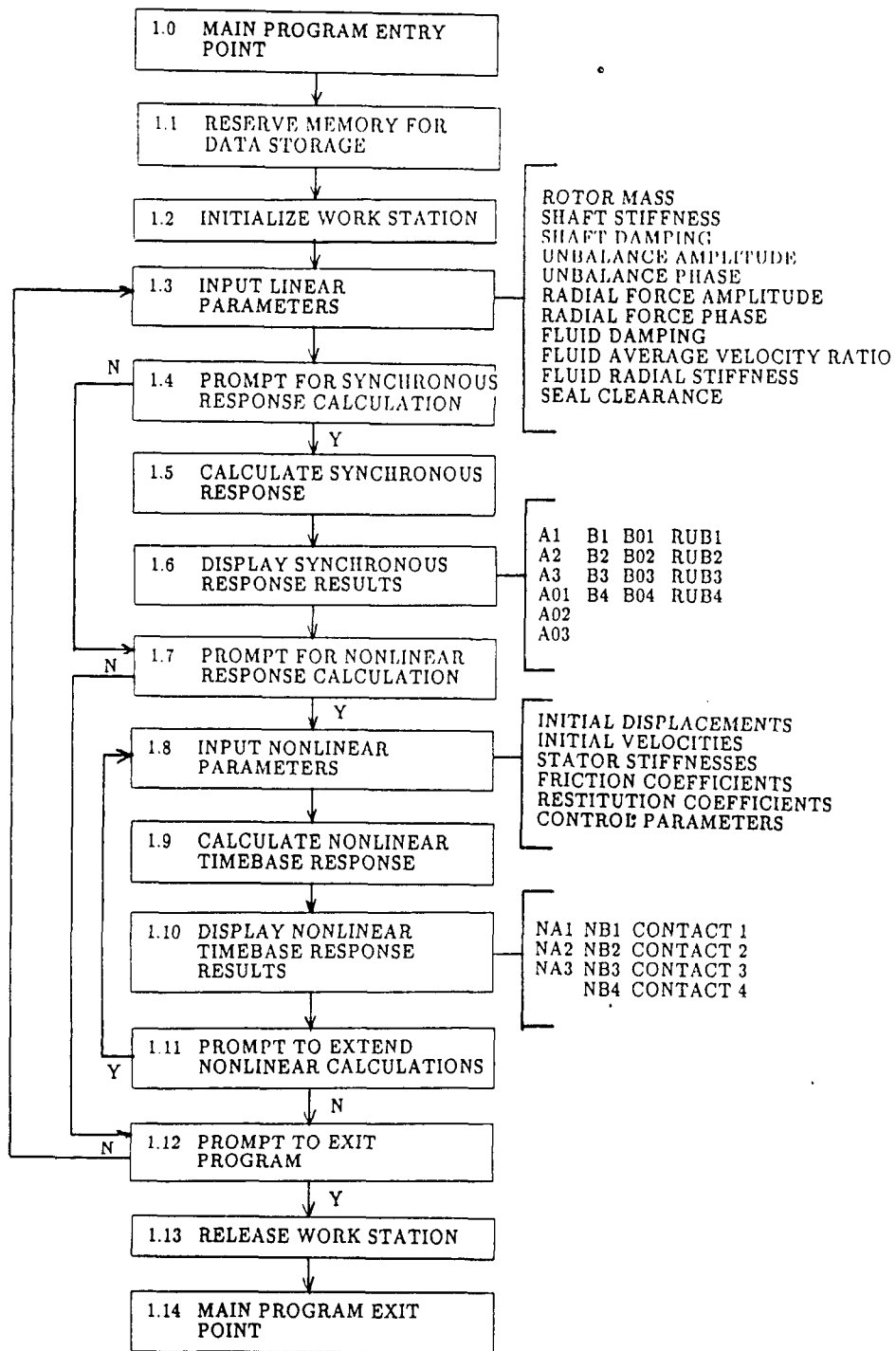


FIGURE 14.2 FLOW CHART OF MAIN PROGRAM SEQUENCE.

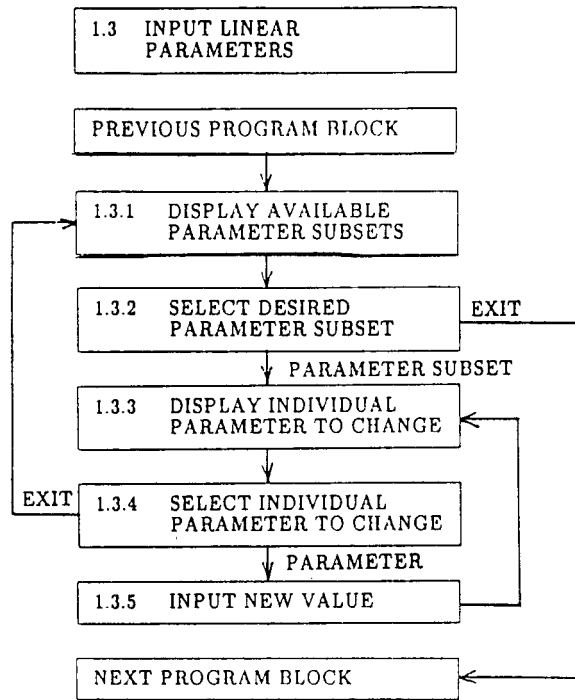


FIGURE 14.3 FLOW CHART OF INPUT LINEAR PARAMETERS SUBPROGRAM SEQUENCE.

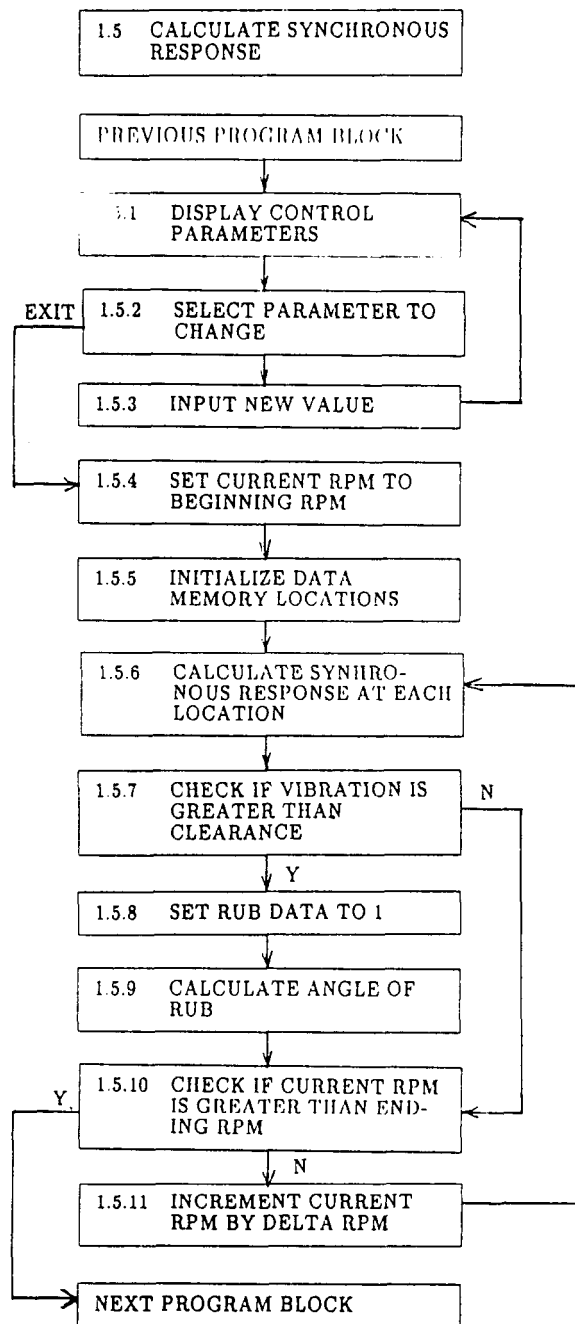


FIGURE 14.4 FLOW CHART OF CALCULATE SYNCHRONOUS RESPONSE SUBPROGRAM SEQUENCE.

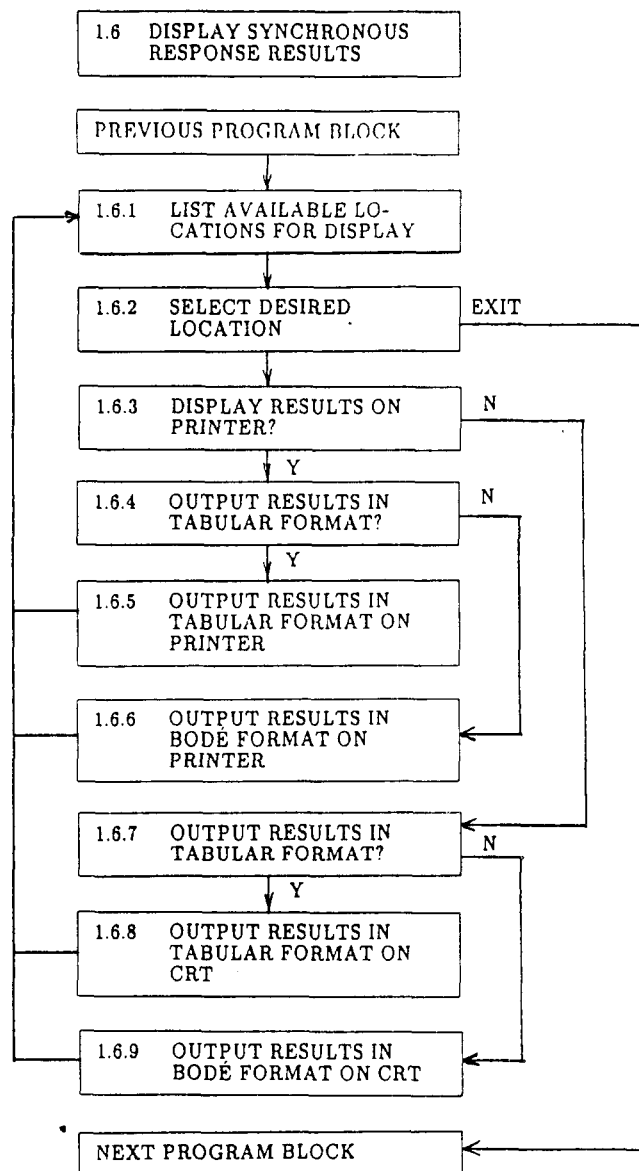


FIGURE 14.5 FLOW CHART OF DISPLAY SYNCHRONOUS RESULTS SUBPROGRAM SEQUENCE.

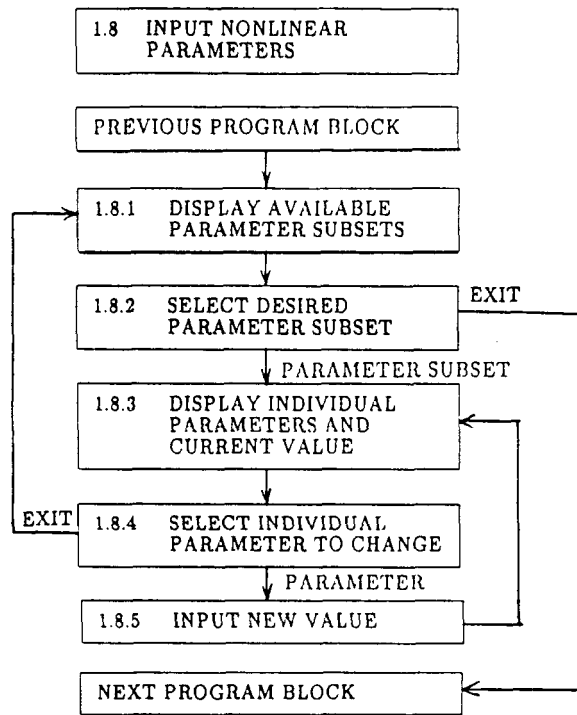


FIGURE 14.6 FLOW CHART OF INPUT NONLINEAR PARAMETERS SUBPROGRAM SEQUENCE.

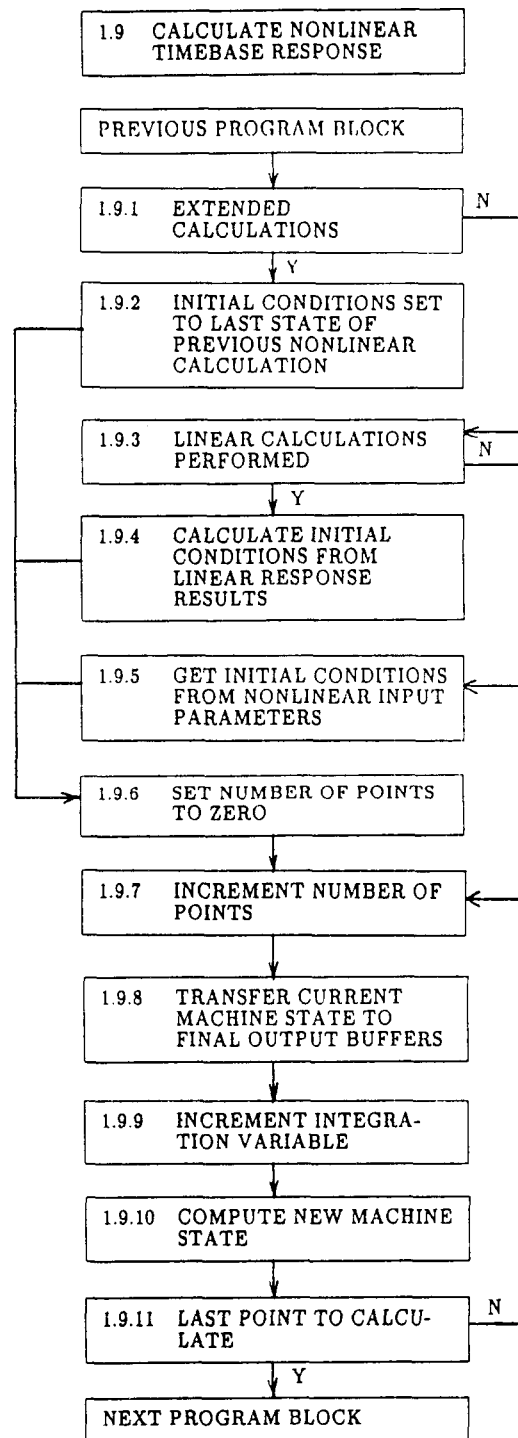


FIGURE 14.7 FLOW CHART OF CALCULATE NONLINEAR TIMEBASE RESPONSE SUBPROGRAM SEQUENCE.

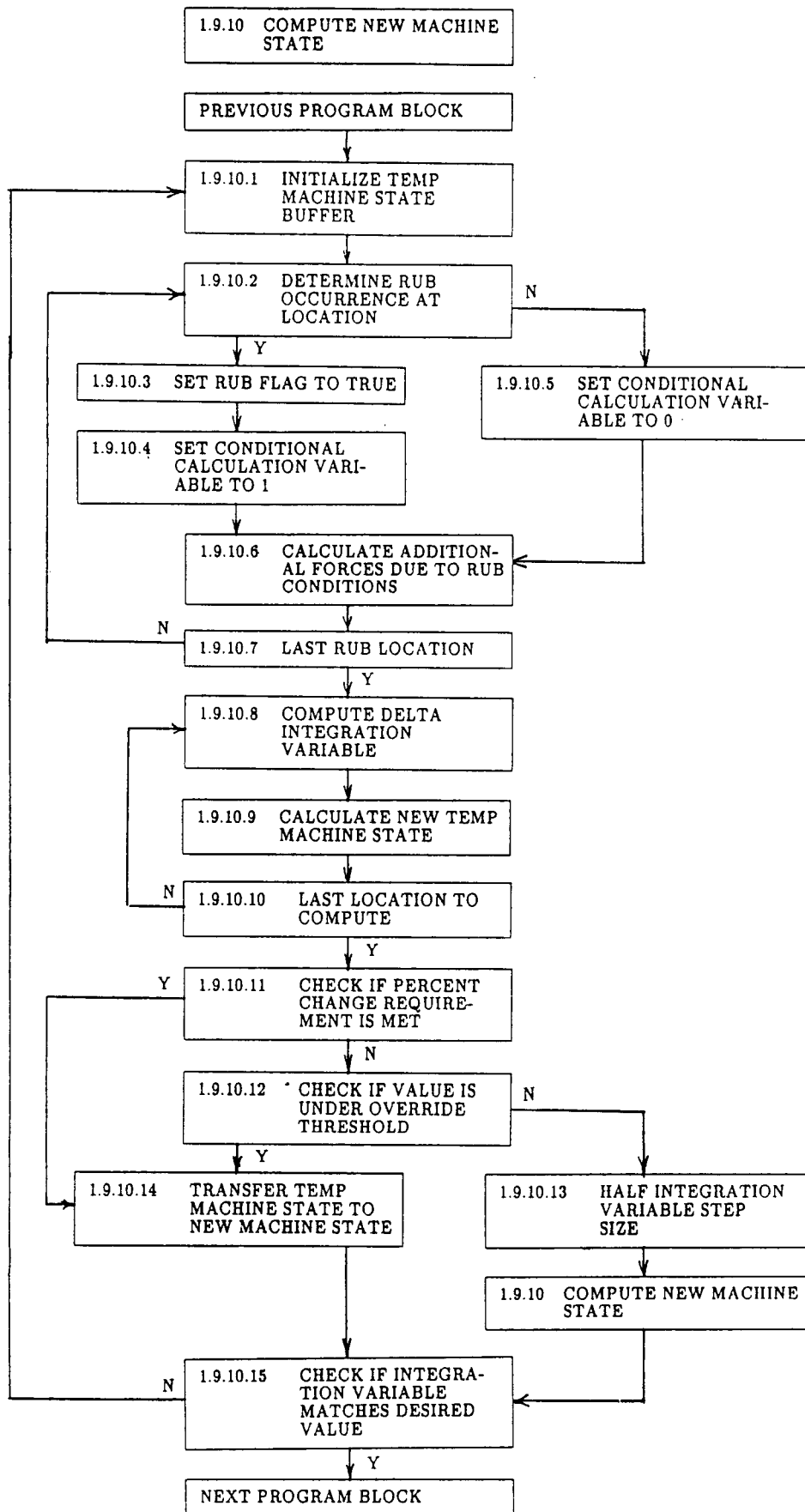


FIGURE 14.8 FLOW CHART OF COMPUTE NEW MACHINE STATE SUBPROGRAM SEQUENCE.

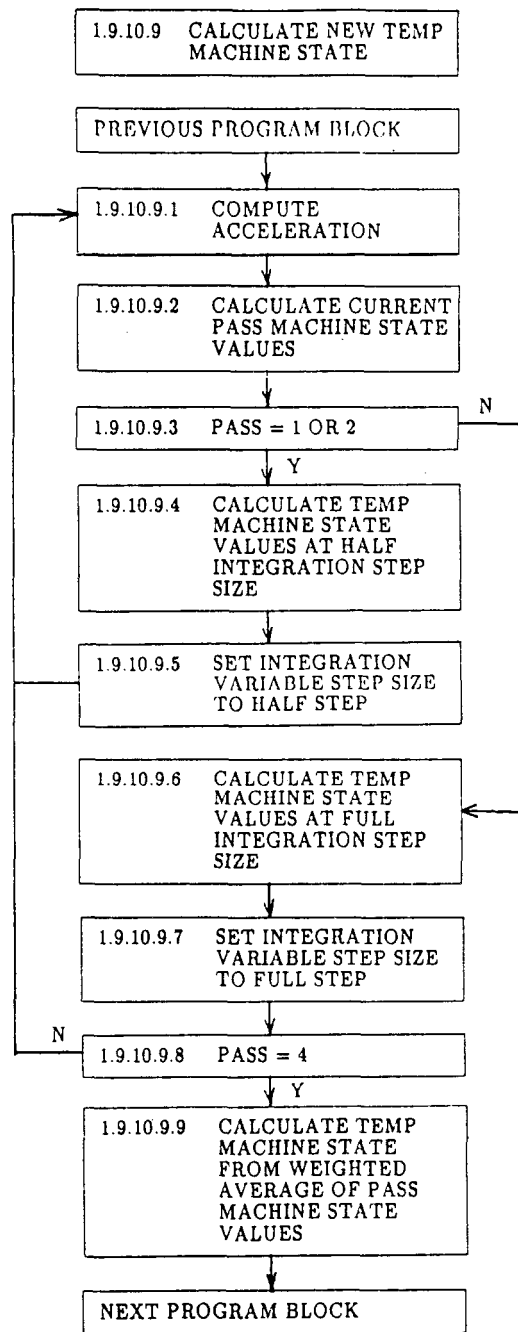


FIGURE 14.9

FLOW CHART OF CALCULATE NEW TEMPORARY MACHINE STATE SUBPROGRAM SEQUENCE.

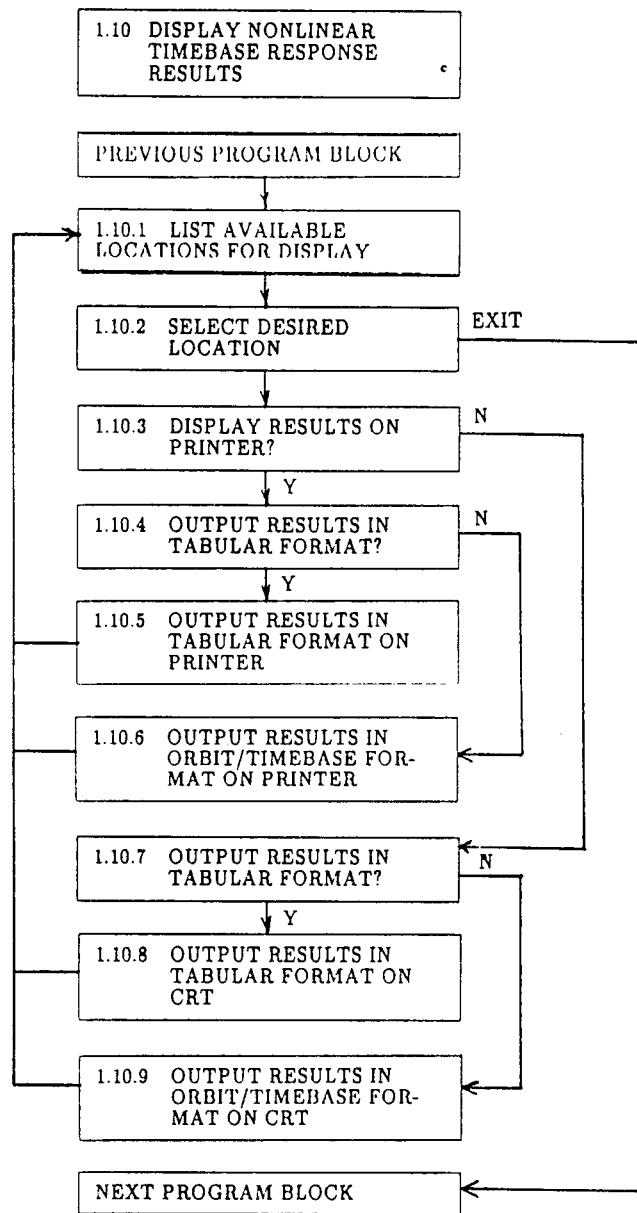
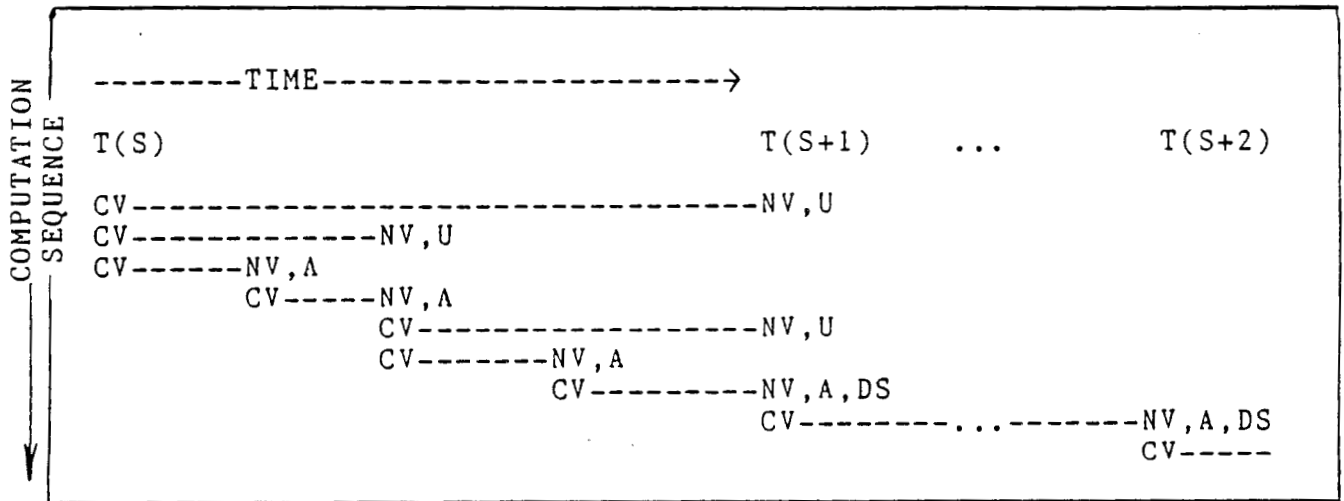


FIGURE 14.10 FLOW CHART OF DISPLAY NONLINEAR TIMEBASE RESPONSE RESULTS SUBPROGRAM SEQUENCE.



T(---) = DATA SAMPLE/STORE TIMES  
 CV = CURRENT VALUE  
 NV = NEW VALUE  
 U = UNACCEPTABLE AMPLITUDE CHANGE  
 A = ACCEPTABLE AMPLITUDE CHANGE  
 DS = DATA STORED

FIGURE 14.11 COMPUTATIONAL SEQUENCE FOR VARIABLE STEP SIZE RUNGE-KUTTA NUMERICAL ALGORITHM.

NEW RUN NUMBER (number)	A
1. SPRING STIFFNESS;K (Lb/in)	100
2. OBSERVED DAMPING;D (Lb sec/in)	0
3. EFFECTIVE ROTOR MASS;Meff (Lb sec <sup>2</sup> /in)	.005
220. DIAM CLEARANCE;Cd (Mils)	20
244. COEFFICIENT OF FRICTION;Mu (value)	40
272. IMPACT DURATION;Im_dur (Sec)	.001
23. PERTURBATION MASS;Mp (Grams)	0
24. PERTURBATION RADIUS;Rp (Inches)	1
166. PERTURBATION WEIGHT ANGLE (Degrees)	0
240. INITIAL RADIAL DISPLACEMENT;R1 (Inches)	.005
249. INITIAL ANGULAR DISPLACEMENT;T1 (Degrees)	0
250. INITIAL RADIAL VELOCITY;Vr1 (In/sec)	0
251. INITIAL ANGULAR VELOCITY;Vt1 (Rpm)	0
13. OPERATING FREQUENCY;Fop (Rpm)	1000
NUMBER OF COMPUTATIONAL STEPS/REVOLUTION (value)	64
NUMBER OF REVOLUTIONS (value)	8
260. MAXIMUM DISPLACEMENT CHANGE;Ch (Percent)	1
261. ITERATION THRESHOLD;It_thresh (Inches)	1.E-6

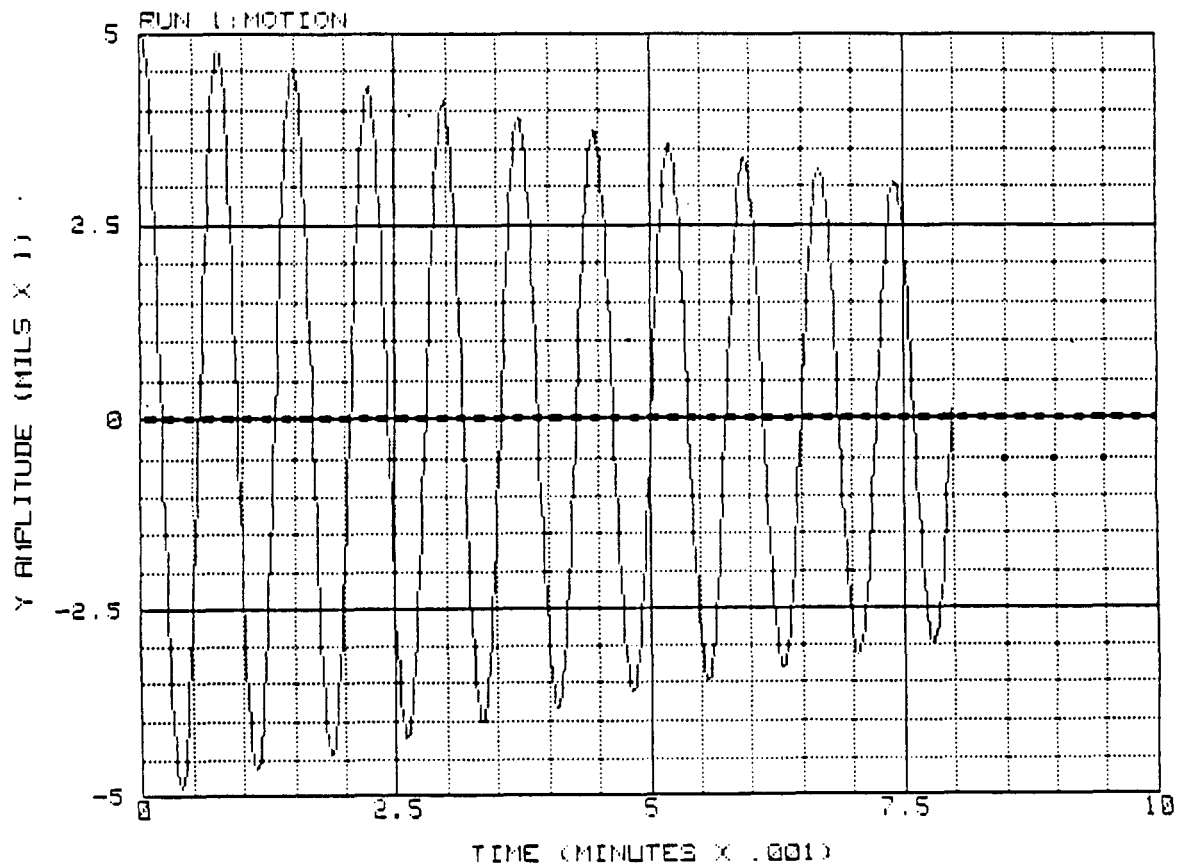


FIGURE 14.12 NUMERICALLY CALCULATED SOLUTION FOR MAXIMUM CHANGE OF 1% AND OVERRIDE THRESHOLD OF  $1 \times 10^{-6}$  INCHES FOR A SYSTEM WITH NO EXTERNAL DAMPING AND 5 MILS OF INITIAL DISPLACEMENT.

NEW RUN NUMBER (number)	8
1. SPRING STIFFNESS;K (Lb/in)	100
2. OBSERVED DAMPING;D (Lb sec/in)	0
3. EFFECTIVE ROTOR MASS;Meff (Lb sec <sup>2</sup> /in)	.005
223. DIAM CLEARANCE;Cd (Mils)	20
244. COEFFICIENT OF FRICTION;Mu (value)	40
272. IMPACT DURATION;Im_dur (Sec)	.001
23. PERTURBATION MASS;Mp (Grams)	0
24. PERTURBATION RADIUS;Rp (Inches)	1
166. PERTURBATION WEIGHT ANGLE (Degrees)	0
248. INITIAL RADIAL DISPLACEMENT;R1 (Inches)	.005
249. INITIAL ANGULAR DISPLACEMENT;T1 (Degrees)	0
250. INITIAL RADIAL VELOCITY;Vr1 (In/sec)	0
251. INITIAL ANGULAR VELOCITY;Vt1 (Rpm)	0
13. OPERATING FREQUENCY;Fop (Rpm)	1000
NUMBER OF COMPUTATIONAL STEPS/REVOLUTION (value)	64
NUMBER OF REVOLUTIONS (value)	8
260. MAXIMUM DISPLACEMENT CHANGE;Ch (Percent)	5
261. ITERATION THRESHOLD;It_thresh (Inches)	1.E-6

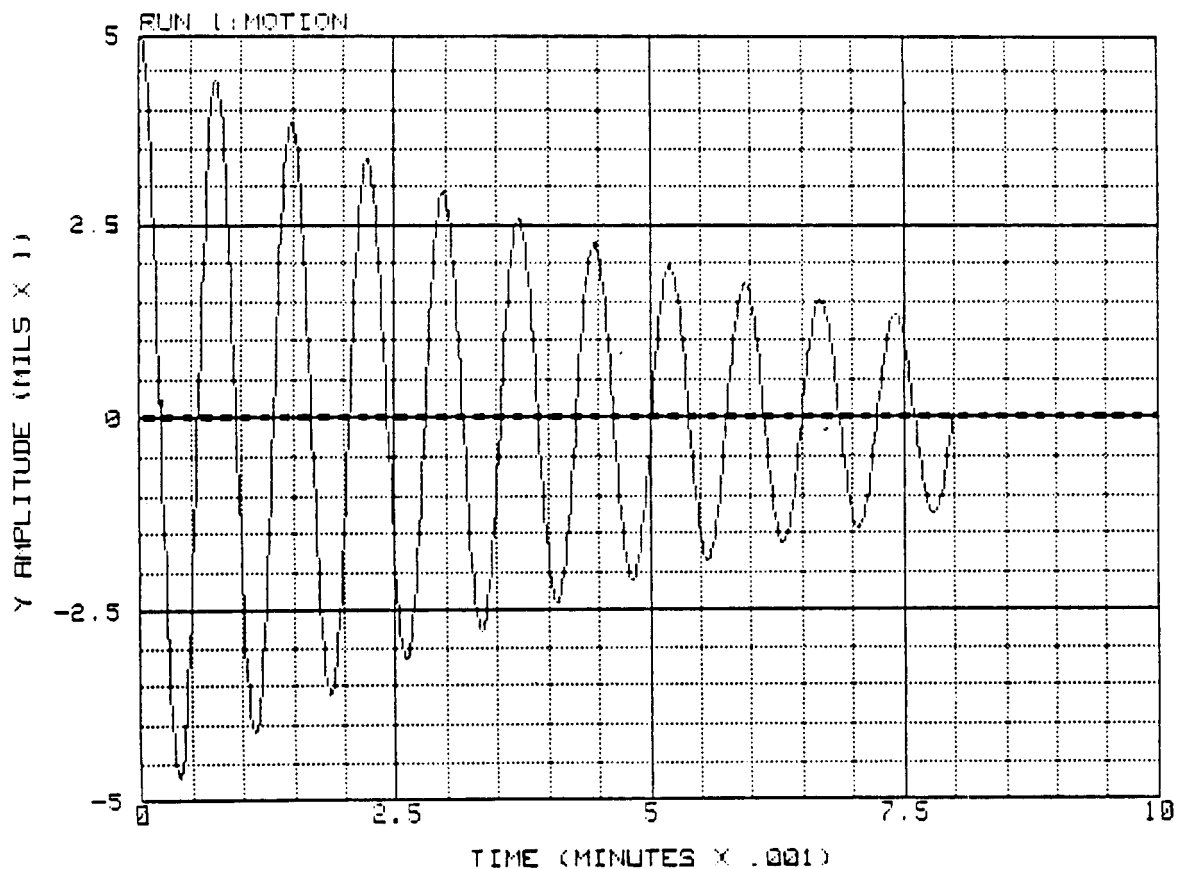


FIGURE 14.13 NUMERICALLY CALCULATED SOLUTION FOR MAXIMUM CHANGE OF 5% AND OVERRIDE THRESHOLD OF  $1 \times 10^{-6}$  INCHES FOR A SYSTEM WITH NO EXTERNAL DAMPING AND 5 MILS OF INITIAL DISPLACEMENT.

NEW RUN NUMBER (number)	C
1. SPRING STIFFNESS;K (Lb/in)	100
2. OBSERVED DAMPING;D (Lb sec/in)	0
3. EFFECTIVE ROTOR MASS;Meff (Lb sec <sup>2</sup> /in)	.005
223. DIAM CLEARANCE;Cd (Mils)	20
244. COEFFICIENT OF FRICTION;Mu (value)	40
272. IMPACT DURATION;Im_dur (Sec)	.001
23. PERTURBATION MASS;Mp (Grams)	0
24. PERTURBATION RADIUS;Rp (Inches)	1
166. PERTURBATION WEIGHT ANGLE (Degrees)	0
249. INITIAL RADIAL DISPLACEMENT;R1 (Inches)	.005
249. INITIAL ANGULAR DISPLACEMENT;T1 (Degrees)	0
250. INITIAL RADIAL VELOCITY;Vr1 (In/sec)	0
251. INITIAL ANGULAR VELOCITY;Vt1 (Rpm)	0
13. OPERATING FREQUENCY;Fop (Rpm)	1000
NUMBER OF COMPUTATIONAL STEPS/REVOLUTION (value)	64
NUMBER OF REVOLUTIONS (value)	8
260. MAXIMUM DISPLACEMENT CHANGE;Ch (Percent)	10
261. ITERATION THRESHOLD;It_thresh (Inches)	1.E-6

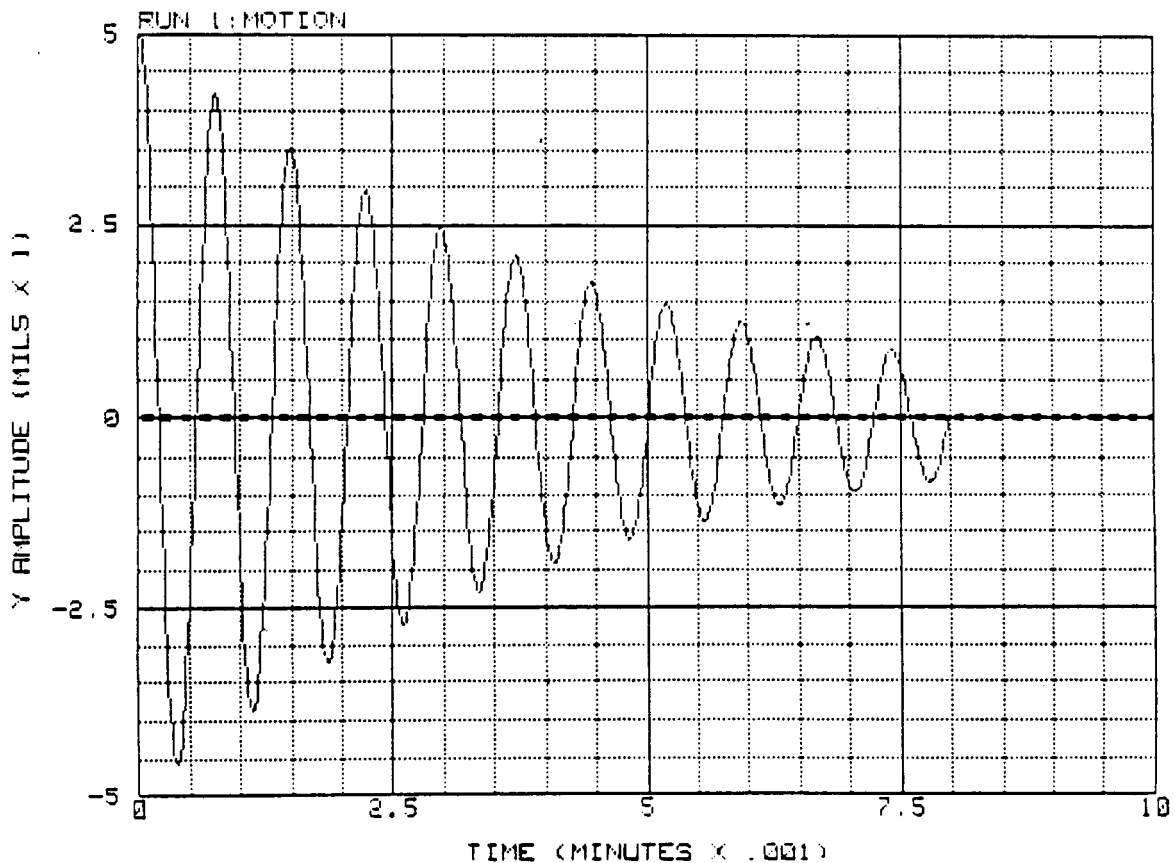


FIGURE 14.14 NUMERICALLY CALCULATED SOLUTION FOR MAXIMUM CHANGE OF 10% AND OVERRIDE THRESHOLD OF  $1 \times 10^{-6}$  INCHES FOR A SYSTEM WITH NO EXTERNAL DAMPING AND 5 MILS OF INITIAL DISPLACEMENT.

NEW RUN NUMBER (number)	D
1. SPRING STIFFNESS;K (Lb/in)	100
2. OBSERVED DAMPING;D (Lb sec/in)	0
3. EFFECTIVE ROTOR MASS;Meff (Lb sec <sup>2</sup> /in)	.005
223. DIAM CLEARANCE;Cd (Mils)	20
244. COEFFICIENT OF FRICTION;Mu (value)	40
272. IMPACT DURATION;Im_dur (Sec)	.001
23. PERTURBATION MASS;Mp (Grams)	0
24. PERTURBATION RADIUS;Rp (Inches)	1
166. PERTURBATION WEIGHT ANGLE (Degrees)	0
248. INITIAL RADIAL DISPLACEMENT;R1 (Inches)	.005
249. INITIAL ANGULAR DISPLACEMENT;T1 (Degrees)	0
250. INITIAL RADIAL VELOCITY;Vr1 (In/sec)	0
251. INITIAL ANGULAR VELOCITY;Vr1 (Rpm)	0
13. OPERATING FREQUENCY;Fop (Rpm)	1000
NUMBER OF COMPUTATIONAL STEPS/REVOLUTION (value)	64
NUMBER OF REVOLUTIONS (value)	8
260. MAXIMUM DISPLACEMENT CHANGE;Ch (Percent)	5
261. ITERATION THRESHOLD;It_thresh (Inches)	.0001

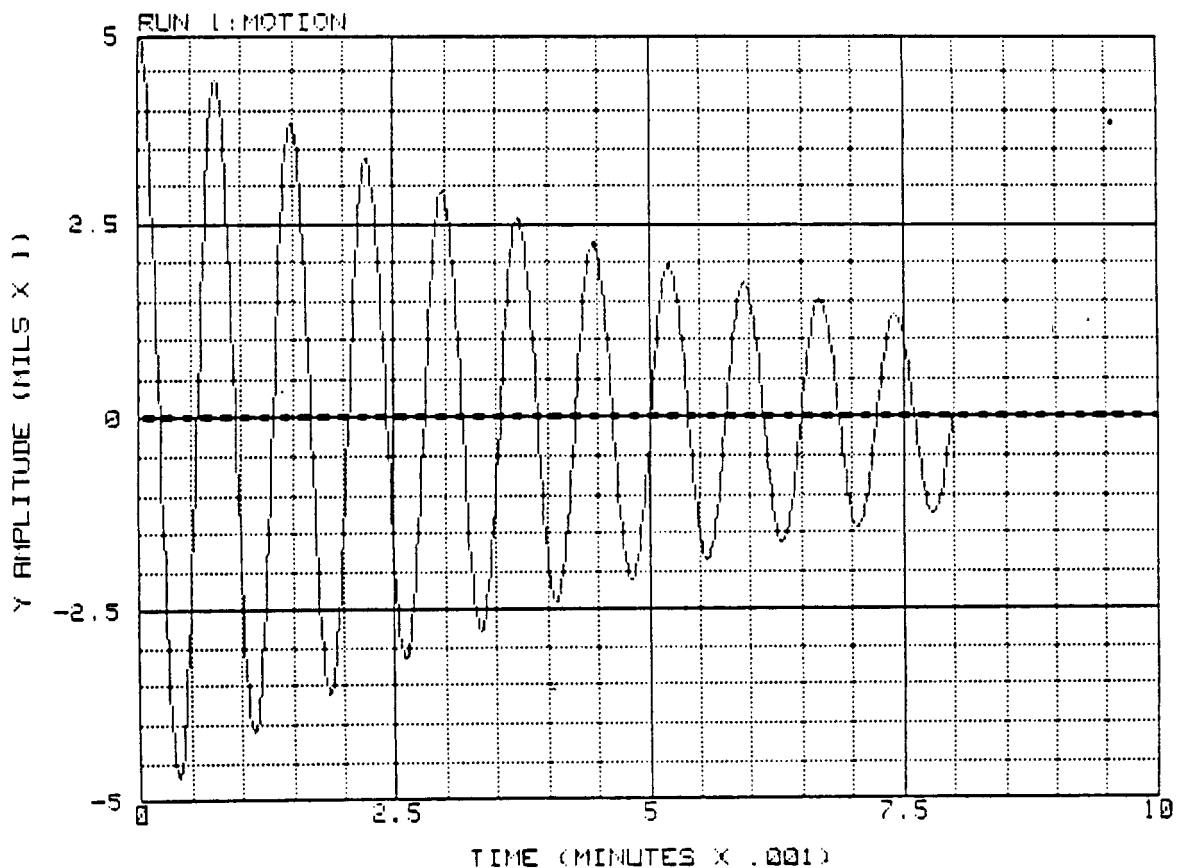


FIGURE 14.15 NUMERICALLY CALCULATED SOLUTION FOR MAXIMUM CHANGE OF 5% AND OVERRIDE THRESHOLD OF  $1 \times 10^{-4}$  INCHES FOR A SYSTEM WITH NO EXTERNAL DAMPING AND 5 MILS OF INITIAL DISPLACEMENT.

NEW RUN NUMBER (number)	E
1. SPRING STIFFNESS;K (Lb/in)	100
2. OBSERVED DAMPING;D (Lb sec/in)	0
3. EFFECTIVE ROTOR MASS;Meff (Lb sec <sup>2</sup> /in)	.005
223. DIAM CLEARANCE;Cd (Mils)	20
244. COEFFICIENT OF FRICTION;Mu (value)	40
272. IMPACT DURATION;Im_dur (Sec)	.001
23. PERTURBATION MASS;Mp (Grams)	0
24. PERTURBATION RADIUS;Rp (Inches)	1
166. PERTURBATION WEIGHT ANGLE (Degrees)	0
248. INITIAL RADIAL DISPLACEMENT;R1 (Inches)	.005
249. INITIAL ANGULAR DISPLACEMENT;T1 (Degrees)	0
250. INITIAL RADIAL VELOCITY;Vr1 (In/sec)	0
251. INITIAL ANGULAR VELOCITY;Vt1 (Rpm)	0
13. OPERATING FREQUENCY;Fop (Rpm)	1000
NUMBER OF COMPUTATIONAL STEPS/REVOLUTION (value)	64
NUMBER OF REVOLUTIONS (value)	8
260. MAXIMUM DISPLACEMENT CHANGE;Ch (Percent)	5
261. ITERATION THRESHOLD;It_thresh (Inches)	.001

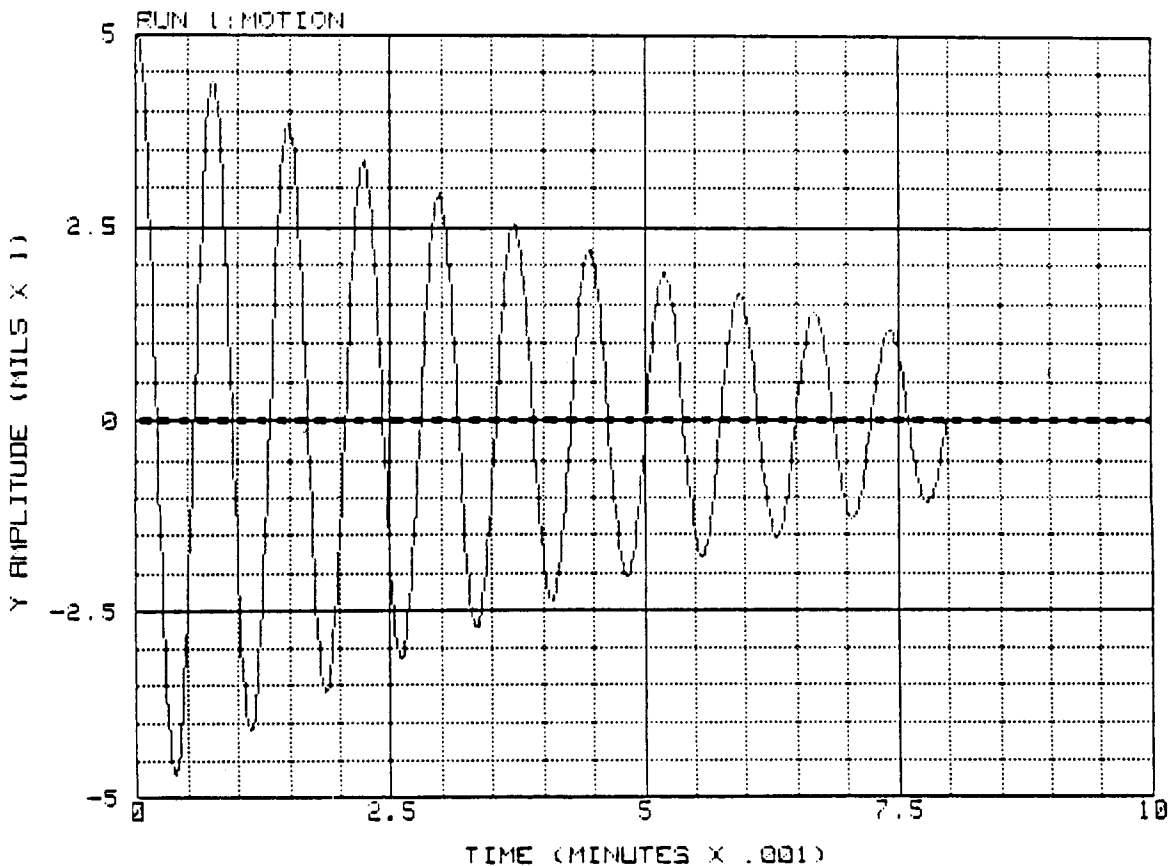


FIGURE 14.16 NUMERICALLY CALCULATED SOLUTION FOR MAXIMUM CHANGE OF 5% AND OVERRIDE THRESHOLD OF  $1 \times 10^{-3}$  INCHES FOR A SYSTEM WITH NO EXTERNAL DAMPING AND 5 MILS OF INITIAL DISPLACEMENT.

NEW RUN NUMBER (number)	F
1. SPRING STIFFNESS;K (Lb/in)	100
2. OBSERVED DAMPING;D (Lb sec/in)	0
3. EFFECTIVE ROTOR MASS;M <sub>eff</sub> (Lb sec <sup>2</sup> /in)	.005
223. DIAM CLEARANCE;C <sub>d</sub> (Mils)	20
244. COEFFICIENT OF FRICTION;Mu (value)	40
272. IMPACT DURATION;Im_dur (Sec)	.001
23. PERTURBATION MASS;Mp (Grams)	0
24. PERTURBATION RADIUS;Rp (Inches)	1
166. PERTURBATION WEIGHT ANGLE (Degrees)	0
248. INITIAL RADIAL DISPLACEMENT;R1 (Inches)	.005
249. INITIAL ANGULAR DISPLACEMENT;T1 (Degrees)	0
250. INITIAL RADIAL VELOCITY;Vr1 (In/sec)	0
251. INITIAL ANGULAR VELOCITY;Vt1 (Rpm)	0
13. OPERATING FREQUENCY;Fop (Rpm)	1000
NUMBER OF COMPUTATIONAL STEPS/REVOLUTION (value)	64
NUMBER OF REVOLUTIONS (value)	8
260. MAXIMUM DISPLACEMENT CHANGE;Ch (Percent)	5
261. ITERATION THRESHOLD;It_thresh (Inches)	.01

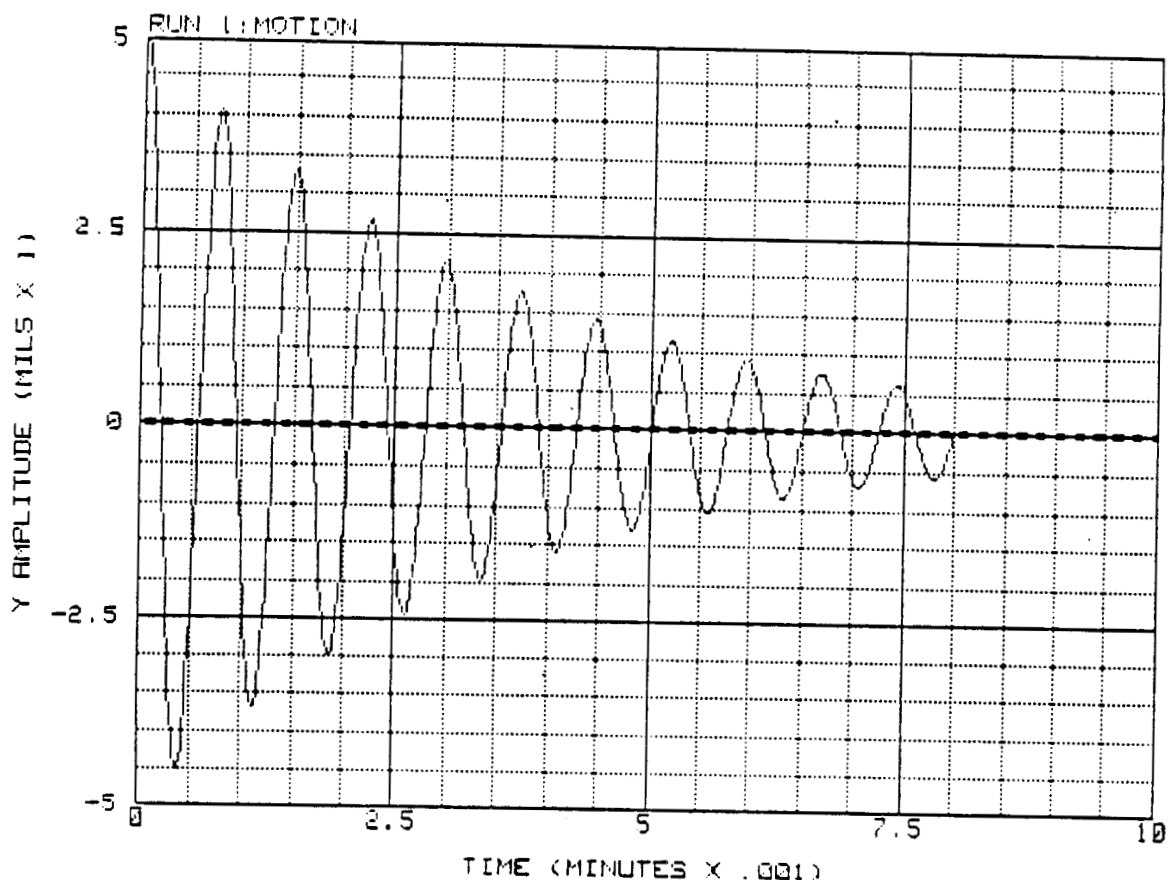


FIGURE 14.17 NUMERICALLY CALCULATED SOLUTION FOR MAXIMUM CHANGE OF 5% AND OVER-RIDE THRESHOLD OF  $1 \times 10^{-2}$  INCHES FOR A SYSTEM WITH NO EXTERNAL DAMPING AND 5 MILS OF INITIAL DISPLACEMENT.

## 15. RESULTS FROM COMPUTER SIMULATION PROGRAM.

### 15.1 Introduction

The computer program described in the previous chapter was written to help explore the effects of rotor-to-stator contact on the vibrational response of rotating machines operating under rubbing conditions. This chapter of the report presents some rotor vibrational responses calculated by the program for conditions similar to those used to produce the data from the HPFTP simulation rotor rig presented in Chapter 12 of this report.

### 15.2 Determination of the System Dynamic Parameters Using the Linear Synchronous Response Part of the Computer Program

The first step in the rub analysis process using this computer program consists of defining the system parameters. As with any simulation process, the computed responses only represent the actual responses of the target system to the degree that the computer model and its parameters match those of the real system. To verify program operation, the parameters were selected to roughly model the HPFTP simulation rub rig. Therefore, it should be possible to determine whether the calculated rub responses exhibit the same characteristics as those obtained experimentally. The system parameters were determined by choosing a set of parameters and then using the linear synchronous portion of the program to get the resonant frequencies and rotor mode shape at each resonance. The parameters were then adjusted and the program run again, until the resonant frequencies approximated those of the simulation rotor rig. The parameters selected for these tests are listed in Table 15.1, and the synchronous responses at each location are presented in Figures 15.1 through 15.7. These can be compared with the experimental results from the simulation rotor rig presented in Chapter 7. Since the parameters are axially symmetrical for ease of selection, the mode shapes only roughly approximate those of the simulation rig.

### 15.3 Results From the Nonlinear Timebase Portion of the Computer Program

Table 15.2 lists the additional parameters necessary for the nonlinear system calculations. As was discussed in the previous section, the values for the system parameters used for the computational tests represent a system similar to, but not identical with, the HPFTP simulation rub rig. This produces calculated linear response resonant frequencies reasonably close to those of the simulation rotor rig, but the mode shape at each of these frequencies only roughly approximates mode shapes of the simulation rotor rig. In order to get results which match the experimental test results more closely, the parameters need to be adjusted from the symmetrical system used for these calculations to a set which more closely approximates the skewed mode shapes produced by the experimental rotor rig. Also, the unbalance and radial preload forces should be distributed amongst the three mass locations, "A," to produce the same once-per-turn synchronous responses and static mode shapes as those generated in the simulation rig by the mass unbalance and radial preload applied for the individual tests. The test sequence used to generate the experimental data was repeated to produce the calculated results. This consists of introducing an unbalance force which does not result with a large enough amplitude to generate rub at the desired rotative speed and then incrementally increasing the static radial preload to initiate rubbing conditions of variable ranges of severity.

Two sets of test data were generated using this test sequence. The first was produced with the unbalance force located at the third disk, the plane  $z_3$  (A3), while the second with the unbalance force located in the second disk, at  $z_2$  (A2). The static radial preload force was applied at the third disk, location  $z_3$  (A3), for both sets of tests.

### 15.3.1 Results From the Calculations With the Unbalance and the Radial Preload at the Third Disk

Even though the model parameters do not exactly match the simulation rub rig, when the computed results from the program, presented in Figures 15.8 through 15.42, are compared with the experimentally obtained data from the rub rig presented in Chapter 12, the similarity is readily apparent.

For comparison purposes, the data for low oil pressures at seal simulation bearing should be used, either 0.0 or 2.5 psi oil pressures, since no seal stiffnesses were introduced in the example of computer model parameters. Vibrational data responses near a primary rub location are represented in the computer results at location NB3, and in the experimental data at probe location 2. Therefore, the vibration responses at these points may be compared for response similarity near a rub location, even though the points are not identical because of the difficulty in installing measurement transducers at the exact location where rub occurs. For comparison of vibration response at different axial locations along the shaft; NA1 should be compared with probe location 3, NA2 with probe location 4, and NA3 with probe location 5. Again, these comparisons cannot be entirely exact since there are no exact matches between calculated points and measurement points.

At low radial preload forces, before rotor-to-stator contact occurs, both systems produce linear responses to the applied forces. As the radial preload (with a chosen vertical direction) is increased until light radial contact occurs, the shaft response orbits become highly nonsymmetrical with the highest amplitudes in the direction from the contact point to the centerline of the system, in this case the vertical direction. This large vertical component of the vibration response is predominantly  $1/2\times$  for both the calculated and experimental data while the horizontal vibration response remains predominantly  $1\times$  with a much smaller  $1/2\times$  component. At the highest forces used in the calculated results, which correspond with the medium preload results from the experimental data, the larger preload have reduced the  $1/2\times$  vibration component in the vertical direction producing a vibration response that is moving back toward predominantly  $1\times$  components, with the addition of some higher harmonics. The horizontal vibration response has increased, mostly due to a large increase in the  $1/2\times$  component in the computer-calculated responses. The experimental data also shows an increase in the horizontal response; however, the major increase is in the  $1\times$  component instead of the  $1/2\times$ . This could be attributed to the difference in contact and measurement planes that exist between the computer and experimental models, or differences in the rub parameters such as friction coefficients, restitution coefficients, or maybe even the increased restraint added due to the stator stiffness. Additional parametric studies using the computer program would have to be conducted to determine the exact cause for the observed variation. A comparison of the results calculated by the computer program with the experimental results obtained from the HPFTP simulation rotor rig indicates that the computer program produces responses similar to those obtained experimentally for operating conditions including rotor-to-stator rubbing.

### 15.3.2 Results From the Calculations With the Unbalance in the Second Disk and the Radial Preload at the Third Disk

The calculated responses for this series of tests are presented in Figures 15.43 through 15.70. As with the experimental results from the simulation rotor rig, the basic trends for the rub responses are the same as those determined from the test with the unbalance in the third disk. Again the same basic trends are seen in both the experimental and calculated vibrational responses.

#### 15.4 Summary

This chapter presented the calculated responses from the computer simulation program and compared these with the data experimentally obtained from the HPFTP simulation rotor rig. Even though the system parameters in the computer program have not been perfectly matched to those of the HPFTP rub rig, there is strong similarity between the responses produced using the computer program and those obtained experimentally from the rub rig. The results presented in this chapter represent only a sample of the computer program use and abilities. This program may have a wide range of applications in rotor dynamic problems.

TABLE 15.1 SYSTEM PARAMETERS USED IN THE COMPUTER SIMULATION PROGRAM TO APPROXIMATE THE HPFTP SIMULATION ROTOR RIG.

RUB CONDITIONING

LINEAR PARAMETER	VALUE	
MASS 1	0.00250000	
MASS 2	0.00180000	
MASS 3	0.00250000	
SHAFT STIFFNESS 1	200.000	
SHAFT STIFFNESS 2	400.000	
SHAFT STIFFNESS 3	400.000	
SHAFT STIFFNESS 4	400.000	
SHAFT STIFFNESS 5	400.000	
SHAFT STIFFNESS 6	200.000	
SHAFT STIFFNESS 7	0.000	
SHAFT DAMPING 1	0.050000	
SHAFT DAMPING 2	0.050000	
SHAFT DAMPING 3	0.050000	
UNBALANCE AMPLITUDE 1	TEST VARIABLE-- SEE INDIVIDUAL PLOT CAPTIONS FOR THE VALUE OF THESE PARAMETERS USED TO PRODUCE THE PLOT	
UNBALANCE AMPLITUDE 2		
UNBALANCE AMPLITUDE 3		
UNBALANCE PHASE 1 in degrees	0.000	
UNBALANCE PHASE 2 in degrees	0.000	
UNBALANCE PHASE 3 in degrees	0.000	
RADIAL FORCE 1	TEST VARIABLE-- SEE INDIVIDUAL PLOT CAPTIONS FOR THE VALUE OF THESE PARAMETERS USED TO PRODUCE THE PLOT	
RADIAL FORCE 2		
RADIAL FORCE 3		
FORCE PHASE 1 in degrees	0.000	
FORCE PHASE 2 in degrees	0.000	
FORCE PHASE 3 in degrees	90.000	
FLUID DAMPING 1	0.050	
FLUID DAMPING 2	0.010	
FLUID DAMPING 3	0.010	
FLUID DAMPING 4	0.050	
FLUID VELOCITY RATIO 1	0.000000	
FLUID VELOCITY RATIO 2	0.000000	
FLUID VELOCITY RATIO 3	0.000000	
FLUID VELOCITY RATIO 4	0.000000	
FLUID RADIAL STIFFNESS 1	100.00000	
FLUID RADIAL STIFFNESS 2	0.00000	
FLUID RADIAL STIFFNESS 3	0.00000	
FLUID RADIAL STIFFNESS 4	100.00000	
SEAL CLEARANCE 1	10.00000000	
SEAL CLEARANCE 2	0.05000000	
SEAL CLEARANCE 3	0.05000000	
SEAL CLEARANCE 4	10.00000000	
BEGINNING RPM => 10	ENDING RPM => 10000	DELTA RPM => 20

TABLE 15.2 ADDITIONAL SYSTEM PARAMETERS NECESSARY TO PERFORM  
NONLINEAR TIMEBASE RESPONSE CALCULATIONS USING THE  
COMPUTER SIMULATION PROGRAM.

RUB CONDITIONING		
NONLINEAR PARAMETER		VALUE
INITIAL X DISPLACEMENT	A1	0.00000000
INITIAL X DISPLACEMENT	A2	0.00000000
INITIAL X DISPLACEMENT	A3	0.00000000
INITIAL X DISPLACEMENT	B1	0.00000000
INITIAL X DISPLACEMENT	B2	0.00000000
INITIAL X DISPLACEMENT	B3	0.00000000
INITIAL X DISPLACEMENT	B4	0.00000000
INITIAL Y DISPLACEMENT	A1	0.00100000
INITIAL Y DISPLACEMENT	A2	0.00100000
INITIAL Y DISPLACEMENT	A3	0.00100000
INITIAL Y DISPLACEMENT	B1	0.00100000
INITIAL Y DISPLACEMENT	B2	0.00100000
INITIAL Y DISPLACEMENT	B3	0.00100000
INITIAL Y DISPLACEMENT	B4	0.00100000
INITIAL X VELOCITY	A1	0.000
INITIAL X VELOCITY	A2	0.000
INITIAL X VELOCITY	A3	0.000
INITIAL X VELOCITY	B1	0.000
INITIAL X VELOCITY	B2	0.000
INITIAL X VELOCITY	B3	0.000
INITIAL X VELOCITY	B4	0.000
INITIAL Y VELOCITY	A1	0.000
INITIAL Y VELOCITY	A2	0.000
INITIAL Y VELOCITY	A3	0.000
INITIAL Y VELOCITY	B1	0.000
INITIAL Y VELOCITY	B2	0.000
INITIAL Y VELOCITY	B3	0.000
INITIAL Y VELOCITY	B4	0.000
STATOR STIFFNESS	1	100000.000
STATOR STIFFNESS	2	100000.000
STATOR STIFFNESS	3	100000.000
STATOR STIFFNESS	4	100000.000
FRICITION COEFFICIENTS	1	0.40000000
FRICITION COEFFICIENTS	2	0.40000000
FRICITION COEFFICIENTS	3	0.40000000
FRICITION COEFFICIENTS	4	0.40000000
RESTITUTION COEFFICIENT	1	1.000
RESTITUTION COEFFICIENT	2	1.000
RESTITUTION COEFFICIENT	3	1.000
RESTITUTION COEFFICIENT	4	1.000
OPERATING SPEED		4000
NUMBER OF SAMPLES PER REVOLUTION		150
NUMBER OF REVOLUTIONS		4

Point ID: B 1 and BETA 1

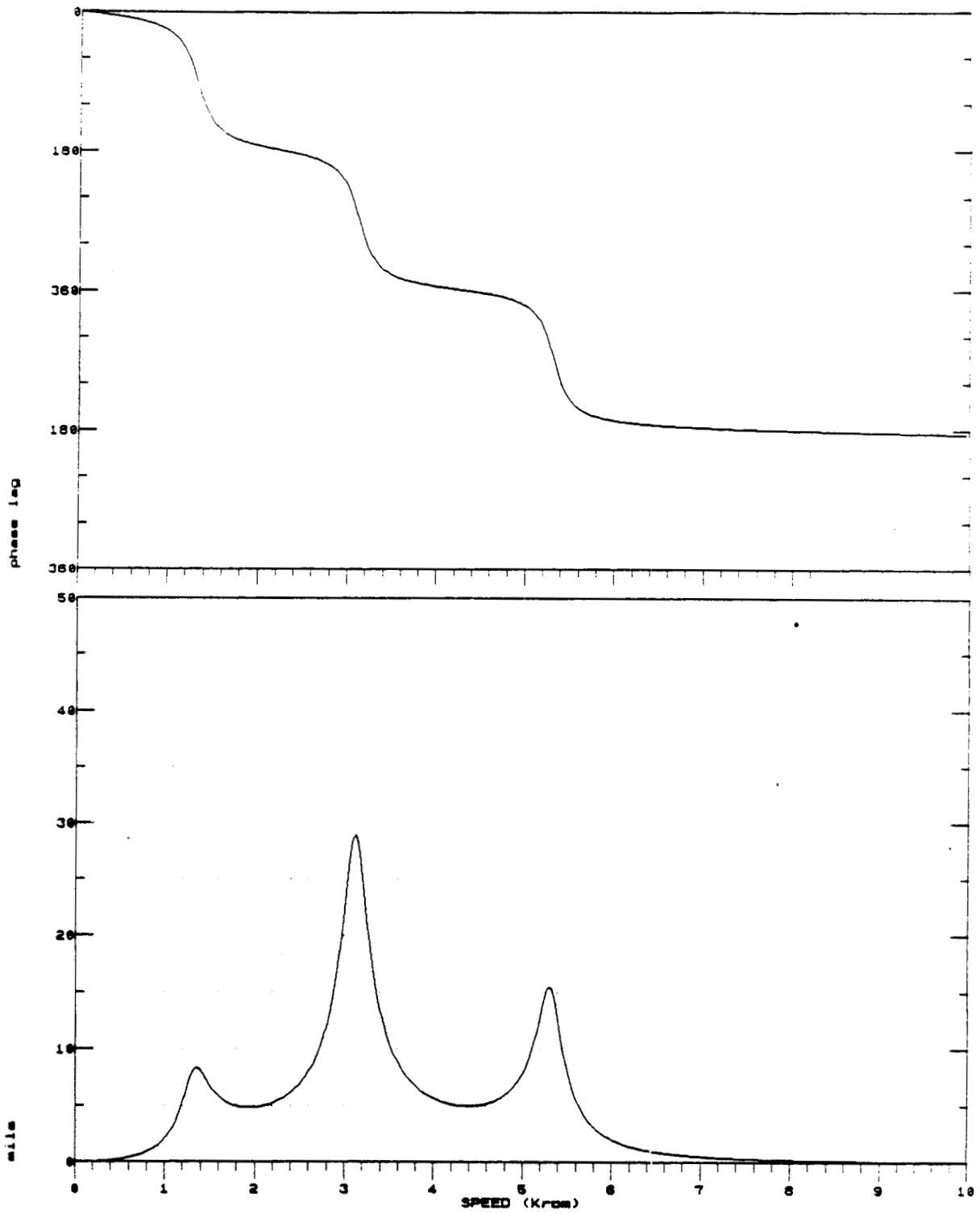


FIGURE 15.1 CALCULATED TRANSIENT RESPONSE USING LINEAR PORTION OF COMPUTER SIMULATION PROGRAM FOR LOCATION B1.

Point ID: A 1 and ALPHA 1

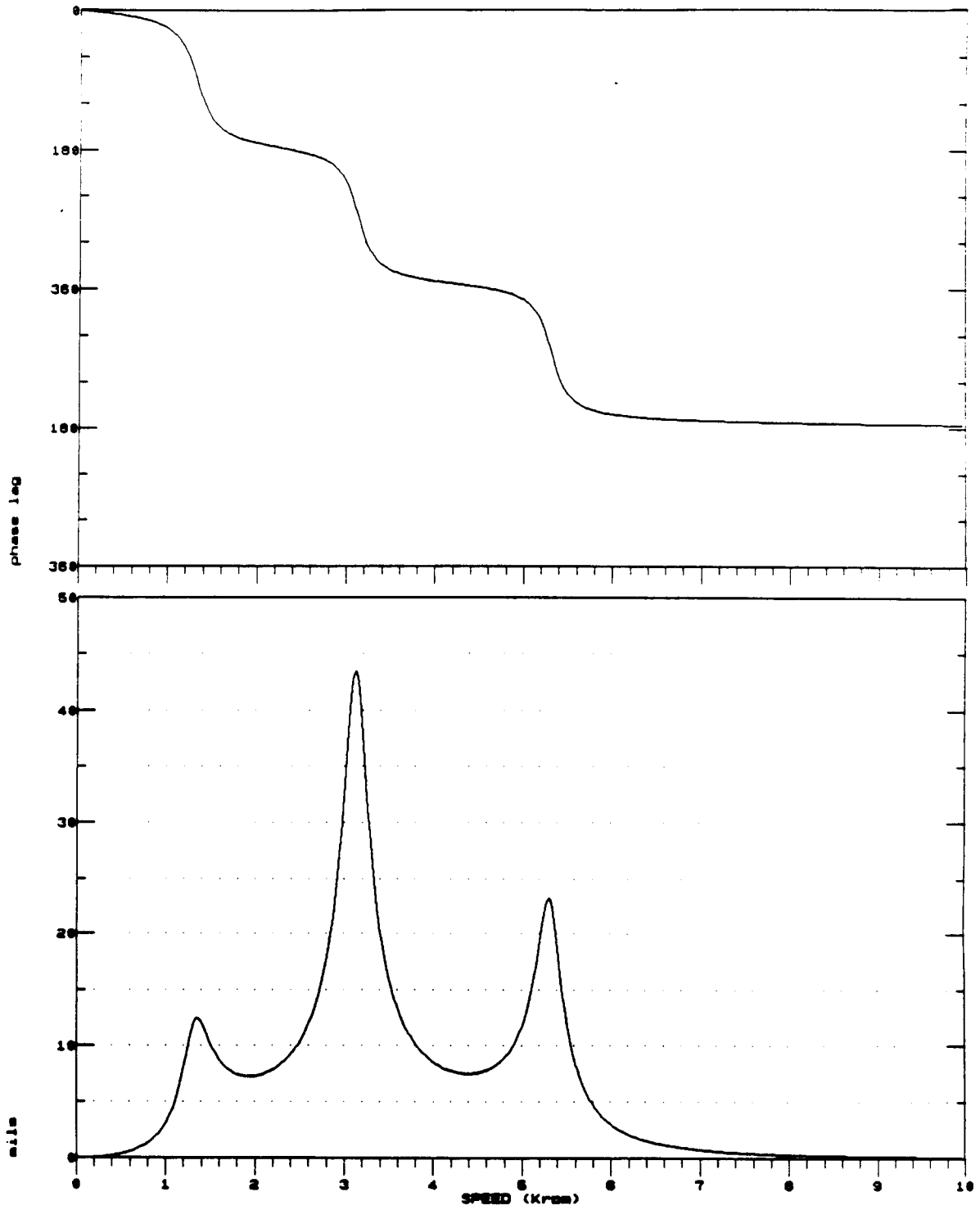


FIGURE 15.2 CALCULATED TRANSIENT RESPONSE USING LINEAR PORTION OF COMPUTER SIMULATION PROGRAM FOR LOCATION A1.

Point ID: B 2 and BETA 2

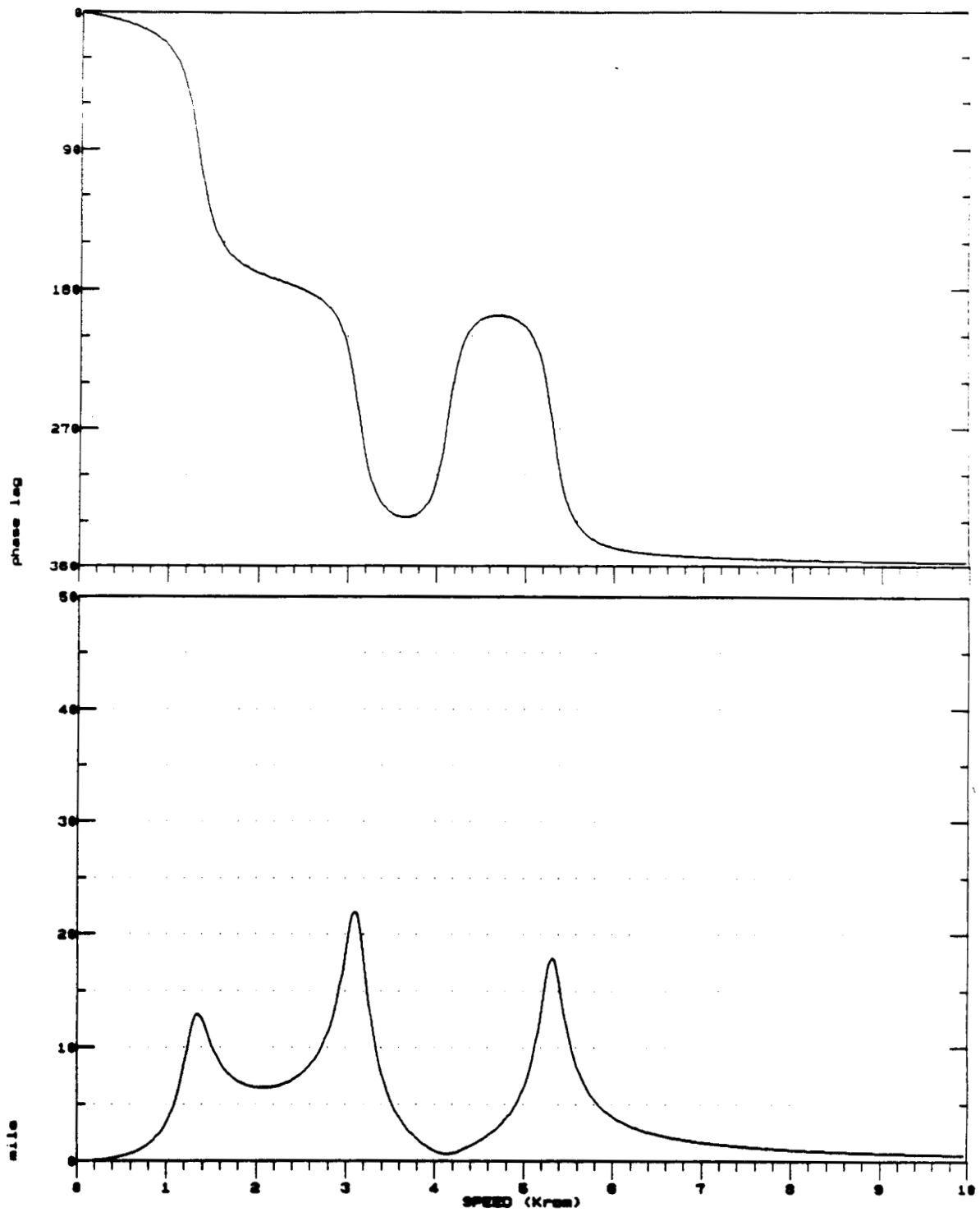


FIGURE 15.3 CALCULATED TRANSIENT RESPONSE USING LINEAR PORTION OF COMPUTER SIMULATION PROGRAM FOR LOCATION B2.

Point ID: A 2 and ALPHA 2

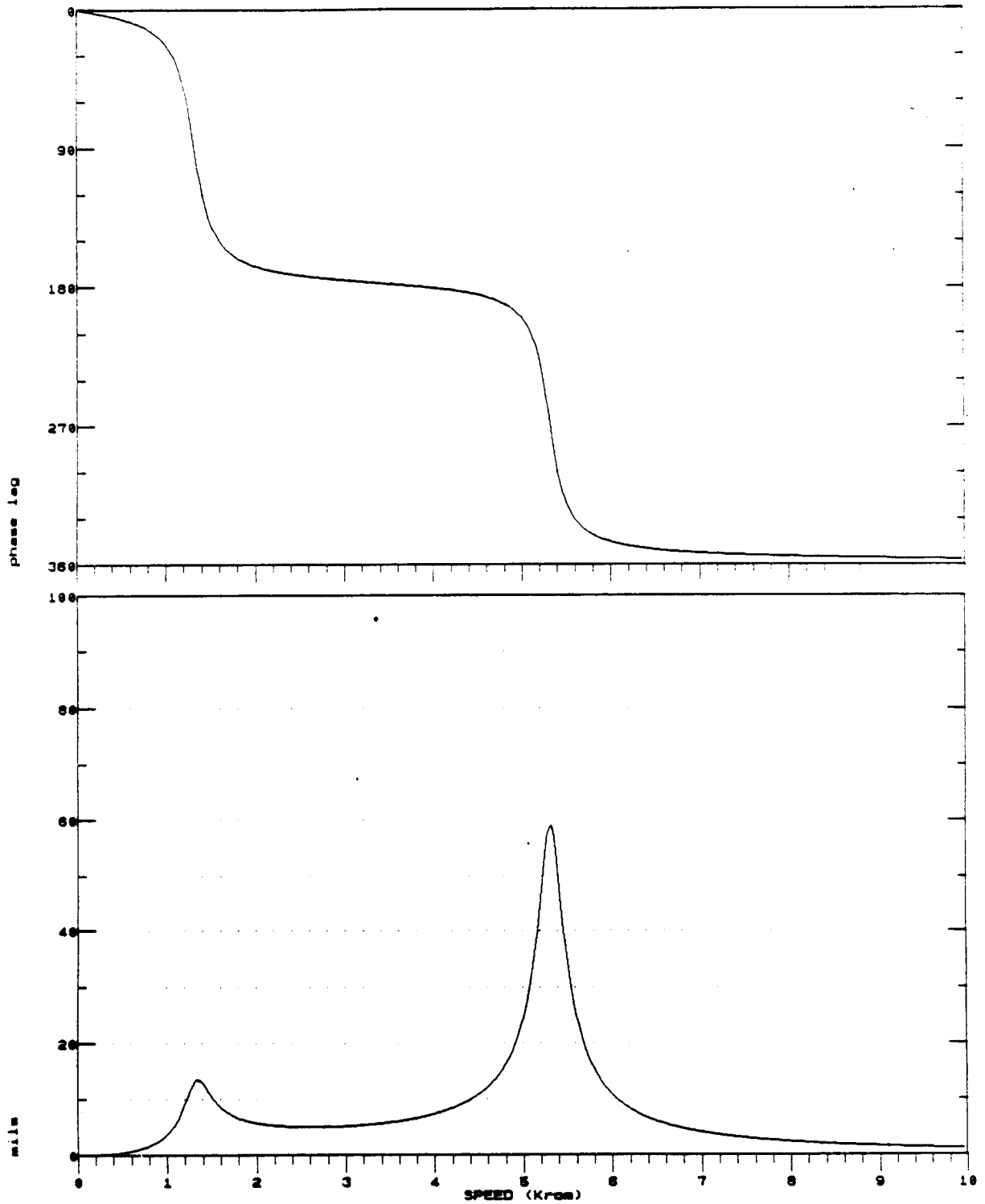


FIGURE 15.4 CALCULATED TRANSIENT RESPONSE USING LINEAR PORTION OF COMPUTER SIMULATION PROGRAM FOR LOCATION A2.

Point ID: B 3 and BETA 3

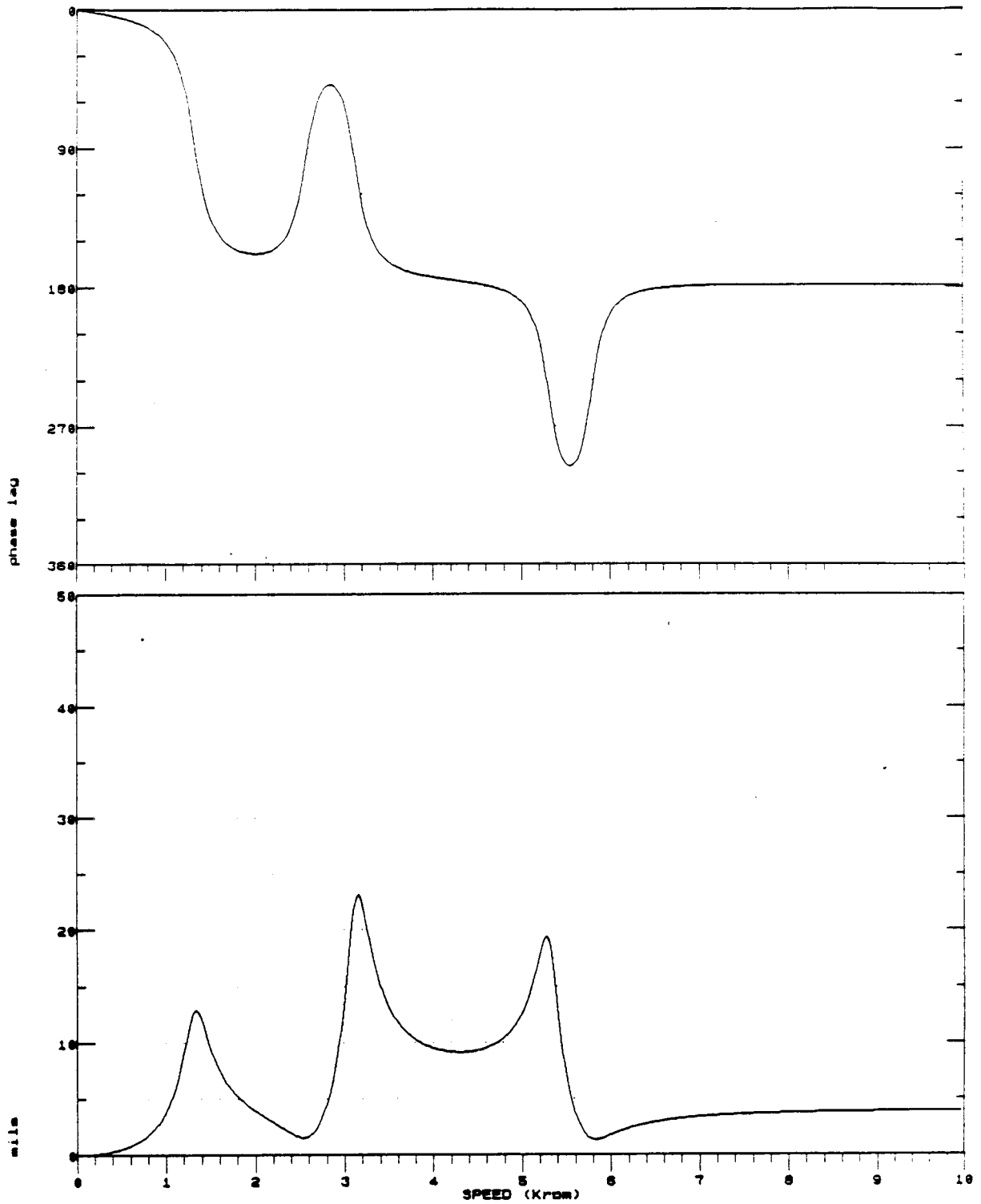


FIGURE 15.5 CALCULATED TRANSIENT RESPONSE USING LINEAR PORTION OF COMPUTER SIMULATION PROGRAM FOR LOCATION B3.

Point ID: A 3 and ALPHA 3

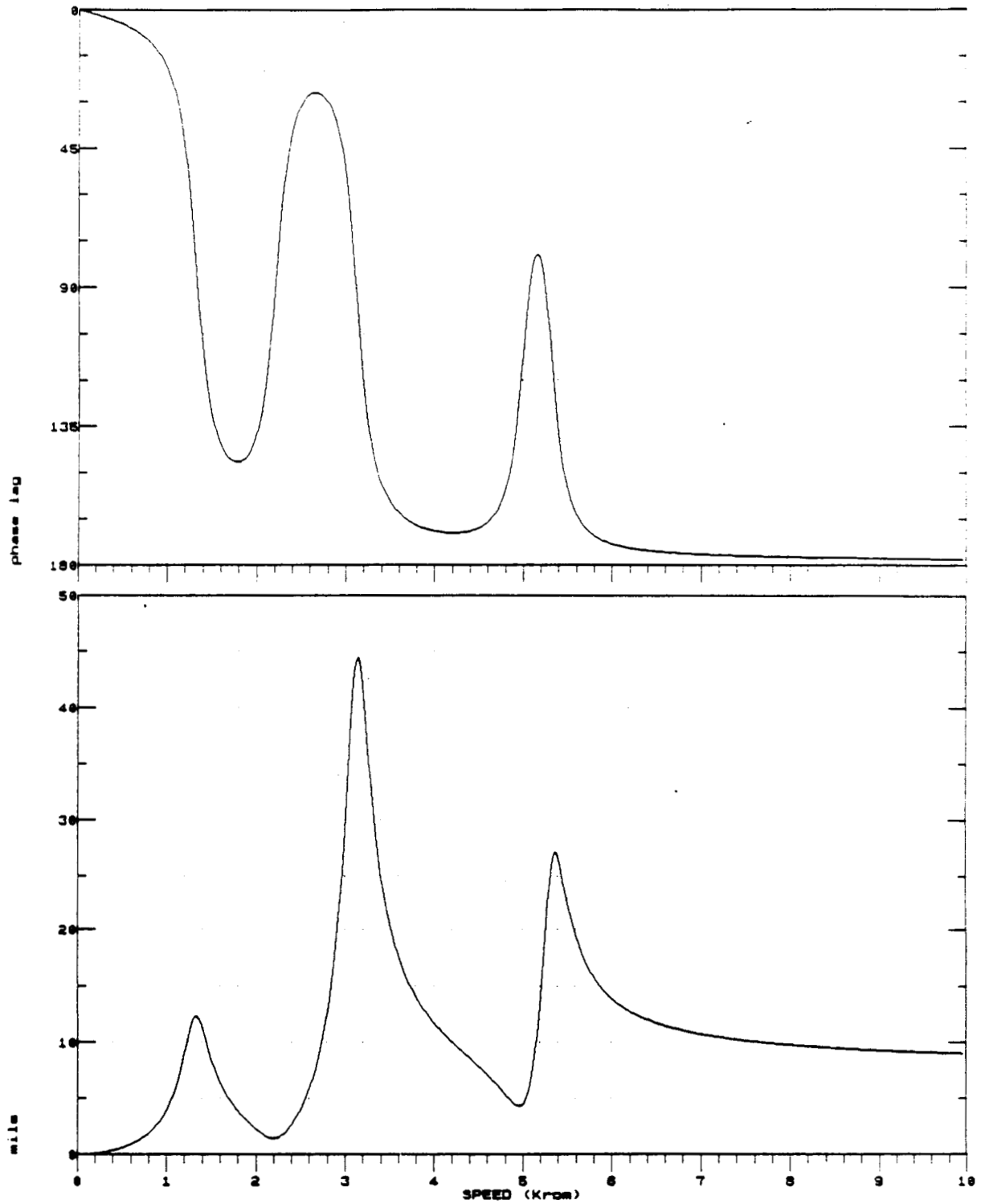


FIGURE 15.6 CALCULATED TRANSIENT RESPONSE USING LINEAR PORTION OF COMPUTER SIMULATION PROGRAM FOR LOCATION A3.

Point ID: B 4 and BETA 4

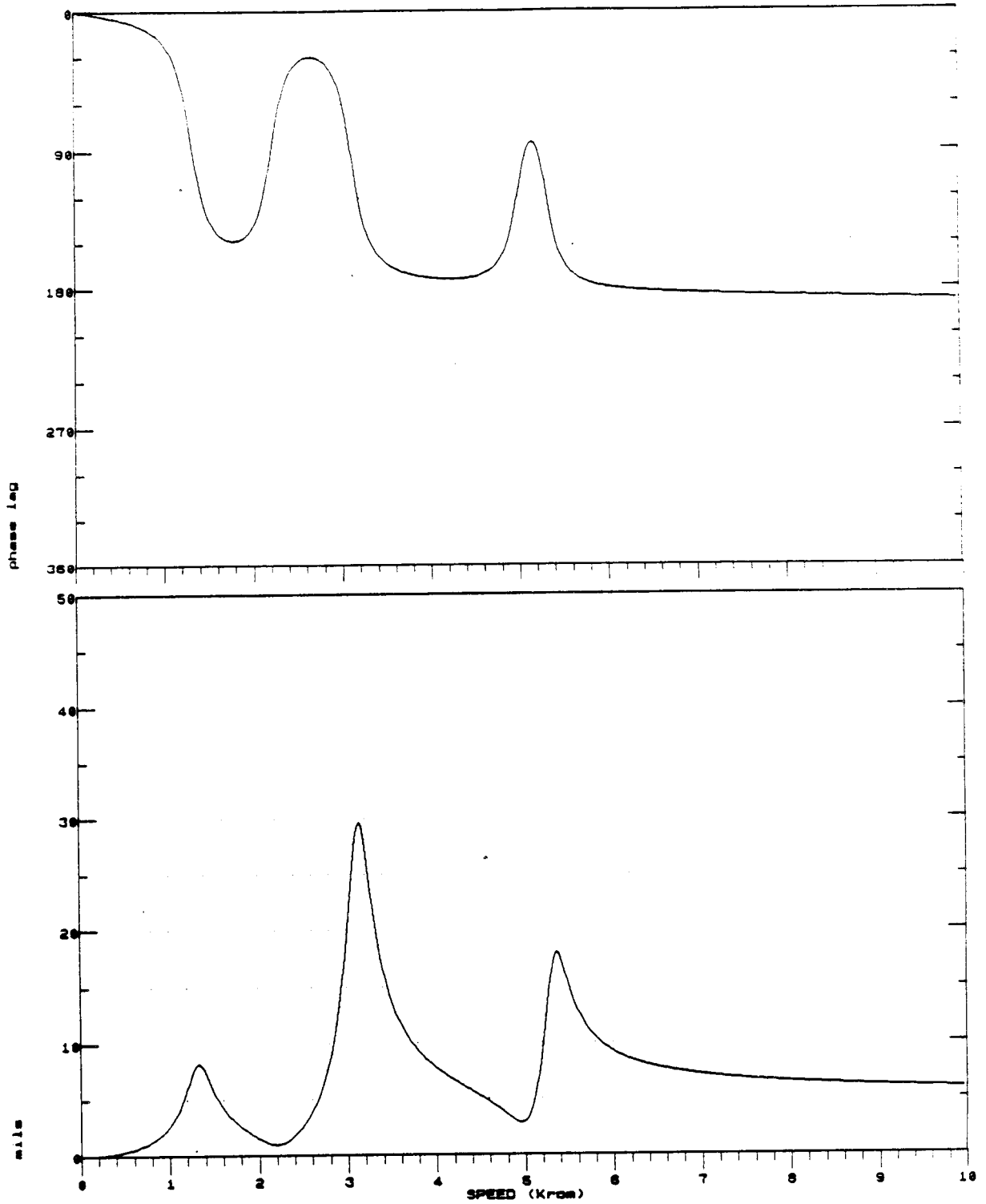
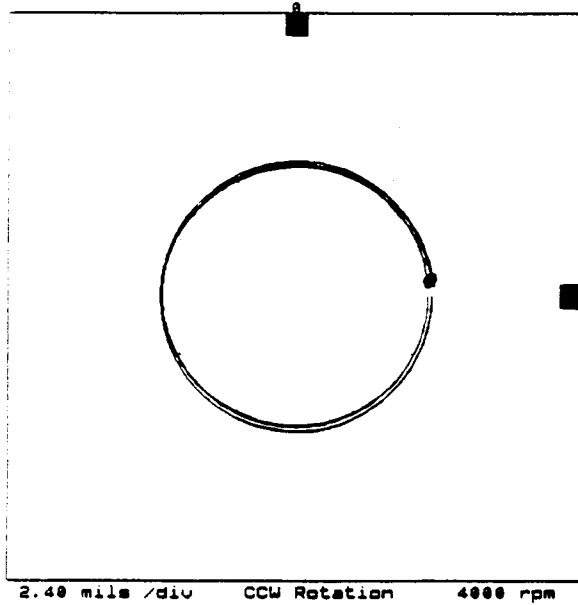


FIGURE 15.7 CALCULATED TRANSIENT RESPONSE USING LINEAR PORTION OF COMPUTER SIMULATION PROGRAM FOR LOCATION B4.

ORIGINAL PAGE IS  
OF POOR QUALITY

Point ID: NBy 1 0 deg  
Point ID: NBx 1 270 deg  
Plot:



Variable:

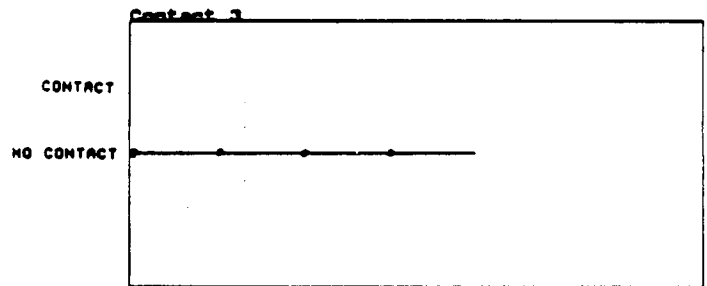
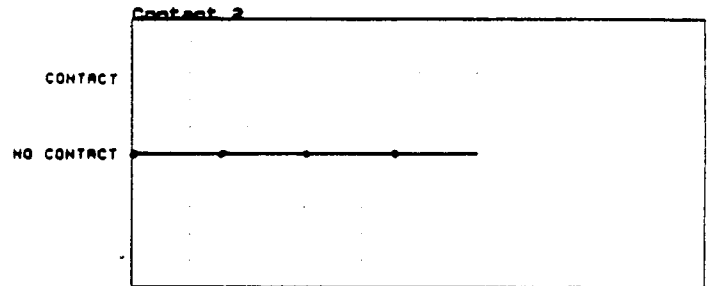
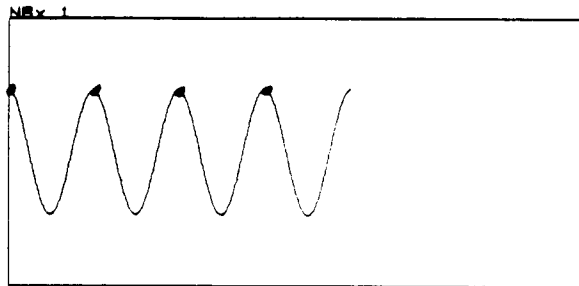
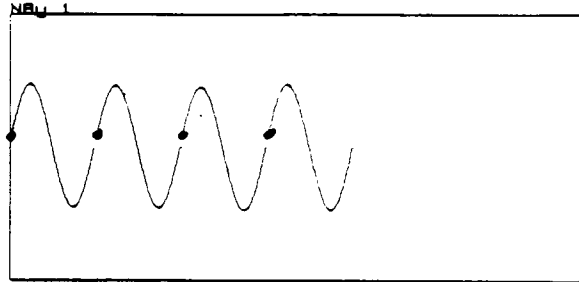
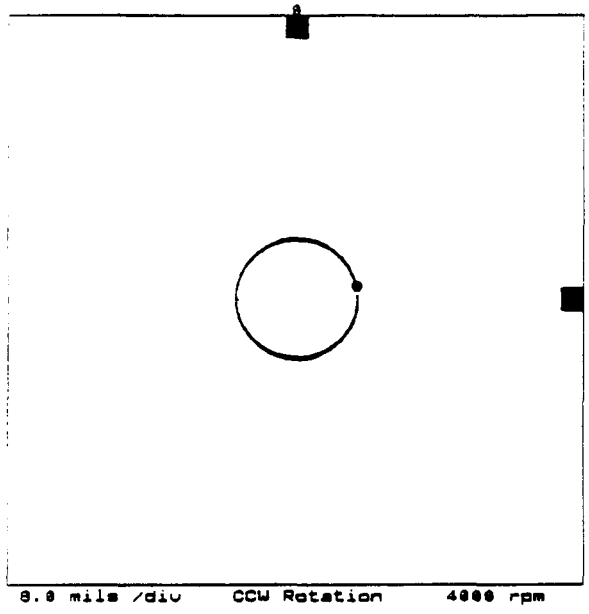


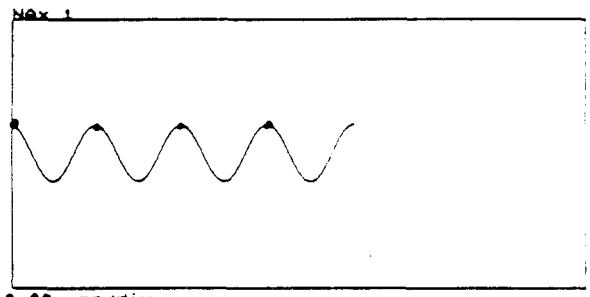
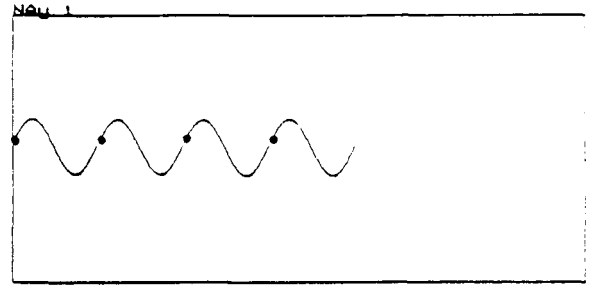
FIGURE 15.8 CALCULATED STEADY-STATE RESPONSE AT LOCATION B1 USING NONLINEAR PORTION OF COMPUTER SIMULATION PROGRAM FOR 4000 RPM, A 0.00002 IN-LB UNBALANCE IN A3 AND A 0.0 LB. RADIAL PRELOAD.

Point ID: NAY 1 0 deg  
Point ID: NAX 1 270 deg  
Plot:



8.8 mils /div CCW Rotation 4000 rpm

Variable:



0.00 ms/div

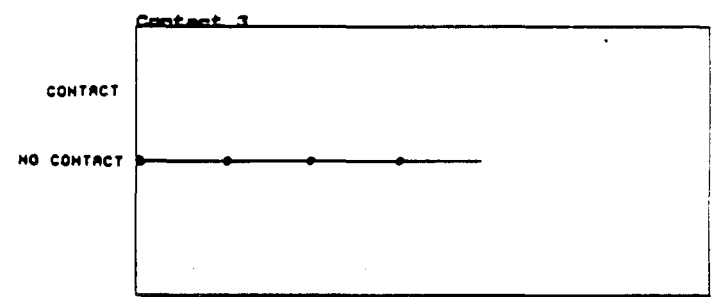
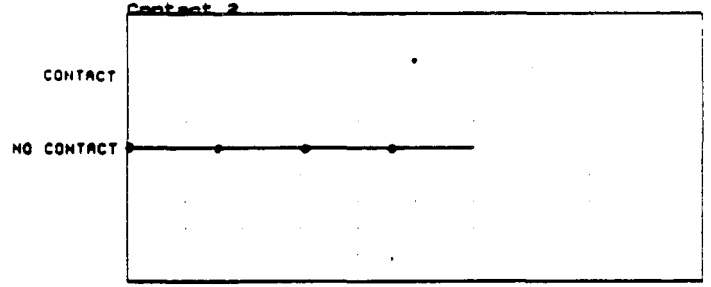


FIGURE 15.9 CALCULATED STEADY-STATE RESPONSE AT LOCATION A1 USING NONLINEAR PORTION OF COMPUTER SIMULATION PROGRAM FOR 4000 RPM, A 0.00002 IN-LB UNBALANCE IN A3 AND A 0.0 LB. RADIAL PRELOAD.

ORIGINAL PAGE IS  
OF POOR QUALITY

Point ID: Nby 2 0 deg  
Point ID: Nbx 2 270 deg  
Plot:

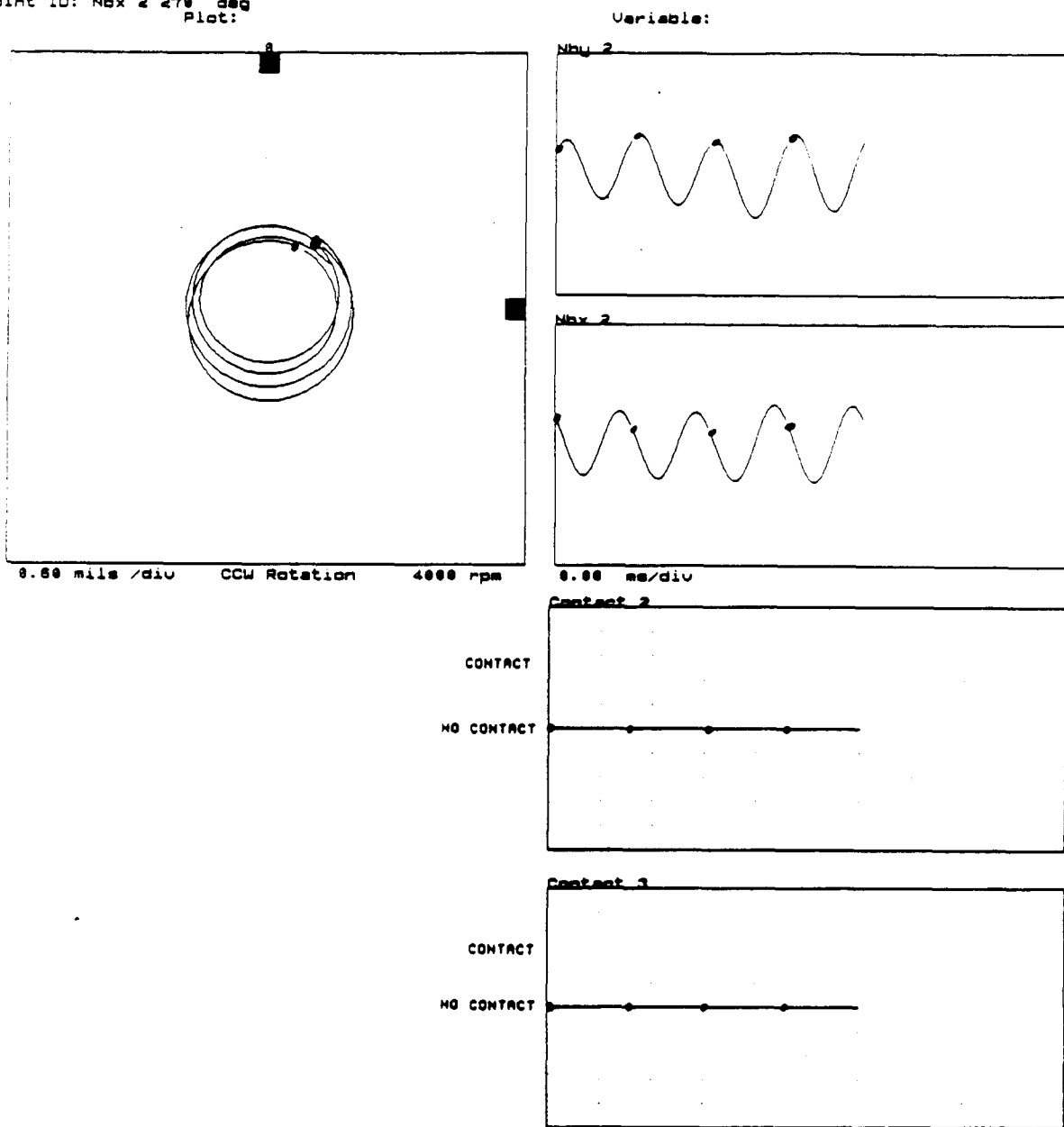
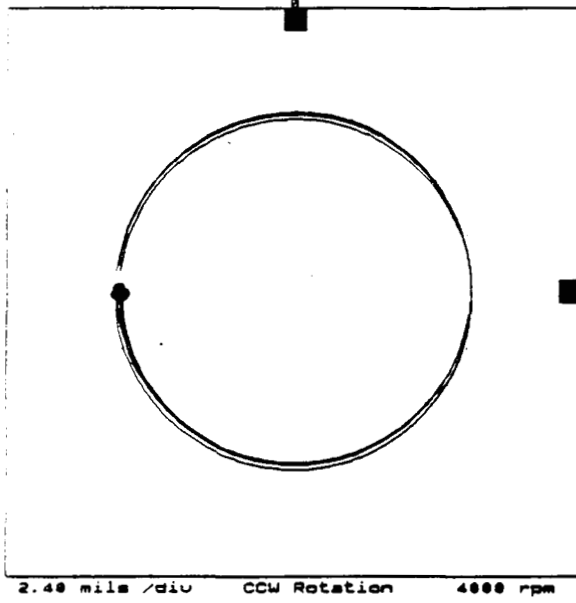


FIGURE 15.10 CALCULATED STEADY-STATE RESPONSE AT LOCATION B2 USING NONLINEAR PORTION OF COMPUTER SIMULATION PROGRAM FOR 4000 RPM, A 0.00002 IN-LB UNBALANCE IN A3 AND A 0.0 LB. RADIAL PRELOAD.

Point ID: NAY 2 0 deg  
Point ID: NAX 2 270 deg  
Plot:



Variable:

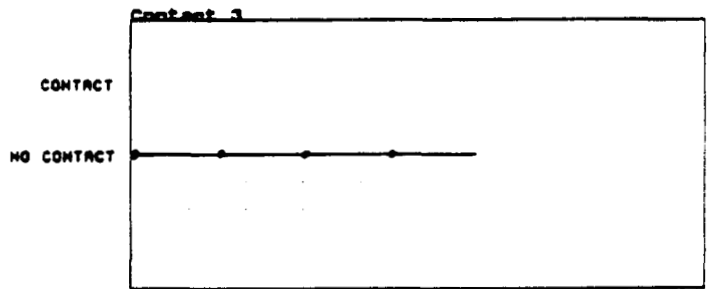
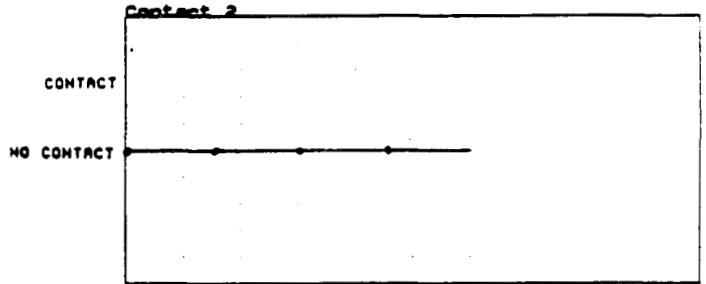
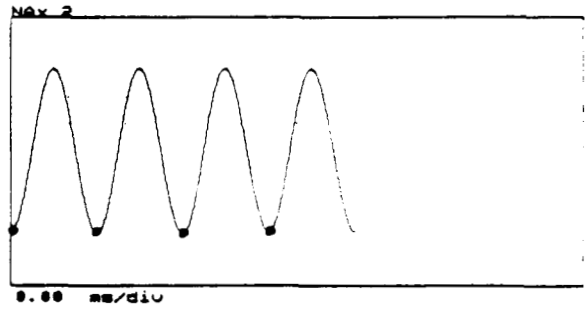
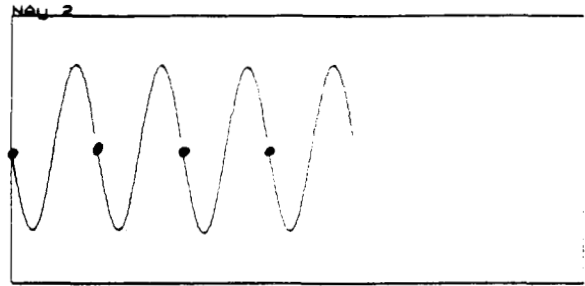
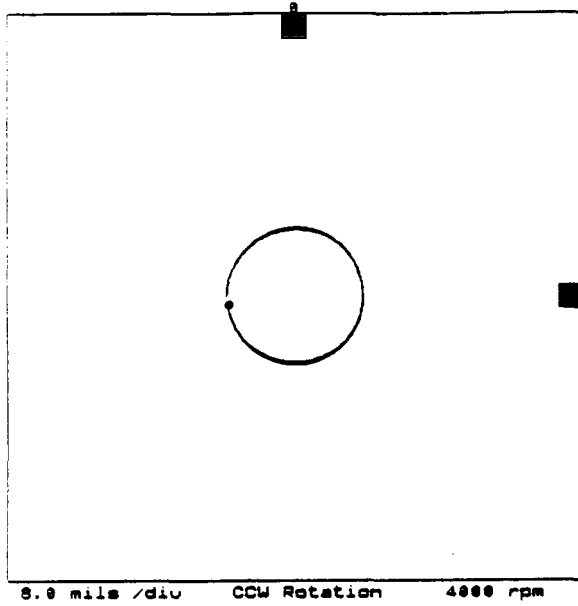


FIGURE 15.11 CALCULATED STEADY-STATE RESPONSE AT LOCATION A2 USING NONLINEAR PORTION OF COMPUTER SIMULATION PROGRAM FOR 4000 RPM, A 0.00002 IN-LB UNBALANCE IN A3 AND A 0.0 LB. RADIAL PRELOAD.

Point ID: NBY 3 0 deg  
Point ID: NBX 3 270 deg  
Plot:



Variable:

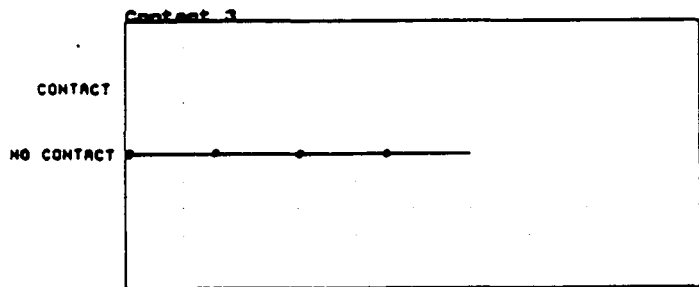
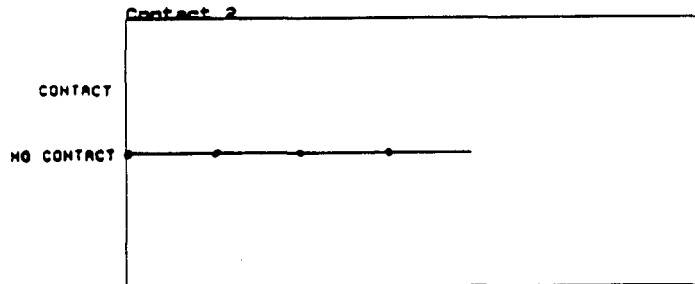
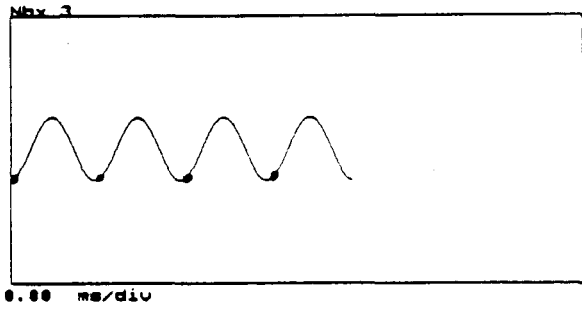
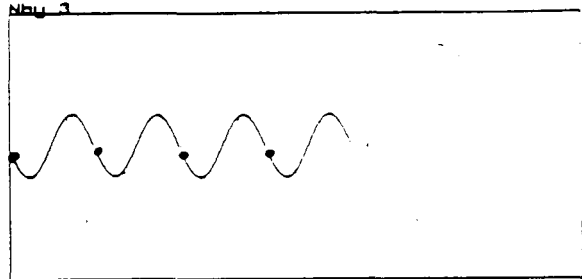


FIGURE 15.12 CALCULATED STEADY-STATE RESPONSE AT LOCATION B3 USING NONLINEAR PORTION OF COMPUTER SIMULATION PROGRAM FOR 4000 RPM, A 0.00002 IN-LB UNBALANCE IN A3 AND A 0.0 LB. RADIAL PRELOAD.

Point ID: NAY 3 0 deg  
Point ID: NAX 3 270 deg  
Plot:

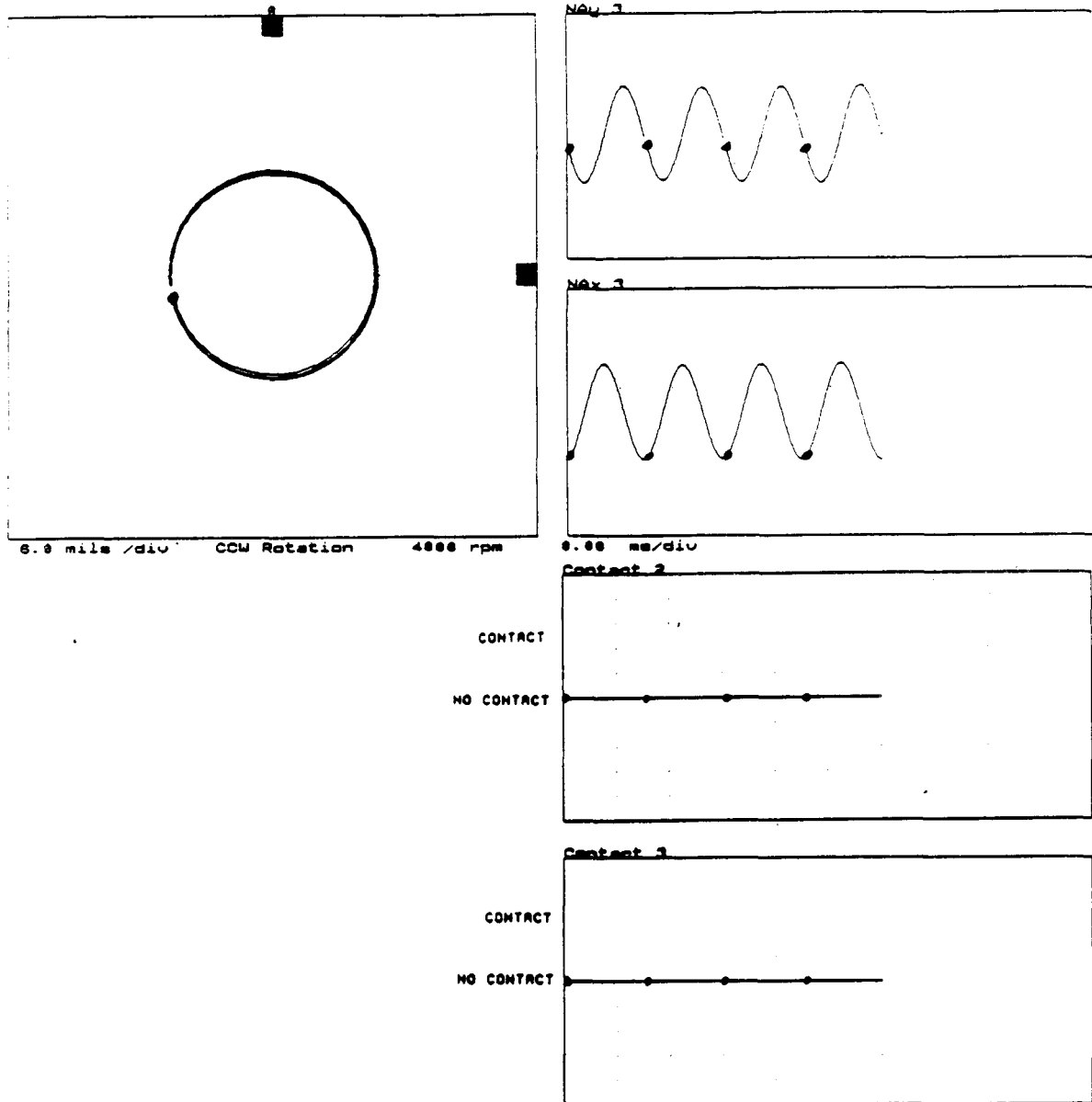
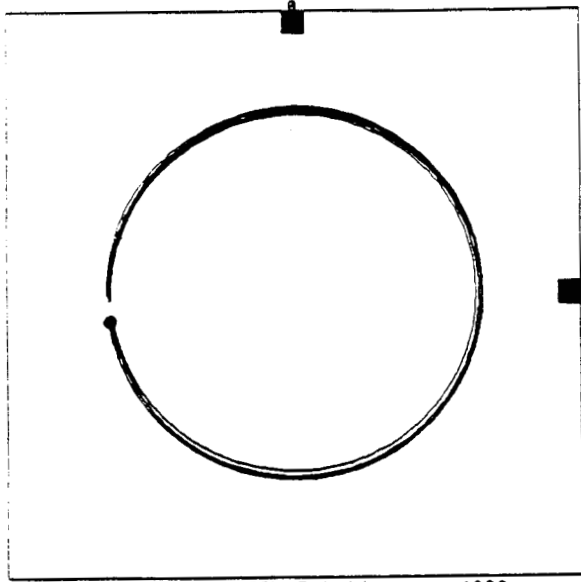


FIGURE 15.13 CALCULATED STEADY-STATE RESPONSE AT LOCATION A3 USING NONLINEAR PORTION OF COMPUTER SIMULATION PROGRAM FOR 4000 RPM, A 0.00002 IN-LB UNBALANCE IN A3 AND A 0.0 LB. RADIAL PRELOAD.

Point ID: NBY 4 0 deg  
Point ID: NBX 4 270 deg  
Plot:



Variable:

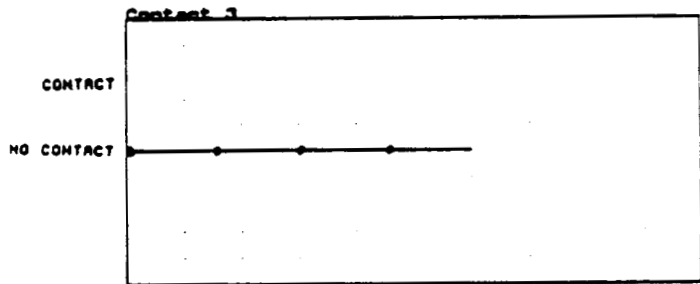
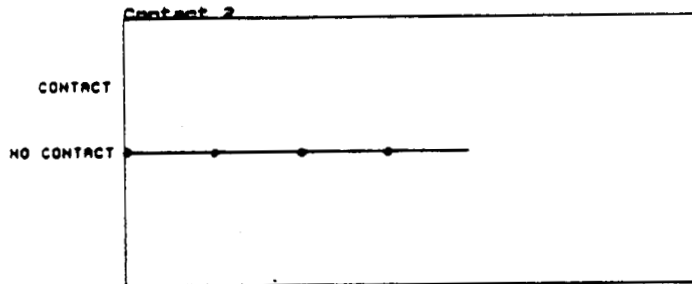
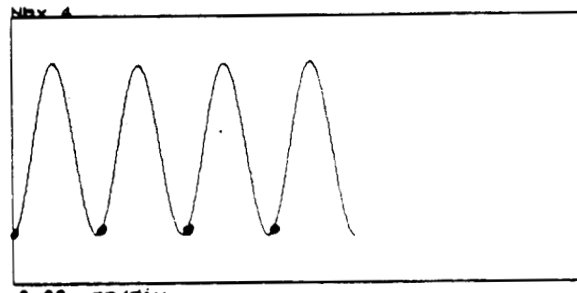
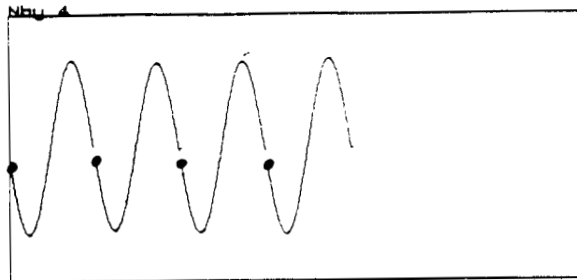


FIGURE 15.14 CALCULATED STEADY-STATE RESPONSE AT LOCATION B4 USING NONLINEAR PORTION OF COMPUTER SIMULATION PROGRAM FOR 4000 RPM, A 0.00002 IN-LB UNBALANCE IN A3 AND A 0.0 LB. RADIAL PRELOAD.

ORIGINAL PAGE IS  
OF POOR QUALITY

Point ID: NBu 1 0 deg  
Point ID: NBx 1 270 deg  
Plot:

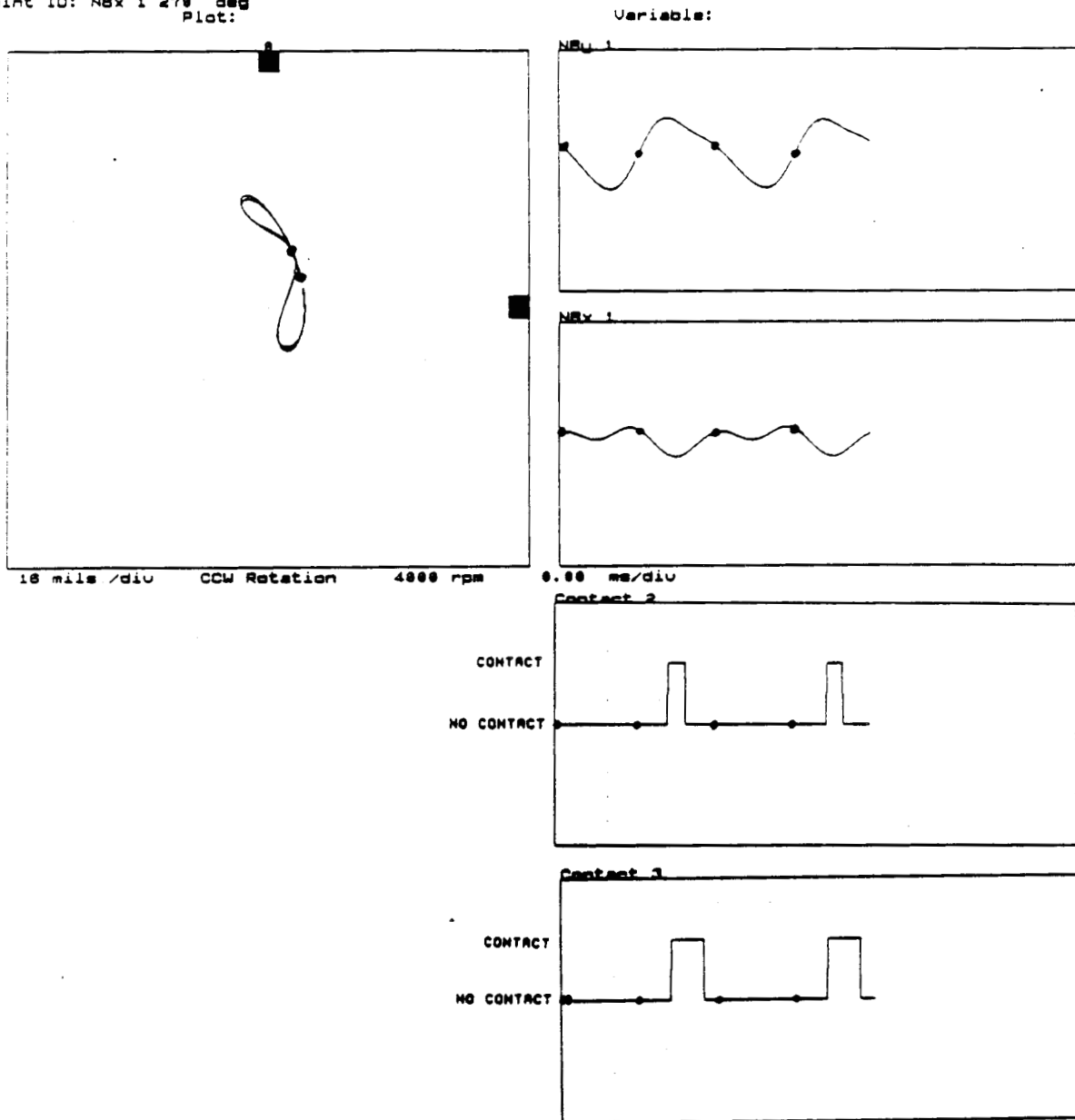


FIGURE 15.15 CALCULATED STEADY-STATE RESPONSE AT LOCATION B1 USING NONLINEAR PORTION COMPUTER SIMULATION PROGRAM FOR 4000 RPM, A 0.00002 IN-LB UNBALANCE IN A3 AND A 6.0 LB. RADIAL PRELOAD AT A3.

Point ID: XDL 1 0 deg  
 Point ID: XDL 1 27 deg  
 Plot:

Variable:

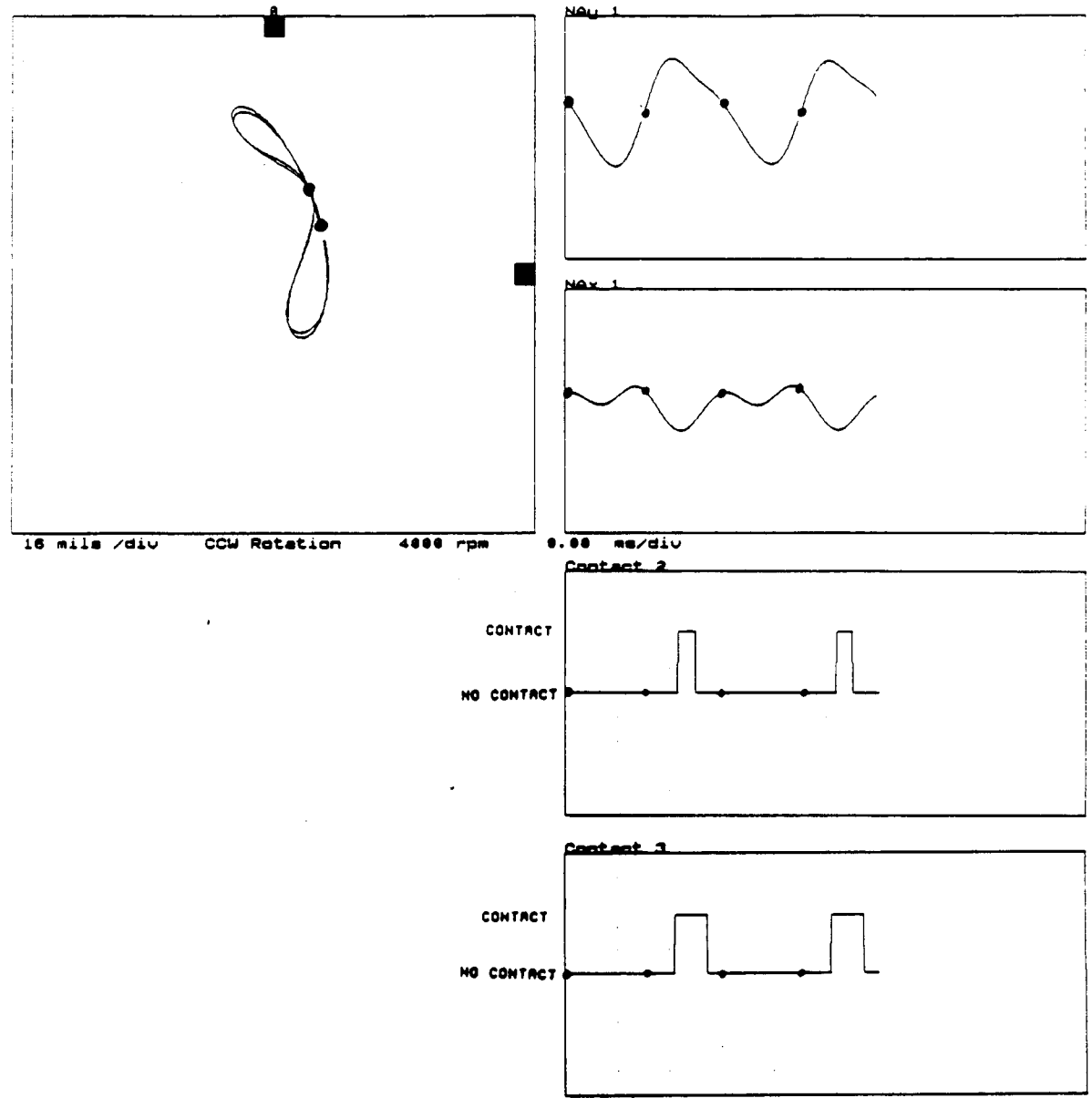


FIGURE 15.16 CALCULATED STEADY-STATE RESPONSE AT LOCATION A1 USING NONLINEAR PORTION OF COMPUTER SIMULATION PROGRAM FOR 4000 RPM, A 0.00002 IN-LB UNBALANCE IN A3 AND A 6.0 LB. RADIAL PRELOAD AT A3.

Point ID: Z0U 2 0 deg  
 Point ID: Z0X 2 270 deg  
 Plot:

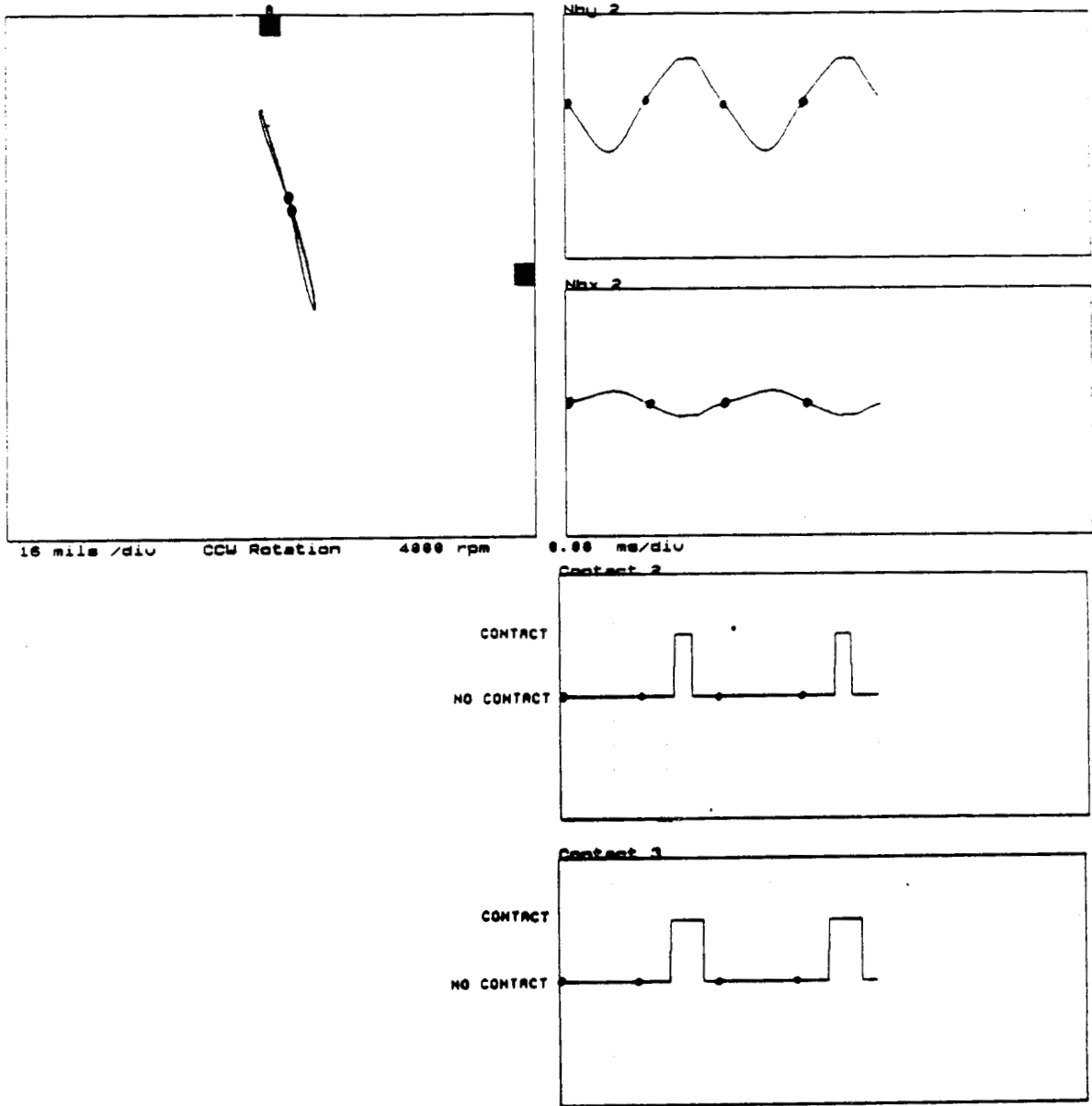


FIGURE 15.17 CALCULATED STEADY-STATE RESPONSE AT LOCATION B2 USING NONLINEAR PORTION COMPUTER SIMULATION PROGRAM FOR 4000 RPM, A 0.00002 IN-LB UNBALANCE IN A3 AND A6.0 LB. RADIAL PRELOAD AT A3.

Point ID: NAY 2 0 deg  
 Point ID: NAX 2 270 deg  
 Plot:

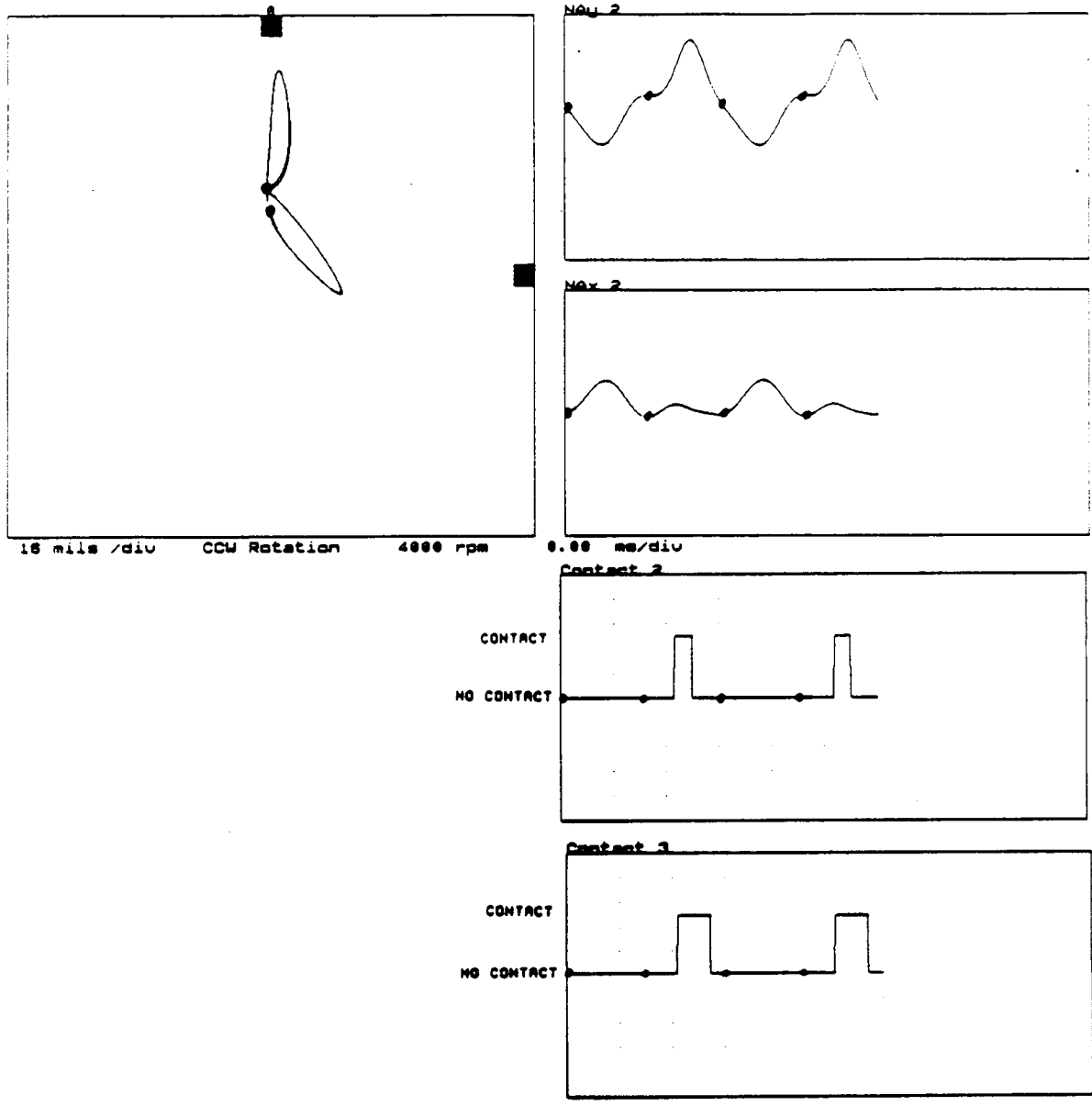


FIGURE 15.18 CALCULATED STEADY-STATE RESPONSE AT LOCATION A2 USING NONLINEAR PORTION COMPUTER SIMULATION PROGRAM FOR 4000 RPM, A 0.00002 IN-LB UNBALANCE IN A3 AND A6.0 LB. RADIAL PRELOAD AT A3.

Point ID: Nbu 3 0 deg  
Point ID: Nbx 3 270 deg  
Plot:

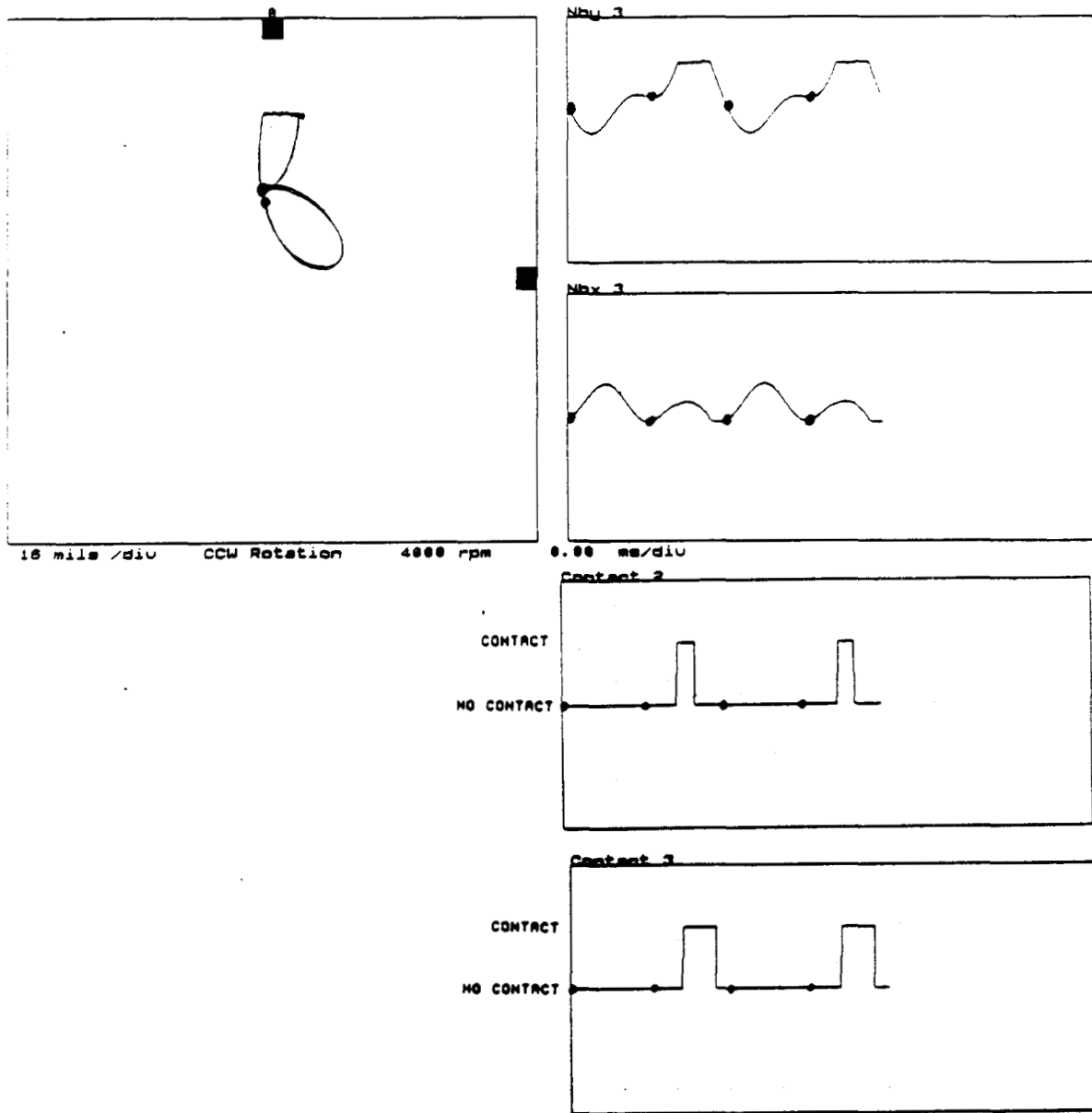


FIGURE 15.19 CALCULATED STEADY-STATE RESPONSE AT LOCATION B3 USING NONLINEAR PORTION COMPUTER SIMULATION PROGRAM FOR 4000 RPM, A 0.00002 IN-LB UNBALANCE IN A3 AND A6.0 LB. RADIAL PRELOAD AT A3.

Point ID: NAY 3 0 deg  
 Point ID: NAX 3 270 deg  
 Plot:

Variable:

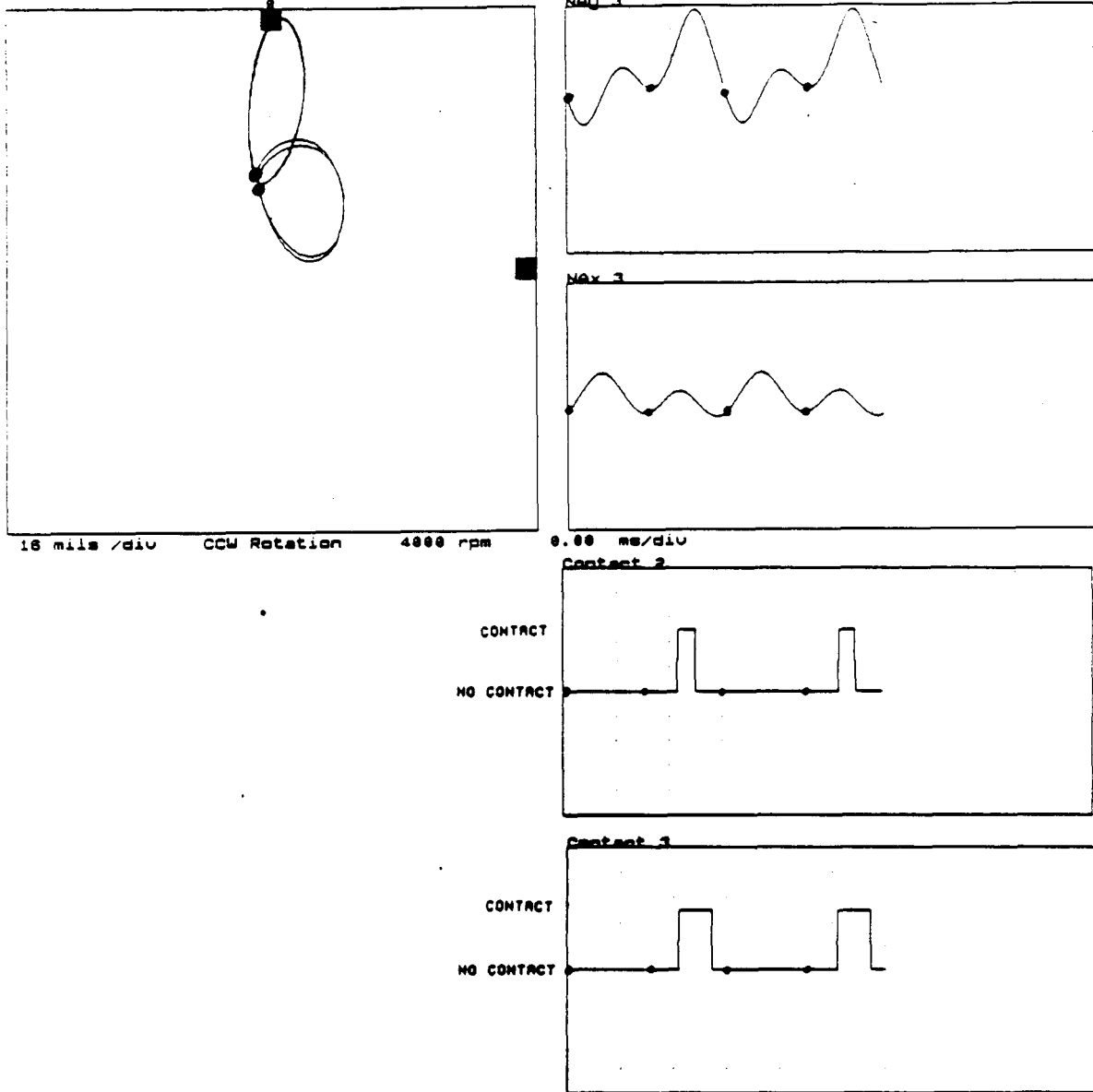


FIGURE 15.20 CALCULATED STEADY-STATE RESPONSE AT LOCATION A3 USING NONLINEAR PORTION COMPUTER SIMULATION PROGRAM FOR 4000 RPM, A 0.00002 IN-LB UNBALANCE IN A3 AND A6.0 LB. RADIAL PRELOAD AT A3.

Point ID: Nby 4 0 deg  
Point ID: Nbx 4 270 deg  
Plot:

Variable:

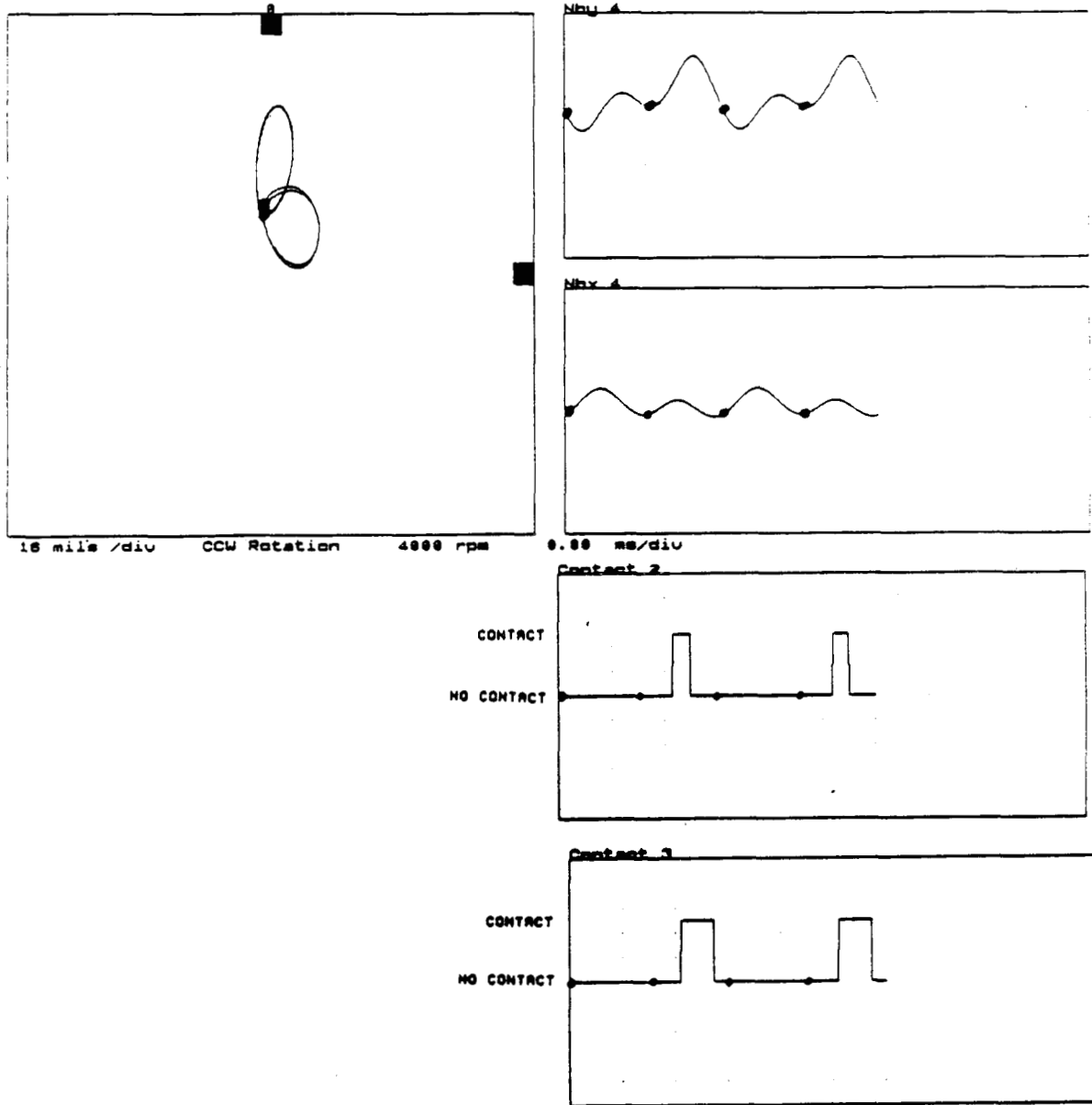


FIGURE 15.21 CALCULATED STEADY-STATE RESPONSE AT LOCATION B4 USING NONLINEAR PORTION COMPUTER SIMULATION PROGRAM FOR 4000 RPM, A 0.00002 IN-LB UNBALANCE IN A3 AND A6.0 LB. RADIAL PRELOAD AT A3.

ORIGINAL PAGE IS  
OF POOR QUALITY

Point ID: NBU 1 0 deg  
Point ID: NBx 1 270 deg  
Plot:

Variable:

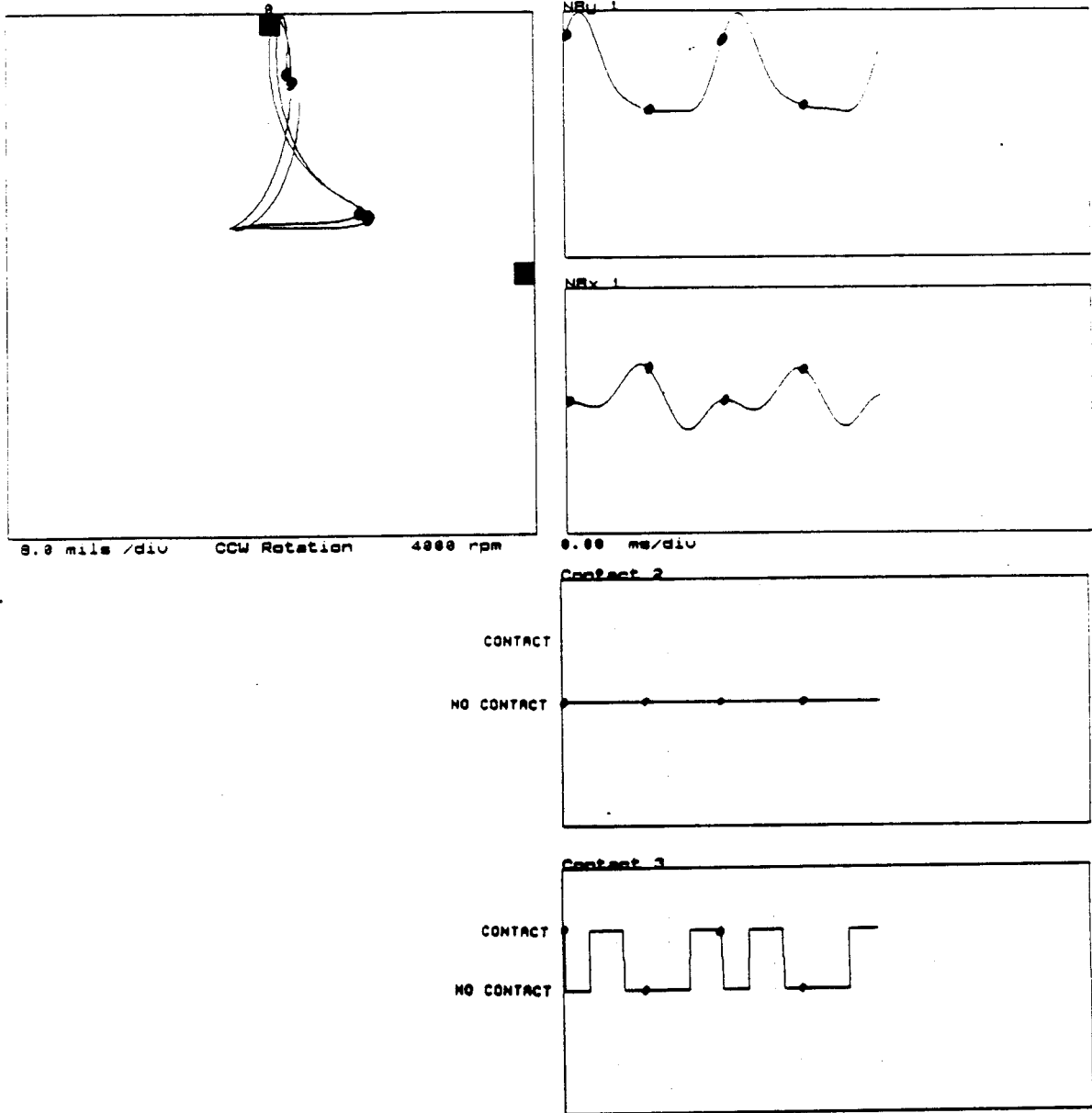


FIGURE 15.22    CALCULATED STEADY-STATE RESPONSE AT LOCATION B1  
USING NONLINEAR PORTION COMPUTER SIMULATION  
PROGRAM FOR 4000 RPM, 0.0002 IN-LB UNBALANCE IN A3,  
AND 9.0 LB. RADIAL PRELOAD AT A3.

Point ID: Nax 1 8 deg  
 Point ID: Nax 1 270 deg  
 Plot:

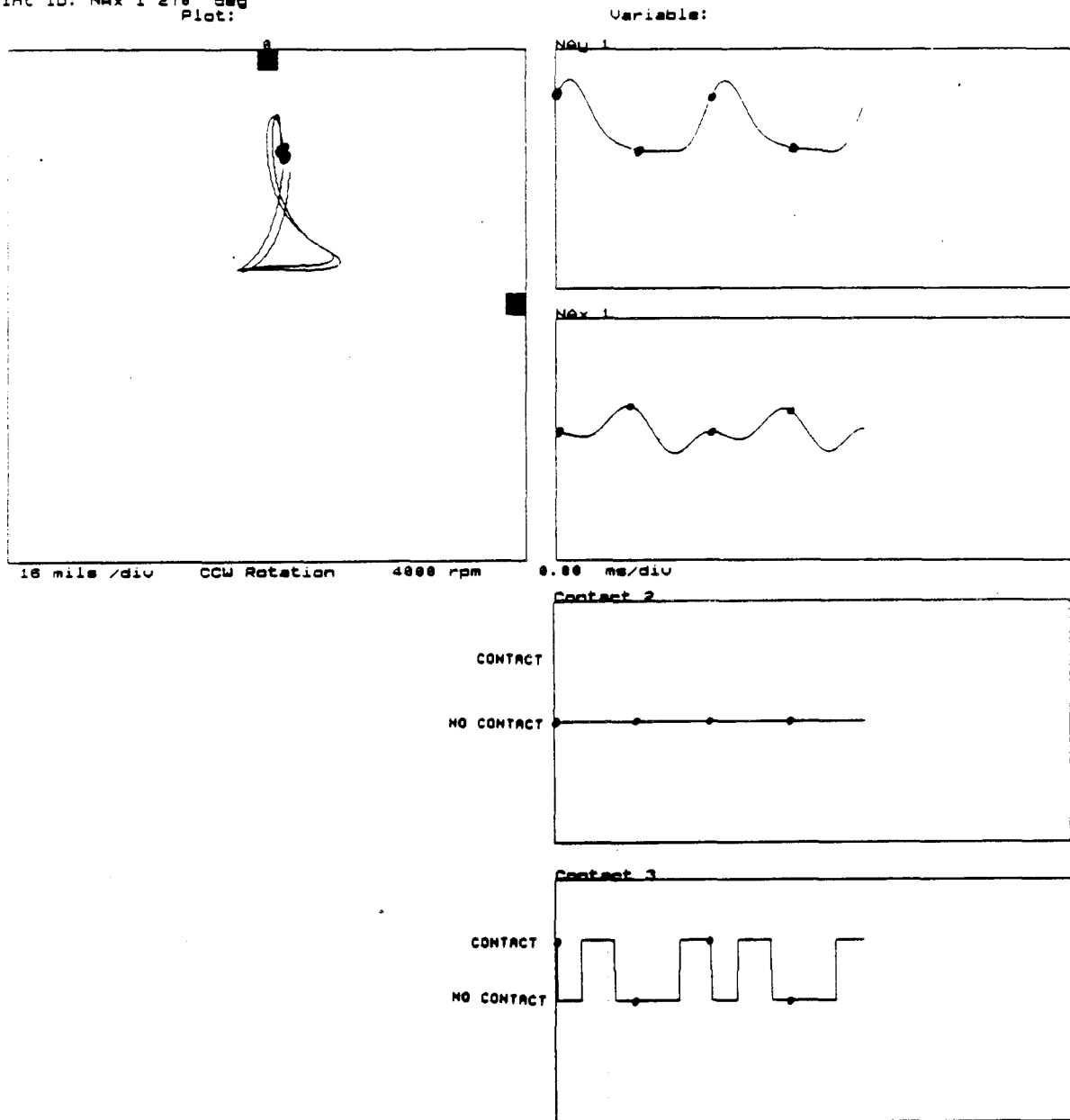


FIGURE 15.23 CALCULATED STEADY-STATE RESPONSE AT LOCATION A1 USING NONLINEAR PORTION COMPUTER SIMULATION PROGRAM FOR 4000 RPM, 0.0002 IN-LB UNBALANCE IN A3, AND 9.0 LB. RADIAL PRELOAD AT A3.

Point ID: Nby 2 0 deg  
Point ID: Nbx 2 270 deg  
Plot:

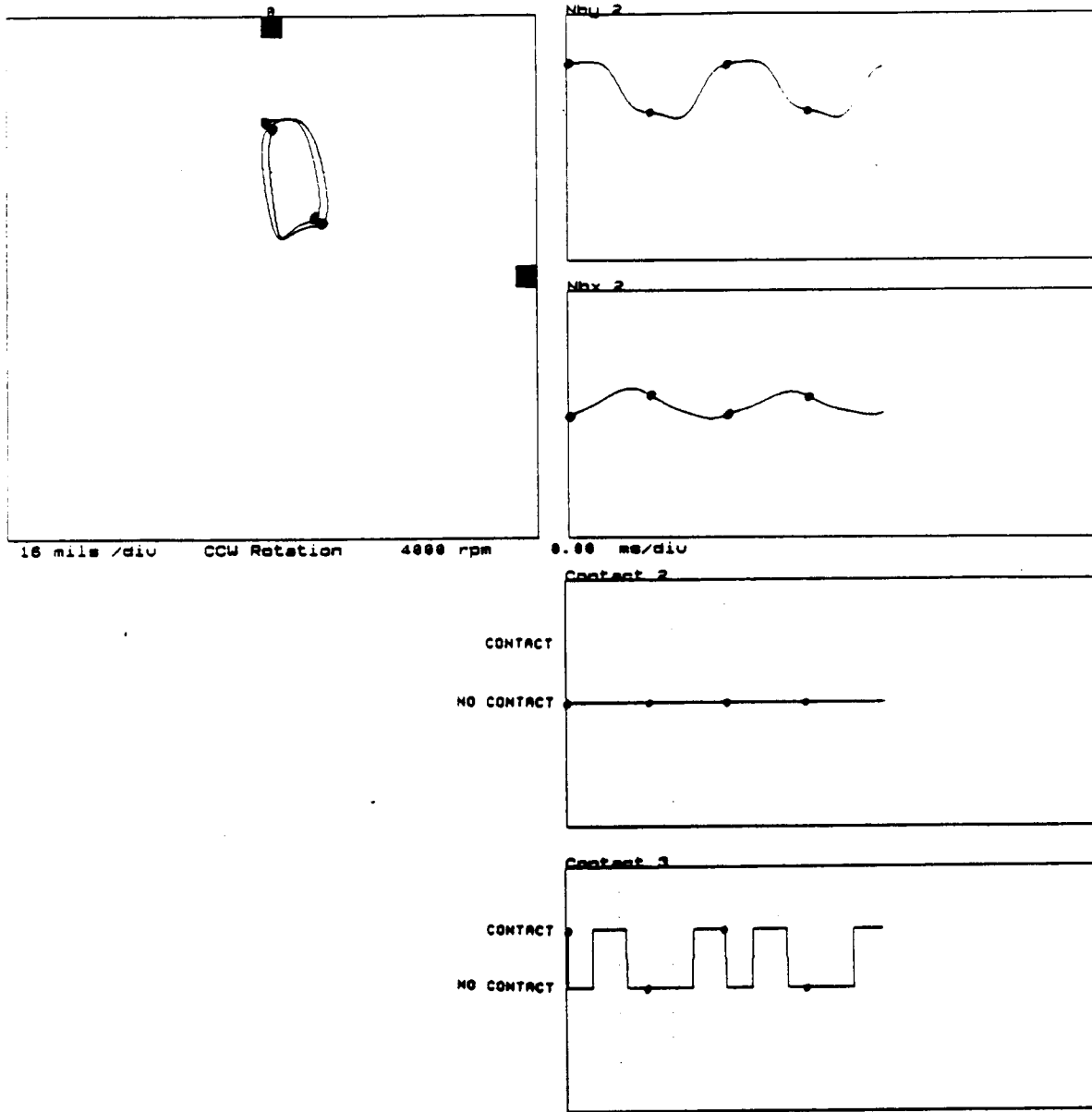


FIGURE 15.24    CALCULATED STEADY-STATE RESPONSE AT LOCATION B2 USING NONLINEAR PORTION COMPUTER SIMULATION PROGRAM FOR 4000 RPM, 0.0002 IN-LB UNBALANCE IN A3, AND 9.0 LB. RADIAL PRELOAD AT A3.

Point ID: NAL 2 2 deg  
 Point ID: NAX 2 270 deg  
 Plot:

Variable:

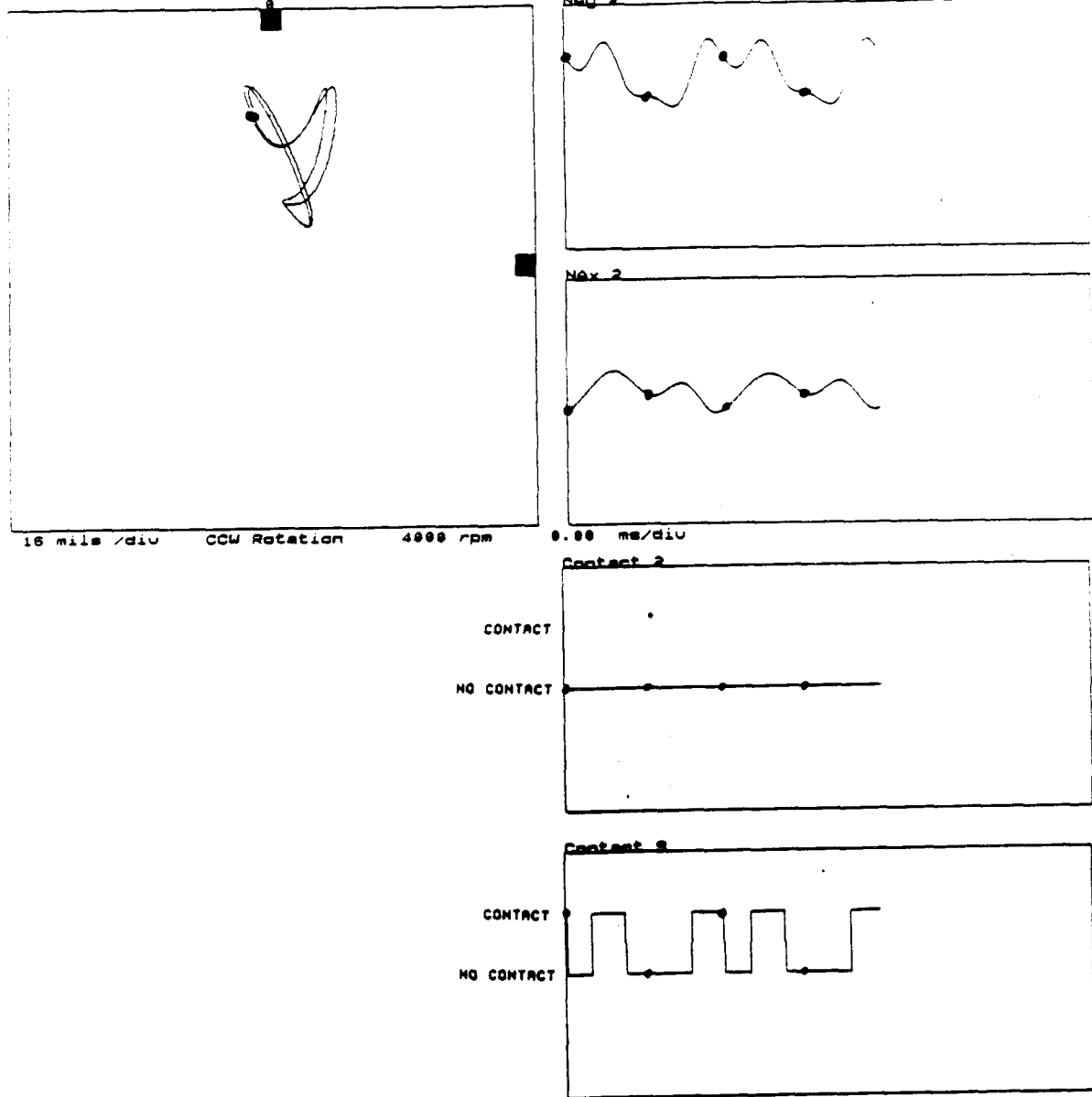


FIGURE 15.25 CALCULATED STEADY-STATE RESPONSE AT LOCATION A2 USING NONLINEAR PORTION COMPUTER SIMULATION PROGRAM FOR 4000 RPM, 0.0002 IN-LB UNBALANCE IN A3, AND 9.0 LB. RADIAL PRELOAD AT A3.

Point ID: Nbc 3 0 deg  
 Point ID: Nbx 3 270 deg  
 Plot:

Variable:

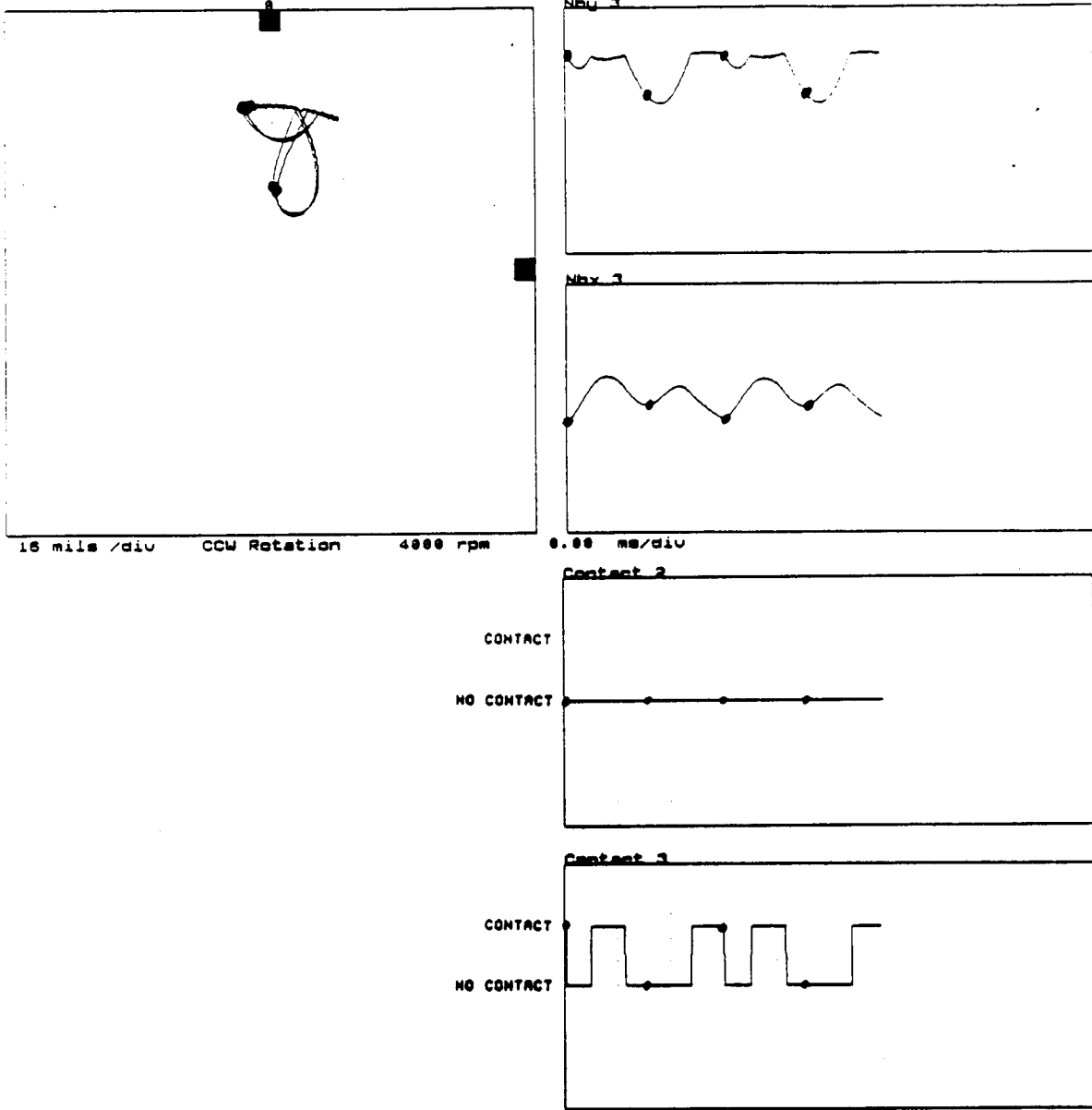


FIGURE 15.26 CALCULATED STEADY-STATE RESPONSE AT LOCATION B3 USING NONLINEAR PORTION COMPUTER SIMULATION PROGRAM FOR 4000 RPM, 0.0002 IN-LB UNBALANCE IN A3, AND 9.0 LB. RADIAL PRELOAD AT A3.

Point ID: NAY 3 0 deg  
Point ID: NAX 3 270 deg  
Plot:

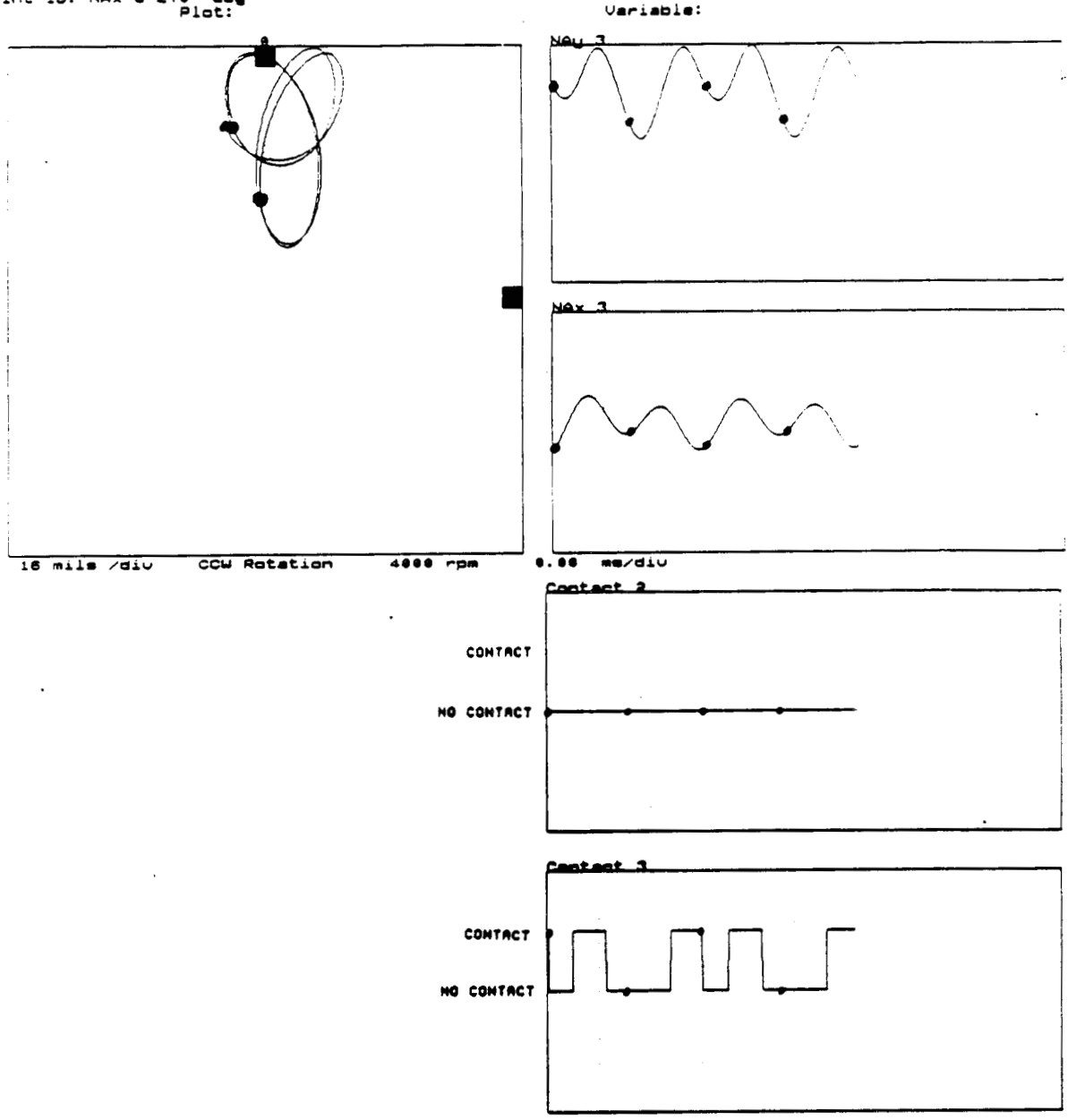
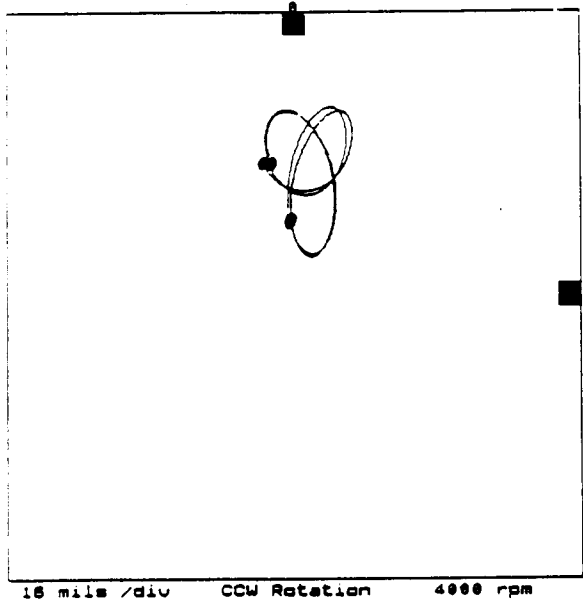


FIGURE 15.27 CALCULATED STEADY-STATE RESPONSE AT LOCATION A3 USING NONLINEAR PORTION COMPUTER SIMULATION PROGRAM FOR 4000 RPM, 0.0002 IN-LB UNBALANCE IN A3, AND 9.0 LB. RADIAL PRELOAD AT A3.

Point ID: Nbu 4 0 deg  
 Point ID: Nbx 4 270 deg  
 Plot:



Variable:

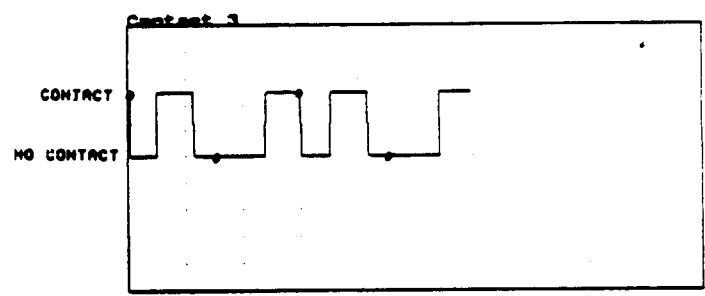
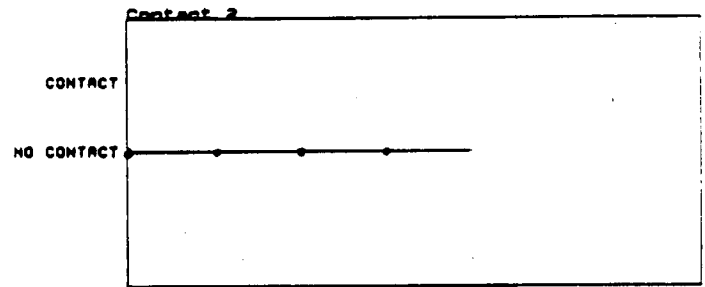
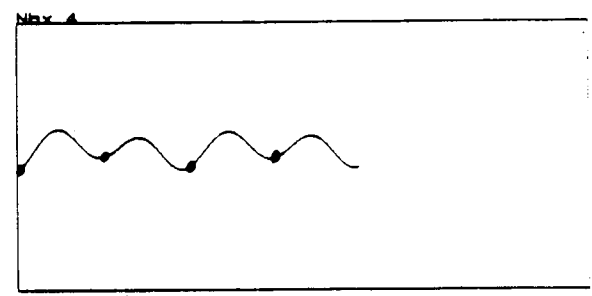
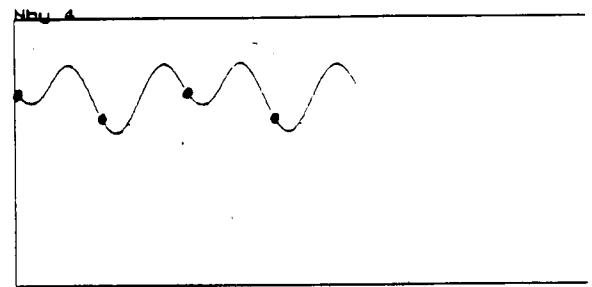
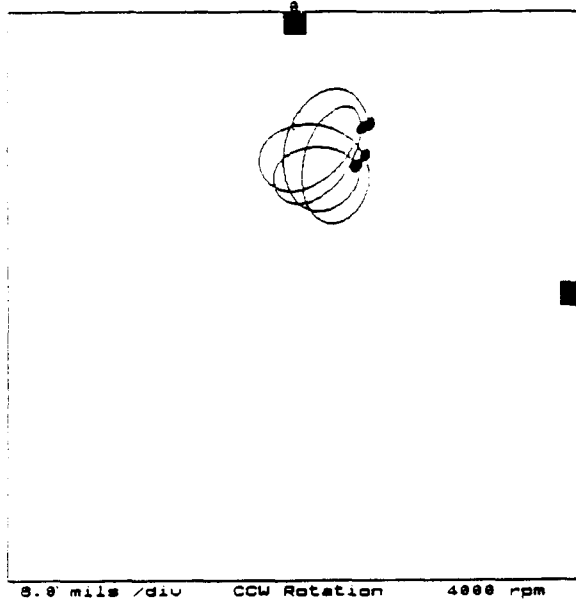


FIGURE 15.28 CALCULATED STEADY-STATE RESPONSE AT LOCATION B4 USING NONLINEAR PORTION COMPUTER SIMULATION PROGRAM FOR 4000 RPM, 0.0002 IN-LB UNBALANCE IN A3, AND 9.0 LB. RADIAL PRELOAD AT A3.

Point ID: NBx 1 0 deg  
Point ID: NBx 1 270 deg  
Plot:



Variable:

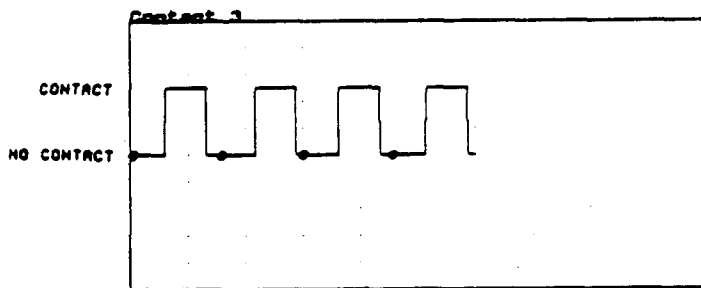
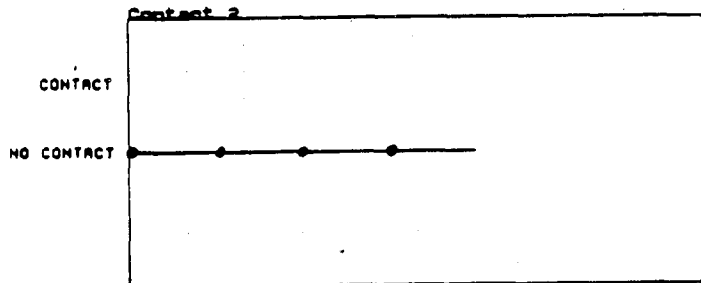
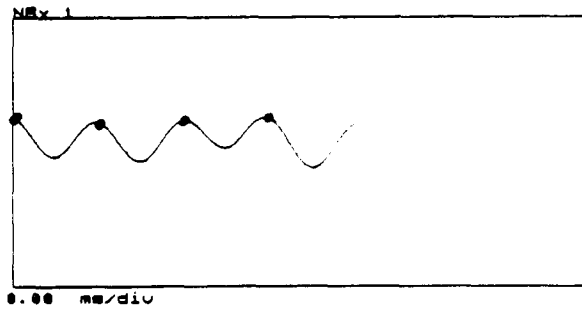
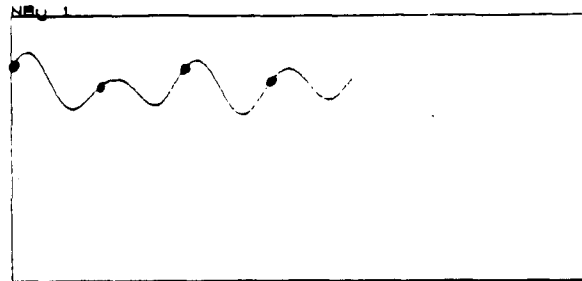


FIGURE 15.29 CALCULATED STEADY-STATE RESPONSE AT LOCATION B1 USING NONLINEAR PORTION OF COMPUTER SIMULATION PROGRAM FOR 4000 RPM, 0.00002 IN-LB UNBALANCE IN A3, AND 12.0 LB RADIAL PRELOAD AT A3.

Point ID: NAY 1 0 deg  
Point ID: NAX 1 270 deg  
Plot:

Variable:

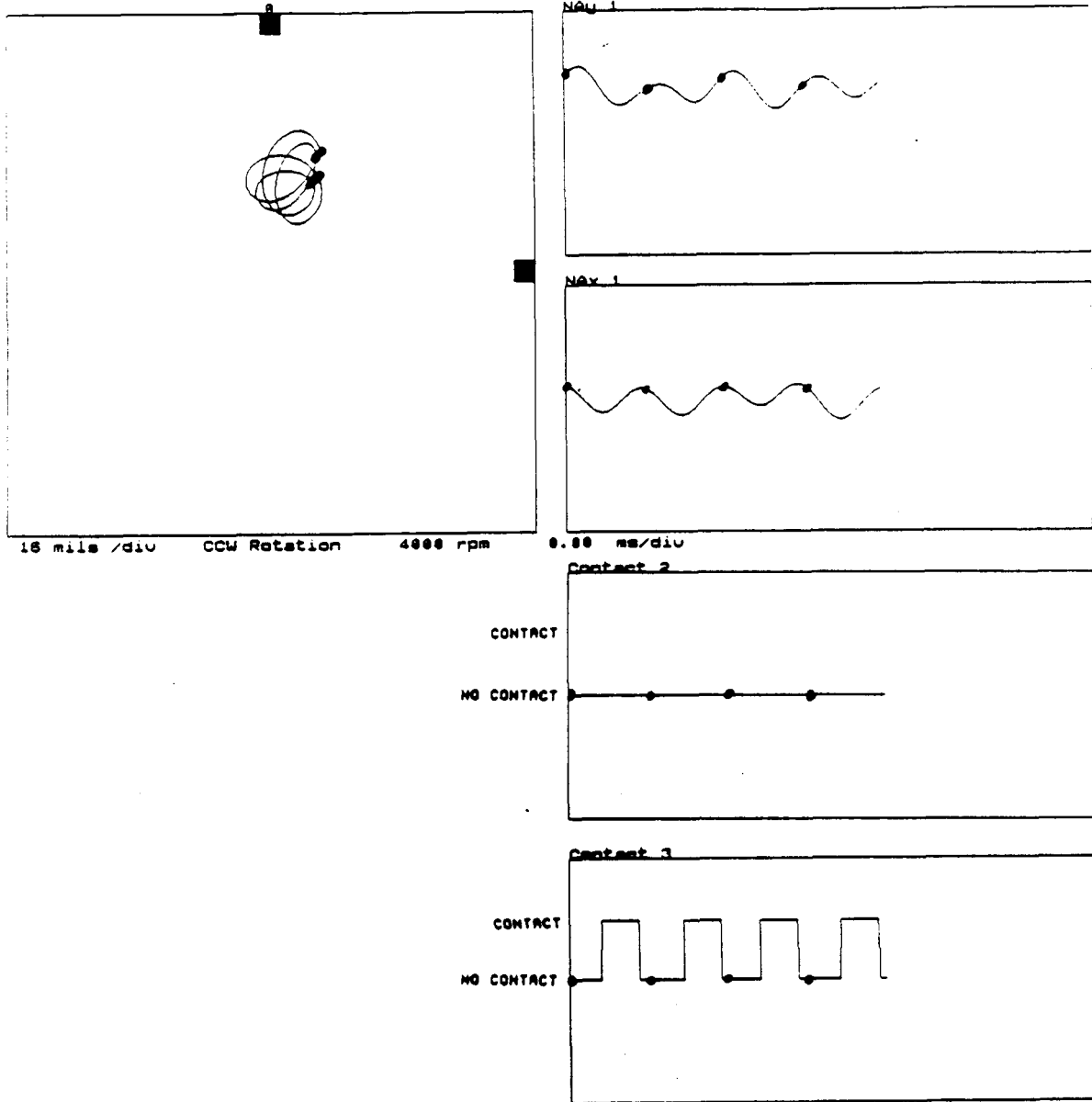
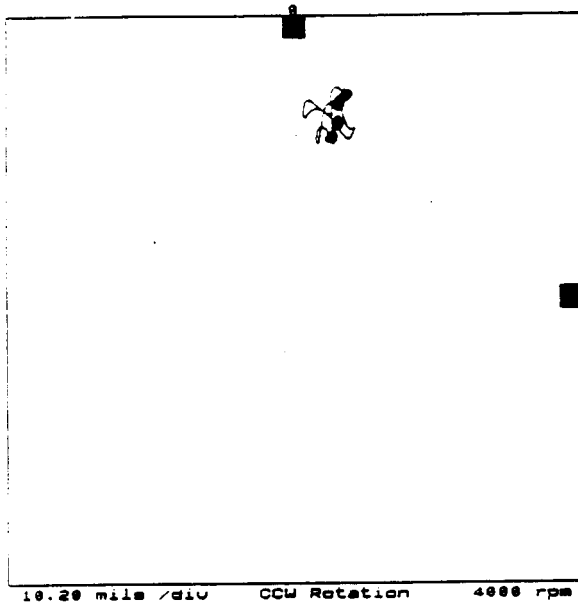


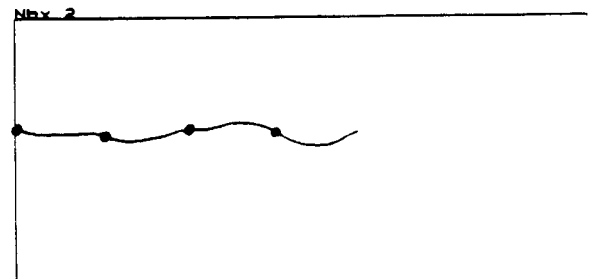
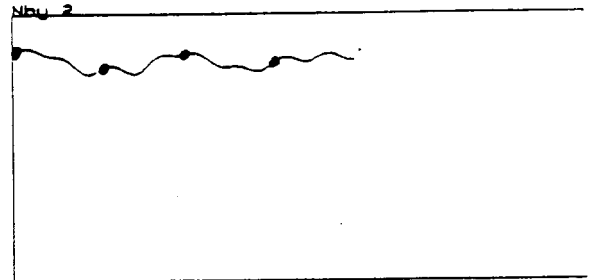
FIGURE 15.30 CALCULATED STEADY-STATE RESPONSE AT LOCATION A1 USING NONLINEAR PORTION OF COMPUTER SIMULATION PROGRAM FOR 4000 RPM, 0.00002 IN-LB UNBALANCE IN A3, AND 12.0 LBRADIAL PRELOAD AT A3.

Point ID: ZBC 2 8 deg  
 Point ID: ZBC 2 278 deg  
 Plot:



10.20 mils /div CCW Rotation 4000 rpm

Variable:



0.00 ms/div

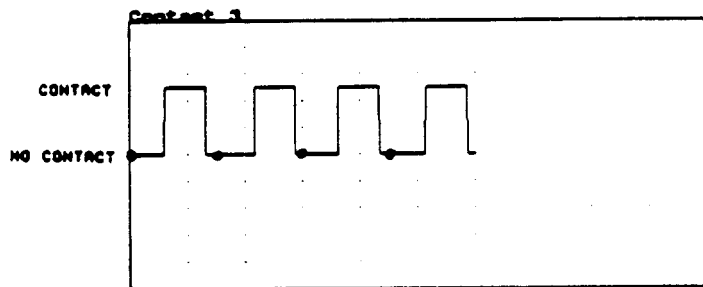
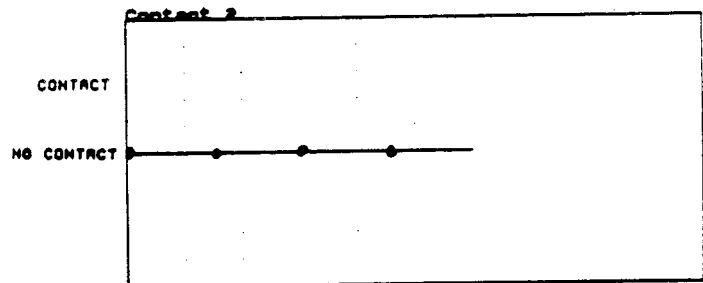


FIGURE 15.31 CALCULATED STEADY-STATE RESPONSE AT LOCATION B2 USING NONLINEAR PORTION OF COMPUTER SIMULATION PROGRAM FOR 4000 RPM, 0.00002 IN-LB UNBALANCE IN A3, AND 12.0 LBRADIAL PRELOAD AT A3.

Point ID: NAY 2 0 deg  
Point ID: NAX 2 270 deg  
Plot:

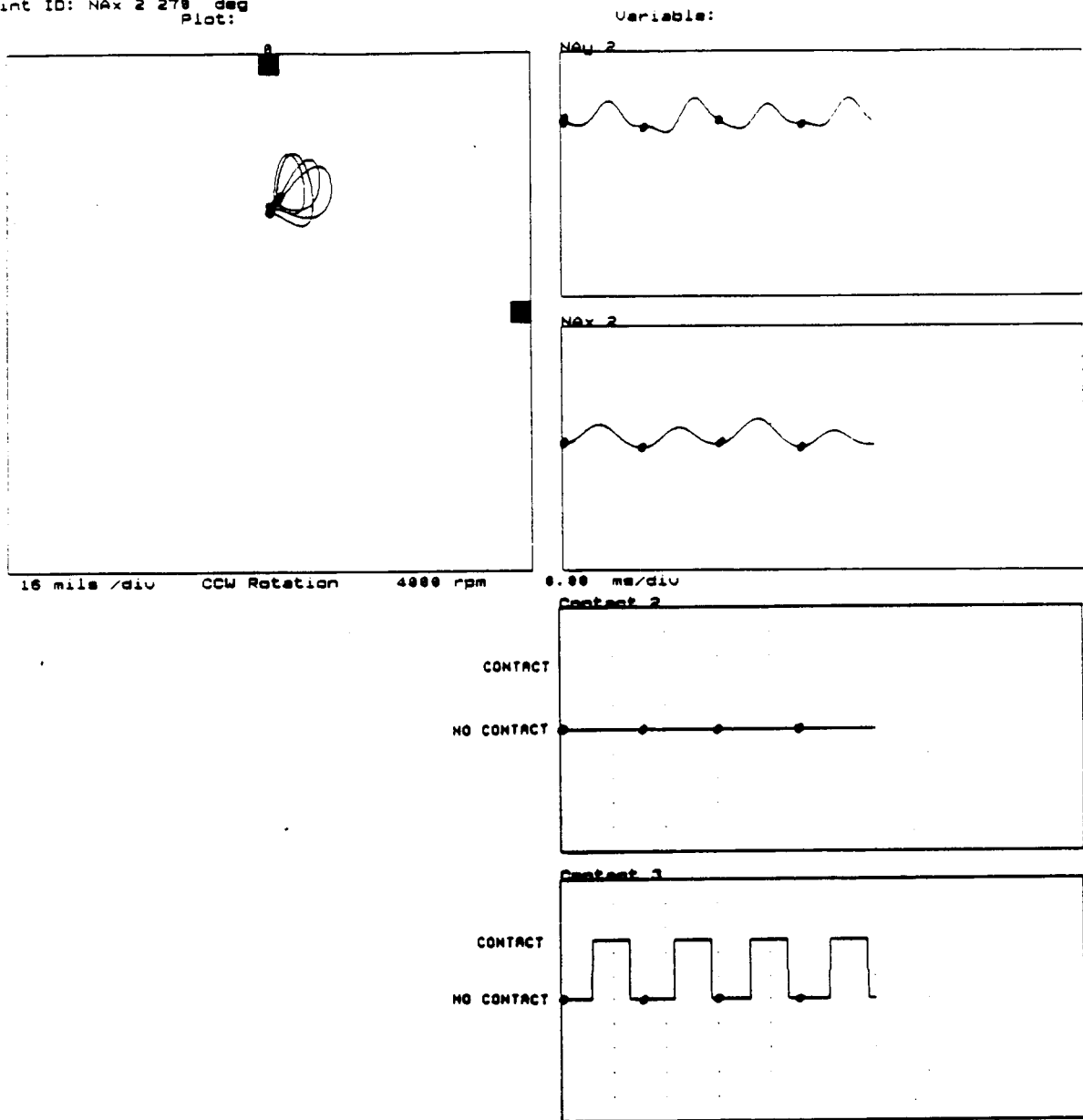


FIGURE 15.32    CALCULATED STEADY-STATE RESPONSE AT LOCATION A2 USING NONLINEAR PORTION OF COMPUTER SIMULATION PROGRAM FOR 4000 RPM, 0.00002 IN-LB UNBALANCE IN A3, AND 12.0 LB RADIAL PRELOAD AT A3.

Point ID: Nby 3 0 deg  
 Point ID: Nbx 3 270 deg  
 Plot:

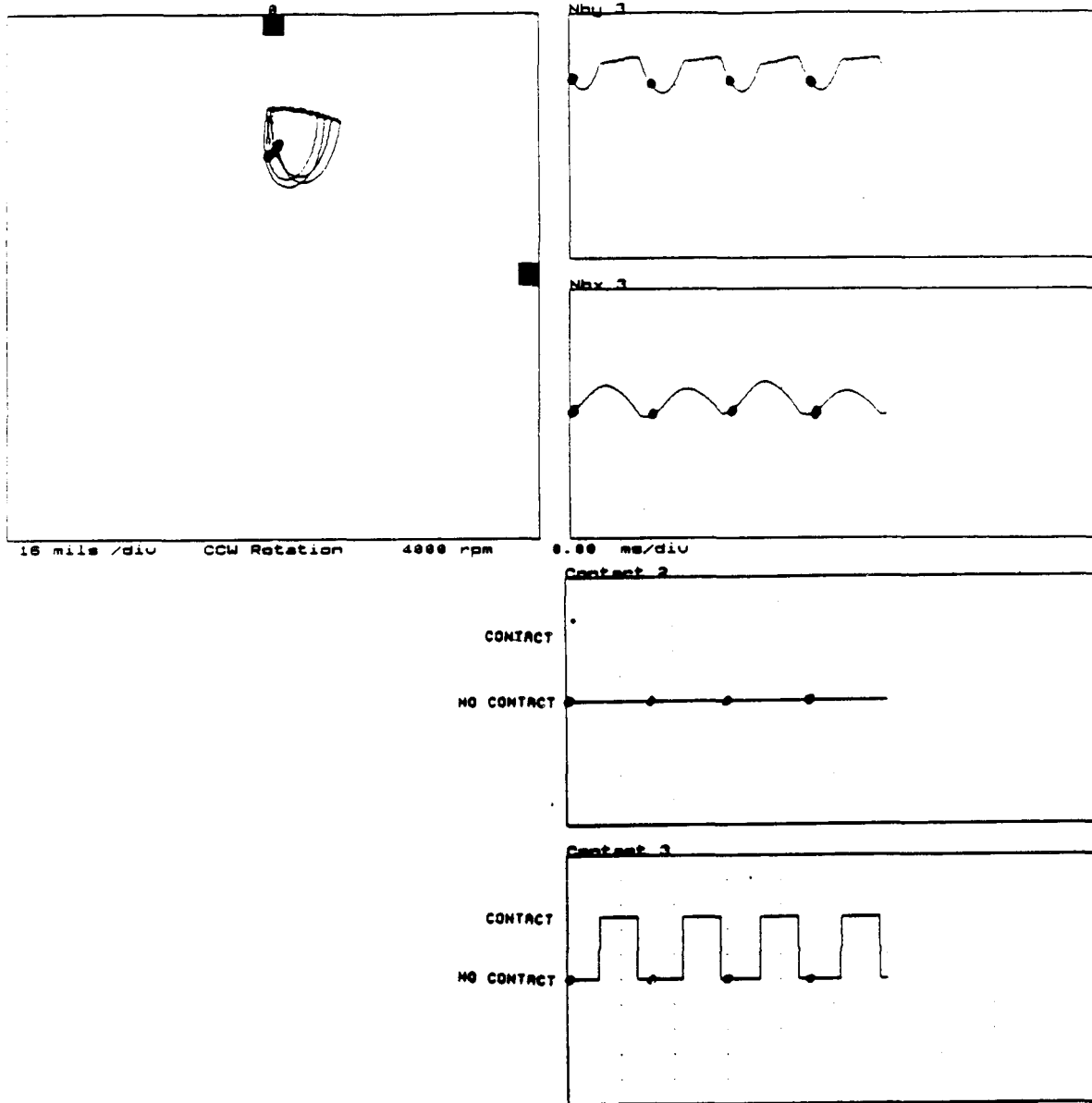


FIGURE 15.33 CALCULATED STEADY-STATE RESPONSE AT LOCATION B3 USING NONLINEAR PORTION OF COMPUTER SIMULATION PROGRAM FOR 4000 RPM, 0.00002 IN-LB UNBALANCE IN A3, AND 12.0 LBRADIAL PRELOAD AT A3.

Point ID: NAY 3 8 deg  
Point ID: NAX 3 270 deg  
Plot:

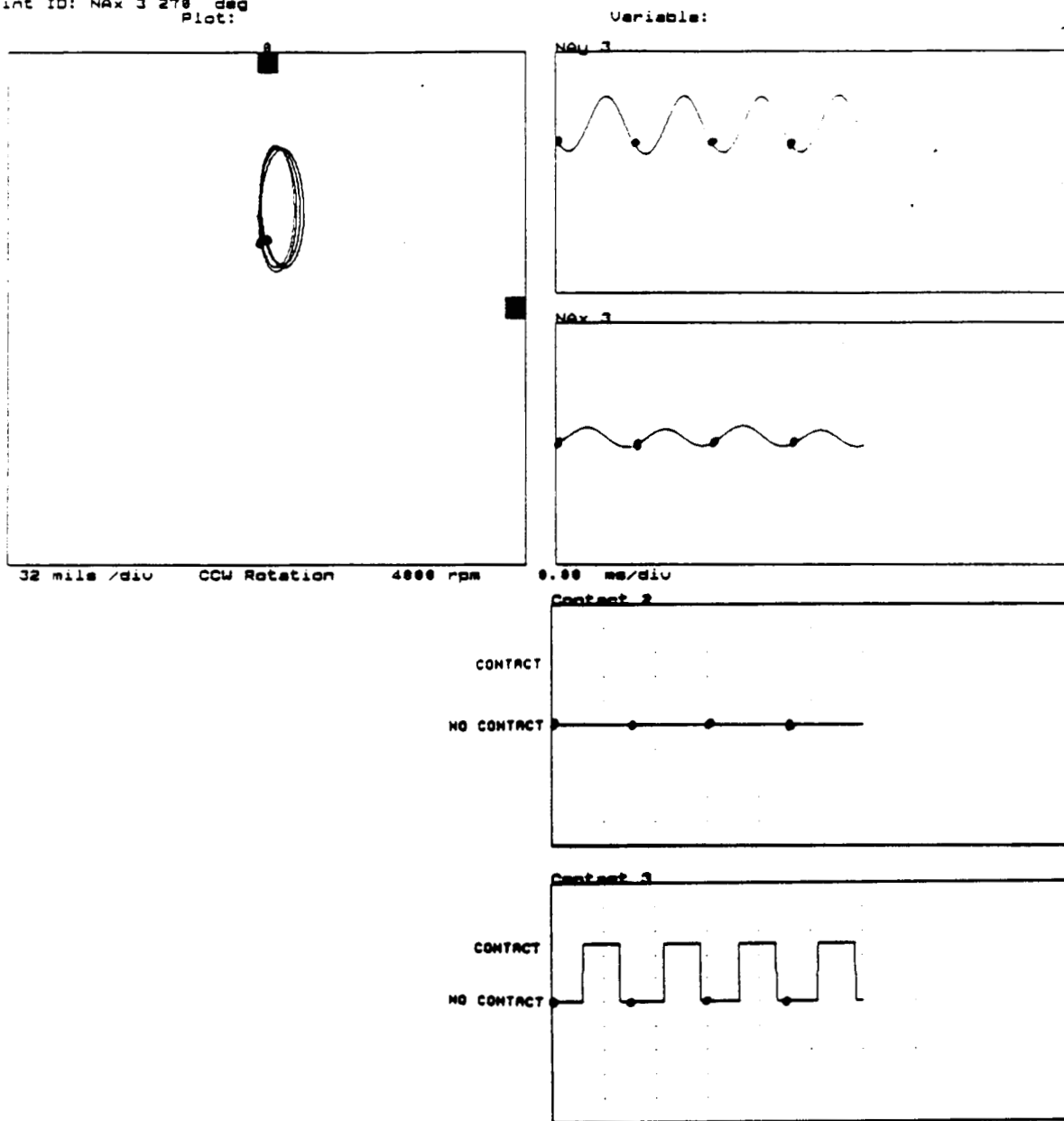


FIGURE 15.34 CALCULATED STEADY-STATE RESPONSE AT LOCATION A3 USING NONLINEAR PORTION OF COMPUTER SIMULATION PROGRAM FOR 4000 RPM, 0.00002 IN-LB UNBALANCE IN A3, AND 12.0 LB RADIAL PRELOAD AT A3.

Point ID: Nby 4 0 deg  
Point ID: Nbx 4 270 deg  
Plot:

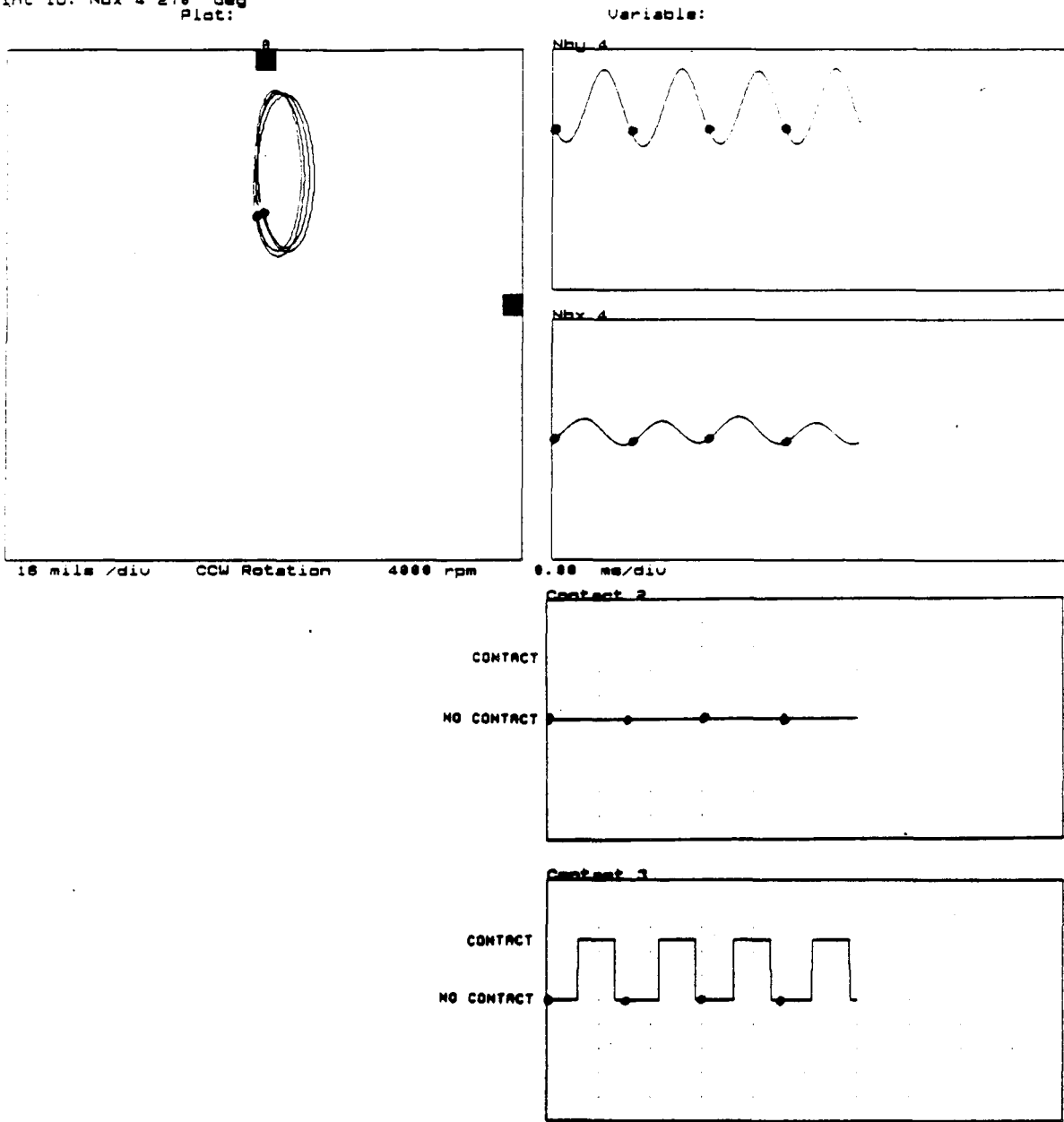


FIGURE 15.35    CALCULATED STEADY-STATE RESPONSE AT LOCATION B4 USING NONLINEAR PORTION OF COMPUTER SIMULATION PROGRAM FOR 4000 RPM, 0.00002 IN-LB UNBALANCE IN A3, AND 12.0LB RADIAL PRELOAD AT A3.

Point ID: NBy 1 0 deg  
Point ID: NBx 1 270 deg  
Plot:

Variable:

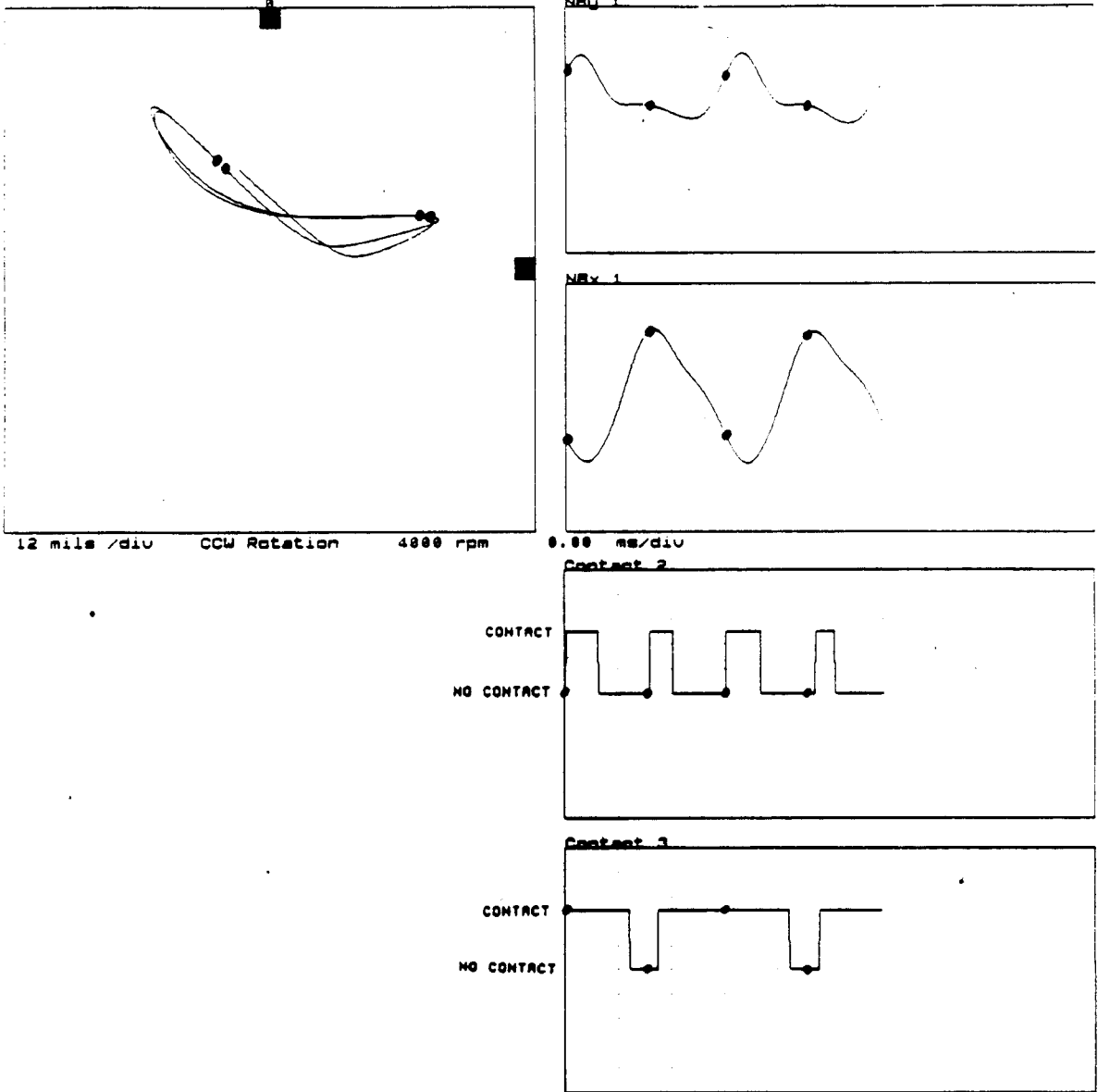


FIGURE 15.36 CALCULATED STEADY-STATE RESPONSE AT LOCATION B1 USING NONLINEAR PORTION COMPUTER SIMULATION PROGRAM FOR 4000 RPM, 0.00002 IN-LB UNBALANCE IN A3, AND 15.0 LB. RADIAL PRELOAD AT A3.

Point ID: NAY 1 0 deg  
Point ID: NAX 1 270 deg  
Plot:

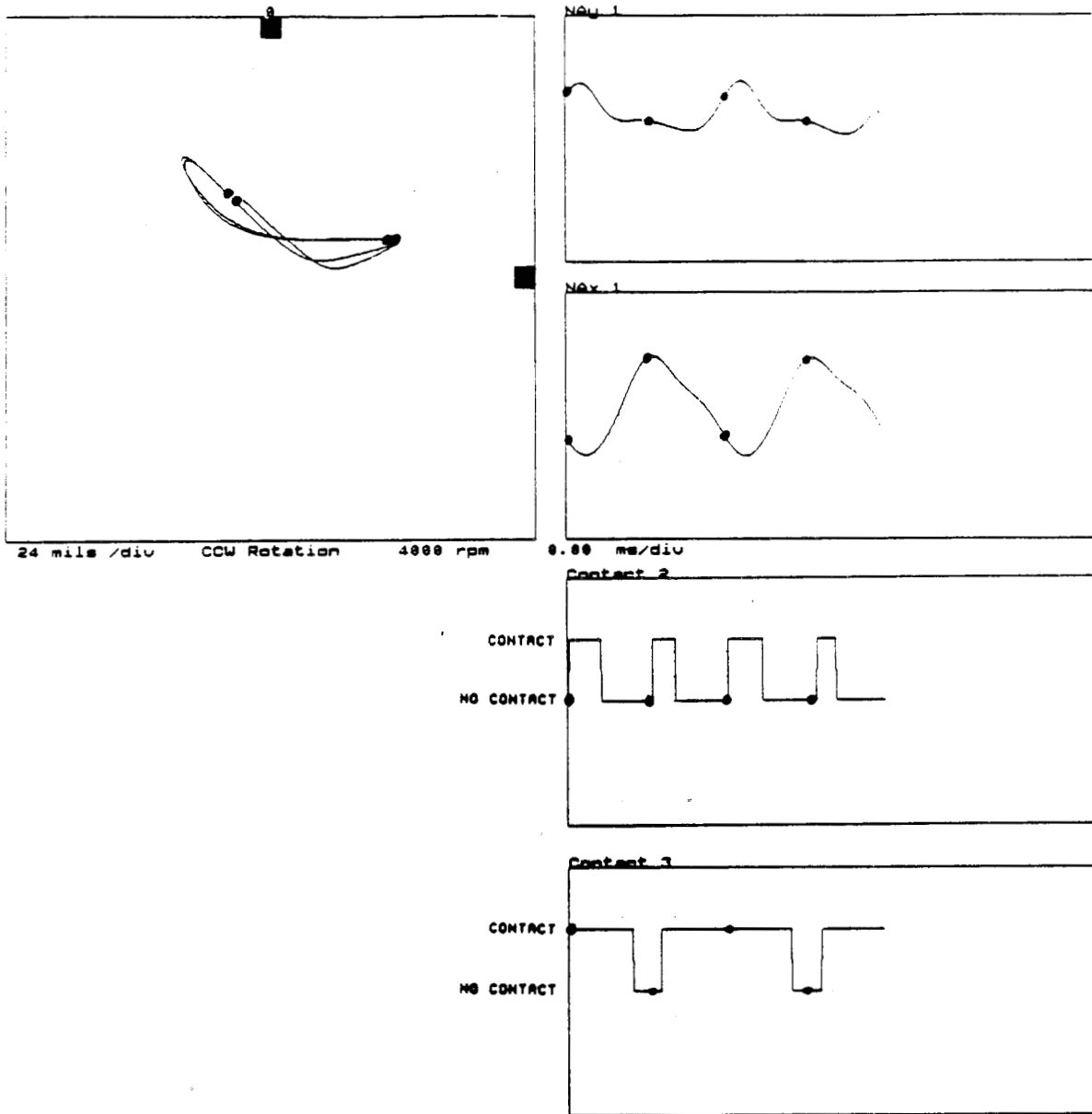


FIGURE 15.37 CALCULATED STEADY-STATE RESPONSE AT LOCATION A1 USING NONLINEAR PORTION COMPUTER SIMULATION PROGRAM FOR 4000 RPM, 0.00002 IN-LB UNBALANCE IN A3, AND 15.0 LB. RADIAL PRELOAD AT A3.

Point ID: NBV 2 0 deg  
Point ID: NBX 2 270 deg  
Plot:

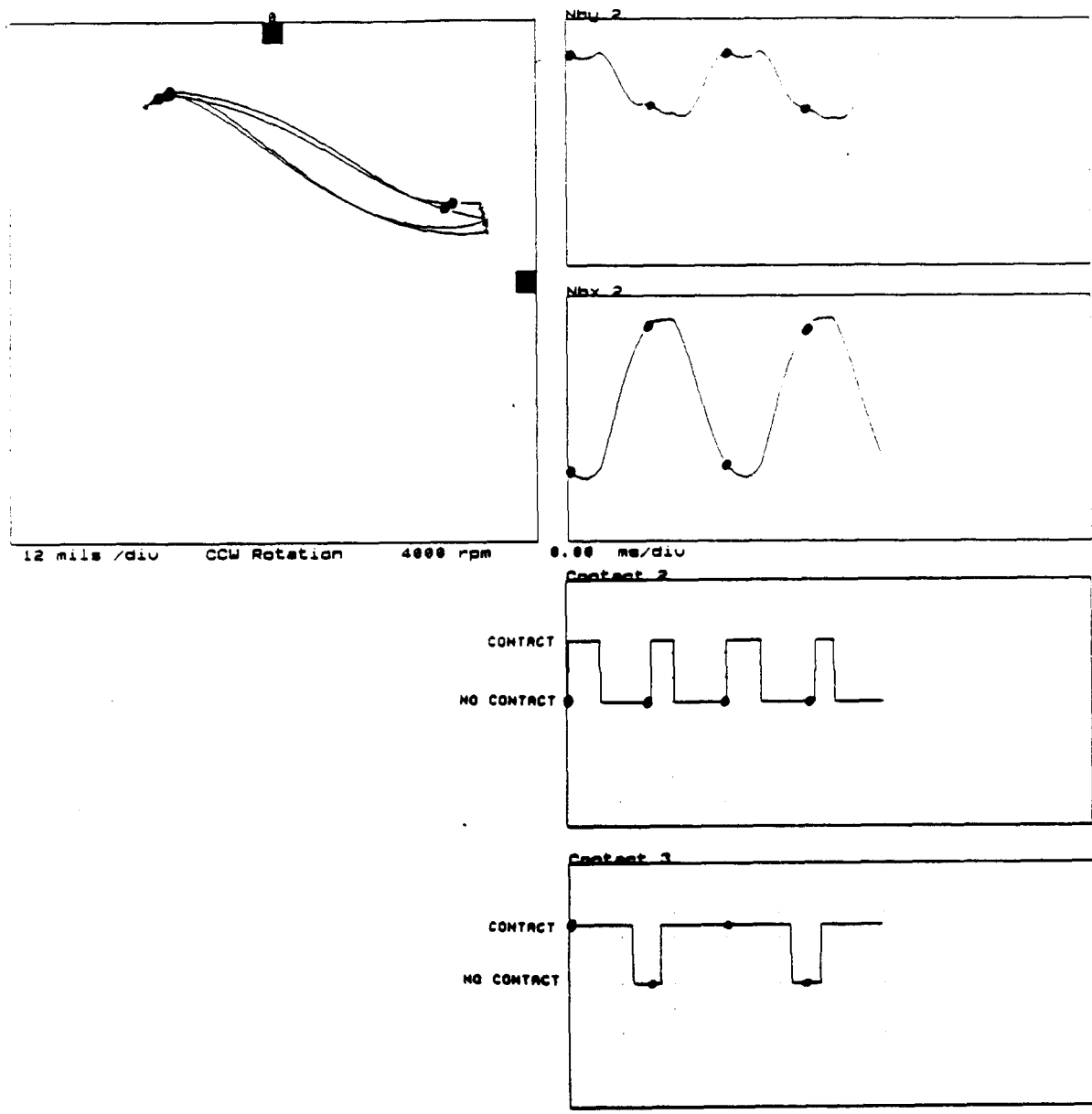
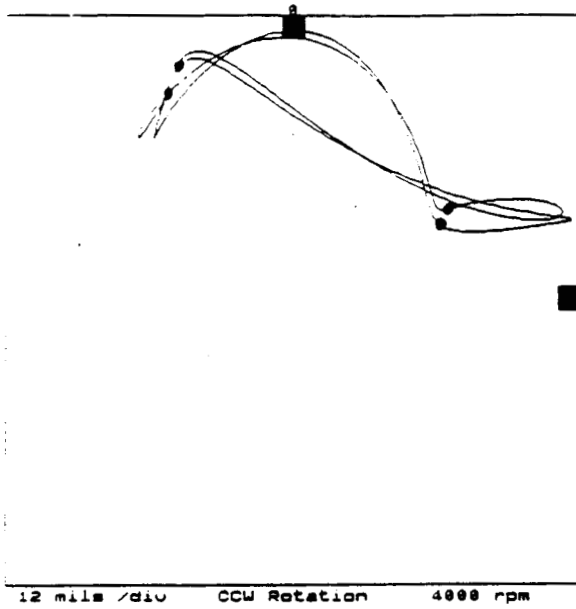


FIGURE 15.38 CALCULATED STEADY-STATE RESPONSE AT LOCATION B2 USING NONLINEAR PORTION COMPUTER SIMULATION PROGRAM FOR 4000 RPM, 0.00002 IN-LB UNBALANCE IN A3, AND 15.0 LB. RADIAL PRELOAD AT A3.

Point ID: NAX 2 0 deg  
Point ID: NAX 2 270 deg  
Plot:



Variable:

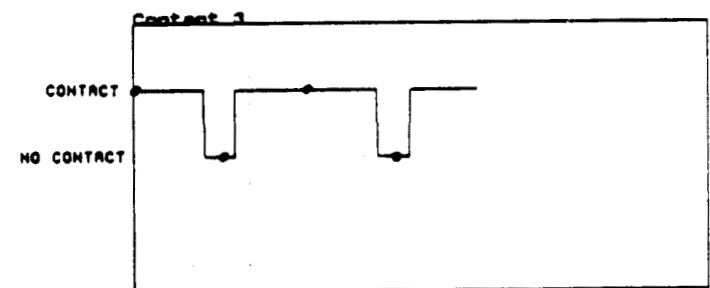
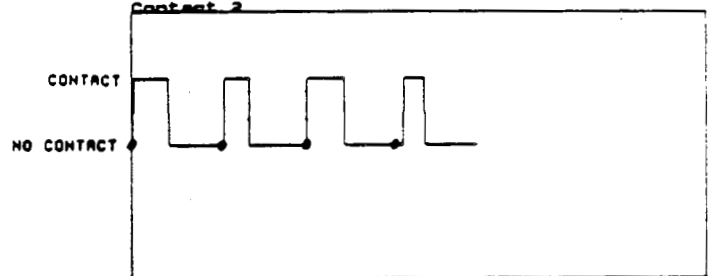
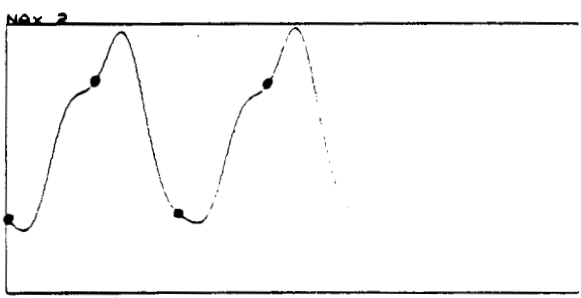
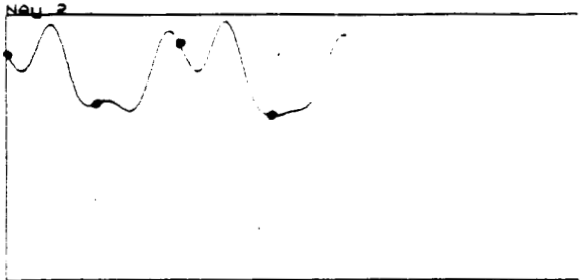


FIGURE 15.39 CALCULATED STEADY-STATE RESPONSE AT LOCATION A2 USING NONLINEAR PORTION COMPUTER SIMULATION PROGRAM FOR 4000 RPM, 0.00002 IN-LB UNBALANCE IN A3, AND 15.0 LB. RADIAL PRELOAD AT A3.

Point ID: Nby 3 0 deg  
Point ID: Nbx 3 270 deg  
Plot:

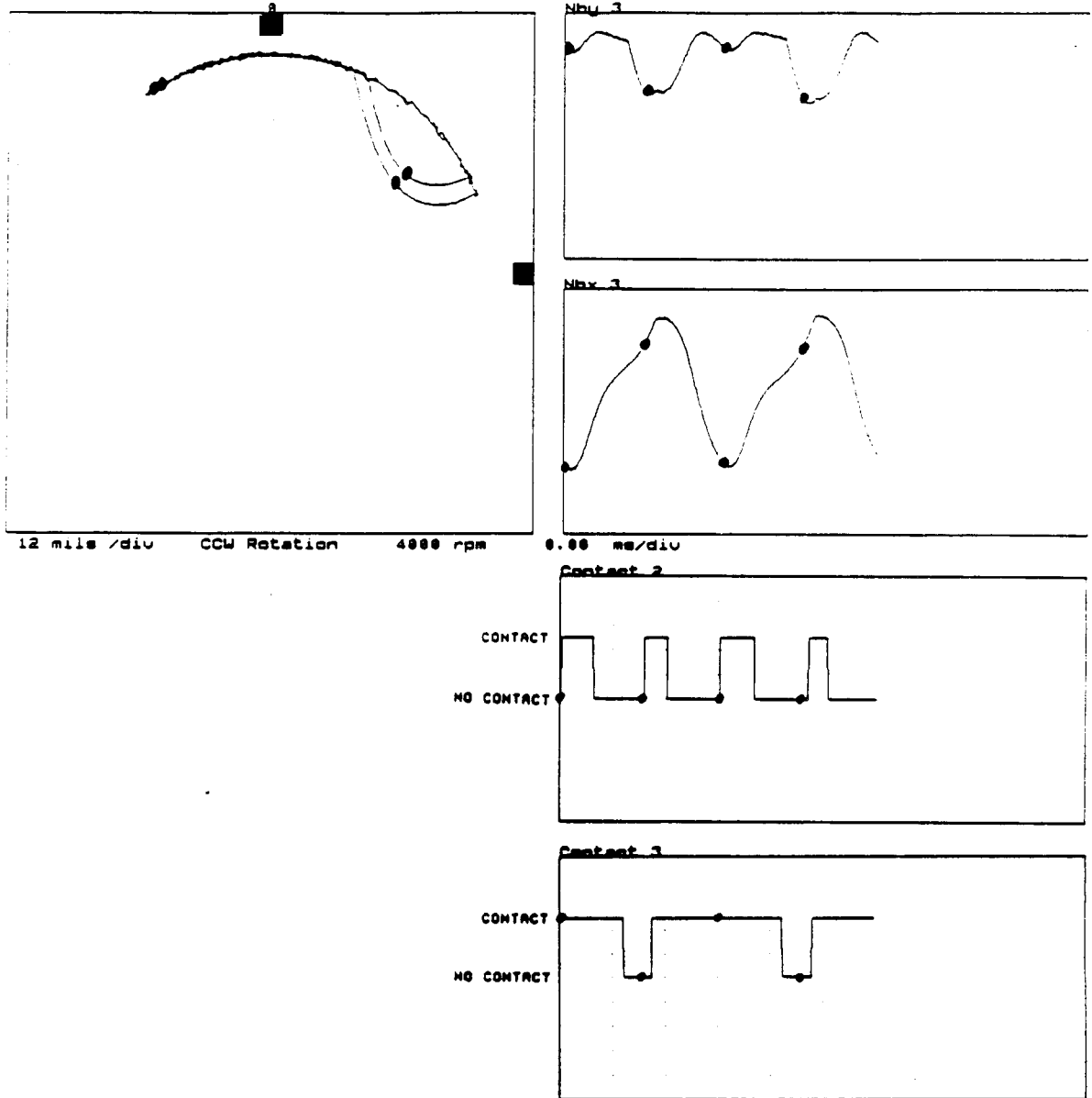
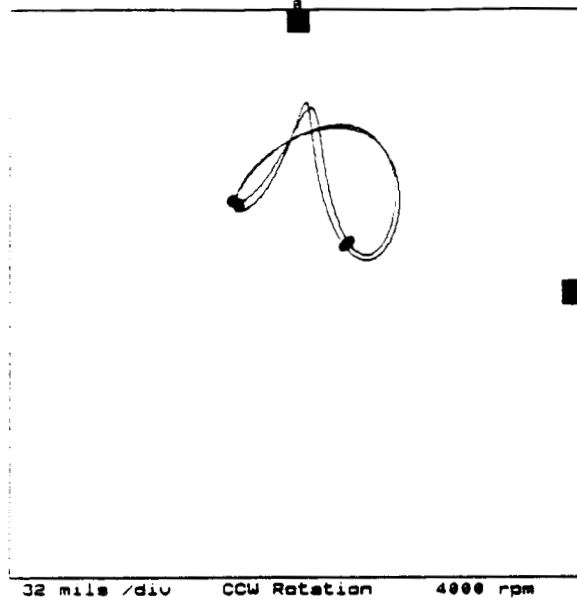


FIGURE 15.40 CALCULATED STEADY-STATE RESPONSE AT LOCATION B3 USING NONLINEAR PORTION COMPUTER SIMULATION PROGRAM FOR 4000 RPM, 0.00002 IN-LB UNBALANCE IN A3, AND 15.0 LB. RADIAL PRELOAD AT A3.

Point ID: N0y 3 0 deg  
Point ID: N0x 3 270 deg  
Plot:



Variable:

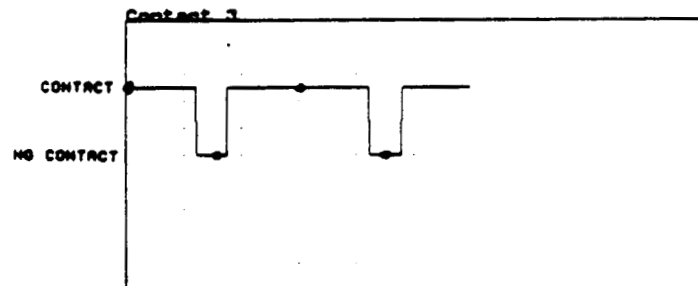
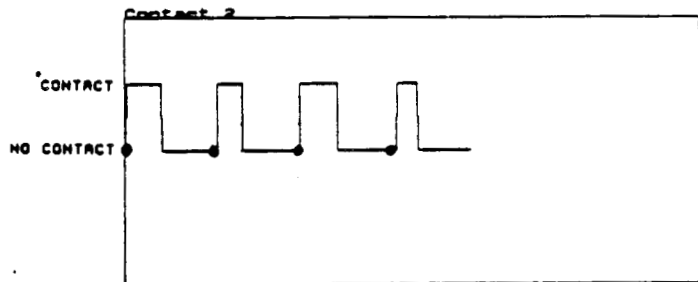
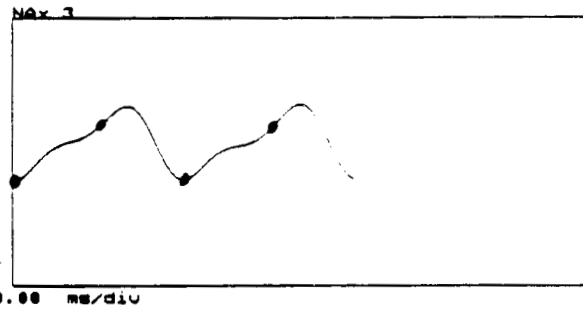
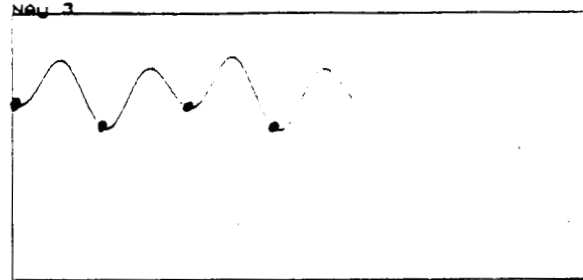
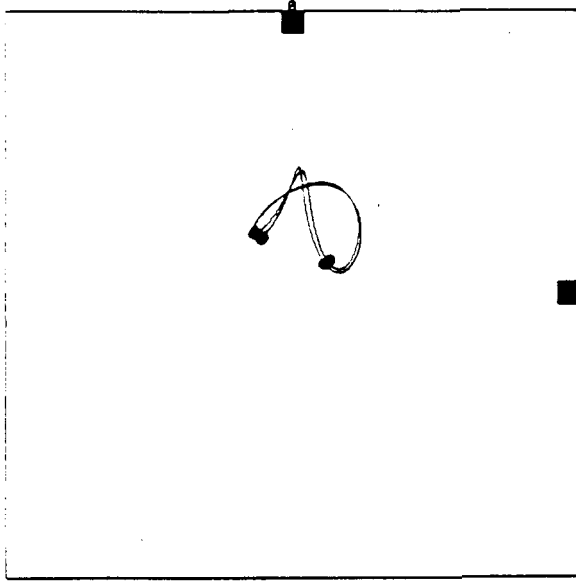
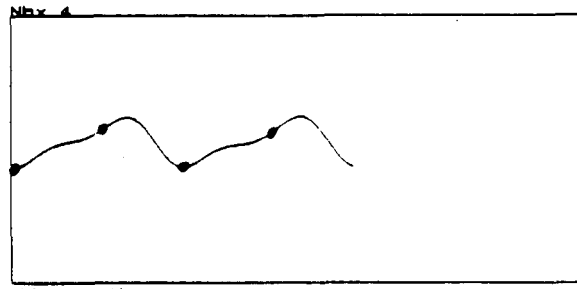
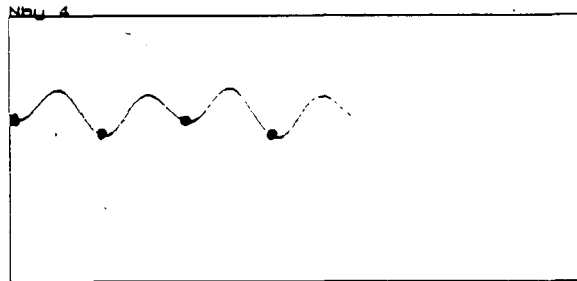


FIGURE 15.41 CALCULATED STEADY-STATE RESPONSE AT LOCATION A3 USING NONLINEAR PORTION COMPUTER SIMULATION PROGRAM FOR 4000 RPM, 0.00002 IN-LB UNBALANCE IN A3, AND 15.0 LB. RADIAL PRELOAD AT A3.

Point ID: Nby 4 0 deg  
Point ID: Nbx 4 270 deg  
Plot:



Variable:



32 mils /div CCW Rotation 4000 rpm

0.00 ms/div

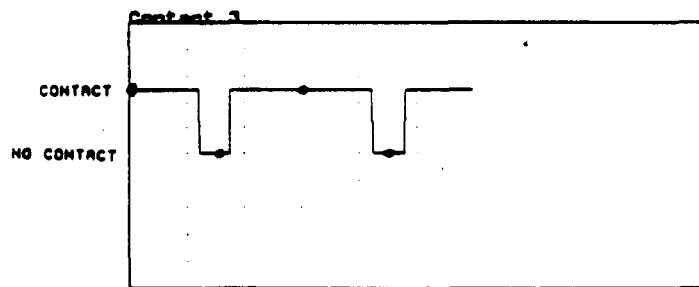
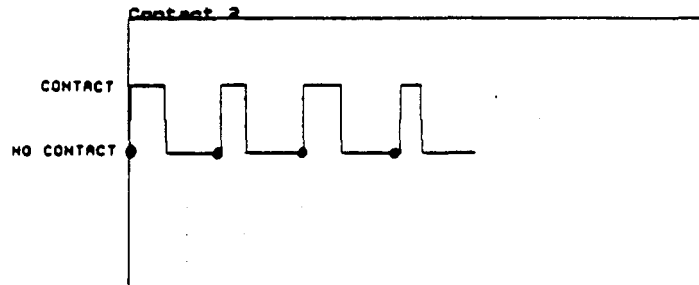
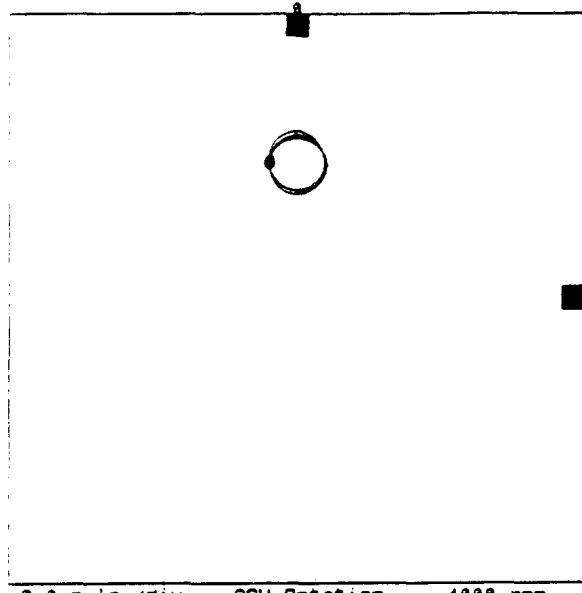


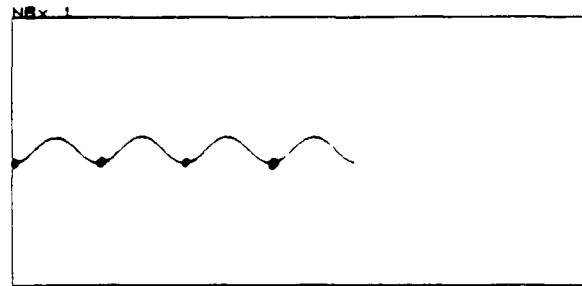
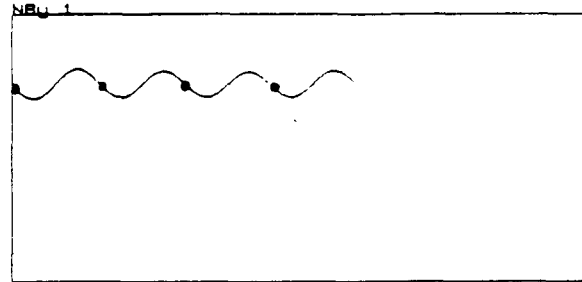
FIGURE 15.42 CALCULATED STEADY-STATE RESPONSE AT LOCATION B4 USING NONLINEAR PORTION COMPUTER SIMULATION PROGRAM FOR 4000 RPM, 0.00002 IN-LB UNBALANCE IN A3, AND 15.0 LB. RADIAL PRELOAD AT A3.

Point ID: NBU 1 0 deg  
 Point ID: NBY 1 270 deg  
 Plot:



9.8 mils /diu CCW Rotation 4000 rpm

Variable:



9.88 ms/diu

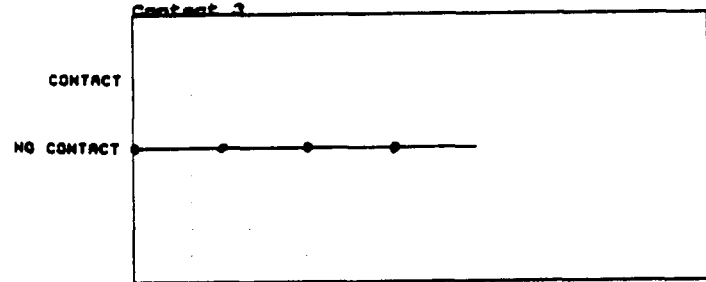
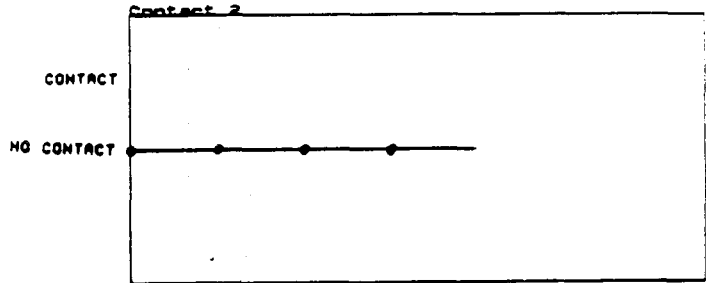
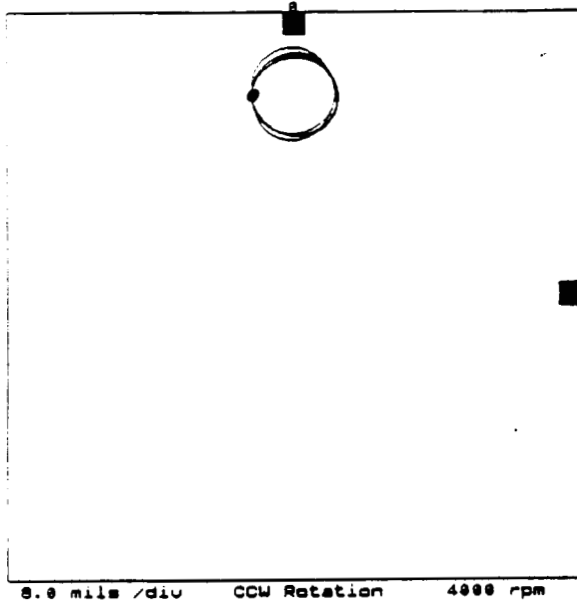


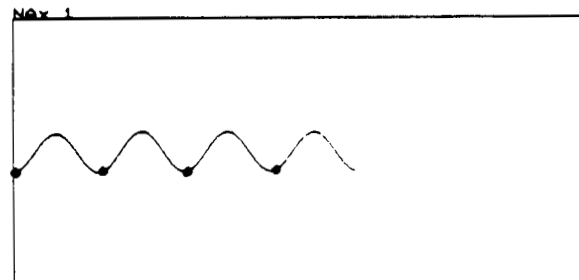
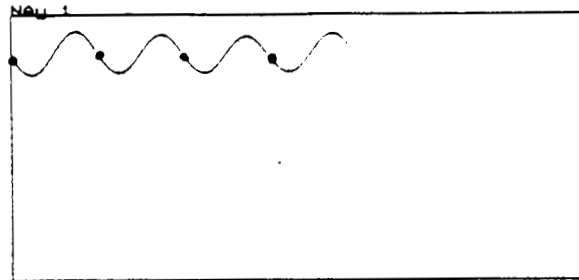
FIGURE 15.43 CALCULATED STEADY-STATE RESPONSE AT LOCATION B1 USING NONLINEAR PORTION OF COMPUTER SIMULATION PROGRAM FOR 4000 RPM, 0.00016 IN-LB UNBALANCE IN A2, AND 5.0 LB. RADIAL PRELOAD AT A3.

Point ID: ZDx 1 0 deg  
Point ID: ZDx 1 270 deg  
Plot:



0.0 mils/div CCW Rotation 4000 rpm

Variable:



0.00 ms/div

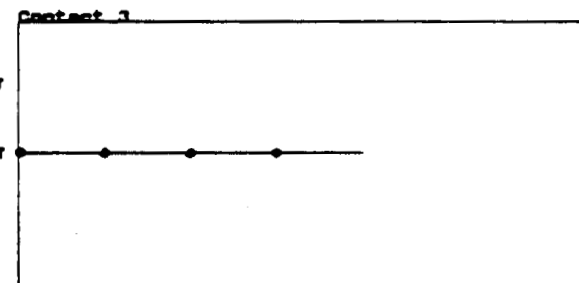
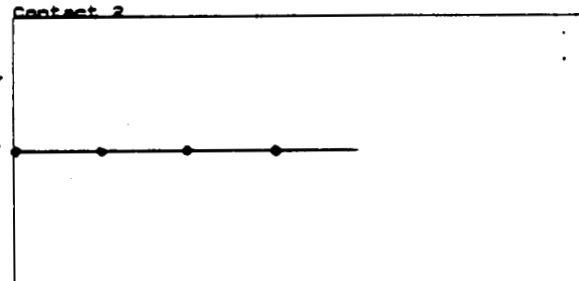
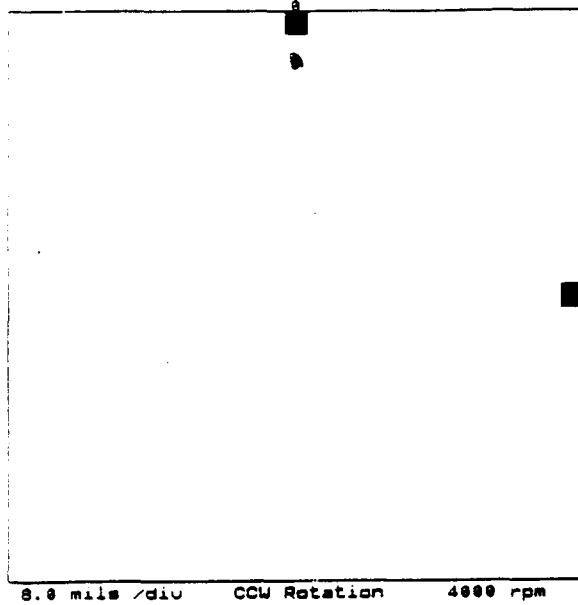
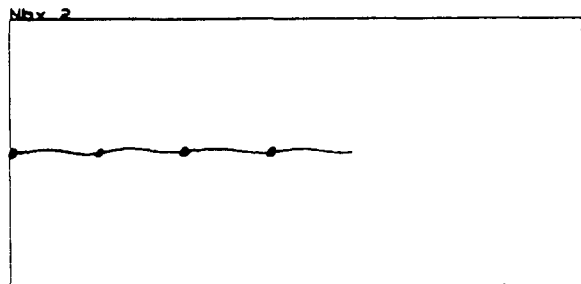
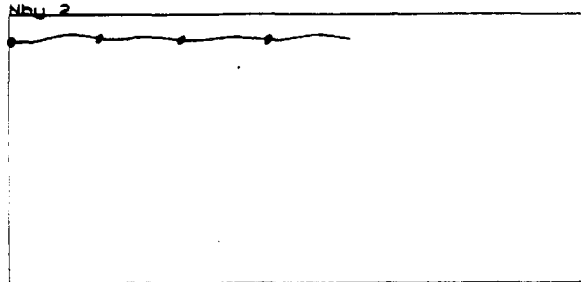


FIGURE 15.44 CALCULATED STEADY-STATE RESPONSE AT LOCATION A1 USING NONLINEAR PORTION OF COMPUTER SIMULATION PROGRAM FOR 4000 RPM, 0.00016 IN-LB UNBALANCE IN A2, AND 5.0 LB. RADIAL PRELOAD AT A3.

Point ID: Nby 2 0 deg  
Point ID: Nbx 2 270 deg  
Plot:



Variable:



0.00 ms/div

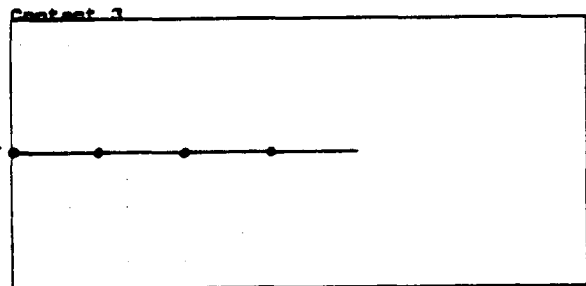
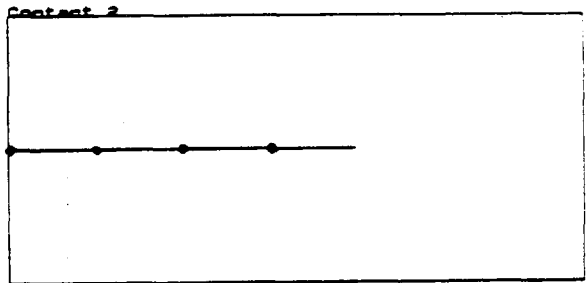


FIGURE 15.45 CALCULATED STEADY-STATE RESPONSE AT LOCATION B2 USING NONLINEAR PORTION OF COMPUTER SIMULATION PROGRAM FOR 4000 RPM, 0.00016 IN-LB UNBALANCE IN A2, AND 5.0 LB. RADIAL PRELOAD AT A3.

Point ID: NAY 2 0 deg  
Point ID: NAX 2 270 deg  
Plot:

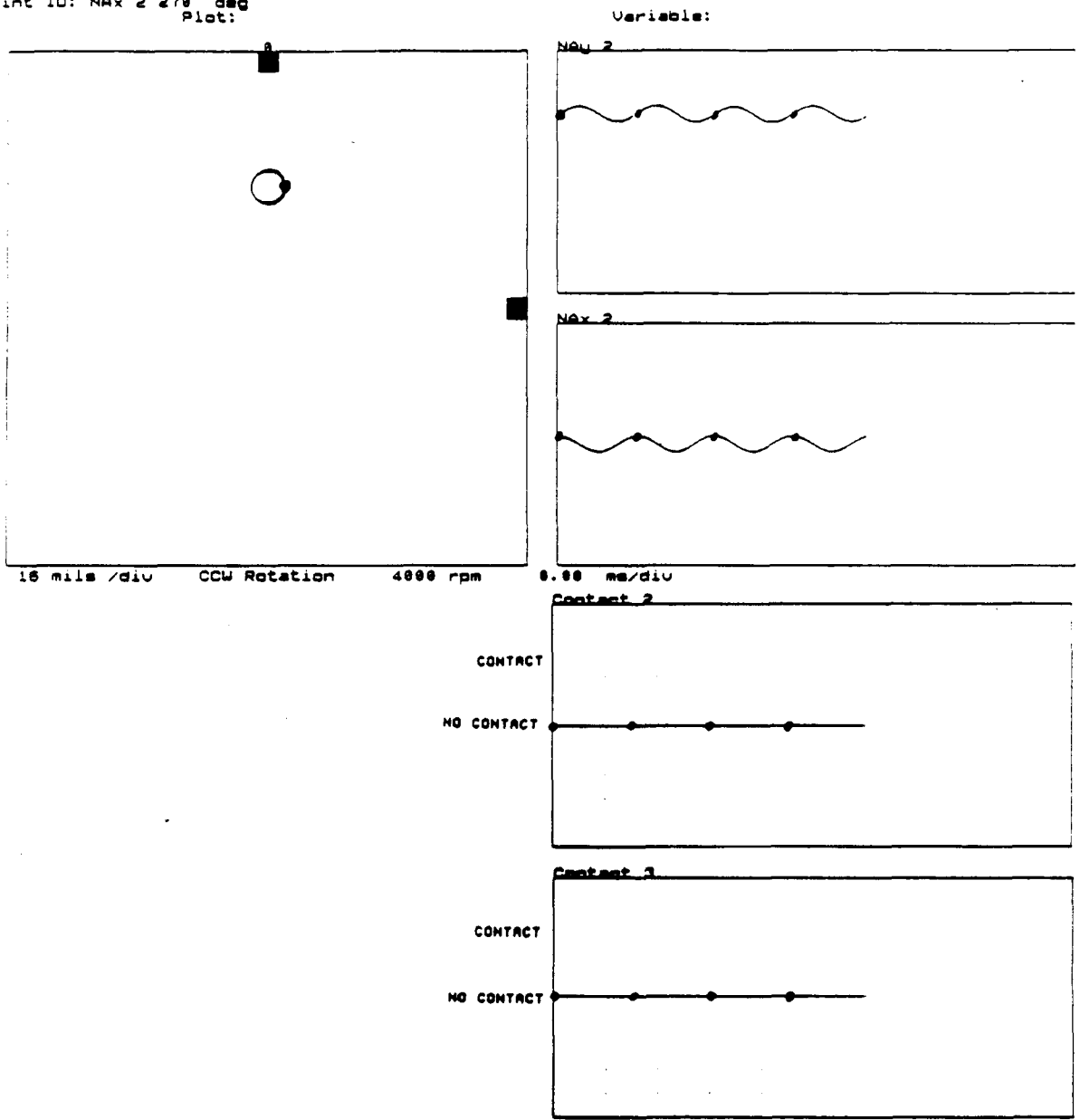


FIGURE 15.46 CALCULATED STEADY-STATE RESPONSE AT LOCATION A2 USING NONLINEAR PORTION OF COMPUTER SIMULATION PROGRAM FOR 4000 RPM, 0.00016 IN-LB UNBALANCE IN A2, AND 5.0 LB. RADIAL PRELOAD AT A3.

Point ID: Nby 3 0 deg  
Point ID: Nbx 3 270 deg  
Plot:

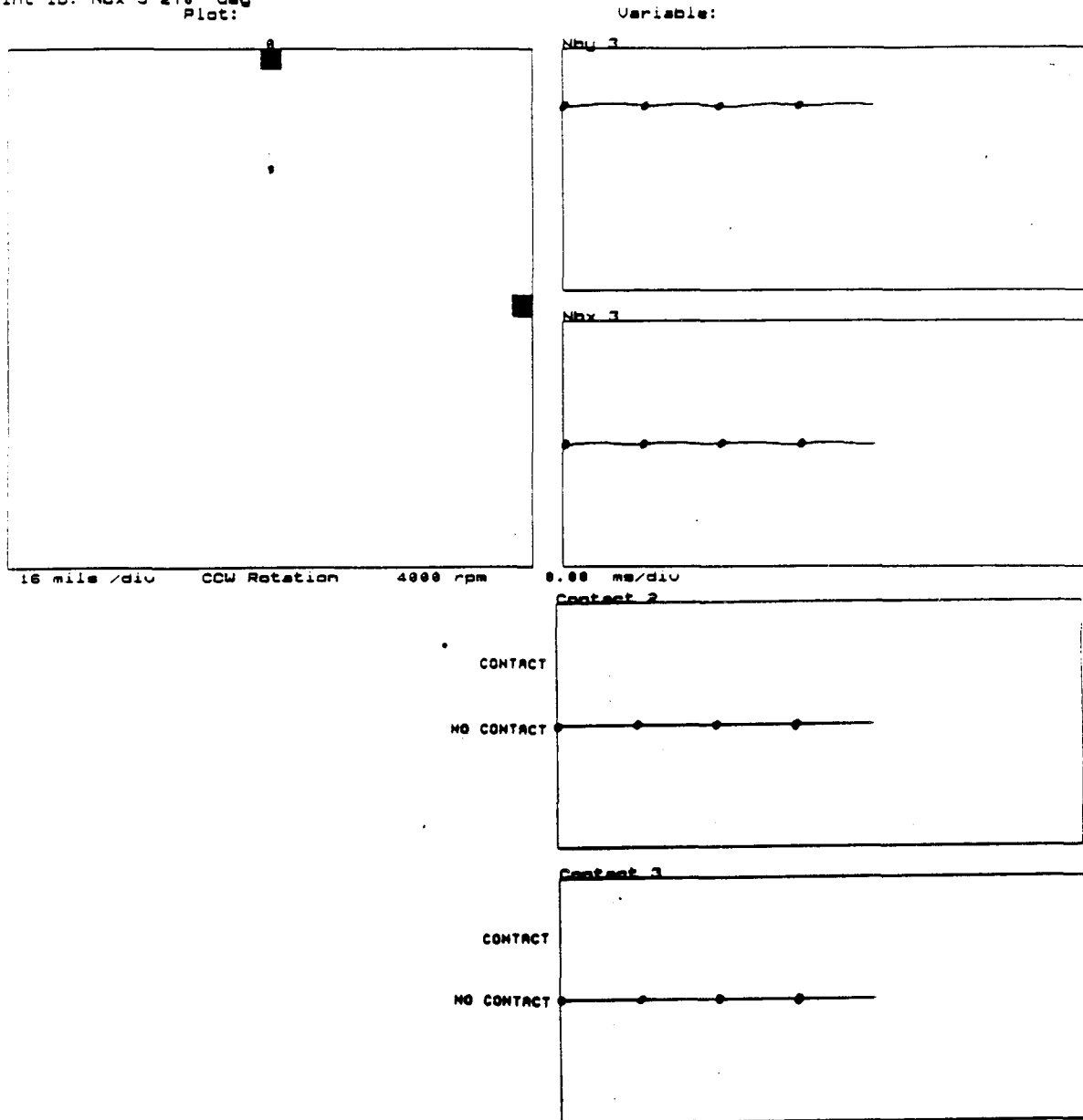


FIGURE 15.47 CALCULATED STEADY-STATE RESPONSE AT LOCATION B3 USING NONLINEAR PORTION OF COMPUTER SIMULATION PROGRAM FOR 4000 RPM, 0.00016 IN-LB UNBALANCE IN A2, AND 5.0 LB. RADIAL PRELOAD AT A3.

Point ID: NAY 3 0 deg  
Point ID: NAX 3 270 deg  
Plot:

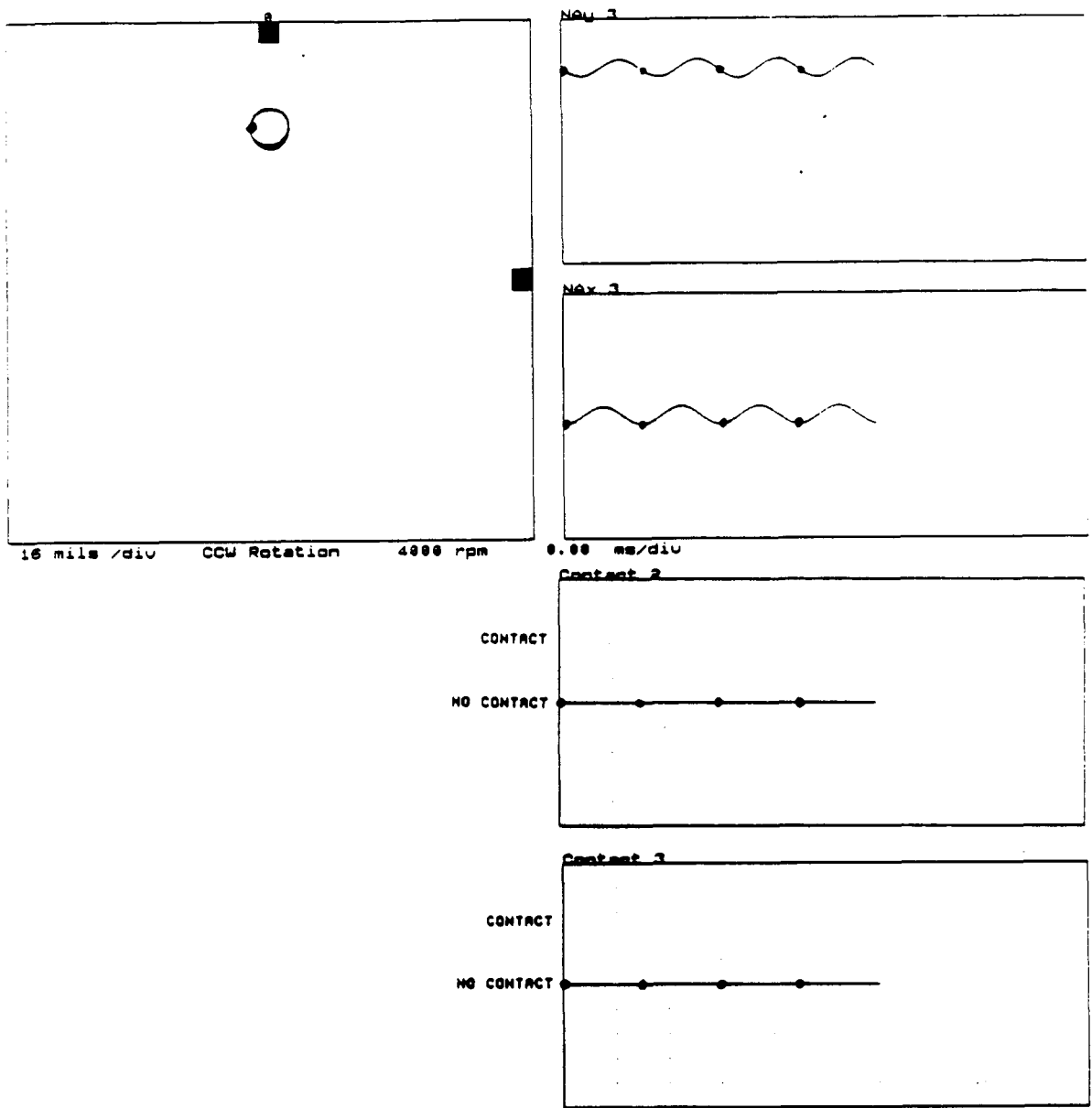


FIGURE 15.48 CALCULATED STEADY-STATE RESPONSE AT LOCATION A3 USING NONLINEAR PORTION OF COMPUTER SIMULATION PROGRAM FOR 4000 RPM, 0.00016 IN-LB UNBALANCE IN A2, AND 5.0 LB. RADIAL PRELOAD AT A3.

Point ID: Nbu 4 8 deg  
 Point ID: Nbx 4 278 deg  
 Plot:

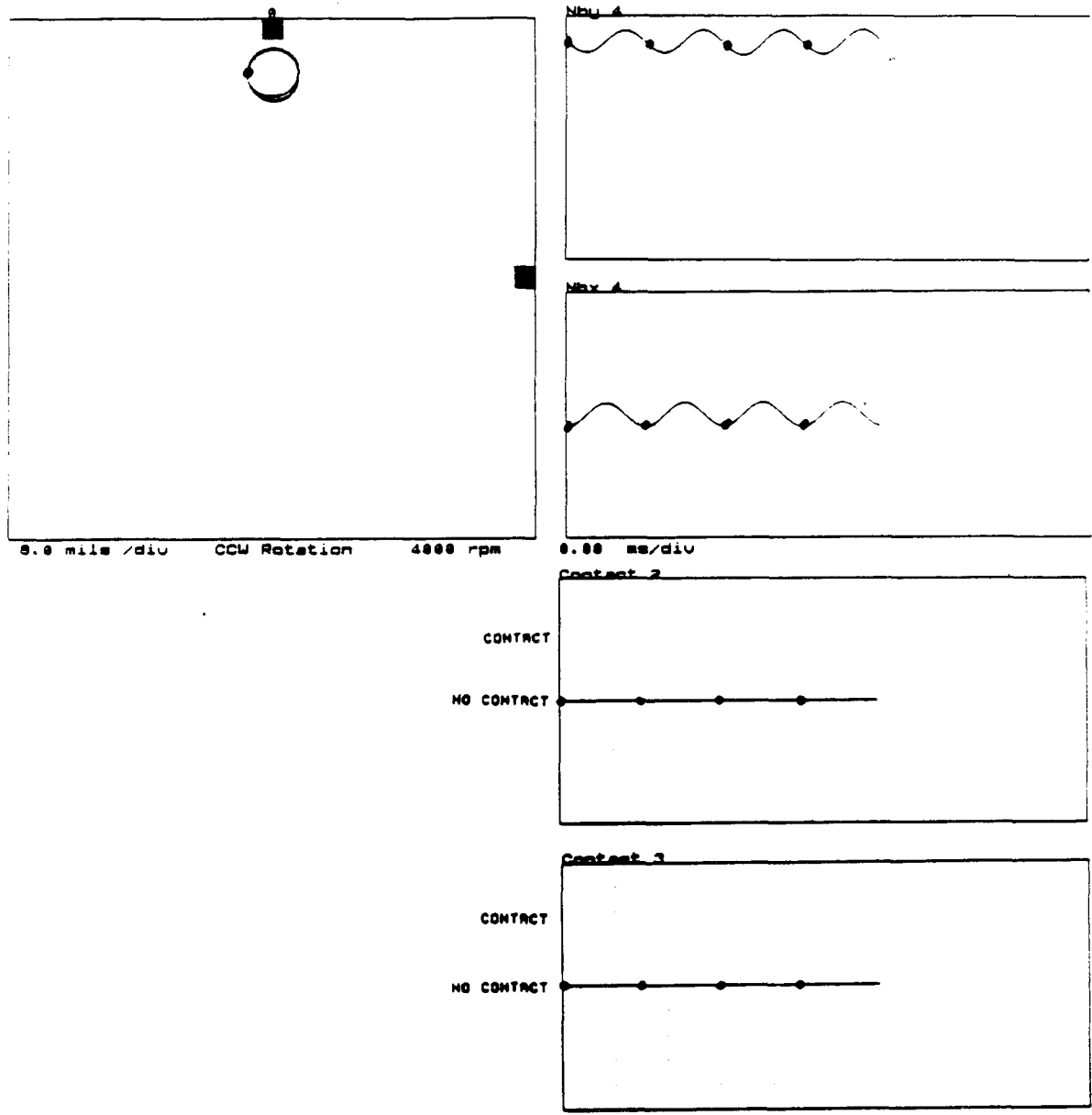


FIGURE 15.49 CALCULATED STEADY-STATE RESPONSE AT LOCATION B4 USING NONLINEAR PORTION OF COMPUTER SIMULATION PROGRAM FOR 4000 RPM, 0.00016 IN-LB UNBALANCE IN A2, AND 5.0 LB. RADIAL PRELOAD AT A3.

ORIGINAL PAGE IS  
OF POOR QUALITY

Point ID: NBy 1 0 deg  
Point ID: NBx 1 270 deg  
Plot:

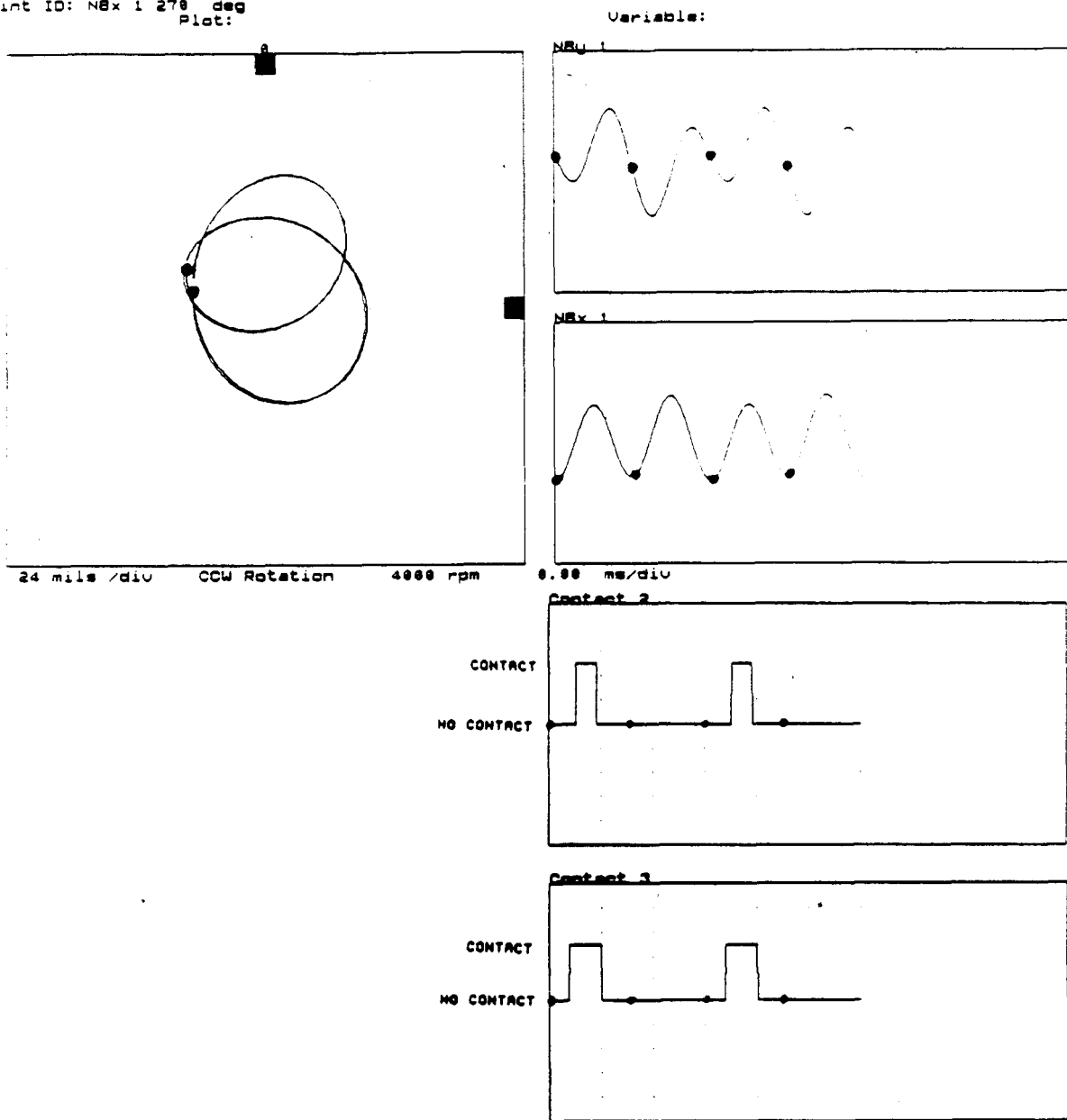


FIGURE 15.50 CALCULATED STEADY-STATE RESPONSE AT LOCATION B1 USING NONLINEAR PORTION OF COMPUTER SIMULATION PROGRAM FOR 4000 RPM, 0.00016 IN-LB UNBALANCE IN A2, AND 6.0 LB. RADIAL PRELOAD AT A3.

Point ID: NAX 1 0 ddd  
Point ID: NAX 1 270 ddd  
Plot:

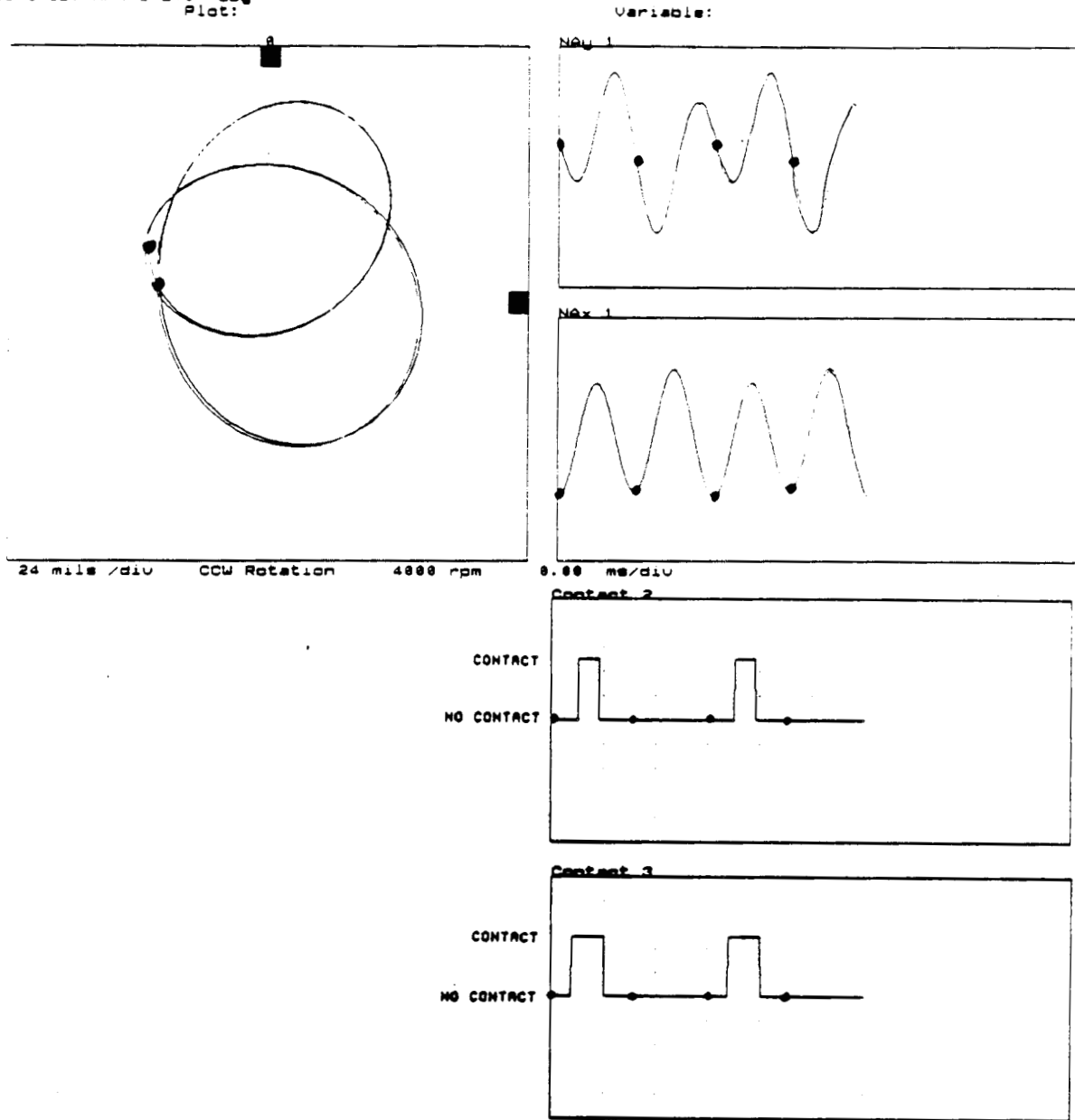
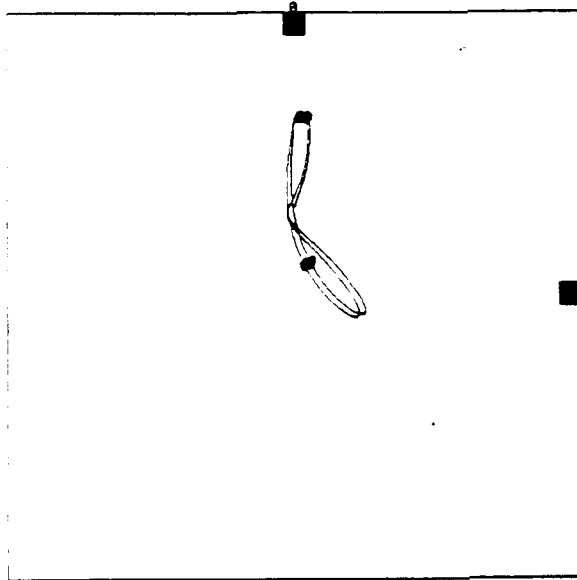


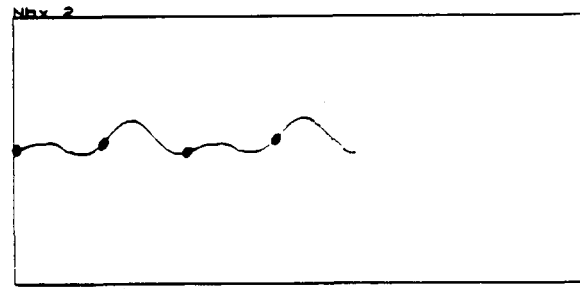
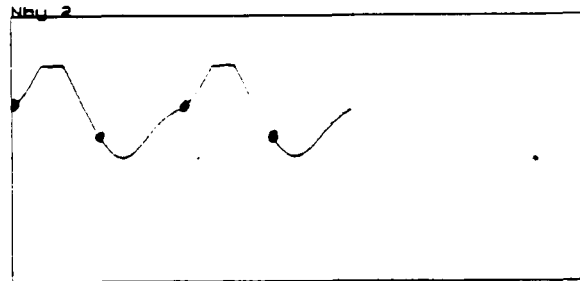
FIGURE 15.51    CALCULATED STEADY-STATE RESPONSE AT LOCATION A1 USING NONLINEAR PORTION OF COMPUTER SIMULATION PROGRAM FOR 4000 RPM, 0.00016 IN-LB UNBALANCE IN A2, AND 6.0 LB. RADIAL PRELOAD AT A3.

Point ID: Nby 2 0 deg  
Point ID: Nbx 2 270 deg  
Plot:



16 mils/div CCW Rotation 4000 rpm

Variable:



0.00 ms/div

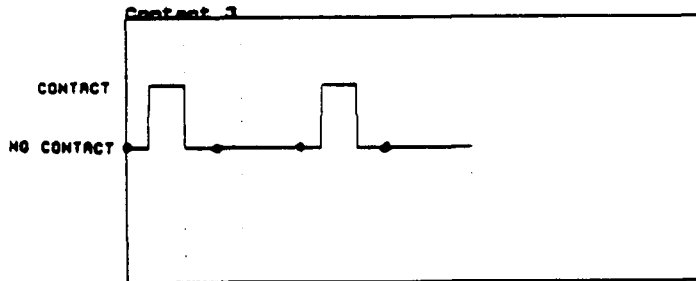
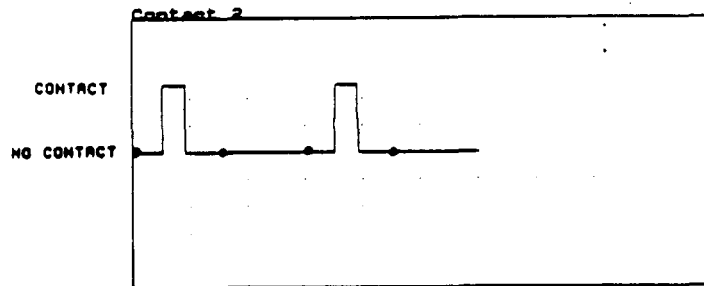


FIGURE 15.52 CALCULATED STEADY-STATE RESPONSE AT LOCATION B2 USING NONLINEAR PORTION OF COMPUTER SIMULATION PROGRAM FOR 4000 RPM, 0.00016 IN-LB UNBALANCE IN A2, AND 6.0 LB. RADIAL PRELOAD AT A3.

Point ID: NAX 2 0 deg  
 Point ID: NAY 2 270 deg  
 Plot:

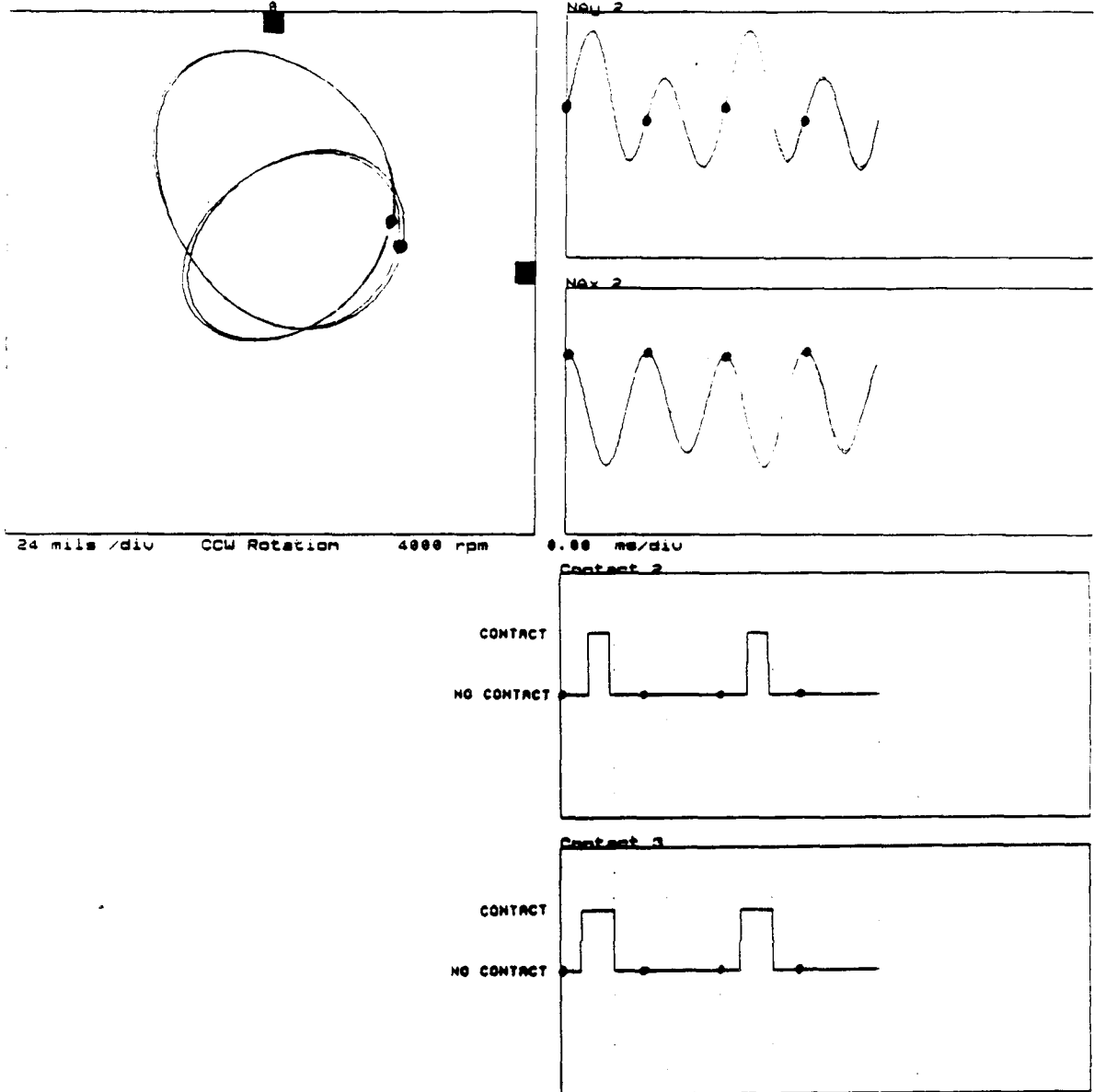


FIGURE 15.53 CALCULATED STEADY-STATE RESPONSE AT LOCATION A2 USING NONLINEAR PORTION OF COMPUTER SIMULATION PROGRAM FOR 4000 RPM, 0.00016 IN-LB UNBALANCE IN A2, AND 6.0 LB. RADIAL PRELOAD AT A3.

Point ID: Nbu 3 0 deg  
Point ID: Nbx 3 270 deg  
Plot:

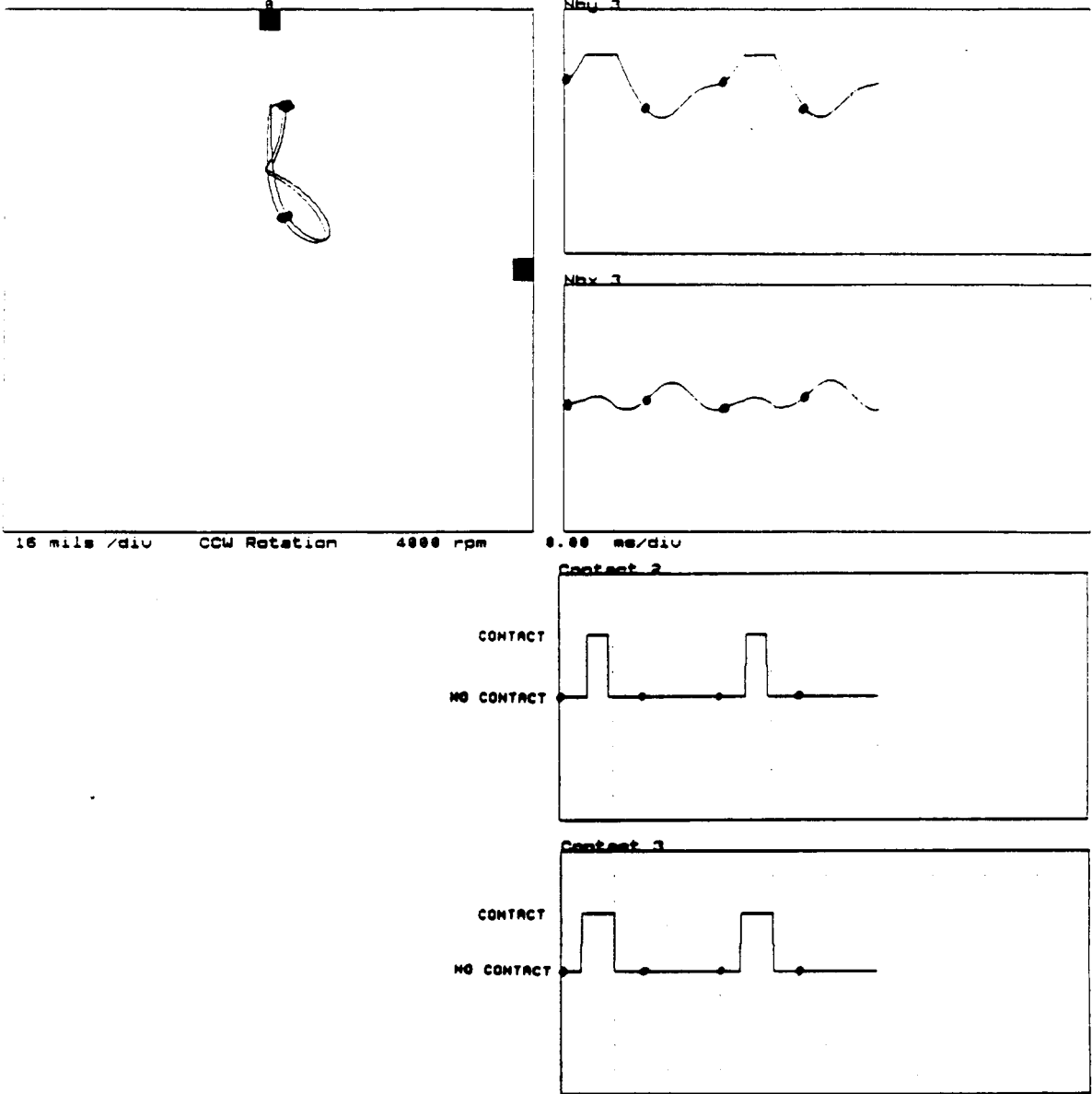


FIGURE 15.54 CALCULATED STEADY-STATE RESPONSE AT LOCATION B3 USING NONLINEAR PORTION OF COMPUTER SIMULATION PROGRAM FOR 4000 RPM, 0.00016 IN-LB UNBALANCE IN A2, AND 6.0 LB. RADIAL PRELOAD AT A3.

Point ID: NAX 3 0 deg  
Point ID: NAX 3 270 deg  
Plot:

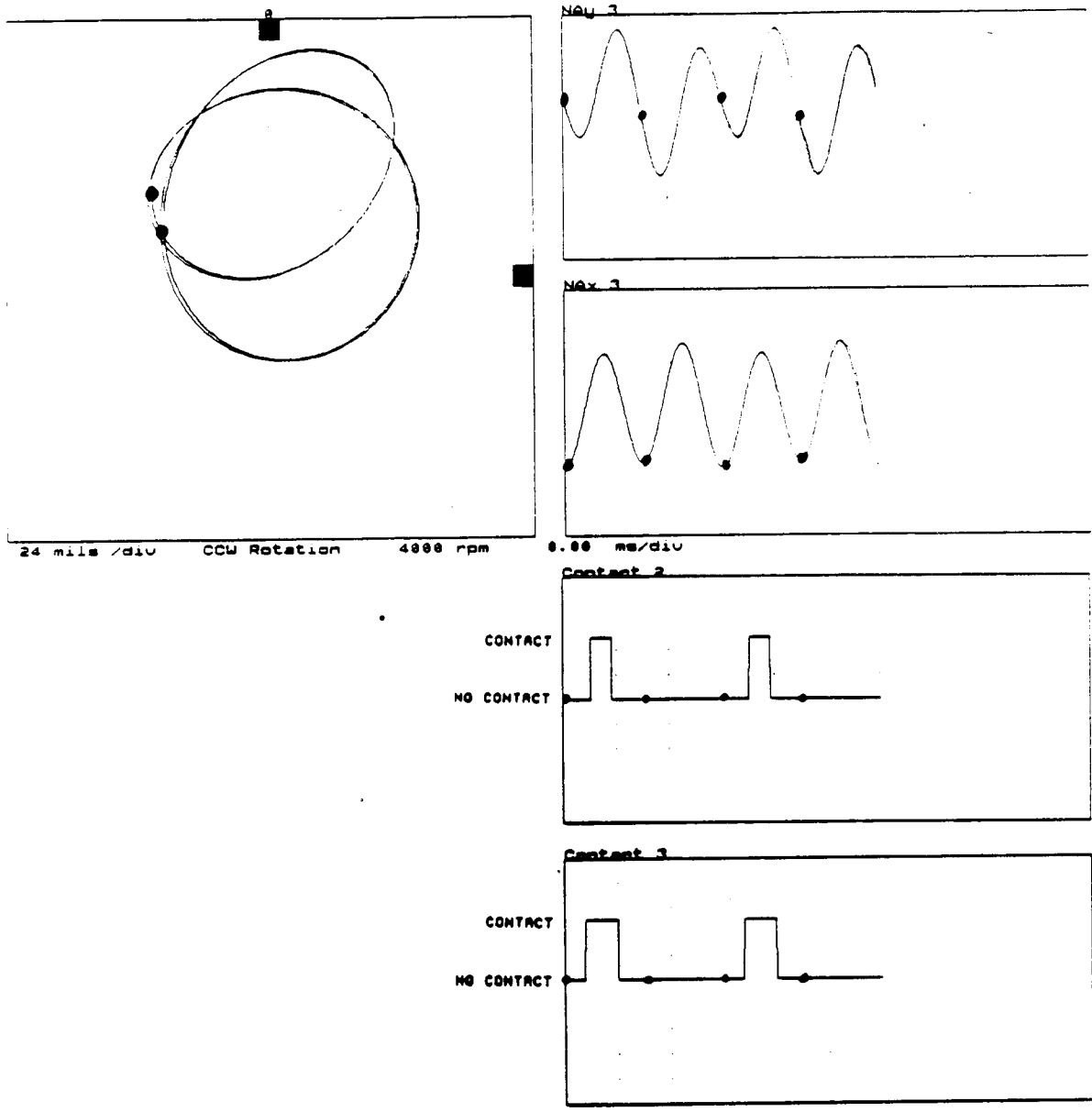


FIGURE 15.55 CALCULATED STEADY-STATE RESPONSE AT LOCATION A3 USING NONLINEAR PORTION OF COMPUTER SIMULATION PROGRAM FOR 4000 RPM, 0.00016 IN-LB UNBALANCE IN A2, AND 6.0 LB. RADIAL PRELOAD AT A3.

ORIGINAL PAGE IS  
OF POOR QUALITY

Point ID: Nbu 4 8 deg  
Point ID: Nbx 4 270 deg  
Plot:

Variable:

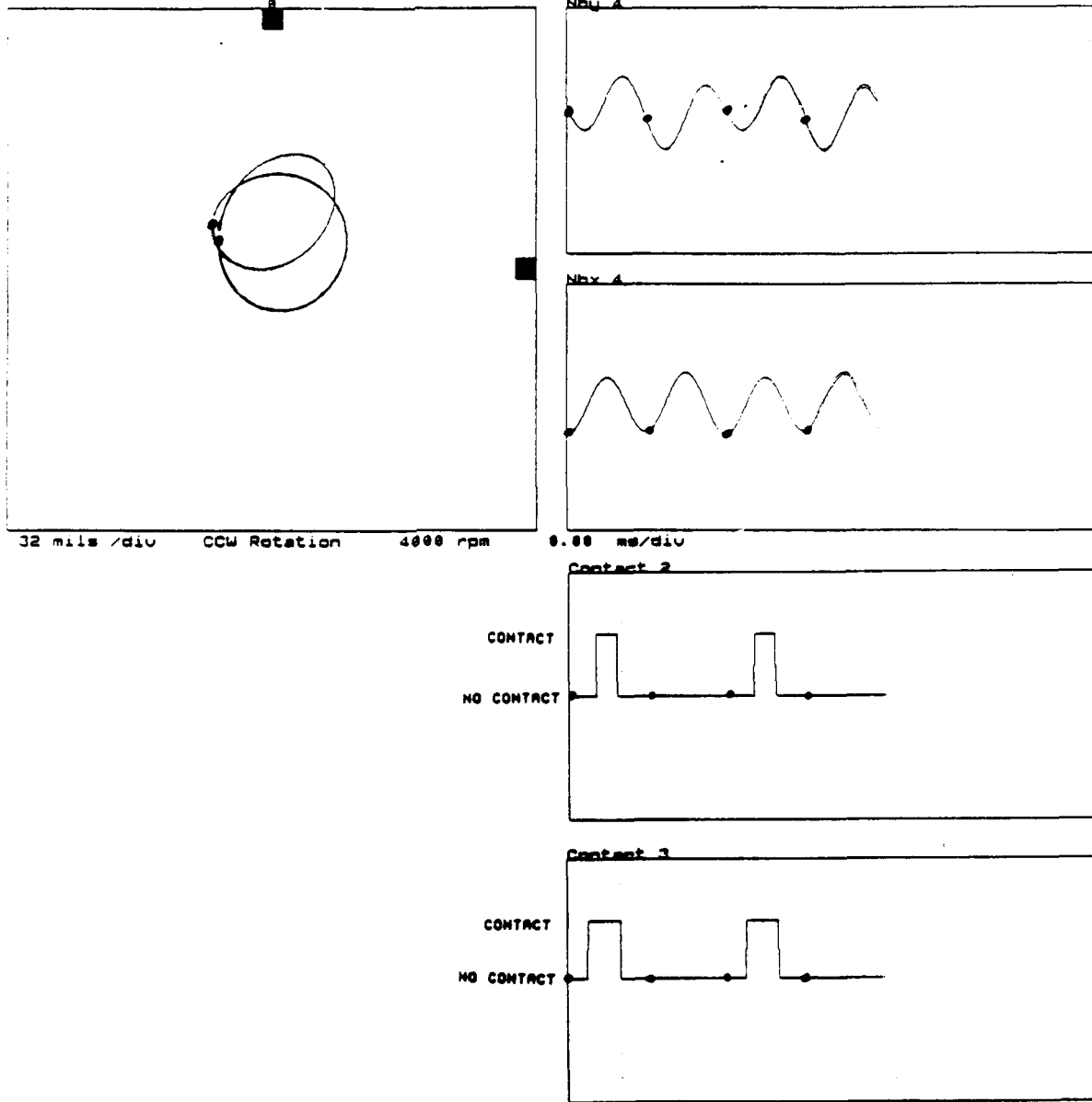
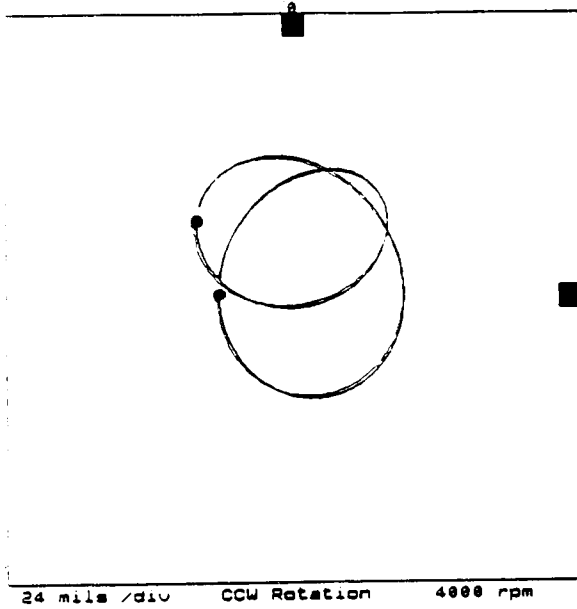


FIGURE 15.56    CALCULATED STEADY-STATE RESPONSE AT LOCATION B4  
USING NONLINEAR PORTION OF COMPUTER SIMULATION  
PROGRAM FOR 4000 RPM, 0.00016 IN-LB UNBALANCE IN A2,  
AND 6.0 LB. RADIAL PRELOAD AT A3.

Point ID: NBy 1 0 deg  
Point ID: NBx 1 270 deg  
Plot:



Variable:

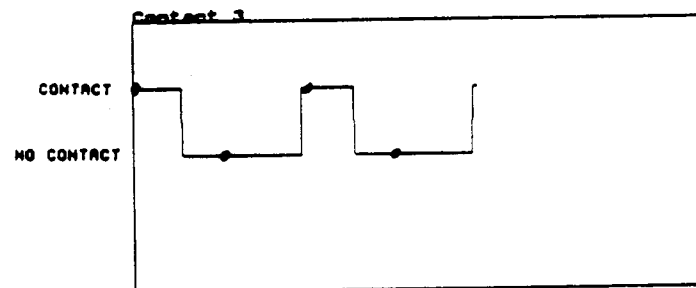
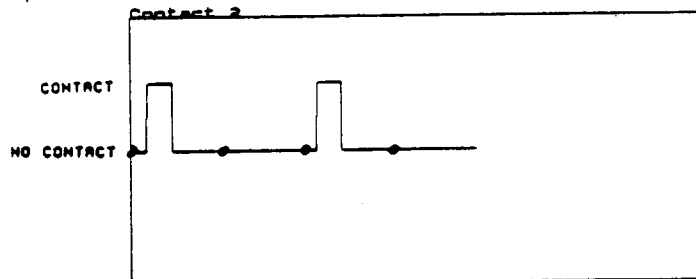
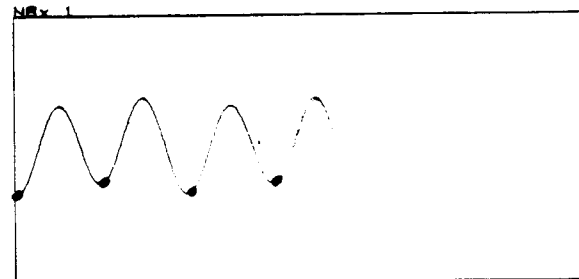
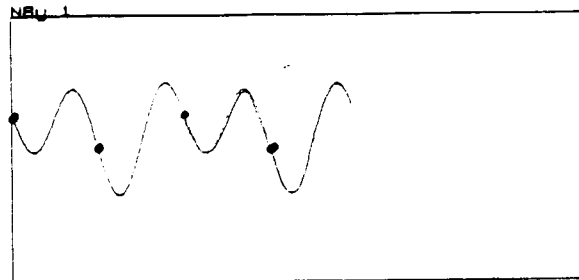


FIGURE 15.57 CALCULATED STEADY-STATE RESPONSE AT LOCATION B1 USING NONLINEAR PORTION OF COMPUTER SIMULATION PROGRAM FOR 4000 RPM, 0.00016 IN-LB UNBALANCE IN A2, AND 7.0 LB. RADIAL PRELOAD AT A3.

ORIGINAL PAGE IS  
OF POOR QUALITY

Point ID: NAY 1 0 deg  
Point ID: NAX 1 270 deg  
Plot:

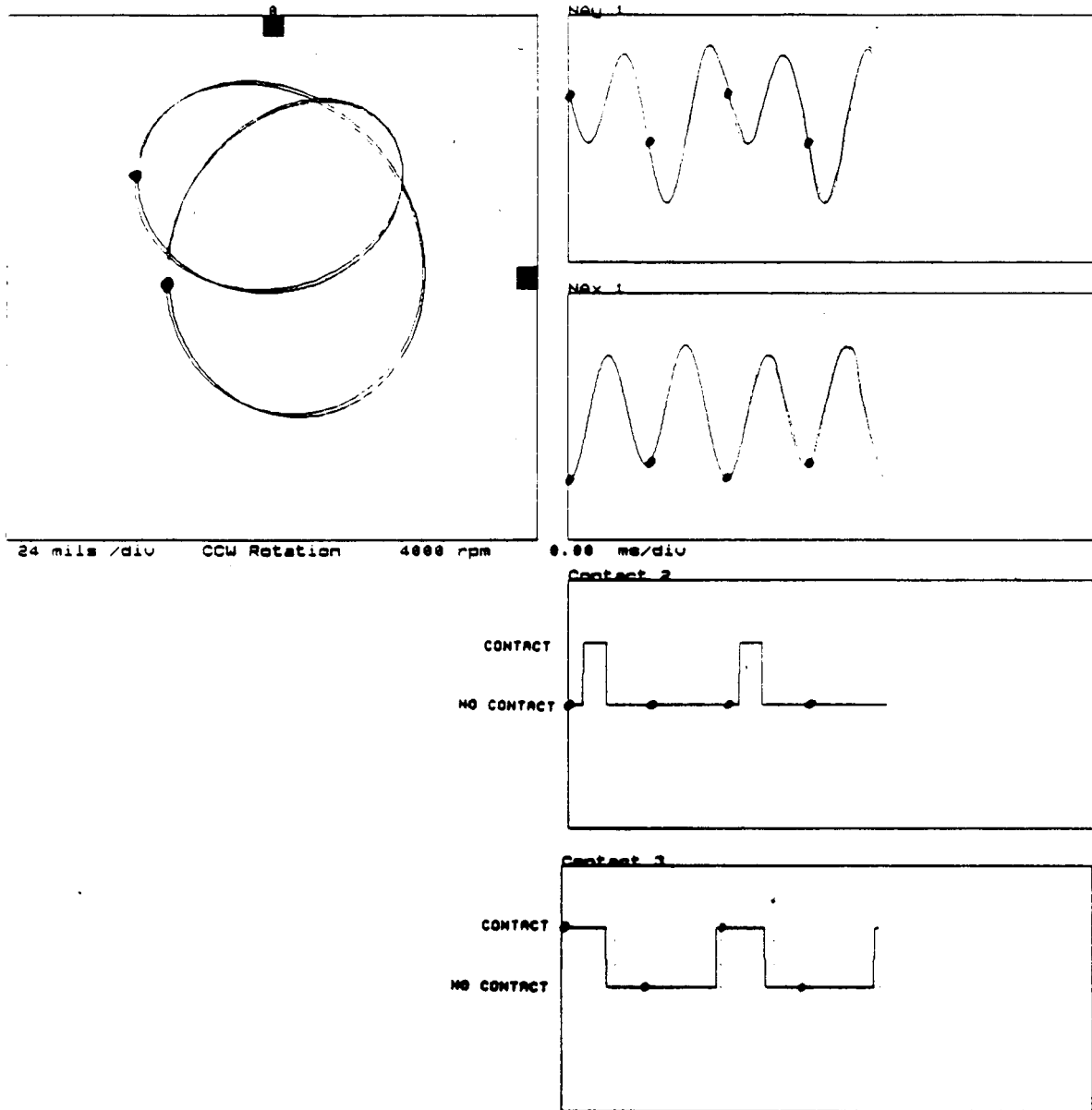


FIGURE 15.58 CALCULATED STEADY-STATE RESPONSE AT LOCATION A1 USING NONLINEAR PORTION OF COMPUTER SIMULATION PROGRAM FOR 4000 RPM, 0.00016 IN-LB UNBALANCE IN A2, AND 7.0 LB. RADIAL PRELOAD AT A3.

Point ID: ZBC 270 0 00  
 Point ID: ZBX 270 0 00  
 Plot: 00

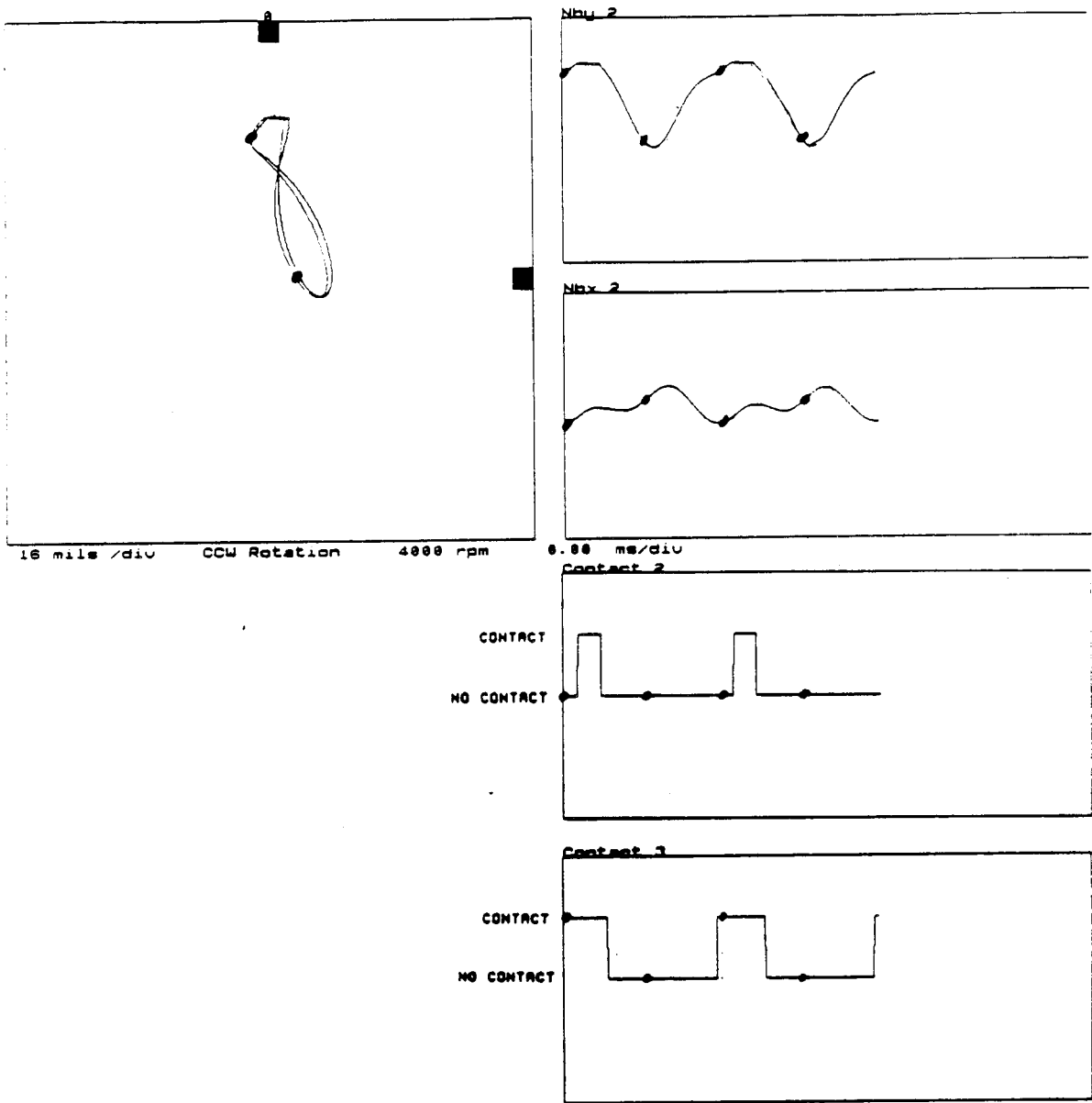


FIGURE 15.59 CALCULATED STEADY-STATE RESPONSE AT LOCATION B2 USING NONLINEAR PORTION OF COMPUTER SIMULATION PROGRAM FOR 4000 RPM, 0.00016 IN-LB UNBALANCE IN A2, AND 7.0 LB. RADIAL PRELOAD AT A3.

ORIGINAL PAGE IS  
OF POOR QUALITY

Point ID: NAY 2 0 deg  
Point ID: NAX 2 270 deg  
Plot:

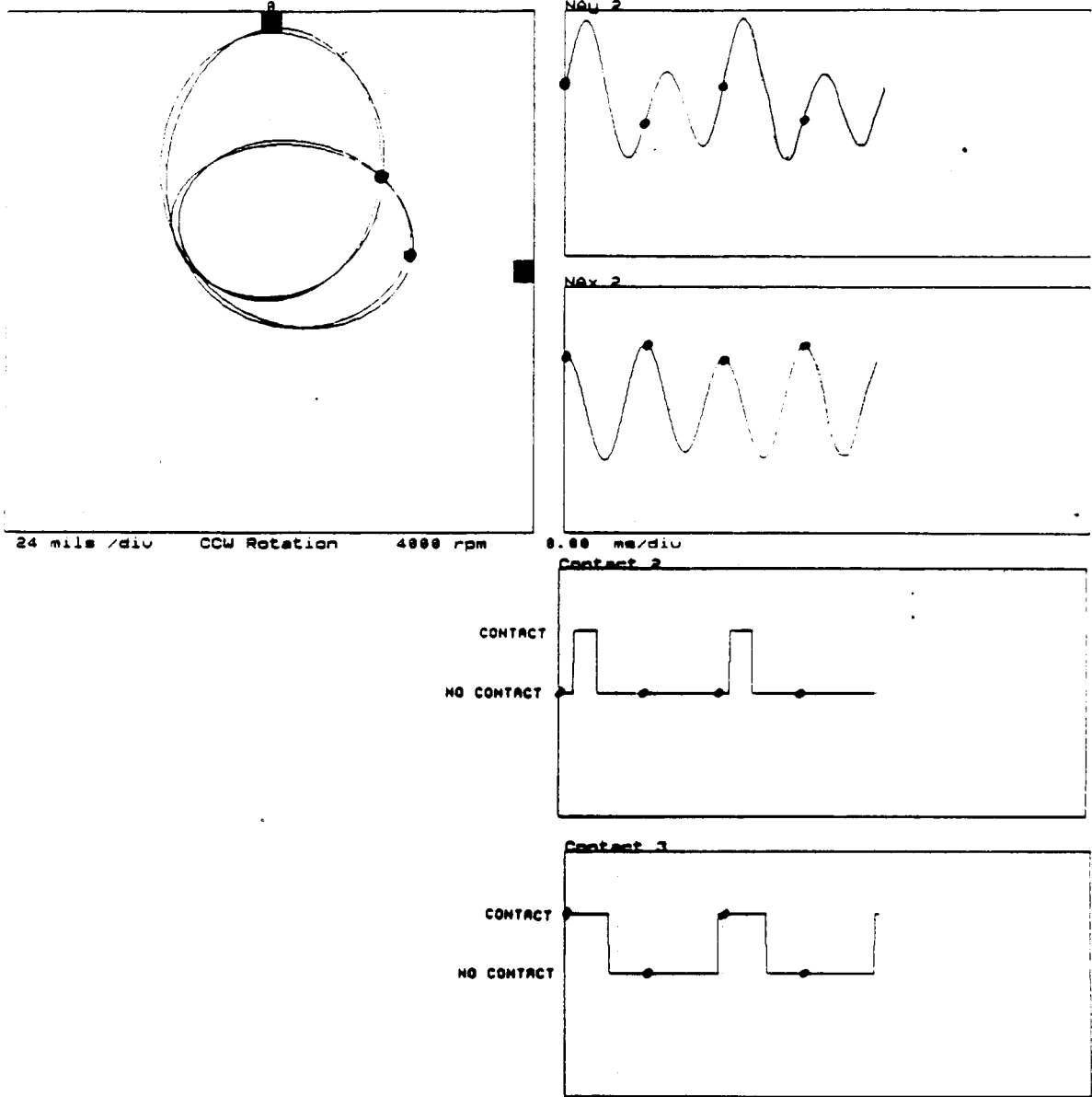


FIGURE 15.60 CALCULATED STEADY-STATE RESPONSE AT LOCATION A2 USING NONLINEAR PORTION OF COMPUTER SIMULATION PROGRAM FOR 4000 RPM, 0.00016 IN-LB UNBALANCE IN A2, AND 7.0 LB. RADIAL PRELOAD AT A3.

Point ID: NBY 3 0 deg  
Point ID: NBX 3 270 deg  
Plot:

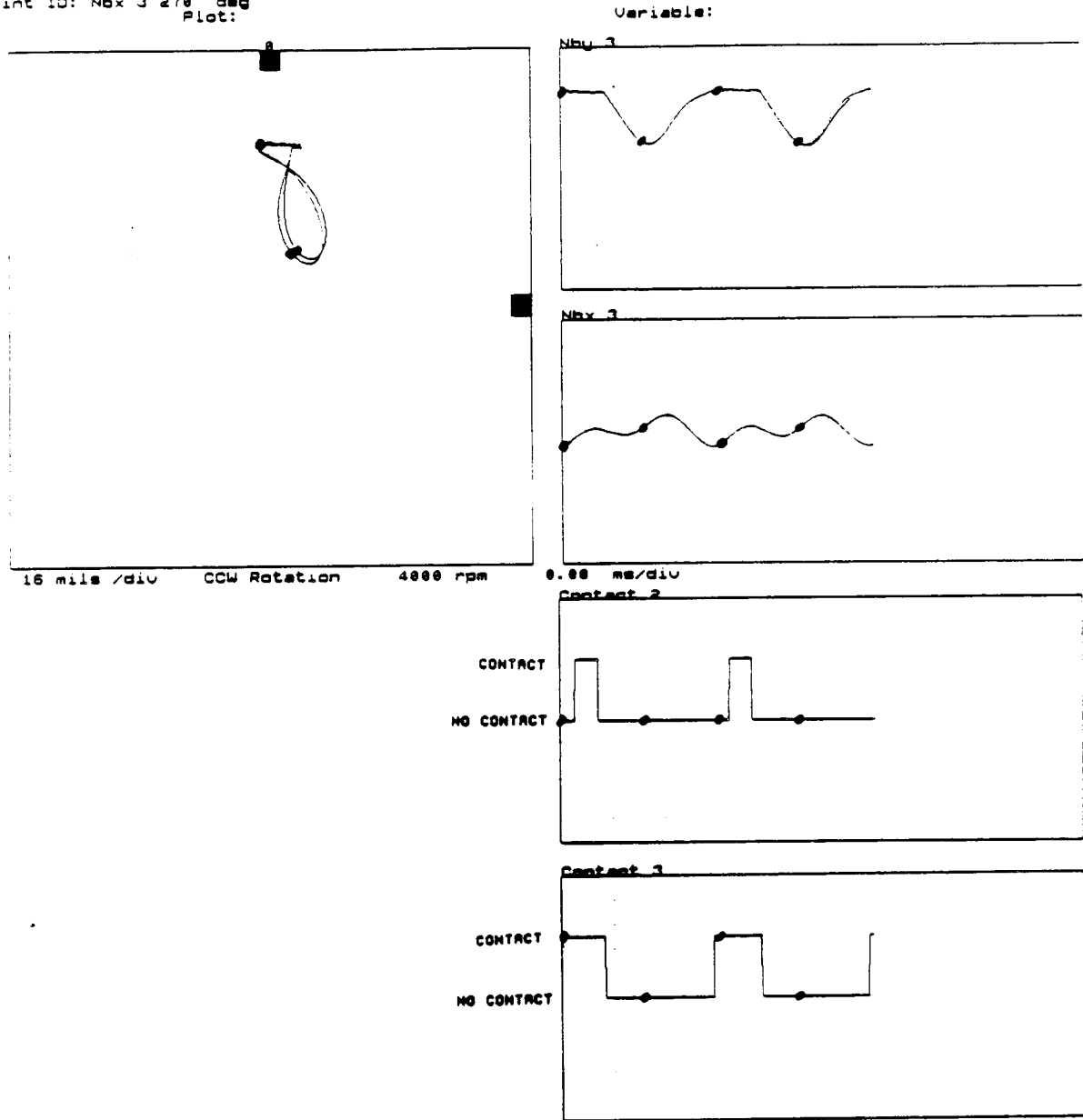


FIGURE 15.61 CALCULATED STEADY-STATE RESPONSE AT LOCATION B3 USING NONLINEAR PORTION OF COMPUTER SIMULATION PROGRAM FOR 4000 RPM, 0.00016 IN-LB UNBALANCE IN A2, AND 7.0 LB. RADIAL PRELOAD AT A3.

Point ID: Z6y 3 0 deg  
Point ID: Z6x 3 270 deg  
Plot:

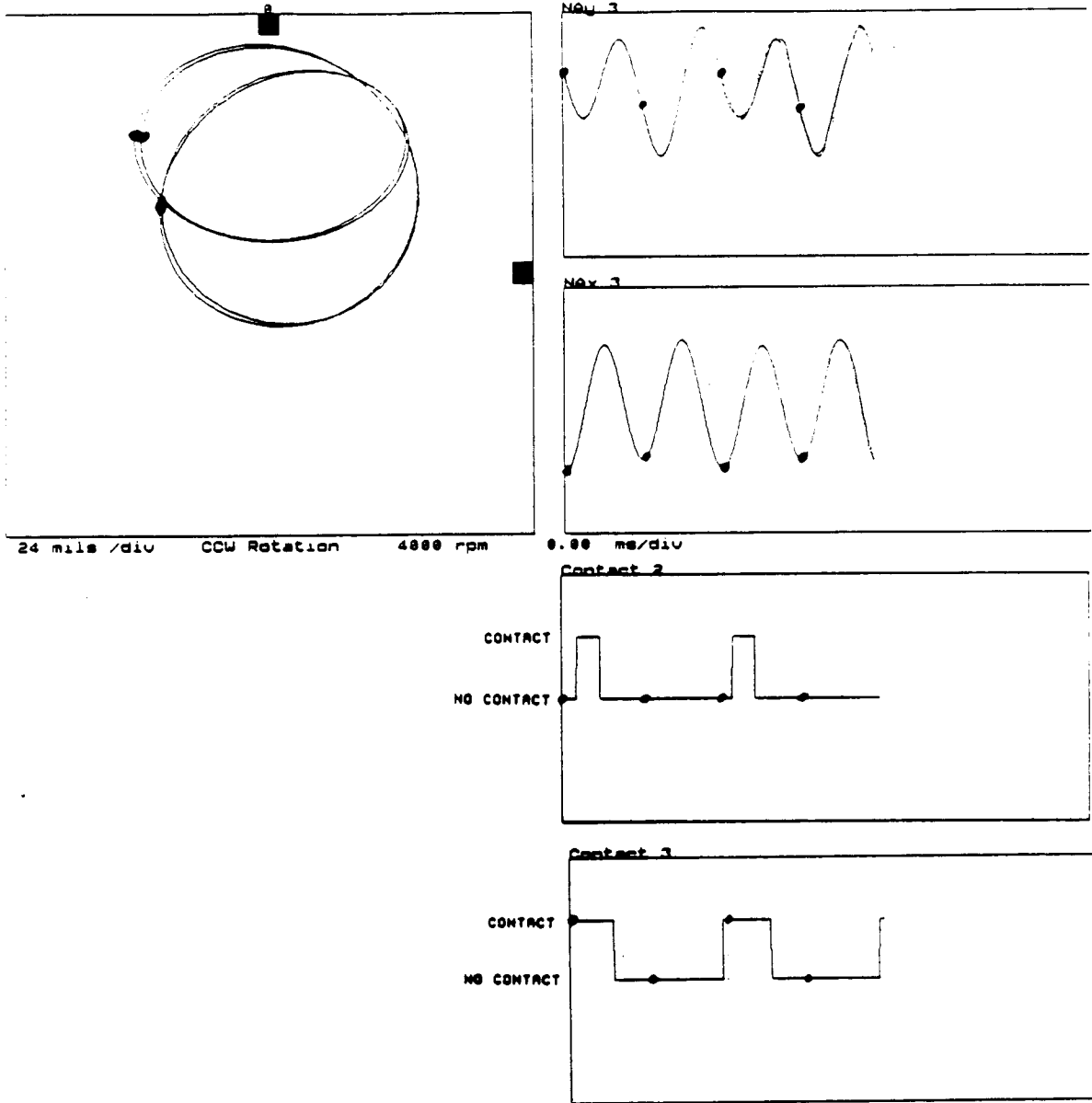


FIGURE 15.62 CALCULATED STEADY-STATE RESPONSE AT LOCATION A3 USING NONLINEAR PORTION OF COMPUTER SIMULATION PROGRAM FOR 4000 RPM, 0.00016 IN-LB UNBALANCE IN A2, AND 7.0 LB. RADIAL PRELOAD AT A3.

Point ID: Nby 4 9 deg  
Point ID: Nbx 4 279 deg  
Plot:

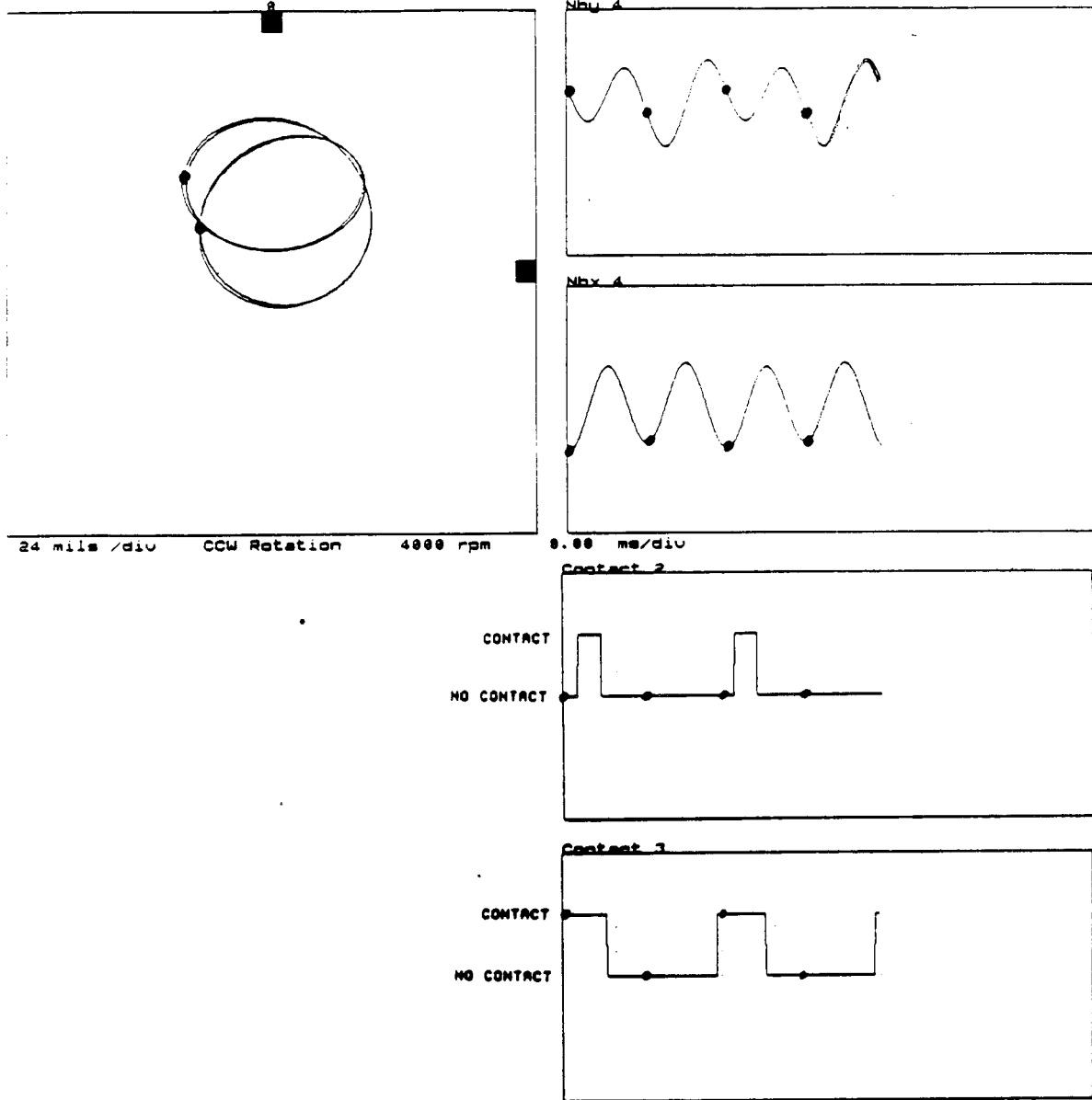


FIGURE 15.63 CALCULATED STEADY-STATE RESPONSE AT LOCATION B4 USING NONLINEAR PORTION OF COMPUTER SIMULATION PROGRAM FOR 4000 RPM, 0.00016 IN-LB UNBALANCE IN A2, AND 7.0 LB. RADIAL PRELOAD AT A3.

Point ID: NBu 1 0 deg  
Point ID: NBx 1 270 deg  
Plot:

Variable:

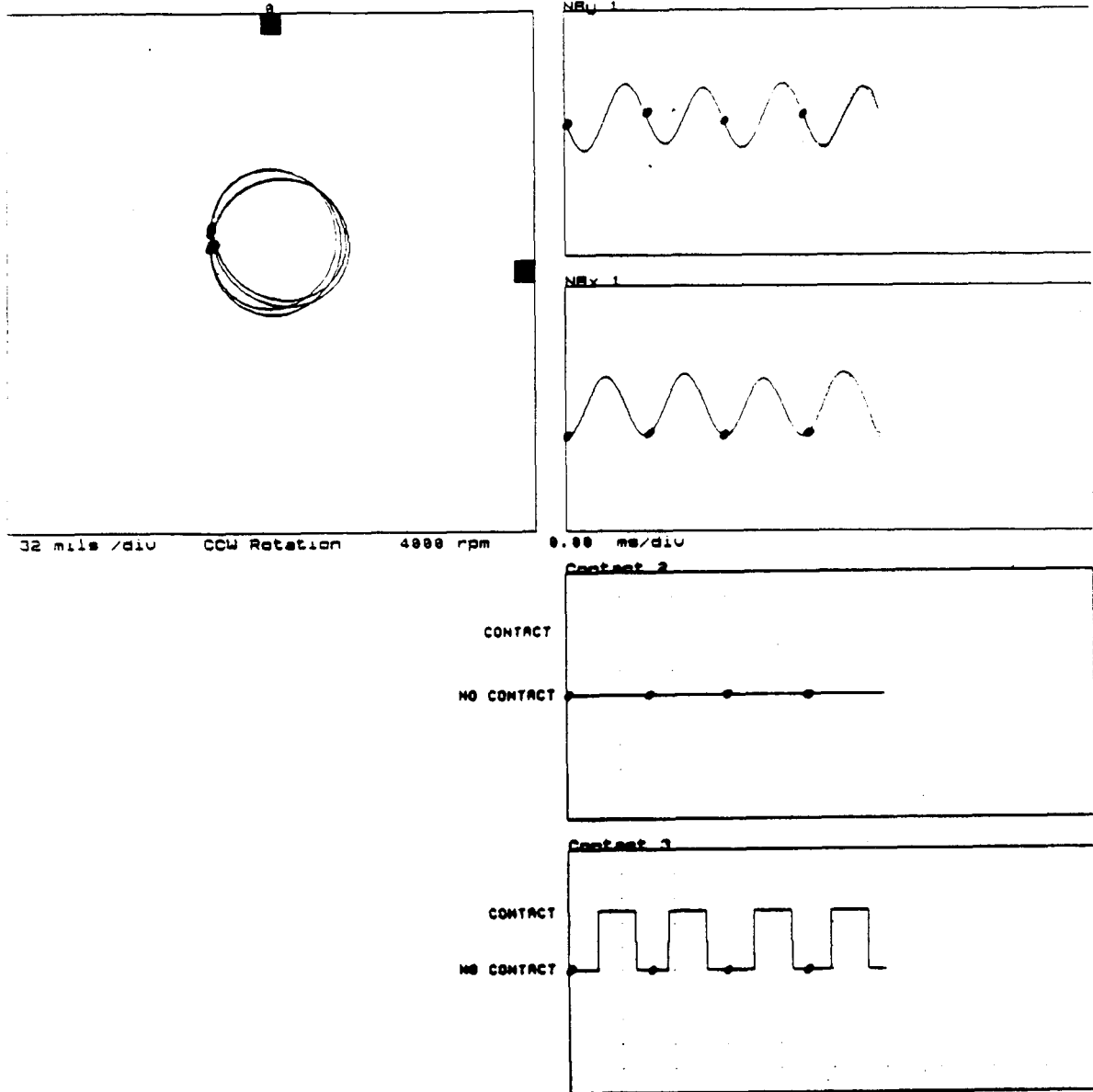


FIGURE 15.64 CALCULATED STEADY-STATE RESPONSE AT LOCATION B1 USING NONLINEAR PORTION OF COMPUTER SIMULATION PROGRAM FOR 4000 RPM, 0.00016 IN-LB UNBALANCE IN A2, AND 10.0 LB RADIAL PRELOAD AT A3.

Point ID: NAY 1 0 000  
Point ID: NAX 1 270 000  
Plot:

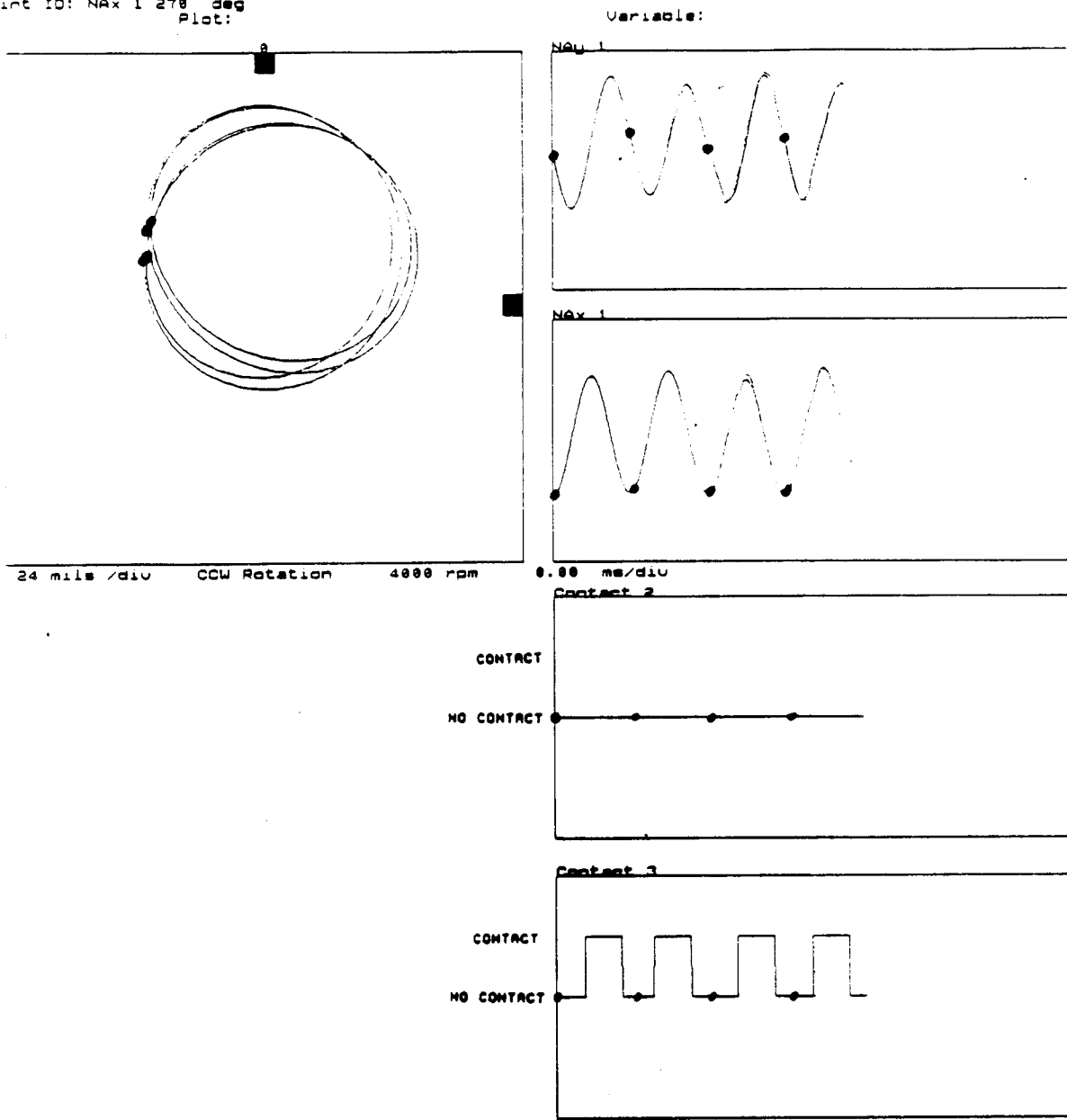
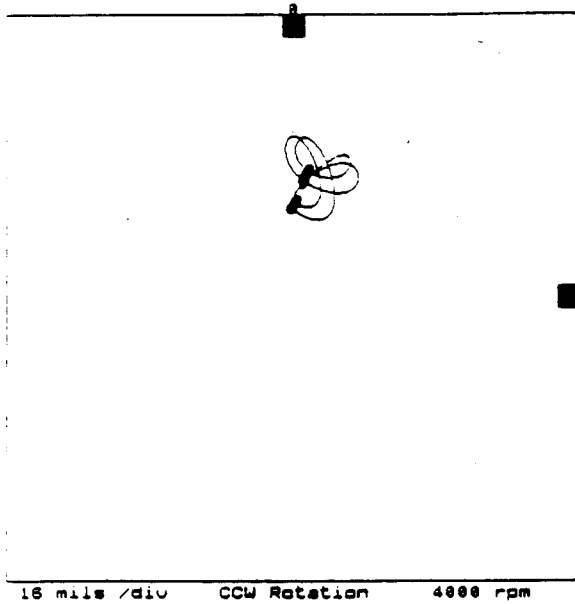


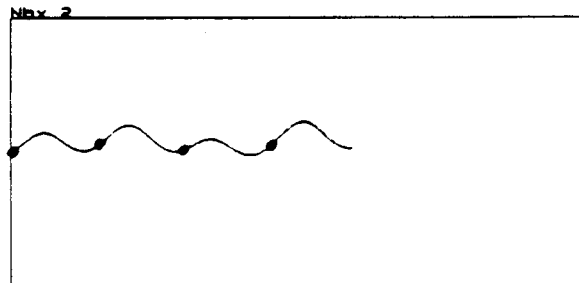
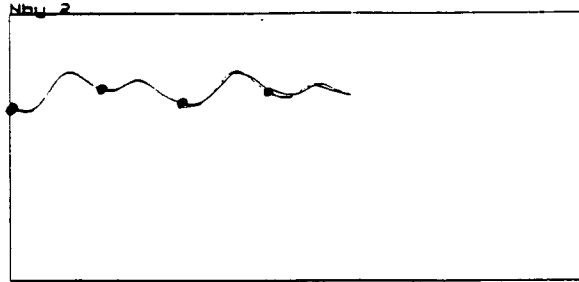
FIGURE 15.65 CALCULATED STEADY-STATE RESPONSE AT LOCATION A1 USING NONLINEAR PORTION OF COMPUTER SIMULATION PROGRAM FOR 4000 RPM, 0.00016 IN-LB UNBALANCE IN A2, AND 10.0 LB RADIAL PRELOAD AT A3.

Point ID: Nby 2 0 deg  
Point ID: Nbx 2 270 deg  
Plot:



16 mils /diu CCW Rotation 4000 rpm

Variable:



0.00 ms/diu

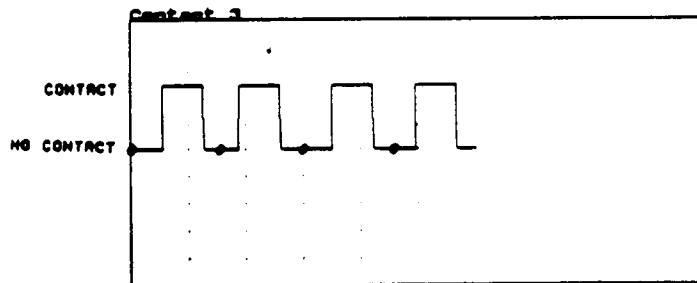
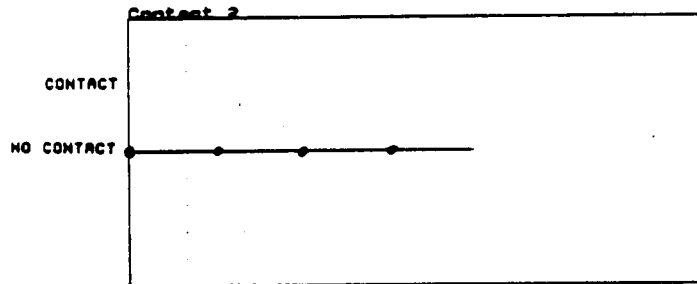


FIGURE 15.66 CALCULATED STEADY-STATE RESPONSE AT LOCATION B2 USING NONLINEAR PORTION OF COMPUTER SIMULATION PROGRAM FOR 4000 RPM, 0.00016 IN-LB UNBALANCE IN A2, AND 10.0 LB RADIAL PRELOAD AT A3.

Point ID: NAY 2 0 deg  
Point ID: NAY 2 270 deg  
Plot:

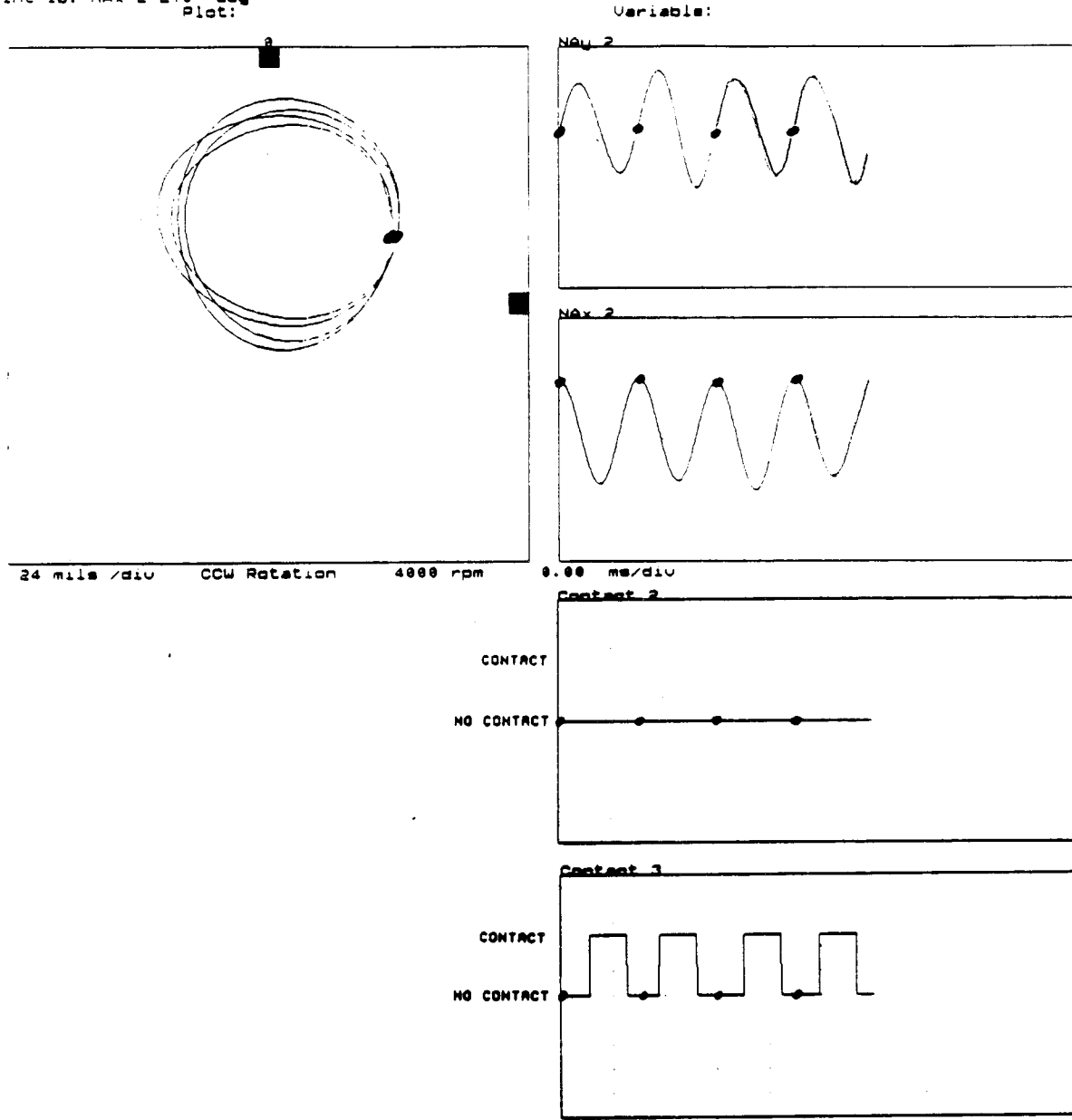


FIGURE 15.67    CALCULATED STEADY-STATE RESPONSE AT LOCATION A2 USING NONLINEAR PORTION OF COMPUTER SIMULATION PROGRAM FOR 4000 RPM, 0.00016 IN-LB UNBALANCE IN A2, AND 10.0 LB RADIAL PRELOAD AT A3.

Point ID: Nby 3 0 deg  
Point ID: Nbx 3 270 deg  
Plot:

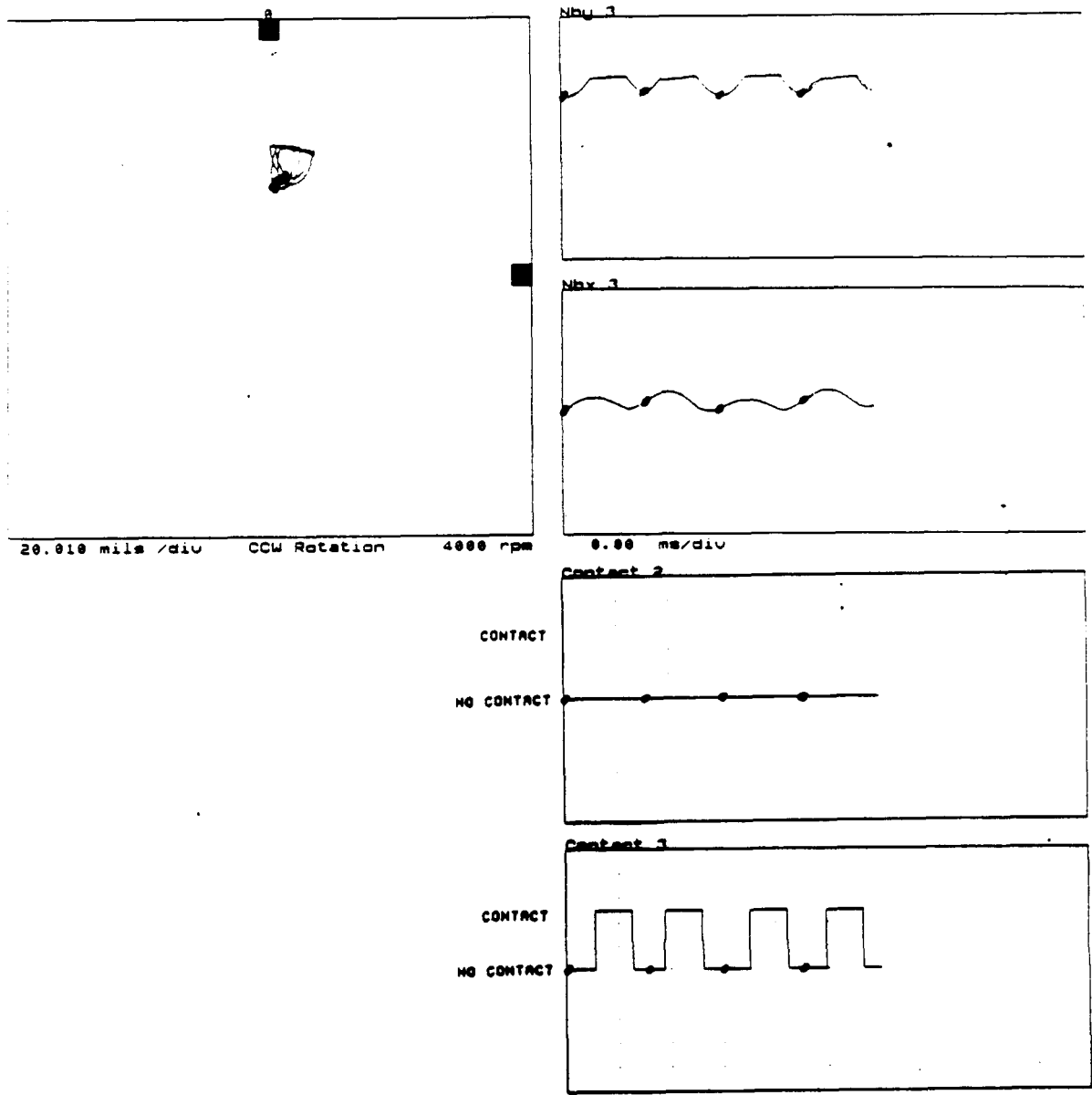
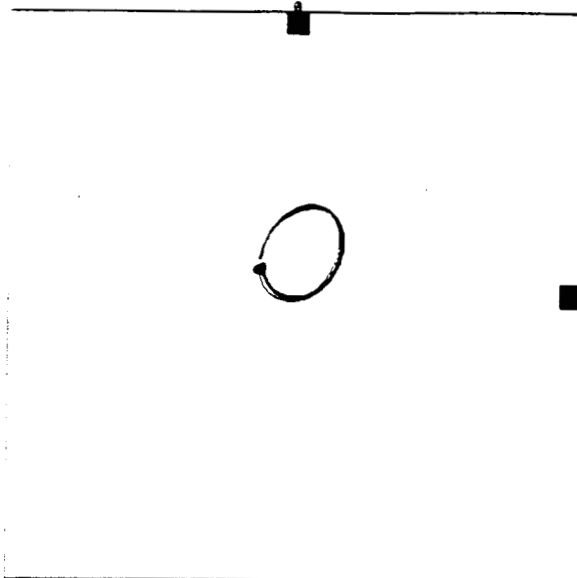


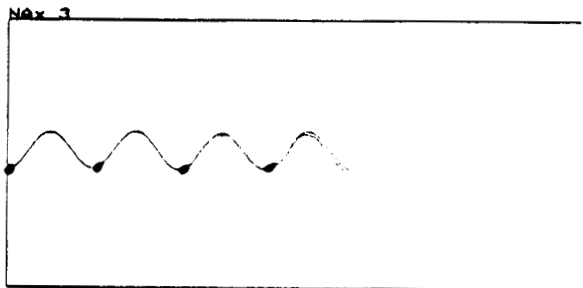
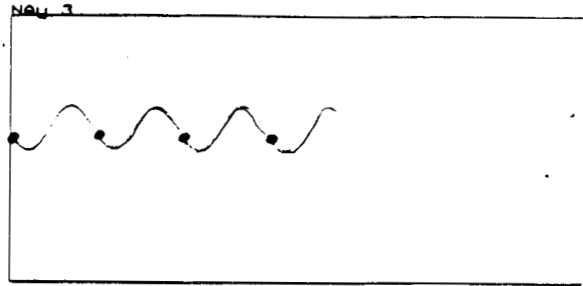
FIGURE 15.68 CALCULATED STEADY-STATE RESPONSE AT LOCATION B3 USING NONLINEAR PORTION OF COMPUTER SIMULATION PROGRAM FOR 4000 RPM, 0.00016 IN-LB UNBALANCE IN A2, AND 10.0 LB RADIAL PRELOAD AT A3.

Point ID: NAY 3 0 deg  
 Point ID: NAX 3 270 deg  
 Plot:



88 mils / div CCW Rotation 4000 rpm

Variable:



0.88 ms/div

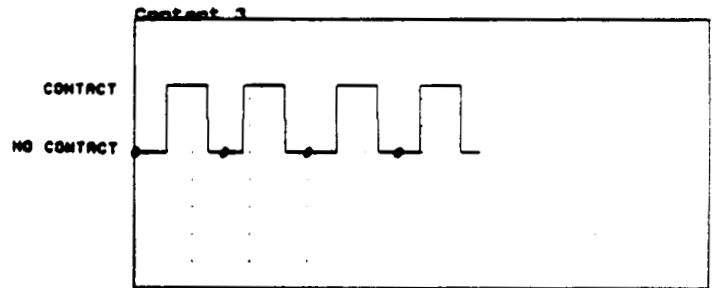
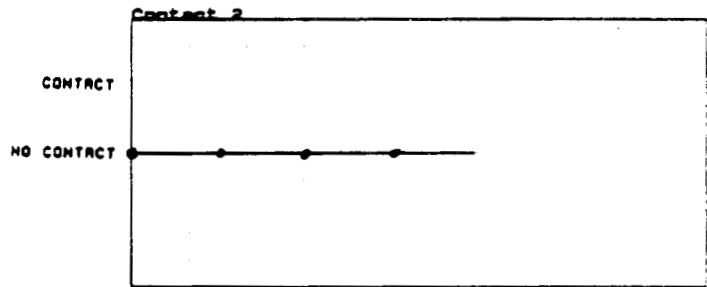


FIGURE 15.69 CALCULATED STEADY-STATE RESPONSE AT LOCATION A3 USING NONLINEAR PORTION OF COMPUTER SIMULATION PROGRAM FOR 4000 RPM, 0.00016 IN-LB UNBALANCE IN A2, AND 10.0 LB RADIAL PRELOAD AT A3.

Point ID: Nby 4 8 deg  
Point ID: Nbx 4 278 deg  
Plot:

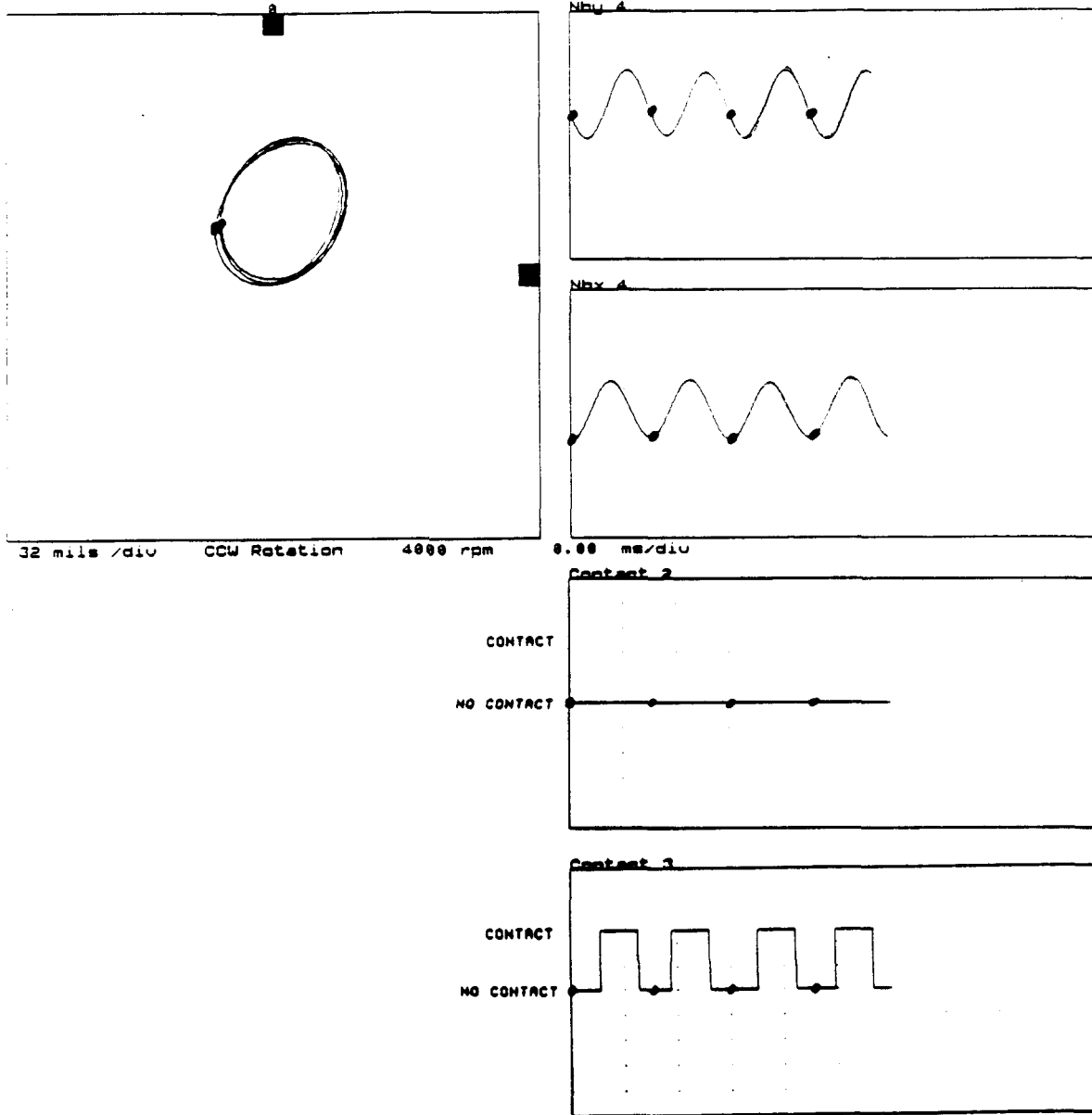


FIGURE 15.70 CALCULATED STEADY-STATE RESPONSE AT LOCATION B4 USING NONLINEAR PORTION OF COMPUTER SIMULATION PROGRAM FOR 4000 RPM, 0.00016 IN-LB UNBALANCE IN A2, AND 10.0 LB RADIAL PRELOAD AT A3.

## 16. CONCLUSIONS

### 16.1 General Remarks

Rotor-to-stator rub-affected vibrational phenomena experienced by rotors can be considered in the framework of the chaos theory: in a seeming randomness due to a multitude of factors and parameters affecting rotor responses, which in turn exhibit a rich manifold of occurrences, there exist some regularities and well pronounced, dominant patterns. These patterns represent strong attractors to make the rub-affected rotor dynamics better ordered in its apparent randomness. The attractors defined by the chaos theory are represented here by steady-state regimes of rotor vibrational responses. Steady-state processes can be maintained during a prolonged time, provided that all conditions remain unchanged. From the point of view of correct operation of the rotating machine a practical question arises on how much damage these steady-state rotor vibrations bring to the machine. For rub-related attractors the answer is always the same: an extreme damage, with the possibility of ultimate failure included.

The definition of steady-state processes, as existing during a prolonged time should be modified in the case of rubbing: the conditions which determine the steady-state rotor vibrations are usually changing relatively fast. Among these changing conditions the surface wear is the most significant. It can lead to two extreme situations: either clearances become opened, thus the rotor loses contact with the stationary part, and without further damage comes back to the normal operation (no-rub attractor), or the damage increases, leading possibly to the ultimate failure of the machine.

The characterization of rotor-to-stator rub phenomena in rotating machines exposed a rich array of parameters which have influence on the rotating system vibrational responses. Some of these parameters can be rationally controlled in order to prevent the rotor from rubbing and, if rubbing occurs, to limit its damaging effects.

Rub is always a secondary phenomenon, preceded by rotor motion exceeding the allowable clearance within the stationary element. The tendency to reduce clearances in order to increase fluid-handling machine efficiency contribute considerably to more often occurrences of rotor rubbing. The first preventive measure is therefore maintaining rotor eccentricities and vibration level low, compromising with the clearance requirements. The recommendation regarding low vibration level refers to prevention or elimination of all possible malfunctions resulting in rotor vibrations. Among the most common malfunctions there are unbalance, inappropriate choice of the rotative operating speed versus natural frequency spectrum: too close to any of the systems natural frequencies, their fractions (especially  $1/2\times$ ), or their multiples (especially  $2\times$ ), internal/structural friction, such as results from stacked-type rotors, and finally fluid flow-related instabilities of rotors. The latter can be prevented by controlling circumferential flow around the rotating shaft, by applying for instance anti-swirl devices.

The other contributor to rotor rub is the operation of the rotor at high eccentricities. The rotor displacement from concentric to an eccentric position is a result of some radial preload forces, such as generated by fluid flow, or rotor misalignment. The amount of rotor preload should be compromised with the rotor eccentricity-related control of fluid circumferential flows, the most often used measure to prevent rotor instabilities in fluid-lubricated bearings. There is a very narrow dividing line between a "friendly" preload, controlling fluid-induced instabilities of rotors and an entirely "unfriendly" preload, possibly leading to rubs. A compromise can be achieved here by controlling fluid flow using other means than radially preloading the rotors (mainly using anti-swirl arrangements and externally pressurized, ("hydrostatic") bearings). This will allow the

application of the second preventive measure, namely a reduction of rotor radial preloads below the margin of potential rubs.

There exist two main steady-state attractors in rotor rub-affected vibrational response patterns: a partial rub and a full annular rub ("dry whip"). The first, less damaging pattern is characterized by occasional rotor/stator contact during the rotor precessional motion. The contact may occur once, or several times (and not necessarily at the same angular location of the stator) per precessional period. The ratio of the "contact time" to the "no-contact time" per precessional period rarely exceeds a half. The partial rub most often occurs when the rotor is preloaded and rotates at higher eccentricity. With reduced eccentricity and increasing vibration amplitude the partial rub inside a circular seal gradually evolves from single location rub to multiple location, exhibiting star-like orbits.

The second main steady-state attractor is rotor full annular rub. Characterized by lateral symmetry, it usually occurs when rotor eccentricity is low, but vibration amplitudes high. The threshold of stability for full annular rub occurs at high rotative speed. The multi-partial rub can be instantaneously replaced by the full annular rub due to any random impulse (e.g., sudden change of speed or load). The full annular rub is much more damaging to both stator and rotor, as their contact, accompanied by significant normal and tangential forces, is maintained the whole 360 degrees of the precessional period. In barely a few rotations, the damage to the machine may become ultimate. Preventive measures against full annular rub should be taken into consideration, because full annular rub is the most destructive to the machine integrity. Again, one of these preventive measures is the "friendly" radial preload, and carefully controlled rotor vibration level.

The steady-state partial rub vibrations exhibit a manifold of occurrences. There exists, however, a very well determined rule regarding frequency of these vibrations. At rotative speeds lower than twice first balance resonance (first natural frequency of the shaft bending mode) the rotor rubbing against the stationary part modifies vibrational amplitudes, but does not change the lowest frequency of vibration: If the original (no-rub) response was synchronous ( $1\times$ ) vibration due to unbalance, the rubbing rotor response remains mainly synchronous ( $1\times$ ) (accompanied however by higher frequency components). When the rubbing is light, at twice or above the twice first balance resonance speed the situation changes: A new subsynchronous component appears in the rotor vibrational spectrum. This component has a distinct subsynchronous half rotative frequency ( $1/2\times$ ). The rotor rubs against the stator once per two rotations. If however the rubbing is more severe (when a radial preload force results in rotor eccentricity, and the rotor/stator normal force becomes higher) then again, only  $1\times$  is the fundamental frequency component. The threshold between these two patterns for a constant rotative speed is however difficult to quantify, as it depends on several geometric and physical factors of the system.

The clean frequency-related pattern of rub continues also for higher rotative speeds: For example, when the rub is light, and rotative speed exceeds three times first balance resonance value the  $1/3\times$  subsynchronous component may appear in the rotor response spectrum. A larger radial preload resulting in rotor higher eccentricity, and more severe rubbing causes the  $1/3\times$  component to be replaced by  $1/2\times$ , and eventually, with increasing eccentricity, by  $1\times$  as the lowest frequency component. The partial rub is, therefore, characterized by frequencies proportional to the rotative speed. The partial rub is repeatable phenomenon, but it can also be accompanied by some chaotic action of transient processes.

The full annular rub vibration also has a clean frequency pattern: its frequency is equal to the natural frequency of the significantly more rigid coupled rotor/seal system, and is

entirely independent from the actual rotative speed. The full annular rub is very stable, and persists even if the rotative speed is reduced below first balance resonance.

When the conditions leading to steady-state regimes change, the system responds with a transient process, usually leading to another steady-state regime. This transient process has also a distinct frequency characterization: the rotor responds with its natural frequency free vibrations.

Amplitudes of either rotor steady-state or transient regimes are much more difficult to predict, as nonlinear factors of the system are usually involved. The latter are not easy to quantify.

Rubbing arc, i.e., the time of rotor/stator contact, as a possible measure of the severity of rub was investigated. A parameter to vary was again the rotative speed. It was shown that the time of this contact depends significantly on the rotor original vibrational amplitude versus the available clearance. Particular patterns of these rotor orbital responses after the contact was broken were however somewhat chaotic.

It should be well understood that rotor-to-stator rubbing is not an isolated phenomenon. It is a dynamic process determined by the entire system dynamic characteristics. In order to properly interpret the rotor rub-affected motion it is necessary to identify first these characteristics. The system dynamic characteristic identification methodology developed and used during this study is described in this report.

Ideally, system analysis provides insight leading to an improved design yielding better, more reliable performance of machines. Application of the knowledge acquired from analysis should, if possible, be implemented at the most elementary design stage.

System response may be considered as the fingerprint of a particular machine, representative of the fundamental operational dynamic properties for these type of machines. The most important basic dynamic properties are characterized by modal behavior of the system. The latter can be investigated by the modal identification testing and dynamic stiffness approach used in this project. The practical two-mode identification procedure for the rotor/bearing system was developed and eventually applied for identification of more mode characteristics. The latter include system modal masses, stiffnesses and dampings related to specific modes. The identification is based on presumed linear system behavior. It gives, however, some insight into nonlinearity-related changes in the characteristics. The model complexity can increase rapidly, however, when considering nonlinearities, such as fluid-related effects, and of particular interest in this study, friction forces, impacting, and irregular or periodic modifications to system stiffness. The latter effects caused by rotor-to-stator rub are highly nonlinear, with lateral nonsymmetry, greatly modifying the vibrational responses of the machine.

Modelling the interface of rubbing surfaces proves to be quite challenging. In order to provide adequate results the rub model should comprise local micro elastic and plastic effects, wear and heat transfer, as well as global effects, i.e., the rotor system dynamics in the macro scale.

The model developed during this study was not that highly ambitious. The micro-local part was omitted, and only averaged macro effects were taken into consideration. The developed computer code, enabling to calculate rotor response for an array of input parameters, brought some promising results which could be adequately compared with obtained experimental results. A limited time and resources for this project prevented,

however, obtaining wider matrix of computer parametric studies. The proposed code might eventually be adapted to a main frame computer programs for rotor dynamics.

Experimentally tested rotor responses compared with computer calculated results suggest that a simple "dead band" (noncontinuous stiffness of the system) model is not adequate to describe the rub phenomena. Both friction and impacting play significant roles in the rub occurrences, thus they cannot be neglected in the model.

Being an undesired malfunction of the machine, rub is relatively easy to detect and diagnose as it causes specific modifications of the rotor system vibrational patterns. The rubbing, however, is always not a primary, but secondary malfunction. By monitoring the growth trend of both rotor eccentricity and vibration magnitude which both result from a primary malfunction, the rub inception can be predicted. Once rub occurs it modifies the previous rotor response vibrational pattern. The most pronounced effect consists of an increase of response components in the frequency spectrum: from subharmonic to superharmonic components. The previously existing components undergo amplitude and phase changes. By using appropriate vibration monitoring systems these effects are easily detected.

At this point it is necessary to mention what is considered an "appropriate" vibration monitoring system. The heart of the system consists of adequately selected and installed transducers. For diagnosing rotating machine malfunctions the best are noncontacting shaft-observing displacement probes. The advantage from the use of such probes has two aspects: (i) rotor is the main source of the machine vibration, thus observation is direct, and not affected by transmissibility of the supporting structure, and (ii) displacement transducer highest sensitivity falls in the low frequency vibration range, including zero-frequency, static displacements of the rotor. It should be well understood that the low frequency subsynchronous vibrations of rotors are the most important indicators of machine malfunctions, thus from the diagnostic point of view bring direct information. The subsynchronous vibrations usually acquire high amplitudes, thus are most dangerous for the machine integrity. The higher frequency components result most often from the secondary effects, and appear as harmonics of the low-frequency components.

Accelerometers mounted on the machine casing, as sensitive to higher frequency vibrations easily detect these high frequency components. The accelerometer readings are, however, affected by casing transmissibility, and for rigid, thick, and vibration wave absorbing/dispersing supporting structures the accelerometers would not be able to detect a major malfunction. In the instance of softer casings, when accelerometers are the only used transducers, the relative strength of higher frequency harmonics can give a meaningful diagnostic signal about rub malfunction. Quantification of the rub "severity" might be however difficult, when only accelerometers are in use.

Another important part of the rotating machine monitoring system should be mentioned. One of the shaft-observing displacement transducers should play a role of the KEYPHASOR, the once-per-turn marker. The information provided by such transducer enables one to relate rotor vibrations to its rotational motion, which, as a matter of fact, is the most important source of all dynamic processes in the system. Relation to the rotative motion bring therefore the relation to the main source, thus providing a most significant diagnostic tool.

The monitoring system for a rotating fluid-handling machine should also contain fluid flow and pressure transducers, which would provide a meaningful information regarding rotor load. Combined with vibration information constitutes a powerful diagnostic base.

Advancements in the modern electronic technology result in efficient data acquisition and processing systems which quantify and display the required cross-correlated information in meaningful formats.

## 16.2 Conclusions Related to HPFTP

Based on the diversity of information obtained through the research on rotor-to-stator rubbing it seems imperative the rub be studied for a particular application. Otherwise, the investigator can get lost in a sea of confusion due to the many varieties of rub and the multiplicity of factors contributing to the phenomena associated with the rub dynamic process. By studying a specific application, both the varieties of rub and their contributing factors may be reduced to a tolerable level. This study centered on the effects of rub on the vibrational response of the rotor and stator of a rotating machine caused by partial rubs generated due to a limited level of unbalance-related synchronous vibration and a static displacement of the rotor due to a radial preload force. Both dry and lubricated contact surfaces were used in the tests. From a macroscopic view of the rub process, both types of rub could be reduced to a set of parameters that describe the additional forces on the rotor and stator caused by the rub. The experiments with dry contact surfaces allowed the acquisition of actual rotor-to-stator contact initiation times and contact durations, monitored by electrical contact devices. The rotating systems analyzed and used for experimental tests were limited to not more than three vibrational modes and the operating rotative speeds kept below the third balance resonance. Some preliminary testing was performed to determine the change in rotor vibrational response due to rub caused by excessive synchronous vibrations and limited radial displacement (eccentricity) of the rotor. The testing indicated that rub causes significant alterations in the vibrational response of rotating systems. A correctly functioning rotating system, without malfunctions, produces a small synchronous vibration response due to residual unbalances plus a small static centerline deflection due to constant radial preloads such as gravity, process flows, or other external forces. Often, especially for pumps, the forces from process flows can be significantly larger than the force generated by gravity and the rotor mass. As was mentioned earlier, rub was induced and its severity controlled by using a radial static preload force which results in a static radial displacement (eccentricity) of the rotor. Under these conditions, and when the rotative operating speed exceeds twice first balance resonance frequency which is true for the HPFTP, as well as the HPFTP simulation rig cases, light rubbing produces predominantly subsynchronous vibration with a half of the operating speed frequency (i.e.,  $1/2\times$ ).

The  $1/2\times$  frequency component in the vibration response usually exhibits a very flat reverse orbit which produces the "figure eight" shaped orbits when mixed with the  $1\times$  component normally associated with rotor unbalance response. As the rub increases in severity, the subsynchronous components tend to decrease in amplitude until they virtually disappear. They are then replaced by  $1\times$  vibrational components along with increasing amplitudes of super synchronous harmonics ( $2\times$ ,  $3\times$ ,  $4\times$ , etc.), and components with natural frequencies of the system. This results in flattened, elliptically shaped orbits that seem to bounce around a center location. Rub at one discrete axial location along the rotor produces changes in the vibrational response of the rotor at all axial locations. The changes are more severe at the axial position of the rub occurrence and tend to decrease, or soften, as the distance from the rub location increases.

The stiffness of the stationary element against which the rotor rubs, has a large effect on the rotor response during rub. The vibrational response modifications due to rub described in the previous paragraph would occur in a system in which the stator stiffness was relatively high. Most rotating systems would probably fall within this category. As the

stator stiffness is decreased the rotor response would be affected less and less. The entire energy would be then transferred to the stator.

The rotor vibrational response modification discussed earlier were for preload-induced rubs. The situation gradually changes when the preload and resulting rotor eccentricity are reduced and rotor unbalance increased. Preliminary tests indicate that for light rub conditions the fractional subharmonics generated for preload induced rubs are not present when rubbing is generated by excessive synchronous vibrations. Instead, the response frequency content is synchronous, with components at system natural frequencies also appearing in the spectrum. This produces a star-shaped orbit, instead of the "figure eight". The star shape indicates largely reverse orbiting. These types of rubs tend to progress into a full annular rub for increasing rub severity. The comments pertaining to axial propagation of the vibration modification, and the role of stator stiffness in these modifications discussed above are also valid for this class of rubs.

Surface conditions of the rubbing elements have an influence on the vibration response modification. They do not change the qualitative description given above, but have a drastic effect in determining the transition point from light to heavy rubs. However, due to the destructive nature of the rub, surface preparations to minimize the effects of friction would probably be ineffective. The damage to the contacting surfaces continually changes the surface conditions of the rotor and stator at the rub location. Rotors and stators with several initial surface finishes of the contact areas were tested under rubbing conditions. Over the duration of the tests the differences in the surface initial characteristics had little or no effect on the vibration response modifications described earlier. However, material removal from one surface which is deposited on the other can have drastic effects on the vibration response. For example, the build up of aluminum on the steel rotor during contact with an aluminum stator assembly changes the coefficient of friction between the two contacting surfaces from 0.47 for aluminum on steel to approximately 1.5 for aluminum on aluminum. This drastic increase in the coefficient of friction between the contacting surfaces produced extremely violent rubs during the tests on the HPFTP simulation rig until the steel shaft was cleaned, thereby reducing the coefficient of friction to its original value. The changes in the surface characteristics of the rubbing surfaces and the material removal/deposition encountered in the rubbing process are virtually impossible to predict or control under operating conditions.

In order to study the rub phenomena from a parametric viewpoint, a mathematical model of the target system was generated. This model includes all the parameters that influence the linear system response as well as those governing the motion at the contact. Due to the high nonlinearities and impact-related accelerations encountered during the sudden rotor/stator contact, the appropriate numerical algorithm used in the calculations had to be selected for the stability of its solution. The RUNGE-KUTTA algorithm chosen for the computer simulation program developed during this study is very stable and produces accurate results as long as the integration variable step size multiplied by the acceleration term is kept small. To maintain reasonable size data buffers, some form of variable integration step size was mandatory. In other words, if an integration variable step size is selected for the impact conditions, the personal size computer memory would be filled before enough revolutions of the shaft had been computed to allow the initial transient responses to decay enough to reach the steady-state response for the system. The simulation program developed can be used to identify the effects on the rotor vibrational response due to parameters that are difficult to control during experimental tests, such as stator stiffnesses, coefficients of friction, and impact restitution coefficients.

The hypothetical sequence of conditions leading to the possibility of rub in the HPFTP focuses on the increasing preload on the rotor generated by the hydrogen exiting the final

pump stage. This sequence of events would result in a static radial displacement of the rotor. Based on the discussion of the rub variety presented earlier, the following vibration response changes should occur. Since the operating speed of the HPFTP falls between two and three times the system first natural frequency, when the flow increases enough to provide a preload adequate to initiate light rub conditions the vibration response should shift from predominantly  $1\times$  frequency components to  $0.5\times$  components. The pump would probably not survive the transition to the heavy rub condition; therefore, the change from  $0.5\times$  frequency components back to  $1\times$  and higher harmonics for the heavy rub might never be seen.

It is obvious that in the dynamics of the HPFTP the flow plays the major role. The flow provides the major radial preload force, and the flow irregularities act as instantaneous impulse forces applied to the rotor. Finally the flow circumferential shaft rotation-generated component is responsible for possible whirl/whip instabilities of the rotor. Rub occurs as a secondary effect of rotor high eccentricity resulting from the load, or high amplitude transient motion due to flow impulse forces, or finally due to whirl/whip vibrations. The control of the flow would provide better performance of the HPFTP, and prevent rotor rubbing.

The appearance of the close-to-a-half rotative speed subsynchronous frequency component in the HPFTP hot fire test results proves that there is a problem. The HPFTP operational speed falls between second and third natural frequencies of the rotor lateral modes. The rotative speed to first natural frequency ratio is 2.26. When the rotor rubs the system stiffness increases and natural frequencies increase. This causes the operating speed to first natural frequency ratio to decrease, and become closer to 2, however in a dynamic transient manner, following the irregularity of rub occurrences. This explains differences in frequencies of the subsynchronous components of vibration. The latter most probably should be correlated to the first natural frequency of the system. The flow irregularities certainly contribute to impulse excitation of this transient component.

A redesigned version of the HPFTP should take into consideration specific ratios of operational speed versus natural frequencies in order to avoid magnification of the subsynchronous vibration by combining two effects: the half-frequency partial rub and impulse-related transients.

The method of rub detection within the HPFTP explored in this study is based on the modification of the rotor vibrational response due to the rub and how this response might couple through to the casing. In order to obtain and evaluate the rotor response some form of displacement transducers measuring direct rotor motion need to be installed in the HPFTP. The frequencies of interest generated by the rub phenomena, at least at the inception of rub when it should be detected, are predominantly subsynchronous. This would suggest that at least for hot fire testing, the eddy current displacement transducers observing shaft motion should be used, since they provide high sensitivity at low frequencies, including zero frequency rotor static displacement. Test results indicate that for low casing stiffnesses a sufficient motion due to rub is transmitted through the casing. Under these conditions, casing mounted transducers (such as accelerometers or velocity pickups) might be used to detect the inception of rub. However, as the casing stiffness is increased, less and less rub-related motion would be transmitted through the casing to the transducers, eliminating the effectiveness of the casing-mounted transducers to detect rubs. In addition, these types of transducers have limited sensitivity to detect low frequency vibration components. The proximity transducers properly located along the rotor, and enhanced by once-per-turn, KEYPHASOR-type marker would provide additional information valuable for determining operating conditions, such as rotor

centerline movement, vibration amplitudes and rotor mode shapes, resonant frequencies of the system, fluid-induced whirl/whip instabilities, etc.

## APPENDIX 1

### DATA REDUCTION OF THE HPFTP HOT FIRE TAPES

#### A.1.1 Introduction

The data from the HPFTP hot fire test provided by NASA was reduced to determine the factors contributing to the HPFTP rotor dynamic behavior. Of special interest was a small subsynchronous vibration occurring at approximately one-half running speed frequency.

#### A.1.2 Data Reduction

Transducer locations at the HPFTP are as shown in Figure A.1 supplied by NASA along with the data tapes. The first run selected for data reduction was number 750-268 (NASA notation). Figure A.2 presents the relationship between HPFTP rotative speed and time, the data supplied by NASA. Since the recorded data did not contain the Keyphasor channel (once-per-turn marker), the first step in the data reduction process was to locate a signal suitable for use as a Keyphasor. The signals from the radial probes indicated the existence of a glitch (discontinuity in vibration amplitude), caused probably by a notch or irregularity on the impeller surface being observed by the noncontacting proximity probe. It would serve as a Keyphasor signal. The probe at the 8 o'clock radial position was selected as the Keyphasor. For rotor dynamic behavior, probes mounted 180 degrees apart produce redundant information; therefore, only the data from two of the four radial probes was reduced. The data from the probes at 8 and 11 o'clock were selected for processing. The first reduction pass consisted of recording the variation of the rotative speed (Figure A.3) and  $1\times$  filtered vibration component (Figures A.4 and A.5) as functions of time for the test duration. The speed profile obtained from the tape matches the one supplied by NASA (Figure A.2) almost perfectly. The  $1\times$  filtered amplitude is very small and is inversely proportional to rotative speed changes. It also shows some transient behavior at approximately 3 minutes into the test. The data from the pressure transducers (Figure A.6) shows at the same time a sudden pressure drop at the 8 o'clock location. This would indicate that the transient process in the vibration data was a transient reaction to this pressure drop.

The next step in the data reduction process was to obtain orbit, timebase, and spectral information on vibration of the HPFTP rotor at the radial probe locations for different operating time points during the test. This data is presented in Figures A.7 to A.22. The shaft orbits are basically circular with two excursions caused by the signal spike (glitch) being used as the Keyphasor signal. There is only one Keyphasor mark on the orbit, indicating the motion is predominantly synchronous with the rotative frequency ( $1\times$ ). This synchronous motion is probably caused by the residual unbalance in the rotor being restrained by supports with laterally symmetrical stiffnesses. The spectral information confirms that the majority of the motion is  $1\times$  with small amounts of higher harmonics  $2\times$ ,  $3\times$ , and subsynchronous component with frequency close to 19,000 rpm. The  $2\times$  and  $3\times$  components can be caused by nonlinearities in the system, including the impeller surface notch-correlated signal spike. The latter can be well seen in the time-base waveforms and orbits presented in Figures A.7, A.9, A.11, A.13, A.15, A.17, A.19, and A.21. The signal spike resulting in a high irregularity of the sine waveform is most likely the highest contributor to the occurrence of higher harmonics in the rotor response spectrum. The small subsynchronous signal at slightly less than 19,000 rpm is probably caused by background noise forces exciting the first balance resonance vibration (with natural frequency of the first lateral mode of the system). The probability of two other major causes of subsynchronous vibrations, namely rub and fluid-induced whirl/whip, is reduced for the

following reasons. The rub should rather produce an exact  $0.5\times$  subsynchronous component as it is strongly rotative speed dependent. The observed subsynchronous component seems to be independent of rotative speed. The flow-related whirl/whip is harder to discount. The whirl is easily rejected as it again would be a function of rotative speed; however, the whip would appear to be independent of rotative speed and excite the first balance resonance of the system. One of the two reasons that background noise forces were selected as the probably cause over whip is that whip most often produces large response amplitudes, usually larger than the  $1\times$  vibration amplitude. The other reason background noise was selected is based on the relative amplitude of the subsynchronous displacement peak to the adjacent frequency signal levels. The peak is only 2 to 3 times higher than the signal level around it, indicating selective amplification of a general broadband noise force. Other plot formats emphasizing the independence of the subsynchronous signal from rotative speed and its relationship to surrounding vibration levels are shown in Figures A.23 to A.27.

The last piece of information obtained is the spectral content from two of the axial probes. This data (Figures A.28 to A.31) show small  $1\times$  vibration amplitudes due to cross coupling between the lateral and axial vibrations.

### A.1.3 Conclusions and Recommendations

The major vibration response in the system is represented by a small  $1\times$  (synchronous) component which is mostly due to the residual unbalance in the system. There are some  $2\times$  and  $3\times$  components (higher harmonics) in the response, generated by system nonlinearities, including a signal spike from some surface irregularity on the impeller (it might be an initiation of a crack!). This effect was discussed in the previous section. The other signal of interest was the small subsynchronous vibration with the frequency approximately 19,000 rpm. This is probably the first balance resonance vibration (bending mode) being excited by broadband background noise due to uneven process fluid flow, background vibration coupled through the test stand support, etc. It was unfortunate that the operating speed for the HPFTP occurs at almost twice first balance resonance.

Another area of concern that needs to be addressed is the number and location of the transducers — the eddy current proximity probes, as well as the correctness of the vibration data acquisition system. The vibration data obtained from the current probe location allowed some conclusions to be drawn concerning the rotor behavior; however, much more could have been learned with better probe placement. For instance, if radial probes had been located at several axial locations along the rotor, accurate mode shapes for the rotor could have been determined. If the number of probes are limited by some structural or other considerations, they should be placed where major vibration problems are expected. Only two XY probes per axial section of the shaft are required (four of them give redundant information). Probes in the vicinity of the fuel exit could show rotor bow and misalignment caused by the process flow and also would be more sensitive to associated vibration data (due to rubs, etc.). In order to correlate the vibration signal frequencies to the rotative speed, one Keyphasor probe (producing one-per-turn signal) is required. The Keyphasor probe provides also important phase measurements. For future tests, we strongly urge considering selecting probe locations to maximize the useful vibration data. Along these same lines, it would also be beneficial if the start-up data before the test, and the coast-down data after the test, could also be recorded on tape.

The proximity probes provide extremely useful vibrational information for signals with low frequency, including static position of the shaft. The position of shaft centerline during dynamic motion represents extremely important information. From this information, flow

dynamic actions, as well as rotor-to-stator rubs, can be estimated. The lack of the shaft centerline position data from the HPFTP hot fire test leaves a broad margin for guessing, not substantiated by test recorded evidences.

HPFTP 2708 INSTRUMENTED PUMP

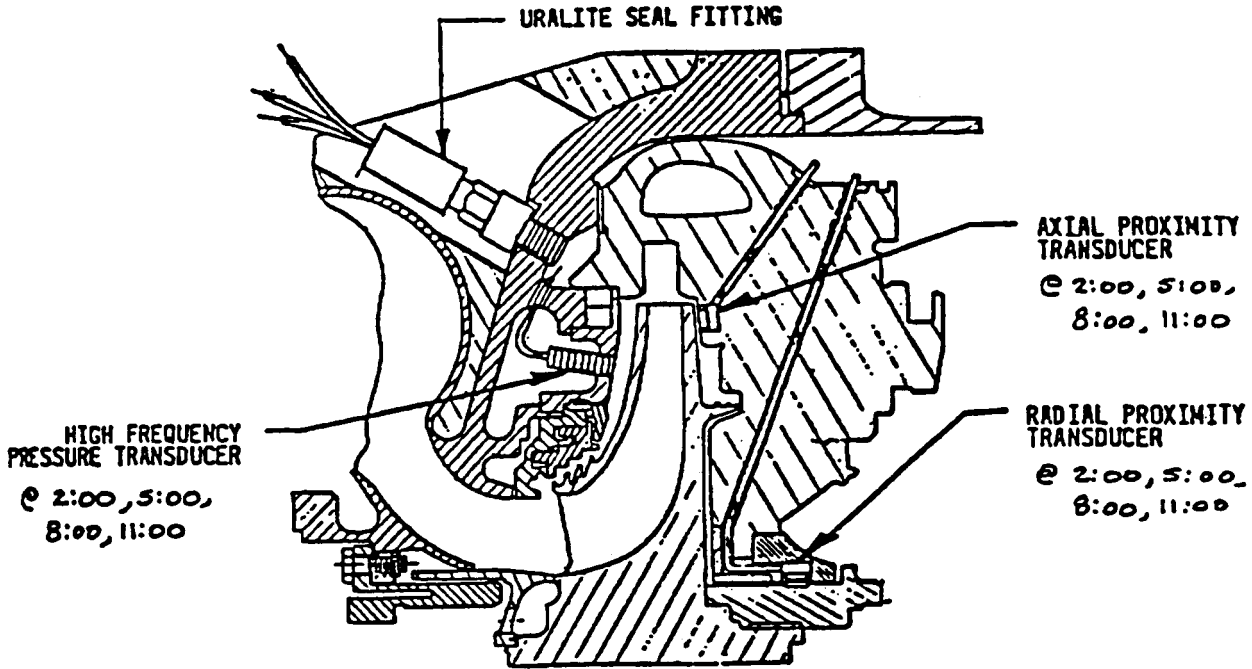


FIGURE A.1 PROBE LOCATIONS FOR HPFTP HOT FIRE TESTS.

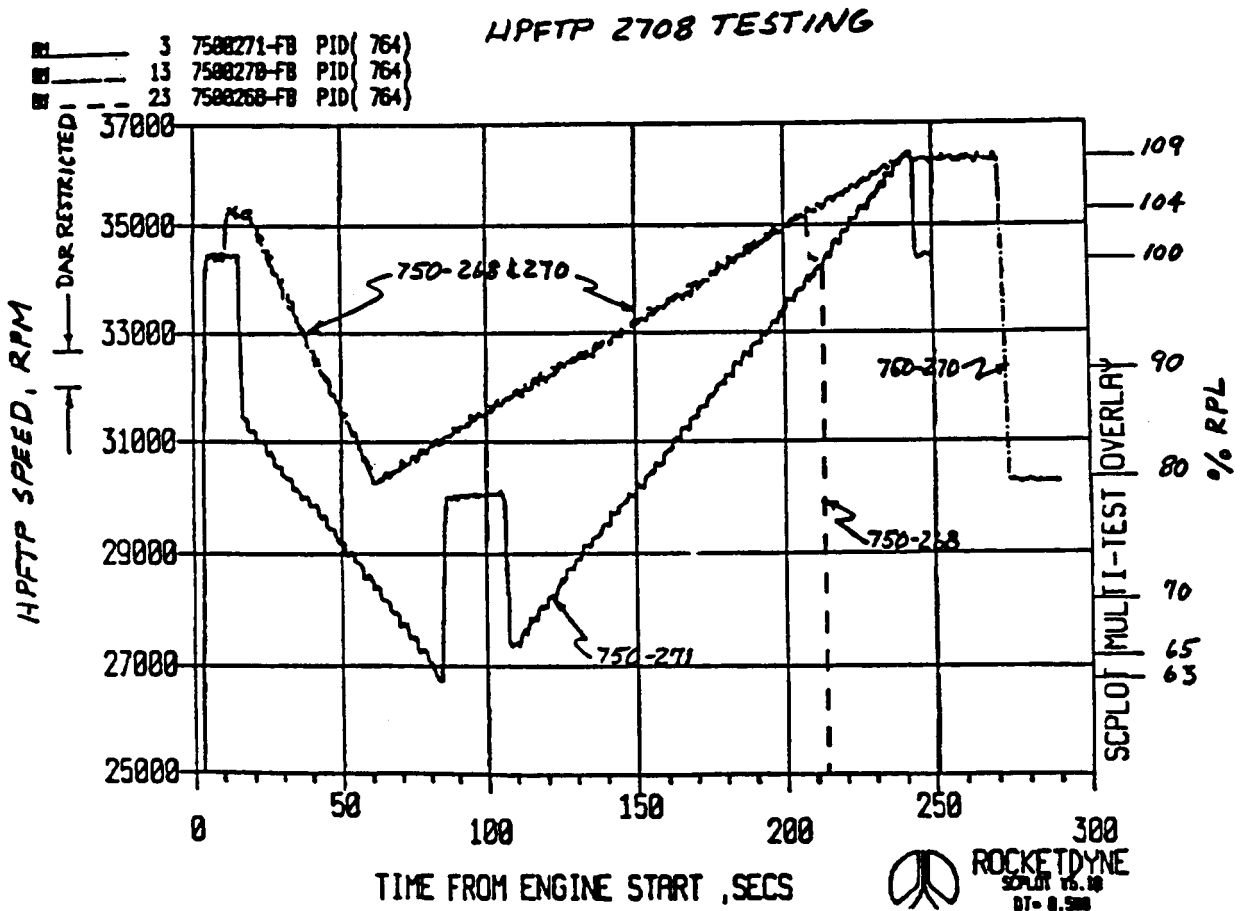


FIGURE A.2 ROTATIVE SPEED PROFILE SUPPLIED BY MSFC FOR HPFTP HOT FIRE TESTS.

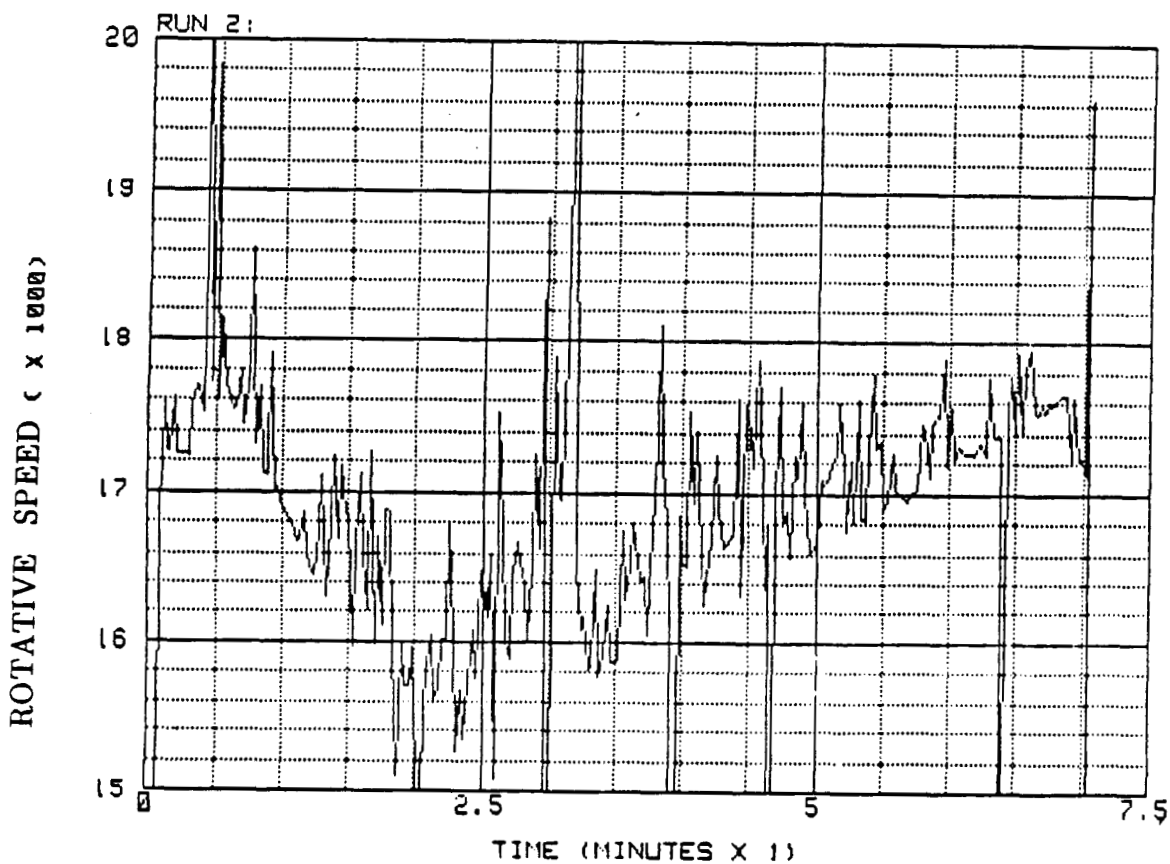
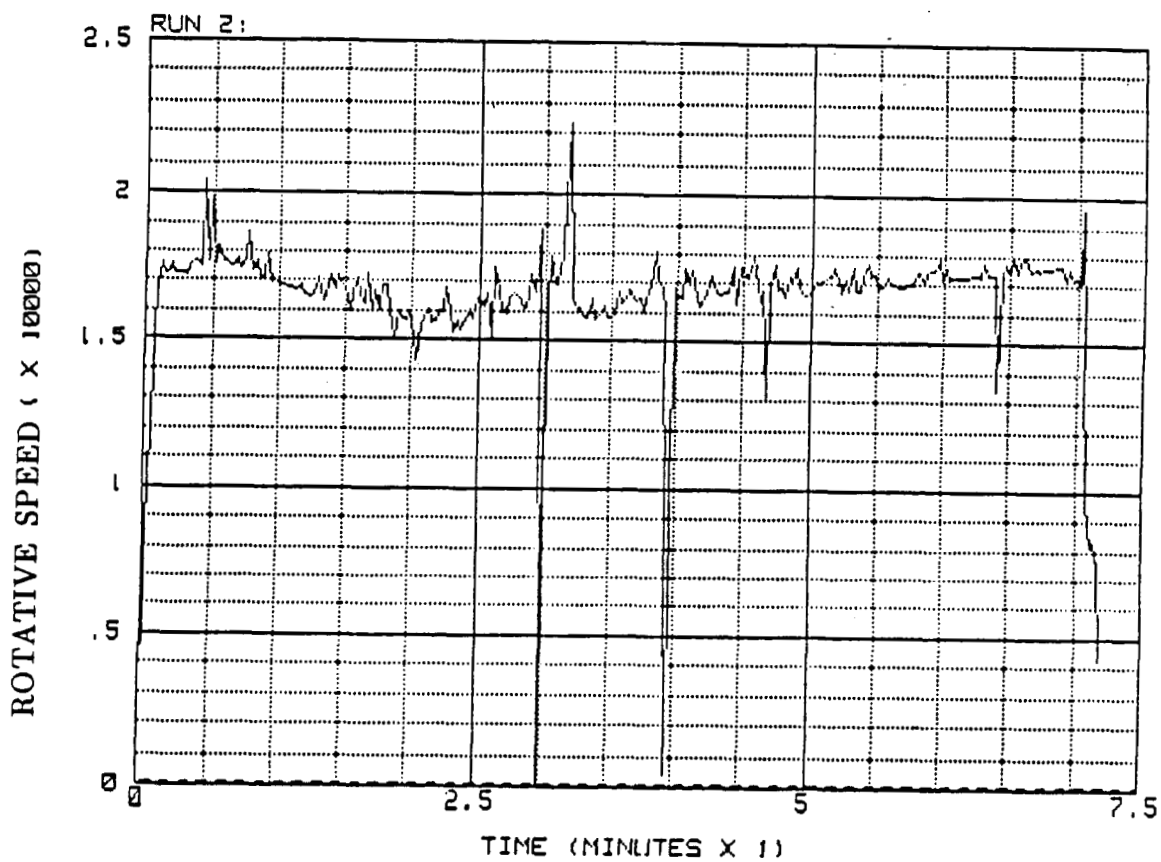


FIGURE A.3 ROTATIVE SPEED PROFILE FOR TEST 750-268 REDUCED FROM NASA SUPPLIED TAPES.

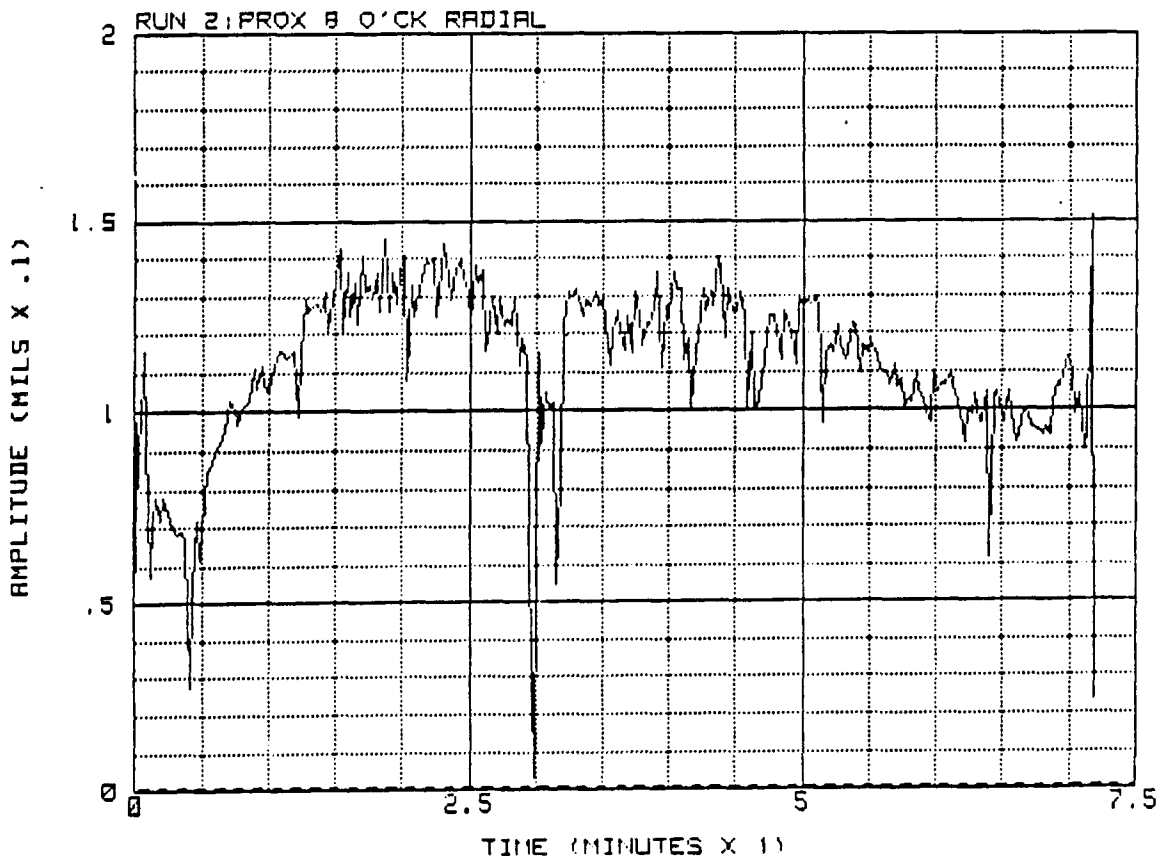
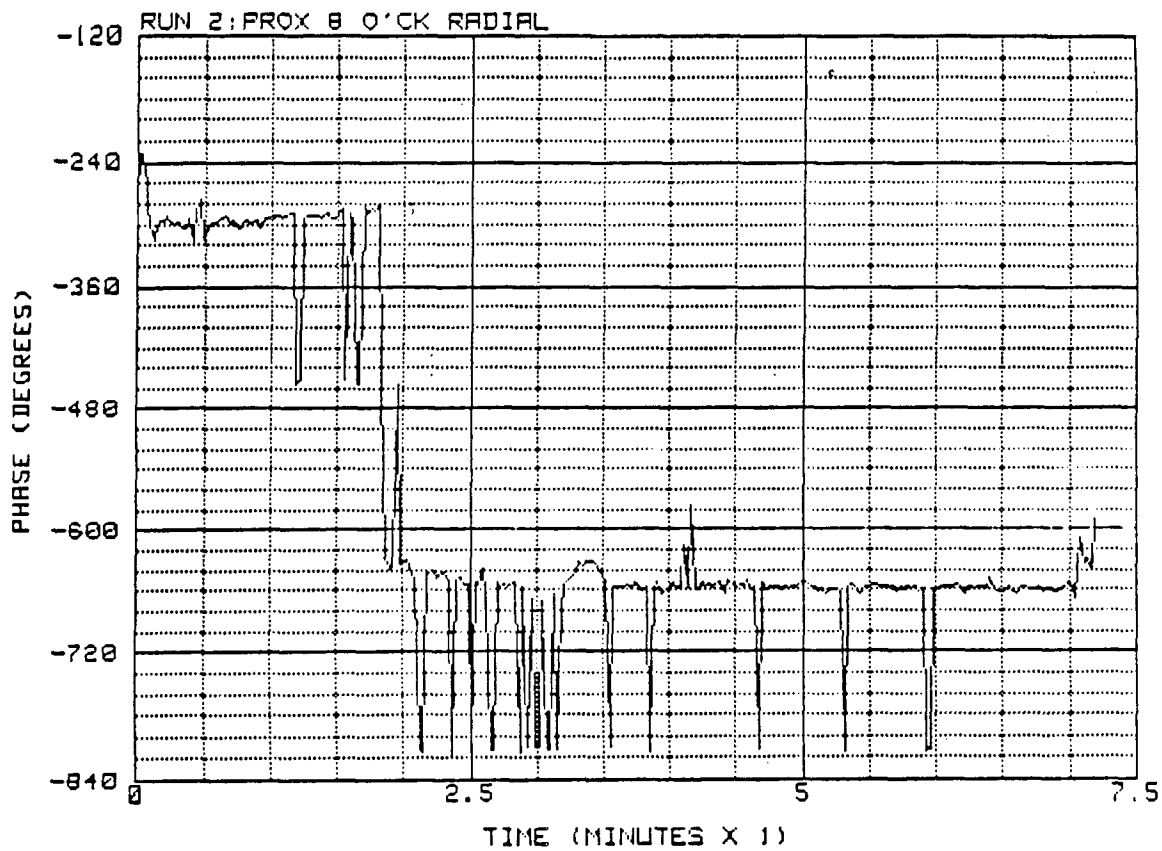


FIGURE A.4 1X FILTERED VIBRATION DATA FOR TEST 750-268, FROM 8 O'CLOCK LOCATION PROBE.

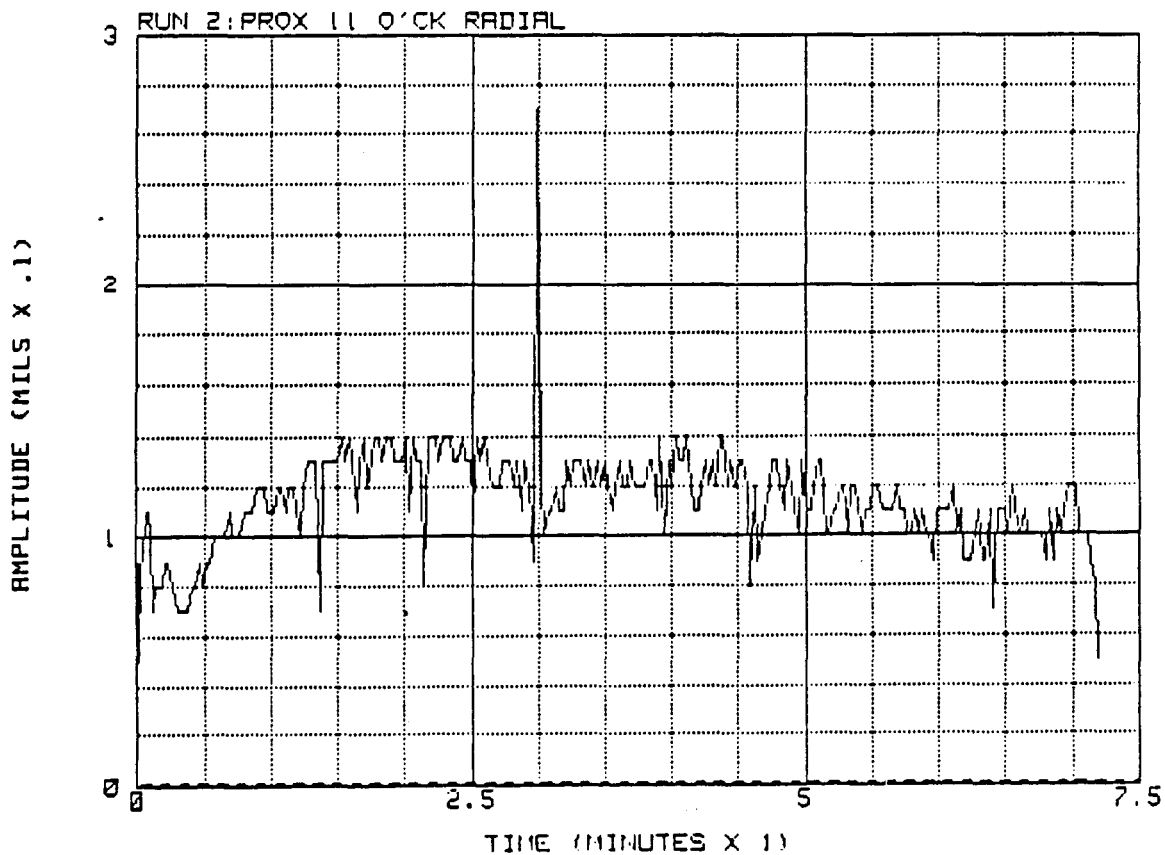
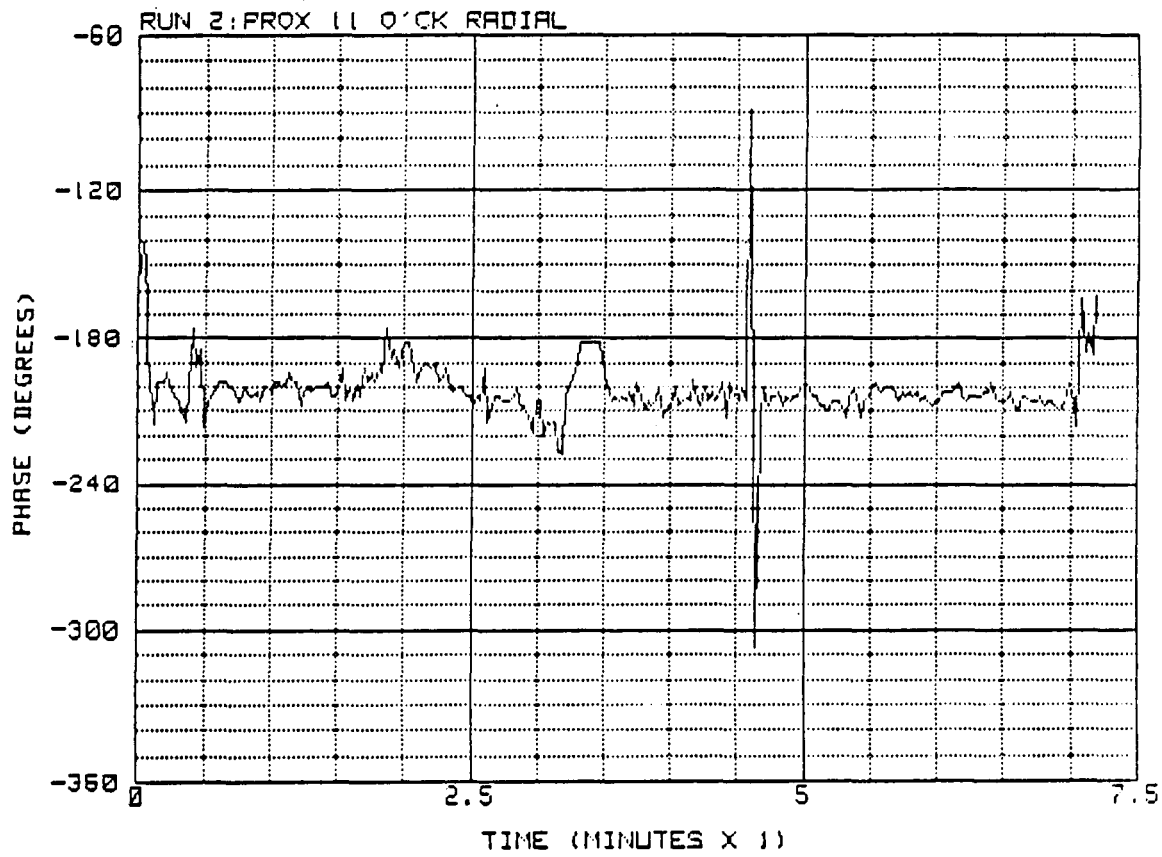


FIGURE A.5 1X FILTERED VIBRATION DATA FOR TEST 750-268, FROM 11 O'CLOCK LOCATION PROBE.

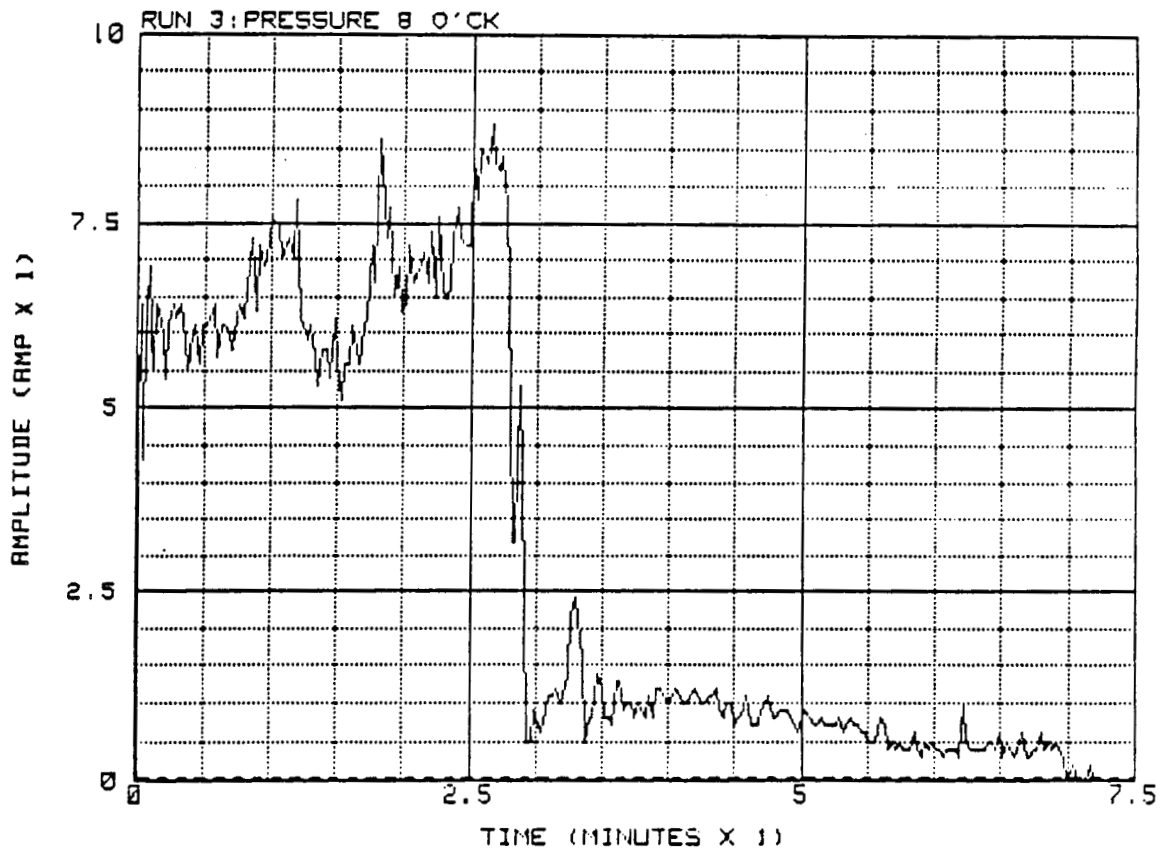


FIGURE A.6.A PRESSURE PROFILE FOR TEST 750-268, FROM 8 O'CLOCK LOCATION PROBE.

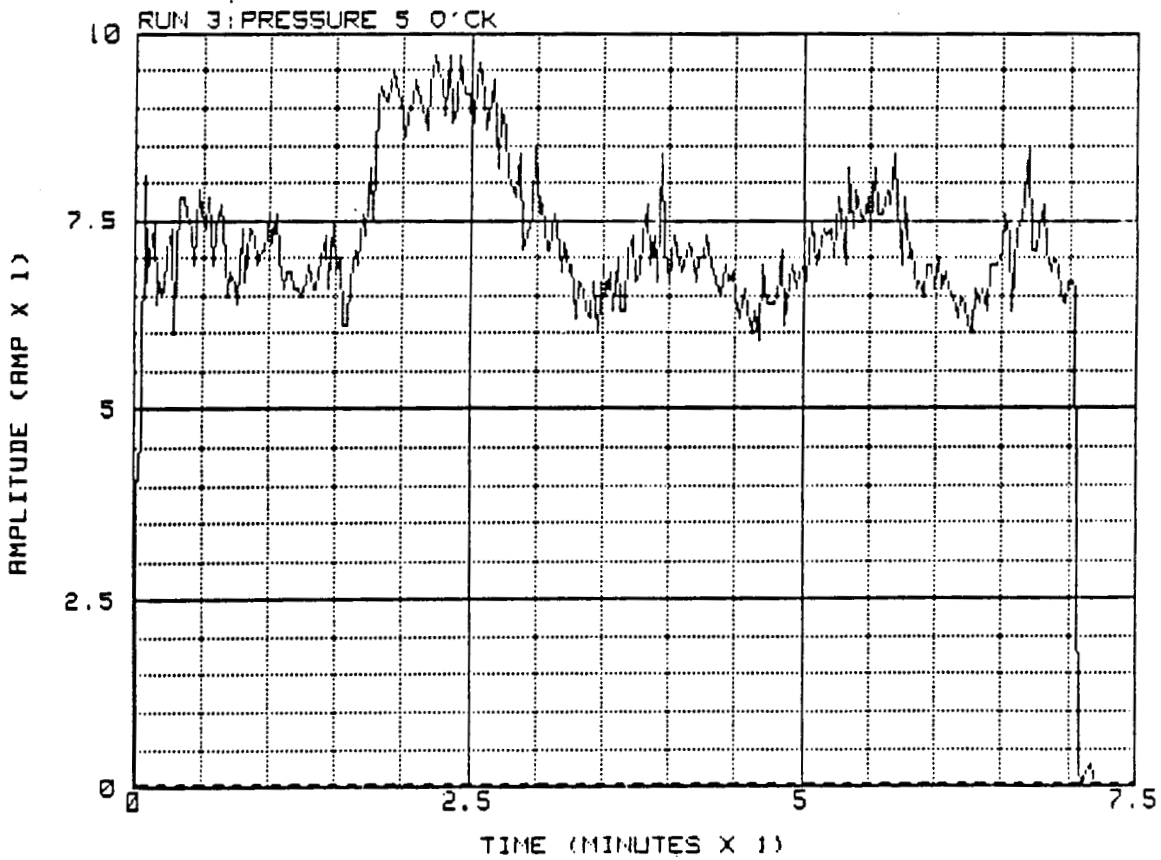


FIGURE A.6.B PRESSURE PROFILE FOR TEST 750-268, FROM 5 O'CLOCK LOCATION PROBE.

BENTLY  
NEVADA  
CORP.

PLANT ID: B.R.D.R.C.  
TRAIN ID: NASA TEST 750-268  
MACHINE ID: ENGINE 2012

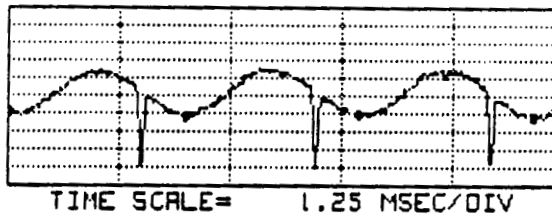
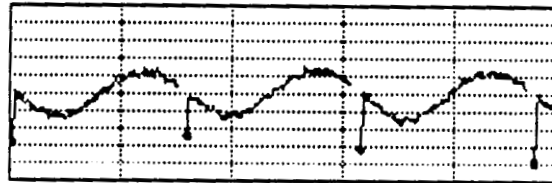
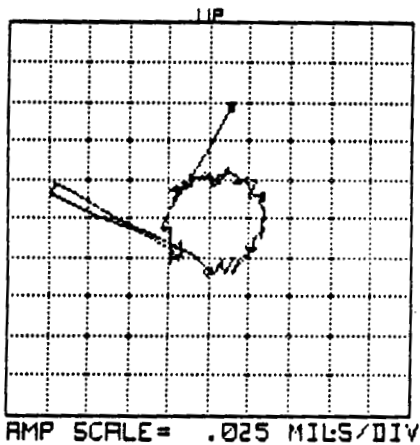
PLOT NO:

RUN: 1      DATE:      TIME: 08:25:51

PROBE #1 ID: PROX 8 O'CK RADIAL      ORIENTATION= 240 DEG  
1X FILTERED      1X VECTOR= .14 MILS PK-PK @-270

PROBE #2 ID: PROX 11 O'CK RADIAL      ORIENTATION= 330 DEG  
1X FILTERED      1X VECTOR= .14 MILS PK-PK @-180

ROTATION: CCW  
RPM(START)= 30424 RPM(END)= 30420



OTB PLOT CORRESPONDS TO 60 SECONDS FROM ENGINE START

FIGURE A.7 ORBIT AND TIMEBASE DATA FOR TEST 750-268, TAKEN 60 SECONDS FROM ENGINE START.

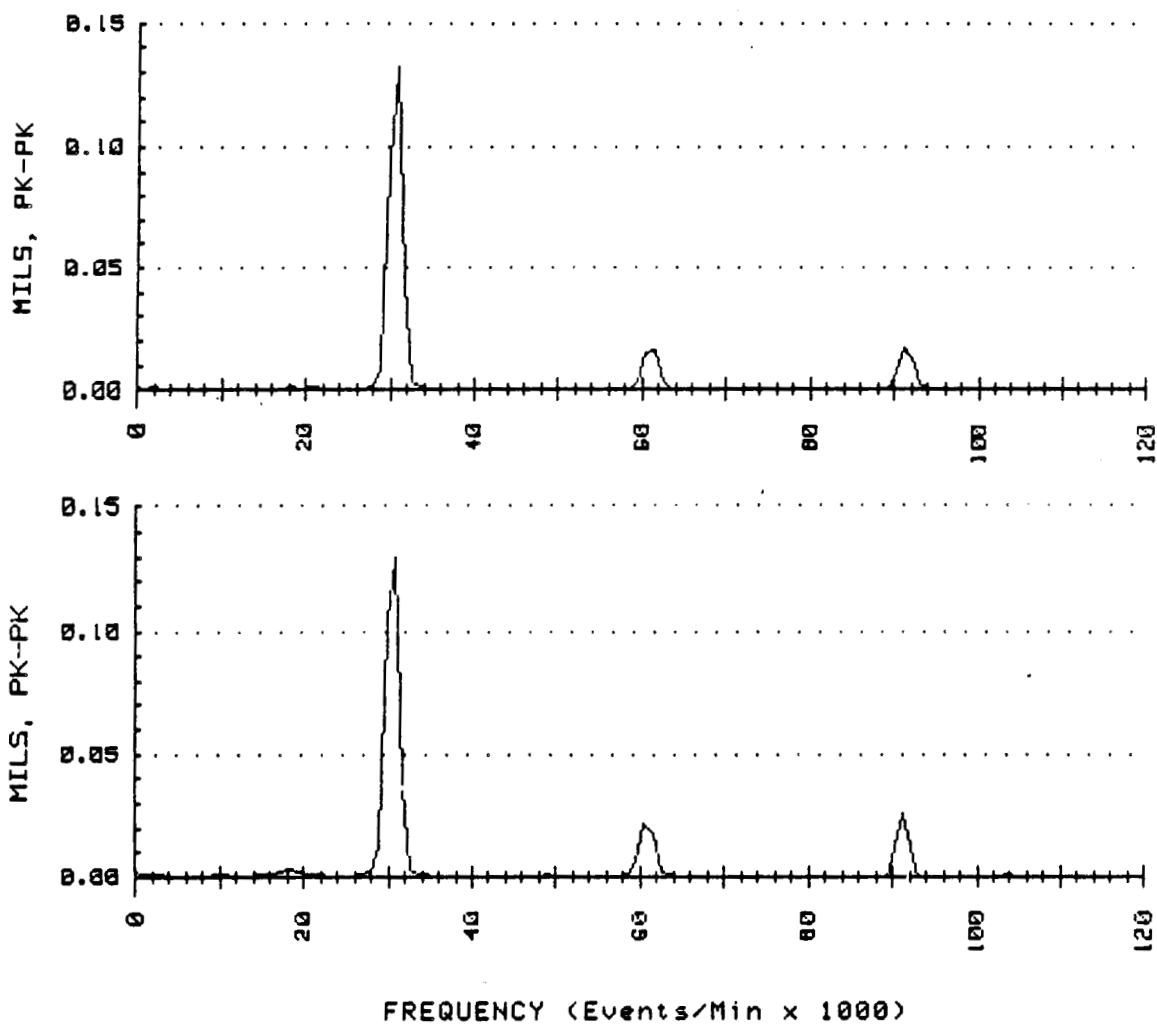
BENTLY  
NEVADA  
CORP.

PLANT ID: B.R.D.R.C.  
TRAIN ID: NASA TEST 750-268  
MACHINE ID: ENGINE 2012

PLOT NO:

RUN: 1A DATE: TIME: 08:50:13 PROBE ID: PROX 8 O'CK RADIAL  
1X FILTERED AMP = .14 TO .15 MILS, PK-PK  
1X = 30485 RPM TIME AVERAGED - 16 SAMPLES

RUN: 1A DATE: TIME: 08:51:27 PROBE ID: PROX 11 O'CK RADIAL  
1X FILTERED AMP = .14 TO .14 MILS, PK-PK  
1X = 30421 RPM TIME AVERAGED - 16 SAMPLES



SPEC PLOT CORRESPONDS TO 60 SECONDS FROM ENGINE START

FIGURE A.8 SPECTRAL DATA FOR TEST 750-268, 8 AND 11 O'CLOCK PROBES, TAKEN 60 SECONDS FROM ENGINE START.

BENTLY  
NEVADA  
CORP.

PLANT ID: B.R.D.R.C.  
TRAIN ID: NASA TEST 750-268  
MACHINE ID: ENGINE 2012

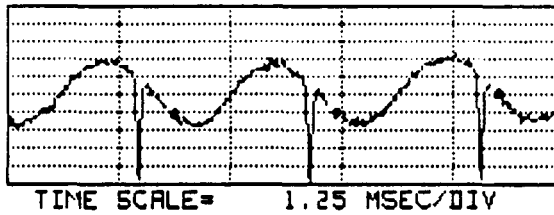
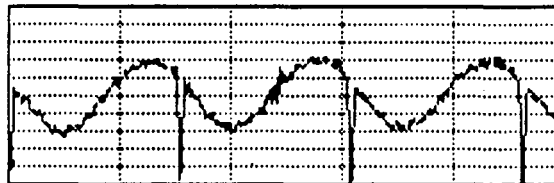
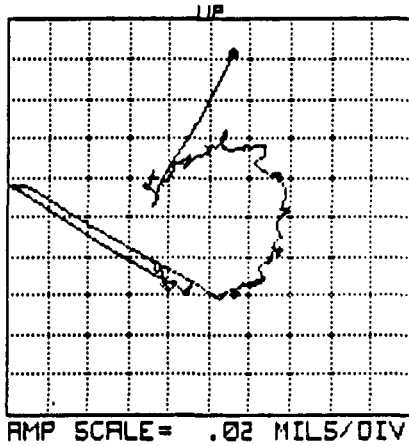
PLOT NO:

RUN: 3      DATE:      TIME: 10:49:16

PROBE #1 ID: PROX 8 O'CK RADIAL      ORIENTATION=      240 DEG  
1X FILTERED      1X VECTOR=      .15 MILS PK-PK @-286

PROBE #2 ID: PROX 11 O'CK RADIAL      ORIENTATION=      330 DEG  
1X FILTERED      1X VECTOR=      .14 MILS PK-PK @-196

ROTATION: CCW  
RPM(START)= 34388 RPM(END)= 30892



P  
OTB RESULTS 80 SECONDS FROM ENGINE START

FIGURE A.9 ORBIT-TIMEBASE DATA FOR TEST 750-268, TAKEN 80 SECONDS FROM ENGINE START.

BENTLY  
NEVADA  
CORP.

PLANT ID: B.R.D.R.C.  
TRAIN ID: NASA TEST 750-268  
MACHINE ID: ENGINE 2012

PLOT NO:

RUN: 3A DATE:  
1X FILTERED AMP =  
1X = 31510 RPM

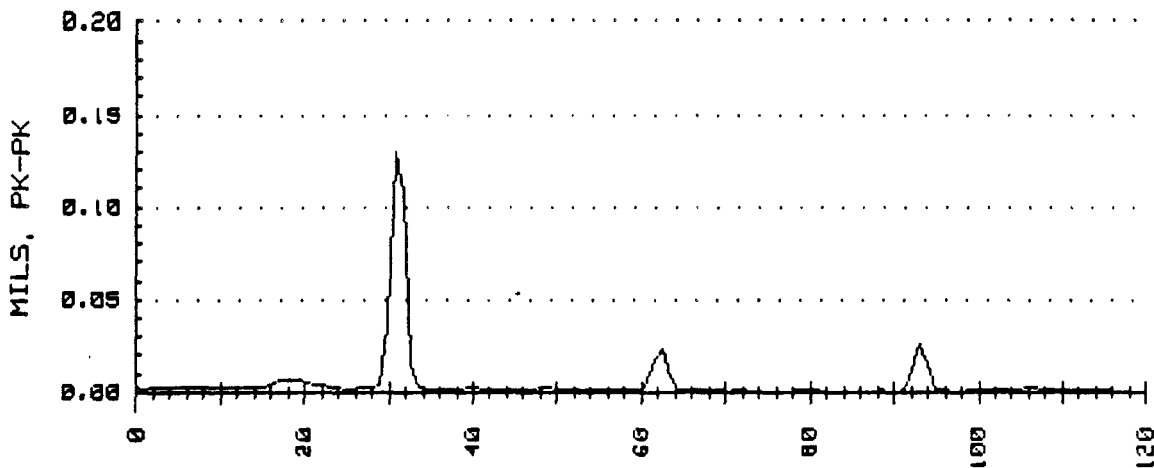
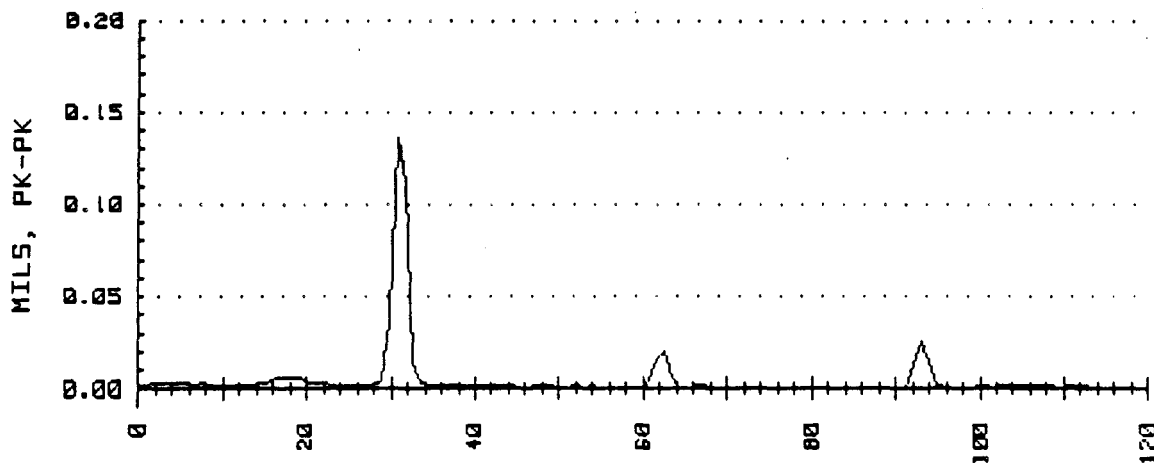
TIME: 10:59:27  
.13 TO .15 MILS, PK-PK  
AVERAGED - 16 SPECTRA

PROBE ID: PROX 8 O'CK RADIAL

RUN: 3A DATE:  
1X FILTERED AMP =  
1X = 31691 RPM

TIME: 11:00:16  
.12 TO .14 MILS, PK-PK  
AVERAGED - 16 SPECTRA

PROBE ID: PROX 11 O'CK RADIAL



FREQUENCY (Events/Min x 1000)

SPEC RESULTS 80 SECONDS FROM ENGINE START

FIGURE A.10 SPECTRAL DATA FOR TEST 750-268, 8 AND 11 O'CLOCK PROBES, TAKEN 80 SECONDS FROM ENGINE START.

BENTLY  
NEVADA  
CORP.

PLANT ID: B.R.D.R.C.  
TRAIN ID: NASA TEST 750-268  
MACHINE ID: ENGINE 2012

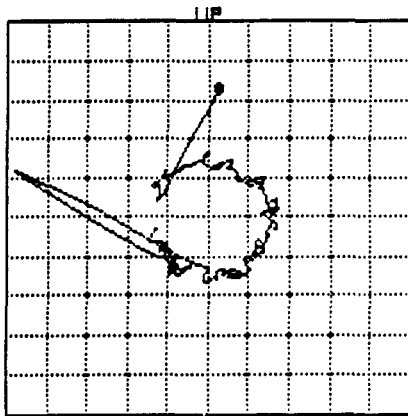
PLOT NO:

RUN: 5      DATE:      TIME: 11:27:51

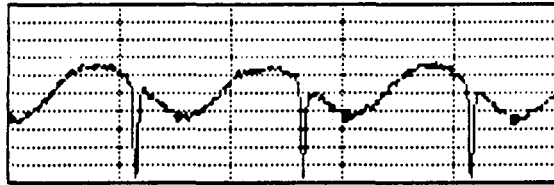
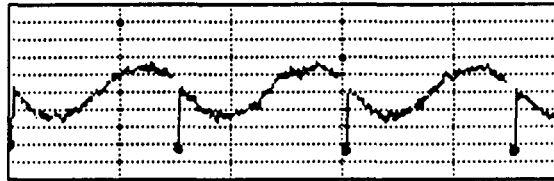
PROBE #1 ID: PROX 8 O'CK RADIAL      ORIENTATION=      240 DEG  
1X FILTERED      1X VECTOR=      .13 MILS PK-PK @-270

PROBE #2 ID: PROX 11 O'CK RADIAL      ORIENTATION=      330 DEG  
1X FILTERED      1X VECTOR=      .13 MILS PK-PK @-178

ROTATION: CCW  
RPM(START)= 31600 RPM(END)= 31712



AMP SCALE= .02 MILS/DIV



TIME SCALE= 1.25 MSEC/DIV

OTB RESULTS 100 SECONDS FROM ENGINE START

FIGURE A.11 ORBIT-TIMEBASE DATA FOR TEST 750-268, TAKEN 100 SECONDS FROM ENGINE START.

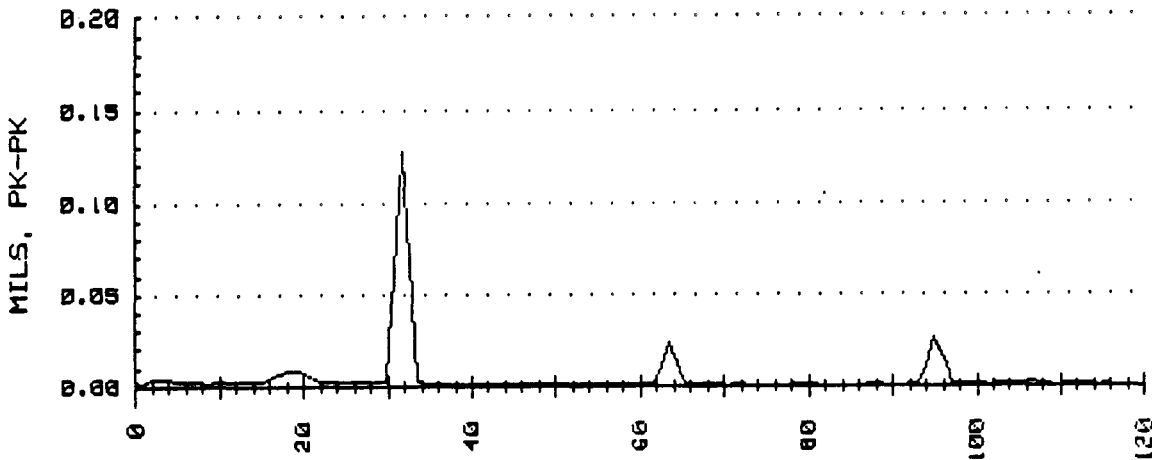
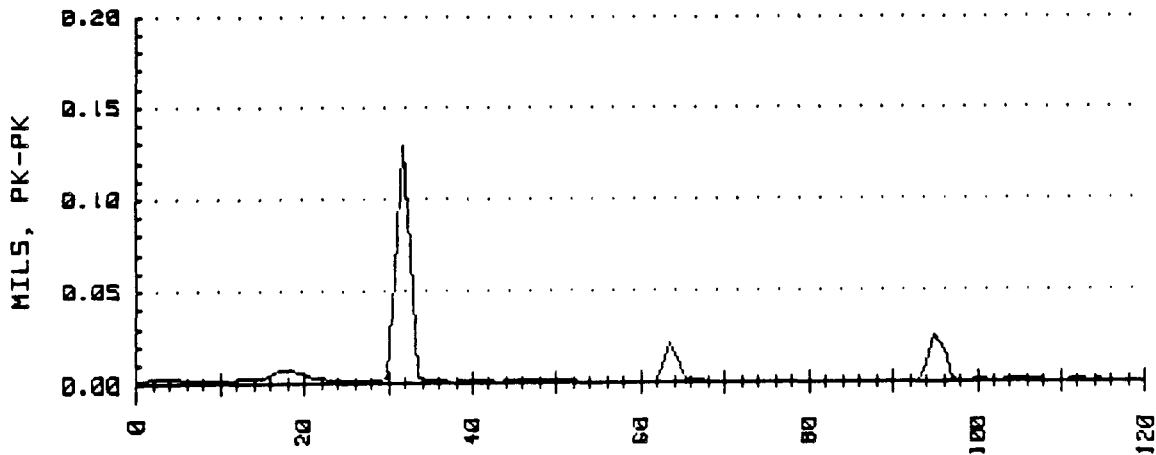
BENTLY  
NEVADA  
CORP.

PLANT ID: B.R.D.R.C.  
TRAIN ID: NASA TEST 750-268  
MACHINE ID: ENGINE 2012

PLOT NO:

RUN: 5A DATE: TIME: 11:32:03 PROBE ID: PROX 8 O'CK RADIAL  
1X FILTERED AMP = .13 TO .14 MILS, PK-PK  
1X = 31734 RPM AVERAGED - 16 SPECTRA

RUN: 5A DATE: TIME: 11:32:53 PROBE ID: PROX 11 O'CK RADIAL  
1X FILTERED AMP = .13 TO .13 MILS, PK-PK  
1X = 31736 RPM AVERAGED - 16 SPECTRA



FREQUENCY (Events/Min x 1000)

SPEC RESULTS 100 SECONDS FROM ENGINE START

FIGURE A.12 SPECTRAL DATA FOR TEST 750-268, 8 AND 11 O'CLOCK PROBES, TAKEN 100 SECONDS FROM ENGINE START.

BENTLY  
NEVADA  
CORP.

PLANT ID: B.R.D.R.C.  
TRAIN ID: NASA TEST 750-268  
MACHINE ID: ENGINE 2012

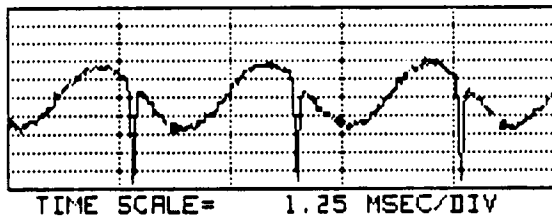
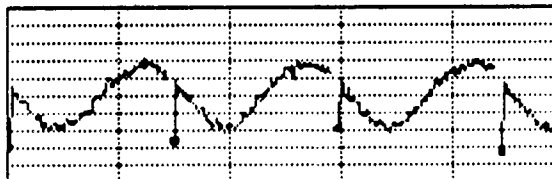
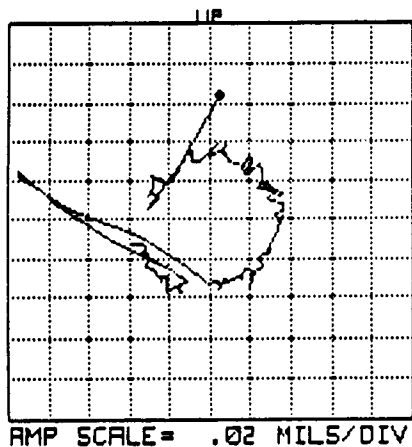
PLOT NO:

RUN: 6      DATE:      TIME: 11:37:13

PROBE #1 ID: PROX 8 O'CK RADIAL      ORIENTATION= 240 DEG  
1X FILTERED      1X VECTOR= .14 MILS PK-PK @-288

PROBE #2 ID: PROX 11 O'CK RADIAL      ORIENTATION= 330 DEG  
1X FILTERED      1X VECTOR= .14 MILS PK-PK @-198

ROTATION: CCW  
RPM(START)= 32274 RPM(END)= 32442



OTB RESULTS 120 SECONDS FROM ENGINE START

FIGURE A.13 ORBIT-TIMEBASE DATA FOR TEST 750-268, TAKEN 120 SECONDS FROM ENGINE START.

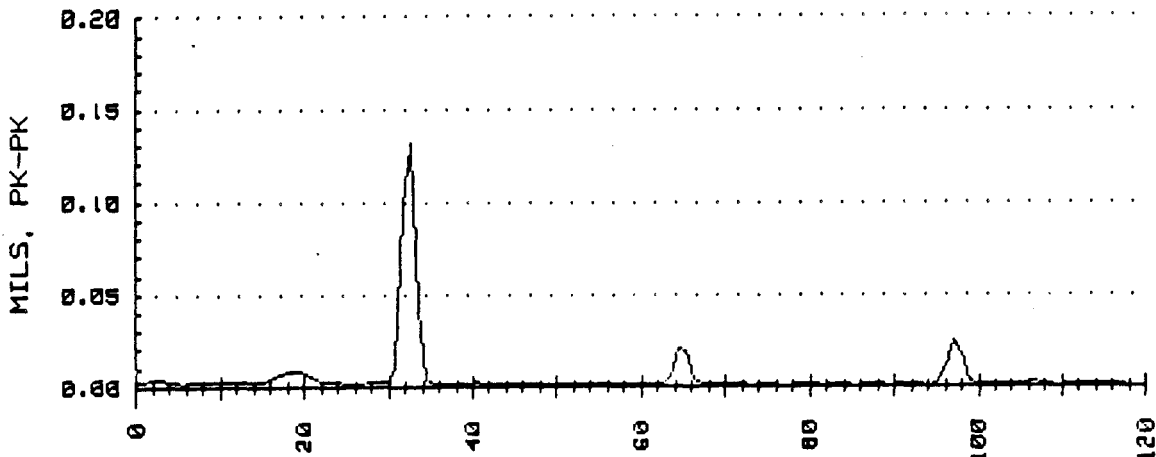
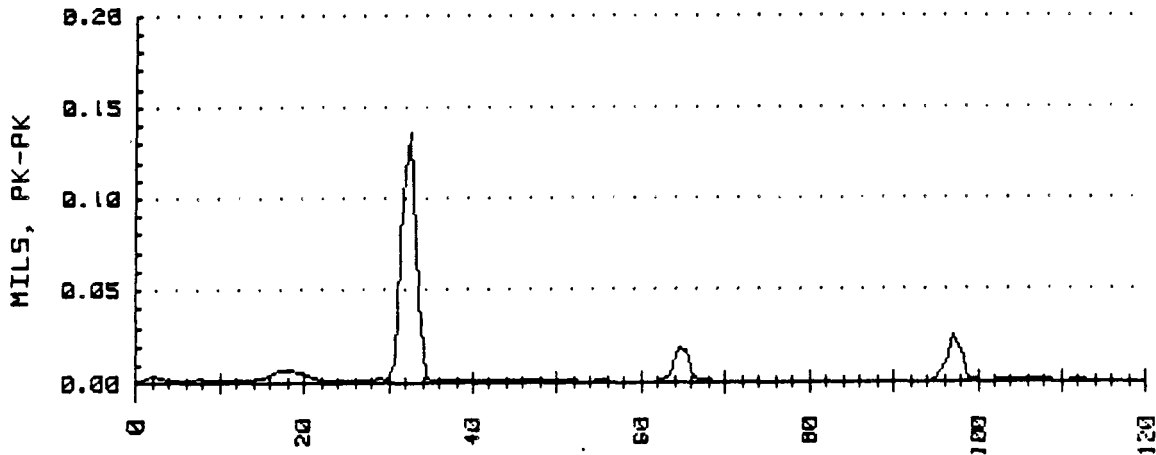
BENTLY  
NEVADA  
CORP.

PLANT ID: B.R.D.R.C.  
TRAIN ID: NASA TEST 750-268  
MACHINE ID: ENGINE 2012

PLOT NO:

RUN: 6A DATE: TIME: 11:40:10 PROBE ID: PROX 8 O'CK RADIAL  
1X FILTERED AMP = .14 TO .15 MILS, PK-PK  
1X = 32395 RPM AVERAGED - 16 SPECTRA

RUN: 6A DATE: TIME: 11:40:46 PROBE ID: PROX 11 O'CK RADIAL  
1X FILTERED AMP = .13 TO .14 MILS, PK-PK  
1X = 32396 RPM AVERAGED - 16 SPECTRA



FREQUENCY (Events/Min x 1000)

SPEC RESULTS 120 SECONDS FROM ENGINE START

FIGURE A.14 SPECTRAL DATA FOR TEST 750-268, 8 AND 11 O'CLOCK PROBES, TAKEN 120 SECONDS FROM ENGINE START.

BENTLY  
NEVADA  
CORP.

PLANT ID: B.R.D.R.C.  
TRAIN ID: NASA TEST 750-268  
MACHINE ID: ENGINE 2012

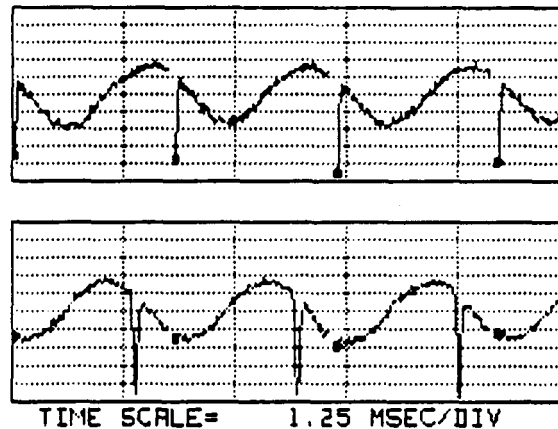
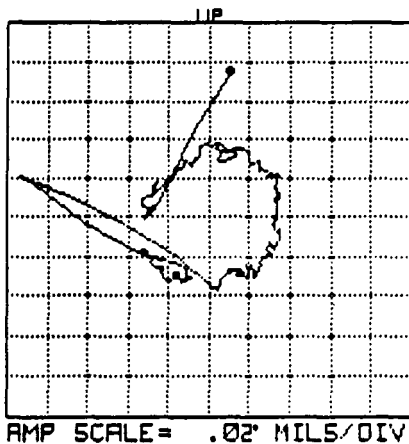
PLOT NO:

RUN: 7      DATE:      TIME: 13:00:21

PROBE #1 ID: PROX 8 O'CK RADIAL      ORIENTATION= 240 DEG  
1X FILTERED      1X VECTOR= .14 MILS PK-PK @-290.

PROBE #2 ID: PROX 11 O'CK RADIAL      ORIENTATION= 330 DEG  
1X FILTERED      1X VECTOR= .13 MILS PK-PK @-196

ROTATION: CCW  
RPM<START>= 32952 RPM<END>= 33052



OTB RESULTS 140 SECONDS FROM ENGINE START

FIGURE A.15 ORBIT-TIMEBASE DATA FOR TEST 750-268, TAKEN 140 SECONDS FROM ENGINE START.

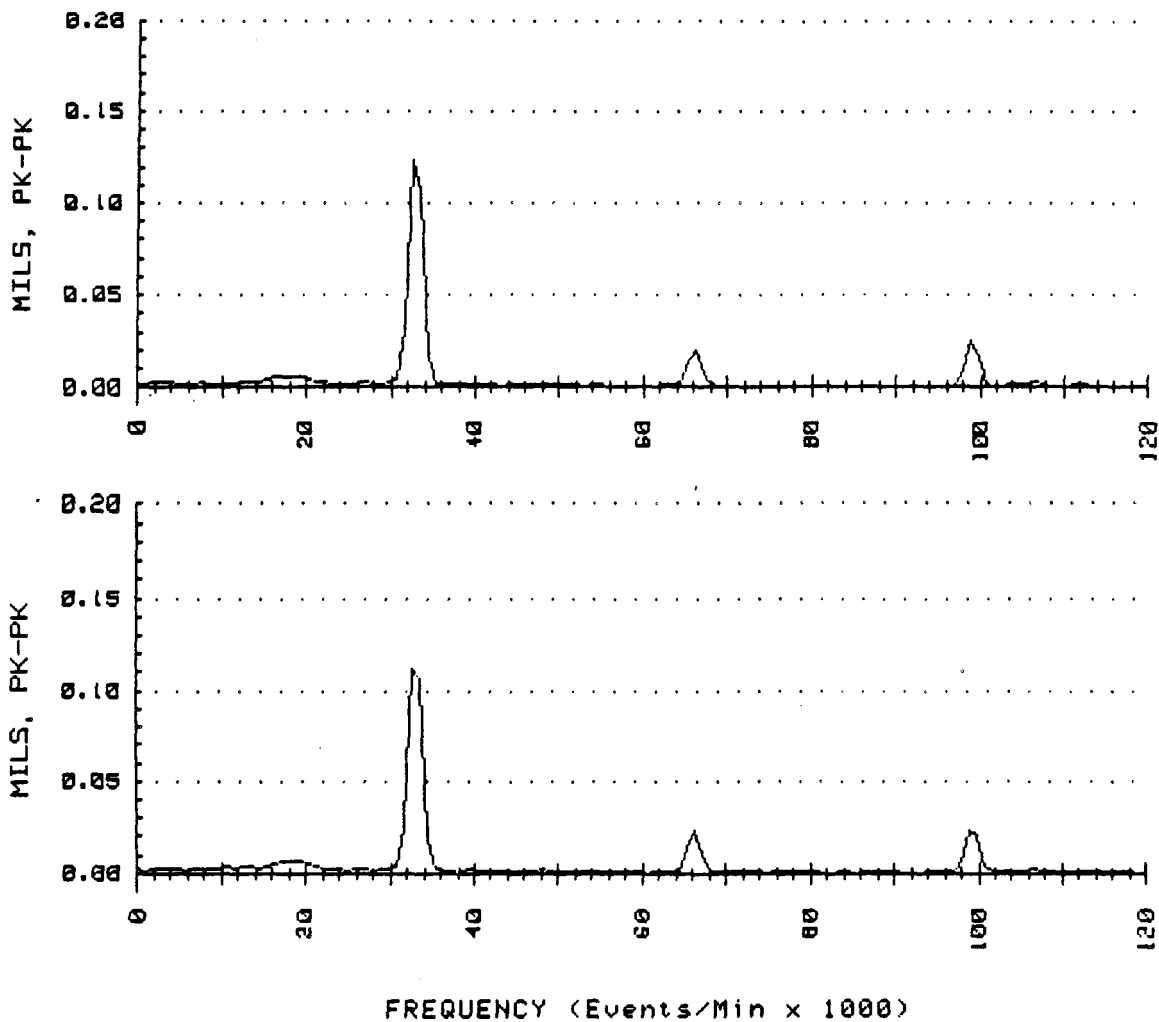
BENTLY  
NEVADA  
CORP.

PLANT ID: B.R.D.R.C.  
TRAIN ID: NASA TEST 750-268  
MACHINE ID: ENGINE 2012

PLOT NO:

RUN: 7A DATE: TIME: 13:04:17 PROBE ID: PROX 8 O'CLOCK RADIAL  
1X FILTERED AMP = .13 TO .14 MILS, PK-PK  
1X = 33037 RPM AVERAGED - 16 SPECTRA

RUN: 7A DATE: TIME: 13:04:55 PROBE ID: PROX 11 O'CLOCK RADIAL  
1X FILTERED AMP = 0.00 TO .13 MILS, PK-PK  
1X = 28198 RPM AVERAGED - 16 SPECTRA



SPEC RESULTS 140 SECONDS FROM ENGINE START

FIGURE A.16 SPECTRAL DATA FOR TEST 750-268, 8 AND 11 O'CLOCK PROBES, TAKEN 140 SECONDS FROM ENGINE START.

BENTLY  
NEVADA  
CORP.

PLANT ID: B.R.D.R.C.  
TRAIN ID: NASA TEST 750-268  
MACHINE ID: ENGINE 2012

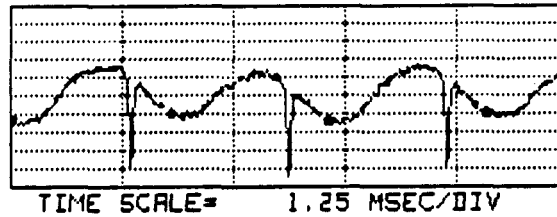
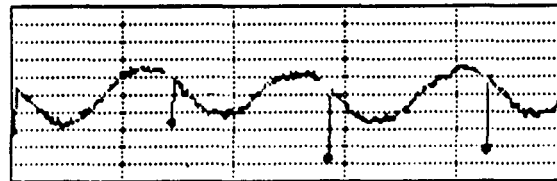
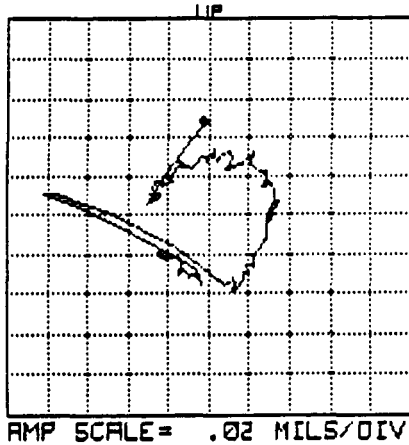
PLOT NO:

RUN: 8      DATE:      TIME: 13:08:44

PROBE #1 ID: PROX 8 O'CK RADIAL      ORIENTATION= 240 DEG  
1X FILTERED      1X VECTOR= .12 MILS PK-PK @-294

PROBE #2 ID: PROX 11 O'CK RADIAL      ORIENTATION= 330 DEG  
1X FILTERED      1X VECTOR= .12 MILS PK-PK @-200

ROTATION: CCW  
RPM(START)= 33708 RPM(END)= 33708



OTB RESULTS 160 SECONDS FROM ENGINE START

FIGURE A.17 ORBIT-TIMEBASE DATA FOR TEST 750-268, TAKEN 160 SECONDS FROM ENGINE START.

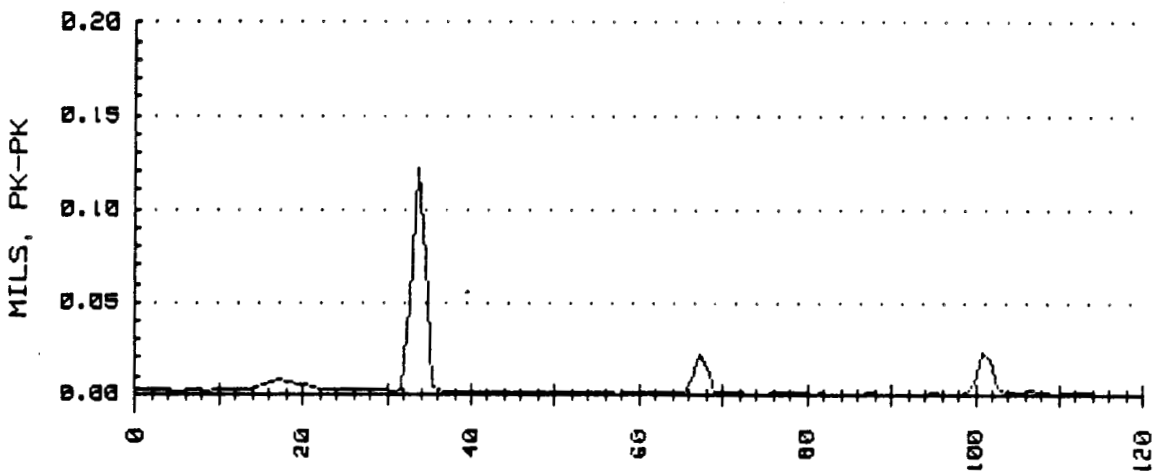
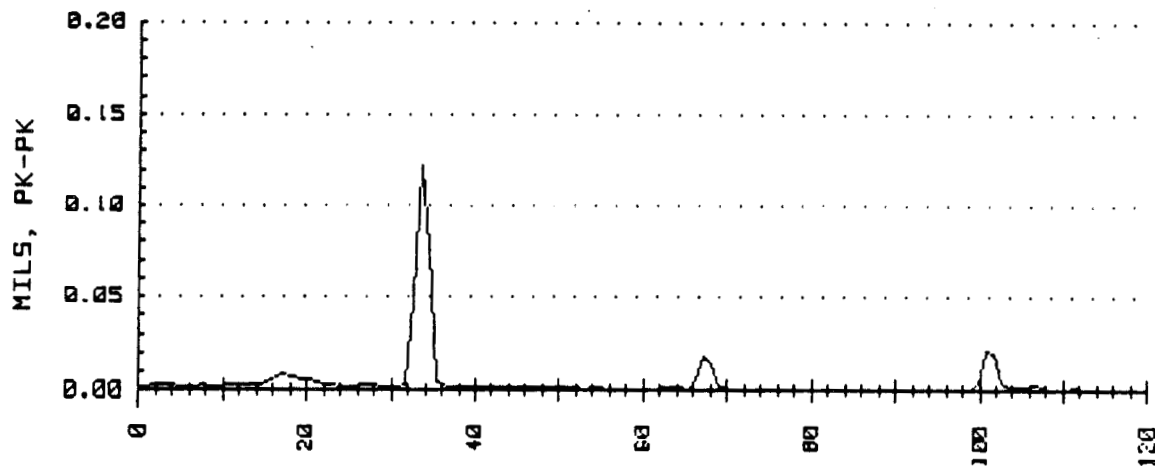
BENTLY  
NEVADA  
CORP.

PLANT ID: B.R.D.R.C.  
TRAIN ID: NASA TEST 750-268  
MACHINE ID: ENGINE 2012

PLOT NO:

RUN: 8A DATE: TIME: 13:12:29 PROBE ID: PROX 8 O'CK RADIAL  
1X FILTERED AMP = .12 TO .13 MILS, PK-PK  
1X = 33770 RPM AVERAGED - 16 SPECTRA

RUN: 8A DATE: TIME: 13:13:22 PROBE ID: PROX 11 O'CK RADIAL  
1X FILTERED AMP = .12 TO .13 MILS, PK-PK  
1X = 33748 RPM AVERAGED - 16 SPECTRA



FREQUENCY (Events/Min x 1000)

SPEC RESULTS 160 SECONDS FROM ENGINE START

FIGURE A.18 SPECTRAL DATA FOR TEST 750-268, 8 AND 11 O'CLOCK PROBES, TAKEN 160 SECONDS FROM ENGINE START.

BENTLY  
NEVADA  
CORP.

PLANT ID: B.R.D.R.C.  
TRAIN ID: NASA TEST 750-268  
MACHINE ID: ENGINE 2012

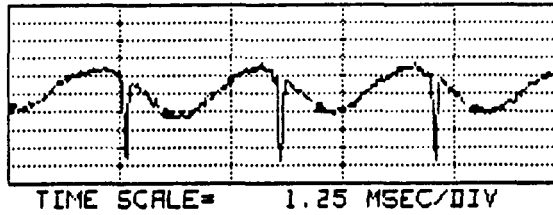
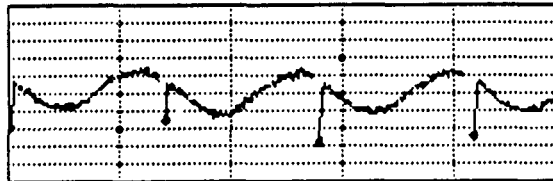
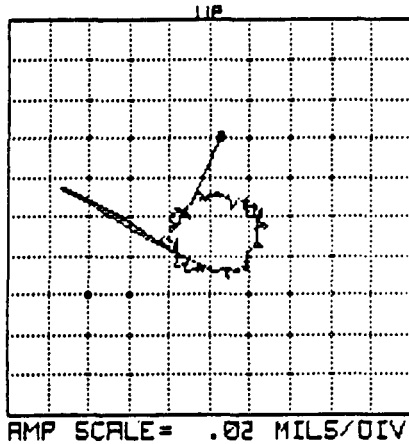
PLOT NO:

RUN: 9      DATE:      TIME: 13:34:51

PROBE #1 ID: PROX 8 O'CK RADIAL      ORIENTATION=      240 DEG  
1X FILTERED      1X VECTOR=      .11 MILS PK-PK @-296

PROBE #2 ID: PROX 11 O'CK RADIAL      ORIENTATION=      330 DEG  
1X FILTERED      1X VECTOR=      .11 MILS PK-PK @-200

ROTATION: CCW  
RPM(START)= 34466 RPM(END)= 34446



OTB RESULTS 180 SECONDS FROM ENGINE START

FIGURE A.19 ORBIT-TIMEBASE DATA FOR TEST 750-268, TAKEN 180 SECONDS FROM ENGINE START.

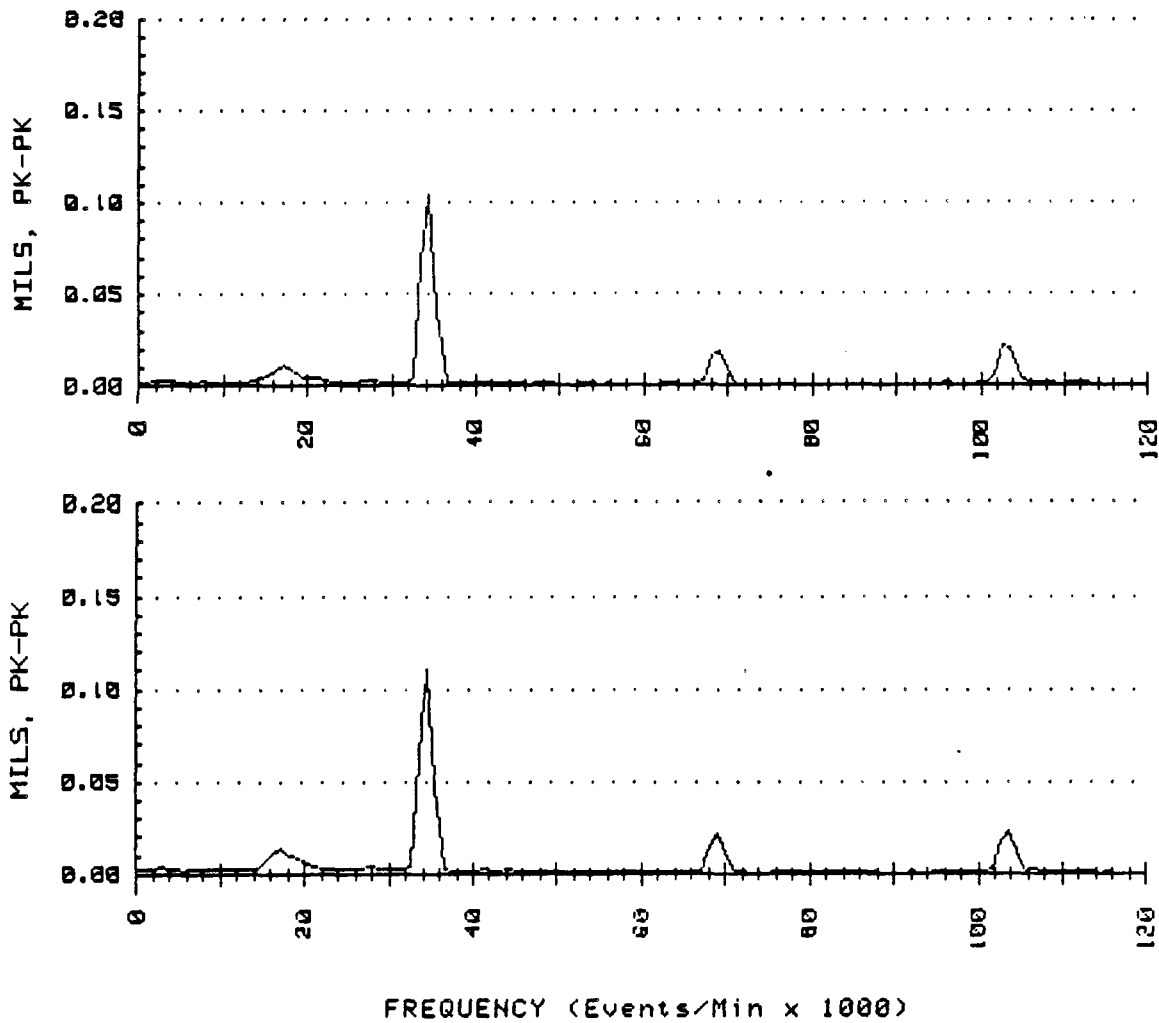
BENTLY  
NEVADA  
CORP.

PLANT ID: B.R.D.R.C.  
TRAIN ID: NASA TEST 750-268  
MACHINE ID: ENGINE 2012

PLOT NO:

RUN: 9A DATE: TIME: 13:41:07 PROBE ID: PROX 8 O'CK RADIAL  
1X FILTERED AMP = .10 TO .11 MILS, PK-PK  
1X = 34428 RPM AVERAGED - 16 SPECTRA

RUN: 9A DATE: TIME: 13:41:53 PROBE ID: PROX 11 O'CK RADIAL  
1X FILTERED AMP = .10 TO .11 MILS, PK-PK  
1X = 34482 RPM AVERAGED - 16 SPECTRA



SPEC RESULTS 180 SECONDS FROM ENGINE START

FIGURE A.20 SPECTRAL DATA FOR TEST 750-268, 8 AND 11 O'CLOCK PROBES, TAKEN 180 SECONDS FROM ENGINE START.

BENTLY  
NEVADA  
CORP.

PLANT ID: B.R.D.R.C.  
TRAIN ID: NASA TEST 750-268  
MACHINE ID: ENGINE 2012

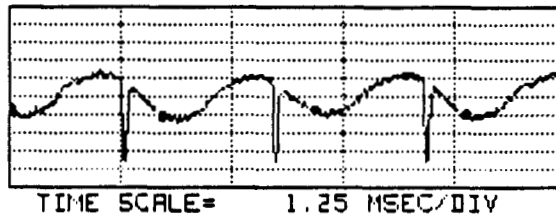
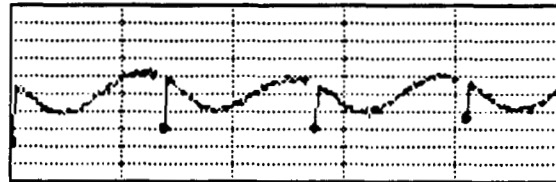
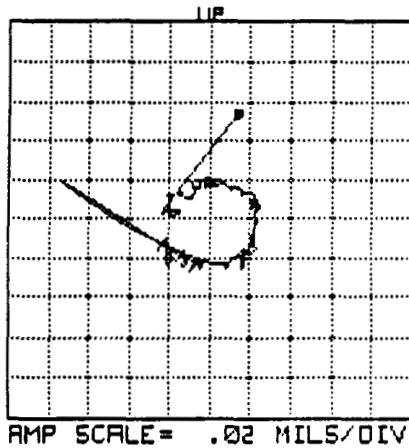
PLOT NO:

RUN: 10      DATE:      TIME: 13:45:52

PROBE #1 ID: PROX 8 O'CK RADIAL      ORIENTATION= 240 DEG  
1X FILTERED      1X VECTOR= .10 MILS PK-PK @-298

PROBE #2 ID: PROX 11 O'CK RADIAL      ORIENTATION= 330 DEG  
1X FILTERED      1X VECTOR= .10 MILS PK-PK @-204

ROTATION: CCW  
RPM(START)= 35066 RPM(END)= 35168



OTB RESULTS 200 SECONDS FROM ENGINE START

FIGURE A.21 ORBIT-TIMEBASE DATA FOR TEST 750-268, TAKEN 200 SECONDS FROM ENGINE START.

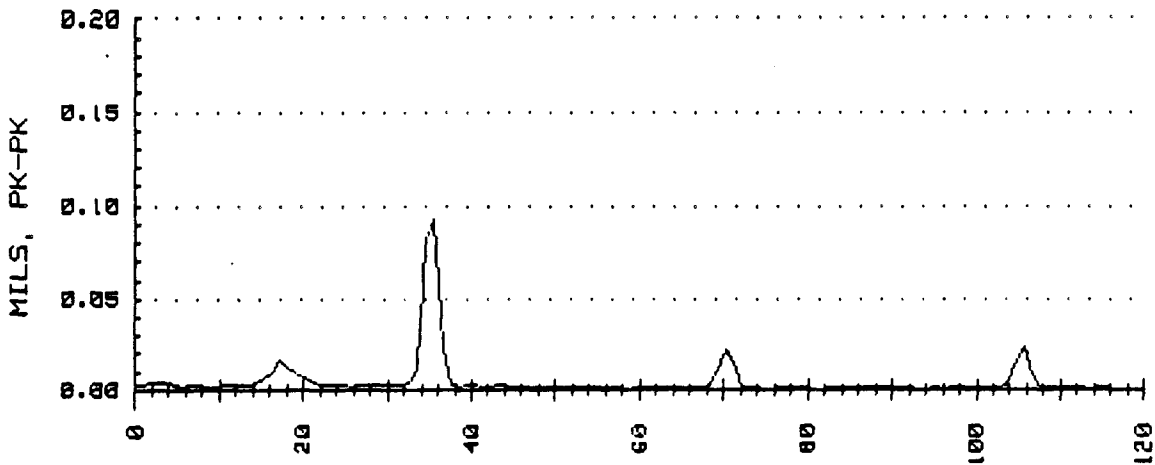
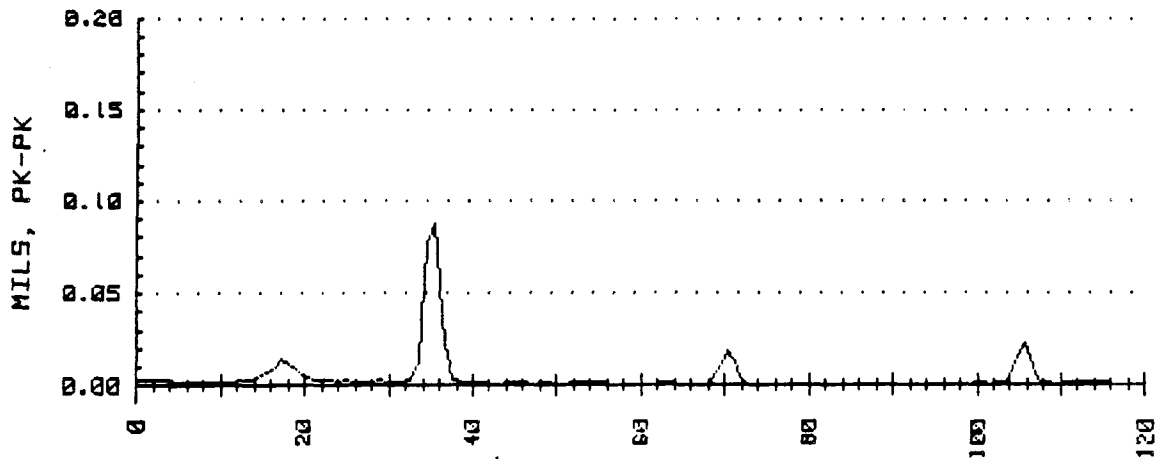
BENTLY  
NEVADA  
CORP.

PLANT ID: B.R.D.R.C.  
TRAIN ID: NASA TEST 750-268  
MACHINE ID: ENGINE 2012

PLOT NO:

RUN: 10A DATE: TIME: 14:14:30 PROBE ID: PROX 8 O'CLOCK RADIAL  
1X FILTERED AMP = .09 TO .10 MILS, PK-PK  
1X = 35164 RPM AVERAGED - 16 SPECTRA

RUN: 10A DATE: TIME: 14:15:14 PROBE ID: PROX 11 O'CLOCK RADIAL  
1X FILTERED AMP = .10 TO .11 MILS, PK-PK  
1X = 35167 RPM AVERAGED - 16 SPECTRA



FREQUENCY (Events/Min x 1000)

SPEC RESULTS 200 SECONDS FROM ENGINE START

FIGURE A.22 SPECTRAL DATA FOR TEST 750-268, 8 AND 11 O'CLOCK PROBES, TAKEN 200 SECONDS FROM ENGINE START.

BENTLY  
NEVADA  
CORP.

PLOT NO:

PLANT ID:  
TRAIN ID:  
MACHINE ID:  
PROBE ID:

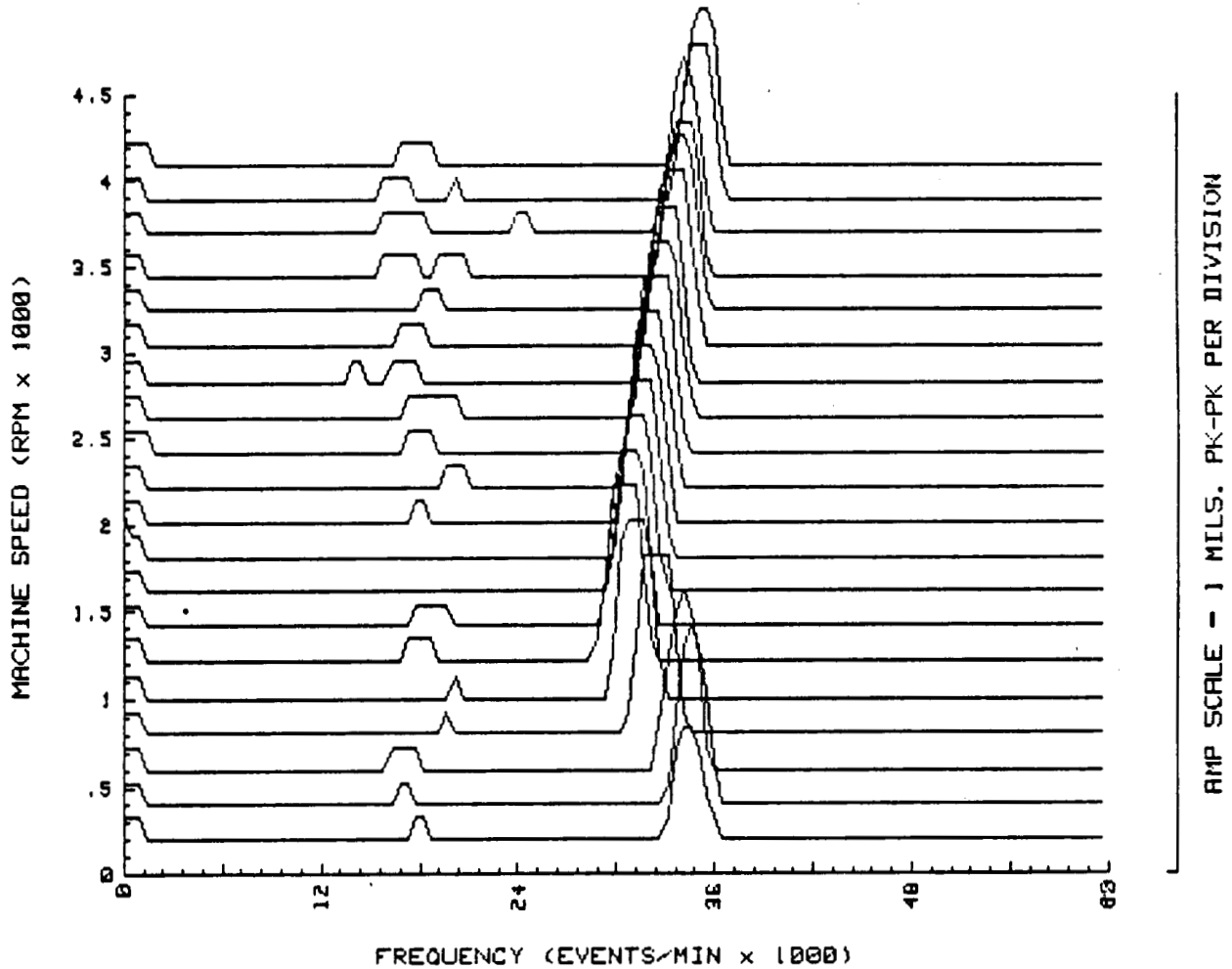
B.R.D.R.C.  
NASA TEST 750-268  
ENGINE 2012  
PROX 8 O'CK RADIAL

RUNUP

RUN: 2

DATE: 14 JULY 87

TIME: 11:11



THE RPM SCALE IS INACCURATE. THE RPM SCALE SHOULD BE A TIME SCALE  
WITH EVERY 500 RPM CORRESPONDING TO 25 SECONDS OF ENGINE RUN TIME.

FIGURE A.23 TIME CASCADE VIBRATION SPECTRUM DATA FOR RUN  
750-268, 8 O'CLOCK PROBE LOCATION.

BENTLY  
NEVADA  
CORP.

PLOT NO:

PLANT ID:  
TRAIN ID:  
MACHINE ID:  
PROBE ID:

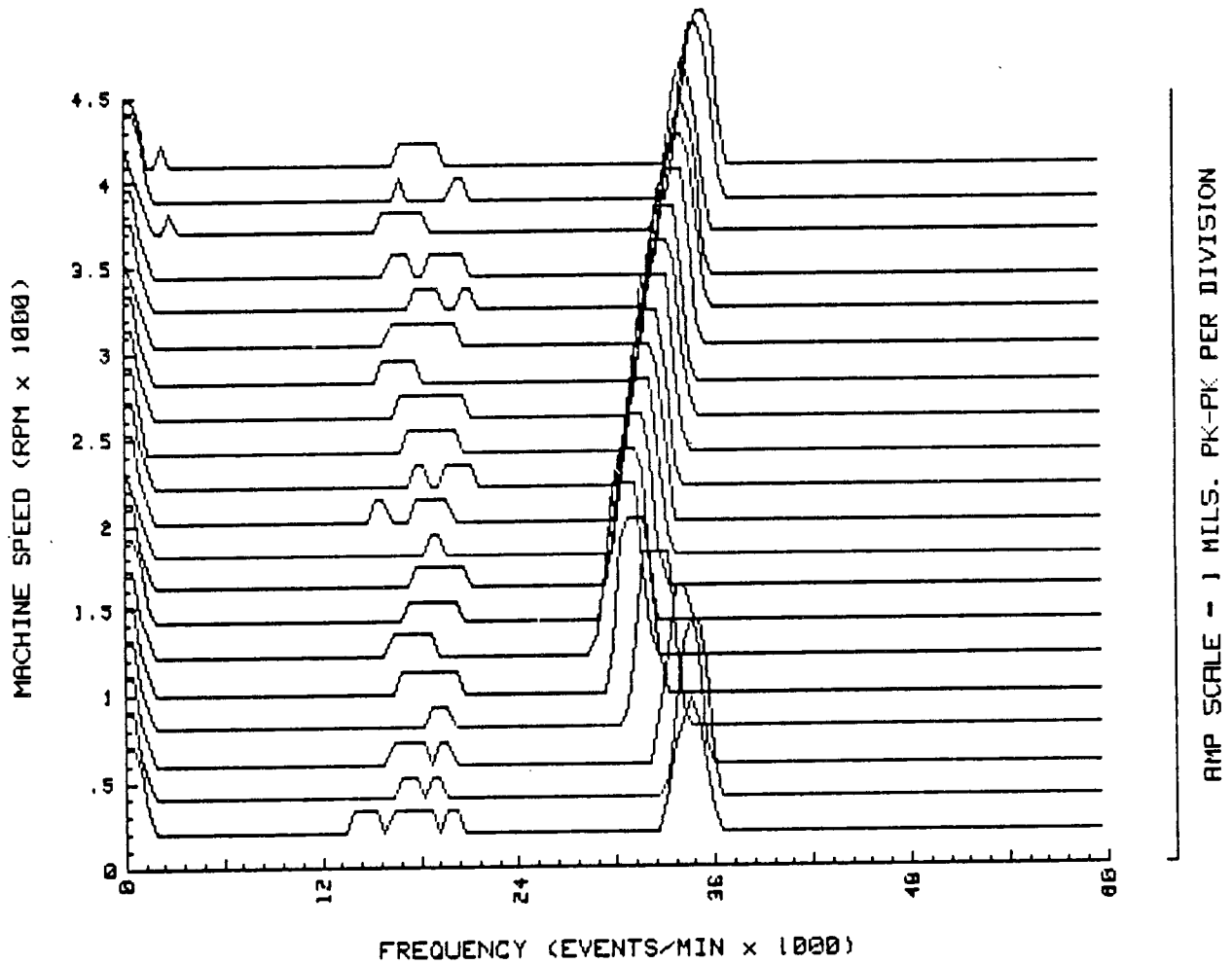
B.R.D.R.C.  
NASA TEST 750-268  
ENGINE 2012  
PROX 11 O'CK RADIAL

RUNUP

RUN: 2

DATE: 14 JULY 87

TIME: 11:11



THE RPM SCALE IS INACCURATE. THE RPM SCALE SHOULD BE A TIME SCALE WITH EVERY 500 RPM CORRESPONDING TO 25 SECONDS OF ENGINE RUN TIME.

FIGURE A.24 TIME CASCADE OF VIBRATION SPECTRUM DATA FOR RUN 750-268, 11 O'CLOCK PROBE LOCATION.

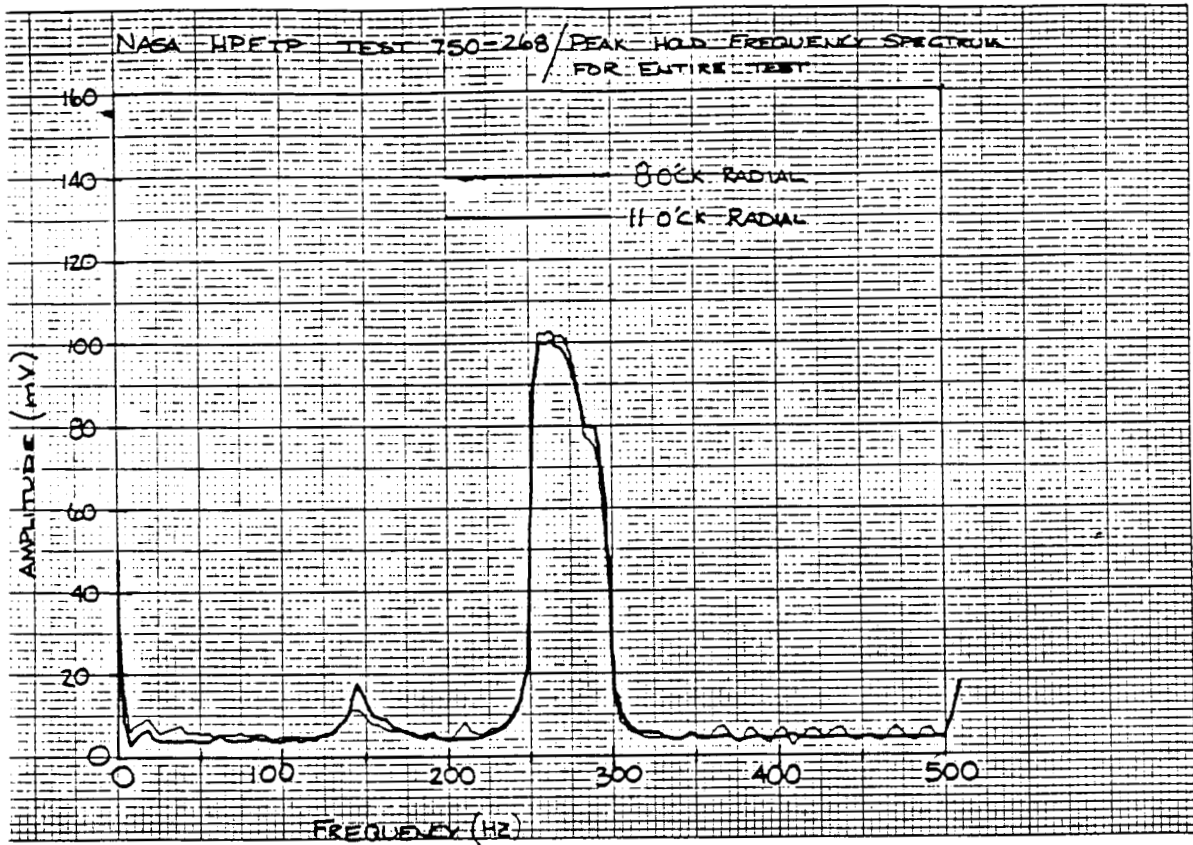


FIGURE A.25 PEAK HELD SPECTRAL DATA PROFILE FOR RUN 750-268.

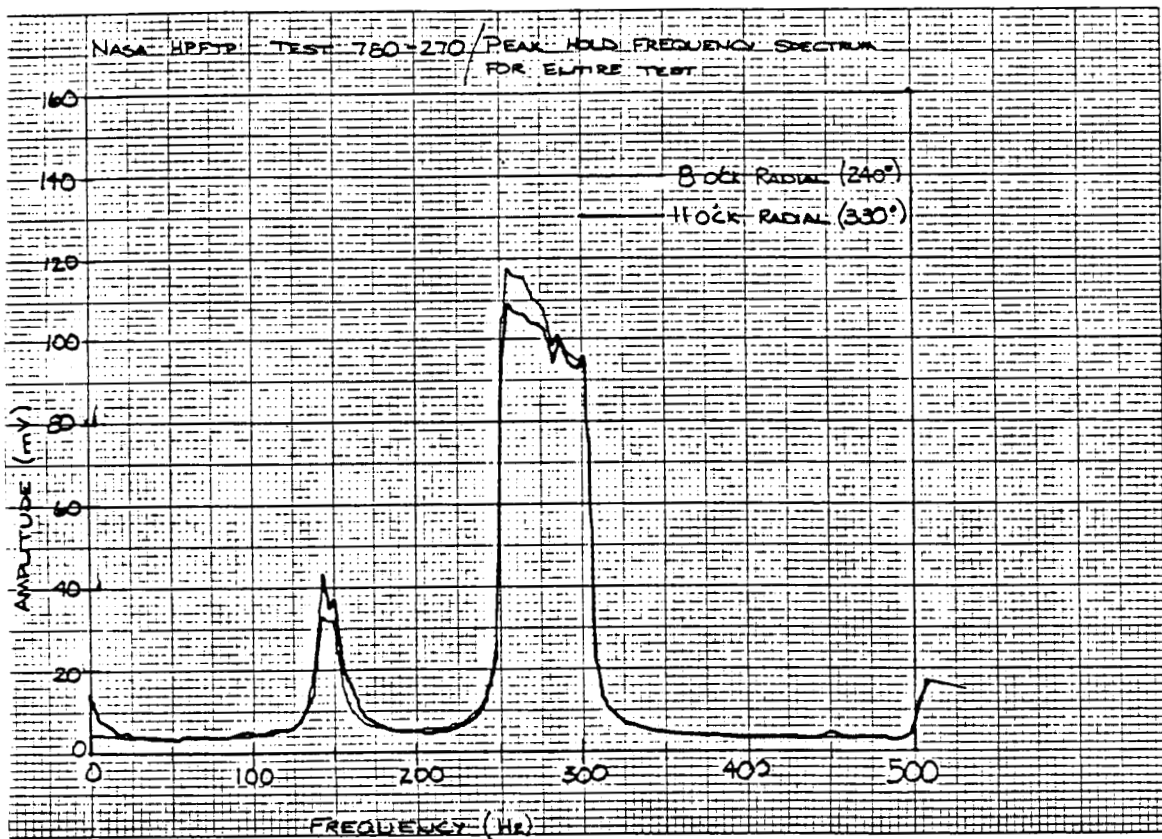


FIGURE A.26 PEAK HELD SPECTRAL DATA PROFILE FOR RUN 750-270.

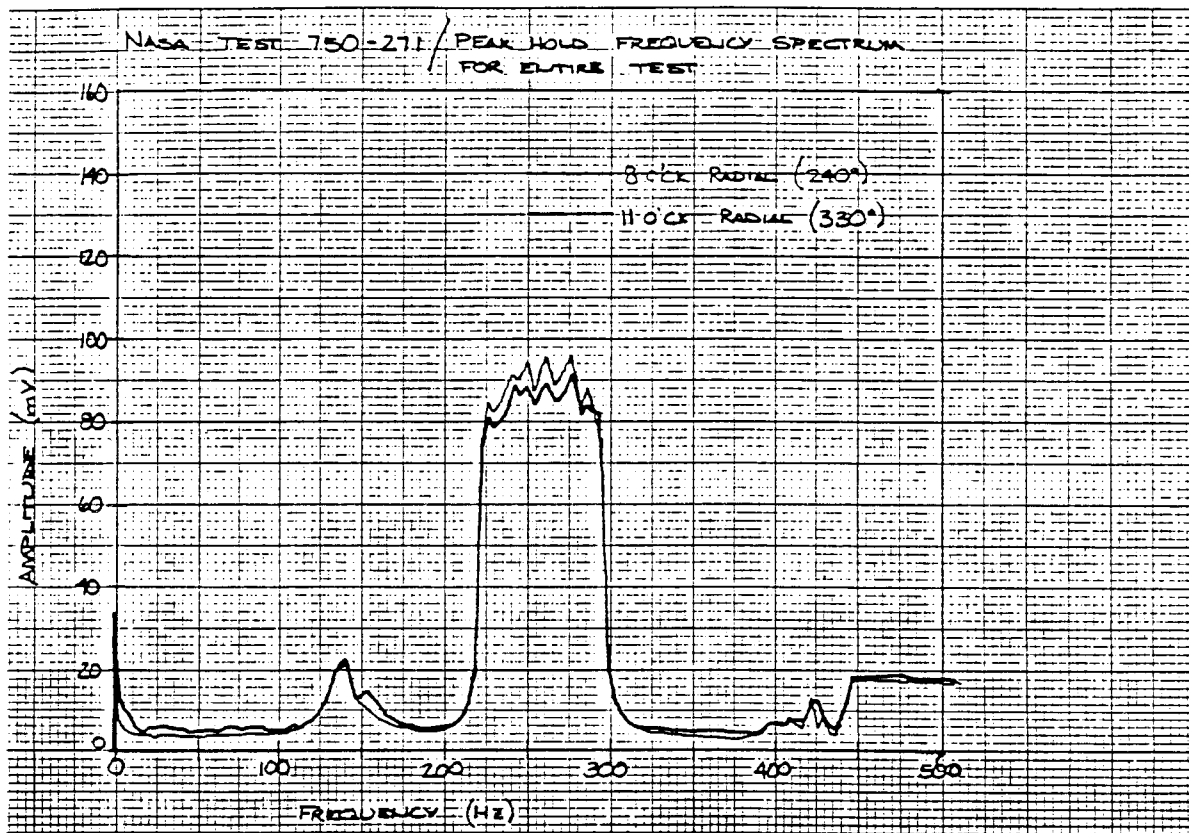


FIGURE A.27 PEAK HELD SPECTRAL DATA PROFILE FOR RUN 750-271.

ORIGINAL PAGE IS  
OF POOR QUALITY

BENTLY  
NEVADA  
CORP.

PLANT ID: B.R.D.R.C.  
TRAIN ID: NASA TEST 750-268  
MACHINE ID: HPFTP/ENGINE 2012

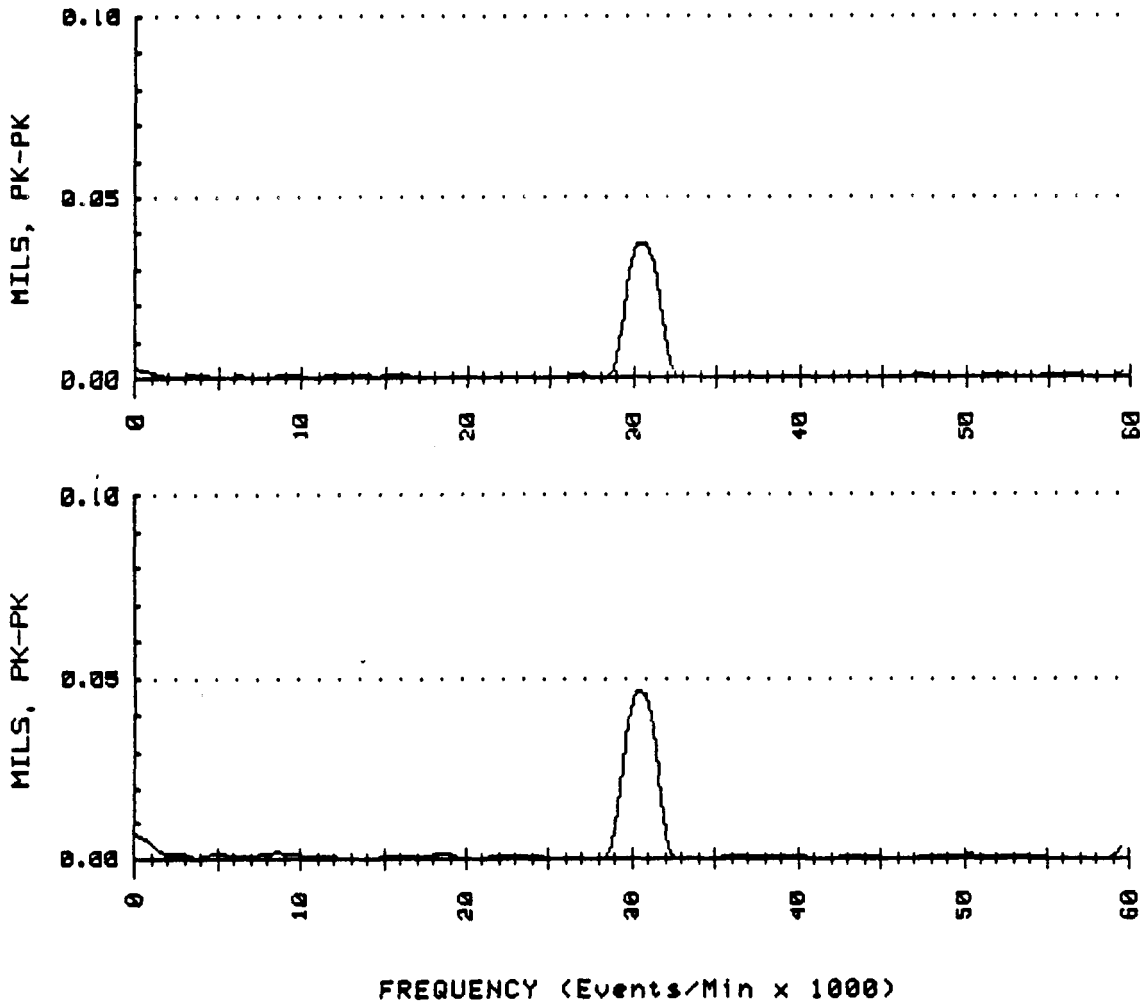
PLOT NO:

RUN: 1 DATE:  
1X FILTERED AMP =  
1X = 30509 RPM

TIME: 14:37:30 PROBE ID: 8 O'CK AXIAL  
.04 TO .05 MILS, PK-PK  
TIME AVERAGED - 16 SAMPLES

RUN: 1 DATE:  
1X FILTERED AMP =  
1X = 30476 RPM

TIME: 14:38:06 PROBE ID: 11 O'CK AXIAL  
.05 TO .06 MILS, PK-PK  
TIME AVERAGED - 16 SAMPLES



SPECTRUM RESULTS CORRESPOND TO 60 SECONDS FROM ENGINE START

FIGURE A.28 SPECTRAL DATA FOR TEST 750-268, AXIAL PROBES, TAKEN 60 SECONDS FROM ENGINE START.

BENTLY  
NEVADA  
CORP.

PLANT ID: B.R.D.R.C.  
TRAIN ID: NASA TEST 750-268  
MACHINE ID: HPFTP/ENGINE 2012

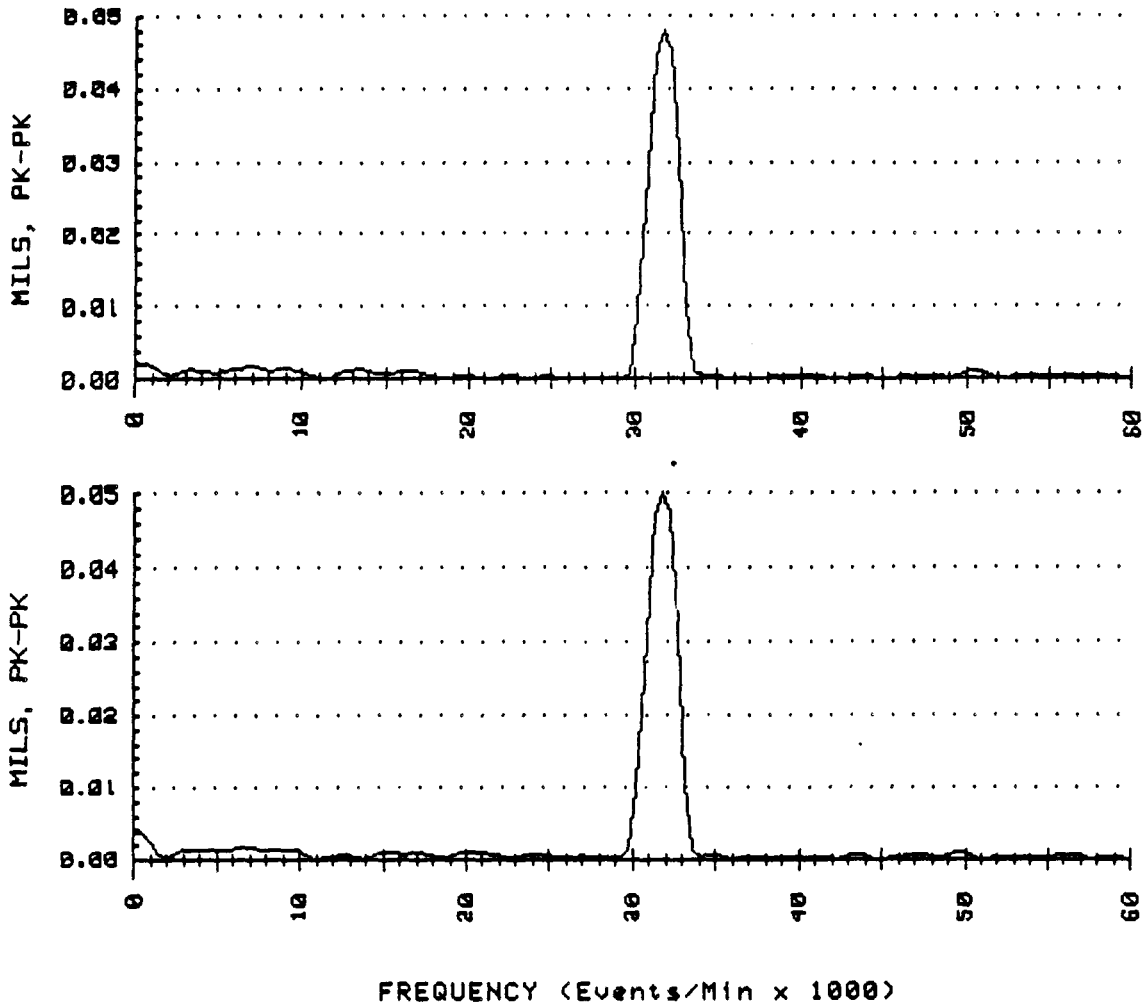
PLOT NO:

RUN: 2 DATE:  
1X FILTERED AMP =  
1X = 31689 RPM

TIME: 13:49:42 PROBE ID: 8 O'CK AXIAL  
.04 TO .05 MILS, PK-PK  
TIME AVERAGED - 16 SAMPLES

RUN: 2 DATE:  
1X FILTERED AMP =  
1X = 31689 RPM

TIME: 13:49:42 PROBE ID: 11 O'CK AXIAL  
.05 TO .06 MILS, PK-PK  
TIME AVERAGED - 16 SAMPLES



SPECTRUM RESULTS CORRESPOND TO 100 SECONDS FROM ENGINE START

FIGURE A.29 SPECTRAL DATA FOR TEST 750-268, AXIAL PROBES, TAKEN 100 SECONDS FROM ENGINE START.

BENTLY  
NEVADA  
CORP.

PLANT ID: B.R.D.R.C.  
TRAIN ID: NASA TEST 750-268  
MACHINE ID: HPFTP/ENGINE 2012

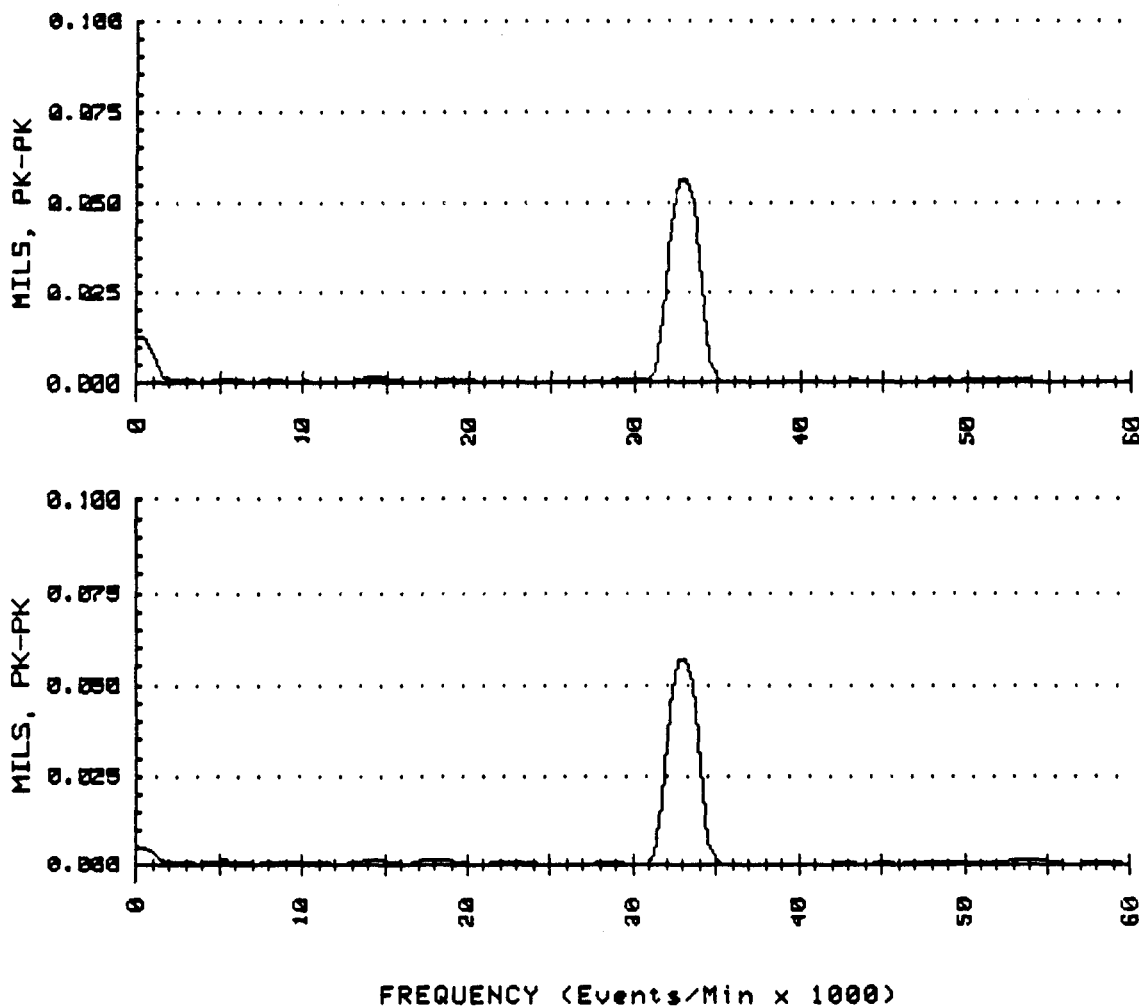
PLOT NO:

RUN: 3 DATE:  
1X FILTERED AMP =  
1X = 33128 RPM

TIME: 13:56:49 PROBE ID: 8 O'CK AXIAL  
.06 TO .06 MILS, PK-PK  
TIME AVERAGED - 16 SAMPLES

RUN: 3 DATE:  
1X FILTERED AMP =  
1X = 33128 RPM

TIME: 13:56:49 PROBE ID: 11 O'CK AXIAL  
.05 TO .06 MILS, PK-PK  
TIME AVERAGED - 16 SAMPLES



SPECTRUM RESULTS CORRESPOND TO 140 SECONDS FROM ENGINE START

FIGURE A.30 SPECTRAL DATA FOR TEST 750-268, AXIAL PROBES, TAKEN 140 SECONDS FROM ENGINE START.

BENTLY  
NEVADA  
CORP.

PLANT ID: B.R.D.R.C.  
TRAIN ID: NASA TEST 750-268  
MACHINE ID: HPFTP/ENGINE 2012

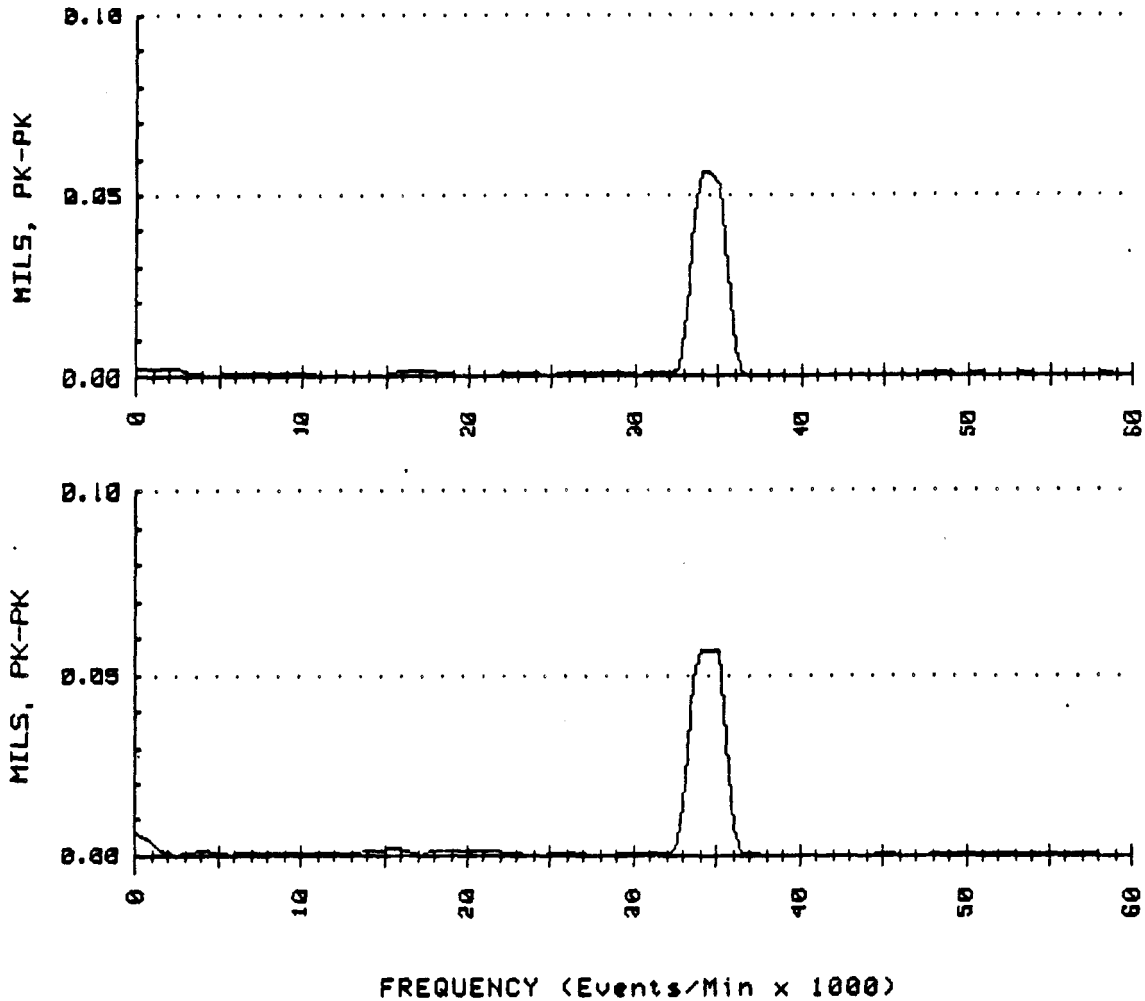
PLOT NO:

RUN: 4 DATE:  
1X FILTERED AMP =  
1X = 34414 RPM

TIME: 14:32:28 PROBE ID: 8 O'CK AXIAL  
.06 TO .07 MILS, PK-PK  
TIME AVERAGED - 16 SAMPLES

RUN: 4 DATE:  
1X FILTERED AMP =  
1X = 34412 RPM

TIME: 14:34:03 PROBE ID: 11 O'CK AXIAL  
.07 TO .08 MILS, PK-PK  
TIME AVERAGED - 16 SAMPLES



SPECTRUM RESULTS CORRESPOND TO 180 SECONDS FROM ENGINE START

FIGURE A.31 SPECTRAL DATA FOR TEST 750-268, AXIAL PROBES, TAKEN 180 SECONDS FROM ENGINE START.

APPENDIX 2

*NASA Conference Publication 3012*

# **Advanced Earth-to-Orbit Propulsion Technology 1988**

*Volume II*

*Edited by  
R. J. Richmond  
George C. Marshall Space Flight Center  
Huntsville, Alabama*

*S. T. Wu  
The University of Alabama in Huntsville  
Huntsville, Alabama*

**Proceedings of a conference held at  
NASA George C. Marshall Space Flight Center  
Huntsville, Alabama  
May 10-12, 1988**

**NASA**

**National Aeronautics  
and Space Administration**

**Scientific and Technical  
Information Division**

**1988**

## INFLUENCE OF RUBBING ON ROTOR DYNAMICS

Agnes Muszynska, Ph.D.  
Wesley D. Franklin  
Robert D. Hayashida

Bently Nevada Corporation  
Minden, NV 89423

### ABSTRACT

This paper presents the progress report from the experimental and analytical studies on the influence of rubbing in rotating machines, with direct application to the space shuttle hydrogen turbopump. The dynamic response and vibrational pattern of the rotor when rubbing occurs is carefully measured and correlated with various physical factors such as rotative speed, impacting conditions, dry/lubricated friction, system stiffness modifications, mode shapes, and unbalance.

A categorization of rub-related dynamic responses of rotors, as well as pattern recognition for identification of such machine malfunction, emerges from this study. Mathematical models of the observable physical phenomena are built. These models can be implemented in more complex, computerized rotor dynamic analyses.

### 1. INTRODUCTION

Improving machine efficiency, by increasing the power and operational velocity of machines, represents a significant trend in technology. In rotative machines, higher efficiency is often achieved by tightening operating clearances between stationary and rotating elements. Reduced clearances lead more frequently to rotor-to-stator rubs. The most common types of rubs in rotating machinery are blade tip rubs and seal rubs. Both are caused either by casing distortion or by the displacement of the rotor centerline and/or high rotor vibrations, which are, in turn, caused by imbalance, gravity force, various radial preloads, fluid dynamic forces, thermal expansion, misalignment, etc.

Rub occurs, therefore, as a secondary effect of some initial machine malfunction. Once a rotor starts rubbing, however, this effect becomes dominant in the dynamic response. Vibrations may become violent. They can easily cause serious damage and even lead to machine catastrophic failure.

### 2. CHARACTERIZATION OF RUB PHENOMENA IN ROTATING MACHINERY

#### 2.1 Definitions

The normal operation of a rotating machine is related to an appropriate torque/load balance and consists of main rotative motion of the shaft (together with all rotating elements associated with the shaft) performed with an appropriate rotative speed around the appropriate axis. This main motion can be accompanied

by a limited level of lateral/torsional/longitudinal vibrations (parasitic motion) of the rotor itself and a limited level of vibration of stationary (nonrotating) parts.

Rub in a rotating machine is a malfunction condition associated with the physical contact of rotating and stationary parts which otherwise should not be in contact. As a result of rub the "normal operation" of the machine is affected. Rub changes the system force balance and dynamic stiffness, which results in modifications of the machine motion. The effect is usually associated with a decrease of the amount of energy in the main motion and an increase in the level of "parasitic" motion.

## 2.2 Rub-related changes in the rotating machine force balance and dynamic stiffness

2.2.1 Coupling effect. Due to the physical contact of the rotating and stationary parts, the mechanical structure will be involved in motion changes. This effect is similar to coupling an additional structure to the existing ("normal") structure. Since the rub-related coupling is usually time dependent (on/off periodic type), the system dynamic stiffness also becomes periodically time dependent. The rub coupling effect will vary with:

- contact normal forces
- contact surface area
- flexibility (degrees of freedom) of the contacting elements dynamic stiffnesses of the normally operating structure and the additional, coupled additional, coupled structure (strong/weak coupling)
- time of contact versus time of separation:

Parameters of concern for mathematical modelization are:

- "normal operation system" and "coupled system" spectra of natural frequencies and corresponding modes
- function of coupling and decoupling relationship versus time and its relation to rotor unbalance.

2.2.2 Stiffening effect. An additional effect of rub-coupling results in stiffening of the shaft as it is forced to rotate in a bent position. This results in an increase of the system rigidity and a slight increase of the natural frequencies.

Parameters of concern for mathematical modelization:

- stiffnesses of the normally supported shaft and bent shaft.

2.2.3 Friction effect. Friction accompanies the relative motion of rotor/stationary parts during their contact. It produces the usual friction-related effects: wear (grinding, pitting) of the rubbing surfaces together with heat generation (up to metal melting temperatures). Since the rubbing surface relative tangential velocity is usually high, the destructive effects of friction can be extremely strong producing significant damage within very short time. Friction is a nonlinear phenomenon. Due to the wear effect, the surface rubbing conditions change very fast with time. This may lead to either widening clearances and elimination of the contact or to an enlargement of the contact surface

area (breaking-in effect). Therefore, in a short time either rub stops (causing some short-time transient conditions for the rotor system) or rub will continue with further continuous modification of conditions and dynamic responses.

Parameters of concern for mathematical modelization:

- normal forces at the contact surfaces and contact stresses
- surface area of contact
- friction conditions (dry/fluid lubricated) leading to realistic model of the friction force
- time intervals of contact/separation.

2.2.4 Impacting effect. Impact conditions occur when the contact of rotor/stationary part occurs instantaneously. An impact generates a wide frequency spectrum of exciting forces; however, repetitive periodic impacts can result in a definite spectrum of periodic excitation.

Impacts create an "after impact" response -- most often, a rebounding motion (separation) with the initial direction depending on impact conditions (material, and its rigidity in particular) and relative tangential velocities. From the dynamic point of view, impacting is a highly nonlinear phenomenon.

Parameters of concern for mathematical modelization:

- impact surface conditions, restitution coefficient/function, incoming velocities
- time intervals of contact/separation.

2.2.5 Fluid dynamic forces and thermal unbalance. Rub-related wear of seal surfaces causes an increase of clearances and changes in the flow pattern of the working fluid. This generates new fluid dynamic forces and modifications of thermal conditions which, in turn, can change clearance situations due to thermal expansion. Both effects have to be investigated when rub-results in the conditions of slowly or rapidly increasing clearances.

### 2.3 Rub location

Generally rub locations can be classified in terms of occurrence along the shaft axis:

- at one axial location
- at several axial locations.

At each axial location, rub can occur:

- at one angular radial location (seals or other stationary parts) with determined area of contact
- at several angular radial locations (e.g. rebounding motion inside a seal)
- continuously maintaining the shaft/seal contact (for an obviously limited time).

Relating to the shaft axis, the rubbing surfaces can be located radially, axially, or conically.

## 2.4 Conditions leading to rub

Rub is a secondary phenomenon usually resulting from a primary cause which perturbs the "normal operating conditions." This primary cause can originate from various sources (such as unbalance, misalignment, fluid dynamic forces in main flow/bearings/seals leading to instability, etc.). The occurrence of the "primary source" results in:

- changes of shaft centerline position
- and/or shaft vibrations (most often lateral mode).

The amount of the centerline displacement and the vibration amplitude have to be considered in relationship to clearance values (together with their tolerances). By taking into account the most probable mode of the shaft centerline bow for the operational conditions, the most probable "weak" point, which is susceptible to rub can be determined. The first "weak point" is the one where rub starts. This causes a modification in system properties which eventually may lead to rubbing in other locations. The conditions leading to rub must, therefore, be considered in a sequential form.

## 2.5 Transient character of rub-related effects

Most of rub-related dynamic phenomena are characterized by continuously changing conditions due to "grinding effect" at the rubbing surfaces. Steady-state conditions can be maintained during significantly long (but limited) time only if:

- rub is very light (short contact time and/or low contact normal forces), or
- there are full annular backward rub conditions (the regime which is most often destructive for the machine i.e., the "steady state" lasts a limited time before transforming into a transient regime of destruction).

## 2.6 Expected modifications of the rotating machine vibrational response

2.6.1 Frequency. The starting point is no-rub machine operation. Machine vibrational response frequencies of interest are:

- shaft actual rotative speed,  $\omega$
- spectrum of machine natural frequencies,  $\omega_n$ ,  $n = 1, 2, 3, \dots$

Rub can cause machine element vibrational responses with frequencies being:

- a fraction ( $p/r$ ) of the rotative speed  $\omega$  ( $p$ ,  $r$  are integers)
- one (or more) system natural frequencies  $\omega_n$  (note the coupling and stiffening effects causing modifications in the natural frequency spectrum)
- higher harmonics (multiples) of the lowest frequency component ( $q\omega(p/r)$  and/or  $q\omega_n$ ;  $q = 2, 3, 4, \dots$ )
- combinations of the above.

Note: Higher harmonics (multiples) are generated (or significantly magnified if they already exist in limited amount in the vibrational response) due to strong

nonlinear effects of rub-related friction, impacting, and the on/off type of motion.

2.6.2 Amplitude, phase. Both amplitude and phase (the latter for synchronous  $1\times$  and multiples of synchronous  $2\times, 3\times, \dots$  components) of the system responses are modified by rub.

Response frequency content, amplitudes, phases of the response components, static displacement position, and shaft orbital motion carry significant rub-diagnostics information.

2.6.3 Mode of shaft-centerline. Rub can modify the shaft-centerline modal deflection shape. The information can be significant for localization of rub area.

### 3. MATHEMATICAL MODELLING

In the mathematical model of the rubbing rotor the modal concept is applied. The rotor model is limited to one, two, or three lateral modes. At the first approximation, the rotor is considered laterally symmetric (isotropic). Up to four rub axial locations are possibly considered in the model. Since rub most probably occurs at the seal locations, the additional flow-related forces are introduced in the model. The rub forces included in the model describe the main physical phenomena taking place, when rotor-to-stator rub occurs, namely friction, system stiffness modifications and impacting. The rub forces are expressed in an "averaged" sense.

The rotor model is, therefore, as follows (Fig. 1):

$$M_i \ddot{z}_i + \alpha_i K_{2i-2} (z_i - z_{i-1}) + \alpha_{i+1} K_{2i} (z_i - z_{i+1}) + D_{s_i} \dot{z}_i + \alpha_i F_i + \alpha_{i+1} \beta_{2i} F_{i+1} = \quad (1)$$

$$= m_i r_i \omega^2 e^{j(\omega t + \epsilon_i)} + P_i e^{j\gamma_i}, \quad i = 1, 2, 3, \quad K_0 = z_0 = z_4 = 0, \quad z_i = x_i + jy_i, \quad j = \sqrt{-1}$$

where

$$\alpha_i = \frac{1}{1 + \beta_{2i-2}}, \quad \beta_{2i} = \frac{K_{2i}}{K_{2i+1}}$$

Eqs. (1) describe the rotor lateral motion ( $x_i, y_i$  are horizontal and vertical displacements of the rotor corresponding axial locations "i" respectively).  $M_i, K_i, D_{s_i}$  are modal masses, stiffnesses and damping coefficients respectively. The parameters  $\alpha_i$  and  $\beta_{2i}$  take into consideration that rub location does not

coincide with the modal mass axial location.  $M_i r_i e^{j\epsilon_i}$  are modal unbalance vectors,  $\omega$  is rotative speed,  $P_i e^{j\gamma_i}$  are constant radial force vectors. The rub and fluid forces are described by the functions  $F_i$ , and impact velocity relationships:

$$F_i = \sum_{\ell=0}^n f_{\ell i}(\Omega t) [K_{r_i} |\dot{\tilde{z}}_i| + N_{\ell i} (1 + j\mu_{\ell i})] e^{j\delta_{\ell i}} + D_i (\dot{\tilde{z}} - j\lambda_i \omega \tilde{z}_i) + K_{b_i} \tilde{z}_i \quad (2)$$

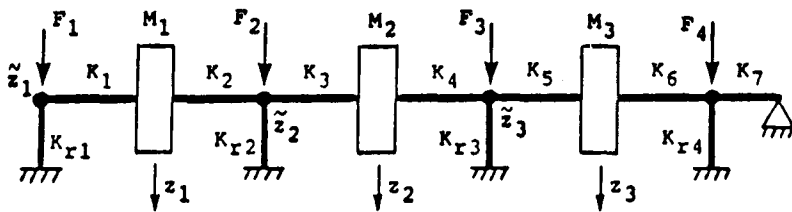


FIG. 1 RUBBING ROTOR/BEARING/SEAL MODEL.

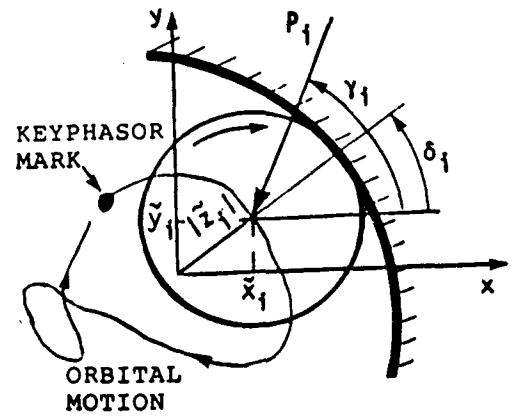


FIG. 2 RADIAL LOCATION OF RUB.

$$\ddot{z}_i(t_\ell) = -\kappa \ddot{z}_i(t_{\ell-1}), \quad i = 1, 2, 3, 4, \quad \ell = 0, \dots, n \quad (3)$$

where  $\ell=0, 1, \dots, n$  indicates number of the consecutive rotor-to-stator contact within one period  $\Omega t$  of rotor precessional motion ( $t$  is time). The functions  $f_{\ell i}$  describe the timing of "contact" versus "no contact."  $K_{r i} |z_i|$  is radially applied additional stiffness force due to rub.  $N_{\ell i}$  is the normal force at rubbing surfaces;  $\mu_{\ell i}$  is friction coefficient. The angle  $\delta_i$  indicates rub location (Fig. 2).  $D_i, k_{b i},$  and  $\lambda_i$  are fluid film radial dampings, stiffness, and circumferential velocity ratios respectively, at seal and bearing locations.  $D_i, K_{b i},$  and  $\lambda_i$  are nonlinear functions of  $|z_i| = \sqrt{x^2 + y^2}$ . Eq. (3) gives the impacting condition;  $\kappa$  is the coefficient of restitution. Due to rotation-related tangential velocity component,  $\kappa$  might acquire more complex form.

Eqs. (1), (2), and (3) represent the mathematical model of the rubbing rotor. Note that three modes are coupled in Eq. (1). The modal masses and stiffnesses can be obtained from numerical analysis (transfer matrix or FE methods followed by reduction to three modes), and/or identified from an experiment, using dynamic stiffness concept. The classical modal approach would leave each mode uncoupled from the others, thus would make the analysis much simpler. The uncoupled model of a rubbing rotor is a particular case of Eqs. (1), (2), and (3) and was analyzed in [1]. In the model proposed here a more general case is considered. It may provide results which correlate rub phenomena with rotor modal responses.

#### 4. ROTOR-TO-STATOR RUB EXPERIMENTAL RESULTS

##### 4.1 Scope

A rub fixture used in conjunction with the rotor system shown in Fig. 3 allows the exploration of rotor vibrational response during partial rub conditions. In this part of the study, emphasis has been placed on the comparison of results from rotor vibrational responses generated by rotor-to-stator partial rubs with varying stator compliances.

**4.1.1 Rub Fixture Mechanism.** The rub fixture (Fig. 4) consists of a plunger supported in two bearings allowing for its linear motion. The rub block is located at one end of the plunger to allow its positioning along the rotor shaft. The plunger is both positioned and restrained axially by a compression spring located in the fixture body. Adjustments to the spring allow for axial position

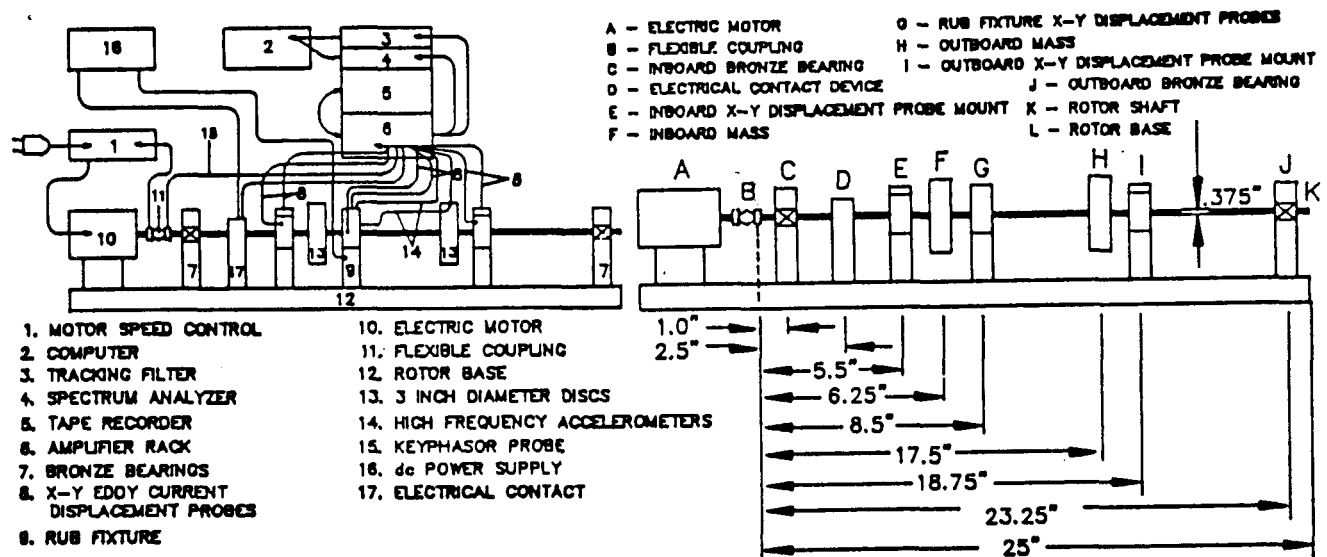


FIG. 3 RUB TEST RIG.

and preload to be made independently of one another. Located at the plunger end opposite the rub block is a displacement probe monitoring the axial motion of the plunger.

4.1.2 System Configuration. The rub test rig presented in Fig. 3 shows both the rotor and data acquisition system configuration. The slender shaft rotor incorporates two masses and is supported in bronze sliding bearings at both ends of the shaft. The rig allows for various modifications, such as mass, stiffness, modes, unbalance, preload rub materials, rub surface conditions, etc., thus, providing a rich matrix of parameters for the investigation of the rub-related dynamic phenomena.

4.1.3 Transducer Selection/Application. All rotor vibrational data are captured via X-Y eddy current noncontacting displacement probes mounted at three axial positions along the shaft. These probes are specifically helpful when identification of low frequency vibrations are of interest. To measure high frequency vibrations, two accelerometers are used. One accelerometer is mounted vertically on the rub fixture base, the other horizontally on the rub plunger. It should be noted that appropriate applications of proximity probes and accelerometers are necessary to obtain useful and interpretable vibration information. Accelerometers measure casing vibrations, not the vibration main source, rotor vibrations. Thus, the casing transmissibility plays a significant role in the results. In addition, the accelerometers do not provide enough sensitivity to detect low frequency components and, therefore, high amplitude low frequency, potentially destructive vibration may not be detected. On the other hand, accelerometers provide useful information when looking at the higher order frequency vibration components generated during rub. A Keyphasor<sup>®</sup> probe provides rotative speed and an angular reference for rotor phase measurements.

An extremely light rub may not be detected by either vibration signals or a significantly altered orbit shape. Therefore, an electrical contact device is used to more accurately identify the rotor-to-stator contact. Utilizing 1-volt dc potential, any mechanical contact between the rotor shaft and rub block pro-

vides a circuit that can be monitored with continuity position/timing correlated to the Keyphasor signal and plunger movements. Information obtained from this device is quite useful, as a rub condition does not require any detectable plunger movement. This is due to the fact that as plunger compliance decreases (spring preload increases), a greater impact force is necessary to overcome the spring force and thus produce motion.

#### 4.2 Test Procedure

After achieving the desired balance state of the rotor, a controlled unbalance was introduced at the inboard plane, this unbalance being used to obtain a required level of synchronous vibrations in order to initiate a rotor-to-stator rub. Both transient (during start-ups) and steady-state data (at constant rotative speed) have been monitored and presented in spectrum cascade and orbit formats respectively. Operating speeds (for data recording) range from 300 to 10,000 rpm, running well above the first and second balance resonances (1600 and 4200 rpm respectively) for this rotor rig.

The controlled unbalance weight is 0.48 grams at 0.0 degrees relative to the Keyphasor notch. The slow roll amplitude was maintained less than 0.5 mils at all times. The sample results of the experiment are presented in the next section. For the series of data presented, all runs were with the unbalance located at the inboard plane. The rub block material was aluminum with a plunger spring stiffness of 107 lb/in.

#### 4.3 Results

The data presented in Figs. 5 to 8 are from runs with two plunger preloads of 3.34 lb and 10.03 lb respectively. The chosen preloads are representative of a rotor system with high and low stator compliances.

Transient rub data from displacement probes show the presence of both subsynchronous and supersynchronous vibration components. Data from the horizontal accelerometer mounted on the plunger shows highly defined, well-ordered harmo-

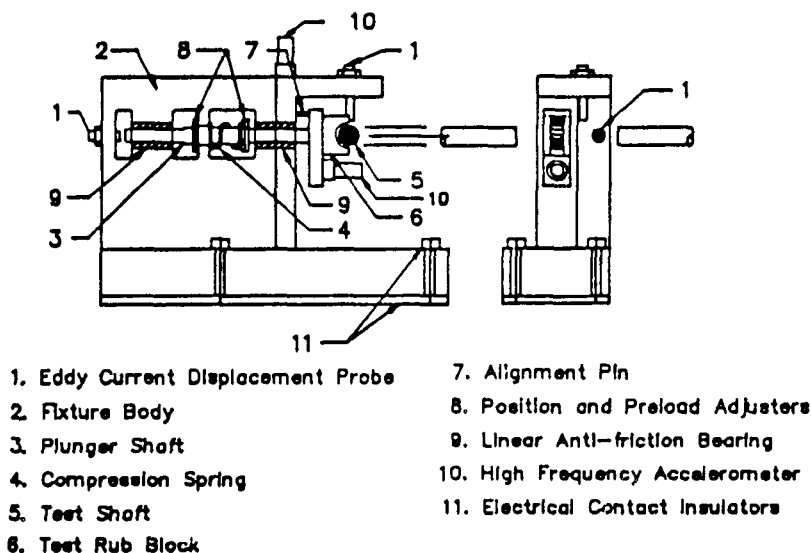


FIG. 4 RUB FIXTURE.

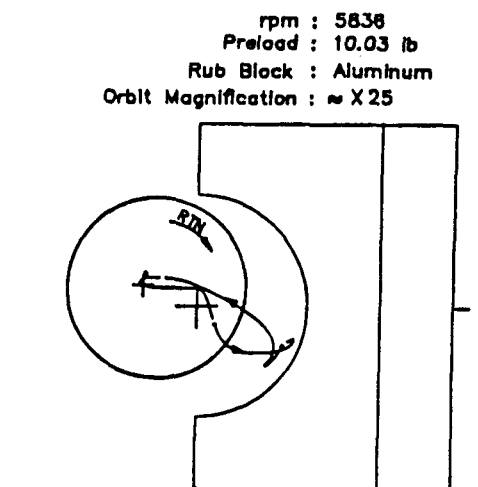


FIG. 5 ORBIT OF THE SHAFT RUBBING AGAINST RUB BLOCK.

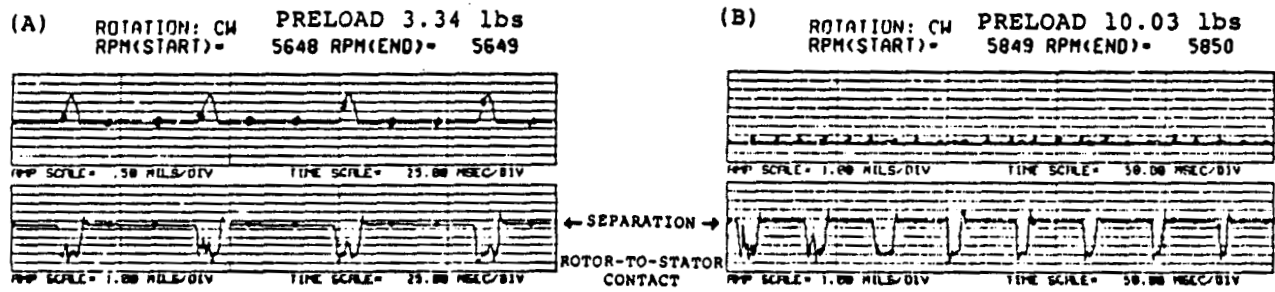


FIG. 6 TIME BASE RESPONSE OF THE PLUNGER (TOP) AND ELECTRICAL CONTACT SIGNAL (BOTTOM) FOR THE CASE OF 3.34 LB PLUNGER PRELOAD (A) AND 10.03 LB PRELOAD (B). PLUNGER MOTION AT THIS ROTATIVE SPEED OCCURS EVERY THIRD ROTATION OF THE SHAFT (SEE KEYPHASOR MARK). ITS MOTION IS CONSISTENT WITH THE ROTOR-TO-STATOR CONTACT/NO CONTACT PERIODICITY. HIGHER PRELOAD REDUCES PLUNGER AMPLITUDE (B).

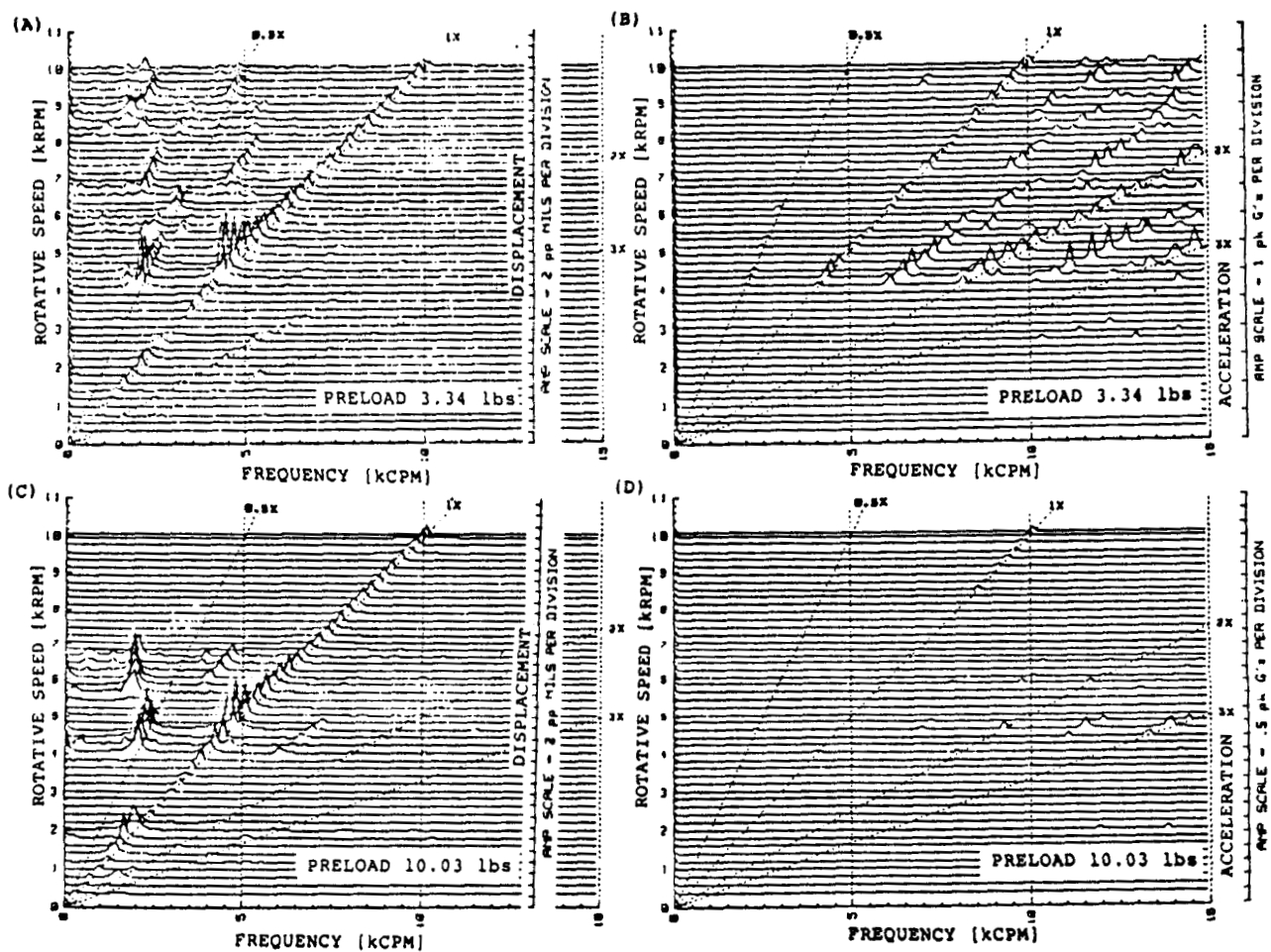


FIG. 7 SPECTRUM CASCADE OF RUBBING ROTOR VIBRATIONAL RESPONSE DURING START-UP, MEASURED BY RUB FIXTURE HORIZONTAL DISPLACEMENT PROBE ((A) AND (C)) AND ACCELEROMETER ON PLUNGER MECHANISM ((B) AND (D)) FOR TWO VALUES OF THE PLUNGER PRELOAD: 3.34 LBS ((A) AND (B)) AND 10.03 LBS ((C) AND (D)). NOTE RUB-RELATED SUBSYNCHRONOUS VIBRATIONS MEASURED BY THE DISPLACEMENT PROBE AND LACK OF SUBSYNCHRONOUS COMPONENTS IN THE ACCELERATION SPECTRUM. NOTE A DECREASE OF HIGHER FREQUENCY COMPONENT AMPLITUDES WITH INCREASE OF STATOR RIGIDITY.

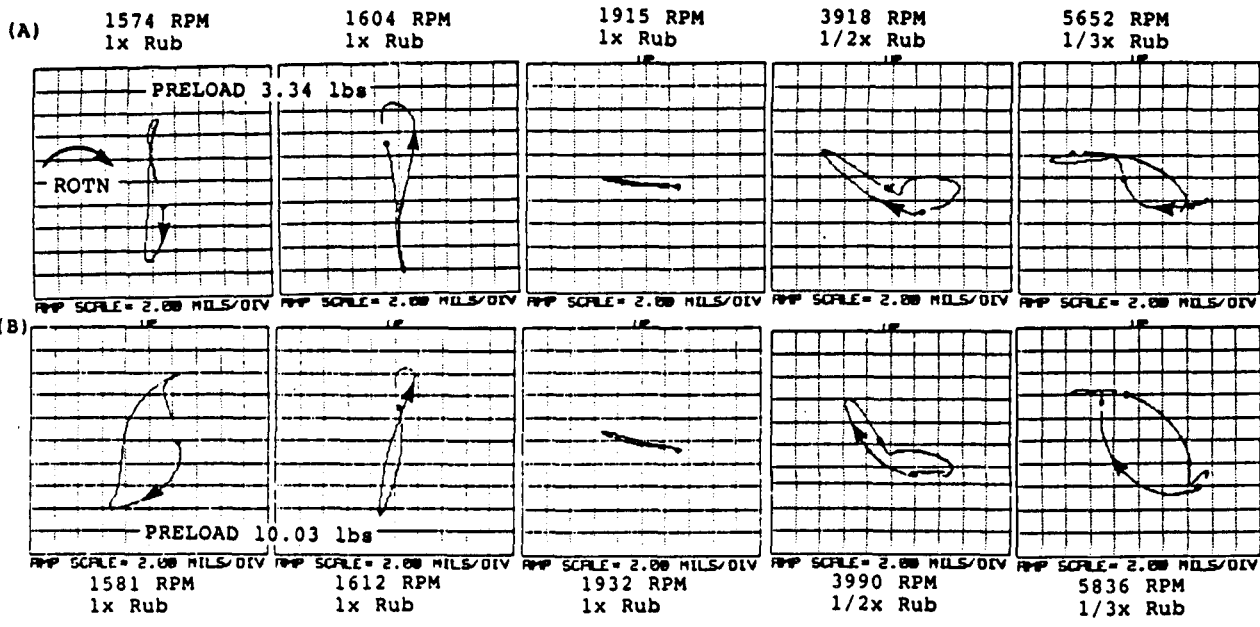


FIG. 8 SHAFT ORBITAL MOTION FOR A SEQUENCE OF ROTATIVE SPEEDS, AS SEEN BY RUB FIXTURE X-Y DISPLACEMENT PROBES FOR TWO VALUES OF THE PLUNGER PRELOAD: 3.34 LBS (A) AND 10.03 LBS (B). NOTE THE VARIETY OF THE ORBITAL PATTERNS.

tics. However, the prevalence of these components diminishes with increasing preload (decreasing compliance) of the plunger mechanism.

Steady-state data for both plunger preloads presented in orbit format also supports the presence of both subsynchronous and supersynchronous vibration components indicated by multiple Keyphasor marks and external loops. Orbit plots represent the rotor shaft centerline motion. As an example, to better illustrate the relationship between rub and shaft motion, the orbital (precessional) motion of the rotor can be overlaid with a figure of the rub block Fig. 5. Note that the orbit is highly magnified while the rub block and shaft sizes are reduced, so the figure represents the actual behavior in qualitative terms only. The orbit very clearly indicates the rebounding effect of the rotor shaft caused by the rub.

With less preload on the plunger mechanism (greater casing/stator compliance), accelerometer data from the plunger indicates significant excitation of lower frequency components in the range from 5 kcpm to 15 kcpm, (83.3-250 Hz), with displacement probes showing significant subsynchronous components (1/4x, 1/3x, 1/2x). As plunger compliance decreases, accelerometer, as well as displacement probe data indicate decreasing excitation of lower frequency subsynchronous components. Relatively speaking, lower frequency vibrations correspond to large displacements over long time intervals. As plunger preload increases, its displacement must decrease, providing external forces remain constant, thus resulting in the progressive lack of lower frequency components.

Data captured while observing plunger motion is presented together with data from electrical contact device (Fig. 6). This data clearly represents the time of contact versus separation, as well as transient vibrational process of the plunger when the contact is broken.

#### 4.4 Conclusions

From the rub data presented, it becomes apparent that rub plays a large role in the rotor vibrational response. This particular study allows manipulation of the casing compliance, which may also be correlated to stator compliance in the event of a rotor-to-stator rub. The effect in either case, is a periodic modification of the system stiffness during rub and modification of impacting conditions. The large amplitude subsynchronous vibration response indicated by the displacement probes can be correlated to increasing plunger preload. The increase in plunger preload effectively increases the coefficient of restitution, thus the velocity of the rotor shaft after impact and resultant displacements are accordingly greater.

#### 5. APPLICATION TO SSME: HPFTP SIMULATING RIG EXPERIMENTAL RESULTS

In order to develop a high pressure fuel turbo pump (HPFTP) simulating system to study rotor-to-stator rubs that was safe for experimentation in the laboratory, the rotational kinetic energy of the system needed to be reduced. This has been accomplished by designing and building a simulation system with both lower rotational inertia and reduced rotative velocity (Fig. 9). To maintain a recognizable relationship between the vibrational data taken using the simulation system and that of the HPFTP, the simulation system first three mode shapes have been matched to the predicted HPFTP mode shapes (Fig. 10), and the ratiometric relationship between the first three natural frequencies maintained (Table 1). These constraints dictated a system consisting of a 0.375" diameter steel shaft with four 1.5" diameter disks mounted on the shaft to simulate pump and turbine stages (Fig. 9). The pump stage disks are 0.5" thick while the turbine disk is slightly thicker (0.75"). Axial dimensions of the rig and HPFTP rotors are the

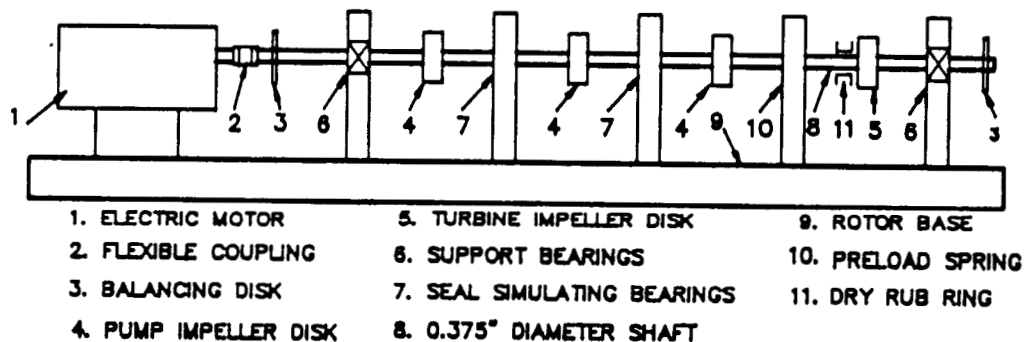


FIG. 9 HPFTP SIMULATION RUB RIG.

TABLE 1 SUMMARY OF RESONANT SPEED FOR HPFTP AND RUB RIG AT DIFFERENT PRESSURES.

Mode	HPFTP rpm	SCALED HPFTP rpm	0 psi	5 psi	10 psi	15 psi
1st	16828	1870	1650	1900	2200	2300
2nd	30881	3435	3000	3100	3350	3750
3rd	46286	5150	5400	4800	5100	5200

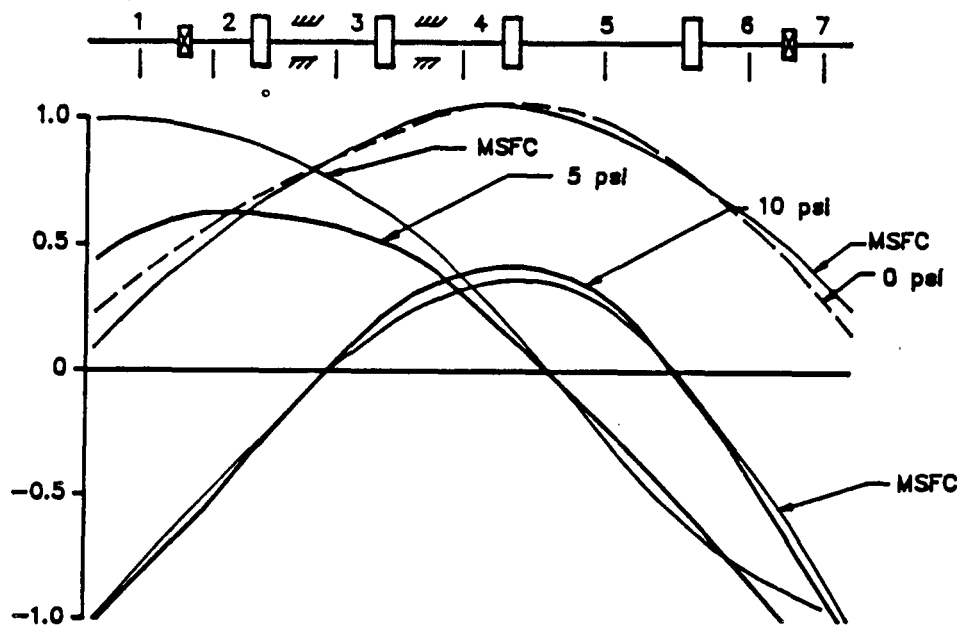


FIG. 10 COMPARISON OF MSFC HPFTP MODE SHAPES WITH SIMULATION RUB RIG MODE SHAPES AT CORRESPONDING OIL PRESSURES IN THE SEAL-SIMULATING BEARINGS. THE NUMBERS ON THE RIG SKETCH INDICATE DISPLACEMENT PROBE LOCATIONS.

same. The shaft is supported by rolling element bearings suspended within a rigid frame with four radial springs positioned 90 degrees apart. This configuration produces a relatively soft support with light damping. The interstage seals between the pump stages are simulated with externally pressurized oil bearings. The system stiffness at these locations can be modified by varying the inlet oil pressure. This allows the simulation of different flow conditions within the turbo pump. The principal rub locations are at the two seal simulating bearings, and at a third non-lubricated rub ring mounted inboard of the turbine disk. All the rub positions have a 10 mil diametral clearance and are instrumented with an electrical circuit which indicates the rotor-to-stator contact, i.e., the occurrence of rub. An additional rolling element bearing suspended with weak springs in a rigid frame is located inboard of the last pump stage to simulate the shaft unidirectional radial preload induced by the fuel flow in the HPFTP.

Representative rub data is shown in Fig. 11. The data was obtained at a constant rotative speed of 4000 rpm by introducing a sequence of preload forces at point P. Seal simulation bearings were run with no lubrication. The data consists of orbits and horizontal and vertical spectral information at the axial shaft locations for three different rub conditions, following the increasing radial preload: no rub, light rub, and heavy rub. As can be seen in the data, there is a definite change in both orbit shapes and spectral content for the three different rub conditions. In the no-rub case the rotor vibrates predominately with once-per-turn frequency. Some small free vibration components with system natural frequencies may appear in the spectrum. The orbits are circular with jitter. The introduction of light rub increases the relative importance of the subsynchronous half-per-turn frequency component which transforms the orbit to the "figure eight" shape. During heavy rubs the twice and three times per turn components become more dominant, along with stronger excitation of the system natural frequencies, producing orbits with more elliptic shapes and jitter.

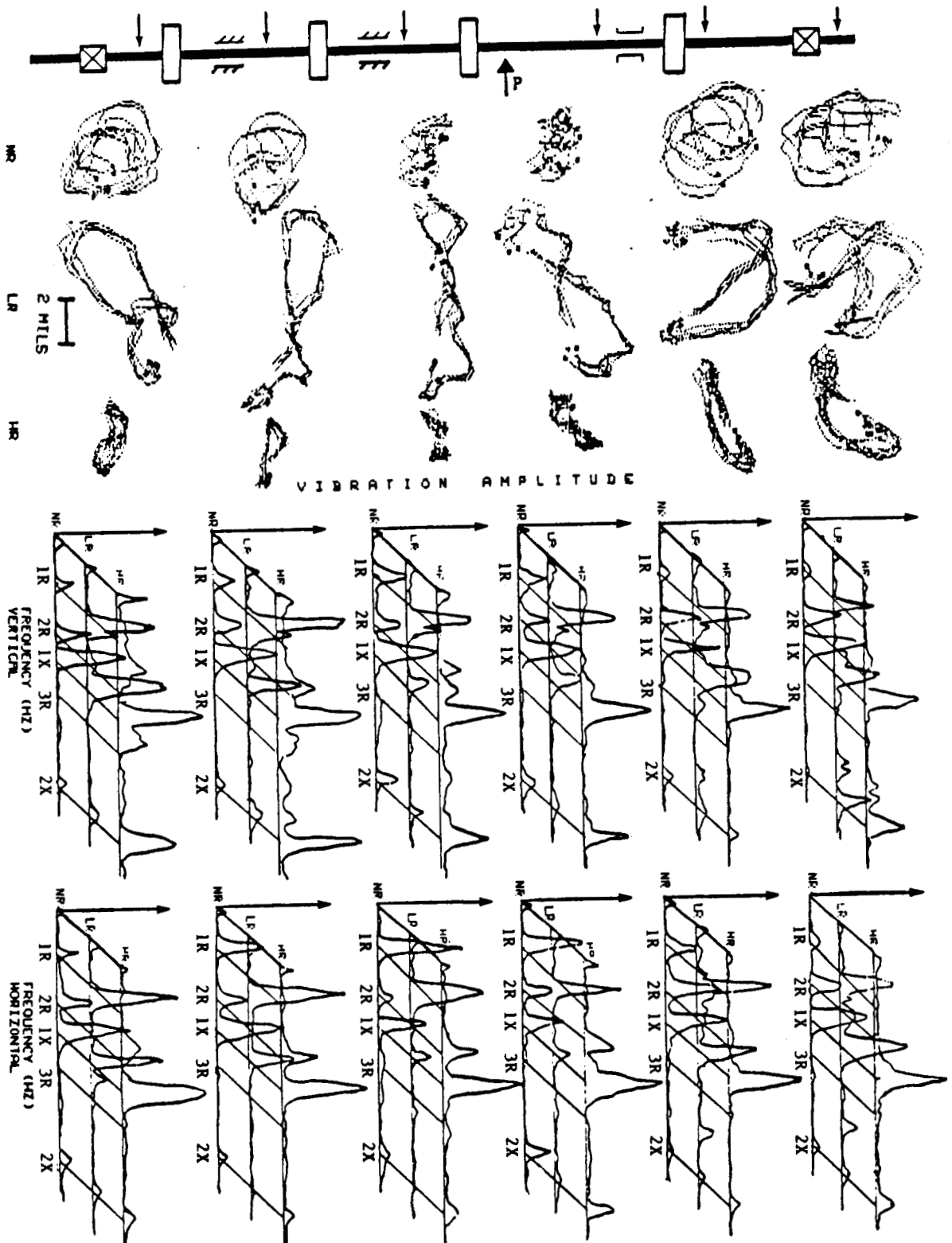


FIG. 11 ORBIT AND SPECTRAL SIGNAL CONTENT AT SIX AXIAL LOCATIONS FOR NO RUB (NR), LIGHT RUB (LR), AND HEAVY RUB (HR) CONDITIONS GENERATED BY INCREASING PRELOAD AT POINT P. 1R, 2R, 3R DENOTE CORRESPONDING NATURAL FREQUENCIES OF THE SYSTEM.

Another test performed, at MSFC request, was the effect of rub during rotor subsynchronous self-excited vibrations due to fluid flow interaction, known as whirl/whip instability. This test was done using a brass rub screw fixture located inboard of the third pump impeller to provide a controlled rub. Data was taken again for three separate rub conditions: "no rub", "intermittent rub", and "continuous rub" (Fig. 12). The data labeled "no rub" provides reference level indicating the systems response in the absence of rub. Severe whirl/whip vibrations are present in the spectrum. The screw was then moved close enough to the shaft to provide rub at the higher vibration levels encountered during unstable operation (when whirl/whips occurs), but not during normal operation. For the third condition the screw was moved close enough to the shaft to provide light contact at all vibration levels. As can be seen from the data, the intermittent rub case shows an instability similar to the no-rub case pattern, however, with reduced amplitudes. In the continuous rub case, the whirl/whip instability is eliminated. This would be expected, since the amplitude of these vibrations is determined primarily by the nonlinearity of the system stiffness which significantly increases in this case. In the intermittent rub case there is some stiffness increase. This results in a reduction of the self-excited vibration limit cycle amplitude, as compared to the no-rub case. In the continuous rub case the stiffness has increased enough to prevent the instability due to fluid-flow in the seal simulating bearings.

## 6. FINAL REMARKS

This paper presented and discussed the selected results obtained during the study on influence of rubbing on rotor dynamics. Lack of space prevented the authors from including results of other accomplished tests, such as rotor-to-stator rubs for various unbalances, rub-related changes in shaft centerline, rotating system dynamic stiffness identification, friction force measurements and metallographic analysis of rubbing surface damage.

Another area of investigation not included within this report is the design and testing of the oil bearings used to simulate the HPFTP interstage seals. This knowledge and the testing methodology of identification of the bearing dynamic characteristics could be used to enhance future seal design efforts.

One more area of study was the reduction of hot fire test data for the HPFTP. The item of greatest concern to us was the lack of appropriately installed instrumentation to monitor the dynamic response of the pump rotor. It is almost impossible to improve a design without obtaining adequate diagnostic information from tests. We feel that for future tests this might be accomplished by better sensor selection and appropriate sensor location.

Rubs in rotating machinery and their dynamic effects on the machine performance represent very complex phenomena. In the adapted approach to study them, a distinct separation of various rub-affecting factors has been attempted.

A relatively simple test rig (as compared with HPFTP simulating rig) with adjustable rub block allows for investigation of the rub influence on the rotor behavior during various operating conditions. The results provide a good insight into the specifics of observable dynamic phenomena and create a basis for adequate mathematical modeling. There still remain several aspects of the rotor-to-stator rubs which require further investigation, in order to accomplish numerical parametric study of mathematical model.

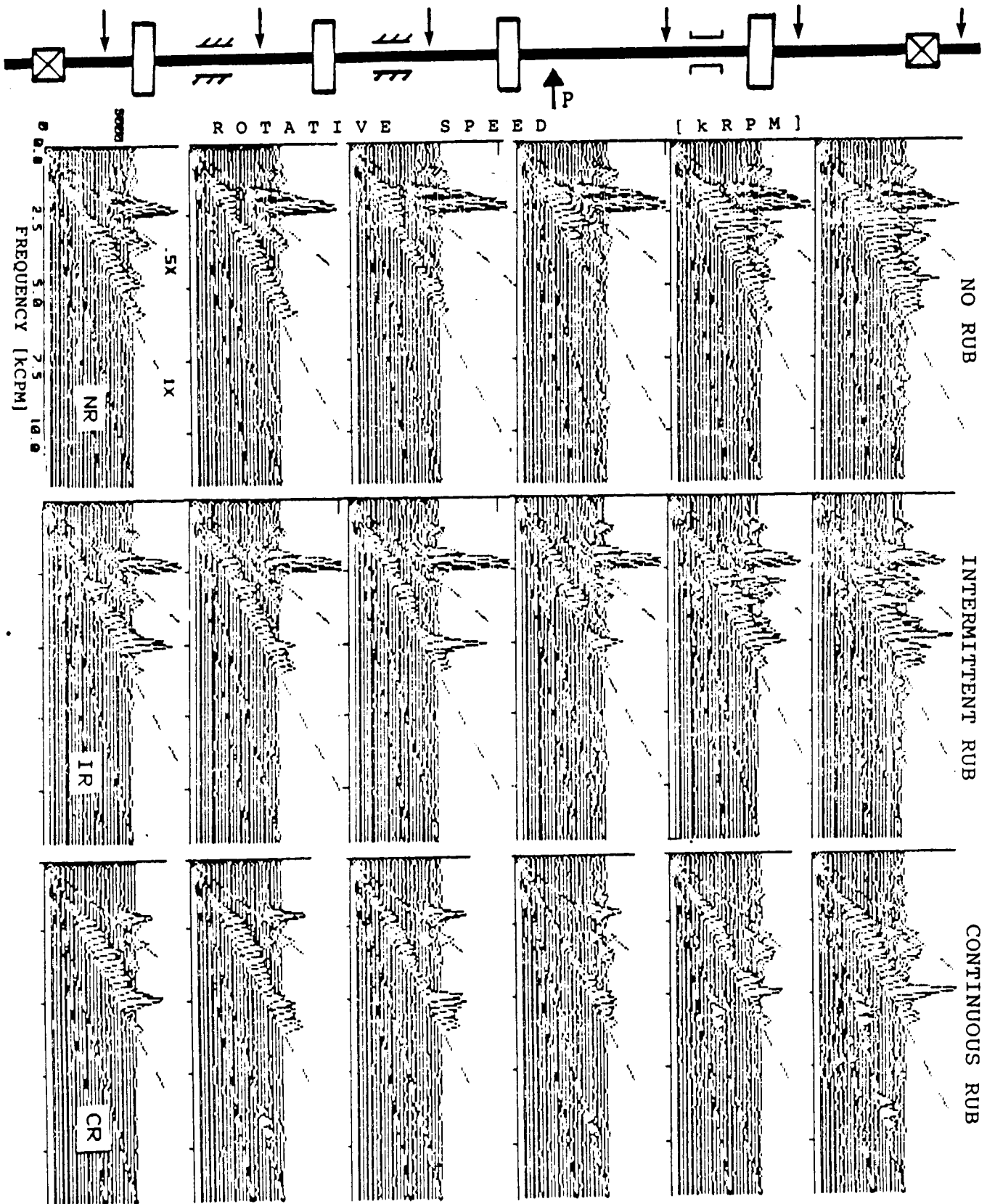


FIG. 12 SPECTRUM DATA FOR NO RUB (NR), INTERMITTENT RUB (IR), AND CONTINUOUS RUB (CR) GENERATED BY THE BRASS SCREW. RUB/FLUID-RELATED INSTABILITY INTERACTION.

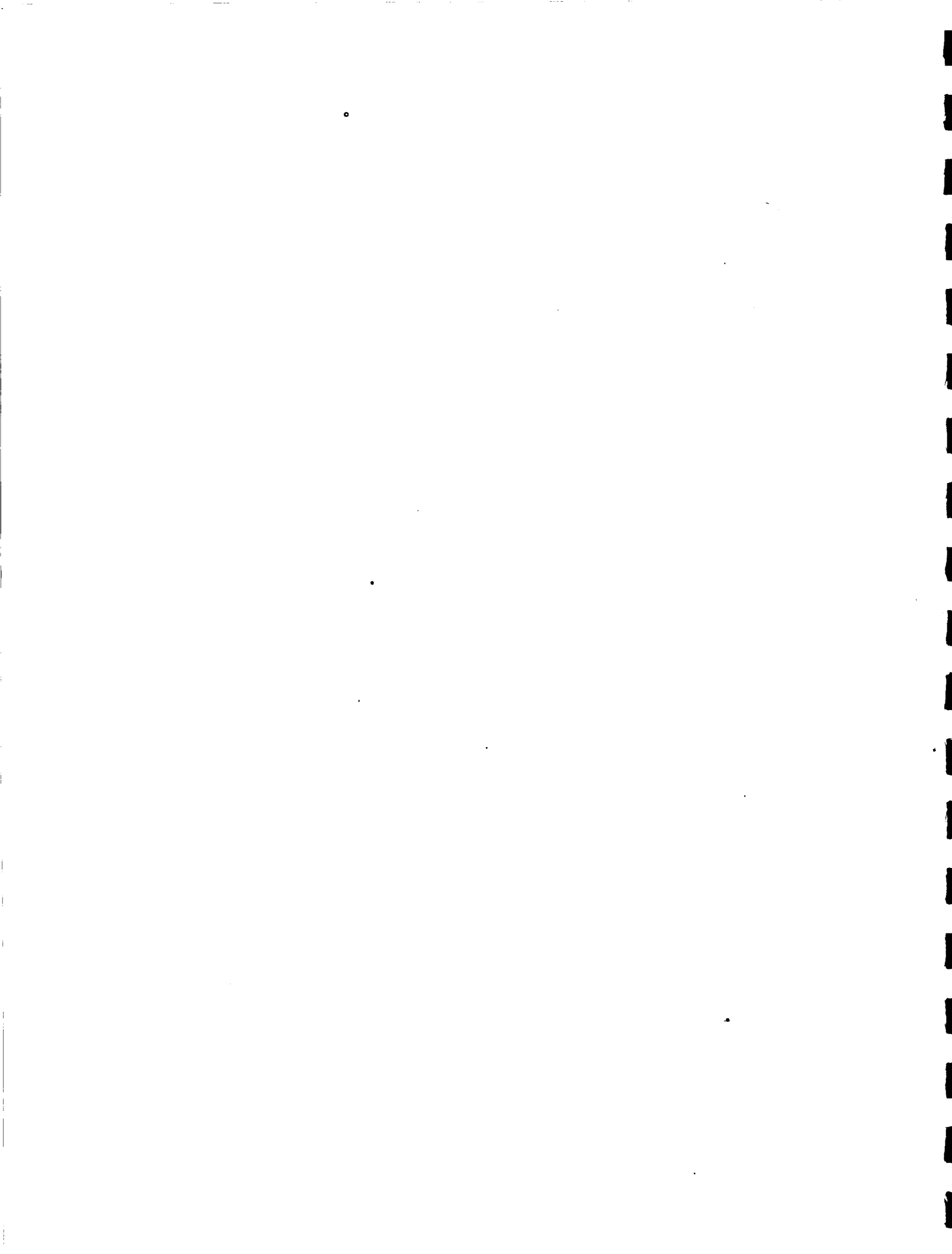
ORIGINAL PAGE IS  
OF POOR QUALITY

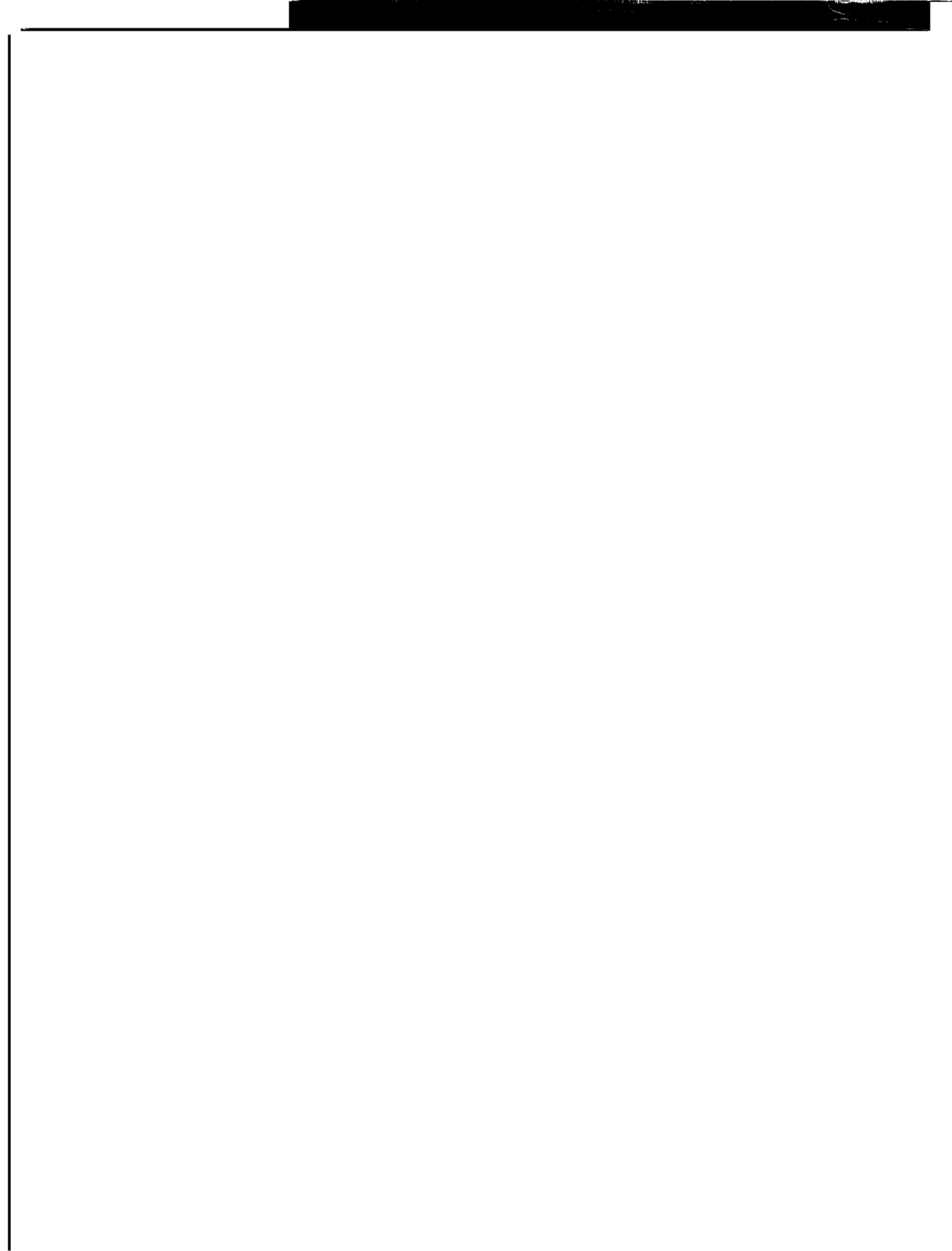
During the design of the HPFTP simulation rotor rig some problems other than rub have been encountered. An occurrence of similar problems on the actual HPFTP was also reported. Of these, two seem to be of interest to NASA. They are internal friction and fluid-related rotor instabilities. Some data showing the effect of rub on the fluid-related instability is included in this paper. Further investigation into this area of rotor dynamics is not a part of the current rub study, but might be considered in the future. Some results pertaining to the rotor internal friction and fluid-interaction instabilities have been obtained. The first were primarily associated with rotor disk attachments. The second cover several bearing and seal types at various operational conditions with shaft low eccentricities. The results are not included in this paper, as they are not directly related to the present rub study.

#### REFERENCE

1. Muszynska, A., Partial Lateral Rotor-to-Stator Rubs, Proceedings of the Third International Conference on Vibrations in Rotating Machinery, C281/84, York, U. K., September, 1984.

APPENDIX 3. INSTRUMENTATION DATA





# 3000 and 7000 Series Proximity Transducer Systems

## Technical/Ordering Information

TRANSDUCERS

### Radial vibration and thrust position measurements on machines requiring a small linear measuring range

The 3000 and 7000 Series Proximity Transducer Systems are ideal for measuring radial vibration and thrust position movements on machines that require only 40 to 50 mils linear range.

Operating on the same principle as Bently Nevada 7200 Series proximity probes, the 3000 Series Proximity Probes have no moving parts. They are not subject to mechanical wear that occurs on other types of transducers, such as shaft riders, Linear Variable Differential Transformers (LVDT), and potentiometers.

The 3000 and 7000 Series Proximity Transducers are not designed for use in API 670 type installations.

The 3000 and 7000 Series Proximity Transducer Systems provide vibration and position information for diagnostics as well as monitoring. You receive measurements of vibration amplitude, frequency, phase angle, and other rotor characteristics for determining specific machine malfunctions. The typical response of 0 Hz to 10 kHz enables you to measure static shaft position as well as dynamic motion.

The 3000 Series transducer systems utilize the 190 or 300 probes. The 7000 Series transducer systems use the 300 probe.

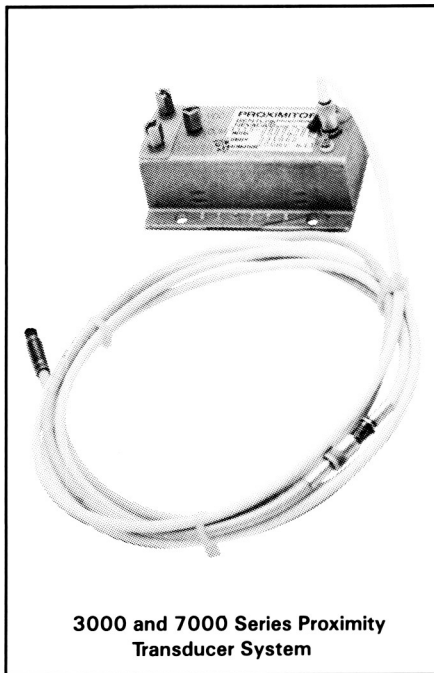
Each transducer system consists of a proximity probe, extension cable, and Proximitor.<sup>®</sup> All 3000 and 7000 Series transducer systems can be used in conjunction with the 7200 Series and 9000 Series Monitoring Systems.

### Types of measurements obtained with a 3000 and 7000 Series Proximity Transducer System

Whether used in static, low rpm, or rapidly-changing conditions, the 7000 Series Proximity Transducer Systems provide accurate linear, gap-to-voltage measurements. They can be used on virtually all types of rotating machines, including turbines, compressors, generators, pumps, and centrifuges, to make the following types of measurements:

Radial vibration for indicating bearing condition, rotor unbalance, and misalignment.

Thrust or axial position for determining bearing wear and potential bearing failure. (3000 Series probes only.)



3000 and 7000 Series Proximity Transducer System

- Shaft attitude angle or axial position, an indicator of rotor stability.
- Vibration amplitude and phase angle for plotting diagnostic information in polar and Bode formats.
- Eccentricity to measure the amount of rotor bow and the steady-state position of the rotor in the journal bearing.
- Peak-to-peak eccentricity to indicate bearing wear, heavy preloads caused by misalignment, lube oil breakdown, and electrostatic discharge.

### 190 and 300 Proximity Probes

The 190 and 300 Proximity Probes are offered in 12 configurations. You have a choice of fiberglass or Tonox<sup>®</sup> construction. Tonox versions are designed for use in high pH environments, but are not recommended for use in pressurized ammonia.

The 300 Proximity Probe is available in two linear measuring ranges: 50 mils with a scale factor of 200 mV/mil using a 3000 Proximitor and 60 mils with a scale factor of 100 mV/mil using a 7000 Proximitor.

The 190 Proximity Probe has a linear measuring range of 40 mils with a scale factor of 200 mV/mil when used with a 3000 Proximitor. It is the smallest standard probe that Bently Nevada offers.

### 3000 and 7000 Proximitors

A three-conductor, shielded cable provides the signal output and power source input interface between the Proximitor and a Bently Nevada monitor. The 3000 and 7000 Proximitors can be placed up to 1,000 feet from standard Bently Nevada monitors without degradation of performance.

The 3000 Proximitor is available in four configurations. The 7000 Proximitor is offered in two configurations.

The 3000 and 7000 Proximitors can be used with the 300 Proximity Probes. The 190 Proximity Probe is used with the 3000 Proximitor.

### Extension Cables

The combination of a probe lead and extension cable is designed to achieve a system length of either 15 or 20 feet. The extension cable is ordered in six-inch increments. It is available with or without protective armor.

Tonox<sup>®</sup> is a registered trademark of Uniroyal Corporation.

### Specifications

#### OUTPUTS

##### Calibrated Range:

**With 3000 Proximitor:** 50 mils for 300 probe; 40 mils for 190 probe. Range begins at approximately 20 mils from target surface.

**With 7000 Proximitor:** 60 mils, for 300 probes only. Range begins at approximately 30 mils from target surface.

##### Scale Factor:

**With 3000 Proximitors:** 200 mV/mil (8 V/mm).

**With 7000 Proximitors:** 100 mV/mil (3.94 V/mm).

**Frequency Response:** 0 to 600,000 cpm  $\pm$  1%

##### Power Requirements:

**With 3000 Proximitors:** -18 Vdc at 8.0 mA nominal.

**With 7000 Proximitors:** -24 Vdc at 8.0 mA nominal.



**BENTLY  
NEVADA**

P.O. BOX 157 • MINDEN, NEVADA USA 89423 • (702) 782-3611

TELEX: 7400983 • FAX: (702) 782-9253

# 3000 and 7000 Series Proximity Transducer Systems

## ENVIRONMENTAL

### Operating Temperature Range:

**3000 Proximito:** -29 °C to +66 °C  
(-20 °F to +150 °F).

**7000 Proximito:** -51 °C to +100 °C  
(-60 °F to +212 °F).

**Probe and extension cable:** -56 °C to +177 °C (-50 °F to +350 °F).

Tonox version probe specifications available upon request.

## DIMENSIONS

### Height:

**3000 Proximito:** 1.60 inches (40.6 mm).

**7000 Proximito:** 2.00 inches (50.8 mm).

### Width:

**3000 Proximito:** 2.14 inches (54.4 mm).

**7000 Proximito:** 2.38 inches (60.4 mm).

### Length:

**3000 and 7000 Proximito:** 3.14 inches (79.8 mm).

### Weight:

**3000 Proximito:** 7.2 ounces (204 grams).

**7000 Proximito:** 6.4 ounces (181 grams).

## Ordering Information

### Standard Mount Probe

A B C D E  
□□□□-□□-□□-□□-□□

### Option Description

- A Probe Catalog Number Option
- B Unthreaded Length Option
- C Case Length Option
- D Cable Length Option
- E Connector Option

A □□□□ Probe Catalog Number Option  
Select from Table 1.

### B □□ Unthreaded Length Option

Order in increments of 0.1 inches [01] for English thread, 10 mm [01] for metric threads.

#### English thread configurations:

Maximum unthreaded length: 9.0 inches [90]

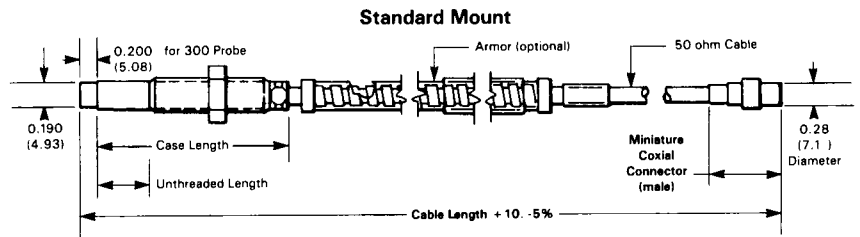
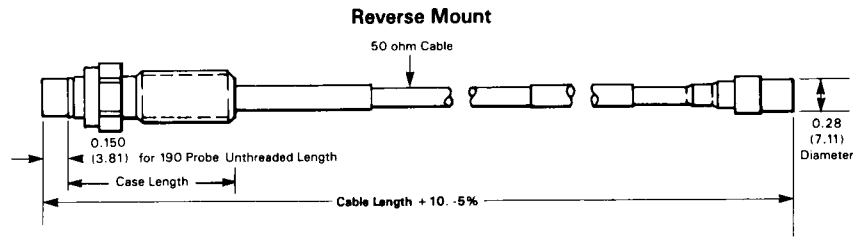
Minimum unthreaded length: 0.0 inches [00]

#### Metric thread configuration:

Maximum unthreaded length: 900 mm [90]

Minimum unthreaded length: 0.0 mm [00]

## 3000 and 7000 Series Probe Configurations



### C □□ Case Length Option

Order in increments of 0.1 inches [01] for English thread, 10 mm [01] for metric thread.

#### English thread configurations:

Maximum case length: 9.8 inches [98]

Minimum case length: 1.0 inches [10]

#### Metric thread configurations:

Maximum length: 250 mm [25]

Minimum length: 20 mm [02]

### D □□ Cable Length Option

Order in increments of 6.0 inches [06] (152 mm). Total length must exceed case length by a minimum of 4.75 inches (120.6 mm).

Maximum cable length: 36.0 inches [36] (914 mm).

Minimum cable length: 6.0 inches [06] (152 mm).

### E □□ Connector Option

- 00 Without connector.
- 02 With miniature male coaxial connector.

### Reverse Mount Probe

Fiberglass A B C  
-□□□-04-02-12-□□-□□

Tonox A B C  
-□□□□-02-12-□□-□□

### Option Description

- A Probe Catalog Number Option
- B Cable Length Option
- C Connector Option

Note: The unthreaded length and case length are supplied in standard, pre-set lengths.

### A Probe Catalog Number Option

□□□□ Fiberglass or □□□□□ Tonox  
Select from Table 1.

### B □□ Cable Length Option\*

Order in increments of 6.0 inches [06] (152 mm). Total length must exceed case length by a minimum of 4.75 inches (120.6 mm).

Maximum cable length: 36.0 inches [36] (914 mm).

Minimum cable length: 6.0 inches [06] (152.40 mm).

\* To obtain the electrical length, multiply the cable length by 2.

# 3000 and 7000 Series Proximity Transducer Systems

- C**  **Connector Option**  
 00 Without connector.  
 02 With miniature male coaxial connector.

**Proximity**

**20929 -  3000 Series Proximitors**

- 01 For combined system electrical length of 15 feet, with 300 tip transducer.  
 02 For combined system electrical length of 15 feet, with 190 tip transducer.  
 03 For combined system electrical length of 20 feet, with 300 tip transducer.  
 04 For combined system electrical length of 20 feet, with 190 tip transducer.

**12237 -  7000 Series Proximitors**

- 01 For combined system electrical length of 15 feet, with 300 probe tip.  
 02 For combined system electrical length of 20 feet, with 300 probe tip.

**Extension Cable**

- 4454 -  Extension cable with armor  
 2789 -  Extension cable without armor

**Cable Length Option**

Order in increments of 12 inches  
 (304.8 mm).  
 Maximum cable length: 468 inches  
 (11.89 meters).  
 Minimum cable length: 12 inches  
 (305 mm).

**TABLE 1**

TIP			CASE		LEAD ARMOR
CATALOG NUMBER		TYPE	CONFIGURATION	THREADS	
FIBERGLASS	TONOX				
300-00	28407	300	Standard	3/8-24	No
300-01	28408	300	Standard	3/8-24	Yes
300-04-02-12 *	28411	300	Reverse	3/8-24	No
300-06	28413	300	Pressure	3/8-24	No
300-11	28416	300	Standard	M10X1	No
300-12	28417	300	Standard	M10X1	Yes
190-00	28400	190	Standard	1/4-28	No
190-01	28401	190	Standard	1/4-28	Yes
190-04-02-12 *	28402	190	Reverse	3/8-24	No
190-06	28404	190	Pressure	1/4-28	No
190-07	28405	190	Standard	M8X1	No
190-08	28406	190	Standard	M8X1	Yes

\* The unthreaded length and case length are set on the reverse mount probe.

**TABLE 2**  
 Required Extension Cable Lengths for Proximitors

CATALOG NUMBERS	PROBE LEAD LENGTHS					
	6 Inches	12 Inches	18 Inches	24 Inches	30 Inches	36 Inches
20929-01, 20929-02, and 12237-01	168 Inches	156 Inches	144 Inches	132 Inches	120 Inches	108 Inches
20929-03, 20929-04, and 12237-01	228 Inches	216 Inches	204 Inches	192 Inches	180 Inches	168 Inches

**Note:** Other cable lengths—up to 25 feet—not listed in Table 2 may be ordered, but are not recommended. Lengths are critical to obtain the correct system performance.

# Acceleration Transducer System

## Technical/Ordering Information

### High frequency measurements for determining overall machine condition

The Acceleration Transducer System is most suited for measuring high frequency vibration on the machine case or bearing housing. Under certain conditions, it also is useful for evaluating the overall mechanical condition of some machines.

The Acceleration Transducer System is easy to install. The transducer is mounted on the machine case, or when feasible, the bearing housing.

The Acceleration Transducer System consists of an accelerometer, interconnect cable, and interface module. It can be used in conjunction with the 7200 Series and 9000 Series Monitoring Systems.

### Applications recommended for acceleration measurements

The Acceleration Transducer System normally should not be used in place of direct shaft vibration measurement, except in specific applications, such as:

- When a supplementary casing measurement may provide pertinent information about the mechanical condition of rotating machinery. Supplemental casing measurements are typically required for measuring gear mesh frequencies and turbine blade passage frequencies.

- When the machine housing, piping, or foundation are suspected of being the source of significant vibration.

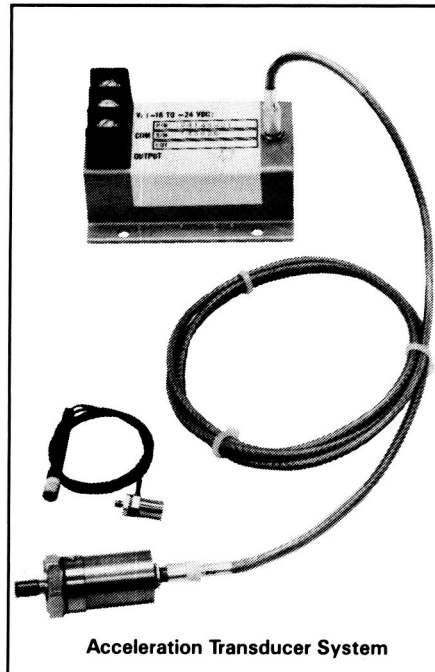
### How an acceleration transducer system works

Acceleration is the measurement of the time rate of change of velocity. To make this measurement, the accelerometer uses a piezoelectric crystal situated between the accelerometer base and an inertial reference mass.

When compression or a tension force excites the crystal, the crystal acts as a precision spring to oppose the compression or tension force. It generates a displaced electric charge. An integral amplifier converts the charge to a voltage, which is transmitted via the interconnect cable to the interface module.

The interface module supplies a constant current to the accelerometer. It also amplifies the signal from the accelerometer.

The interface module has an output sensitivity of 100 mV/g.



### Accelerometer

Two versions of the accelerometer are offered: a standard version for measuring vibration frequencies up to 20 kHz and a high frequency version for measuring vibration frequencies up to 30 kHz.

### Interface Module

The standard accelerometer uses a 23733-03 interface module. The high frequency version utilizes a 24145-02 interface module.

### Interconnect Cable

The interconnect cable is offered with or without armor. It is ordered in one-foot increments.

The standard accelerometer utilizes a 18622 interconnect cable. A radiation-resistant option is available for the 18622 interconnect cable for use in radiation environments.

The high frequency accelerometer uses a 21165 interconnect cable. Both the 21165 and 18622 interconnect cables are available with a stainless steel protective armor.

**NOTE:** If casing acceleration measurements are being made for the overall protection of a machine, thought should be given to the usefulness of the measurement for each application. Most common machine malfunctions, such as unbalance, misalignment, etc., occur on the rotor and originate as an increase (or at least a change) in rotor vibration.

For any casing measurement alone to be effective for overall machine protection, a significant amount of rotor vibration must be faithfully transmitted to the machine casing or mounting location of the transducer.

In addition, care should be exercised in the physical installation of the acceleration transducer on the bearing housing or machine casing. Improper installation may result in a decrease of the transducer amplitude and frequency response and/or the generation of false signals that do not represent actual vibration. For more information, please refer to the appropriate Instruction Manuals and Application Notes.

### Specifications

#### Accelerometer

##### OUTPUT SENSITIVITY

**Standard:** 25 mV/g  $\pm$  5% (2.55 mV/m/sec.<sup>2</sup>).

**High Frequency:** 10 mV/g  $\pm$  10% (1.02 mV/m/sec.<sup>2</sup>).

**Acceleration Range:** 50 g's peak (490 metres/sec.<sup>2</sup>).

##### Frequency Response:

**Standard:** 2 Hz to 20 kHz  $\pm$  3 dB, 5 Hz to 10 kHz  $\pm$  5%.

**High Frequency:** 2 Hz to 30 kHz  $\pm$  3 dB, 7 Hz to 14 kHz  $\pm$  5%.

##### Mounted Resonant Frequency:

**Standard:** 30 kHz minimum.

**High Frequency:** 55 kHz minimum.

**Amplitude Linearity:**  $\pm$  1% to 50g's (490 metre/sec.<sup>2</sup>).

##### ELECTRICAL ISOLATION

Case is internally connected to system common. Isolation from machine case is provided by a built-in isolator.

#### Interface Module

##### OUTPUT SENSITIVITY

**Standard:** 100 mV/g (10.2 mV/metre/sec.<sup>2</sup>).

**High Frequency:** 100 mV/g (10.2 mV/metre/sec.<sup>2</sup>).

##### POWER REQUIREMENTS

**Standard:** -18 to -24 Vdc at 15 mA maximum; 10 mA typical.

**High Frequency:** -22 to -26 Vdc at 30 mA maximum; 21 mA typical.



# Acceleration Transducer System

## ENVIRONMENTAL

**Accelerometer Operating Temperature Range:**  
-20 °F to +250 °F (-29 °C to +121 °C).

**Accelerometer Shock Survivability:**

**Standard:** ± 5000g's (± 49,050 m/sec.<sup>2</sup>)  
peak.

**High Frequency:** ± 10,000g's (+ 98,100  
m/sec.<sup>2</sup>) peak.

**Interface Module Operating Temperature  
Range:** -40 °F to +212 °F (-40 °C to  
+100 °C).

**Interface Module Storage Temperature Range:**  
-60 °F to +302 °F (-51 °C to +150 °C).

## Ordering Information

### Accelerometer

23732-01 Standard Accelerometer

24147-01 High Frequency Accelerometer

### Interface Module

23733-03 Standard Interface Module

24145-02 High Frequency Interface Module

### Extension Cable

**A B**  
18622 -  -  Standard Extension  
Cable

21165 -  -  High Frequency Extension  
Cable

### Option Description

**A Cable Length Option**  
**B Armor Option**

**A  Cable Length Option**  
Order in increments of 1 foot.  
Minimum: 1 foot 1  
Maximum: 30 feet 30

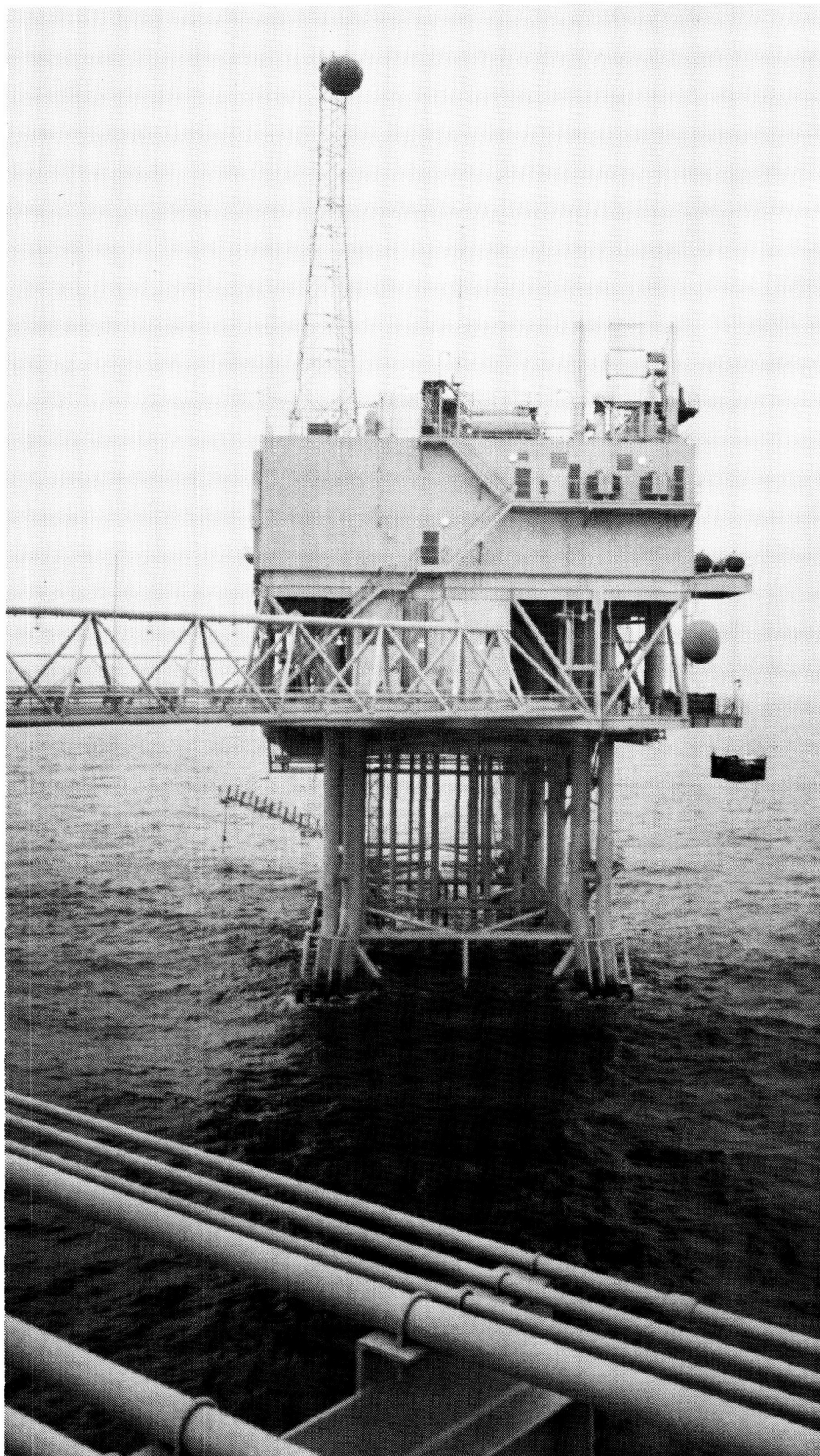
**B  Armor Option**

00 For 18622 and 21165 cables, with-  
out armor.

01 For 18622 and 21165 cables, with  
armor.

02 For 18622 cable used in radiation  
environments, without armor.

03 For 18622 cable used in radiation  
environments, with armor.



# ADRE®

## Technical/Ordering Information

DIAGNOSTICS AND TEST KITS

### Reduces data reduction time for machinery behavior analysis

Bently Nevada's ADRE system (Automated Diagnostics for Rotating Equipment) significantly reduces the time required to analyze and diagnose machinery behavior. A computer-based data acquisition and reduction system, ADRE eliminates the time-consuming task of hand logging and reducing steady-state and transient dynamic vibration data.

Automated reduction of dynamic vibration data, including startup and shutdown information, enables you to analyze and document the mechanical condition of rotating machinery and troubleshoot machine malfunctions. The information received from the ADRE also can be used to balance machines, determine mechanical impedances and multiple resonances, and assist with stability studies.

Transient dynamic vibration data collected during startup and shutdown is presented in Bode, polar, and cascade plots. These plots provide insight into the rotating system's margin of stability and reveal synchronous, sub-, and super-synchronous vibration components.

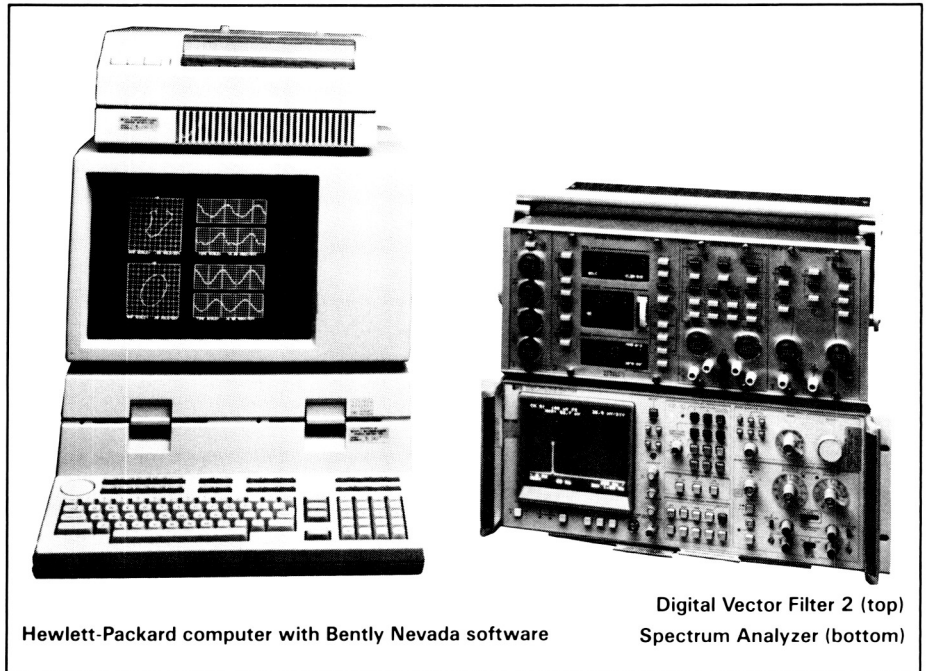
Steady-state dynamic vibration data is presented in orbit, time base, and comparative spectrum plots. This information can be used to examine magnitude, frequency, phase angle, and the shape or path of dynamic motion as well as to track change in spectral content over a period of time.

ADRE is available in a variety of hardware and software options to meet your machinery information needs and budget requirements. The hardware consists of a choice of two Hewlett-Packard (HP) computers, a Bently Nevada Digital Vector Filter (DVF 2), and a spectrum analyzer. Recommended additional hardware includes a multi-channel FM tape recorder and a Recorder Amplifier System.

### Software packages for machine analysis

The heart of the ADRE system is software. Developed by Bently Nevada's engineering staff from years of field experience, the software is tailored for efficient behavior analysis and diagnosis.

Five software packages are available. Transient, Steady-State, Shaft Centerline, and Hardware Diagnostics soft-



Hewlett-Packard computer with Bently Nevada software

Digital Vector Filter 2 (top)  
Spectrum Analyzer (bottom)

ware packages are supplied as standard components of the ADRE system. An additional package — Snapshot Predictive Maintenance — is available as an option and requires additional memory and hardware.

Designed for personnel with minimal computer training, the ADRE software packages are easy to use. Operator input prompts written in simple English make program execution quick and easy.

#### Transient package

The Transient package enables you to acquire data for identifying rotor and structural resonances and their amplification factors, instabilities, misalignment, rubs, and other malfunctions. Data is plotted in polar, Bode, or cascade formats or in tabular listings.

#### Steady-State package

The Steady-State package gives you information on the on-line condition of your machinery at operating speed. Data can be plotted in orbit, time base, or comparative spectrum formats.

#### Shaft Centerline package

The Shaft Centerline package provides information that can be used to determine the margin of stability on rotating machinery and the position of the shaft within its bearing. It also can be used to identify thin-film oil thickness, bearing wear, and the presence of

shaft preloads. Data can be plotted as a function of machine speed or elapsed time.

#### Hardware Diagnostics package

The Hardware Diagnostics package makes it possible to diagnose potential ADRE hardware failures. A series of diagnostic programs allows you to test and verify the correct operation of the instruments and peripheral devices in the ADRE system. The program ensures that all hardware is connected and operating properly.

#### Snapshot Predictive Maintenance (PM) package

The optional Snapshot PM package, used in conjunction with Bently Nevada's Snapshot,® reduces, stores, and plots data for a large number of machine points. This capability enables you to increase the number of machines in your vibration monitoring or predictive maintenance program. Information is presented in trend, spectrum, and time base plots.

The software package requires additional memory. The Snapshot system, when used with the ADRE computer, does not require a DVF 2 or spectrum analyzer for data collection and reduction.

For more details on the Snapshot PM package and the Snapshot system see data sheets L0546 and L0559.

**BENTLY  
NEVADA**

P.O. BOX 157 • MINDEN, NEVADA USA 89423 • (702) 782-3611

ORIGINAL PAGE

BLACK AND WHITE PHOTOGRAPH

• FAX: (702) 782-9253

Software packages operate on the specified computers when they are accompanied by specific hardware and a specific operating system. No claims to software compatibility are expressed or implied for any other computer, hardware, or operating system revision. Call your Bently Nevada representative for details of computer requirements.

## Hardware

Two hardware system models, using the HP Series 200 computer, are available.

The Model 10 system uses the HP Series 200 Model 16S computer.

The Model 10 system consists of:

- Hewlett-Packard Series 200 Model 16S computer with a nine-inch CRT, HP-IB and RS-232 interfaces, RAM BASIC with extensions, and 512 Kbytes of RAM.
- Dual 3 1/2-inch microfloppy disk drive.
- Thermal graphics line printer.
- Bently Nevada DVF 2 with carrying case.
- Spectrum analyzer with carrying case.
- Bently Nevada Transient, Steady-State, Shaft Centerline, and Hardware Diagnostics software packages.

The Model 30 system uses an HP Series 200 Model 36CS computer.

The Model 30 system consists of:

- HP Series 200 Model 36CS with a 12-inch color CRT; an HP-IB interface; built-in, dual 5 1/4-inch microfloppy disk drives; RAM BASIC with extensions and RAM Pascal language systems and 540 Kbytes of RAM.
- Thermal graphics line printer.
- Bently Nevada DVF 2 with carrying case.
- Spectrum analyzer with carrying case.
- Bently Nevada Transient, Steady-State, Shaft Centerline, and Hardware Diagnostics software packages.

## Specifications

### INPUTS

**Power:** 90-125 Vac or 180-250 Vac, 48-66 Hz.

**Consumption:**

- Model 10:** 80 Watts.
- Model 30:** 300 Watts.

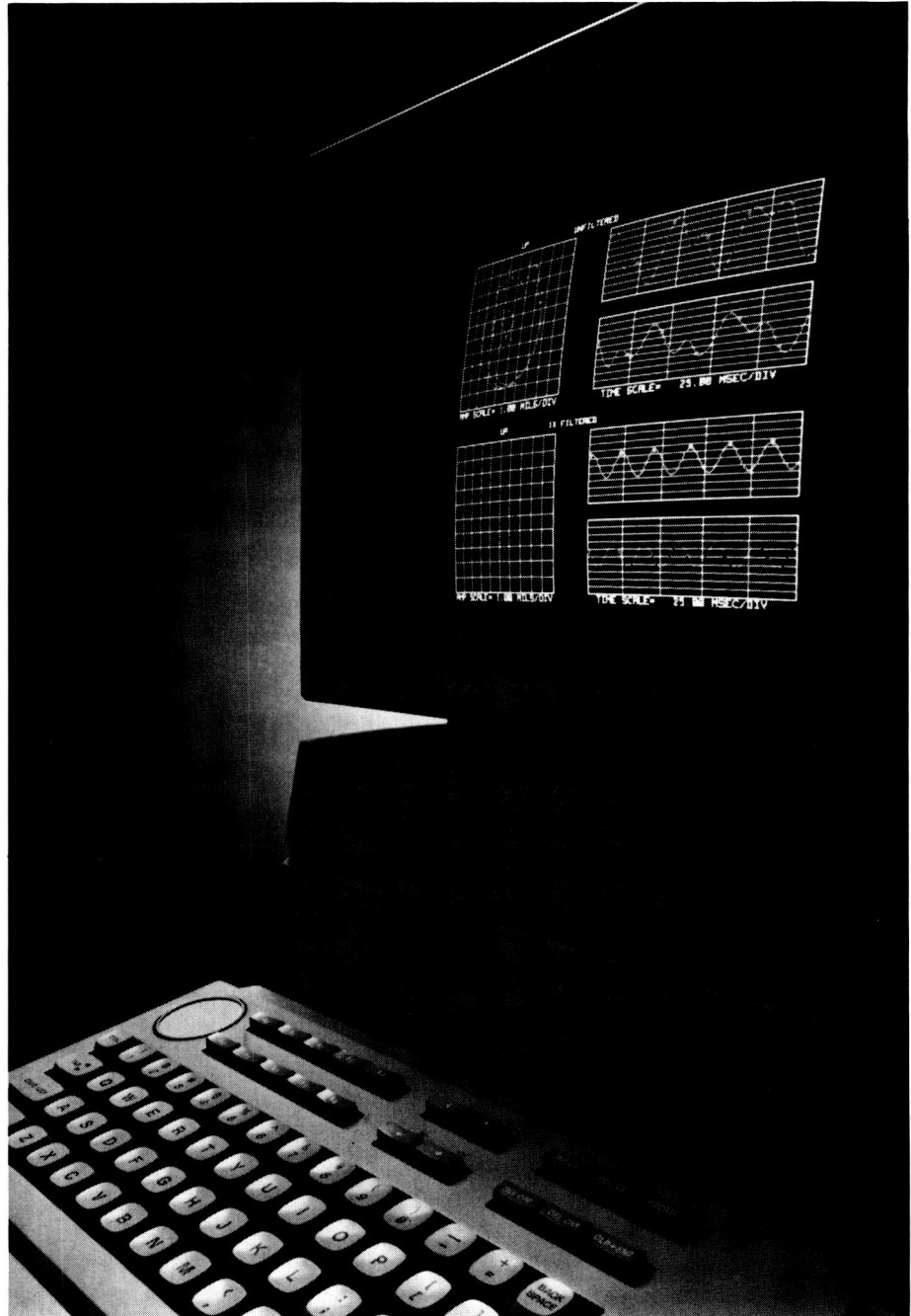
### OUTPUTS

**Display:**

- Model 10:** 9-inch diagonal (229 mm).
- Model 30:** 12.2-inch diagonal (309 mm).

### STORAGE

- Capacity (Mass Storage):** 540 Kbytes.
- Data Sheet Number:** L0453.



The heart of the ADRE is software. Developed by Bently Nevada's engineering staff from years of field experience, the software is tailored for efficient behavior analysis and diagnosis.

## Ordering Information

### Model 10

44163 -  -  -  -  -

#### Option Description

- A Computer Option
- B Peripheral Device Option
- C Instrumentation Option
- D Software Option

- A  Computer Option
  - 10 Standard offering
  - 11 With ROM BASIC
  - 12 With HP 9836 Keyboard
  - 13 With ROM BASIC and HP 9836 Keyboard

- B  Peripheral Device Option
  - 0 Standard offering
  - 1 Without standard printer
  - 2 Without standard disk drive
  - 3 Without standard printer and standard disk drive

- C  Instrumentation Option
  - 0 Standard offering
  - 1 Without standard DVF 2
  - 2 Without standard spectrum analyzer
  - 3 Without DVF 2 and spectrum analyzer

- D  Software Option
 

Ordering ADRE software requires assistance from your Bently Nevada sales representative. The following software packages are available:

- Steady-State Package
- Shaft Centerline Package
- Transient Package
- Snapshot Predictive Maintenance (PM) Package
- Hardware Diagnostics Package

- B  Peripheral Device Option
  - 0 Standard offering
  - 1 Without standard printer

- C  Instrumentation Options
  - 0 Standard offering
  - 1 Without standard DVF 2
  - 2 Without standard spectrum analyzer
  - 3 Without DVF 2 and spectrum analyzer

- D  Software Option
 

Ordering ADRE software requires assistance from your Bently Nevada sales representative. The following software packages are available:

- Steady-State Package
- Shaft Centerline Package
- Transient Package
- Snapshot Predictive Maintenance (PM) Package
- Hardware Diagnostics Package

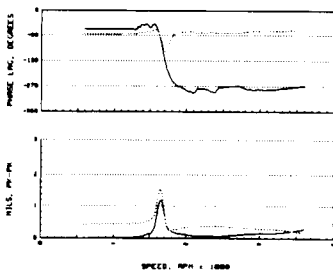
### Model 30

44165 -  -  -  -  -

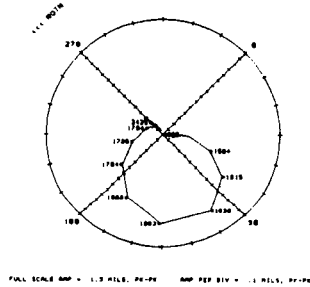
#### Option Description

- A Computer Option
- B Peripheral Device Option
- C Instrumentation Option
- D Software Option

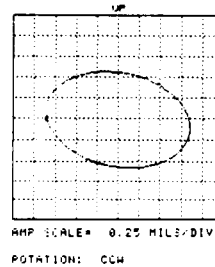
- A  Computer Option
  - 10 Standard offering
  - 11 With ROM BASIC
  - 12 Without color CRT
  - 13 With ROM BASIC and without color CRT



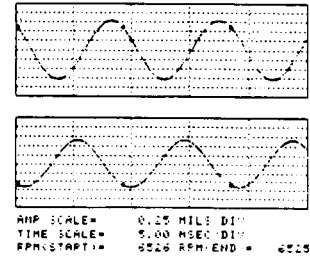
Bode



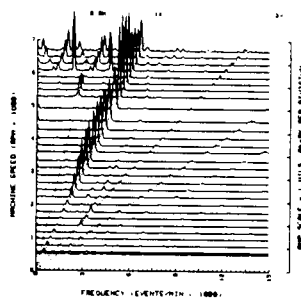
Polar



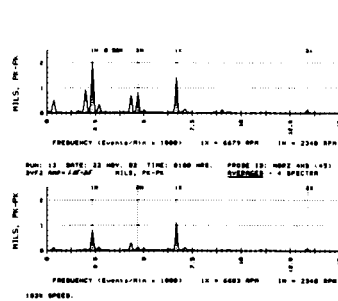
Filtered Orbit



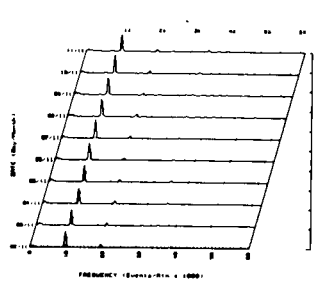
Time Base Spectrum



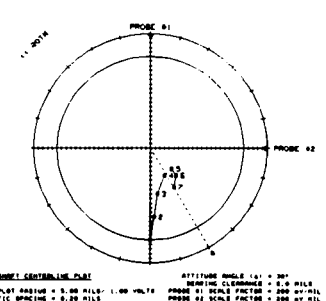
Cascade



Spectrum



Dynamic Trend



Shaft Centerline

The heart of the ADRE is software. Developed by Bently Nevada's engineering staff from years of field experience, the software is tailored

for efficient behavior analysis and diagnosis. The software packages require minimal computer training to operate and are easy to use.

# 24000 Digital Vector Filter 2

## Technical/Ordering Information

### In-place diagnostic and balancing data for rotating machinery

The Digital Vector Filter 2 (DVF 2) gives you amplitude, phase, and speed data for diagnosing, balancing, and detecting shaft cracks on all types of rotating machinery.

Two versions of the DVF 2 are available. One version processes 1/2X, 1X, and 2X rotative speed signals.

The second version processes 1X, 2X, 3X, and 4X rotative speed data. The ability to analyze 1X, 2X, 3X, and 4X rotative speed data is vital for detecting and diagnosing shaft cracks on turbine generators and other rotating machinery.

The DVF 2 can be interfaced with a computer, such as Bently Nevada's ADRE® (Automated Diagnostics for Rotating Equipment) system, via its IEEE 488 computer interface. When used with the ADRE, data can be presented in Bodé, polar, cascade, orbit, time base, and comparative spectrum plots.

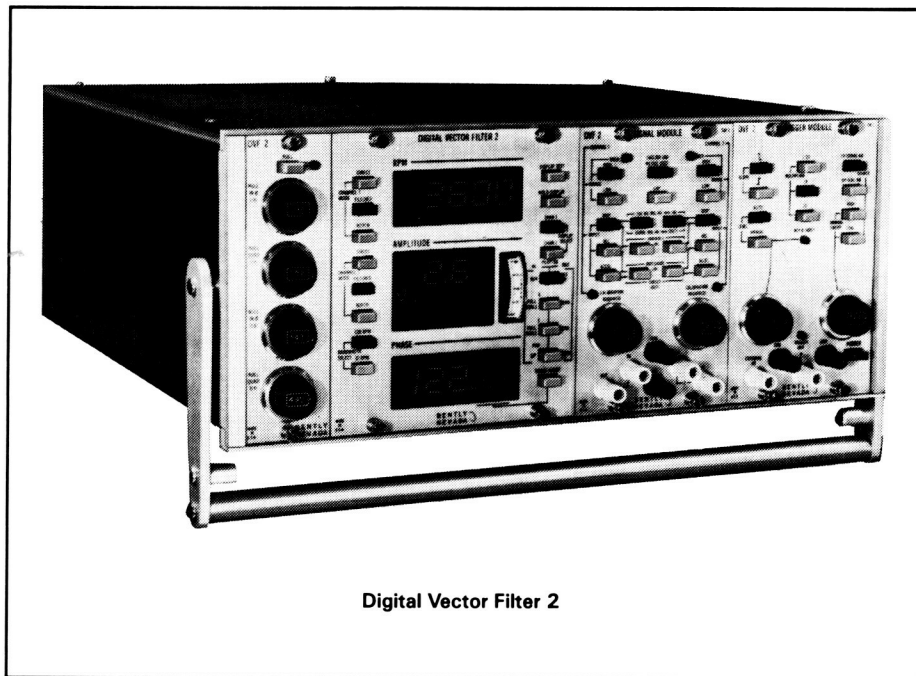
### Applications for the DVF 2

The ability to accurately measure amplitude, phase, and speed data helps answer the questions: What is happening on the machine, when, where, and how? This information can be used on steam, gas, or hydroelectric turbines; electric motors; centrifugal, reciprocating, or screw compressors; generators; pumps; and fans for some of the following applications:

- Detecting and diagnosing shaft cracks, using data on the 1X, 2X, 3X, and 4X rotative speed behavior of turbine generators and other rotating machinery.
- Determining the balance condition of a machine and locating the residual unbalances on a rotor.
- Determining the rpm location of the natural rotor balance resonances, or "criticals," on a machine.
- Establishing the machine response for documenting acceptance tests and for evaluating and diagnosing current and future machine behavior.

The DVF 2 provides two continuous channels of amplitude and phase data, which is filtered at running speed, and one channel of speed data.

Triggering signals from a Keyphasor® and signals from proximity, velocity, or acceleration transducers are converted by the digital circuitry in the DVF 2 to display rotor rpm, vibration amplitude, and phase angle.



Digital Vector Filter 2

## Specifications

### INPUT

**Power:** 95-125 Vac or 190-250 Vac, rear panel switch selectable. 50-60 Hz 1 phase.

**Nominal power consumption:** 100 watts.

### VIBRATION INPUT

#### Scale Factors:

**Displacement:** 200 or 100 mV/mil (8 or 4 V/mm) fixed. 100 to 1,000 mV/mil (4 to 40 mV/mm) variable.

**Velocity:** 100 to 1,000 mV/inch/second (4 to 40 mV/mm/second) variable.

**Acceleration:** 100 to 1,000 mV/G (10 to 100 mV/M/second<sup>2</sup>) variable.

**Input Impedance:** 1.1 M ohms minimum at AC signal frequencies; 2.4 M ohms at DC signal frequencies.

### KEYPHASOR INPUT

**Threshold Range:** ± 15 Vdc.

**Hysteresis:** 0.5V typical (internally adjustable from 0.2 to 2.0V).

### VIBRATION OUTPUT

#### Scale Factors:

**Displacement:** 200 mV/mil (8V/mm) or 100 mV/mil (4 V/mm) for fixed input of 200 mV/mil or 100 mV/mil respectively. For variable input scale factors, an output of 200 mV/mil is standard.

**Velocity:** 500 mV/inch/second (20 mV/mm/second).

**Acceleration:** 100 mV/G (10 mV/M/second<sup>2</sup>).

**Output Impedance:** 100 ohms.

#### Manual Sweep Oscillator Ranges:

**Low:** 100-10,000 rpm.

**High:** 1,000-100,000 rpm.

**Computer Interface:** DVF 2 output data is available through an IEEE 488 compatible interface.

### ENVIRONMENTAL

#### Temperature Range:

**Operating:** 0 °C to +65 °C (+32 °F to +149 °F).

**Storage:** -40 °C to +85 °C (-40 °F to +185 °F).

**Humidity:** To 95% noncondensing.

ORIGINAL PAGE  
BLACK AND WHITE PHOTOGRAPH

# 24000 Digital Vector Filter 2

## DIMENSIONS

	Bench Mounted (includes handle)	Rack Mounted
Height	8 inches (203 mm)	8 inches (203 mm)
Width	18 inches (457 mm)	19 inches (483 mm)
Depth	18 7/8 inches (479 mm)	18 7/8 inches (479 mm)

### Weight:

DVF: 33 pounds (15 kg) nominal.

Case: 28.5 pounds (12.9 kg) nominal.

## Ordering Information

### Digital Vector Filter 2 1/2X, 1X, and 2X Version

24000 -

#### Mounting Option

- 01 Bench Mount (includes case).
- 02 19-inch EIA Rack Mount.

### Digital Vector Filter 2

1X, 2X, 3X, and 4X Version

24000 -

#### Mounting Option

- 03 Bench Mount (includes case).
- 04 19-inch EIA Rack Mount.



The DVF 2 enables you to accurately measure amplitude, phase, and speed for determining the balance condition of rotating machinery,

locating the residual unbalances on a rotor, and diagnosing shaft cracks and other machine malfunctions.

# Digital Vector Filter 3

## Technical/Ordering Information

### The solution for balancing and diagnosing rotating machinery problems at a competitive price

The Digital Vector Filter 3 (DVF 3) provides amplitude, phase, and shaft rotative speed data for detailed vibration analysis including balancing, rotor response evaluation and shaft crack detection on all types of rotating machinery. The instrument's primary application is for documentation of vibration data during machine transient (runup and coastdown) and steady-state (constant speed) conditions.

The DVF 3 accommodates two signal inputs for vibration transducers and a third for a Keyphasor® transducer. Vibration inputs can be from either displacement (proximity), velocity, or acceleration transducers. The Keyphasor input represents a once-per-revolution pulse from either a proximity probe, an optical pickup, or a strobe light. This provides the measurement of shaft rotative speed, and the reference point for measuring phase lag angle. It also provides a trigger signal to tune the tracking filter in each vibration channel to shaft rotative speed.

The instrument provides excellent reliability and outstanding performance in a rugged, lightweight package. Its alphanumeric display and menu-driven setup make the instrument easy to operate. It provides the information accuracy required to make sound decisions regarding machine condition. The DVF 3 can be ordered in several packages, which enables you to select the components best suited for your specific applications without the expenditure for unnecessary functions.

### Easy-to-use functional features

The DVF 3's streamlined design incorporates the features our customers have found most useful from years of experience and adds new features which assist in solving today's machinery problems.

Two channels are simultaneously displayed on the large, highly visible readout, showing vibration amplitude, phase angle, and shaft rotative speed. The display also shows status of instrument setup parameters, such as filter mode and hold.

### Bodé/Polar Plots

A GP-IB interface is provided for connection to a computer or directly to one or up to two digital plotters depending on the type of DVF 3. The DVF 3 is

### ORIGINAL PAGE BLACK AND WHITE PHOTOGRAPH



Digital Vector Filter 3

programmed to produce high quality Bodé and polar plots on-site with the accessory digital plotter(s). These plots can be generated "real-time", on full size blank paper (8 1/2 x 11 in. or A4) with full annotation.

Alternatively, the accessory DVF 3 software package may be used to produce these plots on an IBM AT or compatible computer. See DVF 3 Storage and Plotting Application Software product data sheet L6030.

Bodé and polar plots are useful for evaluating vibration response during machine transient conditions. These plots reveal balance resonances (critical speeds), synchronous amplification factors, and other characteristics for evaluating machine condition.

### Sweep Frequency Plots

For machinery operation under steady-state conditions the DVF 3 will produce sweep frequency spectrum plots. Frequency analysis provides useful additional information for complete evaluation of machinery vibration characteristics.

**Automatic signal sweep** allows:

- Frequency spectrum plotting within user-defined start and end frequencies.
- Frequency component search; instrument pauses at components above a user-defined amplitude threshold.

- Manual (coarse/fine) tuning to pinpoint frequencies of interest.

### Other Features

**Keyphasor error indication** appears when:

- Shaft rotative speed is outside the operating range (50 to 100,000 rpm)
- Consecutive Keyphasor pulses (shaft rotative speed measurements) vary more than 12.5%
- Trigger threshold is set too low or high.

**Peak Hold** stores the maximum vector (for both channels) since the last time the memory was reset; a useful feature for identification of peak amplitudes from transient data.

**Variable Transducer Input** scale factors (0.1 to 9999.9 millivolts per engineering unit) allow connection of virtually all available proximity, velocity and acceleration transducers. Scale factors between input and output are equal, providing convenient interface with other diagnostic instruments.

**Hold** function freezes the display for easy reading and interpretation of the values; useful for identifying 1X vectors at a particular balancing speed.

**Multiple Full Scale Ranges** enhance the accuracy of measured variables and make the instrument extremely useful for a variety of applications.

# Digital Vector Filter 3

**Signal Integration** from acceleration to velocity or from velocity to displacement is available independently on each channel.

**Metric or English Units** can be used for display of measured variables. Displacement values are shown in pk-pk units; velocity and acceleration units can be 0-pk or RMS.

**DC Gap Voltage** measurements are available for both channels. The high resolution of this data allows the determination of shaft average radial position relative to the bearing clearance.

**Triggering in Two Modes** is possible. In the AUTOMATIC mode, the threshold level is determined by the DVF 3; ideal for triggering on a noise-free Keyphasor pulse. In the MANUAL mode, the threshold level is selected by the user, which allows triggering on a poor quality Keyphasor pulse. In addition, the manual mode allows Keyphasor indexing. The index function identifies the location of the Keyphasor reference mark when visual observation is impossible. Indexing, indicated by an asterisk on the display, is performed on the negative slope of the Keyphasor pulse, which for a notch, relates to the leading edge, and for a projection or optical pickup, the trailing edge.

**Amplitude Over/Underrange** conditions are indicated on the display to ensure data integrity.

**Tracking Filter Bandwidth** is selectable between 12 and 120 cpm to provide accurate measurements for low and high speed applications.

**Filtered 1/2X, 1X and 2X** signal outputs are available. These dynamic signals may be used for display on an oscilloscope (e.g. for filtered orbits) or connected to other diagnostic instruments.

**Slow Roll Compensation** is provided in order to eliminate the effects of shaft runout. The runout vectors may be stored automatically with the rotor at slow roll speed, or the previously documented vectors can be entered manually.

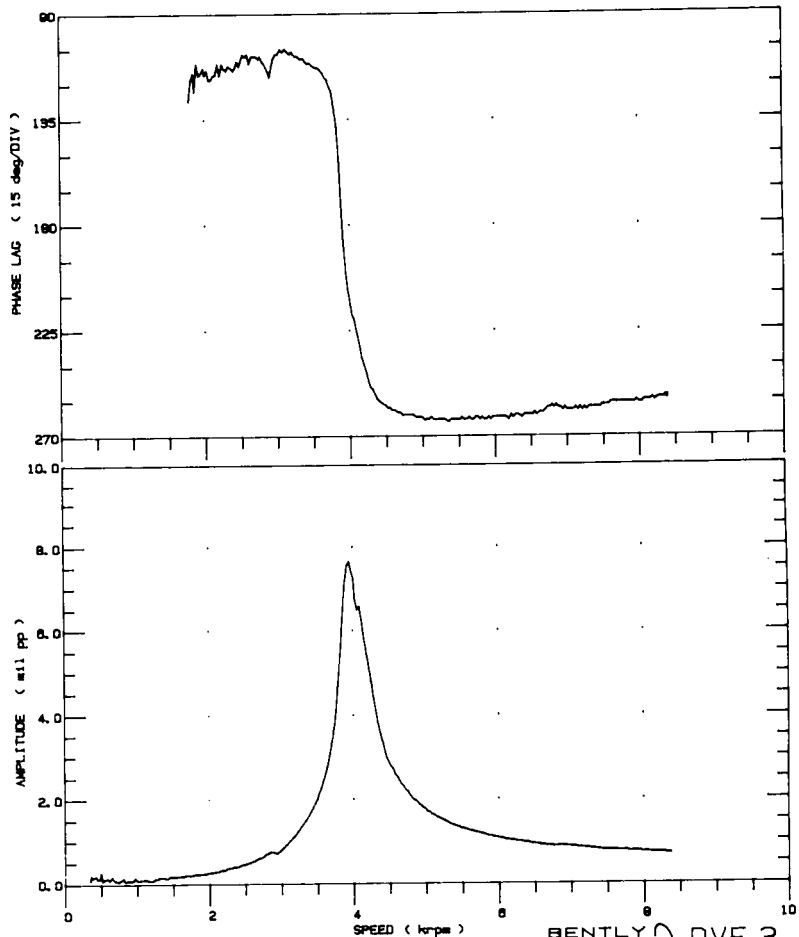
**Coaxial Connectors** on the front and rear panel inputs and outputs provide a reliable interface for transducers and other instruments.

## Useful for a Wide Variety of Applications

The extended operating range of the DVF 3 (50 to 100,000 rpm) allows it to be used on virtually all types of rotating machinery.

- Steam, gas, and hydroelectric turbines
- Electric motors and generators

COMPANY: \_\_\_\_\_  
PLANT: \_\_\_\_\_  
MACHINE TRAIN: \_\_\_\_\_ XDCR ID: \_\_\_\_\_  
DATE: \_\_\_\_\_ STATE: START-UP 1X Filtered Comp  
SLOW ROLL: 1.42 mil pp @ 348 deg Collected at 369 rpm



Bode Plot

- Centrifugal, reciprocating, and screw compressors
- Vertical and horizontal pumps
- Gearboxes
- Fans and blowers
- Centrifuges
- Paper machine rollers
- Propulsion systems

sampled or manually entered by the user. The HOLD function enables the user to freeze the displayed data for easy interpretation at the balancing speed.

The Field Balancing Package option provides a programmable handheld HP 41 CV calculator and Bently Nevada software for multiplane balancing solutions, up to four planes.

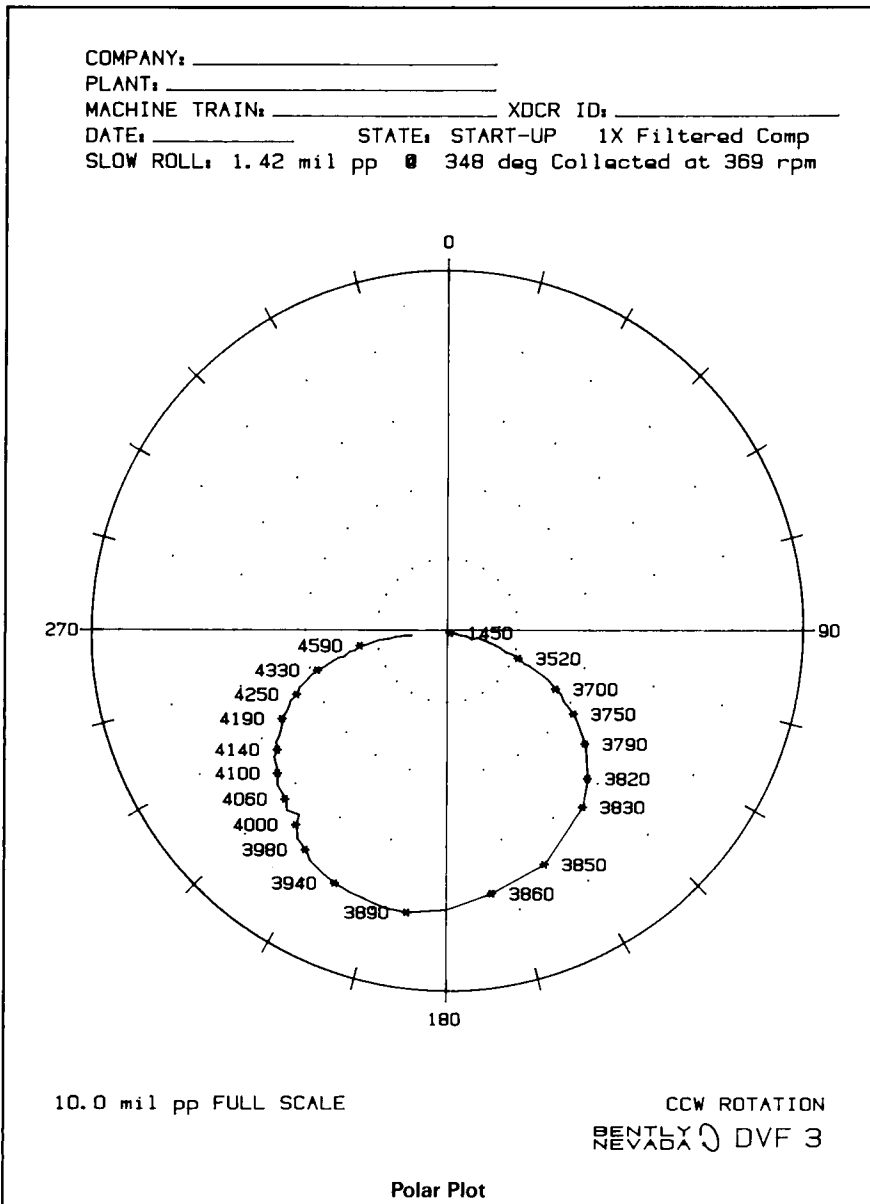
## Using the DVF 3 for balancing

The DVF 3 is ideal for balancing rotating machinery due to its ability to track the 1X vibration response of the machine. The 1X vector on each channel can be slow roll compensated for shaft runout effects to display the true 1X dynamic motion. The slow roll compensation vectors can be automatically

## Using the DVF 3 for REAL TIME Bode and Polar Plotting.

The DVF 3 and the accessory digital plotter(s) can produce Bode or polar plots in "real time"; a useful feature for the engineer faced with deciding whether a machine start-up should continue or not.

# Digital Vector Filter 3



The polar plots are automatically annotated with rpm tic marks at rotative speed increments. This plot is extremely useful for structural resonance and mode shape identification, particularly on balancing exercises where modal consideration is required.

The Bode plot scaling is user-selectable in terms of amplitude, rpm and phase lag angle. This plot allows the exact frequency of resonances to be accurately determined. The damping characteristics of a system resonance can be evaluated by calculating synchronous amplification factors from the presented data.

Both the Bode and polar plots can be made using the 1X or 2X vectors. The 2X plot is very useful in the detection of shaft cracks where lateral stiffness asymmetry due to a crack is to be evaluated.

## Using the DVF 3 with a tape recorder.

Multi-channel tape recording of a startup or shutdown can be easily reduced in the field into report-quality Bode and polar plots for each channel. The DVF 3 and its accessory plotter(s) can produce these quality plots from blank (8 1/2 x 11 inch or A4) paper or previously prepared graph paper. The DVF 3 firmware is programmed to fully label these plots. Plot correlation is possible by replaying data from other transducers or channels and plotting on the same sheet. The multi-pen, multi-color plotter(s) facilitates this feature.

## Using the DVF 3 for Pre- and Post-Maintenance checks.

When a long running machine is being

shutdown for planned maintenance, the DVF 3, digital plotter(s) and a tape recorder can be used to provide quick documentation of the transient characteristics during shutdown. This data can be used either as a baseline transient response curve or compared with the last response curve plotted for that machine. Indications of changes in balance condition, system dynamic stiffness and damping effects can be quickly pinpointed using such methods.

Plots generated from shutdown data can be compared to those made during startup in order to evaluate the effects of any maintenance performed on the machine during shutdown. In addition, the post-maintenance transient response can be used as a reference for the next scheduled maintenance.

## Using the DVF 3 for Acceptance Testing.

A typical acceptance test may include the documentation of measured balance resonances, calculation of synchronous amplification factors (Q), shaft mode shapes and frequency spectra. It may also call for casing measurements which are specified in either O-to-peak or RMS units. The DVF 3 and its accessories can document and display all of this information, making it an ideal test stand instrument.

## Using the DVF 3 with Low Speed Machinery.

The tracking filters on the DVF 3 can operate down to 50 rpm, making the instrument useful for low speed applications. Hydroturbines and cooling tower fans can be balanced accurately using 1X vector information. The 12 cpm bandwidth selection is useful for low speed applications.

The low speed DVF 3 response is also useful for measuring shaft runout at slow roll speeds for eliminating runout effects from subsequent vibration data and detection of shaft cracks.

## Using the DVF 3 with the ADRE II System.

The DVF 3 can be used in place of the DVF 2 with the ADRE II system. When DVF 3 is used with the ADRE II system, one additional useful feature is the ability to manually enter slow roll compensation vectors at the instrument's front panel. This eliminates having to sample real slow roll data from tape recordings before compensation can be performed on any plot.

# Digital Vector Filter 3

## Specifications

The following specifications are intended to provide basic information only.

Specifications provided are at 73 °F (23 °C) with a sine wave input, at input scale factor greater than 3 mV/mil and with a full scale setting of 10 mils. Where required, input signal level is the full scale selection. Specifications given are for a shaft rotative speed of 3600 rpm and with the tracking filter set for 12 cpm bandwidth.

### INPUTS

**Power:** 90-132 Vac or 180-264 Vac, (switch selectable), 47 to 63 Hz, 1 phase. Nominal power consumption 30 Watts.

#### Vibration Signals:

**Sensitivity:** Selectable in 0.1 mV per engineering unit increments from 0.1 to 9,999.9 mV/unit.

**Range:** From one to six full scale ranges are available depending on sensitivity and units selected. For example 2, 5, 10, 20 and 50 mil ranges are available with an input sensitivity of 200 mV/mil.

**Probe Gap Voltage:** ± 25 Vdc.

**Impedance:** 1 MΩ.

#### Keyphasor Signal:

**Input impedance:** 100 kΩ.

**Transducer:** 7200, 7000 or 3000 series transducer system, optical pickup, or stroboscope; one event per shaft revolution.

**Threshold range:** ± 18 Vdc.

**Hysteresis:** Factory set at 0.5 volts. Internally adjustable for 0.2, 0.5 and 1.5 volts.

### OUTPUTS

**Display Accuracy:** Input to front panel display

#### Amplitude (non-integrating):

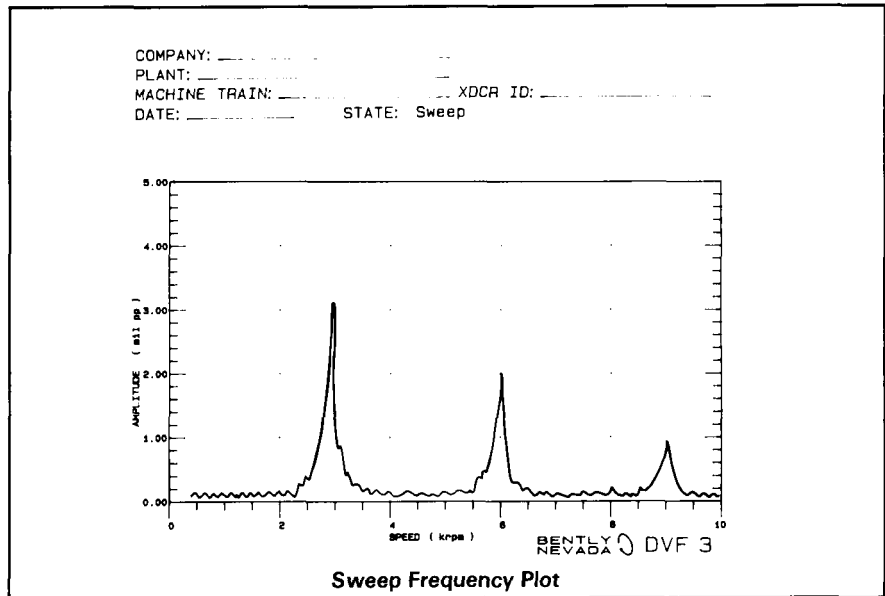
**Direct Mode:** pk-pk and 0-pk; within +2.9%, -3.2% (maximum).

**RMS Mode:** Within +2.8%, -3.1% (maximum).

**Filtered Mode:** Within +2.0%, -2.4% (maximum).

#### Phase:

**Filtered Mode:** Within +0.6%, -2.1% (maximum).



#### Output Accuracy:

##### Input to front/rear outputs

##### Amplitude:

**Direct Mode:** Within +1.3%, -1.7%.

**Filtered Mode:** Within +4.9%, -5.3%.

##### Phase:

**Direct Mode:** Within +0.2°, -1.3°.

**Filtered Mode:** 1X phase shift within +2.1°, -3.6°.

##### RPM:

**50 to 3600 rpm:** Within ± 1 rpm

**3601 to 10,000 rpm:** Within ± 3 rpm

**10,001 to 25,000 rpm:** Within ± 20 rpm

**25,001 to 99,900 rpm:** Within ± 100 rpm

#### Probe Gap Voltages:

**Accuracy:** ± 1.5%.

#### Resolution:

Range	Resolution
-25.0 Vdc to -10.0 Vdc	0.1 Vdc
-9.99 Vdc to +9.99 Vdc	0.01 Vdc
+10.0 Vdc to +25.0 Vdc	0.1 Vdc

#### Trigger Signal:

**Impedance:** 220 Ω.

**Drive Capacity:** 1 TTL load.

### SIGNAL PROCESSING

**Operating Range:** 50 rpm to 99,900 rpm.

#### Integration:

##### 0 dB frequencies:

**Velocity:** 63.9 Hz ± 1.1 Hz.

**Acceleration:** 305 Hz ± 5.0 Hz.

**Amplitude:** Within +1.5%, -2.5% of input signal in addition to vibration measurement deviation.

#### Output Signal Scale Factors:

**Velocity to Displacement:** 0.4 times the input scale factor, ± 1.6%.

**Example:** Input of 500 mV/in/s provides output of 200 mV/mil, ± 1.6%.

**Acceleration to Velocity:** 5.0 times the input scale factor, ± 1.4%.

**Example:** Input of 100 mV/g provides output of 500 mV/in/s, ± 1.4%.

#### Filter:

##### Bandwidths:

**120 ± 10 cpm (2.0 Hz).**

**12 ± 1 cpm (0.2 Hz).**

##### Response Time to 99% of Final Value:

**120 cpm:** 0.65 second.

**12 cpm:** 7.30 seconds.

*Note: Add 0.4 second for RMS measurements*

#### Signal Frequency Sweep:

**Range:** 100 (± 2.0) cpm to 99,900 (± 100) cpm.

**Increments:** 25 cpm increments.

### COMPUTER INTERFACE

The DVF 3 is equipped with a GP-IB and an ADRE II interface.

# Digital Vector Filter 3

## ENVIRONMENTAL LIMITS

### Temperature Range:

**Operating:** +32 °F to +122 °F  
(0 °C to +50 °C).

**Storage:** -40 °F to +185 °F  
(-40 °C to +85 °C).

**Relative Humidity:** Up to 90%, noncondensing.

## HAZARDOUS AREA APPROVALS

**CSA:** Certified safe for general purpose use in laboratory environments.

## PHYSICAL

**Width:** 17.40 in. (440 mm).

**Depth:** 17.25 in. (430 mm).

**Height:** 5.18 in. (130 mm).

**Weight:** 22 lbs. (10 kg).

Rack mountable (19 inches - 482.6 mm) with optional EIA rack-mount kit

## ENGINEERING UNITS

### User Selection:

mils peak-to-peak	..... (mil pp)
micrometres peak-to-peak	..... (µm pp)
inches per second peak	..... (in/s pk)
inches per second rms	..... (in/s rms)
millimetres per second peak	..... (mm/s pk)
millimetres per second rms	..... (mm/s rms)
velocity integrated to displacement in mils peak-to-peak	..... (int mil pp)
velocity integrated to displacement in micrometres peak-to-peak	..... (int µm pp)
g's peak	..... (g pk)
g's rms	..... (g rms)
metres per second per second peak	..... (m/ss pk)
metres per second per second rms	..... (m/ss rms)
acceleration integrated to velocity in inches per second peak	..... (int in/s pk)
acceleration integrated to velocity in inches per second rms	..... (int in/s rms)
acceleration integrated to velocity in millimetres per second peak	..... (int mm/s pk)
acceleration integrated to velocity in millimetres per second rms	..... (int mm/s rms)

### Abbreviation:

## Ordering Information

The DVF 3 and commonly-used accessories comprise the DVF 3 Field Packages. You can design your package by using the accessories list for maximum flexibility.

## BASIC FIELD PACKAGES

### 81496-01

#### Includes:

- 1 DVF 3 Type 77581-01
- 1 DVF 3 soft carrying case
- 1 Digital plotter
- 1 Set of interconnect cables

### 81496-02

#### Includes:

- 1 DVF 3 Type 77581-02 
- 1 DVF 3 soft carrying case
- 2 Digital plotters
- 1 Set of interconnect cables

## BALANCING PACKAGE

### 82246-01

#### Includes:

- 1 HP-41CV calculator with card reader and printer
- 1 HP Infrared printer with interface module
- 1 Bently Nevada Multiplane Balancing software package (4-plane maximum)

## TRANSDUCER FIELD PACKAGE

### 82705-01

#### Includes:

- 1 Proximitor® panel.
- 4 Proximity probes and cables.
- 2 Velocity transducers and mounting accessories.
- 1 Optical Keyphasor® and mounting accessories.
- Co-axial to Banana adapters.
- Co-axial cables
- Banana cables
- 1 TK15 Keyphasor Conditioner/Power Supply.
- 2 Manuals
- 1 Hard carrying case.

## ACCESSORIES

77581-01	DVF 3
77581-02	DVF 3 
79981-01	DVF 3 test cable kit 
76285-01	DVF 3 hard transit case
78858-01	DVF 3 soft carrying case
75237-01	DVF 3 rack-mount kit
82292-01	DVF 3 Users Guide 
02198937	DVF 3 power cord 
83194-01	DVF 3 Storage and Plotting Application Software 
02290871	Tektronix HC100 digital plotter 
04160166	HC100 Hard carry case
02290003	HP-IB Computer Interface card
02260372	HP-IB Cable
02290381	HP 7440A digital plotter
9200-09-01-01	Velocity transducer 
80705-02	Velocity interconnect cable, 6 ft (2 m)
16707-01	Adapter (3 to 2 wire) 
46000-01	Super Mag 100 magnetic base
7989-01	Extension rod, for use with 9200 velocity transducer
10798-03	Optical pickup
20545-25	Optical pickup cable (25ft)
20211-05	Optical pickup mounting package (Includes: locking pliers, magnetic base, gooseneck transducer holder)
81769-01	Reflective tape roll
02290947	HP 41CV programmable calculator

## Digital Vector Filter 3

- 43980-01 Bently Nevada multiplane balancing software (HP 41CV or CX)
- 02290948 HP card reader
- 02290951 HP infrared printer
- 02290949 Printer interface module
- 76131-01 Stroboscope kit with 12 Vdc battery pack and 240 Vac, 50/60 Hz charger
- 76131-02 Stroboscope kit with 12 Vdc battery pack and 120 Vac, 50/60 Hz charger
- 76131-04 Stroboscope kit with 120 Vac, 50/60 Hz power supply
- 76131-03 Stroboscope kit with 240 Vac, 50/60 Hz power supply
- 73783-01 Keyphasor Multiplier/Divider
- 81663-01 Keyphasor Conditioner/Power Supply

*▲ Supplied with DVF 3 and all packages*

*▲ Other velocity transducers are available.*

*▲ For use with Bently Nevada 16699 3-wire velocity transducers.*

*▲ Test cable kit consists of a set of short coaxial cables with BNC connectors for use with the DVF 3 self test function.*

*▲ DVF 3 type 77581-02 has additional features; -18, -24 Vdc power supply to drive Proximitors and the ability to drive two digital plotters simultaneously.*

*▲ See product data sheet L6030 for details on DVF 3 software for IBM AT and compatible computers.*

*▲ US style plug, 110 V ac. Other power and mains plug configurations available for UK, European, Swiss, Australian and North American users.*

**BENTLY  
NEVADA** 

### WORLDWIDE SALES AND SERVICE

**United States of America:** Phoenix, Arizona  Los Angeles, California  San Diego, California  San Francisco, California   
St. Petersburg, Florida  Charlotte, North Carolina  Atlanta, Georgia  Chicago, Illinois  Kansas City, Kansas

Baton Rouge, Louisiana  Boston, Massachusetts  Chester, New Jersey  Buffalo, New York  Cincinnati, Ohio  Tulsa, Oklahoma   
Portland, Oregon  Philadelphia, Pennsylvania  Pittsburgh, Pennsylvania  Dallas, Texas  Houston, Texas

**International:** Argentina  Australia  Brazil  British Columbia  Canada  Chile  Columbia  Egypt  France   
Germany  Greece  India  Indonesia  Italy  Japan  Korea  Kuwait  Malaysia  Mexico  The Netherlands  New Zealand   
Nigeria  Norway  Pakistan  People's Republic of China  Qatar  Quebec  Saudi Arabia  Singapore  South Africa  Sweden   
Taiwan  Turkey  United Arab Emirates  United Kingdom  USSR  Venezuela

**Corporate Office:** P.O. Box 157 • Minden, Nevada, U.S.A. • Telephone: 702-782-3611 • Telex: 7400983 BNC UC • Fax: 702-782-9253

© 1989 Bently Nevada Corporation

## ADRE® 3

### Technical/Ordering Information

#### Fast acquisition and reduction of dynamic vibration data for rotating machinery behavior analysis

The ADRE® 3 system (Automated Diagnostics for Rotating Equipment) provides affordable, fast and simple acquisition and reduction of vibration data for diagnostics on rotating machinery.

The system's ability to simultaneously capture eight channels of dynamic vibration data during machine transient conditions (startup or shutdown), or while the machine is operating at a constant speed, makes ADRE 3 essential for rotating equipment specialists.

An ADRE 3 data acquisition and reduction system consists of:

- One (or up to ten) Bently Nevada 108 Data Acquisition Instrument(s)
- Bently Nevada ADRE 3 application software
- Computer system

With ADRE 3's application software, dynamic waveform records and static data records (vector and scalar values) are retrieved from the 108 Data Acquisition Instrument (108 DAI) or floppy disk, and reduced in a variety of plotting formats suitable for diagnosis of rotating machinery malfunctions.

Ease of use and low cost make it economical to utilize ADRE 3 as part of a (predictive) vibration analysis program. Its ease of operation enables acquisition and reduction of vibration data for analysis with minimal training.

Low weight and compact size make the ADRE 3 system (with "portable" computer) the ideal setup for "in the field" work, on acceptance test and balancing stands, control rooms and laboratories.

ADRE 3 is specifically designed to analyze rotating machinery; in particular, steam and gas turbines, electric motors, centrifugal and screw compressors, vertical and horizontal pumps, turbogenerator sets, hydro turbine-generator sets, turbo expanders, ship propulsion systems, aircraft engines, fans, blowers, reciprocating engines and compressors.

#### 108 Data Acquisition Instrument

The 108 DAI is a highly versatile instrument with many features aimed at application flexibility and easy user interface.



The ADRE 3 system consists of one (or up to 10) 108 DAI Data Acquisition Instrument(s) (left) and computer system with ADRE 3 software (right).

- Vibration input signals can be from acceleration, velocity and displacement transducers.
- Scale factors are user selectable (default values or manual entry).
- Single integration may be performed on each of the eight channels.
- English and metric engineering units can be displayed in pk-pk values for displacement and 0-pk or RMS for velocity and acceleration.
- Independent channel overload and Keyphasor® error LEDs ensure that the user is alerted of irregularities during data collection.

Setup keys on the 108 DAI make it simple to configure the instrument to acquire data. Selections which can be made using the clearly labeled keys include the transducer units, scale factor, full scale range, trigger mode, filter mode (1X or 2X) and bandwidth. The user selects whether data will be acquired based on elapsed time ( $\Delta$ TIME), change in shaft rotative speed ( $\Delta$ RPM), or both.

For ease of use and efficiency, the 108 DAI enables the user to configure and store (in non-volatile EEPROM) up to seven instrument setup configurations. Eight setup configurations can be recalled. The eighth is a factory programmed setup.

For complete system integrity, the user can initiate nine different self tests simply by pressing two dedicated keys simultaneously. The 108 DAI display indicates completion and results of a performed self test. Individual channels can be tested, using the test signal at the rear panel.

Automatic data collection can be pre-programmed, based on elapsed time ( $\Delta$ TIME), changes in machine speed ( $\Delta$ RPM), or both.

Data also can be acquired manually, by pressing the MANUAL SAMPLE key on the 108 DAI front panel, or by a (remote) contact closure.

Each channel on the 108 DAI can store up to 32 dynamic waveform records and 320 static data records. Under  $\Delta$ TIME or  $\Delta$ RPM control, a waveform record is sampled concurrently with each tenth static data record.

When using MANUAL SAMPLE, both a waveform record and a static data record are sampled and stored.

A dynamic waveform record consists of 512 data samples and represents the "real time" vibration waveform from the measured points. The first 256 samples are used for orbit and time base waveform reconstruction and presentation. Antialiasing filters are not used when these samples are taken because such filters introduce phase errors in the data.